EPHEMERAL STREAM-AQUIFER INTERACTION

by

Peter James Dillon , B.E.(Civil)(Hons.)

A thesis presented to the Faculty of Engineering
of the University of Adelaide for the
degree of Doctor of Philosophy

The Department of Civil Engineering
University of Adelaide

March 1984

TABLE OF CONTENTS

LIST OF FIGURES

LIST OF PLATES

LIST OF TABLES

SUMMARY

This study was aimed at exploring the nature of the interaction between a 16 km length of the Little Para River and the underlying Quaternary aquifer, through monitoring and numerical modelling. After a review of the literature revealed no investigation of the process of hydraulic connection of ephemeral streams and aquifers, a boundary integral equation model was constructed to satisfy this need. The model was successfully applied to a range of conceptual stream-aquifer interaction problems for which solutions were available. It was then used to explore the process of hydraulic connection which was observed on the Little Para.

A field study was undertaken over a period of three and a half years to monitor discharge losses in the Little Para River and groundwater elevation changes on a regional scale. During that time a series of controlled releases were made into the stream from the Little Para Reservoir upstream of the study area. In addition a streambed test pond experiment was conducted to observe hydraulically disconnected streambed infiltration on a smaller scale. Data from this overall study were used to derive a recharge release rule for the reservoir. Field data were also used to calibrate and validate the numerical model at five cross-sections on the stream and an analysis of stream discharge loss residuals was performed.

The investigation has led to a better understanding of the process and significance of hydraulic connection between ephemeral streams and aquifers. It has revealed the latent potential for enhancing groundwater recharge by flow regulation in ephemeral streams, both in theory and in a prototype example.

STATEMENT OF ORIGINALITY

I certify that this thesis does not contain material previously submitted for the award any other degree or diploma in any university and that to the best of my knowledge and belief it contains no material previously published or written by another person except when due reference is made in the text.

Peter Dillon

ACKNOWLEDGEMENTS

The author is indebted to his supervisor Mr. R. Culver, Reader in Civil Engineering, for providing the opportunity to undertake this study, for his encouragement and assistance throughout and for his review of the thesis. The contribution of Prof. J. Liggett (on leave from Cornell University) in introducing the author to the Boundary Integral Equation Method, providing a seed computer program and offering constructive criticism during the early stages of program development is gratefully acknowledged.

The Director-General and Engineer-in-Chief of the Engineering and Water Supply Department (EWS) which funded the Little Para field investigation permitted the author to have independent and controlling oversight of the project and to publish results during the progress of the work. Many officers of that department have assisted with field construction, data acquisition, data processing and administration. Particular credit is due to Poh Soon Chong who served as an enthusiastic EWS project liaison officer for over three years. Dr. G. Schrale, S.A. Department of Agriculture loaned tensiometers and numerous personnel of the Department of Mines and Energy drilled observation bores and furnished information.

The author wishes to thank Prof. R. Warner for making available material assistance in the later stages of thesis writing, Mr. S. Woithe, instrumentation technician, who was responsible for the ultimately very successful development of the digital recording system and Civil Engineering Department laboratory and workshop staff, under the direction of Mr. H. Tabalotny and Mr. C. Hunter, for providing assistance as needed. The help of Mr. G. De Vries, Mrs. B. Hope and Mrs. I. Rebellato with manuscript preparation is gratefully acknowledged.

Finally, I am indebted to my wife Ruth for her moral support throughout my candidature.

PRINCIPAL NOTATION

A	region defined by boundary, S (ch 4)
b	saturated medium thickness (ch 3), streambed base width (ch 5)
B	streambed hydraulic impedance (eqn 4.37)
C	specific moisture capacity
{c}	vector of knowns for right hand side (eqn 4.27)
D	initial aquifer saturated thickness (ch 5)
DE	change in storage below the free surface during a time step
DLTS	net flux through the boundaries during a time step
[E]	combination of matrices [R] and [L] in eqn 4.27
{FCORN}	product of [L] and $\frac{\partial h}{\partial n}$ which are known at boundary (eqn 4.57)
g	gravitational acceleration
h	hydraulic head
h_c	effective capillary drive (eqn 3.47)
h_s	elevation of stream stage
h_2	is the greater of h_s and y_m
h_o	maximum change in stream stage (section 5.3.2)
H	elevation of stream stage after step change (section 5.3.1)
H_w	height of stream stage above base of semipermeable layer (approximated by stream depth)
i	infiltration rate
k	intrinsic permeability of a porous medium
K	hydraulic conductivity of a fluid in a porous medium
K_B	hydraulic conductivity of semipermeable streambed blanket
ℓ	thickness of semipermeable streambed blanket
L	depth from soil surface to a wetting front (ch 3), characteristic length for BIEM model (eqns 4.42,4.43) lateral extent of an aquifer (ch 5)
[L]	matrix of coefficients of normal hydraulic gradient (eqn 4.24)
$\overline{M}$	mean model groundwater elevation change (ch 9)

n	Mannings roughness coefficient, neutron moisture meter count rate ratio (ch 7)
n'	neutron moisture meter count rate ratio adjusted for density
n_e	effective porosity of a porous medium
n_g	gamma-gamma density meter count rate ratio
p	fluid pressure (called soil suction pressure when negative), with respect to atmospheric pressure
PDER	percentage mass balance error for a time step
PTER	percentage mass balance error since t=0
q	exchange flowrate between stream and aquifer (recharge is +ve)
Q	stream discharge rate (section 8.1)
Q_m	model stream discharge loss (ch 9)
Q_p	prototype stream discharge loss (ch 9)
Q_R	recharge rate due to stream discharge rate, Q (section 8.1)
$[R]$	matrix of coefficients of h in BIE's (eqn 4.24)
RMSS	root mean sum of squares of differences between prototype observations and model values
s	fractional saturation of pore space in a porous medium
S	storage coefficient of an aquifer boundary of region, A (ch 4)
S_C	sensitivity index used by Cunningham and Sinclair (eqn 9.7)
S_D	sensitivity index used in thesis (eqn 9.8)
S_s	specific storage of a porous medium
S_y	specific yield of unconfined aquifer
t	time
t^*	time as a dimensionless variable (eqn 4.42)
T	aquifer transmissivity, or fluid temperature
TDE	change in storage below the free surface since t=0
TLTS	net inflow since t=0
TR	time ratio (ch 9)
u	local coordinate used in boundary integration

$\{u\}$	vector of boundary unknowns to be solved (eqn 4.27)
v	Darcy fluid velocity = discharge rate / cross-section area local coordinate used in boundary integration
V	bank storage (ch 5)
w	dimensionless infiltration rate = W/K
W	groundwater recharge rate (infiltration rate at the water table)
W_b	width of base of trapezoidal channel (section 5.4.2)
x	axial coordinate
y	axial coordinate
y_b	elevation of the base of an aquifer
y_m	elevation of the base of a semipermiable layer below a streambed
z	axial coordinate
α	interior angle at a boundary node between adjacent elements aquifer diffusivity (ch 5)
β	angle between free surface and horizontal axis
$\bar{\beta}$	dimensionless expression for width of an aquifer (eqn 5.27)
δ	constant fixing skewness of stream stage oscillation (eqn 5.21)
ΔS_D	change in S_D due to a change in parameter value (ch 9)
Δt	time increment in BIEM model
$\frac{\partial h}{\partial n}$	normal hydraulic gradient at a boundary
$(\frac{\partial h}{\partial n})_1$	norm. hyd. grad. approaching a node in a clockwise direction
$(\frac{\partial h}{\partial n})_2$	norm. hyd. grad. leaving a node in a clockwise direction
$(\frac{\partial h}{\partial n})_b$	norm. hyd. grad. at the base of an aquifer
ϵ	weighting factor in implicit time stepping procedure (eqn 4.46)
ψ	pressure head (fluid pressure in metres of fluid)
ψ_{cr}	water entry value of ψ in an unsaturated soil (eqn 3.32)
Ψ	depth of water in the stream (section 5.3.2, eqn 5.20)
ϕ	head of node which initially is on the free surface where it intersects the line of symmetry
ϕ_s	elevation of constant stream head (section 5.4)

η	elevation of the free surface
ρ	density of fluid (ch 3) or bulk dry density of soil (ch 7)
ρ'_{wet}	modified bulk wet density of soil (ch 7)
θ	volumetric moisture content (ch 3)
θ_T	total volumetric moisture content ($\theta + \theta_e$) (ch 7)
θ_e	equivalent vol. moisture content of constitutional hydrogen
τ	period of stream stage (eqn 5.21)
ω	frequency of stream stage oscillation
χ^2_C	metric of closeness of fit of model to prototype data (eqn 9.3)
χ^2_D	metric of closeness of fit of model to prototype data (eqn 9.4)

CHAPTER 1

INTRODUCTION

1.1 Study Origin

This study arose due to problems encountered in estimating mean annual groundwater recharge from flow in the Little Para River, South Australia. Uniform releases from a reservoir gave rise to time-varying discharge losses over a 16km length of stream. Observation bores adjacent the stream revealed that goundwater levels rose and fell in response to streamflow. During sustained flow groundwater intercepted the streambed in some reaches and discharge losses declined. This feedback effect of groundwater levels on discharge losses was important in estimating the mean annual recharge.

Consequently an investigation commenced having two major thrusts. The first was to monitor discharge losses and groundwater elevations in a full scale field study on the Little Para River. The second was to develop a numerical model to describe the hydraulics of all phases of ephemeral stream-aquifer interaction including the process of interception of a streambed by a rising groundwater mound.

1.2 Objectives

The study had two principal objectives. The first was to explore the fundamentals of streambed hydraulics which govern the exchange of water between ephemeral streams and aquifers. Secondly a solution was sought to a practical reservoir operation problem for the Little Para Reservoir.

Answers were sought to a number of questions on streambed hydraulics. How is the exchange flow rate affected when the groundwater mound impinges on the streambed? What effect has the hydraulic conductivity of a semipervious blanket on the streambed on exchange flow rate? These and

many other questions were answered with the use of a numerical model.

The reservoir operation problem had two aspects. It required the selection of a reservoir release rule to ensure that the mean annual streambed recharge downstream is not reduced by the presence of the dam. This in turn demanded that the mean annual recharge prior to dam construction be quantified. A field study was conducted on the Little Para River to give the necessary information to satisfy these requirements.

1.3 Limitations

The field study was confined to the Little Para River only and to a duration of three and a half years. The river contained reaches which were intersected by the groundwater mound and reaches permanently elevated above the mound. The results reflect the condition of the streambed between February 1979 and June 1983. Changes in streambed geometry and consequently recharge performance are expected to occur due to an increase in the urban catchment area and the effect of the dam.

The limitation of computer speed was a significant constraint on the study. The numerical model for investigating stream-aquifer interaction processes could not be applied to long discharge records (more than about two months), simply because execution times became excessive. Simulation runs to determine mean annual recharge and test reservoir release policies used 14 to 30 years of discharge data. Thus a simple lumped parameter management model was developed and used to solve the reservoir operation problem.

1.4 Organization of Report

Chapter 2, which is summarized in Appendix C.1, covers a review of the pertinent literature on stream aquifer interaction models and investigations with emphasis on the founding assumptions of the models. This leads into a discussion of the equations of groundwater flow and infiltration presented in Chapter 3.

The fourth and fifth chapters deal exclusively with the two

dimensional boundary integral equation model of stream-aquifer interaction developed by the author and based on a seed program of Professor James A. Liggett of the School of Civil and Environmental Engineering, Cornell University. Chapter 4 describes the mathematical basis of the model and the various boundary conditions which distinguish it from other models. This is followed in chapter 5 by a description of applications of the model to test problems, hydraulically disconnected and connected stream-aquifer problems and to the process of hydraulic connection. The effect of varying major parameters on exchange flow rate and groundwater elevation below the stream centre line is shown for a simple example. An illustration of the effect of flow regulation on recharge is given and this is used to investigate aspects of linearity, system memory and time variance of stream-aquifer interaction.

Chapter 6 outlines the purpose and conduct of the Little Para Recharge Study, including data acquisition, processing and analysis. Chapter 7 describes an experimental infiltration pond constructed in the Little Para River. The instrumentation, procedure and results of the experiment are documented.

Chapter 8 reports the effect on recharge of stream discharge regulation and describes the approach used to derive a recharge release rule for the Little Para Reservoir.

Chapter 9 brings together the numerical model and data from the Little Para Recharge Study. A three stage calibration procedure is described. The model is calibrated and validated at five cross-sections on the stream and the fit of the model against field data is analysed.

The conclusions to be drawn from the study are presented in chapter 10 and reference is made to the potential for recharge enhancement by discharge regulation in ephemeral streams.

CHAPTER 2

LITERATURE REVIEW

The relationship between flow in rivers and groundwater is fundamentally important to the science of hydrology. A wealth of theoretical, experimental and field work has been documented on this subject yet there are still uncertainties about the physical processes which govern the interaction of surface and groundwater at and below the streambed. This review identifies and critically assesses the assumptions upon which stream-aquifer interaction models are founded. These models will be classified as groundwater models, surface water models and integrated models (open channel flow and groundwater models coupled together as a composite model) (see figure 1 in Appendix C.1).

2.1 Groundwater Models

Investigations of the nature of the interaction between streams and aquifers have resulted in two broad classifications: the hydraulically connected and the hydraulically disconnected stream. See figure 2.1 (after Ward, 1974). Sheshtakov and Kravchenko (1967) applied the terms "supported seepage regime" and "free seepage regime" to the same conceptual models. Bear (1979) and Rushton and Tomlinson (1979) expanded on this classification by considering circumstances in which different parts of the same streambed exhibited each type of behaviour (figure 2.2).

A hydraulically connected stream is assumed to have a completely saturated streambed below the elevation of the water in the stream. The hydraulic head in the aquifer immediately adjacent to and below the stream is assumed to be the same elevation as the water level in the stream. In groundwater modelling, such a stream is generally taken to be a line of

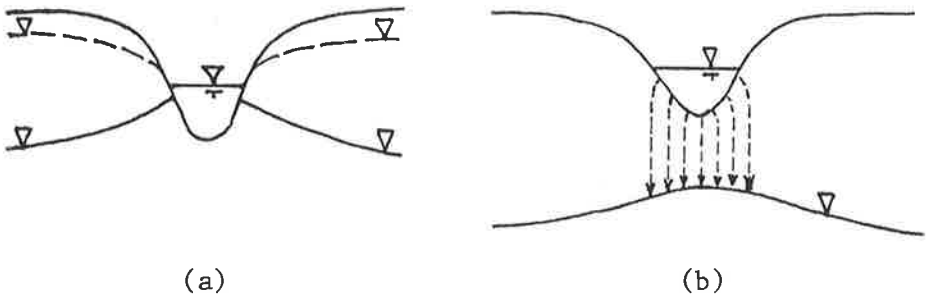

(a) (b)

Figure 2.1 Stream and aquifer (a) hydraulically connected and (b) hydraulically disconnected.

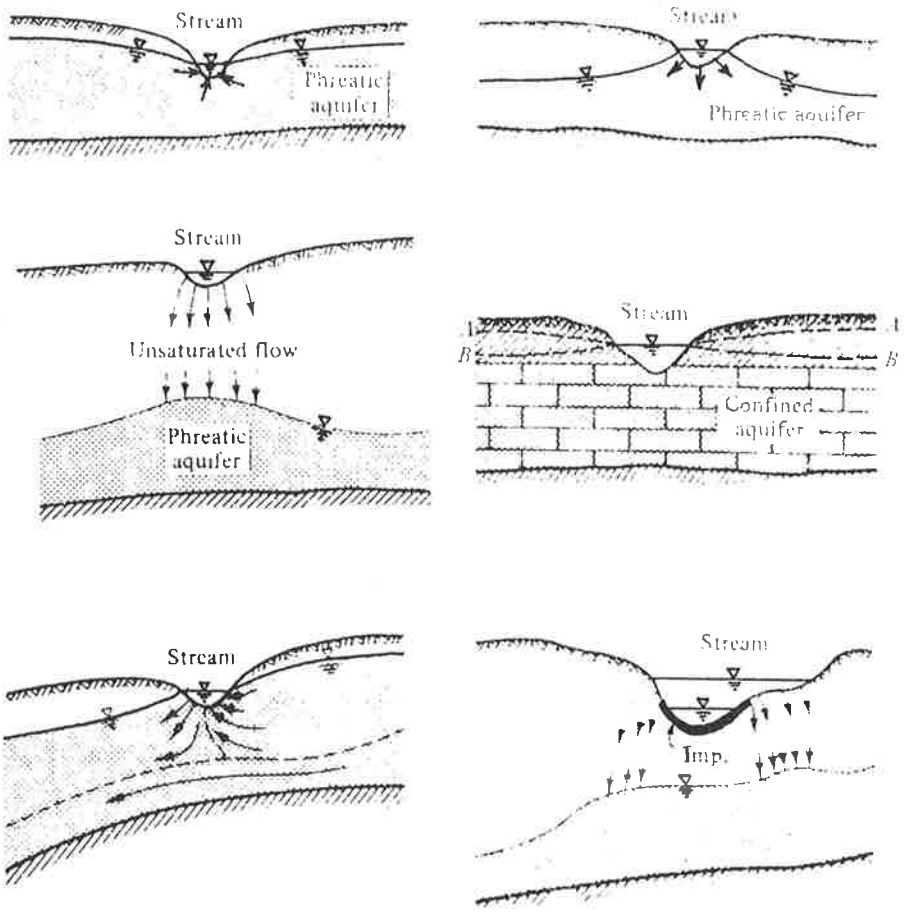

Figure 2.2 A range of relationships between streams and aquifers (after Bear, 1979, figure 3-9).

known or specified hydraulic head and groundwater flow is assumed horizontal.

A hydraulically disconnected stream has an unsaturated zone below the streambed. A change in head in the aquifer below the stream is assumed to have no influence on the water level in the stream nor on the seepage rate. In groundwater modelling the stream is generally considered a line source of water with seepage rate specified. Vertical flow is assumed to occur between the streambed and the watertable where a groundwater mound or ridge develops and spreads laterally.

Walton et al (1967) and Burkham (1970) depict a transition from a hydraulically disconnected stream to a hydraulically connected stream if the groundwater mound rises until it intersects the streambed. Most of the subsequent integrated models adopt a similar criterion. There is a notable absence in the literature of numerical or experimental studies concerning the nature of this transition.

A hydraulically disconnected stream is also called an influent or losing stream and is typical of the ephemeral streams or wadis found in arid and semi-arid areas of low relief. A hydraulically connected stream may alternate between being influent or effluent (gaining) depending on whether the stream stage at the section considered is rising or falling respectively. Such a stream may be perennial and commonly has its source in a humid or alpine zone. Future references to hydraulically connected streams, emphasise groundwater recharge, (seepage from the stream into the aquifer) as opposed to baseflow (seepage from the aquifer into the stream).

2.1.1 Hydraulically connected streams

The assumptions on which many hydraulically connected stream models are based were critically reviewed by Sharp (1977) and are included in the following list.

(1) The alluvial aquifer has a horizontal impermeable base.

(2) All porous media flow is saturated.

(3) Water is discharged from storage instantaneously upon reduction in head.

(4) The alluvial aquifer is homogeneous, isotropic and infinite in extent.

(5) The Dupuit-Forchheimer conditions are valid i.e.

(a) In any vertical section the groundwater flow is horizontal.

(b) The velocity is uniform over the depth of flow.

(c) The head is constant along any vertical line for the whole thickness of the aquifer.

(d) The slope (β) of the free surface is small enough that $\tan \beta \doteq \sin \beta$.

(6) The stream penetrates the full thickness of the aquifer (or alternatively the head throughout the aquifer below the stream bed is always equal to the river stage).

(7) The aquifer is solely confined or solely unconfined. If the aquifer is unconfined the fluctuations in the water table are a small fraction of aquifer thickness so that the transmissivity remains constant.

(8) The system is isothermal.

(9) The quality of water in the stream has no cummulative effect on the stream-aquifer interaction processes.

(10) Groundwater flow in a direction parallel to the stream does not affect the stream-aquifer interaction.

Sharp accepts the first three assumptions as being applicable to the real world. Each assumption is reviewed below.

(1) The alluvial aquifer has a horizontal impermeable base.

Most of the analytical models make this assumption. Four exceptions

were found. McWhorter and Brookman (1972) allow uniform leakage from a confined aquifer. Singh (1968) considers an unconfined aquifer with uniform leakage or evapotranspiration. Bouwer (1975) and De Wiest (1967) allow leakage or evapotranspiration from an unconfined aquifer at a rate which is proportional to hydraulic head in the aquifer. While numerical models are capable of handling sloping and semipervious aquifer bases these effects on stream aquifer interaction have not been referred to explicitly in the literature. If permeabilities of the underlying layer are sufficiently low (less than one tenth the permeability of the aquifer according to Bouwer, 1969, p. 148) and the slope is small, as is usually the case, these assumptions are satisfactory. The case of leakage from perched mounds beneath the streambed is not considered here as it is reviewed in detail in section 2.1.2.2.

(2) All porous media in the region of flow is saturated.

The saturated flow assumption has been examined by several writers. Bouwer (1964) concluded that negative pressure flow could be neglected for horizontal flow and for perched layers where the capillary fringe thickness is very small in comparison with the thickness of the saturated zone. Skaggs and Tang's (1976) investigation of flow to parallel drains, and Luthin et al's (1975) investigation of radial flow to a well with constant drawdown support Bouwer's conclusion.

(3) Water is discharged instantaneously from storage upon reduction in head.

The assumption of spontaneous discharge with decline in head is refuted by Vachaud (1967). He claimed that during draining or recharge the vertical moisture profile in the vicinity of the phreatic surface is not in equilibrium. That is specific yield is not a constant but increases towards a constant value with time. For the sand samples he tested approximately 4 days was required for complete draining. Narasimhan and Yanehiro (1980) concluded that specific yield could be considered constant

provided that sediments were rigid and were only subject to slow variations of pore pressure with time. For hydraulically connected streams, unconfined groundwater flow is activated by hydraulic head changes which are conveyed by mass transfer through the porous medium at slow rates. Thus the spontaneous discharge assumption (constant specific yield) is unlikely to be violated except in the small zone within the banks immediately in contact with the river water following rapid stage changes.

(4) The alluvial aquifer is homogeneous, isotropic and infinite in extent.

The assumption of homogeneous isotropic alluvial aquifers is an obvious starting point when data are scanty. Sharp (1977) found typical river alluvium in central United States had increasing permeability with depth. Numerical solutions for hydraulic head distribution in an aquifer with this observed permeability distribution were compared with those for homogeneous permeability for a step change in river stage. Large discrepancies in hydraulic head were observed particularly in the vicinity of the streambed. Bouwer (1969,p.147) described investigations using an electrical resistance analogue to determine steady state seepage rates from a trapezoidal channel into a two layered porous medium. These compared favourably with results adapted from Ernst over a more comprehensive range of geometric configurations of the two layered medium. If the second layer is more than five times the channel width below the channel bed, then it has only a very small influence on the seepage rate. As the top of the second layer approaches the channel bed its effect becomes important, particularly if the underlying layer is more permeable as in the cases reported by Sharp. These results indicate that flow in heterogeneous media may be poorly modelled by homogeneous medium models.

In analytical models anistropy may be accounted for by transforming the medium to an equivalent isotropic medium with a permeability of $(K_x K_z)^{0.5}$ by multiplying the vertical dimensions by $(K_x / K_z)^{0.5}$ where

K_x is the horizontal permeability and K_z is the vertical permeability (Bouwer, 1969, p 145). No cases were found within the literature in which the effects of anisotropy on seepage rates were explicitly evaluated for hydraulically connected streams.

Bianchi and Haskell (1968) observed that differences between field observations and theoretical predictions for alluvial aquifers were much more dependent upon the ability to define the domain and properties of the porous media than on approximations in groundwater flow theory. Typical descriptions of alluvial aquifers include "discontinuous and interbedded lenticular deposits of silts, sands or gravels" (Miles, 1952).

Streambed hydraulic conductivities may change in time as well as in space. Scour during high stream stages and deposition of fine materials on the streambed during low flow may also affect the rate of exchange of water between streams and aquifers. Jordan (1977), Lang and Rhodehamel (1962), Norris (1970), Randall (1978) and Tixeront and Daniel (1967) all refer to increased seepage where scour occurs or relate the infiltration rate to the velocity of surface flow for particular streams.

The effect of finite distances between streams and aquifer boundaries has been investigated for analytical models. Marino (1973) and Cooper and Rorabough (1963) described transient flow with impermeable boundaries and Sharma and Chawla (1979) investigated the case of steady state flow with drains at the boundary. These authors showed that the effects of various boundary conditions can be readily incorporated into their models. Similarly, numerical models allow a range of boundary conditions to be specified without mathematical complications.

(5) The Dupuit-Forchheimer conditions apply.

The set of assumptions known as the Dupuit-Forchheimer (DF) assumptions are used to reduce the number of dimensions of a problem. Even with the DF assumptions the resulting Boussinesq equation is still nonlinear and solutions to it are difficult to obtain (Lin, 1972). Several

methods of linearizing the Boussinesq equation have been described in detail by Bear (1972).

Gelhar (1974) compared spectral response characteristics of phreatic aquifers modelled with and without the DF assumptions. (Models which do not use the DF assumptions are called potential flow models.) Only when the degree of penetration of the river into the aquifer was small or the aquifer was significantly anisotropic the results of the two models diverged. Otherwise the DF model results were in good agreement with those of the potential flow model.

Results based on studies of growth and dissipation of groundwater mounds for disconnected streams with both models (Khan, Kirkham and Handy, 1976 and Brock, 1976b) indicate that for small mound heights DF and potential models give good agreement. Marino (1967) showed DF results agreed within 5% of Hele-Shaw analogue results for mound heights up to 50% of the initial saturated depth. These conclusions when applied to aquifer connected streams indicate that DF is a valid assumption to use if the stream is fully penetrating a homogeneous aquifer. Sharp (1977) however found this was not the case for the rivers he studied.

(6) The stream penetrates the full thickness of the aquifer.

Complete penetration of the aquifer by a stream appears from the literature to be the exception rather than the rule. Vertical flow usually occurs immediately beneath the streambed. Granneman and Sharp (1979), Lang and Rhodehamel (1962) and Pluhowski and Kantrowitz (1962) all observed vertical hydraulic gradients within the streambed of hydraulically connected rivers. Walton et al (1967) showed that drawdown on one side of a river would occur when pumping on the other side was sufficient to cause disconnection of the stream and aquifer. Ferris et al (1962, p 129) accounted for partially penetrating streams by considering the head change in the aquifer adjacent the stream rather than the river stage change as the driving head for transient groundwater flow. This method also accounts

for semipervious stream banks, but does not give an understanding of the physical processes occurring in the immediate vicinity of the streambed.

Hall and Moench (1972) and Marino (1973) used an equivalent method by considering semipervious banks on a fully penetrating stream as an approximation to a partially penetrating stream. Herbert (1970) used an electric analogue to study steady state seepage from a partially penetrating river of semi-circular cross-section to a pumping well. Ernst (1979) and Streltsova (1974) used superposition in analytical methods for determining seepage rates. Herbert's results indicate that complete penetration assumptions may overestimate seepage rates by 30%. Bouwer (1978, p 288) also using an electrical resistance analogue gives the maximum depth of the active region for a narrow stream overlying a deep isotropic aquifer as about equal to the width of the recharge area. He suggests the use of a reduced or "effective" transmissivity for this zone.

Rushton and Tomlinson (1979) considered the recharge mechanism and its relationship to penetration of a stream into an aquifer. For partially penetrating streams the vertical flow component may complicate the measurement of hydraulic gradient below the streambed. Rushton and Tomlinson proposed that the vertical flow be neglected and using the Dupuit-Forchheimer approximations assigned a single value for the head in the aquifer underlying the river. They proposed a series of possible relationships between the leakage rate through the river bed and the head difference between the river and aquifer. They concluded that leakage rate may be modelled best by the sum of linear and exponential head difference terms. That is they added a nonlinear component to Darcy's law. Their model did not distinguish between increase in stream head and decrease in aquifer head, nor account for the aquifer head at which hydraulic connection was broken. Hadgraft and Volker (1981) followed the same approach in modelling stream-aquifer interaction in the Burdekin Delta, Queensland, Australia.

Narasimhan et al (1978) use a finite element model to simulate groundwater levels subject to pumping and infiltration from a partially penetrating stream. They assume Darcy's law for seepage until the maximum rate is reached at the aquifer head where the hydraulic connection with the stream is broken. The transmissivity varies with aquifer head as does the seepage rate while the stream is hydraulically connected. For this reason the problem becomes nonlinear.

(7) The aquifer is solely confined or solely unconfined.

The change from unconfined to confined states complicates modelling both on a regional scale (Rushton and Tomlinson, 1975) and on a local scale (Sharp, 1977). These problems can be countered by careful selection of spacial grid and time increments for use in numerical modelling.

Assumptions 8 to 11 apply to both hydraulically connected and disconnected streams.

(8) The system is isothermal.

Norris (1970) found a 35% increase in streambed leakage due to an 11^{o}C increase in stream temperature, reducing the viscosity of water. Similar effects were presented by Walton and Ackroyd (1966). Worstell (1976) reports temperature changes affecting gas pressures in the soil thereby affecting soil hydraulic conductivity. Seasonal and even diurnal temperature variations may significantly influence seepage rates and should be accounted for. Thermally stratified flow is possible when recharged water is significantly warmer than the underlying groundwater.

(9) Water quality has no affect on stream aquifer interaction.

Suspended sediments as well as chemical and biological constituents warrant study for each particular stream being considered. In many cases this assumption is valid. For catchments exhibiting changes in land use, water quality may change (Cordery, 1976) and disturb the interaction between surface water and groundwater. Some investigations performed on

the Burdekin Delta, Queensland have identified the effects of siltation on recharge rates (James and Henry, 1977 and Watson and Whisler, 1977) and some of the biological problems (Jackes, 1981) for artificial recharge from strip basins. Warner and Doty (1967) examined feasible chemical reactions between recharged surface water and groundwater which may precipitate compounds causing a reduction in aquifer permeability. Nightingale and Bianchi (1977) recorded a transient increase in turbidity of water drawn from wells following recharge into a bore. Although these studies were based on artificial recharge operations they may be extended to account for changes in stream aquifer interaction for cases where stream water quality is changing due to catchment land use changes or the diversion of water from other streams.

An implicit assumption in (9) is that the density difference between stream water and aquifer water is sufficiently small to preclude density stratified groundwater flow. Grodzensky (1967) did not make this assumption and examined the volume of fresh water leaking from canals to form lenses overlying saline groundwater. His paper illustrates an exceptional case. For natural losing streams the stream is the source of water in the alluvial aquifer which justifies the assumption that the density difference is negligible.

(10) Stream-aquifer interaction is independent of underflow.

Analytical models which considered the effects of groundwater movement in the direction parallel to the stream were not found within the literature. Numerical modellers were not explicit in their findings on this subject either. Pinder and Sauer (1971) precluded this effect in their bank storage model, by their selection of boundary conditions.

In summary the effectiveness of modelling the interaction of streams hydraulically connected to aquifers depends more on how account is taken of partial penetration, spatial variability of the porous medium, temperature

effects and the choice of boundary conditions than on the mathematical simplification of the flow equations. Spatial discretization of the medium should therefore be in accordance with the amount of stratigraphic data available. The success of a number of models in matching sand tank, electric resistance and Hele-Shaw experimental results is unlikely to be extended into the field unless adequate definition of the actual flow field is successful (Bianchi and Haskell, 1968).

2.1.2 Hydraulically disconnected streams

Models of porous media flow beneath hydraulically disconnected streams fall into three categories -

1) vertical flow models
2) groundwater mound models

and 3) combined models of vertical flow and groundwater mounds.

A tree diagram of the classification of stream-aquifer models appears as figure 1 in Appendix C.1.

The vertical flow or infiltration models are useful during the advance of flow in an ephemeral stream for predicting transient seepage rates and the advance of the wetting front until steady seepage occurs. Groundwater mound models predict the shape of the free surface developing under this seepage source. Their importance for stream-aquifer interaction is in predicting if or when the groundwater mound will rise to the streambed. At this point the stream would become hydraulically connected and in general the groundwater mound models would cease to be applicable. Combined models generally rely on Richards equation (discussed in chapter 3) requiring detailed information on porous media hydraulic properties and time consuming solutions. An analysis of the underlying assumptions of these models will be restricted to their effect on stream-aquifer interactions.

2.1.2.1 Vertical Flow Models

Analytical steady state vertical flow models have been developed to investigate the effects of anisotropy of soil (Reddy and Basu, 1976) and of channel shape (Hunt, 1972) on seepage rates and on the location of the flow boundary. Their results showed that seepage rates were insensitive to both these parameters for the cases they considered. A large number of vertical flow models however dealt with transient conditions. The common assumptions are:

1) Flow is one-dimensional (vertical).

2) A sharp wetting front occurs.

3) The soil is initially dry.

4) Resistance to the flow of air displaced by water is negligible.

Freeze (1969) gives an excellent summary of literature preceding his paper, indicating the major assumptions of each. Therefore papers published prior to 1969 are not reviewed here. Each of the four listed assumptions are examined by considering models in which they were not used.

(1) Flow is one dimensional.

Bouwer (1969) used an electrical resistance analogue to investigate saturated flow beneath trapezoidal channels with a range of channel stages. He found the effect of stage on seepage rate to be more pronounced for hydraulically disconnected streams than for hydraulically connected streams. As stream stage increased the stream width increased and widened the strip of vertical flow below the channel. For this case gravity provides the driving force. Talsma (1969) investigated the case of unsaturated infiltration from semi-circular furrows over a short time span when adsorption is the major force and gravity forces can be very small in comparison. For larger scale sources or longer time intervals it appears that the one dimensional assumption is satisfactory. This is supported by the location of the flow boundaries for seepage from channels in two

dimensional variational inequality methods presented by Bruch and Sloss (1978) and Bruch, Sayle and Sloss (1978).

(2) A sharp wetting front occurs.

The assumption that a sharp wetting front occurs allows the use of various one dimensional infiltration and drainage equations as compared by Whisler and Bouwer (1970). Green and Ampt's equation is most commonly used as all parameters have a physical meaning and are measurable in the field (Bouwer, 1969, p.158). This implies a horizontal wetting front moves downwards until it reaches the water table, or in the case where permeability increases with depth, the wetting front stabilizes at an equilibrium position (Bouwer, 1976). Numerical modelling using Richards equation for unsaturated infiltration requires a knowledge of the soil moisture versus suction head (for the wetting curve at least) and unsaturated hydraulic conductivity versus suction head relationships for the porous medium. The results of this modelling provide vertical profiles of moisture content and hydraulic head at any given time after commencement of infiltration. See Webb and Watson (1977) for a typical example. However the data requirements and computer time required for long term transient solutions put constraints on the applicability of this method to the study of full scale stream-aquifer interaction.

(3) The soil is initially dry.

A disadvantage of the piston flow method of Green and Ampt is that it fails to provide for redistribution of moisture within the soil profile. Watson (1981) showed that the moisture profile in the unsaturated zone has a significant influence on the rate and volume of groundwater accretion due to intermittent infiltration at the soil surface. Hence the piston flow model is not expected to give a correct account of transient infiltration rates at the streambed resulting from intermittent flow in the stream. For this reason the proviso is made that the soil is initially dry (Bouwer, 1969, p 157). Field moisture capacity provides another simple initial soil

moisture profile condition. Philip (1969, p 282), Wallace (1977) and Freeze (1969) underlined the importance of initial soil moisture. Freeze wrote "of all the parameters controlling infiltration and recharge it is likely that antecedent soil mositure regime is most important". Although he was referring to catchment surface conditions, it would seem desirable to incorporate initial moisture conditions in some way with the Green and Ampt equation to have an improved but still simple model for ephemeral streambed infiltration.

(4) Resistance to flow of air is negligible.

The models considered above all assume that the displacement of air as the voids became saturated during the advance of the wetting front does not retard the advance of the wetting front. De Backer (1975) pointed out that the flow of two phases air and water is occurring simultaneously resulting in a reduction of the infiltration rate. He suggested that the resistance to the flow of air of the upper layer of soil be incorporated in Darcys law to account for this. Curtis and Watson (1980) performed experiments on sand columns to observe the buildup of pressure of entrapped air flow below an advancing wetting front, and the rate of advance of the front. For the sample tested the rate of advance of the front was reduced by a factor of three compared to the case of free air escape. Also the zone above the wetting front did not saturate completely owing to the upward escape of air. It appears that De Backers suggestion ought to be incorporated into a model for vertical flow. The modified Green-Ampt equation proposed by Morel-Seytoux and Khanji (1974) attempts to account for the viscous resistance to the flow of air and is discussed in chapter three.

2.1.2.2 Groundwater Mound Models

The assumptions on which models of the growth and decay of groundwater mounds are based are similar to those for hydraulically

connected streams. The only difference is that for groundwater mounds the flux of water is specified as a function of time over a particular source line or area whereas for hydraulically connected streams the head in the aquifer below the streambed is specified as a function of time. Assumptions applying to ground water mound models are as listed in section 2.1.1 with the exception of assumption (6). The complete penetration assumption is replaced by specifying the rate of groundwater accretion. The full list of assumptions is :

(1) The aquifer has a horizntal impermeable base.

(2) All flow is saturated.

(3) Water is discharged instantaneously upon reduction in head.

(4) The alluvial aquifer is homogeneous isotropic and infinite in extent.

(5) The Dupuit-Forchheimer (DF) conditions are valid.

(6) The rate of groundwater accretion is constant once the wetting front reaches the water table.

(7) The aquifer is solely confined or unconfined.

(8) The system is isothermal.

(9) The quality of water in the stream has no cummulative effect on the stream aquifer interaction processes.

(10) Groundwater flow in a direction parallel to the line source does not affect the stream aquifer interaction processes.

Only assumptions 1,4,5 and 6 are discussed here. The other assumptions are reviewed in sequence in section 2.1.1.

(1) The aquifer has a horizontal impermeable base.

Perched mounds may occur if the medium is layered or has a semipervious base. Wilson and de Cook (1968) investigating seepage from the Santa Cruz River identified the formation of two sets of perched mounds between the streambed and the regional watertable.

In 1962 Marmion presented the results of an analytical and experimental study of the steady state shape of groundwater mounds perched on discontinuous impermeable and continuous semi-permeable strata. Experimental mound heights exceeded the calculated values by 10%. Marmion considered the discrepancy arose from air entrainment among the glass beads used in his model during the rise of the free surface.

Khan, Kirkham and Handy (1976) compared the steady state perched mound height at the centre of the mound below strip and circular basins using potential theory and a linearized DF model. Mousavi and Kirkham (1978) provided experimental support for the potential theory solution. Brock (1976a) used a nonlinear DF model to calculate transient mound shape under strip and circular basins, and found an exact solution for the steady state perched mound under a strip basin. All the theoretical models assumed atmospheric pressure in the soil immediately below the semi-confining layer. Providing the mound slopes are relatively shallow then DF theory underestimates perched mound heights by 5% (Brock) to 7% (Khan et al) for a strip basin. For all other groundwater mound models the aquifer base is considered impermeable. Baumann (1965, p 222) considered the case of an unsteady groundwater mound forming over an inclined impermeable base, the aquifer initially having a uniform saturated thickness.

(4) The aquifer is homogeneous, isotropic and infinite in extent.

Baumann (1965) also accounted for the effect of drains in the aquifer at a distance from the source on the development of the groundwater mound Amar (1975), Maasland (1959), and Marino (1974a) considered drains symmetrically located on each side of a strip recharge mound. The effect of drains on the shape of a groundwater mound is best illustrated by Marino (1974b) who examined the case of a drain on one side of a strip mound, the other side being regarded as a semi-infinite aquifer. For his example more than 75% of infiltration flowed towards the drain. For a more distant drain the mound approached the symmetric case. In the literature no

explicit reference was found for impermeable lateral boundaries affecting the development of groundwater mounds. Neither nonhomogeneous nor anisotropic aquifers were considered in the analytical models of groundwater mounds found in the literature (except for Marmion, 1962). While most numerical models were capable of dealing with these features no literature reporting such investigations was uncovered.

(5) The Dupuit-Forchheimer conditions are valid.

The Dupuit-Forchheimer assumptions applying to perched mounds are examined in section 2.1.1. For mounds on an impermeable base Marino (1967) compared a linearized DF approximation with a Hele-Shaw analogue and found agreement of mound heights within 5% for mound heights up to 50% of the initial saturated depth. Singh (1976) compared transient mound heights under strip and circular basins for potential flow and DF models and found good agreement in each case. Smiles and Knight (1979) solved the non-linear Boussinesq equation in two ways to give consistent results as expected. Most models considered mound heights within the range specified by Marino. However for initially thin saturated aquifers and for steep mounds, vertical flow components are significant and the DF theory underestimates mound heights considerably, Khan et al (1976).

(6) The rate of groundwater accretion is constant.

Most models assume that the rate of groundwater accretion is constant with respect to time. Glass et al (1977) however allow a transient seepage rate in accordance with the Green and Ampt equation for a circular pond and mound. Youngs (1977) and Smiles and Knight (1979) use Barenblatts transformation which may be aplied for strip seepage at a rate which is proportional to some constant power of time. Marino (1974a) considers a groundwater mound between drains with uniform spatial recharge at a rate which reduces exponentially with time. Providing continuous infiltration occurs at the streambed the constant recharge assumption for the development of the groundwater mound is satisfactory. However for

intermittent infiltration, input to the saturated zone model should be consistent with drainage from the vertical flow model. Models which combine the vertical flow and groundwater mound models have the advantage that continuity across the water table is automatically maintained.

2.1.2.3 Combined Models

The array of constraining assumptions which are used to simplify vertical flow models and groundwater mound models are not required in these more complex models. The few common assumptions of these models are attributed to experimental convenience for easier verification of the models rather than on limitations of the applicability of the theory or numerical procedure. For instance homogenous media and horizontal impermeable bases are used in most cases. Similarly convenient initial conditions are chosen. These also ensure that the model starts from the steady state. One remaining assumption is that of no air entrainment.

Freeze (1971) describes a 3 dimensional transient saturated-unsaturated flow model. The model requires vast amounts of data. For instance the relationships between pore pressure and density of water, compressibility of the medium and the soil moisture content, porosity and specific permeability are required as inputs for each soil type. The equation for flow is a combination of the Jacob-Cooper equation for saturated flow and the Richards equation for unsaturated flow. Freeze used the model to investigate the formation of a perched mound (1971), and also the variation of baseflow in a stream (1972). In each case processing time for the finite difference solution prevented more than 2 dimensions being modelled. Taylor and Luthin (1969) and Luthin et al (1975) used a saturated- unsaturated transient flow model based on Richard's equation for potential distribution around a discharging well. The model is in a form suitable for use in predicting potential distributions below circular recharge ponds.

Vauclin et al (1979) investigated the formation of a groundwater

mound below a strip source at constant infiltration rate with parallel drains at a finite distance on each side. Hydraulic head and moisture content were measured in a sand tank analogue and compared favourably with the results of a numerical model. Between the bed of the source and the downward moving wetting front the water pressure becomes constant (and negative) giving gravitational flow. Further away from the source, flow is predominantly horizontal with a small upward component. Results were compared with those from saturated flow models. These cannot predict the duration of the time of transfer of water to the water table. They also underestimate the growth of the groundwater mound and overestimate the storage beneath it. Vauclin et al (1979) concluded that these models failed to account for the very small change of water storage resulting from very large changes in water pressure in the zone immediately above the moving water table. The assumption of a time invariant specific yield is invalid for these saturated flow models in agreement with Vachaud (1967).

The saturated models, such as Marino (1967) also assume that the temporal and spatial distribution of flux reaching the water table is the same as the infiltration rate at the source but delayed by a constant time factor. Vauclin et al showed that the recharge rate (rate at which water reaches the water table) increases from zero at the time of transfer to eventually reach the infiltration rate. During this time the width of the recharge zone increases and the rate of recharge at each point increases (figure 2.3). The same paper also indicates the relationship between the time of transfer of water and the infiltration rate and water table depth for the particular case considered.

The numerical analysis used consisted of a finite difference solution to Richards equation which was applied to both the saturated and unsaturated zones. An alternating direction implicit scheme was used and results gave excellent agreement with the sand tank analogue. However stability requirements demanded small time steps and the computer time for

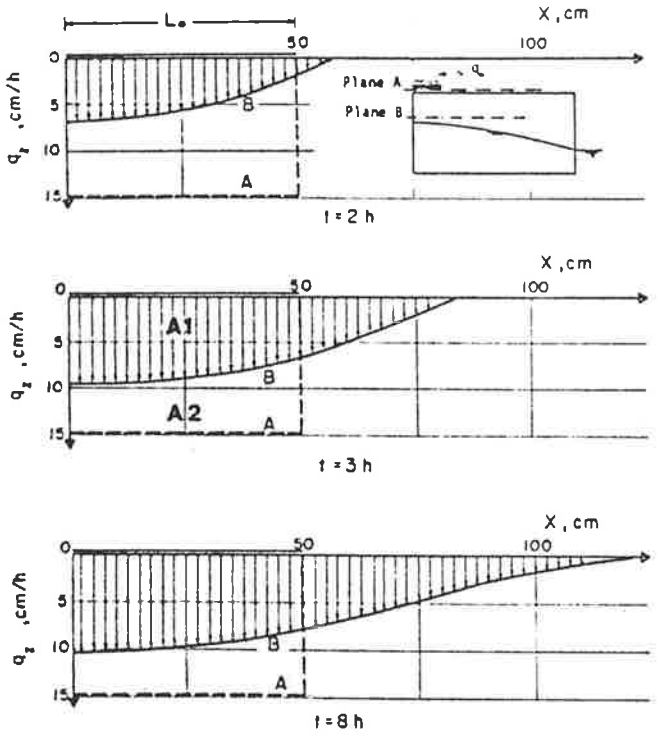

Figure 2.3 Distribution of recharge at the water table below a strip source of infiltration at 15 cm/h over a 50 cm width at 2, 3 and 8 hours after the start of infiltration (after Vauclin et. al., 1979, figure 14).

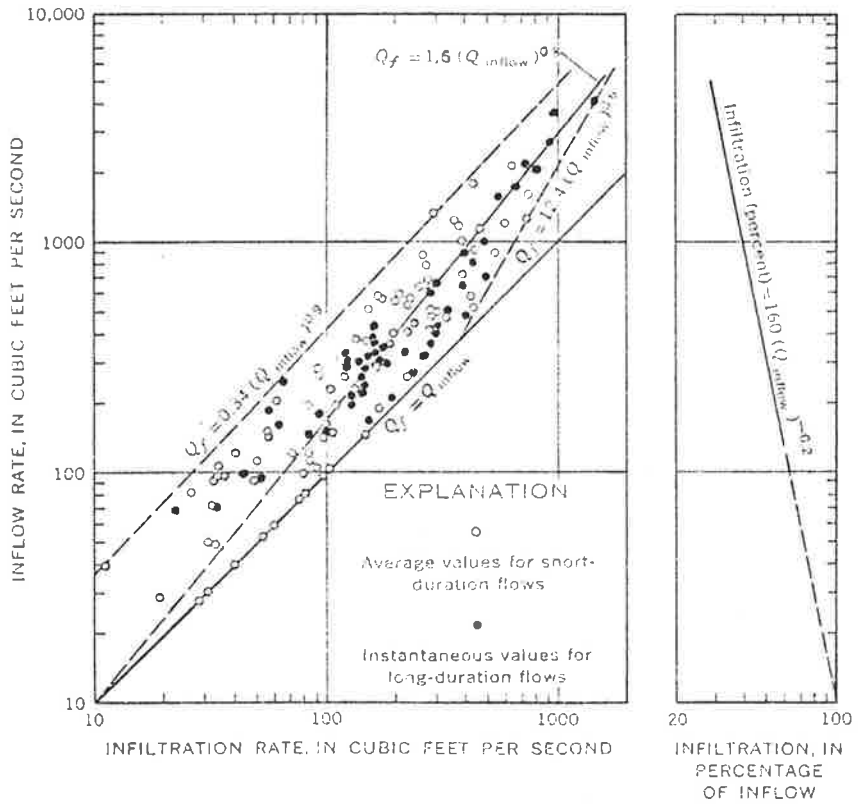

Figure 2.4 Relationship between upstream discharge rate and infiltration rate for the 46 km reach of the Santa Cruz River from Continental to Tuscon, Arizona (after Burkham, 1970, figure 3).

solution was 18 times the real time of the 8 hour experiment. For a grid of 396 nodes the calculation time on a IBM 1130 computer was 3 minutes per time step. Clearly this form of solution is not feasible for field studies but it does provide an understanding of the physical processes occurring during recharge operations.

Up to this point consideration has been given only to flow within the porous medium. It may be necessary to give attention to surface flow if this dictates the spatial and temporal distribution of water available for recharge. The quality of the surface water and the effect of flow history on the shape of the river channel and the composition of the streambed and banks also affect recharge.

2.2 Surface water models

Observations of streamflow at pairs of gauging stations on a stream have been used to determine infiltration rates for reaches of various streams. Todd (1959) lists seven independent studies of stream discharge losses (Irwin (1931), Baker and Conkling (1930), Burgess (1911), Lee (1912), Meinzer (1917), Babcock and Cushing (1942) and Turner (1943)), each of which reported that infiltration rates increased as the discharge rate in the stream increased. Most mentioned that the presence of silt layers in the streambed reduced the rate of infiltration. Burkham (1970) plotted the relationship of infiltration rate to discharge rate for a 46 km reach of the Santa Cruz River in Arizona (figure 2.4). He expected infiltration rate to be proportional to the breadth of the stream, the depth of flow and the velocity of flow each of which can be defined by a power relationship with respect to discharge rate. Howver he found considerable scatter beyond the range of measurement error in relating infiltration rate to discharge rate. The reach of stream he examined was disconnected from the alluvial aquifer. Burkham's implicit assumptions of isothermal and time invariant infiltration rates are a source of error as would be expected in consideration of the discussion of groundwater

models.

Most surface water models which consider the transient interaction with groundwater are concerned with streams which are hydraulically connected to aquifers during a decline in surface water stage. Hall (1968) summarized the mathematical treatment of baseflow recessions, and pointed out the failures of empirical models, and that most natural hydrologic systems are nonlinear.

However some models based on linear assumptions have been applied to the interaction of streams with bank storage or aquifers. Todd (1955) used a Hele-Shaw model of bank storage with a sinusoidal stage hydrograph to relate storage volume with the product of amplitude and period of the flood wave. He also found a logarithmic relationship for recession with time. Cooper and Rorabough (1963) derived analytic equations for transient seepage and bank storage for an asymmetric sinusoidal flood wave in a completely penetrating stream.

Venetis (1968 and 1970) used Cooper and Rorabough's analysis to define unit step and unit implulse response functions relating head in the aquifer to stage in a hydraulically connected stream. This was extended by Hall and Moench (1972) who used discrete convolution to determine recharge for an arbitrary stream stage hydrograph.

Subsequently this technique has been used to determine recharge in a coupled groundwater-surface water model (Moench, Sauer and Jennings, 1974) and Besbes et al (1978) with the aid of a kriging technique. Several papers have demonstrated that the reverse technique, deconvolution, may be used to identify aquifer parameters if the stream stage hydrograph and bore hydrographs are available (Pinder, Bredehoeft and Cooper (1969), Rowe (1960),Singh and Sagar (1977) and Yeh (1975)).

The value of diffusivity so obtained is thought to be extremely sensitive to variations in head measurements at the observation well. For example reanalysis of the data of Pinder et al (1969) reveals that an

increase in head change at the well of 1% would double the value of diffusivity. Yeh, Singh and Sagar warned that noisy data could invalidate the analysis. Sagar and Singh (1979) performed a statistical sensitivity analysis and found a weaker relationship between errors in data and the expected value of diffusivity and its coefficient of variation. They added various levels of random error to their sand tank experimental data, both for the rate of rise of stream stage (during a sinusoidal flood wave) and the initial slope of the free surface at the streambank which fully penetrated the sand layer. By increasing error levels from 5% to 50% they found the expected value for diffusivity changed by only 14% whereas its coefficient of variation increased from 5% to 78%. Sensitivity analyses, as will be reported later, are not reliably generalized as they depend on the particular geometry, boundary conditions and parameter values chosen for the test case.

Another approach to surface water modelling of streambed infiltration has been followed by Smith (1972). He extended a border (furrow) irrigation advance solution to the advance of plane flow in broad dry alluvial channels. Combining the kinematic wave equations and Horton's infiltration equation he located the position of the moving front by the method of characteristics and also using a finite difference approximation. Smith's technique allows the calculation of infiltration in a reach during the passage of an ephemeral flood wave. This appears to be a promising surface water model for recharge due to advancing ephemeral flood waves in streams hydraulically disconnected from aquifers.

2.3 Integrated Stream-Aquifer Models

In many cases the interaction between groundwater and streamflow is significant for either or both systems. The processses governing the interaction take place at the streambed. For groundwater models and surface water models the streambed is a model boundary. This requires that either the hydraulic head or the flow rate through the boundary is

specified at all times. Rushton and Tomlinson (1979) demonstrated that this could invalidate model results. To avoid these restrictions on the modelling of the interaction process the streambed must not be an external boundary. Two techniques have been employed to internalize the streambed within the model. Freeze (1972) classifies the coupling between the two parts of the model as external or internal.

External coupling exists when the output of one system becomes the input to the other without satisfying any internal boundary conditions between the two systems. Internal coupling occurs when the internal boundary conditions are satisfied at each time step. See Appendix C.1, Table V, for a summary of coupling for integrated models.

External coupling requires significantly less computer time but should only be used when the mathematical description of the stream- aquifer interaction is sufficiently representative of the physical process occurring at the internal boundary. One example is when seepage rates are small and have little effect on stream discharge or groundwater levels (Moench et al, 1974).

For the internally coupled models the convergence criterion is the change in either stream stage or leakage rate between successive iterations. Stream stage is derived directly from solving the streamflow routing equations and is less sensitive than seepage rate to changes in groundwater levels.

Sensitivity analyses have been performed by Rovey (1975) and Cunningham and Sinclair (1979). The latter found that river discharge, water table elevation and seepage rate are most sensitive to Mannings roughness coefficient, n , river channel slope and only moderately sensitive to the hydraulic conductivity of the streambed. It should be noted that Cunningham and Sinclair defined sensitivity as the fractional change in model output when model parameters were changed by stated fractions from their assumed values. If other assumed values had been used

the ranking of the sensitivity of the parameters would be different. It is not surprising to find that output was relatively insensitive to streambed hydraulic conductivity as its assumed value was more than four times the hydraulic conductivity of the aquifer.

Rovey using a step function for river discharge and considering unsaturated flow above the water table did not test the effect of varying Manning's n. She reported that the streambed silt layer hydraulic conductivity dominated stream discharge results but had little effect on groundwater levels. A lesser effect was observed when a typical curve for unsaturated hydraulic conductivty with respect to soil suction pressure, p_c was replaced by a step change from zero to saturated hydraulic conductivity at a finite value of p_c. Bouwer (1964) had already quantified the effect of p_c on the steady state seepage rate from a leaky channel. Other unsaturated flow parameters were found to have only small effects on river discharge and groundwater levels.

The results of these two limited analyses are encouraging as the order of decreasing importance of parameters is also the order of increasing difficulty in measurement; channel slope and Manning's n, saturated hydraulic conductivity of the streambed and unsaturated hydraulic conductivity of the streambed. However it would be incorrect to generalize these results in light of the dependence of sensitivity analyses on the model structure and assumed parameter values.

Cunningham and Sinclair (1979) also provided a statistical comparison of observed and predicted observation bore water levels and stream discharge and were able to draw 95% confidence intervals on scatter diagrams. They also performed tests to determine the uniqueness of the values of model parameters for the calibrated model by assuming that the distribution of observed values of piezometric head conformed to the Chi-square distribution (an assumption without sound mathematical support). For their illustrative case study the hypothesis that model predictions and

field observations belong to the same data set was acceptable at a 99% confidence level for parameter changes up to 19% but rejected at 99% confidence level for parameter changes greater than 30%. This affirms the notion of uniqueness for that particular model.

Only two models, those developed by Rovey (1975) and Freeze (1972), consider unsaturated flow in the porous medium. Rovey used a technique for joining a 2D (horizontal plane) and a 3D mesh to enable locations where vertical flow is important to be modelled accurately, without the need of excessive processing time for all other locations. Freeze reported results of a 2D (vertical plane) model as the 3D model was too demanding on core size and processing time.

All other models of the physical flow process in the porous medium use a linearized Boussinesq equation. Of these models all were two dimensional with the exception of Fraser and Jones (1977) one dimensional model of a dendritic alluvial valley aquifer and a model by Moench, Sauer and Jennings (1974). The latter used a one dimensional step response function for a semi-infinite aquifer with a fully penetrating stream and semipervious banks. The function was derived by Hall and Moench (1972) as mentioned in section 2.2.

Morel-Seytoux (1975) uses the 2D linearized Boussinesq equation to find response functions for pumping and pervious reach interaction. He assumes these processes are linear and applies discrete convolution to find groundwater responses to flow in the stream. Taylor and Luckey (1972) take a similar but more simplified approach and consider only the influence on streamflow of pumping from strips parallel to the stream.

While linear system methods adapt well to the description of groundwater flow under gentle hydraulic gradients, they may give a crude approximation of the interaction of ephemeral streams and aquifers. Besbes et al (1978) successfully applied deconvolution to estimate recharge from ephemeral streams in Tunisia by observation of watertable recovery.

Results give good agreement with kriging (estimating the volume changes in groundwater storage). The success of this case relies on consistency in the shape of the groundwater mound for each recharge event, allowing a linear relationship between groundwater levels at a few bores and the volume change in the aquifer. Johnston et al (1973, figure 10) showed that for their field study such a simple relationship could not be established.

For streams hydraulically disconnected from aquifers the unsaturated zone behaviour depends on initial moisture distribution beside the streamflow parameters (depth, velocity, discharge rate). Seepage from hydraulically connected streams depends on initial groundwater levels. In both cases seepage rates will not be consistent for each flood or streamflow event. The amount of variation will determine the applicability of linear theory to stream aquifer interaction. The advantage of linear theory lies in the simple analysis resulting from its use. Morel-Seytoux however builds on the restrictions of linear theory a most complex and costly computer model. His approach while suited to very long term management of a stream aquifer system is inflexible to system changes.

Knapp et al (1975) include surface, upper soil and lower soil moisture stores in their integrated stream-aquifer model. They have the potential to account more accurately for hydrologic processes occurring across the surface of a catchment in this way. Up to forty parameters were required to define storage capacities and water transfer between storages using empirical expressions. As both groundwater levels and streamflow data are used in calibration, the number of degrees of freedom is reduced. Knapp et al claim this enhances the credibility of the calibrated integrated model. It would appear (without proof) that a simpler model with fewer parameters could produce equally valid results and reduce the difficulty of model calibration. Bachmat et al (1980) suggest that the level of sophistication of a management model should match the available data and the cost of acquiring them.

The flow across the streambed is defined by Darcy's law for all except one model. The exception, Freeze (1972) also allows seepage into the stream from a seepage face on the stream bank. Most integrated models consider that the streambed is lined with a thin silt layer of lower permeability than the underlying aquifer (except Cunningham and Sinclair, as previosly discussed). Darcy's law is applied to flow across this silt layer. For hydraulically disconnected streams the bubbling pressure head is used to define the suction head on the lower surface of the silt layer. In the case of hydraulically connected streams the head in the aquifer below the streambed is assumed to act at the lower surface of the silt layer.

One difficulty is to define the head in the aquifer below the streambed. In this zone vertical flow occurs for partially penetrating streams and consequently head variations occur through the aquifer profile. Rushton and Tomlinson's (1979) solution is to neglect the vertical flow component. They use a linearized Boussinesq equation applied over a finite difference grid. The value calculated by the model for aquifer head at the stream is the value they use for the head at the base of the streambed silt layer. All other modellers used the same approximation, with the exception of Freeze.

Only two models consider both hydraulic connection and hydraulic disconnection; Rovey (1975) and Henry (1979). In each case the seepage rate through the silt layer is considered to be proportional to the head difference between the stream level and the aquifer head until a maximum seepage rate is reached for any given stream depth. At this point hydraulic continuity is broken as the bubbling pressure head at the base of the silt layer is reached. The medium below the silt layer desaturates and the maximum seepage rate is governed by the silt layer hydraulic conductivity and thickness. Increases in stream discharge rate continue to raise the seepage rate as the wetted width of the silt layer expands and

the hydraulic gradient across it increases. Freeze's model is the only one to treat the seepage flow with dynamic equations. All other models consider the stream-aquifer interaction to be in steady state equilibrium during the course of each time step.

Two models, Rovey (1975) and Fraser and Jones (1977) use this technique for streamflow simulation also. Their use of Manning's equation alone did not allow for storage or momentum effects to be simulated. Rovey reported poor results for stream discharge routing due to the large effect of unaccounted local runoff and a lack of ability to route flood waves downstream. Moench et al (1974) used linear theory to obtain unit response flow routing (after Sauer, 1973). This was successful in modelling stream discharge rates after routing through one reach of channel.

All other descriptions of streamflow models include one dimensional dynamic equations. Some use the Muskingum equation relating inflow and outflow to stream channel storage. Time steps for streamflow models are much shorter than for groundwater models and in general solved explicitly. All used finite difference equations to advance solutions for stream discharge and aquifer heads through time (except for the linear model of Moench et al). Cunningham and Sinclair (1979) used the finite element method for spatial solutions at each time step and used finite difference equations to advance through time. All others used finite differences for discretizing the flow domain as well as advancing the solution through time.

Problems encountered with models were excessive computer times, (Freeze, Morel-Seytoux), inability to account for initial wetting of dry channels, lack of representation of vertical flow below the phreatic surface, and inability to account for time lag between surface infiltration and recharge at the water table (Rovey and Henry).

There appears to be a large gap between the sophisticated model of Freeze and the other models in the treatment of the streambed behaviour.

The other models use a single value of head in the aquifer below the stream as the head to which stream-aquifer exchange flow rates are tied. It would appear that a model which incorporated a simple treatment of unsaturated flow but a more refined treatment of streambed geometry and the aquifer head nearby (particularly for hydraulically connected cases) is needed. The model described in chapter four was designed with these needs in mind. Chapter three provides the theoretical basis on which that model is founded.

CHAPTER 3

THEORY OF GROUNDWATER FLOW AND INFILTRATION

3.1 Definitions

In this chapter the general equations of groundwater flow are derived. The assumptions which are considered valid from chapter 2 are then introduced and finally an allowance for two phase flow is made.

Firstly, several terms which appear in the text are defined. Pressure head, ψ, is an expression for pressure in metres of fluid,

where $p = \rho g \psi$ 3.1

and p = fluid pressure [$M L^{-1} T^{-2}$]

ρ = fluid density [$M L^{-3}$]

g = gravitational acceleration [$L T^{-2}$]

Hydraulic head, h, is the sum of pressure head, ψ, and elevation, z, of the point at which it is defined, with respect to some constant datum, ie

$$h = \psi + z \qquad [L] \qquad 3.2$$

A number of writers call this the potential or total head. The plane on which $\psi = 0$ is considered to be a phreatic surface above which the medium is unsaturated and ψ is negative. Below the phreatic surface the medium is considered to be saturated and ψ is positive.

Volumetric moisture content, θ, is defined as the total volume of water stored in a unit volume of porous medium.

Effective porosity, n_e, is the maximum fraction of a unit volume of porous medium which may be occupied by water.

Fractional saturation, s, is the proportion of the effective porosity occupied by water.

$$s = \theta / n_e \qquad 3.3$$

Hydraulic conductivity, $K = K(x,y,z,\psi,T)$ is the function associated with a given medium and fluid which satisfied Darcy's law:

$$v_x = -K_x \frac{\partial h}{\partial x} \qquad 3.4$$

where v_x = Darcy velocity, the discharge rate per unit cross-section area of flow, in the direction of the x-axis.

$\frac{\partial h}{\partial x}$ = hydraulic head gradient in the x-direction.

and K_x = hydraulic conductivity in the x-direction.

Replacing x by y or z gives the equations for the other axial directions. K may be dissected into properties attributed to the medium and those attributed to the fluid.

$$K = \frac{k \rho g}{\mu} \qquad 3.5$$

where $k = k(\psi)$ = intrinsic permeability of the medium [L^2]

$\mu(T)$ = dynamic viscosity of fluid [$M\ L^{-1}\ T^{-1}$]

and T = temperature (^oC)

Green and Ampt (1911) suggest that the intrinsic permeability of the medium, $k(\psi)$ varies with suction (negative pressure) in two ways. Firstly, resistance to the flow of air increases as the proportion of saturated pore space increases. Secondly, humus, clay or other colloidal matter in the soil absorb moisture and swell upon wetting, reducing the available pore space and the degree of interconnection between pores. These factors imply a reduction in permeability with increase in moisture content. However, the opposite effect is more commonly observed. Bouwer (1964) shows $K(\psi)$ as a function of suction head derived from 28 experiments in clays, loams and sands (see figure 3.1). It is concluded that the wetting of "capillaries" through which the fluid moves reduces the viscous drag by reducing the absorptive hold of fluid particles by soil particle surfaces. Continuity of the fluid between pores also reduces the surface area per unit volume of fluid thereby diminishing the effect of surface tension. Bouwer suggests the use of a simple relationship between hydraulic conductivity and suction

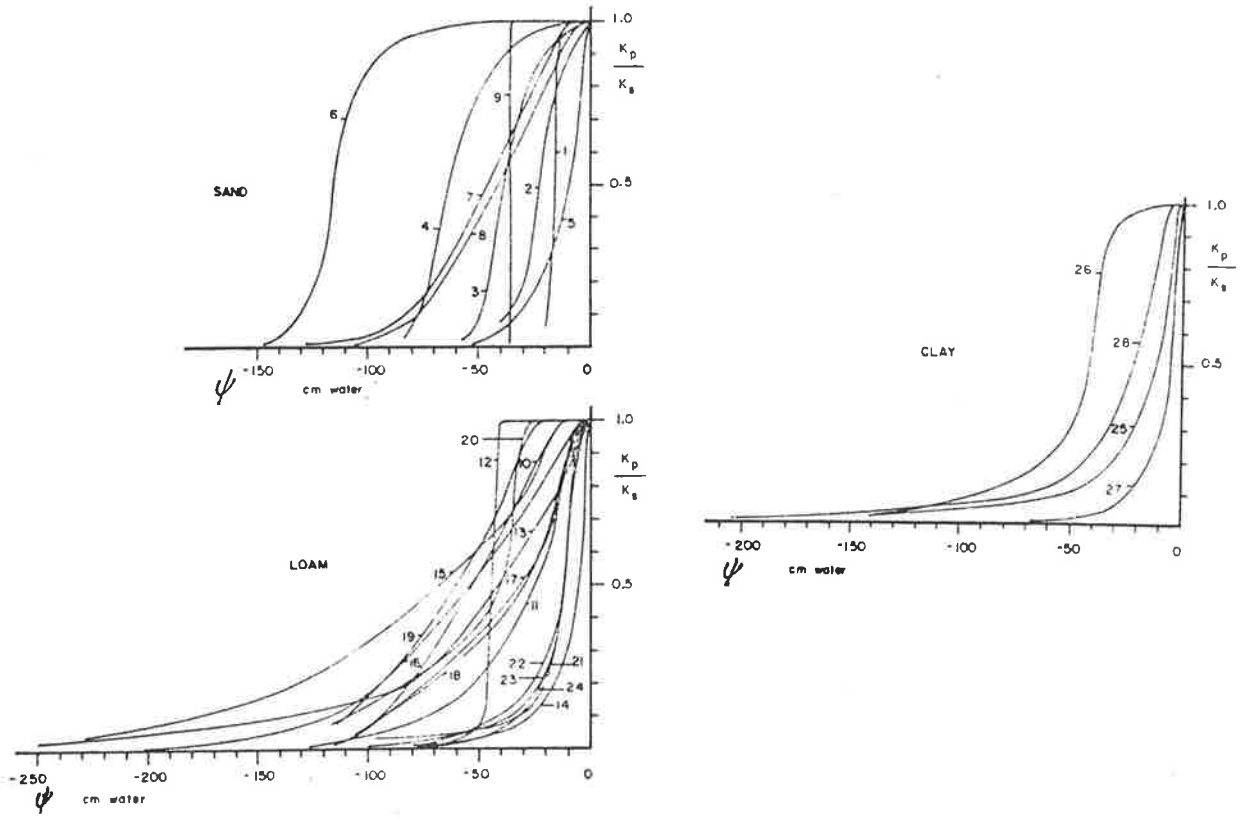

Figure 3.1 Ratio of unsaturated to saturated hydraulic conductivity (K_p/K_s) for a range of suction heads for sand, loam and clay (after Bouwer, 1964, figure 1).

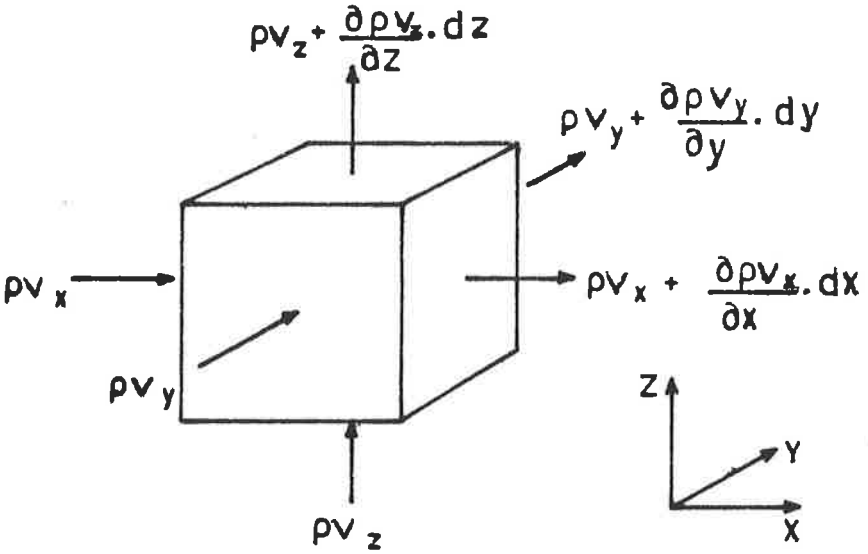

Figure 3.2 An elemental volume of porous medium showing fluid mass fluxes in three dimensions used in deriving equation 3.6.

head where experimental determination is impractical.

$$K = \frac{a}{(-\psi)^n + b} \qquad 3.5a$$

where a, b and n are constants selected from a table (Table 3.1).

Table 3.1

Values of a, b and n for estimating unsaturated hydraulic conductivities for various soil texture classes when experimental data is unavailable (after Bouwer, 1964 table 2).

	K_s (cm/day)	a	b	n
Medium sands	500	5×10^9	10^7	5
River bottom sands	68	1.7×10^9	2.5×10^7	4
Fine sands, sandy loams	50	5×10^6	10^5	3
Structureless loams and clays	1	5×10^3	5×10^3	2

3.2 Governing Equation for Groundwater Flow

Applying the law of conservation of mass to an elemental volume of porous medium (figure 3.2) for one phase flow gives

$$-\left[\frac{\partial \rho v_x}{\partial x} + \frac{\partial \rho v_y}{\partial y} + \frac{\partial \rho v_z}{\partial z}\right] = \frac{\partial}{\partial t}(\rho\theta) \qquad 3.6$$

where x, y, z are orthogonal axial coordinates [L], t = time [T], and v_x, v_y, v_z are the axial components of Darcy velocity [LT^{-1}].

3.2.1 Storage term

The right hand side of equation 3.6 represents the change in mass stored within the elemental volume. Using equation 3.3 this may be expressed as:

$$\frac{\partial}{\partial t}(\rho\theta) = \frac{\partial}{\partial t}(\rho n_e s) = n_e s \frac{\partial \rho}{\partial t} + \rho s \frac{\partial n_e}{\partial t} + \rho n_e \frac{\partial s}{\partial t} . \qquad 3.7$$

Below the phreatic surface all pores in the medium are assumed to be occupied by water and s = 1 and $\frac{\partial s}{\partial t} = 0$. It is assumed that the porous

medium deforms elastically under applied stress as suggested by Jacob (1950). Thus the porosity varies with changes in total stress. The total stress, σ, caused by the weight of overburden above a horizontal section is balanced by the effective stress, σ_e, in the soil matrix and the pressure, p, in the pore space.

$$\sigma = \sigma_e + \chi p \qquad 3.8$$

where $p >$ atmospheric (datum) ; $\chi = 1$

$p <$ atmospheric (datum) ; $0 < \chi < 1$

and χ is a coefficient that is a function of fluid fractional saturation (Narasimhan and Yanehiro, 1980).

In general, the third term on the right hand side of equation 3.7 dominates the description of mass storage change for unsaturated media, but is neglected for saturated media. It is useful to relate $\frac{\partial \rho}{\partial t}$ and $\frac{\partial n_e}{\partial t}$ in equation 3.7 to the rate of change of fluid pressure, $\frac{\partial p}{\partial t}$. The following discussion which assumes $\chi = s = 1$ applies only to saturated media at constant temperature.

The modulus of elasticity for a fluid, E_f, is defined by

$$E_f = \frac{1}{\beta} = - \frac{p}{\partial V_f / V_f} = \frac{\partial p}{\partial \rho / \rho} \qquad 3.9$$

where β = coefficient of compressibility of fluid [M^{-1} L T^2]

and V_f = volume of fluid

Rearranging equation 3.9 and differentiating with respect to time gives

$$\frac{\partial \rho}{\partial t} = \beta \rho \frac{\partial p}{\partial t} \qquad 3.10$$

Similarly an expression for $\frac{\partial n_e}{\partial t}$ may be found as follows. The modulus of elasticity of a bulk volume, V, of soil is given by

$$E_s = \frac{1}{\alpha} = - \frac{\partial \sigma_e}{\partial V / V} \qquad 3.11$$

where α = coefficient of compressibility of soil [M^{-1} L T^2]

and for saturated media

$$V = V_s + V_f \qquad 3.12$$

where V_s = volume of solids

and V_f = volume of fluid

Assuming that the volume of solids, V_s remains constant during consolidation and the centroid of the elemental volume is stationary, after Raudkivi (1979), then for an infinitesimal change, ∂V, in bulk volume

$$\partial n_e = \frac{\partial V}{V}$$

and substituting into equation 3.11 gives

$$\frac{\partial n_e}{\partial \sigma_e} = -\alpha \ . \qquad 3.13$$

Differentiating equation 3.8 with respect to p for saturated media ($\chi = 1$), and assuming that the total stress, σ, remains constant under the effect of pore pressure changes induced by fluid flow (Jacob, 1950 and Narasimhan and Yanehiro ,1980) gives

$$\frac{\partial \sigma_e}{\partial p} = -1 \qquad 3.14$$

Using the chain rule, and noting the assumptions above $\frac{\partial n_e}{\partial t}$ may be expressed as

$$\frac{\partial n_e}{\partial t} = \frac{\partial n_e}{\partial \sigma_e} \cdot \frac{\partial \sigma_e}{\partial p} \cdot \frac{\partial p}{\partial t} \qquad 3.15$$

Substituting equations 3.13 and 3.14 into 3.15 gives

$$\frac{\partial n_e}{\partial t} = \alpha \frac{\partial p}{\partial t} \qquad 3.16$$

and substituting equations 3.10 and 3.16 into 3.7 gives for saturated media (s=1):

$$\frac{\partial}{\partial t}(\rho\theta) = n_e \beta\rho \frac{\partial p}{\partial t} + \rho\alpha \frac{\partial p}{\partial t} \qquad 3.17$$

$$= \rho(\beta n_e + \alpha) \frac{\partial p}{\partial t}$$

Expressing pressure in terms of pressure head, ψ, with equation 3.1 and

using the chain rule to express saturation in terms of pressure head gives

$$\frac{\partial}{\partial t}(\rho\theta) = \rho^2 g(\beta n_e + \alpha)\frac{\partial \psi}{\partial t} \qquad 3.18$$

For unsaturated media ($s < 1$) the elastic storage due to compressibility of the fluid and the soil is usually neglected. Hence

$$\frac{\partial}{\partial t}(\rho\theta) = \rho n_e \frac{\partial s}{\partial t} = \rho C \frac{\partial \psi}{\partial t} \qquad 3.19$$

where $C = C(x,y,z,\psi) = n_e \frac{\partial s}{\partial \psi} = \frac{\partial \theta}{\partial \psi}$

C is called the specific moisture capacity (Freeze, 1971) or capillary capacity (Richards, 1931) and corresponds to the slope of an empirical plot of volumetric moisture content versus pressure head. Noting that the derivation of the elastic storage terms rests on the assumption that the medium is saturated equations 3.18 and 3.19 are written in combined form in the following text. Hence for saturated media $\psi > 0$, $C = 0$ and for unsaturated media, $\psi < 0$, the elastic terms may be neglected.

$$\frac{\partial}{\partial t}(\rho\theta) = [\rho^2 g(\beta n_e + \alpha) + (\rho C)]\frac{\partial \psi}{\partial t} \qquad 3.19a$$

Combined units within the square brackets are [M L^{-4}].

3.2.2. Flux terms

The left hand side of equation 3.6 represents the change in mass flux across the elemental volume in the three axial directions where v_x, v_y and v_z are Darcy velocity components. Applying Darcy's law, equation 3.4, and noting that z (equation 3.2) is constant for the x and y flux components gives

$$-\left[\frac{\partial \rho v_x}{\partial x} + \frac{\partial \rho v_y}{\partial y} + \frac{\partial \rho v_z}{\partial z}\right] = \frac{\partial}{\partial x}\left(\rho K_x \frac{\partial \psi}{\partial x}\right) + \frac{\partial}{\partial y}\left(\rho K_y \frac{\partial \psi}{\partial y}\right) + \frac{\partial}{\partial z}\left(\rho K_z \left(\frac{\partial \psi}{\partial z} + 1\right)\right) \qquad 3.20$$

3.2.3 The general equation for groundwater flow in some of its forms

A general 3D equation for single phase flow in saturated and unsaturated media, allowing spatial changes in fluid density and media properties can be composed by substituting equations 3.18 and 3.20 into equation 3.6.

$$\frac{\partial}{\partial x}\left(\rho K_x \frac{\partial \psi}{\partial x}\right) + \frac{\partial}{\partial y}\left(\rho K_y \frac{\partial \psi}{\partial y}\right) + \frac{\partial}{\partial z}\left(\rho K_z \left(\frac{\partial \psi}{\partial z} + 1\right)\right) = [\rho^2 g\ (\beta n_e + \alpha) + (\rho C)] \frac{\partial \psi}{\partial t} \qquad 3.21$$

Note that spontaneous discharge with reduction in head (2.1.1.(3)) and single phase flow (2.1.2.1.(4)) have been assumed. Equation 3.21 may be simplified by using further assumptions some of which were discussed in the previous chapter.

If the fluid is assumed to be incompressible, that is fluid density is constant, which is a reasonable assumption for most liquids, equation 3.21 may be reduced to

$$\frac{\partial}{\partial x} K_x \frac{\partial \psi}{\partial x} + \frac{\partial}{\partial y} K_y \frac{\partial \psi}{\partial y} + \frac{\partial}{\partial z} K_z \left(\frac{\partial \psi}{\partial z} + 1\right) = [\rho g\ (\beta n_e + \alpha) + C] \frac{\partial \psi}{\partial t} \qquad 3.22$$

This equation is sometimes expressed in terms of hydraulic head, h, rather than pressure head ψ (e.g. Vauclin et al (1979)) by substituting equation 3.2 into equation 3.22

$$\frac{\partial}{\partial x} K_x \frac{\partial h}{\partial x} + \frac{\partial}{\partial y} K_y \frac{\partial h}{\partial y} + \frac{\partial}{\partial z} K_z \frac{\partial h}{\partial z} = [S_s + C] \frac{\partial h}{\partial t} \qquad 3.23$$

where $S_s = \rho g\ (\beta n_e + \alpha)$ 3.24

and S_s is called the specific storage [L^{-1}].

K_x, K_y and K_z are still dependent on the pressure head ψ when $\psi < 0$.

When the medium is saturated, K_x, K_y and K_z become constants and $C = 0$. In the unsaturated zone it is common to neglect the elastic storage term and horizontal unsaturated porous media flow (assumption 2.1.1.(2)). That is flow is assumed to be one dimensional (vertical).

i.e. $\frac{\partial h}{\partial x} = \frac{\partial h}{\partial y} = 0$ where $\psi < 0$.

The Dupuit-Forchheimer assumptions are commonly applied to saturated flow to reduce the problem by one dimension (see assumption 2.1.1.(5)). This has the effect of setting $\frac{\partial h}{\partial z} = 0$ in equation 3.23. If in addition horizontal flow in the unsaturated zone is neglected, equation 3.23 reduces to

$$\frac{\partial}{\partial x} K_x b \frac{\partial h}{\partial x} + \frac{\partial}{\partial y} K_y b \frac{\partial h}{\partial y} + W = (bS_s + S_y) \frac{\partial h}{\partial t} \qquad 3.25$$

where $b(x,y)$ = saturated medium thickness,

S_y = specific yield for unconfined aquifers, the storage change per unit plan area due to unit change in elevation of the free surface

and $W = W(x,y)$ = net surface influx over incremental area

= recharge + vertical leakage inflow

- evapotranspiration - vertical leakage outflow.

For free surface problems ($\psi = 0$ on upper flow boundary) it is commonly assumed that $S_y = n_e$ and $S_s = 0$. For confined problems ($\psi > 0$ on upper flow boundary) only the elastic storage term applies ($S_y = 0$).

If the medium is assumed to be homogeneous and anisotropic, equation 3.25 reduces to

$$K_x b \frac{\partial^2 h}{\partial x^2} + K_y b \frac{\partial^2 h}{\partial y^2} + W = (bS_s + S_y) \frac{\partial h}{\partial t} \qquad 3.26$$

Extending this assumption to the case of an homogeneous, isotropic medium this simplifies to

$$Kb \left(\frac{\partial^2 h}{\partial x^2} + \frac{\partial^2 h}{\partial y^2} \right) + W = (bS_s + S_y) \frac{\partial h}{\partial t} \qquad 3.27$$

Defining the terms transmissivity, $T = K b$, and

storage coefficient, $S = S_s b$, gives

$$T \nabla^2 h + W = (S + S_y) \frac{\partial h}{\partial t} \qquad 3.28$$

a partial differential equation which is linear with respect to h for confined aquifers where b is constant. For unconfined aquifers elastic storage may be neglected and $S_y = n_e$. One way of linearizing the p.d.e. (Bear (1972) shows other alternatives) is to equate b with the initial saturated aquifer thickness. Assuming a horizontal aquifer base at z = 0 allows h replace b in equation 3.27 giving the nonlinear Boussinesq equation

$$Kh\ \nabla^2 h + W = n_e \frac{\partial h}{\partial t} \qquad 3.29$$

which is sometimes written

$$\frac{K}{2} \nabla^2 h^2 + W = n_e \frac{\partial h}{\partial t} \qquad 3.30$$

3.3 Unsaturated Flow in One Dimension

3.3.1 Richards' equation

Vertical flow models as discussed in 2.1.2.1 are also derived from equation 3.22. The assumption that flow is vertical only (2.1.2.1.(1)) simplifies equation 3.22 to one dimension.

$$\frac{\partial}{\partial z} K_z(\psi)\left(\frac{\partial \psi}{\partial z} + 1\right) = C(\psi) \frac{\partial \psi}{\partial t} \qquad 3.31$$

This is the one dimensional form of Richards' equation, named after the man who first derived this expression for unsaturated flow using Darcy's law and accounting for variation in moisture content and hydraulic conductivity with capillary potential (Richards, 1931). To use this equation the functions $C(\psi)$ and $K_z(\psi)$ need to be known for the medium. This is not feasible in a field study of any size due to medium heterogeneity. Numerical solution of Richard's equation also restricts the time increments to relatively short values during the progression of the wetting front through the soil profile.

3.3.2 Green-Ampt equation

The second assumption, (2.1.2.1.(2)) that piston flow infiltration occurs, implies the existence of a transient wetting front above which soil is saturated (C=0) and a hydrostatic pressure gradient ($\frac{\partial\psi}{\partial z} = -1$) prevails. For this zone both sides of equation 3.31 vanish. The pressure head immediately below the wetting front is assumed constant at ψ_{cr}, the critical pressure head (Bouwer, 1978), and the medium is unsaturated.

Where the pressure head is known at the soil surface, for example where water is ponded these assumptions lead to the simpler Green-Ampt equation. Figure 3.3 (after Freyberg et al, 1980, figure 1) diagramatically shows the differences between the Green-Ampt equation and Richard's equation.

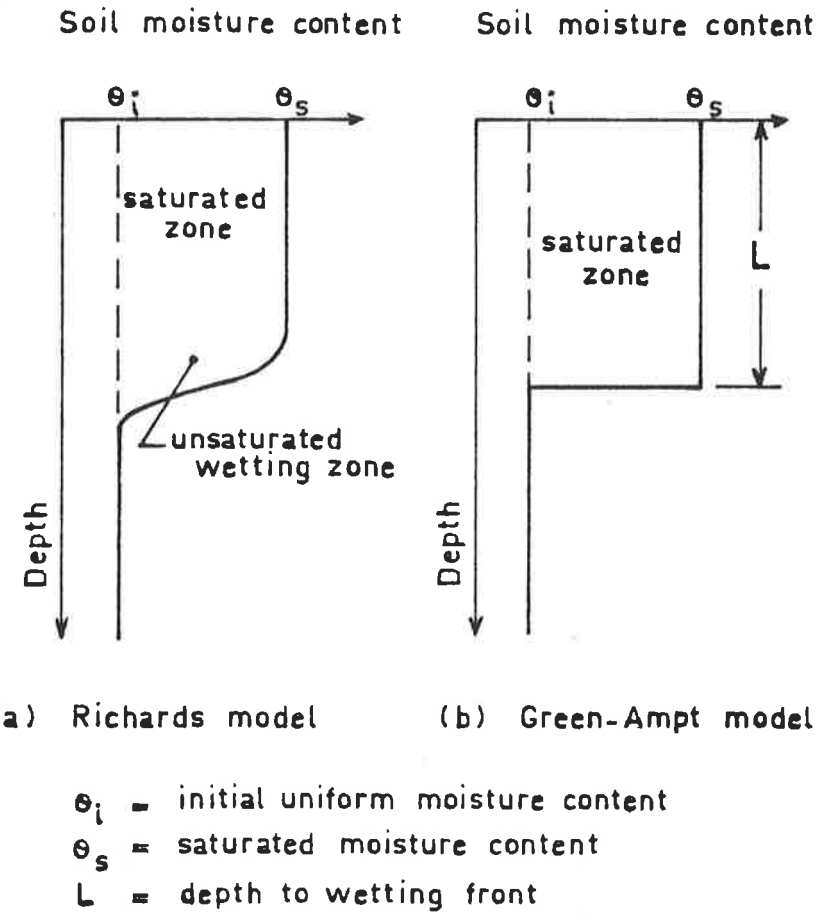

Figure 3.3 Soil moisture profiles during infiltration from a pond for two models (a) Richards model and (b) Green-Ampt model (after Freyberg et. al., 1980, figure 1).

Applying Darcy's law across the depth, L, of soil to the wetting front, at which the critical pressure head equals the water entry value for the soil, ψ_{cr} for a ponded depth, H, the infiltration rate i [$L\,T^{-1}$], is given by (Bouwer, 1969) :

$$i = K\left(\frac{H + L - \psi_{cr}}{L}\right) \qquad 3.32$$

continuity gives the rate of advance of the wetting front as

$$\frac{dL}{dt} = \frac{i}{n_e} \qquad 3.33$$

Substituting equation 3.32 into equation 3.33 gives the equation originally proposed by Green and Ampt (1911, equation 8) :

$$\frac{dL}{dt} = \frac{K}{n_e}\left(\frac{H + L - \psi_{cr}}{L}\right) \qquad 3.34$$

integrating (after Green and Ampt (1911) or Bouwer (1969, p. 158) gives

$$\int_0^t dt = \int_0^L \frac{n_e}{K}\left(\frac{L}{H + L - \psi_{cr}}\right) dL$$

$$t = \frac{n_e}{K}\int_0^L 1 - \frac{H - \psi_{cr}}{H + L - \psi_{cr}}\, dL$$

$$t = \frac{n_e}{K}\left[L - (H - \psi_{cr})\ \ell n\left(\frac{H + L - \psi_{cr}}{H - \psi_{cr}}\right)\right] \qquad 3.35$$

where t is the time elapsed for the wetting front to advance to a depth, L. A modified Green-Ampt equation is discussed in section 3.3.3.3. This piston flow analysis was further developed by Bouwer (1976) in considering infiltration into soils of increasing permeability with depth, as encountered by Sharp (1977) in the alluvium of major river valleys in central United States. Bouwer (1976) allowed for layered media within the saturated zone by substituting the harmonic mean vertical hydraulic conductivity $\bar{K}$, for K in equation 3.32 where

$$\bar{K} = \frac{L}{\sum_{j=1}^{m} \ell_j / K_j} \qquad 3.36$$

where m is the number of layers

and ℓ_j and K_j are the layer thicknesses and saturated vertical hydraulic conductivities.

An analytical solution is available where the saturated hydraulic conductivity increases linearly with depth, that is

$$K_\ell = K_o + c\ell \qquad 3.37$$

where $K_\ell = K_o$ at the soil surface, c is a constant and ℓ is the depth below the soil surface. Then

$$\bar{K} = \frac{K_\ell - K_o}{\ell n \left(\frac{K_\ell}{K_o}\right)} \qquad 3.38$$

The wetting front comesto rest at a depth ℓ_u, where K_{ℓ_u} is equal to the infiltration rate, i, that is

$$i = K_{\ell_u} = \frac{K_{\ell_u} - K_o}{\ell n(K_{\ell_u}/K_o)} \cdot \frac{(H + \ell_u - \psi_{cr})}{\ell_u} \qquad 3.39$$

$$1 + \frac{c}{K_o}\ell_u = \frac{c}{K_o}\frac{H + \ell_u - \psi_{cr}}{\ell n\left(1 + \frac{c\,\ell_u}{K_o}\right)} \qquad 3.40$$

allowing ℓ_u to be calculated iteratively if the remaining parameters are known.

3.3.3. Two phase flow

Resistance to the flow of displaced air has been neglected in deriving all equations up to this point. As discussed in 2.1.2.1.(4) this may be a poor assumption if the escape of air is restricted. This is likely to be the case below wide perched streambeds following the onset of streamflow. De Backer (1975) and Morel-Seytoux and Khanji (1974) proposed methods to account for the effect of the resistance to the flow of air on the water infiltration rate without resorting to a full treatment of two phase flow.

Before examining this simplified approach the actual two phase flow equations are presented in order to grasp the nature of the assumption of single phase flow, 2.1.2.1.(4).

3.3.3.1 Using Fick's Law

Flow of a liquid in a porous medium is described by Darcy's law (equation 3.4). Flow of a compressible gas occurs by diffusion and is thus better described by Fick's law (Dakshanamurthy and Fredlund, 1981) which may be written for one dimensional flow as

$$D \frac{\partial^2 p_a}{\partial x^2} = \frac{\partial m}{\partial t} \qquad 3.41$$

where p_a = absolute air pressure in the pore spaces [$M L^{-1} T^{-2}$]

D = transmission constant [$L T^{-1}$]

m = mass of air in an elemental bulk volume of soil, V_o.

$= (1-s) n_e \rho_a V_o$ [M]

and ρ_a = density of air [$M L^{-3}$]

As the density of a gas changes with pressure and temperature, from the general gas equation

$$p_a V_a = \frac{m R T}{M} \qquad 3.42$$

M = molecular weight of air

V_a = volume of air = $(1-s) n_e V_o$

R = gas constant [$L^2 T^{-2}$]

T = temperature [^oK]

making m the subject of the equation gives

$$m = p_a V_a \frac{M}{RT} \qquad 3.43$$

Substituting for m in equation 3.41 using equation 3.43 in isothermal conditions gives:

$$D \frac{\partial^2 p_a}{\partial x^2} = \frac{M}{RT} V_a \frac{\partial p_a}{\partial t} + \frac{M}{RT} p_a \frac{\partial V_a}{\partial t} \qquad 3.44$$

3.3.3.2 Using Darcy's law

If the change in volume of air over a period of time is small, the second term on the right hand side of equation 3.44 may be neglected. This gives rise to an equation which is very similar in form to the one dimensional homogeneous form of equation 3.22, also a diffusion equation

$$K_x \frac{\partial^2 \psi}{\partial x^2} = C \frac{\partial \psi}{\partial t} \qquad 3.45$$

where	p_a	is analogous to	ψ
	MV_a/RT	"	C
and	D	"	K_x

Equation 3.45 was derived using Darcy's law and continuity. Some writers have made the substitution above to use Darcy's law to represent the flow of gas in porous media (e.g. Nakano (1981) and Morel-Seytoux and Khanji (1974)).

For field studies this substitution is satisfactory as the uncertainty in soils constants is likely to overshadow the mathematical inaccuracy of the zero air volume change assumption.

3.3.3.3 The modified Green-Ampt equation

Morel-Seytoux and Khanji (1974) considered the case of vertical two phase flow and applied Darcy's law and continuity to both phases. They assumed that the compressibility of air was not significant for an open soil column. This is equivalent to neglecting the term for air volume change in equation 3.44. Assuming that the porous medium is non-deforming and that atmospheric air pressure prevails below the wetting front, they derived an equation of infiltration as

$$i = \frac{K}{\beta_M} \left(\frac{H + L - h_c}{L} \right) \qquad 3.46$$

This is almost identical to the form of the Green-Ampt equation given by Bouwer (1969) (equation 3.32)

The two parameters which are new are

(1) $h_c = \int_0^{\psi_{ci}} f_w \, d\psi$ = 'effective capillary drive ' [L] 3.47

where $f_w = \frac{K_w(\psi)}{K_w(\psi) + K_a(\psi)}$ = ratio of relative permeability of water to the sum of relative permeabilities of air and water

$$= \frac{k_w(\psi)\rho_w/\mu_w}{k_w(\psi)\rho_w/\mu_w + k_a(\psi)\rho_a/\mu_a}$$

(from equation 3.5)

and ψ_{ci} = suction head at which $f_w \to 0$ (i.e. the head below which the flow of water is negligible).

An overestimate of the value of ψ_{ci} will have no effect on the value of h_c as f_w is very small when the suction head is large.

(2) $$\beta_M = \frac{\bar{\theta} - \theta_i}{\mu_w} \int_{\theta_i}^{\theta_f} \frac{\frac{d^2 f_w}{d^2\theta}}{k_w(\psi)\rho_w/\mu_w + k_a(\psi)\rho_a/\mu_a} \, d\theta$$ 3.48

where θ_i = initial moisture content

$\bar{\theta}$ = moisture content above wetting front

θ_f = moisture content just below wetting front

β_M is called the viscous resistance correction. This accounts for the effect of a moisture content profile which allows for simultaneous two phase flow. For the Green-Ampt equation where piston flow is assumed, $\beta_M = 1$. In two phase flow the viscous resistance is larger. Morel-Seytoux and Khanji (1974) found values of β_M between 1.1 and 1.7 for loams, sands and clay.

Having investigated the equation of two phase flow in one dimension it can be seen that a modified form of the Green-Ampt equation provides a satisfactory approximation. Parameters h_c and β_M are derived from integrating permeabilities, expressed as functions of suction head. Such functions are impractical to determine for field studies, however, the values of h_c and β_M are confined to predictable ranges. Freyberg et al

(1980) performed sensitivity analyses on the value of h_c for fitting a Green-Ampt model to a model based on Richard's equation (equation 3.31). They found variation in h_c of 50% produced variations in total infiltration of between 3% and 13% for the four cases presented. This is an indication that total infiltration may be relatively insensitive to the value of effective capillary drive. McCuen et al (1981) analysed over 1000 sets of soils infiltration data from a range of soil texture classes and presented means and standard errors for the Green-Ampt parameters for each class. In each class the standard error was less than 10% of the mean value for the effective porosity and for the logs of saturated hydraulic conductivity and wetting front capillary head, implying that a reasonable model of infiltration could be produced with a knowledge of soil texture only. This provides further support for the use of the Green-Ampt equation in modelling ponded infiltration in field studies. Where (K/β_M) and h_c of equation 3.46 or K and ψ_{cr} of equation 3.32 are determined by model fitting (such as in field scale studies) rather than direct measurement, the two equations become interchangeable and the unknown parameters take on the meanings assigned by their respective equations.

3.3.4 Non-isothermal unsaturated flow

Dakshanamurthy and Fredlund (1981) considered the case where unsaturated flow responded to a temperature gradient in addition to a hydraulic head gradient. They included the effect of temperature on pore air pressure using the gas law (equation 3.42), and subsequently adjusted pore water pressures at each time step of their numerical model. While air pressures varied considerably between isothermal and non-isothermal cases, pore water pressures and moisture content profiles were in the authors' words "essentially the same" for each case. The temperature variation for the non isothermal case was 15°C and the material selected was a clay, in which pore pressure gradients could be expected to be large. Therefore it is concluded that for the moderate temperature variations commonly

encountered in field studies, isothermal flow is a satisfactory assumption. However, temperature should be measured to determine the dynamic viscosity of the liquid as required in equation 3.5 to calculate the hydraulic conductivity of the porous medium.

3.4 Application of Theories to Models of Stream-Aquifer Interaction

The purpose in examining the equations of porous media flow with their assumptions is to select a mathematical model for stream-aquifer interaction which has the following attributes. The model is firstly to provide an accurate description of the flow processes. Secondly it is to have realistic data requirements, particularly for alluvial porous media hydraulic properties. Thirdly solutions to the equations should be computationally efficient to enable transient solutions to be processed in reasonable time.

The model described in the next chapter employs equation 3.32 (or, as mentioned in section 3.3.3.3, equation 3.46) to describe flow above the water-table (1D infiltration) and equation 3.23 to describe groundwater flow (in a 2D vertical plane) below the water-table. The latter equation is simplified by neglecting S_s as the compressibility of the medium and of the fluid are insignificant compared with the changes of fluid volume due to the change in the free surface elevation. As C = 0 for saturated media the equation becomes.

$$\frac{\partial}{\partial x} K_x \frac{\partial h}{\partial x} + \frac{\partial}{\partial z} K_z \frac{\partial h}{\partial z} = 0 \qquad 3.49$$

As the DF assumptions have not been used the free surface may be treated as a boundary condition (described in section 4.3). Hence the effective porosity does not occur in this equation. Assuming the medium is homogeneous and isotropic gives Laplace's equation

$$\nabla^2 h = 0. \qquad 3.50$$

This relationship is valid for steady flow in a confined or unconfined aquifer and is an excellent approximation to unsteady flow in an unconfined aquifer. Use of equation 3.50 significantly simplifies the numerical

procedure for the model as is seen in the next chapter.

CHAPTER 4

TWO DIMENSIONAL BOUNDARY INTEGRAL EQUATION MODEL OF STREAM-AQUIFER INTERACTION

A numerical model incorporating the equations governing infiltration and groundwater flow was developed and used to simulate stream-aquifer interaction. The model employs the Green-Ampt infiltration equation (3.32) above the free surface (or water table) and Laplace's equation (3.50) below the free surface.

A two dimensional vertical slice model was used to examine the interaction process at a cross-section through the stream and the surrounding alluvium. The Boundary Integral Equation Method (BIEM) was used to perform numerical solutions for saturated porous media flow. The infiltration equation and an equation for the free surface (derived later) were incorporated in the boundary conditions of the model. The BIEM was used as it reduces this two dimensional problem to one computational dimension. It computes with relative ease the unsteady nonlinear free surface, requires minimal data to specify the spacial domain of the model and it is computationally efficient compared to finite element and finite difference methods.

A description of the application of BIEM to solving potential flow problems follows. Sections describing the principles upon which BIEM is founded and the numerical integration procedure closely follow the text of Liggett and Liu (1983), but are included for the sake of completeness. That text also covers boundary conditions up to equation 4.31. Beyond that point a large part of the presented material, to the author's knowledge, is original.

4.1 The Boundary Integral Equation Method

A formulation of the two dimensional BIEM begins with the statement of Green's second identity

$$\int_A U \nabla^2 V - V \nabla^2 U \, dA = \int_S (U \nabla V - V \nabla U)\cdot\tilde{n} \, ds \qquad 4.1$$

where A is a two dimensional domain bounded by the line, S

U and V are any two functions twice differentiable in A

and $\tilde{n}$ is the unit outward normal to A on S .

The normal component of a gradient with respect to the boundary may be denoted as

$$\frac{\partial V}{\partial n} = \nabla V\cdot\tilde{n} \ , \qquad \frac{\partial U}{\partial n} = \nabla U\cdot\tilde{n} \qquad 4.2$$

If U and V are both chosen to satisfy Laplace's equation

$$\nabla^2 U = \nabla^2 V = 0 \qquad 4.3$$

then equation 4.1 may be rewritten as

$$\int_S \left(U \frac{\partial V}{\partial n} - V \frac{\partial U}{\partial n} \right) ds = 0 \qquad 4.4$$

U is replaced by the function which is to be solved in the domain, that is the hydraulic head, h, which satisfies Laplace's equation below the free surface using the assumptions leading to equation 3.50. V is chosen as a "free space Green's function" which satisfies equation 4.3 except at a singular point, P, where it goes to infinity.

For two dimensional problems

$$V = \ell n \, r \qquad 4.5$$

in which r is the distance between the singular point, P (where r = 0) and another point Q on the boundary. To use equation 4.4 the singular point is excluded by inscribing a small circle of radius r_o around it and connecting this to the boundary S (see figure 4.1). Equation 4.4 becomes

$$\int_S \left[h \frac{\partial}{\partial n}(\ell n \, r) - \ell n \, r \cdot \frac{\partial h}{\partial n} \right] ds + \lim_{r_o \to 0} \int_\sigma \left[h \frac{\partial}{\partial n}(\ell n \, r) - \ell n \, r \cdot \frac{\partial h}{\partial n} \right] d\sigma = 0 \qquad 4.6$$

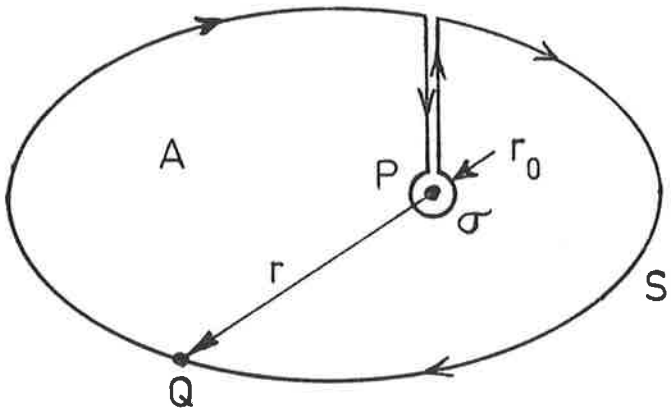

Figure 4.1 The singularity, P is separated from the domain, A by the creation of an artificial boundary, σ of radius, r_o.

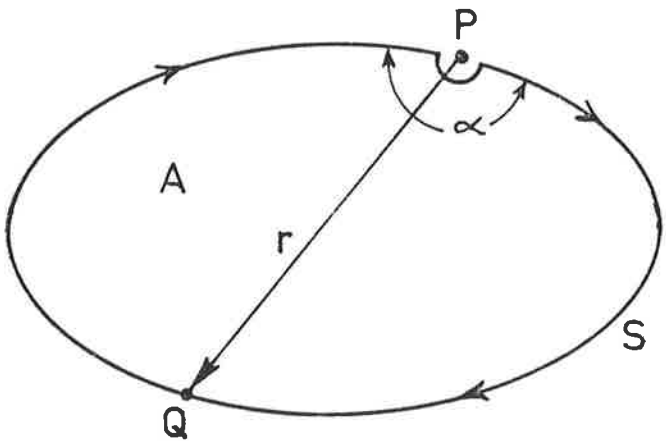

Figure 4.2 The singularity, P is located on the boundary and is separated from the domain, A by a circular arc subtending an angle, α at P.

The portions of the integral along the two lines connecting the circle σ to S will cancel and thus they do not appear in equation 4.6.

On the circle $\sigma(r = r_o)$ the outward normal from A points towards P. Thus the normal derivative of the Green's function is

$$\frac{\partial}{\partial n} (\ell n\ r) = \frac{1}{r} \frac{\partial r}{\partial n} = - \frac{1}{r_o} \qquad 4.7$$

and the integral around the circle becomes

$$\lim_{r_o \to 0} \int_0^{2\pi} \left[- \frac{h}{r_o} - \ell n\ r_o \frac{\partial h}{\partial r} \right] r_o\ d\theta = -2\pi\ h(P) \qquad 4.8$$

Substituting 4.7 and 4.8 into 4.6 defines the hydraulic head at any point P in terms of a boundary integral.

$$2\pi\ h(P) = \int_S \left[h(Q)\ \frac{1}{r} \frac{\partial r}{\partial n} - \ell n\ r \frac{\partial}{\partial n} h(Q) \right] ds \qquad 4.9$$

Hence if h and $\frac{\partial h}{\partial n}$ are known at all points on the boundary then h can be determined at all points in the domain.

By considering the case when the singularity, P is on the boundary, S equation 4.6 still applies. However the circular arc excluding P from the domain will subtend an angle, α, at P where α is less then 2π (see figure 4.2).

Equation 4.9 becomes

$$\alpha\ h(P) = \int_S \left[h(Q)\ \frac{1}{r} \frac{\partial r}{\partial n} - \ell n\ r \frac{\partial}{\partial n} h(Q) \right] ds \qquad 4.10$$

This provides the relationship between the hydraulic head at a point on the boundary and an integral of h and $\frac{\partial h}{\partial n}$ at all points on the boundary. Since P can be chosen at any point on the boundary the equation 4.10 can be written for each such point.

If N node points are chosen on the boundary and each in turn is made a base point, N integral equations in terms of h and $\frac{\partial h}{\partial n}$ at the node points can be written. In a well-conditioned problem the value of h (Dirichlet condition) or $\frac{\partial h}{\partial n}$ (Neumann condition) or the relationship between h and $\frac{\partial h}{\partial n}$

(mixed condition) is known at each boundary node. Thus there are N equations and N unknowns so solution of the unknown boundary values can proceed. Having obtained these the value of the hydraulic head anywhere in the domain can be found with equation 4.9.

4.2 Numerical Integration

To solve equation 4.10 interpolation functions must be chosen to describe the behaviour of h and $\frac{\partial h}{\partial n}$ between boundary nodes. Linear interpolation functions are chosen here for their simplicity. A function is also required to describe the position of the boundary between nodes. There is no advantage in using higher order elements for steam-aquifer problems so linear elements are used.

The hydraulic head and its normal derivative at an intermediate point on a line segment between nodes j and j+1 are described with respect to a local u - v co-ordinate system shown in figure 4.3. Expressions for h and $\frac{\partial h}{\partial n}$ between nodes can then be written (where in each case $v_j < v < v_{j+1}$).

$$h(v) = [(h_{j+1}-h_j)v + v_{j+1}h_j - v_j h_{j+1}]/(v_{j+1}-v_j) \qquad 4.11$$

$$\frac{\partial h}{\partial n}(v) = \left[\left(\left(\frac{\partial h}{\partial n}\right)_{j+1} - \left(\frac{\partial h}{\partial n}\right)_j\right)v + v_{j+1}\left(\frac{\partial h}{\partial n}\right)_j - v_j\left(\frac{\partial h}{\partial n}\right)_{j+1}\right]/(v_{j+1}-v_j) \qquad 4.12$$

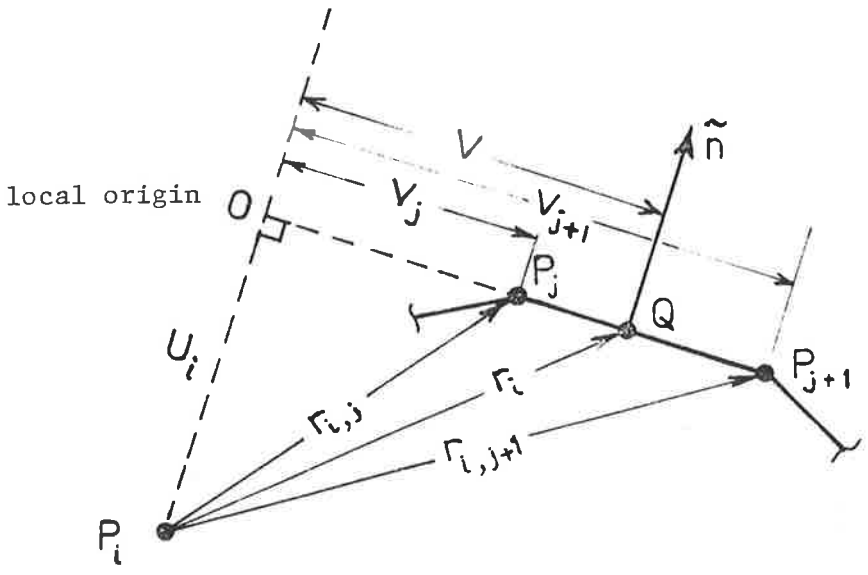

Figure 4.3 The u-v local coordinate system.

The component of the integral in equation 4.10 which is contributed by the boundary element between P_j and P_{j+1} is

$$I_{ij} = \int_{v_j}^{v_{j+1}} \left(\frac{h(v)}{r_i} \frac{\partial r_i}{\partial n} - \ell n\, r_i \frac{\partial h}{\partial n}(v) \right) dv \qquad 4.13$$

expanding 4.13 by substituting 4.11 and 4.12 and using

$$r_i = \sqrt{u_i^2 + v^2} \qquad 4.14$$

and

$$\frac{\partial r_i}{\partial n} = \frac{\partial r_i}{\partial u_i} = \begin{cases} u_i/r_i \text{ when } \vec{P_i 0} \text{ is in the same direction as } \tilde{n} \\ -u_i/r_i \text{ when } \vec{P_i 0} \text{ is in the opposite direction to } \tilde{n} \end{cases} \qquad 4.15$$

gives

$$I_{ij} = \int_{v_j}^{v_{j+1}} \left[(h_{j+1} - h_j)v + v_{j+1}h_j - v_j h_{j+1} \right] \left[\frac{(\pm)u_i}{(u_i^2+v^2)(v_{j+1}-v_j)} \right]$$

$$\frac{-\ell n(\sqrt{u_i^2+v^2})}{v_{j+1}-v_j} \left[\left(\left(\frac{\partial h}{\partial n}\right)_{j+1} - \left(\frac{\partial h}{\partial n}\right)_j \right) v + v_{j+1}\left(\frac{\partial h}{\partial n}\right)_j - v_j \left(\frac{\partial h}{\partial n}\right)_{j+1} \right] dv \qquad 4.16$$

rearranging gives

$$I_{ij} = (h_{j+1} - h_j) \int_{v_j}^{v_{j+1}} \frac{(\pm)u_i\, v\, dv}{(u_i^2+v^2)(v_{j+1}-v_j)}$$

$$+ (v_{j+1}h_j - v_j h_{j+1}) \int_{v_j}^{v_{j+1}} \frac{(\pm)u_i\, dv}{(u_i^2+v^2)(v_{j+1}-v_j)}$$

$$- \left(\left(\frac{\partial h}{\partial n}\right)_{j+1} - \left(\frac{\partial h}{\partial n}\right)_j \right) \int_{v_j}^{v_{j+1}} \frac{v \cdot \ell n \sqrt{u_i^2+v^2}\, dv}{v_{j+1}-v_j}$$

$$- \left(v_{j+1}\left(\frac{\partial h}{\partial n}\right)_j - v_j \left(\frac{\partial h}{\partial n}\right)_{j+1} \right) \int_{v_j}^{v_{j+1}} \frac{\ell n \sqrt{u_i^2+v^2}\, dv}{v_{j+1}-v_j} \qquad 4.17$$

Replacing the integrals by appropriate notation gives

$$I_{ij} = (h_{j+1} - h_j)\, I_{ij1} + (v_{j+1}h_j - v_j h_{j+1})\, I_{ij2} - \left(\left(\frac{\partial h}{\partial n}\right)_{j+1} - \left(\frac{\partial h}{\partial n}\right)_j\right) I_{ij3} - \left(v_{j+1}\left(\frac{\partial h}{\partial n}\right)_j - v_j\left(\frac{\partial h}{\partial n}\right)_{j+1}\right) I_{ij4} \qquad 4.18$$

and rearranging in matrix from gives

$$I_{ij} = \begin{bmatrix} -I_{ij1} + v_{j+1}I_{ij2} & I_{ij1} - v_j I_{ij2} \end{bmatrix} \begin{Bmatrix} h_j \\ h_{j+1} \end{Bmatrix} + \begin{bmatrix} I_{ij3} - v_{j+1}I_{ij4} & -I_{ij3} + v_j I_{ij4} \end{bmatrix} \begin{Bmatrix} \left(\frac{\partial h}{\partial n}\right)_j \\ \left(\frac{\partial h}{\partial n}\right)_{j+1} \end{Bmatrix} \qquad 4.19$$

Using tables the integrals are evaluated in terms of the local co-ordinates u and v.

$$I_{ij1} = \frac{(\pm)u_i}{v_{j+1}-v_j}\int_{v_j}^{v_{j+1}} \frac{v}{u_i^2+v^2}\,dv = \frac{(\pm)u_i}{v_{j+1}-v_j}\left[\frac{1}{2}\,\ell n(u_i^2+v^2)\right]_{v_j}^{v_{j+1}} = \frac{(\pm)u_i}{2(v_{j+1}-v_j)}\,\ell n\left[\frac{u_i^2+v_{j+1}^2}{u_i^2+v_j^2}\right] \qquad 4.20$$

$$I_{ij2} = \frac{1}{v_{j+1}-v_j}\int_{v_j}^{v_{j+1}} \frac{(\pm)u_i}{u_i^2+v^2}\,dv = \frac{(\pm)1}{v_{j+1}-v_j}\left[\tan^{-1}\frac{v}{u_i}\right]_{v_j}^{v_{j+1}} = \frac{(\pm)1}{v_{j+1}-v_j}\left[\tan^{-1}\left(\frac{v_{j+1}}{u_i}\right) - \tan^{-1}\left(\frac{v_j}{u_i}\right)\right] \qquad 4.21$$

$$I_{ij3} = \frac{1}{v_{j+1}-v_j}\int_{v_j}^{v_{j+1}} v\cdot\frac{1}{2}\ell n(u_i^2+v^2)\,dv = \frac{1}{4(v_{j+1}-v_j)}\left[(u_i^2+v^2)\,\ell n(u_i^2+v^2)-1\right]_{v_j}^{v_{j+1}}$$

$$= \frac{1}{4(v_{j+1}-v_j)}\left[(u_i^2+v_{j+1}^2)(\ell n(u_i^2+v_{j+1}^2)-1)-(u_i^2+v_j^2)(\ell n(u_i^2+v_j^2)-1)\right] \qquad 4.22$$

$$I_{ij4} = \frac{1}{v_{j+1}-v_j}\int_{v_j}^{v_{j+1}} \frac{1}{2}\ell n(u_i^2+v^2)dv$$

$$= \frac{1}{2(v_{j+1}-v_j)}\left[v\ell n(u_i^2+v^2)-2v+2u_i \tan^{-1}\frac{v}{u_i}\right]_{v_j}^{v_{j+1}}$$

$$= \frac{1}{2(v_{j+1}-v_j)}\left[v_{j+1}\ \ell n(u_i^2+v_{j+1}^2) - v_j\ \ell n(u_i^2+v_j^2) - 2(v_{j+1}-v_j)\right.$$

$$\left. + 2u_i\left(\tan^{-1}\left(\frac{v_{j+1}}{u_i}\right) - \tan^{-1}\left(\frac{v_j}{u_i}\right)\right)\right] \qquad 4.23$$

These four integrals defined in equations 4.20 to 4.23 depend only on the boundary geometry, specifically on the values of u_i, v_j and v_{j+1}. The right hand side of equation 4.10 is obtained by summing the contributions of each boundary element given by equation 4.19 from j = 1 to j = N, where N is the number of nodes. This gives the integral equation for boundary node i. By changing the base node to each node in turn and performing the boundary integration a set of N such equations is obtained.

The equations written in matrix form are

$$[\ R\ ]\left\{h\right\} = [\ L\ ]\left\{\frac{\partial h}{\partial n}\right\} \qquad 4.24$$

where [R] and [L] are N x N matrices and $\left\{h\right\}$ and $\left\{\frac{\partial h}{\partial n}\right\}$ are N x 1 column vectors.

The term in row i and column j of [R], for example, is

$$(-I_{ij1} + v_{j+1}I_{ij2}) + (I_{i,j-1} - v_{j-1}I_{i,j-1,2}) - \delta_{i,j}\alpha_i \qquad 4.25$$

where the first term (bracketted) arises from integration between nodes j and j+1 and the second term from integration between nodes j-1 and j. It is noted that the local co-ordinates for the second term are not necessarily those of the first. (The local co-ordinate system is defined in Figure 4.3) The last term arises by subtracting the left hand side of equation 4.10 from both sides, where α_i is the interior angle between

boundary elements meeting at base node i (in radians) and δ_{ij} is the Dirac delta function such that

$$\delta_{ij} = \begin{cases} 0 & \text{if} \quad i \neq j \\ 1 & \text{if} \quad i = j \end{cases} \qquad 4.26$$

When the known boundary conditions are substituted into equation 4.24 the resulting set of equations in the unknown variables are ready for solving by Gaussian elimination and back substitution.

$$[E]\{u\} = \{c\} \qquad 4.27$$

where $\{u\}$ is a vector of unknowns (either h or $\frac{\partial h}{\partial n}$),

$[E]$ is a combination of the assembled [R] and [L] matrices as defined by equation 4.24

and $\{c\}$ is the assembled vector for the right hand side (known)

With the unknowns determined, h and $\frac{\partial h}{\partial n}$ are known at all points on the boundary. The value of the hydraulic head anywhere within the flow domain can then be found using equation 4.9. Usually the determination of the unknowns on the boundary is all that is required in a vertical slice groundwater flow problem.

As each node connects two boundary elements, and the value of $\frac{\partial h}{\partial n}$ depends on the direction of the outward normal, $\tilde{n}$, it may be necessary to define $\frac{\partial h}{\partial n}$ twice for each node, where the normal is taken to be perpendicular to each element in turn. This complication is discussed at length in section 4.5.

Boundary conditions must be defined in order to obtain equation 4.27 from 4.24. A description of the various types of boundary conditions follows. In the 2-dimensional vertical slice model, the x axis corresponds to the horizontal direction and the y axis the vertical direction, positive upwards.

4.3 Boundary Conditions

The two most common boundary conditions are specified head, h (Dirichlet condition) and specified normal derivative $\frac{\partial h}{\partial n}$ (Neumann condition).

A seepage face is represented by the boundary condition

$$h = y \qquad 4.28$$

because the hydraulic head is the same as the vertical elevation, y of any node on the seepage face.

For steady flow a free surface is represented by the boundary conditions

$$\frac{\partial h}{\partial n} = 0 \qquad 4.29$$

and $$h = \eta(x) \qquad \text{where} \quad y = \eta(x) \qquad 4.30$$

The steady free surface is a streamline hence the normal flux vanishes, and the hydraulic head at the free surface is the free surface elevation, η.

Mixed boundary conditions occur where only the relationship between h and $\frac{\partial h}{\partial n}$ is defined on the boundary . An example is the unsteady free surface boundary condition which is derived in Appendix A.

This boundary condition is specified as

$$\frac{\partial h}{\partial t} = - \frac{K}{n_e} \frac{1}{\cos \beta} \frac{\partial h}{\partial n} + \frac{W}{n_e} \qquad 4.31$$

where K is the saturated hydraulic conductivity of the medium

n_e is the effective porosity of the medium

β is the angle between the free surface and the horizontal axis

and W is the rate of recharge [$L\ T^{-1}$], or evaporation if $W < 0$.

Bear (1972, p255) suggests that n_e used in equation 4.31 is not constant. This follows from the observation that change in storage, particularly for a receding free surface, is not instantaneous with the free surface movement. (see assumption 2.1.1.(3)). If there is residual moisture above a declining watertable due to insufficient time for drainage to restore an equilibrium moisture profile in the capillary fringe, then

the effective porosity would be reduced should the free surface start to rise. In the model n_e is assumed constant. This is compatible with the isotropic, homogeneous assumption used in the model.

The remaining boundary condition is that for the streambed nodes when the stream is hydraulically connected to the aquifer. This is also a mixed boundary condition and derived from Darcy's law applied across the semipermeable streambed blanket and in the medium.

The Darcy velocity of water across a layer of thickness, ℓ and hydraulic conductivity, K_B, using equation 3.4 is given by

$$v = K_B(h_s - h)/\ell \qquad 4.32$$

where h_s is the hydraulic head at the top of the layer (the stream stage) and h is the hydraulic head in the porous medium (with hydraulic conductivity K) at the base of the semipermeable blanket.

By continuity the Darcy velocity of the fluid in the underlying medium is identical, and is given by Darcy's law as

$$v = K \frac{\partial h}{\partial n} \qquad 4.33$$

There is no negative sign on the right hand side of this equation as the outward normal derivative of the head always opposes the direction of v, where the direction of v is determined by the relative magnitudes of h_s and h. Equating 4.32 and 4.33 gives

$$\frac{\partial h}{\partial n} = \frac{K_B}{K\ell} (h_s - h) \qquad 4.34$$

or rearranged

$$h = h_s - \frac{K\ell}{K_B} \frac{\partial h}{\partial n} \qquad 4.35$$

which may be abbreviated to

$$h = h_s - B \frac{\partial h}{\partial n} \qquad \text{for } h_s > y_m \text{ and } h > y_m \qquad 4.36$$

where

$$B = \frac{K\ell}{K_B} \qquad 4.37$$

and B is called the streambed hydraulic impedance.

Equation 4.36 gives the boundary condition for a node on the base of

the semipermeable blanket, at an elevation y_m, when h_s exceeds y_m and h exceeds y_m. That is, the aquifer is hydraulically connected to the stream at this node.

On the recession limb of a stream hydrograph a hydraulically connected node undergoes a further transition. The head in the aquifer drops more slowly than the stream head and at some time the head at the node may exceed the elevation of the streambed which in turn exceeds the stream head. A seepage face forms at the streambed surface above the node. As the node is located at the base of the semipermeable layer the seepage face boundary condition equation 4.28 is not applicable. Instead h_s is replaced by y_m in equation 4.36.

$$h = y_m - B \frac{\partial h}{\partial n} \qquad \text{for} \quad h > y_m > h_s \qquad 4.38$$

Here the assumption is made that the semipermeable layer thickness is small, allowing the elevation of its base to be used as an approximation for the elevation of the streambed surface. This boundary condition remains operative at the node until the head falls below y_m. Then it reverts to the free surface boundary condition and the node is subject to equation 4.31. A schematic diagram figure 4.4 illustrates this boundary condition transition.

With the onset of flow in a dry streambed the free surface recharge, W is defined with the help of the Green-Ampt equation and Darcy's law.

$$W = \frac{K_B}{\ell}(h_s - y_m - h_c) \qquad \text{for} \quad h < y_m + h_c \qquad 4.39$$

and

$$W = \frac{K_B}{\ell}(h_s - h) \qquad \text{for} \quad y_m + h_c < h < y_m \qquad 4.40$$

where y_m is the elevation of the base of the semipermeable layer above the node and h_c is the critical pressure head, ψ_{cr} (or effective capillary drive as defined in equation 3.47). h_c is less than or equal to zero.

Equation 4.39 gives a constant recharge rate while the capillary

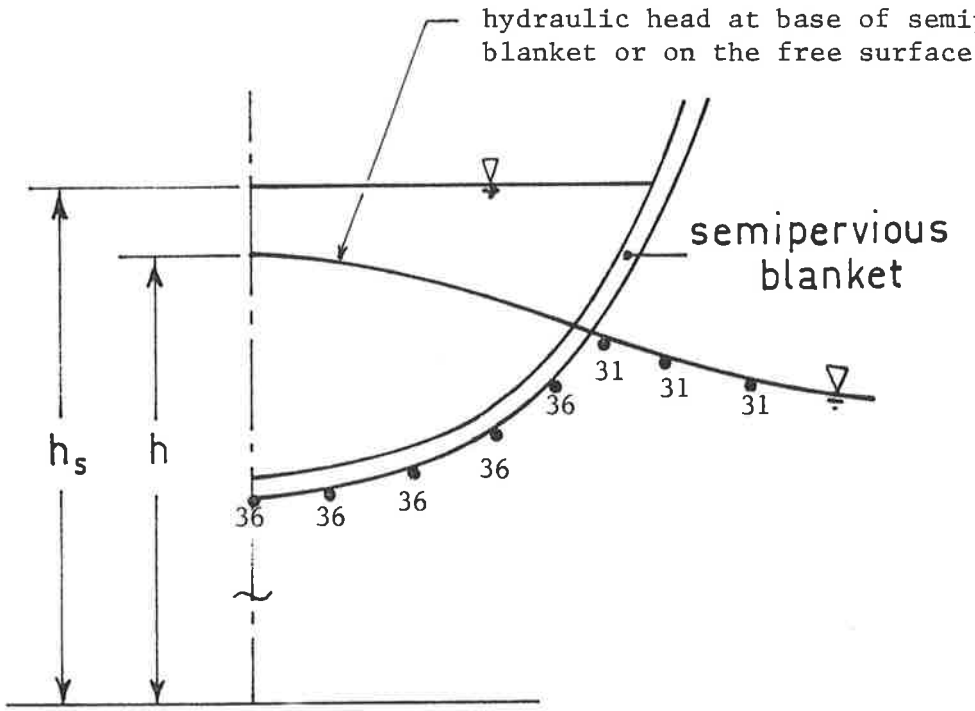

(a) time t_1

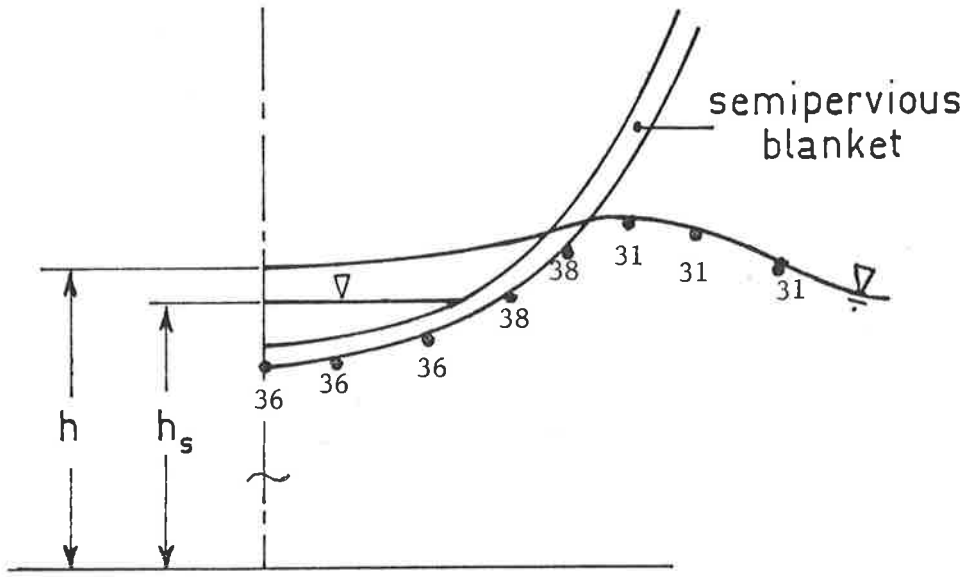

(b) time $t_2 > t_1$; $h_s(t_2) < h_s(t_1)$

Figure 4.4 Change in boundary condition for nodes on the streambed during flow recession for a hydraulically connected stream. The number adjacent each node refers to the boundary condition equation in chapter 4 applying to that node. (36 = streambed node, 38 = node below seepage face, 31 = free surface node)

fringe above the free surface has no effect on the pore water pressure at the base of the semipermeable layer. When the free surface rises beyond that elevation ($y_m + h_c$) the increase in pore water pressure at the base of the semipermeable layer (elevation y_m) reduces the hydraulic gradient across the semipermeable layer. Use of equation 4.40 assumes that the pore pressure head is linear from h_c at a distance ($-h_c$) above the free surface to zero at the free surface. While this approximation is not strictly correct, (for example see the pore pressure distributions above the free surface described in Freyberg et al., 1980) it is considered a satisfactory assumption for use with the Green-Ampt (piston flow) equation for simulating unsaturated porous medium flow.

A time delay, t_d, for recharge to reach the free surface after the onset of streamflow is obtained by integrating the Green-Ampt equation (see equation 3.35) to give

$$t_d = \frac{n_e}{K}\left[y_m - D - (h_s - h_c)\ln\left(\frac{h_s - h_c + y_m - D}{h_s - h_c}\right)\right] \qquad 4.41$$

in which D is the initial elevation of the free surface.

Once a free surface node reaches the base of the semipermeable layer it is transformed into a streambed node and satisfies the boundary condition of equation 4.36. In this way the boundary condition applied to a streambed node varies according to the node elevation.

The range of boundary conditions for nodes beneath a streambed are schematically illustrated in figure 4.5. The flux entering the aquifer (boundary integral domain) is shown on the left hand side, and the equations representing each boundary condition on the right. The distinction between hydraulic connection and hydraulic disconnection occurs when the free surface condition disappears or appears. This occurs when the free surface reaches an elevation y_m, the base of the semipermeable layer on the streambed. In the case when h_c is zero the elevation of the free surface has no influence on stream infiltration rates when $h < y_m$.

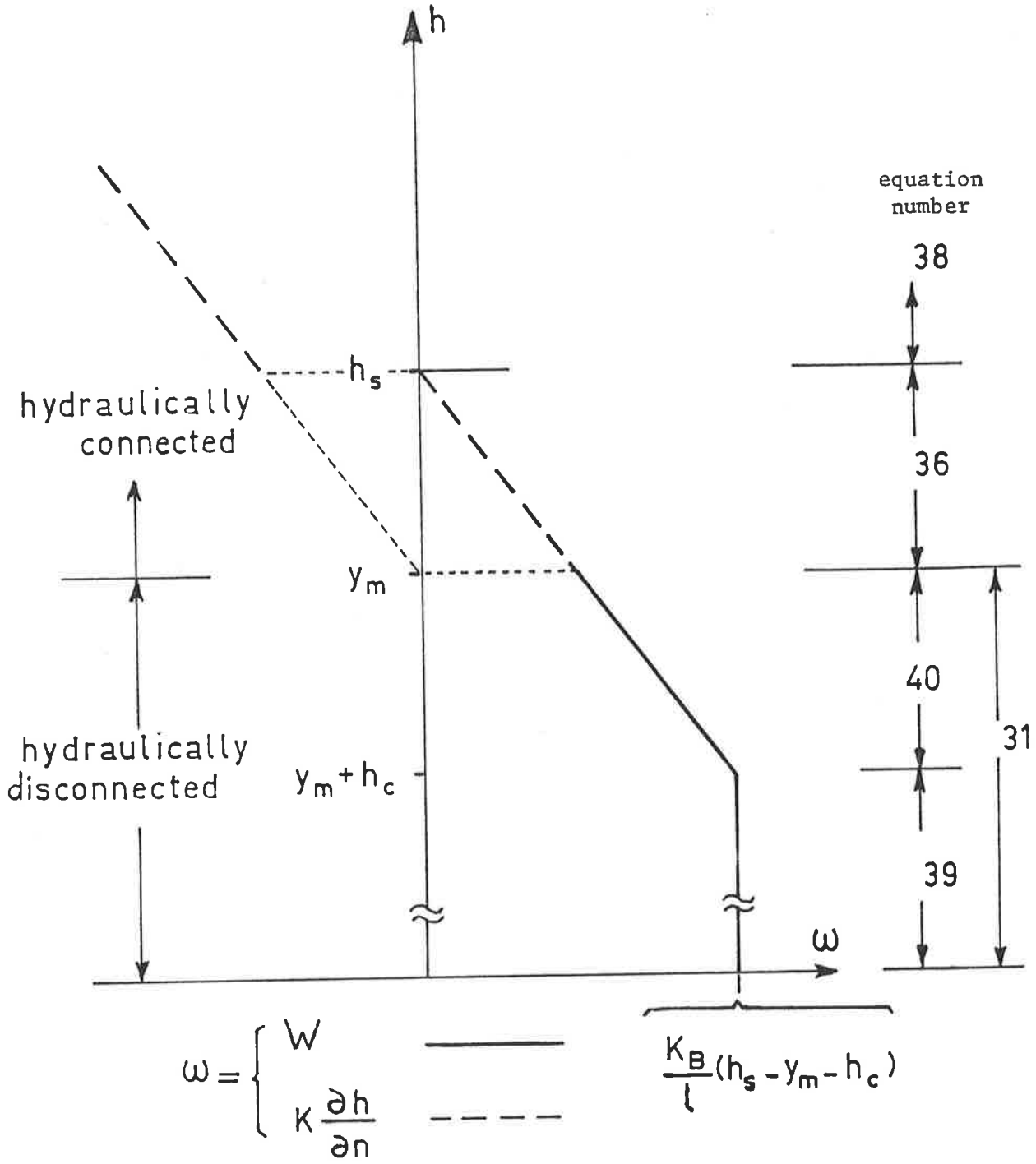

Figure 4.5 Effect of nodal hydraulic head on recharge rate or exchange flow rate. Corresponding boundary condition equations (from chapter 4) are shown at right.

When h_c is less than zero, however, the position of the free surface can influence infiltration rates.

Note that figure 4.5 applies only to single node positions and not to entire streambeds so there is no direct comparison between this figure and models proposed by Rushton and Tomlinson (1979).

4.4 Time Discretization

In order to extend the application of the generalized computer program which solves for the unknowns in equation 4.10 using the boundary conditions described in section 4.3, dimensionless variables are introduced to replace the real variables.

The following substitutions are made

$$t^* = tK/n_e L \tag{4.42}$$

$$(x^*, y^*, y_m^*, h^*, h_s^*, h_c^*, B^*, \tilde{n}^*) = (x, y, y_m, h, h_s, h_c, B, \tilde{n})/L \tag{4.43}$$

$$w = \frac{W}{K} \tag{4.44}$$

where L is a characteristic length scale.

All quantities with asterisks are non dimensional quantities.

Making t, h and W the subjects of equation 4.42, 4.43 and 4.44 respectively and substituting into equation 4.31 gives the non dimensional unsteady free surface boundary condition as

$$\frac{\partial h}{\partial t} = \frac{-1}{\cos \beta} \frac{\partial h}{\partial n} + w \tag{4.45}$$

For brevity all asterisks are dropped in this equation and for the rest of this chapter.

This equation can be written in finite difference form by considering a small time step Δt between time levels k and k+1.

$$h^{k+1} = h^k - \frac{\Delta t}{\cos \beta^k}\left[\varepsilon \left(\frac{\partial h}{\partial n}\right)^{k+1} + (1-\varepsilon)\left(\frac{\partial h}{\partial n}\right)^{k}\right] + \Delta t[\varepsilon\, w^{k+1} + (1-\varepsilon)w^k] \tag{4.46}$$

in which ε is a weighting factor to position the normal hydraulic gradient and the non dimensional recharge between time $k\Delta t$ and $(k+1)\Delta t$. Writing equation 4.24 at time k+1 gives

$$[R]\{h\}^{k+1} = [L]\left\{\frac{\partial h}{\partial n}\right\}^{k+1} \qquad 4.47$$

Considering the column vector $\{h\}^{k+1}$ of nodal heads on the free surface and using equation 4.46 in 4.47 gives

$$[R]\{h^k - \frac{\Delta t}{\cos \beta^k}\left[\varepsilon\left(\frac{\partial h}{\partial n}\right)^{k+1} + (1-\varepsilon)\left(\frac{\partial h}{\partial n}\right)^{k}\right] + \Delta t[\varepsilon w^{k+1}+(1-\varepsilon)w^k]\} = [L]\left\{\frac{\partial h}{\partial n}\right\}^{k+1} \qquad 4.48$$

Rearranging to obtain an expression for the normal derivative at time k+1

$$\left[[L] + \frac{\varepsilon\Delta t}{\cos \beta^k}[R]\right]\left\{\frac{\partial h}{\partial n}\right\}^{k+1} = [R]\left\{h^k - \frac{(1-\varepsilon)\Delta t}{\cos \beta}\left(\frac{\partial h}{\partial n}\right)^{k} + \varepsilon\Delta t\, w^{k+1} + (1-\varepsilon)\Delta t\, w^k\right\} \qquad 4.49$$

Here all variables on the right hand side have known values because they occur at time k for which solutions have already been obtained. The exception is w^{k+1} which is unknown if h^{k+1} falls between y_m+h_c and y_m. To overcome this problem w^{k+1} is initially equated with w^k and the right hand side of equation 4.49 is calculated. A solution is obtained for $\left\{\frac{\partial h}{\partial n}\right\}^{k+1}$ and then with the use of equation 4.46 the new position of the phreatic surface is found $\{h\}^{k+1}$. A second iteration of the time step from time k to k+1 is performed if for any node $y_m + h_c < h^{k+1} < y_m$, that is, $w^{k+1} \neq w^k$.

If $h^{k+1} > y_m$ the node ceases to be free surface node and the boundary condition is changed to equation 4.36 if $h_s^{k+1} > y_m$ or equation 4.38 if $h_s^{k+1} < y_m$. A change in boundary condition requires a second iteration from time step k to k+1 using the new boundary condition for that node to replace the free surface boundary condition.

The premature change in boundary condition at a node introduces a

small error. If time steps are too large the error will manifest itself in the boundary condition at the node oscillating from free surface to streambed types in successive iterations. This arises from oscillation of h about y_m due to the reduction in recharge as the head increases. If time steps are small at the time of the changing boundary condition a stable transition occurs and the resultant error is small.

A third reason for a second iteration of the time step from k to k+1 occurs when $\left| h^{k+1} - h^k \right| > \text{THRESH}$. That is the change in elevation of a node or nodes on the free surface exceeds a specified threshold. Under these circumstances the value of β^k in equation 4.46 may not be a satisfactory approximation to $[\varepsilon\beta^{k+1} + (1-\varepsilon)\beta^k]$ due to large changes in slope of the free surface from time k to k+1. Secondly the boundary integrals contained in matrices [R] and [L] of equation 4.47 depend on the geometry of the boundary. If this changes significantly [R] and [L] require recalculation.

In all cases during the second iteration all nodes which are free surface nodes at time k+1 are assumed to be positioned midway between the elevation of the node at time k (h^k if a free surface node or y_m if a streambed node) and h^{k+1}, the elevation obtained from the first iteration. Matrices [R] and [L] and the free surface slope β are calculated using this assumed position but h^k and $\left(\frac{\partial h}{\partial n}\right)^k$ retain their original values. Equation 4.49 is reemployed to evaluate a new vector $\left\{\frac{\partial h}{\partial n}\right\}^{k+1}$ which in turn gives the new free surface position $\{h\}^{k+1}$.

The remaining mixed boundary condition which by definition invokes terms on both sides of equation 4.47 is the streambed boundary condition

$$h^{k+1} = h_2^{k+1} - B\left(\frac{\partial h}{\partial n}\right)^{k+1} ; \qquad h \geq y_m \tag{4.50}$$

where $h_2^{k+1} = h_s^{k+1}$ for $h_s^{k+1} \geq y_m$

or $h_2^{k+1} = y_m$ for $h_s^{k+1} < y_m$

Note h^{k+1} is independent of h^k so equation 4.50 may be written explicitly at time k+1. (The weighting factor $\varepsilon = 1$). That is this equation represents a series of steady states and not a transient condition, unlike the free surface boundary condition.

Substituting equation 4.50 into 4.47 gives

$$[R]\left\{h_2^{k+1} - B\left(\frac{\partial h}{\partial n}\right)^{k+1}\right\} = [L]\left\{\frac{\partial h}{\partial n}\right\}^{k+1} \qquad 4.51$$

hence

$$\left[[L] + B[R]\right]\left\{\frac{\partial h}{\partial n}\right\}^{k+1} = [R]\{h_2\}^{k+1} \qquad 4.52$$

With h_2 known the right hand side can be calculated and $\left\{\frac{\partial h}{\partial n}\right\}^{k+1}$ determined. Back substitution using equation 4.50 completes the solution. No second iteration is initiated by any streambed node unless it has undergone a change from a free surface node to a streambed node during the time step from k to k+1. Under these circumstances the elevation of the node during the second iteration is assumed to be y_m when calculating [R] and [L].

Time steps for the model may be either uniform or increase logarithmically. Alternatively the times at which solutions are required may be specified. Several parameters are used to control time stepping. These enable efficient use of computer time and contain the mass balance error. The mass balance error is described in section 4.6.

4.5 Node Types

As has been illustrated for the mixed boundary conditions the assembly of equation 4.27 from equation 4.24 is not necessarily as simple as it may first appear. Similarly, complications occur where two different boundary conditions meet at a node. Figure 4.6 contains schematic diagrams of the node types which may occur.

Boundary integration proceeds in a clockwise direction. In figure 4.6 $\left(\frac{\partial h}{\partial n}\right)_1$ and $\left(\frac{\partial h}{\partial n}\right)_2$ represent the hydraulic gradient at the node in the direction normal to the boundary element approaching the node and leaving

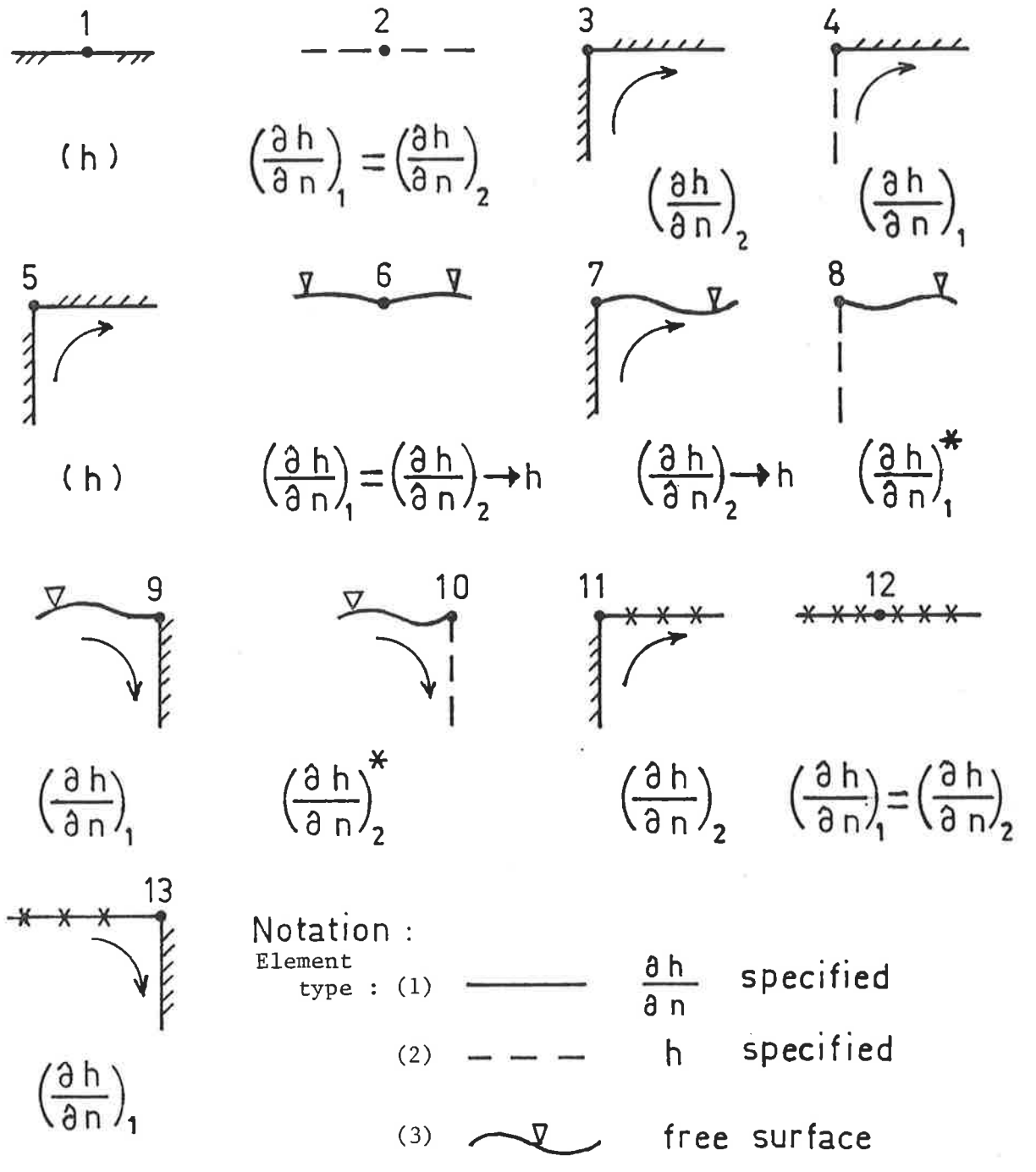

Figure 4.6 Schematic diagram of node types.

the node respectively. For node type 1 there is no change in angle at the boundary and $\left(\frac{\partial h}{\partial n}\right)_1 = \left(\frac{\partial h}{\partial n}\right)_2$. For node type 6 the angle, β the free surface makes with the horizontal is calculated from the derivative of the quadratic function passing through the node and the two adjacent nodes. Hence β and the direction normal to the free surface at the node are unique and $\left(\frac{\partial h}{\partial n}\right)_1 = \left(\frac{\partial h}{\partial n}\right)_2$.

β is calculated as follows at (x_1, y_1) with adjacent nodes (x_o, y_o) and (x_2, y_2).

Defining the parabola passing through the three points as

$$y = Ax^2 + Bx + C \qquad 4.53$$

the derivative at x (which is the tangent of β) is

$$\frac{dy}{dx} = 2Ax + B \qquad 4.54$$

fitting the parabola to the points gives the derivative at x_1, as

$$\left(\frac{dy}{dx}\right)_{x=x_1} = \tan\beta = \frac{(y_0-y_1)(x_2-x_1)^2-(y_2-y_1)(x_0-x_1)^2}{(x_0-x_1)(x_2-x_1)(x_2-x_0)} \qquad 4.55$$

For all other node types $\left(\frac{\partial h}{\partial n}\right)_1$ and $\left(\frac{\partial h}{\partial n}\right)_2$ are not necessarily equal. In order to account for both normal derivatives for these node types equation 4.47 is expanded to include a vector $\{FCORN\}$.

$$[R]\{h\}^{k+1} = [L]\left\{\frac{\partial h}{\partial n}\right\}^{k+1} + \{FCORN\} \qquad 4.56$$

where $$\{FCORN\} = [L]\left\{\frac{\partial h}{\partial n}\right\}^{k+1}_{known} \qquad 4.57$$

$\{FCORN\}$ is used as a means of restricting the number of rows in matrix [L] to N, the number of boundary nodes. That is only one of $\left(\frac{\partial h}{\partial n}\right)_1$ and $\left(\frac{\partial h}{\partial n}\right)_2$ at each node appears in the vector $\left\{\frac{\partial h}{\partial n}\right\}^{k+1}$ of equation 4.56. The other value is known (or can be calculated from the boundary condition), hence the product {FCORN} can be calculated during boundary integration. Table 4.1 shows how [L] and {FCORN} are assembled during boundary integration and the effect of node type.

Table 4.1

Effect of node type on assembly of boundary integral equations

Node type	Elt type -Elt type	Node j action	Node j+1 action
1	1 - 1(cont)	a	a
2	2 - 2	a	a
3	1 - 2	a	c
4	2 - 1	b	a
5	1 - 1(discont)	b	c*
6	3 - 3	a	a
7	1 - 3	a	c
8	2 - 3	b	a
9	3 - 1	b	a
10	3 - 2	a	c
11	1 - 4	a	c
12	4 - 4	a	a
13	4 - 1	b	a

Action a $L(i,j) = L(i,j) + PNJ$

$L(i,j+1) = L(i,j+1) + PNJP$

b $FCORN(i) = FCORN(i) + PNJ * \left(\frac{\partial h}{\partial n}\right)_{j,2}$

$L(i,j+1) = L(i,j+1) + PNJP$

c $L(i,j) = L(i,j) + PNJ$

$FCORN(i) = FCORN(i) + PNJP * \left(\frac{\partial h}{\partial n}\right)_{j+1,1}$

L(i,j) represents the element at the ith row and jth column of matrix [L] defined in equation 4.56. {FCORN } is defined by equation 4.57

$PNJ = -I_{ij3} + v_{j+1} I_{ij4}$ see equation 4.19

$PNJP = I_{ij3} + v_j I_{ij4}$

$\left(\frac{\partial h}{\partial n}\right)_{j,2}$ represents $\left(\frac{\partial h}{\partial n}\right)_2$ at node j and

$\left(\frac{\partial h}{\partial n}\right)_{j+1,1}$ represents $\left(\frac{\partial h}{\partial n}\right)_1$ at node j+1

For each segment two actions may be specified by this table. Action b has priority over action c which has priority over action a. The only exception occurs when node j+1 is of type 5 and then action c is taken.

4.6 Mass Balance Check

A necessary condition of any solution is that the law of mass conservation (continuity) is satisfied. That is, the change in storage (increase in area below the free surface), DE, during each time step, equals the net flux through the boundaries, DLTS. The model calculates the components of the mass balance and computes the percentage error at each time step, PDER, from

$$PDER = 100 * (DE - DLTS) / DE \qquad 4.58$$

The total error is found in the same way using the storage change since t = 0, TDE and the net inflow since t = 0, TLTS. The total percentage error, PTER is given by

$$PTER = 100 * (TDE - TLTS) / TDE \qquad 4.59$$

Time steps and node spacings are specified in such a manner that the mass balance error is contained within an acceptable tolerance. The tradeoff between computer execution time and model accuracy for an example problem is discussed in the next chapter (section 5.1.2).

4.7 Node Shifting

For boundaries which expand or contract it is often desirable to maintain the same spacial relationship between node positions, rather than fix all except the end nodes of a side. A technique for shifting nodes was devised to enable this to occur. Node shifting is initiated at the end of a time step if the percentage change in the length of a boundary since the start or the previous shift exceeds a specified threshold value. Linear interpolation between the new positions of the end nodes is used to locate the new positions of intermediate nodes. A choice of either linear or quadratic interpolation between existing node positions is used to determine h and $\frac{\partial h}{\partial n}$ for the new node positions. Shifting of nodes on shifting boundaries is an optional feature in the model. The effect of node shifting on mass balance error is observed for a test problem, TEST5 in the next chapter.

4.8 Summary of Unique Model Features

The BIEM model described in this chapter contains a number of novel features which distinguish it from previous models of stream-aquifer interaction. Firstly it takes account of the variety of boundary conditions occuring at a streambed cross-section at any instant and secondly it allows for these to change naturally with time according to variations in stream stage and free surface position. In this way it can account for the transition from hydraulic disconnection to hydraulic connection of a stream and aquifer. It also allows for the formation of a seepage face on the streambank during flow recession in a hydraulically connected stream. In addition the Green-Ampt equation is used to describe infiltration in the unsaturated zone. The model requires only a few parameters to be defined or recursively estimated making it relatively easy to calibrate compared with previous models. In Chapter 9 this aspect of model utility is described at length. Tests of model performance and the application of the model to problems for which solutions are already known and to new problems are documented in Chapter 5.

CHAPTER 5

APPLICATION OF THE STREAM-AQUIFER INTERACTION MODEL

5.1 Tests of Model Performance

The model was tested first on simple problems having linear distributions of head and normal hydraulic gradient on the boundary. Results agreed with analytical solutions to six significant figures. Stability and accuracy of the model were investigated using the approach of Liu and Liggett (1980).

5.1.1 Sinusoidal free surface test (SINE)

Liu and Liggett present an exact solution to a linearized problem involving a free surface in the shape of a sine wave, of amplitude 2a, in a box with impermeable base and sides (see figure 5.1). As the stability analysis can only be performed on a linearized system of equations, Liu and Liggett linearize the free surface boundary condition by using the mean free surface position ($y = 0$) as the upper boundary with the head $h(x)$ on this boundary equated with the free surface elevation, $\eta(x)$. This freezes nodal positions, making arrays [R] and [L] in equation 4.56 constant, and has the effect of making β the slope of the free surface, equal to zero in equation 4.45. The resulting linear (in h) boundary condition at $y = 0$, derived from equation 4.46 is

$$h^{k+1} = h^{k} - \Delta t\left[\varepsilon\left(\frac{\partial h}{\partial n}\right)^{k+1} + (1-\varepsilon)\left(\frac{\partial h}{\partial n}\right)^{k}\right] \qquad 5.1$$

where ε is a weighting factor to position the normal hydraulic gradient between time $k\Delta t$ and $(k+1)\Delta t$.

With a test case embracing a half wave length, this mode is represented by the wave number, m where $m = \pi / L$.

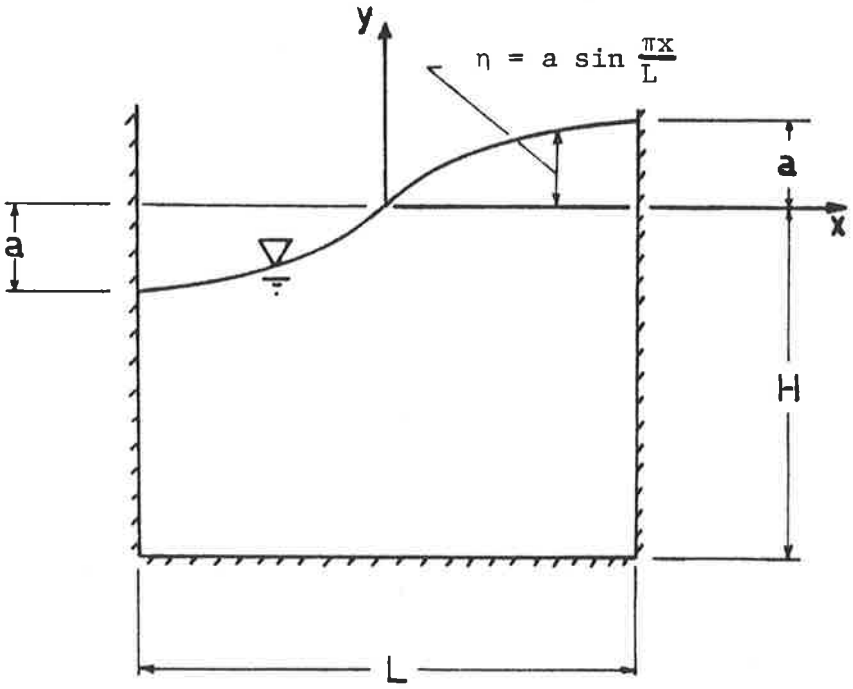

Figure 5.1 Stability test case,SINE. Sinusoidal free surface in a porous medium in an impermeable container : geometry and boundary conditions (after Liu and Liggett, 1980, figure 3).

Liu and Liggett give the exact solution to the linearized problem as

$$h(x,y,t) = a \sin mx \frac{\cosh m(y+H)}{\cosh (mH)} \cdot \exp(-\sigma t) \qquad 5.2$$

where $$\sigma = m \tanh(mH) \qquad 5.3$$

σ, a positive real constant, is the damping coefficient of the linearized physical system. Proof that equation 5.2 is a solution to this linearized problem is given in Appendix B. Substituting equation 5.2 into 5.1 yields (at y = 0);

$$\exp(-\sigma_N \Delta t) = 1 - \Delta t \sigma[\varepsilon \exp(-\sigma_N \Delta t) + (1-\varepsilon)] \qquad 5.4$$

where σ_N is the damping coefficient for the numerical approximation to the free surface boundary condition.

Rearranging gives

$$\sigma_N = -\frac{1}{\Delta t}\,\ell n\left[\frac{1-(1-\varepsilon)\Delta t\sigma}{1+\varepsilon\Delta t\sigma}\right] \qquad 5.5$$

For an ideal model $\sigma_N=\sigma$ and the damping of the free surface sine wave is the same for the model as the linearized system. Defining c as $\sigma_N - \sigma$, the difference between the numerical and the linearized system damping coefficients and substituting equation 5.5 gives

$$c = -\sigma - \frac{1}{\Delta t}\,\ell n\left[\frac{1-(1-\varepsilon)\Delta t\sigma}{1+\varepsilon\Delta t\sigma}\right] \qquad 5.6$$

and defining $q = \Delta t\sigma$ 5.7

gives

$$c\Delta t = -q - \ell n\left(1 - \frac{q}{1+\varepsilon q}\right) \qquad 5.8$$

The best numerical approximation occurs when c is zero. A negative value of c indicates numerical amplification and a positive value indicates numerical damping. Figure 1 of Liu and Liggett (1980) is reproduced here (figure 5.2). For a range of q the best value for ε lies between 0.5 and 0.6. Liu and Liggett observed that:

1. small values of Δt result in less numerical distortion
2. small values of m (longer wavelengths) are less distorted than higher values.
3. optimum values of ε fall between 0.5 and 0.6 when q is less than 1.
4. there is an upper limit on q of $1 / (1-\varepsilon)$ for finite numerical damping.
5. for a given value of q there is a value of ε for which $c = 0$ and there is no numerical distortion (assuming m is single valued).

In most real unconfined groundwater problems there will be a range of wave numbers and the mean depth may vary with time and location giving a range of values of q. For $q < 0.5$ the use of $\varepsilon = 0.53$ results in minimal numerical distortion.

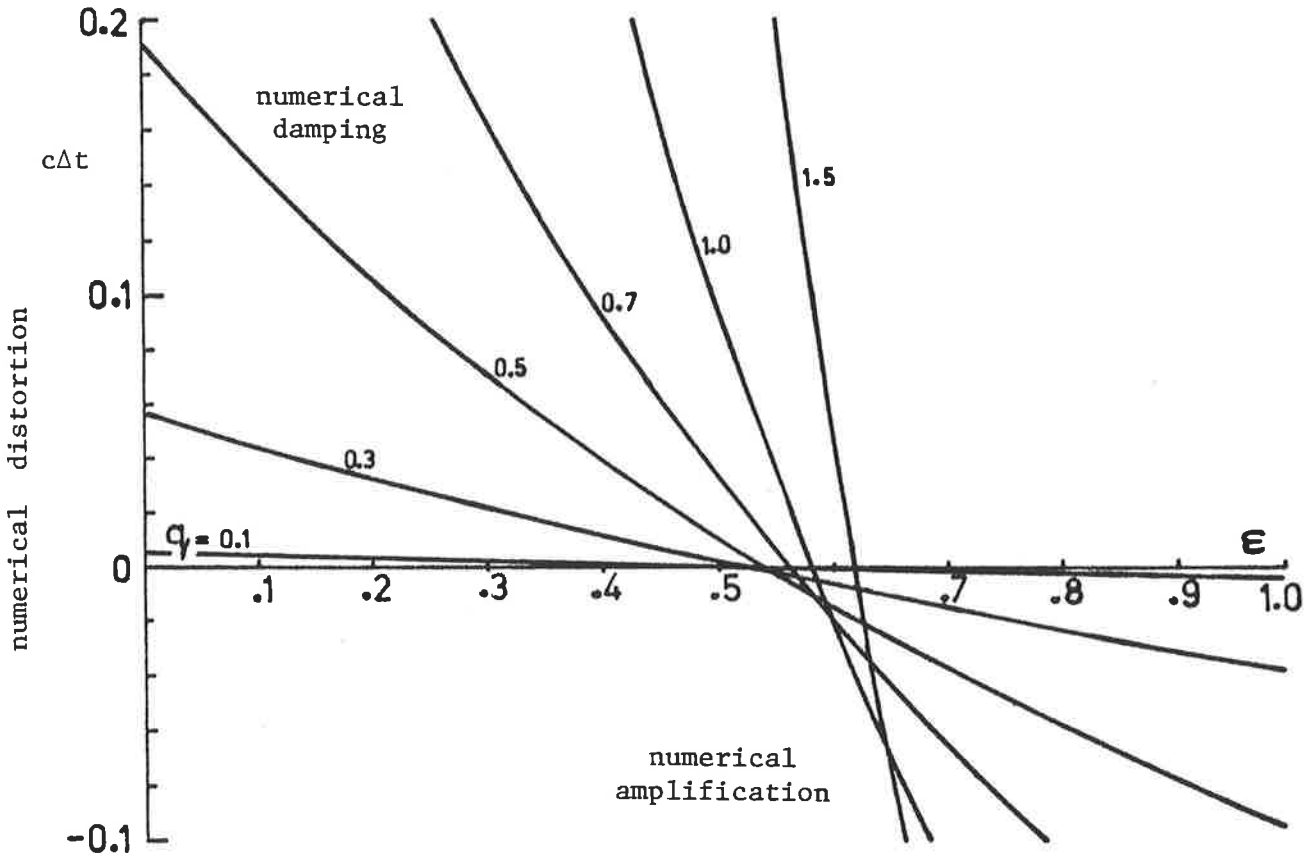

Figure 5.2 Graphical representation of equation 5.8, the numerical distortion ($c\Delta t$) of the linearized problem, related to the implicit weighting factor, ε and the product, q of time increment and damping coefficient (after Liu and Liggett, 1980, figure 1).

Liu and Liggett compare BIEM results for the head at the free surface on the right hand side boundary with the exact solution to the linearized problem. They use H = L =2 and a = 0.1 giving $\sigma = \frac{\pi}{2}\tanh(\pi) \simeq \pi/2$. In figure 5.3 plots of the results of the BIEM model described in chapter 4 are superimposed on their theoretical results.

This figure reveals an excellent agreement on the predicted damping of the sine wave between the linear and nonlinear (chapter 4) model results and the prediction using equation 5.5, for $\varepsilon > 0.5$. This lends support to the case for applying the stability criteria for a linearized model to the nonlinear model.

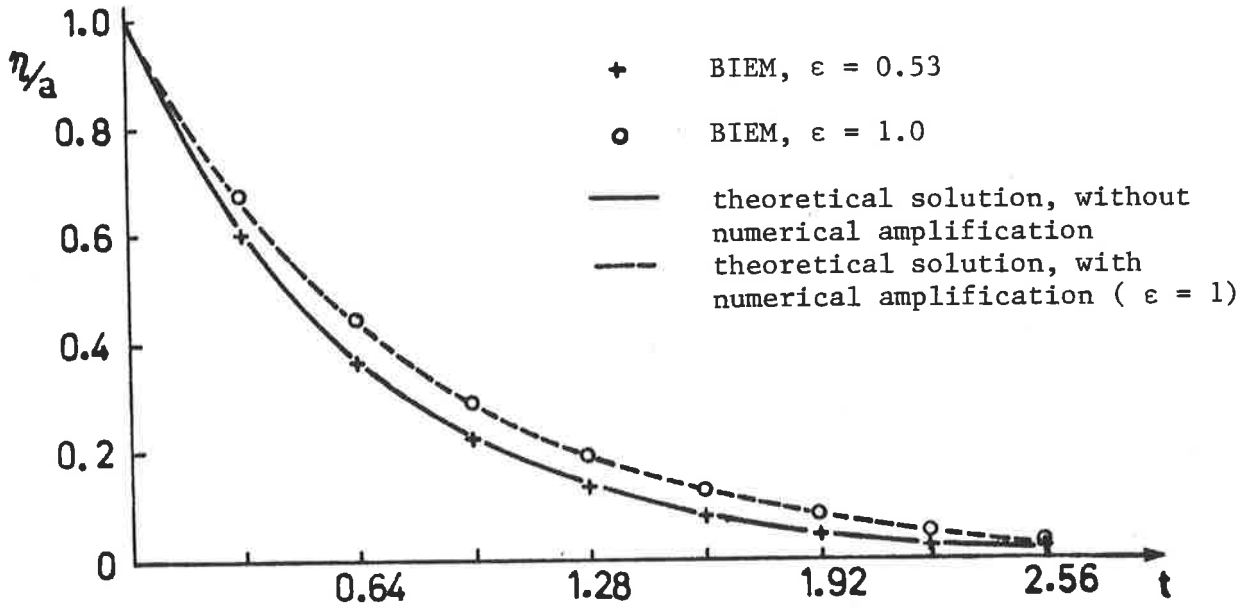

Figure 5.3 Change in head at the free surface at x = L/2 for q = 0.5 and ε = 0.53 and 1.0. These are compared with the theoretical solution to the linearized problem without numerical amplification and with numerical amplification for ε = 1.0.

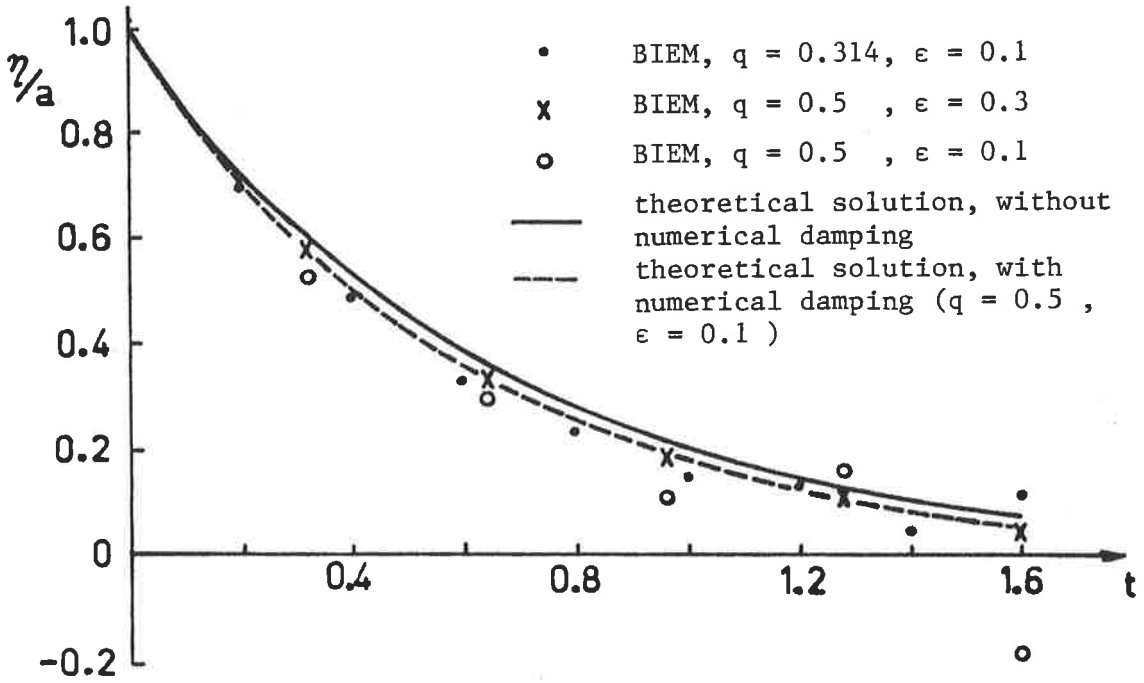

Figure 5.4 Change in head at the free surface at x = L/2 for ε < 0.5 compared with the theoretical solution to the linearized problem without numerical damping and with numerical damping for q = 0.5, ε = 0.1.

A comparison of chapter 4 model results with those of Liu and Liggett for $\varepsilon = 0.1$ shows that the nonlinearity has an unstabilizing effect (Figure 5.4). In the cases of $q = 0.5$, $\varepsilon = 0.1$ and $q = 0.314$, $\varepsilon = 0.1$ amplified oscillations result. This is contrary to the conclusions drawn from the linearized model as shown in figure 2 of Liu and Liggett (repeated here as figure 5.5).

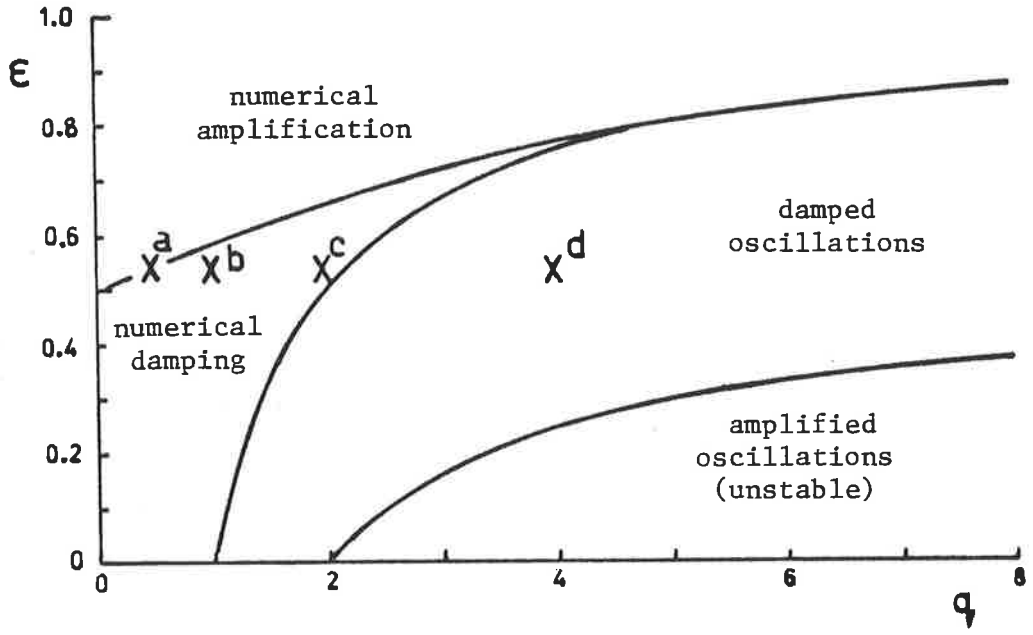

Figure 5.5 Zones of amplification, damping and oscillation as a function of q and ε for the linearized problem (after Liu and Liggett, 1980, figure 2).

A detailed investigation of the onset of oscillation for $\varepsilon < 0.5$ is not performed on the basis that for practical models $\varepsilon > 0.5$ would always be selected (from figure 5.2). However for the value of $\varepsilon = 0.53$ an investigation was made of the effect of q on stability (at points a to d in figure 5.5) and the results are summarized in figure 5.6. For all models reported in this thesis $\varepsilon = 0.53$.

In each case the solution converged to the correct solution. However numerical damping increased as q increased. The difference between the

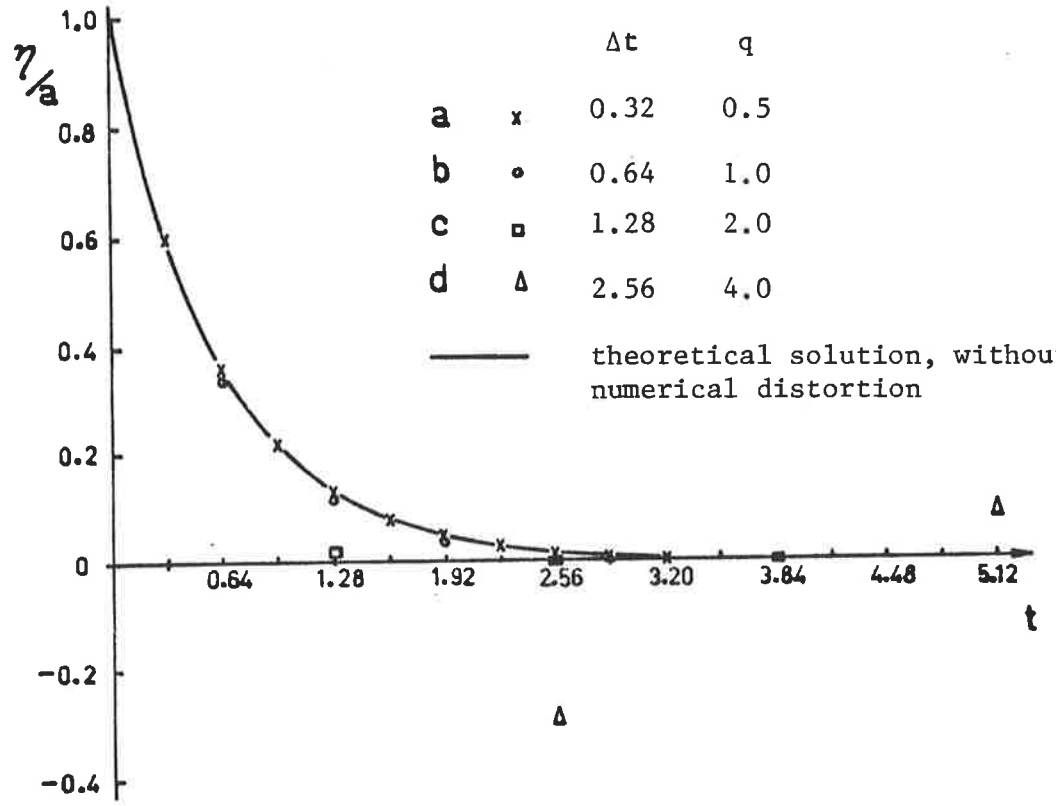

Figure 5.6 Change in head at the free surface at x = L/2 for various values of q when ε = 0.53.

free surface elevation at the right hand boundary for q = 0.5 and q = 1 is less than 0.02a. For q = 2 the damping was excessive resulting in an error of 0.10a for the first time step. For q = 4 damped oscillations resulted. While these ultimately converged to the correct value ($\eta/a = 0$) by t = 10.24, the results are a very poor approximation to the behaviour of the free surface at x = L/2. Halving execution times by doubling the time increment therefore result in initially small errors which become successively larger as the time increment expands. These results agree with figure 5.5.

5.1.2 Lateral inflow with specified hydraulic gradient (TEST5)

A more rigorous test of the effect of numerical damping is contained in problem TEST5, illustrated in figure 5.7. A unit normal hydraulic gradient acts on two sides of an unconfined aquifer on an impermeable base. The rise of the free surface increases the lateral inflow to the flow domain which in turn increases the rate of rise of the free surface. This problem does not reflect the homeostasis or natural equilibrium of real groundwater flow problems. As time approaches infinity, the hydraulic head at all points and the inflow to the domain become infinite. The problem provides a sensitive guide to the effect of the number of boundary nodes, and the time step on mass balance error as is shown in Table 5.1.

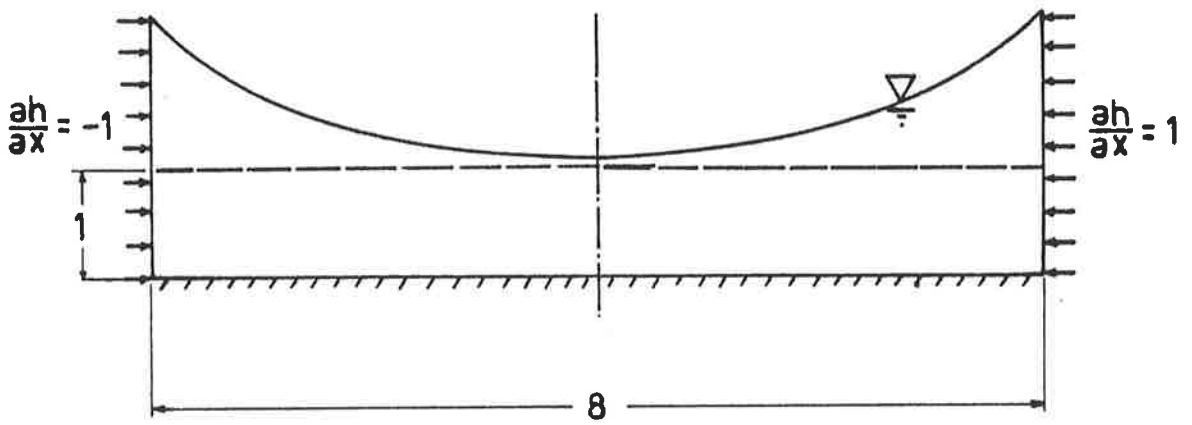

Figure 5.7 Geometry and boundary conditions for problem, TEST5.

For test numbers 5A to 5R the whole flow domain shown in figure 5.7 was modelled. In each case symmetry was preserved in the resulting heads and hydraulic gradients. Hence the hydraulic gradient across the line of symmetry was zero as expected. For test numbers 5T to 5X the line of symmetry was used as a no flow boundary and only half the flow domain was modelled. The use of 42 nodes was equivalent to using 82 nodes for the entire flow domain. Node shifting did not reduce mass balance error.

The head and normal hydraulic gradient on the boundary are shown in

Table 5.1 TEST 5 : Effect of node density and time increment size on mass balance error and computer execution time.

Test No.	No. of Nodes	Time increment	Total Inflow (TLTS)	Storage Change (TDE)	mass balance % error (PTER)	exec. time CP secs.
5 A	14	.10	3.2091	2.7876	-15.1	4.9
5 B	14	.02	3.2222	2.8926	-11.4	12.3
5 C	22	.10	3.3260	2.9160	-14.0	12.2
5 D	22	.02	3.3448	3.0367	-10.1	30.3
5 E	32	1.00	4.2926	1.9639	-118.6	5.0
5 F	32	.50	3.7540	2.6974	-39.2	7.4
5 G	32	.20	3.4984	3.1852	- 9.8	7.6*
5 H	32	.10	3.4782	3.2989	- 5.4	26.6
5 I	32	.04	3.4699	3.3530	- 3.5	35.0
5 J	32	.01	3.4630	3.4302	- 1.0	94.0*
5 K	32_s	.20	3.4801	3.1342	-11.0	14.2
5 L	32_{ss}	.20	3.4942	3.1803	- 9.9	7.8*
5 M	32_s	.10	3.4532	3.2895	- 5.0	25.9
5 N	32_s	.04	3.4511	3.3501	- 3.0	33.9
5 P	32_s	.02	3.4531	3.3955	- 1.7	61.8
5 Q	32_s	.01	3.4555	3.4216	- 1.0	119.9
5 R	32_{ss}	.01	3.4626	3.4296	- 1.0	76.3*
5 T	42^c	.01	3.5078	3.4954	- 0.4	143.0*
5 U	42^c	.02	3.5051	3.4674	- 1.1	66.3*
5 V	42^c	.04	3.5016	3.4134	- 2.6	33.9*
5 W	42^c	.10	3.5188	3.3914	- 3.8	27.3*
5 X	42^c	.20	3.5496	3.2427	- 9.5	14.3*

* higher optimization on compilation (OPT = 2).

s shifting nodes used on side boundaries with linear interpolation.

ss shifting nodes used on side boundaries with quadratic interpolation.

c uses the line of symmetry as an impermeable boundary (equivalent to 82 nodes for the same problem).

TLTS, TDE and PTER are defined in 4.6.

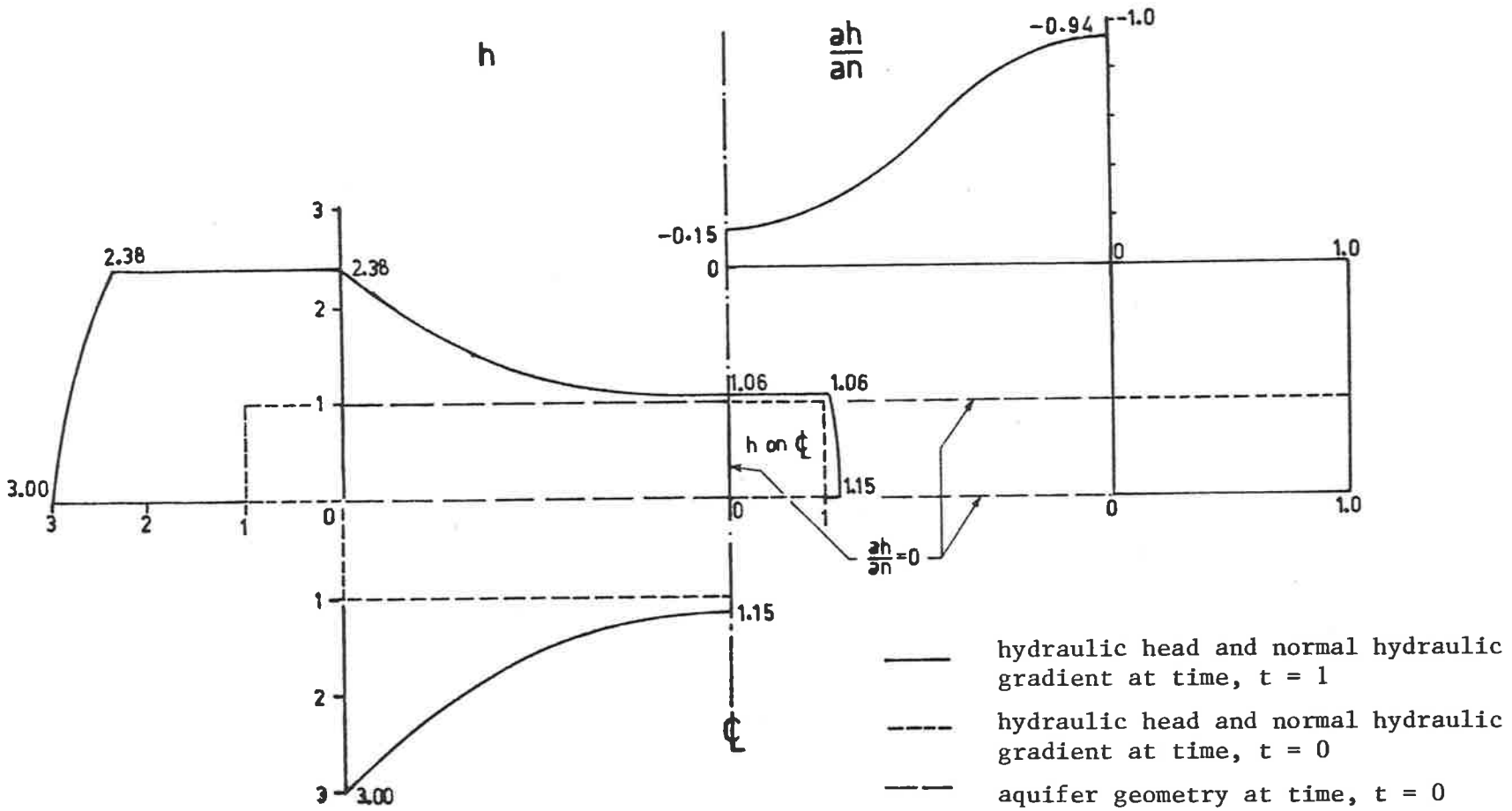

Figure 5.8 Hydraulic head and normal hydraulic gradient on the boundary for problem TEST5 at time, t = 1.
(Test No. 5 T)

figure 5.8 for time t = 1. When smooth curves are drawn through the nodal heads on all boundaries the head distribution is seen to be nonlinear. This also applies to the normal hydraulic gradient on the free surface. It is evident that if more nodes are used, particularly where the curvature of these functions is large, the accuracy of the solution improves. (In section 4.2 the model formulation was shown to rely on linear interpolation of h and $\frac{\partial h}{\partial n}$ between nodes). The improvement in accuracy due to increasing the number of nodes is illustrated by figure 5.9.

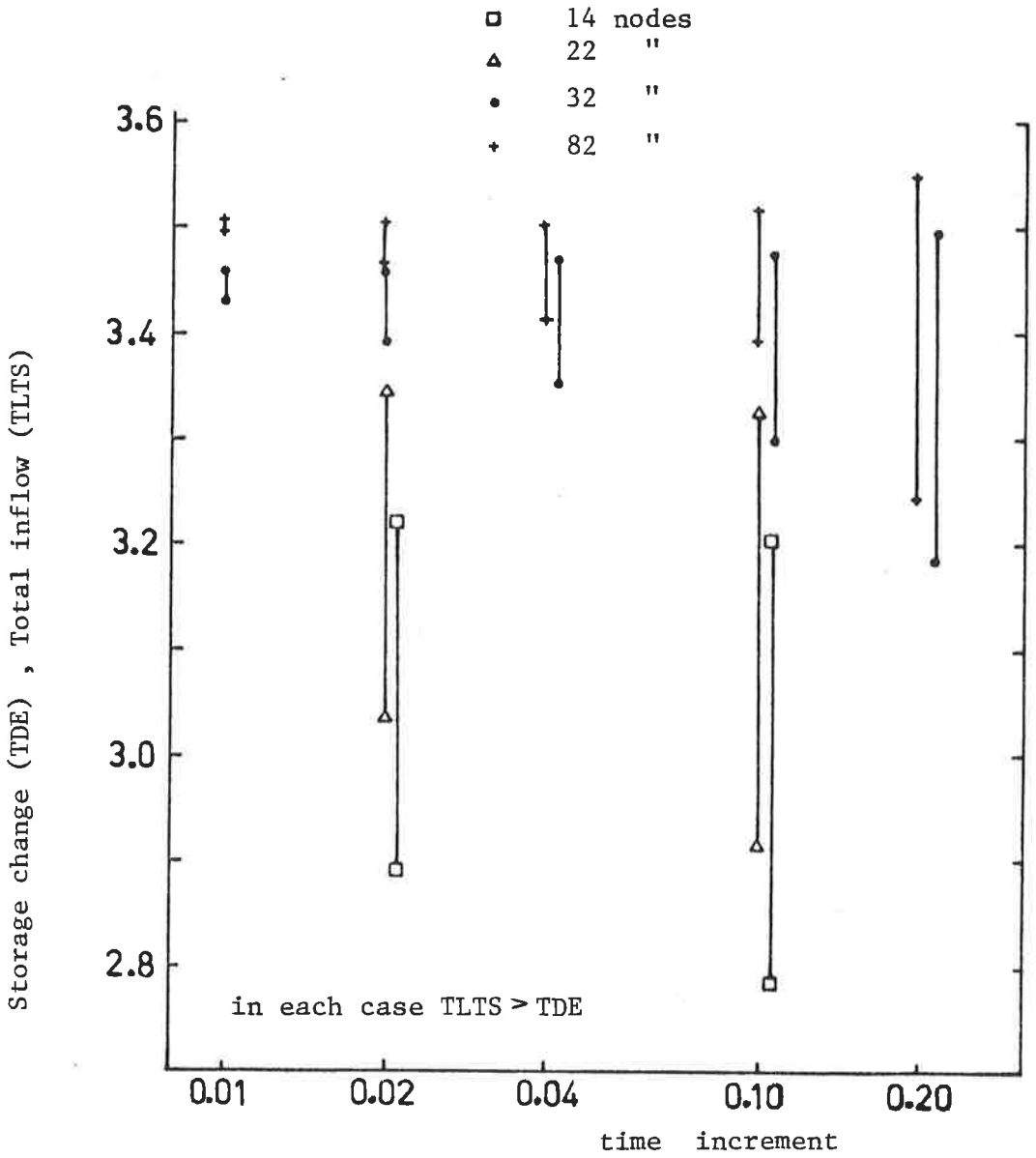

Figure 5.9 Effect of number of nodes and time increment size on total inflow (TLTS) and change in storage (TDE) for problem TEST5 at time, t=1.

The effect of the size of the time increment is also shown in this figure. In each time step the free surface rises, changing the geometry of the boundary. This also produces a larger length of side contributing to inflow. Shorter time steps lead to improved mass balances, and longer computer execution times for any particular node configuration (see Table 5.1). However the value to which the inflow and storage converge for shorter time steps is not necessarily the correct solution. The deviation from the correct solution at small time steps is determined by the ability of linear elements to approximate the nonlinear boundary conditions. In all test cases increasing the number of nodes increased the fluxes at the boundaries and the storage change. For example increasing the number of nodes from 32 to effectively 82 increased the influx through the model by 1.3%. With the law of diminishing returns when representing arcs by line segments of smaller length, one is lead to summize that additional nodes would result in even smaller changes in the total flux. A trade off with computer execution time which increases approximately in proportion to the square of the number of nodes, is necessary.

For most practical applications a tolerance of 5% on the output is acceptable, as the tolerance on the expected effect of variable material hydraulic properties normally exceeds this value.

It should be noted that TEST5 is a particularly rigorous test and for most problems the effect of node spacing and time increment size is much less apparent.

5.2 Hydraulically Disconnected Stream Problems

5.2.1 Marino's Hele-Shaw model

A hydraulically disconnected stream acts as a strip recharge source. Marino (1967) described a Hele-Shaw model study of the growth of a groundwater mound beneath a strip recharge source. The geometry and boundary conditions for his study are shown in figure 5.10, where

W = 0.056 cm/sec , K = 0.42 cm/sec , n_e = 1

b = 23.8 cm , D = 11.3 cm and L = 243.8 cm.

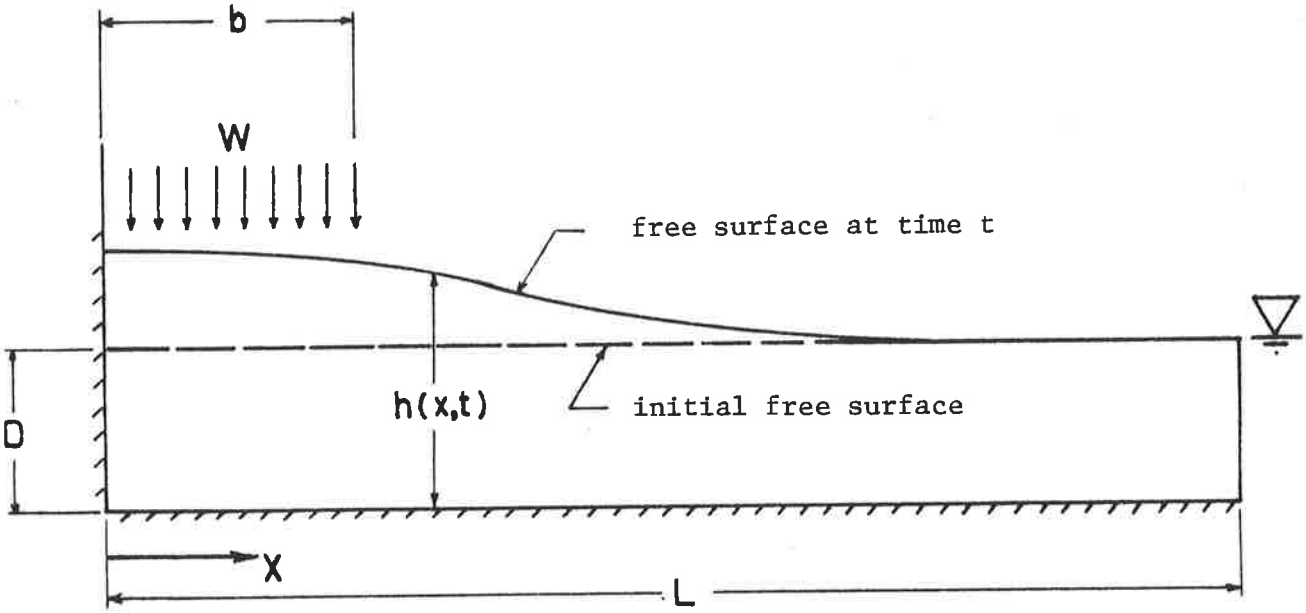

Figure 5.10 Geometry and boundary conditions for growth of a groundwater mound below a strip recharge source.

At time t = 0 a uniform recharge rate, W commenced over a segment of the model. The shape of the mound near its crest after one minute, five minutes and nine minutes from the time infiltrating water reached the free surface is shown in figure 5.11. The increase in storage below the free surface during the first nine minutes exceeded the volume recharged by 9% using Marino's experimental data and extropolating by scaling from the BIEM solution for the region beyond x = 80cm. Marino identified the measurement of percolation rate as a likely source of experimental error. (Alternatively, if Marino's estimate of hydraulic conductivity had been in error, a reduction in K of 17 to 22% would account for the discrepancy between experimental and calculated mound heights.)

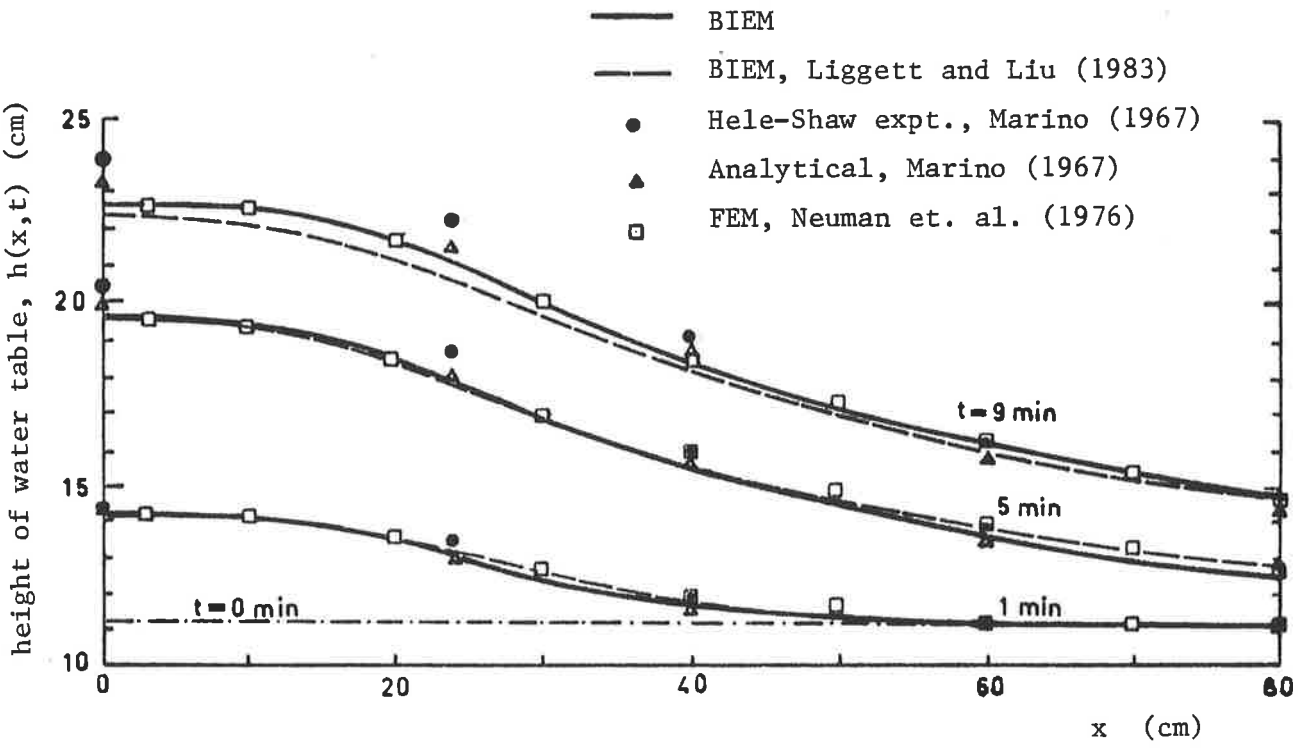

Figure 5.11 Transient free surface profiles for Marino's Hele-Shaw experiment and results of numerical simulations.

An approximate analytical solution to the same type of problem is provided by Hantush (1967) and Marino (1967) by linearizing the one dimensional form of the Boussinesq equation (given for two dimensions by equation 3.29).

Numerical solutions for Marino's experiment were found by Neuman, Narasimhan and Witherspoon (1976) by solving the Boussinesq equation using a one dimensional finite element method. Solutions were also obtained by Liggett and Liu (1983) using the BIEM. In figure 5.11 these results are compared with those of the model described in chapter 4. The mass balance error for the latter is 0.3% using Δt = 20 seconds and 42 nodes. The three numerical methods give excellent agreement. The difference between the BIEM results is due to reiteration when free surface elevation changes exceed a given threshold (see section 4.4) a feature which Liggett and Liu's model lacked. Neuman et al suggested that their discrepancy near the

crest of the ridge is due to "the development of significant vertical hydraulic gradients under the recharging area" which are not taken into account in the Boussinesq equation. This reason is proved incorrect by the BIEM solutions which account for vertical hydraulic gradients. In fact the Boussinesq equation gives excellent agreement with the potential theory solutions and the discrepancy is due to experimental measurement errors.

5.2.2 Brock's analysis of mounds below strip recharge basins.

Brock (1976b) obtained solutions for the maximum mound height below a strip recharge source for long infiltration periods using four different methods. He applied linear and nonlinear DF theory, a linearized potential theory (using a frozen free surface at its initial elevation) and a

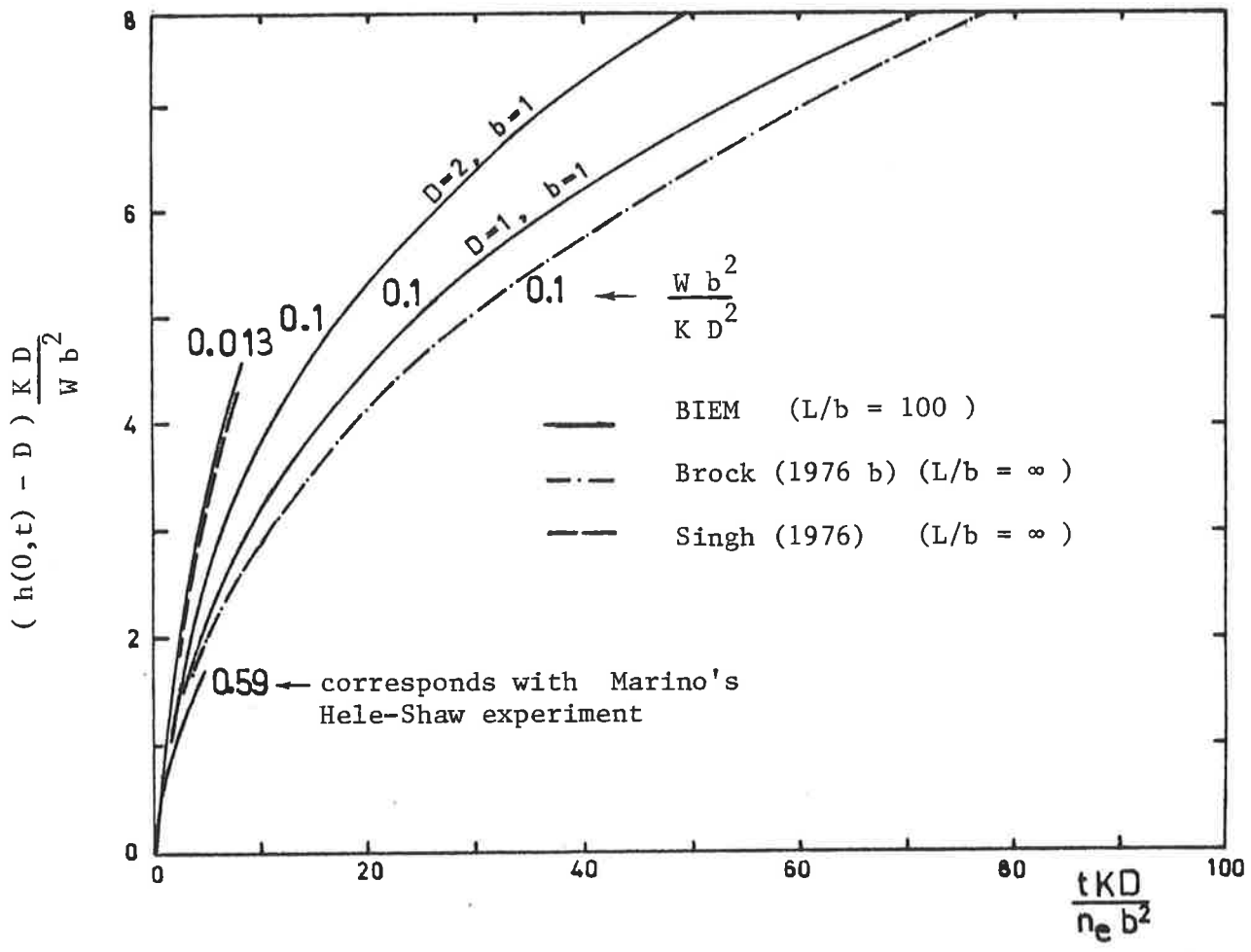

Figure 5.12 Maximum groundwater mound height beneath a strip recharge source : comparison of BIEM with Brock (1976 b).

nonlinear potential theory. In his paper he presents solutions using only nonlinear DF theory. The maximum mound height for the model described in chapter 4, a nonlinear potential theory model, is compared with Brock's nonlinear DF results, for the case of recharge from an infinitely long strip source (see figure 5.12). The results show Brock's choice of nondimensional parameters restricts the application of his results to specific values for those parameters (which are not mentioned in his paper). The BIEM model parameters are : b = 1 m, L = 100 m, K = 1 m/day, $0 < n_e < 1$ and for the four runs shown

(a)	D = 1 m,	W = 0.1 m/day	$W\,b^2 / K\,D^2 = 0.1$
(b)	2 m	0.4 m/day	0.1
(c)	4 m	0.2 m/day	0.0125
(d)	all parameters as for Marino's Hele-Shaw model		0.59

Brock used $L/b = \infty$ and in the BIEM model L/b = 100. These were compatable for the range of t shown in figure 5.12 as the slope of the free surface was negligible at the right hand boundary. Also shown on this figure are comparison of BIEM solutions to Marino's Hele-Shaw experimental results and a numerical solution of Singh (1976). While these both give good agreement they are incompatable with the family of curves drawn by Brock (not shown).

5.2.3. Singh's analysis of mounds below strip recharge basins.

In 1976 Singh presented a potential flow model which used the same nonlinear free surface boundary condition as the model described in chapter 4. The equation employed by Singh is

$$\frac{\partial \eta}{\partial t} = \left(\frac{\partial h}{\partial x}\right)\left(\frac{\partial \eta}{\partial x}\right) - \frac{\partial h}{\partial y} + w \qquad 5.9$$

where all terms are nondimensional and have been previously defined. The relationship between equation 5.9 and the equation used in the BIEM model, equation 4.45 is shown in Appendix A (equation A.24).

Singh solved the problem using an explicit finite difference

procedure. At the start of each time step equation 5.9 was used to predict the free surface position at the end of the time step. Then the head distribution was computed using the new boundary geometry. As an explicit procedure, the time steps were limited by the Courant condition for stability

$$\frac{\Delta t}{(\Delta y)^2} < 0.5 \qquad 5.10$$

where Δt is the size of the time increment (non dimensional) and Δy is the (non dimensional) grid spacing in the vertical direction.

To solve the free surface position equation, Singh found expressions for $\frac{\partial h}{\partial x}$ and $\frac{\partial h}{\partial y}$ at the free surface in terms of $\frac{\partial h}{\partial x}$ and $\frac{\partial h}{\partial y}$, $\frac{\partial^2 h}{\partial y^2}$ and $\frac{\partial^3 h}{\partial y^3}$ at the first grid point below the free surface.

Close agreement between Singh's results and the BIEM solution for the mound profile were expected based on the similarity of assumptions. The differences observed in figure 5.13 are caused by differences in the

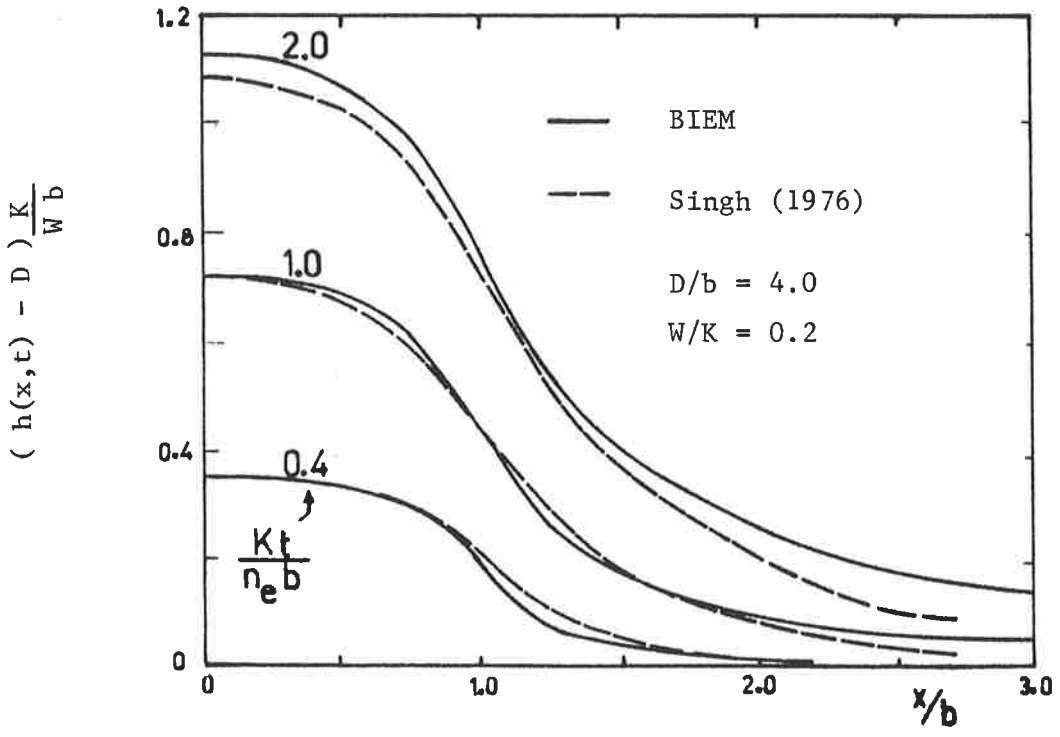

Figure 5.13 Transient free surface profiles for Singh's strip recharge problem : comparison of BIEM with Singh (1976).

computational methods only. At time $Kt/n_e b = 2$, the BIEM model satisfied conservation of mass to within 0.2%. Singh does not state the position of the distant right hand side boundary which he used. The BIEM results still agreed to three significant figures over the range of x/b in figure 5.13 when the BIEM boundary was shifted from x/b = 10 to x/b = 100.

Therefore it is unlikely that Singh's model satisfies conservation of mass and Singh's estimated error based on the ratio of storage change when $0 < x/b < 2.5$ over the entire storage change from the BIEM free surface profile, is 4%. Singh appears to underestimate the maximum mound height by the same amount, with the error increasing as the mound rises (figure 5.14).

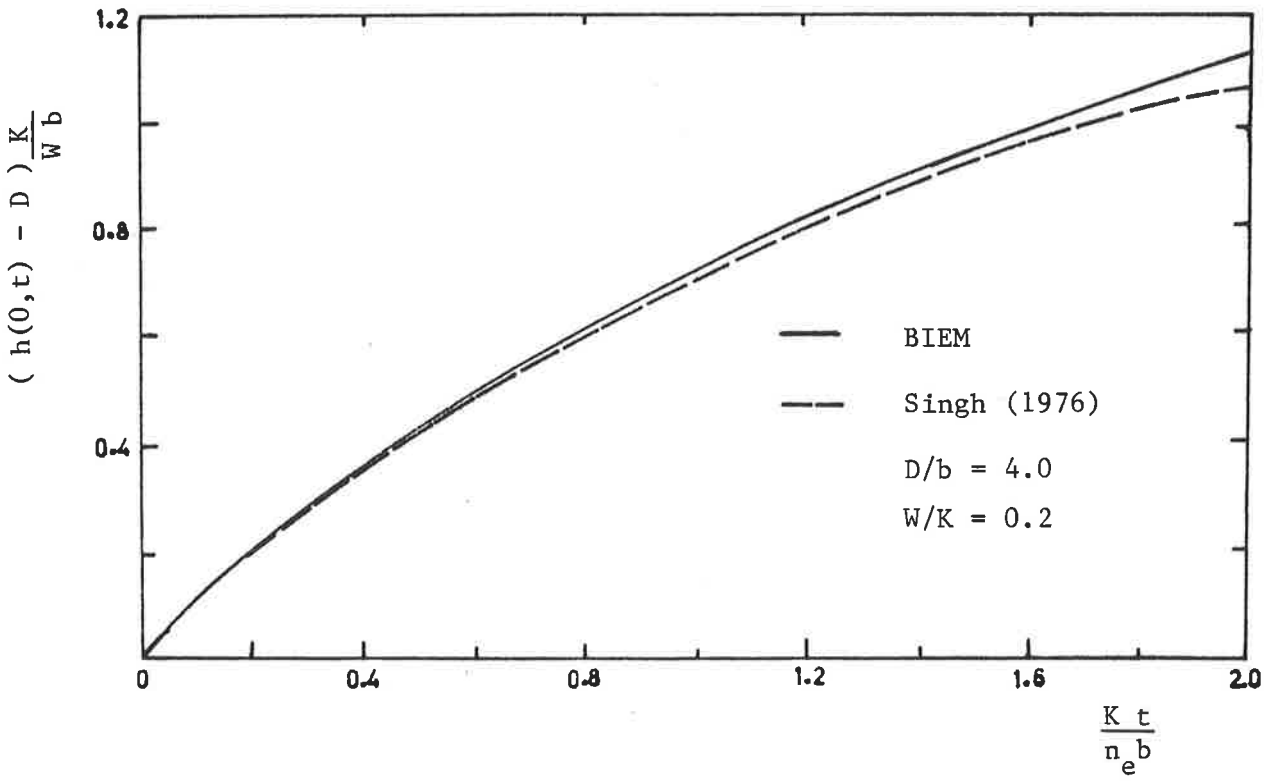

Figure 5.14 Maximum groundwater mound height for Singh's strip recharge problem : comparison of BIEM with Singh (1976).

These three examples of the growth of a strip recharge mound illustrate that the BIEM model described in chapter 4 has advantages over existing models in accuracy and computational integrity.

5.3 Hydraulically Connected Stream Problems

5.3.1 Marino's step change in stream stage

For a hydraulically connected stream the rate of flow between stream and aquifer depends on the head in the aquifer beneath the streambed. Usually the river is assumed to be lined by a semipermeable blanket of fine material which significantly reduces the exchange flow. Analytical models based on impermeable bed and semipervious banks which fully penetrate alluvial aquifers have been described by Marino (1973) and Hall and Moench (1972). However Sharp (1977) found the major alluvial aquifers of central United States were only partially penetrated by their streams and that most of the interchange of water takes place through the riverbed.

In order to test the BIEM model for a hydraulically connected stream for which an analytical solution is available, the configuration shown in figure 5.15 was chosen, noting that this does not represent a good model for real stream aquifer interaction.

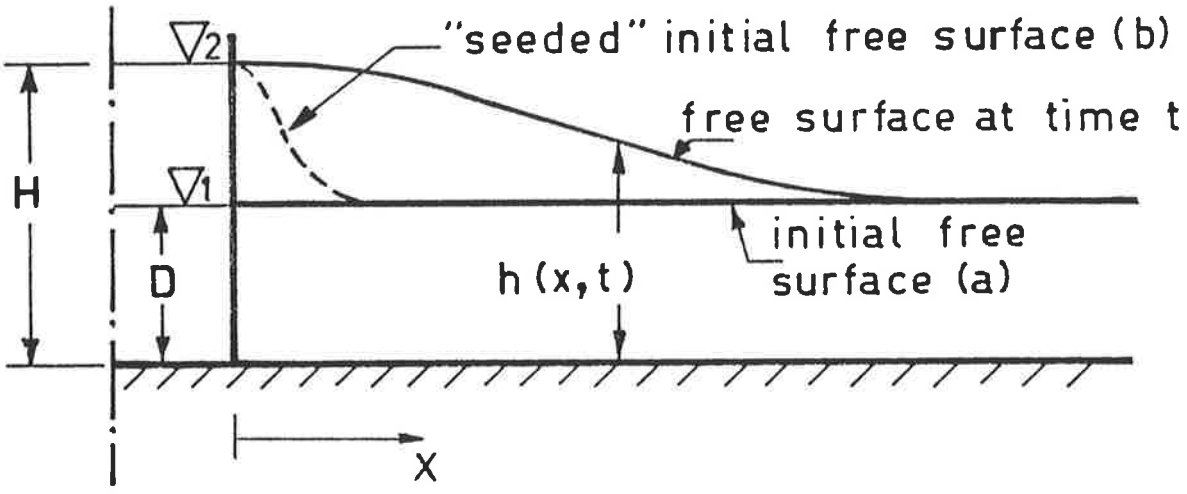

Figure 5.15 Geometry and boundary conditions for aquifer response to a step change in stage (from D to H) of a hydraulically connected stream (after Marino, 1973).

Marino (1973) used the DF assumptions and wrote the diffusion equation as

$$\frac{\partial^2 z}{\partial x^2} = \frac{1}{\alpha}\frac{\partial z}{\partial t} \qquad 5.11$$

where $z = h^2 - D^2$ 5.12

$\alpha = KD/n_e$ 5.13

subject to $z(x,0) = 0$ 5.14

$z(\infty,t) = 0$

and $z(0,t) = H^2 - D^2$ for $t > 0$. 5.15

His solution for the lateral progression of a rise in the free surface with time following a step change in head to H, is

$$h^2(x,t) = D^2 + (H^2-D^2)\,\mathrm{erfc}[x/(4\alpha t)^{\frac{1}{2}}] \qquad 5.16$$

In the problem tested (H - D)/D = 0.1 was chosen to give shallow free surface slopes. Marino (1967) found that results using the DF assumptions agreed within 5% of Hele-Shaw analog results for mounds having (H-D)/D < 0.5.

The exchange flow, q between stream and aquifer is obtained by differentiating equation 5.16 with respect to x at x = 0 and using Darcy's law.

$$q(0,t) = KH\frac{\partial}{\partial t}h(0,t) = K(H^2-D^2)(4\pi\alpha t)^{-\frac{1}{2}} \qquad 5.17$$

Integrating with respect to time gives the bank storage

$$V(0,t) = K(H^2-D^2)(\pi\alpha)^{-\frac{1}{2}}t^{\frac{1}{2}} \qquad 5.18$$

The initial exchange flow rate is infinite according to equation 5.17. This corresponds to a vertical free surface slope at the stream bank. Discrete numerical models are expected to produce errors when faced with such discontinuities. The BIEM model is no exception and for a short period immediately following the step change in stream head, the free

surface profile and the exchange flow rate deviate from the analytical solution.

For the example problem illustrated in figure 5.15, the parameters took the following values

$H = 11$ m, $D = 10$ m, $K = 10$ m/day, $n_e = 0.1$

hence $\alpha = KD/n_e = 10^3$ m^2 / day

The results for two model runs are compared with the analytical solutions for free surface profile (figure 5.16), exchange flow rate and bank storage (figure 5.17).

For model test (a) the initial horizontal free surface position was used. Test (b) consisted of "seeding" the initial free surface in the immediate vicinity of the stream with an approximation of the shape of the analytical free surface at time t = 0.01 day. This removed the initial discontinuity from the numerical problem, and was expected to yield more accurate solutions.

Figure 5.16 shows that seeding the free surface brought the numerical solution closer to the analytical solution for times up to 0.5 day. Beyond that time the differences in free surface elevations from the two tests were less than 0.5% of the maximum elevation change. The error observed at t = 100 days is attributed to the curvature of the free surface over a zone where node spacings are large.

Initial exchange flowrates from the numerical models (figure 5.17) are expected to be smaller than the analytical solutions due to the discontinuity previously discussed. The maximum flowrate for test (b) has been truncated by the choice of the initial free surface position. Similarly this limits the minimum bank storage value. Due to lower exchange flow rates predicted by test (a) its bank storage trails behind the analytical value. After time t = 0.5 day both numerical tests converge to within 0.5% of the analytical values for exchange flow rate and bank storage.

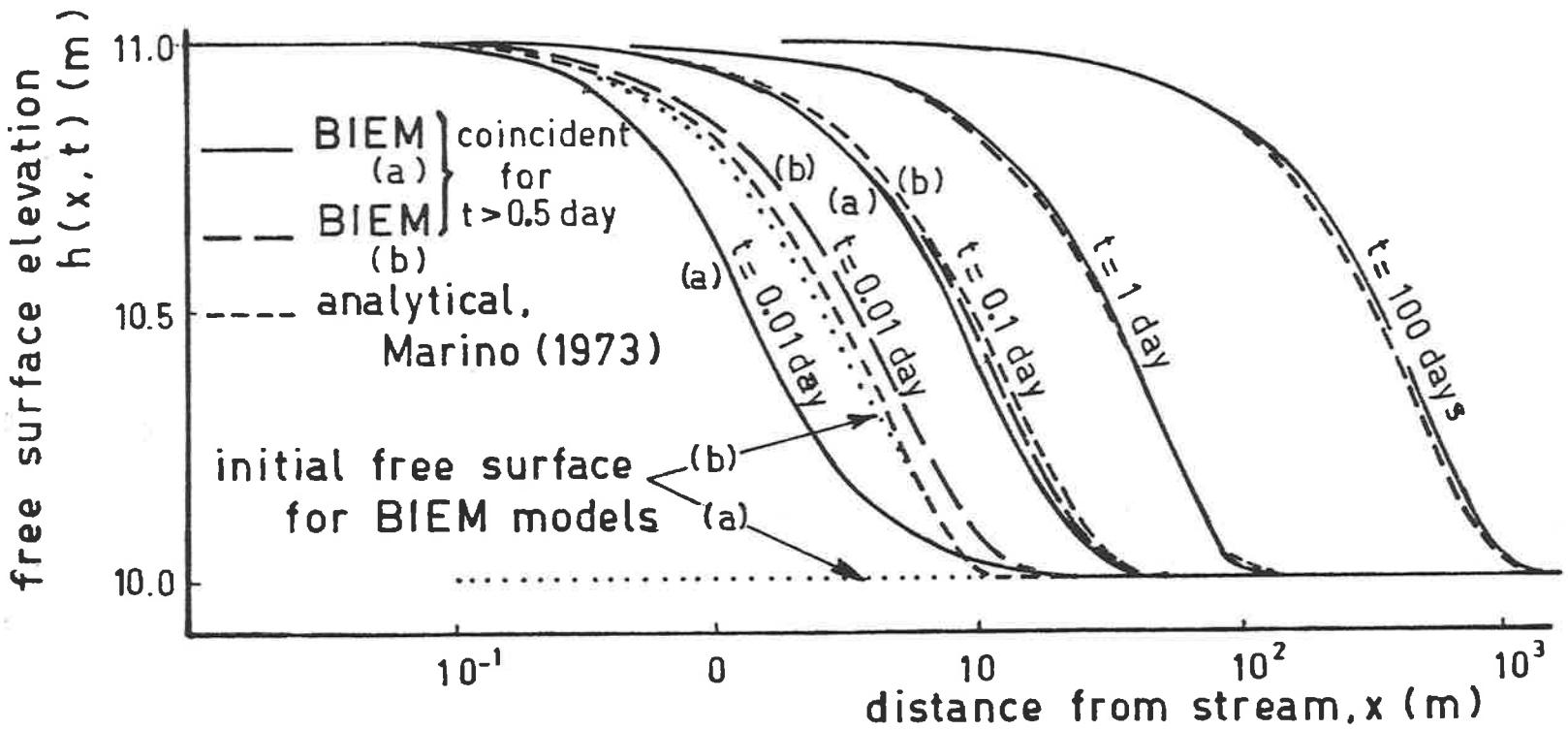

Figure 5.16 Transient free surface profiles after a step change in stream stage : comparison of BIEM with Marino (1973).

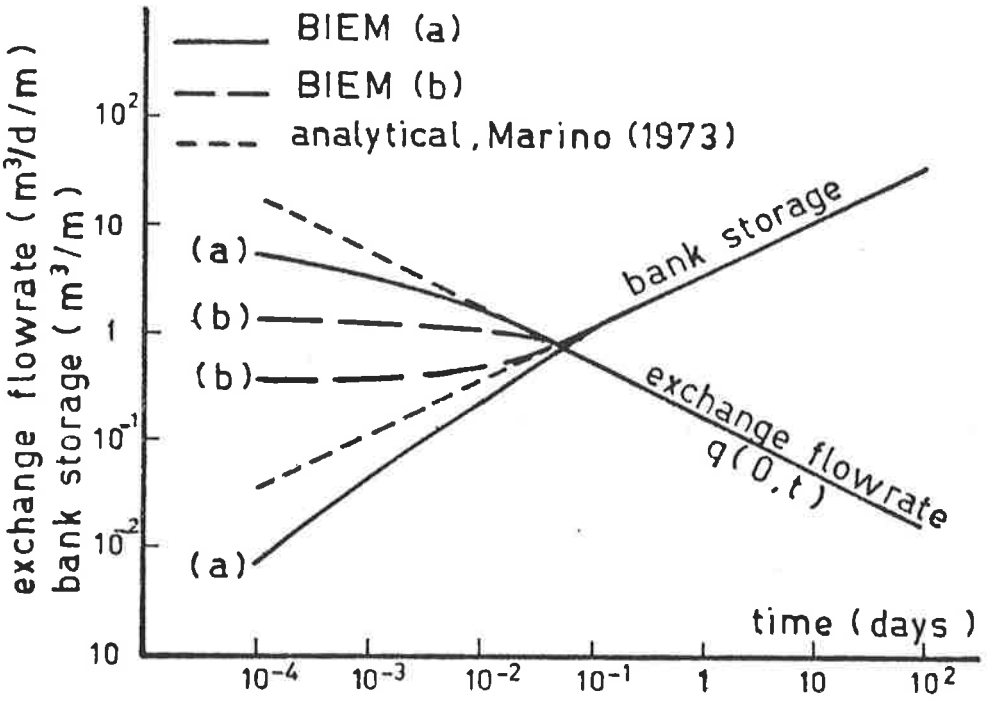

Figure 5.17 Exchange flowrate and bank storage per unit length of stream after a step change in stream stage : comparison of BIEM with Marino (1973).

The effect of free surface seeding is most apparent in examining the mass balance error for the two tests. (figure 5.18). The initial discontinuity causes damped oscillations of free surface node positions adjacent to the streambank for test (a). Very large percentage mass balance errors result. The free surface tends to rise faster than would be predicted by examining the normal hydraulic gradient at the streambank. The mass balance errors for the seeded free surface are not subject to perturbations and remain less than 0.5%. In both tests the mass balance errors become more negative as time exceeds 10 days. From figure 5.16 the curved free surface moves beyond 100 metres and node spacings become larger. The mass balance check, which assumes the free surface is a series of straight line segments connecting nodes, becomes a poorer approximation. Secondly with time increments increasing logarithmically errors are

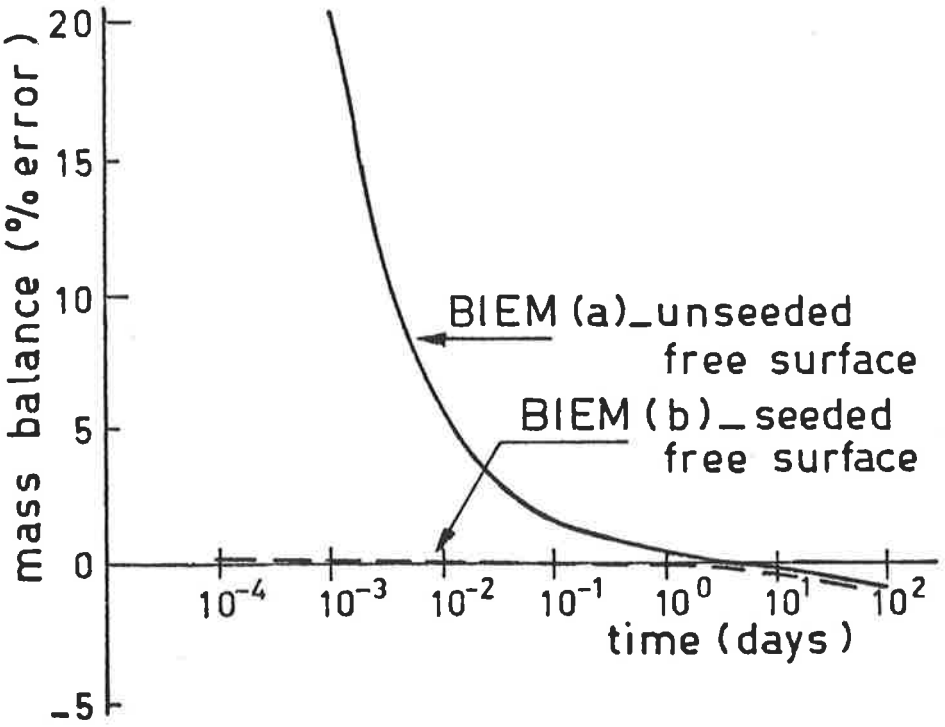

Figure 5.18 Effect of free surface seeding on mass balance error for step change in stream head problem.

expected to increase with time. At t = 100 days the modulus of the mass balance error is less than 1% for both tests.

The use of logarithmic node spacings and time increments is particularly suitable for this problem. Three time steps per log 10 cycle were used starting from t = 10^{-6} day and reaching t = 10^{2} days. Each test took 34 CP seconds execution time (unoptimized) to run. Forty nodes were used in each case, with the first node spacing being 0.1 metre and the most distant nodes 5000 metres from the streambank.

Having examined the case of an instantaneous head change in the stream (the unit step response) the next test is to apply the model to a time varying stream head.

5.3.2 Cooper and Rorabaugh's sinusoidal stream hydrograph.

In 1963 Cooper and Rorabaugh presented analytical solutions for exchange flowrate and bank storage due to skewed and symmetric sinusoidal stream hydrographs. They considered both finite and semi-infinite aquifers. Refering back to figure 5.15 the head along the streambank is

$$H(t) = D + \psi(t) \qquad 5.19$$

where

$$\psi(t) = \begin{cases} N\, h_o (1-\cos\omega t)\exp(-\delta t); & 0 \le t \le \tau \\ 0 \quad ; & t > \tau \end{cases} \qquad 5.20$$

and h_o is the maximum rise in stream stage

ω is the frequency of the stream stage oscillation

τ is the period of the stream stage oscillation

δ is a constant determining the degree of symmetry of the hydrograph (symmetric when $\delta = 0$)

N is a normalizing constant such that at the time of the wave crest $\psi(t_c) = h_o$ where t_c is the time of the flood crest.

hence

$$\tau = 2\pi/\omega$$
$$\delta = \omega\cot(\omega t_c/2) \qquad 5.21$$
$$N = (\exp(\delta t_c))/(1 - \cos\omega t_c)$$

Cooper and Rorabaugh linearized the Boussinesq equation (3.29) in a different way to Marino. The diffusion equation (5.11) still applies but this time

$$z = h - D \qquad 5.22$$

The aquifer diffusivity, α defined in equation 5.13 is unchanged. Note that Marino's equation arises by approximating the depth of flow at the stream bank as (H+D)/2 and using equation 3.30, whereas Cooper and Rorabaugh's equation is derived from equation 3.29 with the depth of flow approximated by D. Boundary conditions 5.14 are unchanged using the new definition of z (equation 5.22). Equation 5.15 becomes

$$z(o,t) = \psi(t) \qquad 5.23$$

and the right hand side is defined in equation 5.20.

The long analytical expressions for the free surface profile, exchange flow and bank storage are given in Cooper and Rorabaugh (1963) and are not repeated here.

The BIEM model was applied to serveral problems and compared with plots of analytical solutions for exchange flow rate and bank storage.

The example problems took the following parameter values:-

h_o = 1 m, D = 10 m, K = 10 m/day, n_e = 0.1

hence $\alpha = KD/n_e = 10^3\ m^2$ / day 5.24

and transmissivity of the aquifer, $T = K\ D = 10^2\ m^2$ / day

τ = 1 day

δ = 0 (symmetric case) $t_c = 0.50\ \tau$

= ω (asymmetric case) $t_c = 0.25\ \tau$

N = 0.5 when $\delta = 0$

= $e^{\pi/2}$ when $\delta = \omega$

Substituting these parameter values into the dimensionless parameters for exchange flow rate, q and bank storage, V (for one streambank only) used as axes in Cooper and Rorabaugh's figures produced:

$$\frac{2q}{h_o(n_e KD\omega)^{\frac{1}{2}}} = 2.52313 * \text{INFLOW} \qquad 5.25$$

$$\frac{2V\omega^{\frac{1}{2}}}{h_o(n_e KD)^{\frac{1}{2}}} = 0.158533 * \text{TDE} \qquad 5.26$$

Where INFLOW and TDE are calculated at each time step in the model's mass balance check algorithm described in section 4.6. INFLOW is the instantaneous flux entering the aquifer at the end of each time step and TDE is the storage change since t = 0.

Cooper and Rorabaugh used a diminsionless term, $\overline{\beta}$ to take account of aquifers having a finite length, l between the streambank and an

impermeable boundary such as a valley wall.

$$\bar{\beta} = \pi\tau\alpha/81^2 \qquad 5.27$$

Substituting parameter values gives $l = 62.67$ m when $\bar{\beta} = 0.1$

Larger values of $\bar{\beta}$ give smaller aquifer lengths. For a semi-infinite aquifer $\bar{\beta} = 0$.

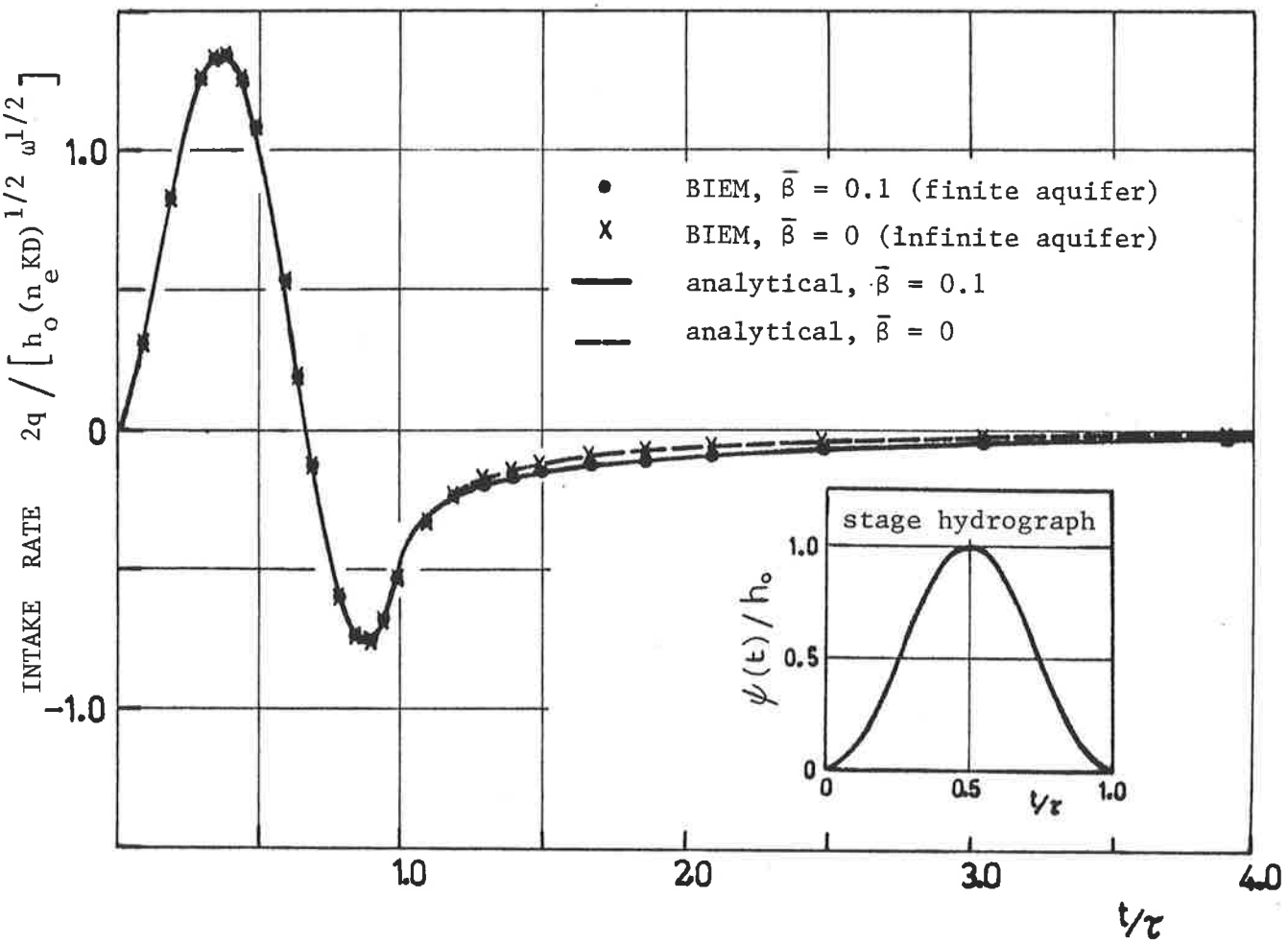

Figure 5.19 Groundwater intake rate due to a symmetric sinusoidal flood wave in a stream connected to a finite ($\bar{\beta} = 0.1$) and semi-infinite aquifer : comparison of BIEM with Cooper and Rorabaugh (1963).

Figure 5.19 compares the exchange flow rate for a finite ($\bar{\beta} = 0.1$) and a semi-infinite aquifer excited by a symmetric ($\delta = 0$) sinusoidal head variation in the stream. The BIEM results give excellent agreement with the analytical solutions. In numerical and analytical results the effect of the impermeable lateral boundary is not apparent until time $t/\tau = 1.2$.

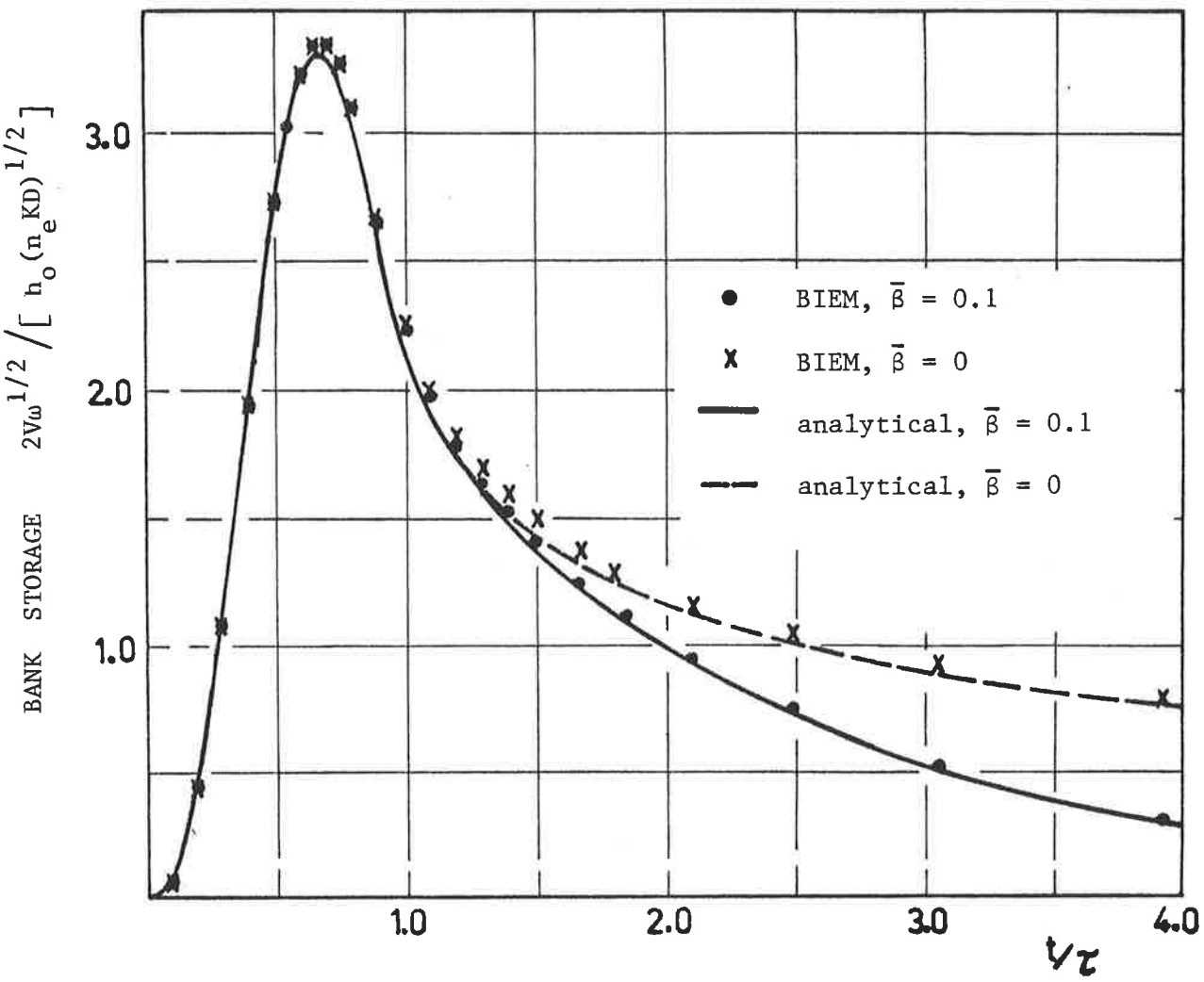

Figure 5.20 Bank storage due to a symmetric sinusoidal flood wave in a stream connected to a finite ($\bar{\beta}$ = 0.1) and semi-infinite aquifer : comparison of BIEM with Cooper and Rorabaugh (1963).

The bank storage graph (figure 5.20) distinguishes the aquifers more clearly. The peak storage volume by BIEM is 1% higher than the analytical value and this additional storage is reflected in the recession curves. The largest deviation, 5% occurs at $t/\tau = 1.5$ for the semi-infinite aquifer. The mass balance error throughout each run is confined to less than 0.5%.

An asymmetric sinusoidal stream stage variation more closely represents a realistic flood hydrograph. A problem was tested using $\delta = \omega$

i.e. $t_c = 0.25\tau$ and compared with the symmetric hydrograph case for a finite aquifer ($\bar{\beta} = 0.1$). The exchange flowrate and bank storage variations are compared in figures 5.21 and 5.22 respectively. Exchange flowrate results give excellent agreement with the analytical solutions. Bank storage for the BIEM model is again 1% higher than the analytical solution. Mass balance errors are less than 0.5%.

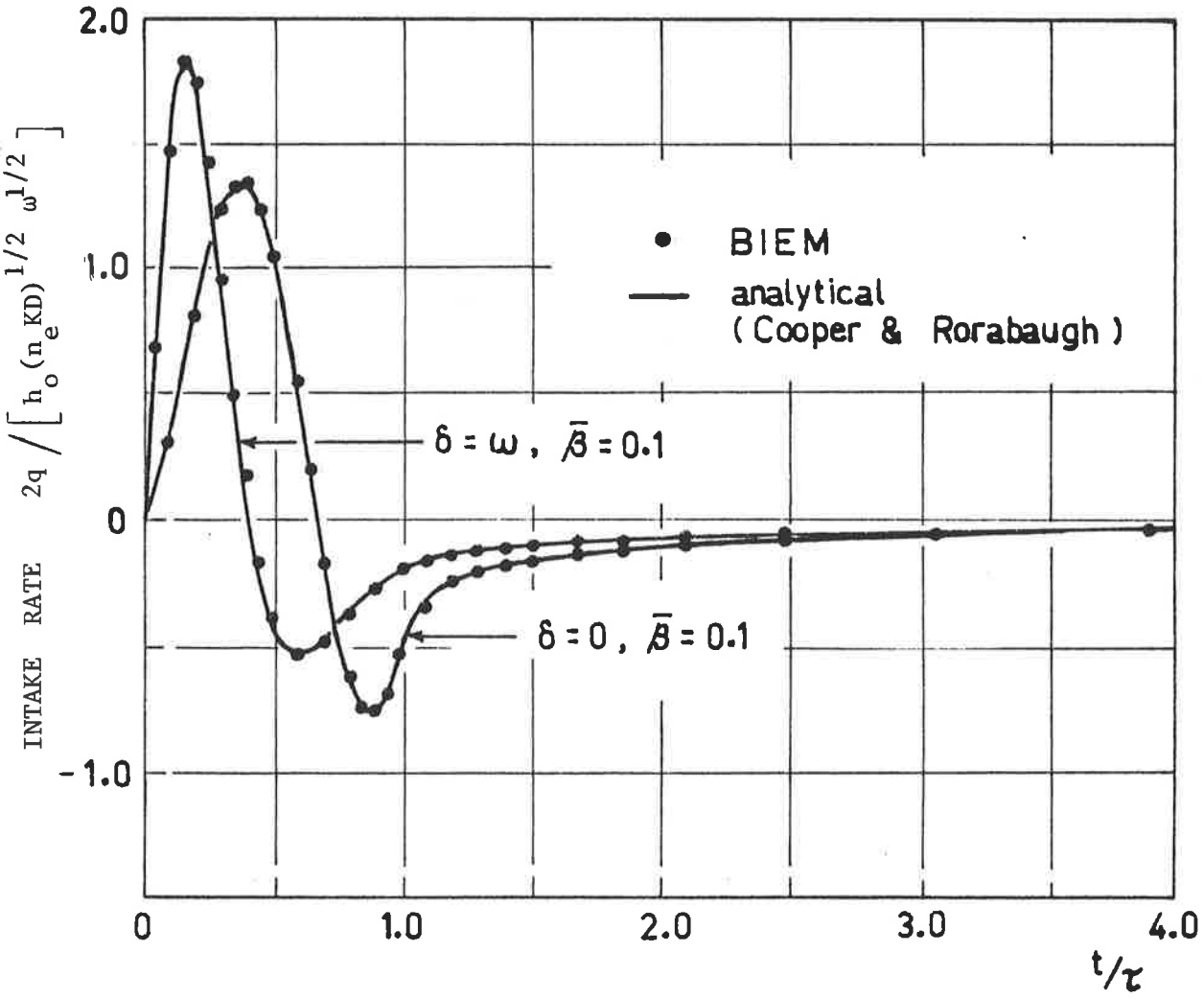

Figure 5.21 Groundwater intake rate due to symmetric and asymmetric sinusoidal flood waves in a stream connected to a finite ($\bar{\beta} = 0.1$) aquifer : comparison of BIEM with Cooper and Rorabaugh (1963).

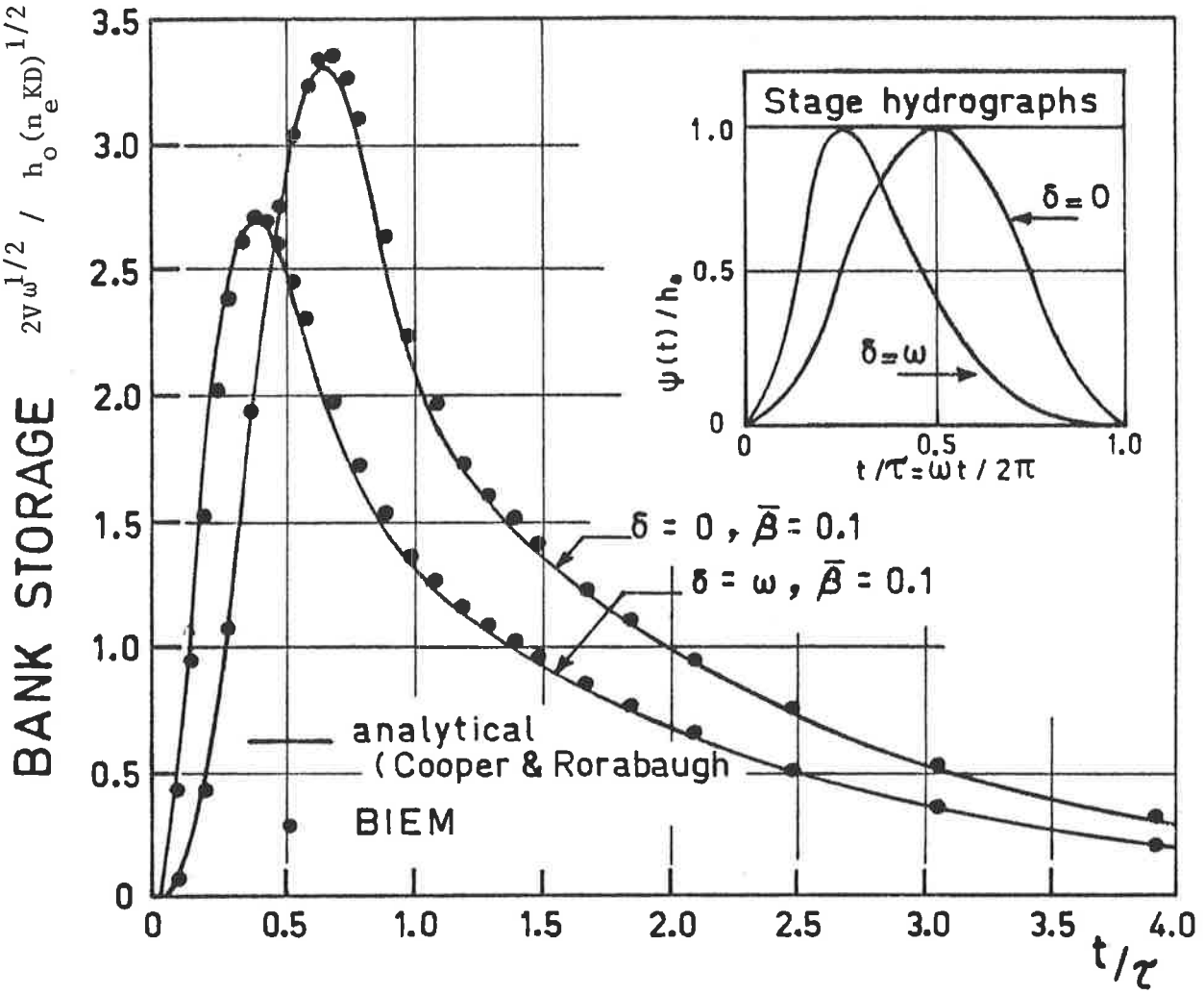

Figure 5.22 Bank storage due to symmetric and asymmetric sinusoidal flood waves in a stream connected to a finite ($\bar{\beta}$ = 0.1) aquifer : comparison of BIEM with Cooper and Rorabaugh (1963).

Exchange flowrates were expected to be marginally higher than the analytical values which were determined from

$$q(t) = -KD \frac{\partial h}{\partial x}(0,t) \qquad 5.28$$

Unlike the BIEM model this equation does not account for the additional height of the saturated streambank due to the flood wave. This factor would be expected to increase the peak bank storage volume marginally beyond the analytical value. Cooper and Rorabaugh plotted a graph of bank storage normalized against the peak value for a symmetric

flood wave and semi-infinite aquifer. Figure 5.23 shows the excellent agreement of the BIEM solution with their results. Todd's experimental curve was constructed from 14 experiments in which h_o and τ were varied. Cooper and Rorabaugh showed that the procedure used by Todd to aggregate the experimental data was not strictly correct. However the agreement is sufficiently close to endorse the analytical solution of Cooper and Rorabaugh and also of the BIEM.

These tests on hydraulically connected stream-aquifer problems confirm the accuracy, stability and versatility of the BIEM model.

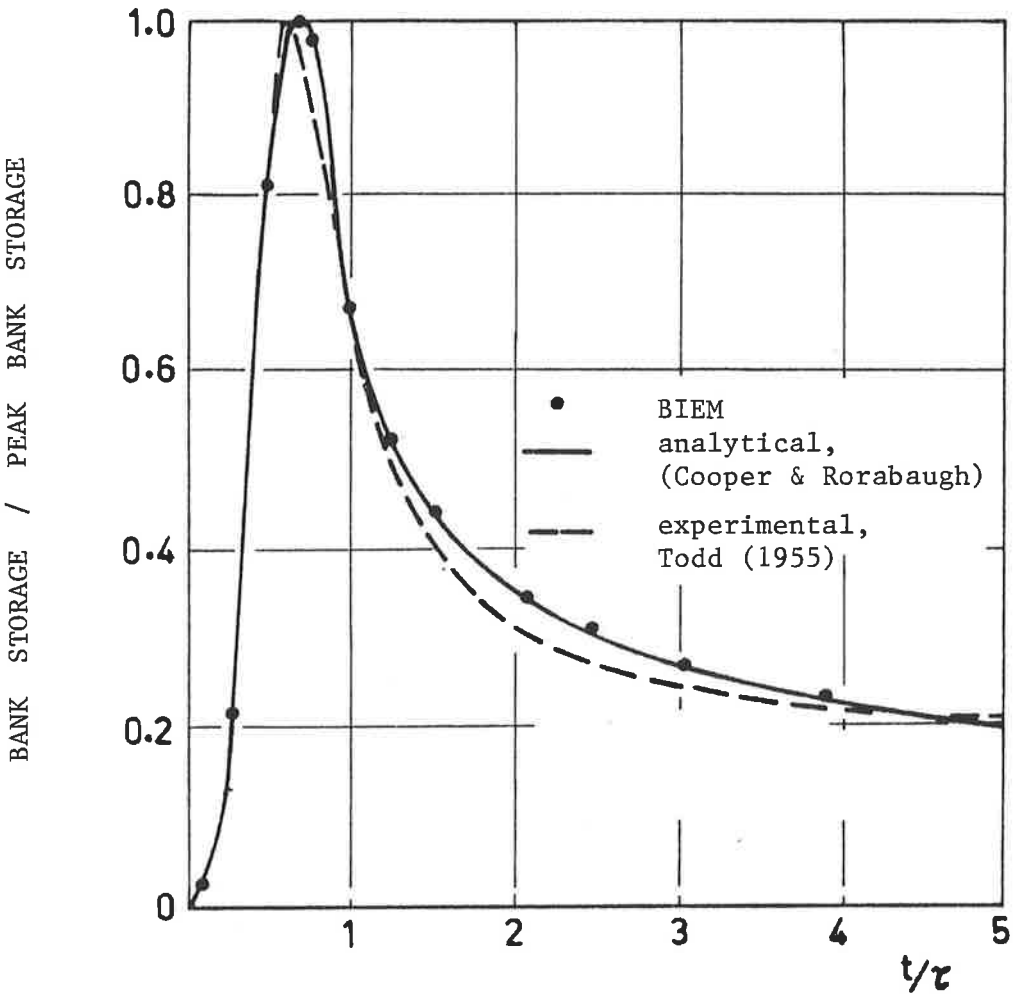

Figure 5.23 Bank storage as a fraction of peak bank storage due to a symmetric sinusoidal flood wave in a stream connected to a semi-infinite aquifer : comparison of BIEM with Cooper and Rorabaugh (1963) and experimental results of Todd (1955).

5.4 Transition from Hydraulically Disconnected to Hydraulically Connected Stream

During sustained flow in an ephemeral stream the induced groundwater ridge may rise until it intersects the streambed. As this occurs the rate of groundwater accretion diminishes due to the reduction in potential gradient across the semipervious streambed material. A review of the literature disclosed no reference to a study of this phenomenon. The BIEM model has been shown to simulate exchange flowrate, bank storage and groundwater levels for hydraulically disconnected streams and hydraulically connected streams and is now applied to this transition problem.

5.4.1 Rectangular stream channel (Problem RECT)

The simple problem of a rectangular stream channel underlain by a semipervious blanket with constant stream head is investigated. Figure 5.24 describes the problem. The initial free surface is horizontal

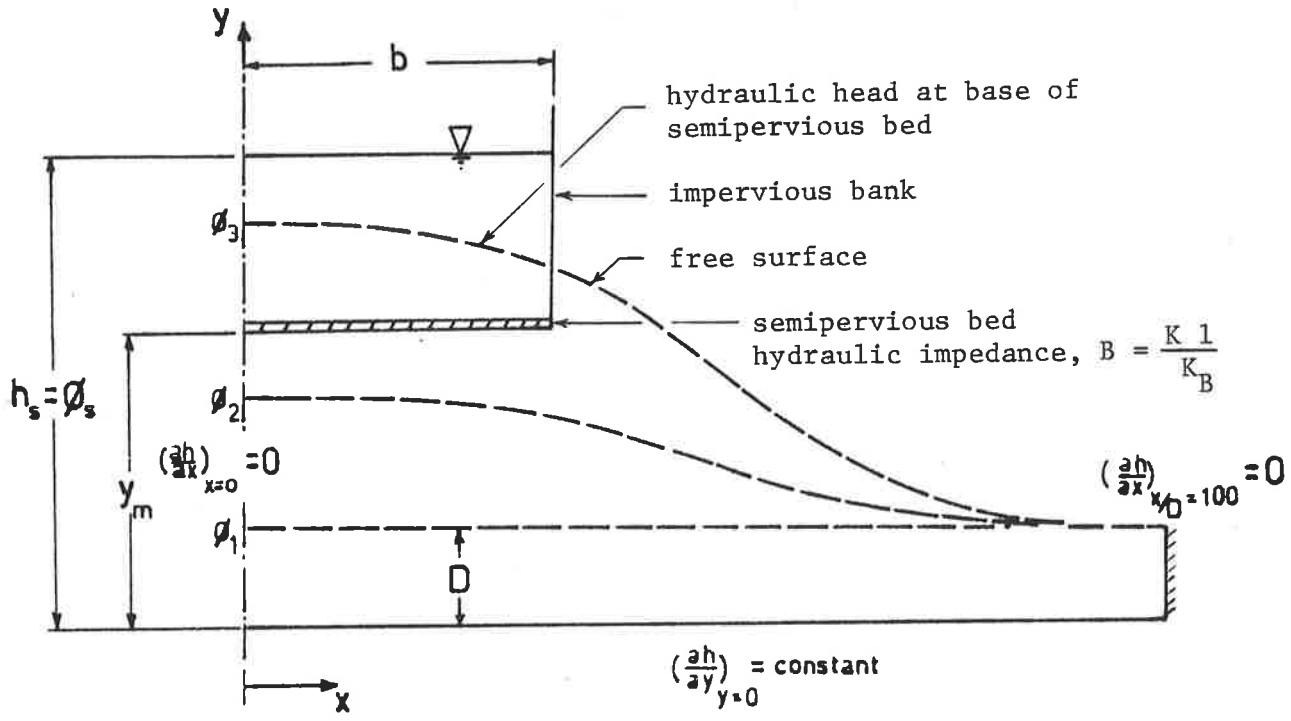

Figure 5.24 Transition from hydraulically disconnected to hydraulically connected stream for a rectangular channel : problem RECT geometry and boundary conditions.

and the aquifer thickness is given by D. The rate of leakage of the basement $K\left(\frac{\partial h}{\partial n}\right)_{y=0}$ is constant (outflow is negative).

The aquifer has sufficient length that the right hand boundary (x = L) has no effect on the seepage processes at the stream during the period modelled. The left hand boundary (x = 0) is taken as a line of symmetry hence $\left(\frac{\partial h}{\partial n}\right)_{x=0} = 0$.

The base of the semipervious blanket is at elevation y_m, and the head in the stream is h_s. In the figures which follow the constant stream head is denoted ϕ_s, and unless specified otherwise $\left(\frac{\partial h}{\partial n}\right)_{y=0} = 0$ and $h_c = 0$. The head of the node where the initial free surface intersects the line of symmetry is denoted ϕ. As this node rises with the free surface, $\phi(t) = \eta(o,t)$ until the base of the semipervious layer is reached. Thereafter ϕ is the head at this elevation and the aquifer in this vicinity is semi-confined.

The recharge rate, W is the rate of accretion at a node on the free surface due to seepage from the stream. Equations 4.39 and 4.40 define the recharge rate in relation to the position of the free surface and the magnitude of the effective capillary drive, h_c. When $h \geq y_m$ the flux through the streambed is $K\frac{\partial h}{\partial n} = \frac{K_B}{\ell}(h_s - h)$ from equation 4.34.

In the following figures, w, on the ordinate axis is taken to mean the integral of exchange flowrate over the width of the streambed where the exchange flowrate at a node is given by $K\frac{\partial h}{\partial n}$ when $h \geq y_m$ or by W when $h < y_m$.

A number of cases were tested and the results for the head, ϕ and the groundwater accretion rate, w are plotted with respect to time on nondimensional graphs. Figures 5.25a and 5.25b show the effect of stream width on the process of hydraulic connection. As streambed width increases with respect to aquifer thickness the duration of the transition process is reduced. For wide streambeds, b/D > 10, the transition is instantaneous once the free surface reaches the base of the semipervious layer.

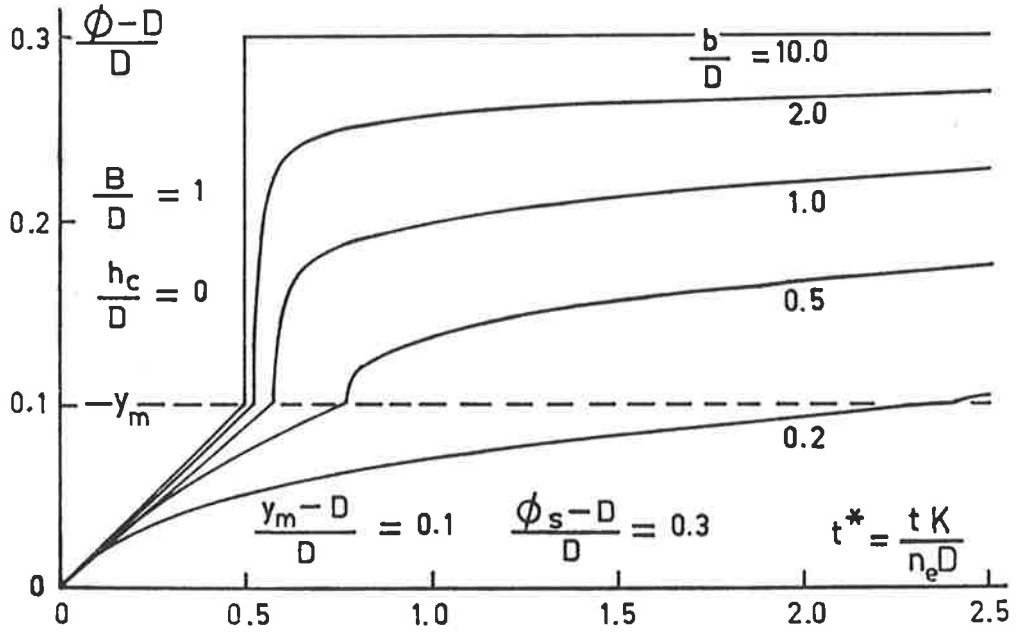

Figure 5.25 (a) Problem RECT : Effect of stream width, b on hydraulic head, ϕ at the stream centreline.

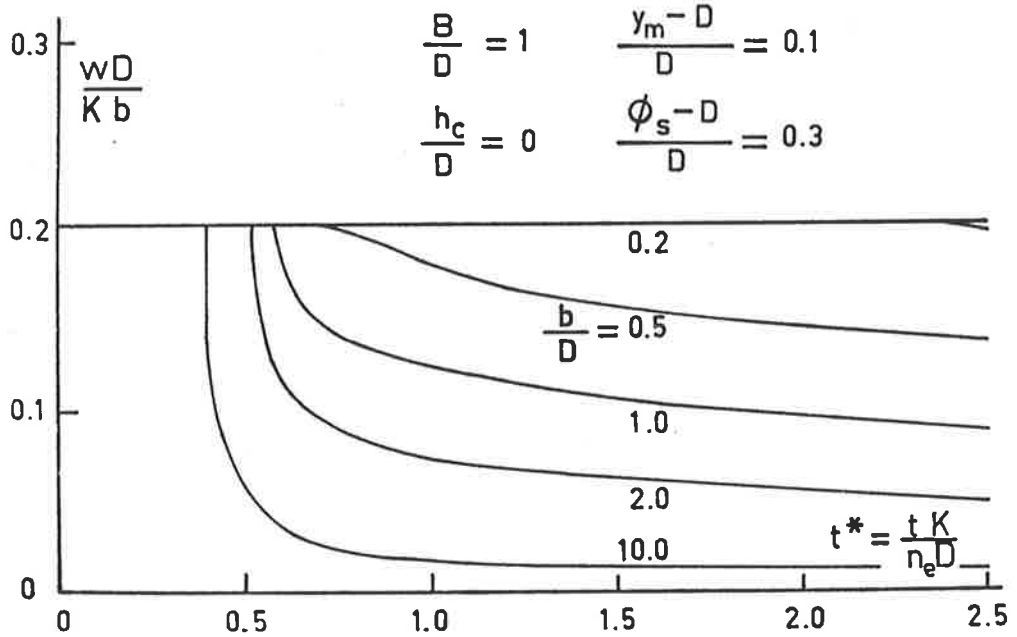

Figure 5.25 (b) Problem RECT : Effect of stream width, b on exchange flow rate, w.

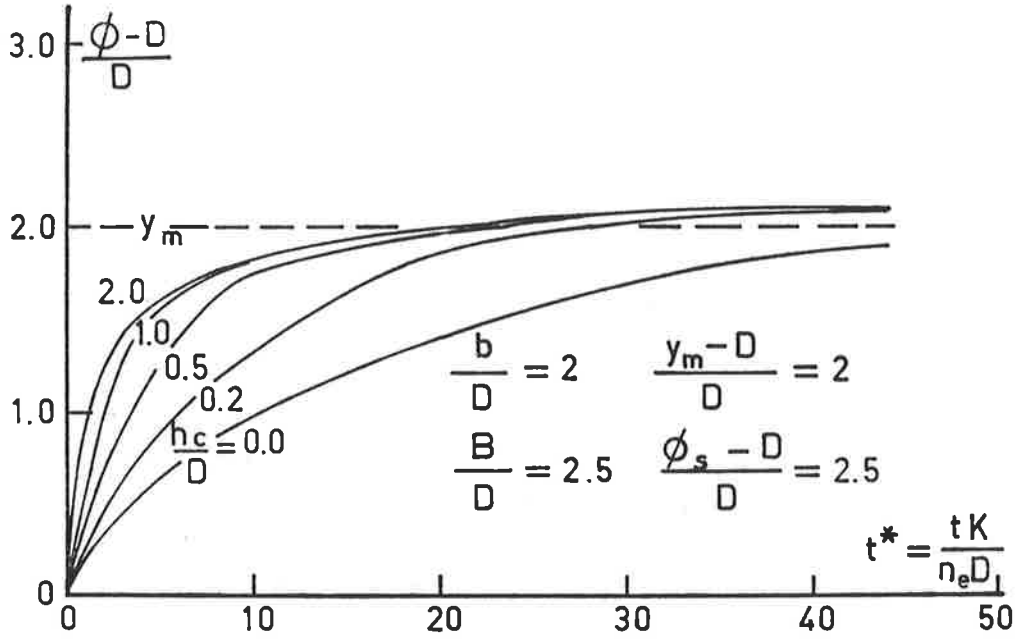

Figure 5.26 (a) Problem RECT : Effect of maximum suction head, h_c on hydraulic head, ϕ at the stream centreline.

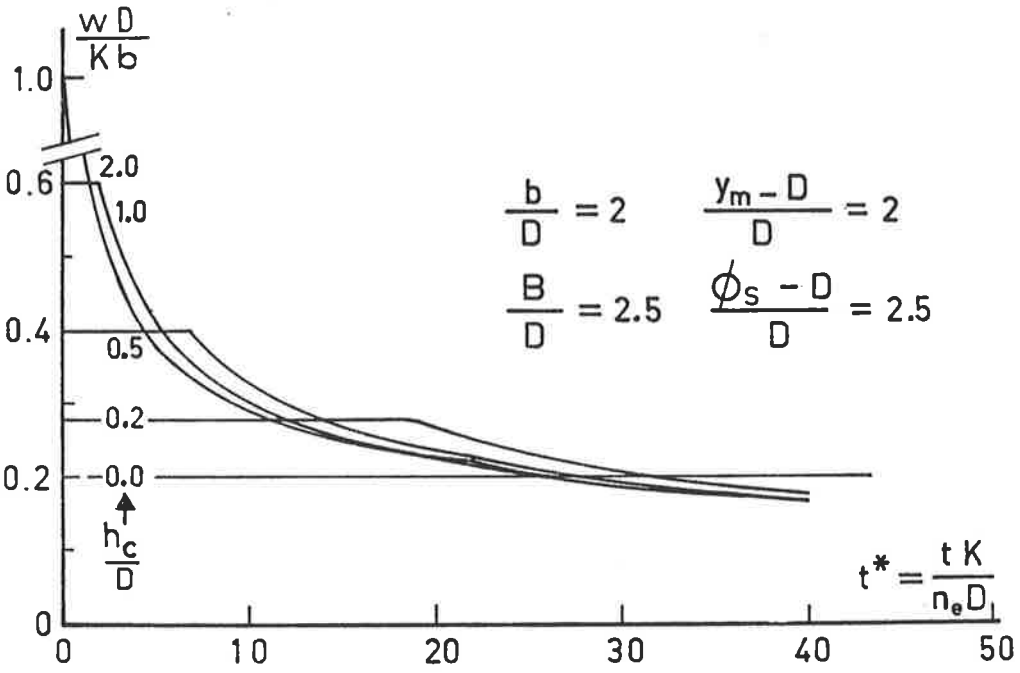

Figure 5.26 (b) Problem RECT : Effect of maximum suction head, h_c on exchange flow rate, w.

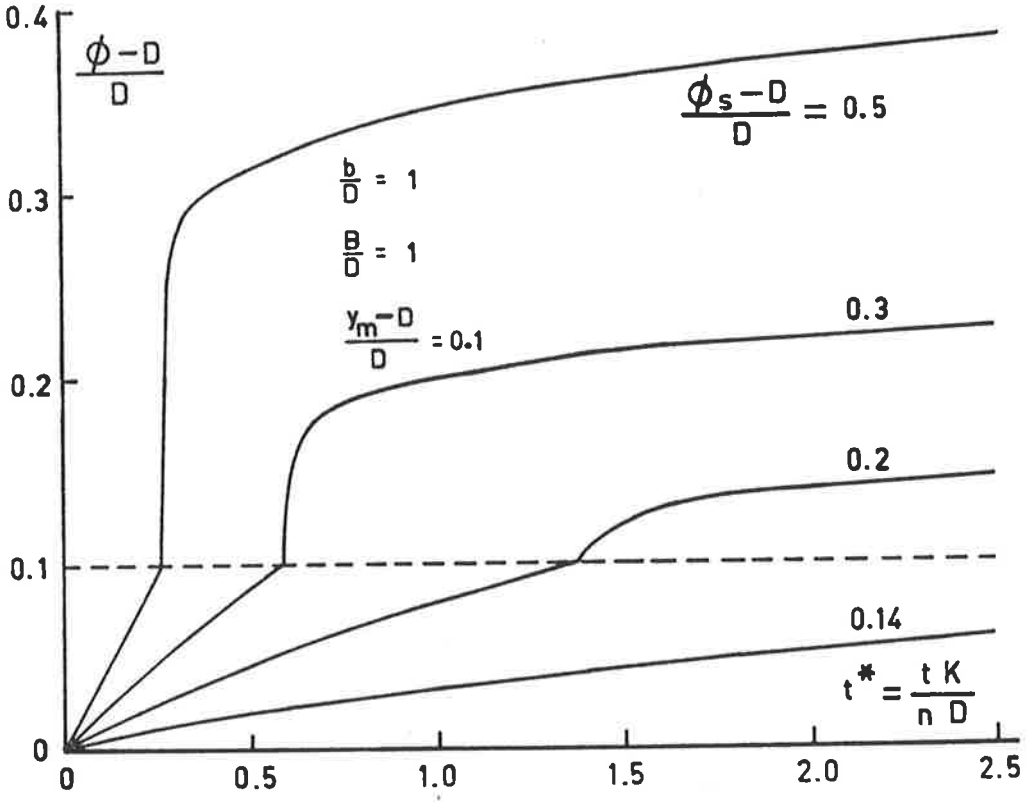

Figure 5.27 (a) Problem RECT : Effect of stream stage, ϕ_s on hydraulic head, ϕ at the stream centreline.

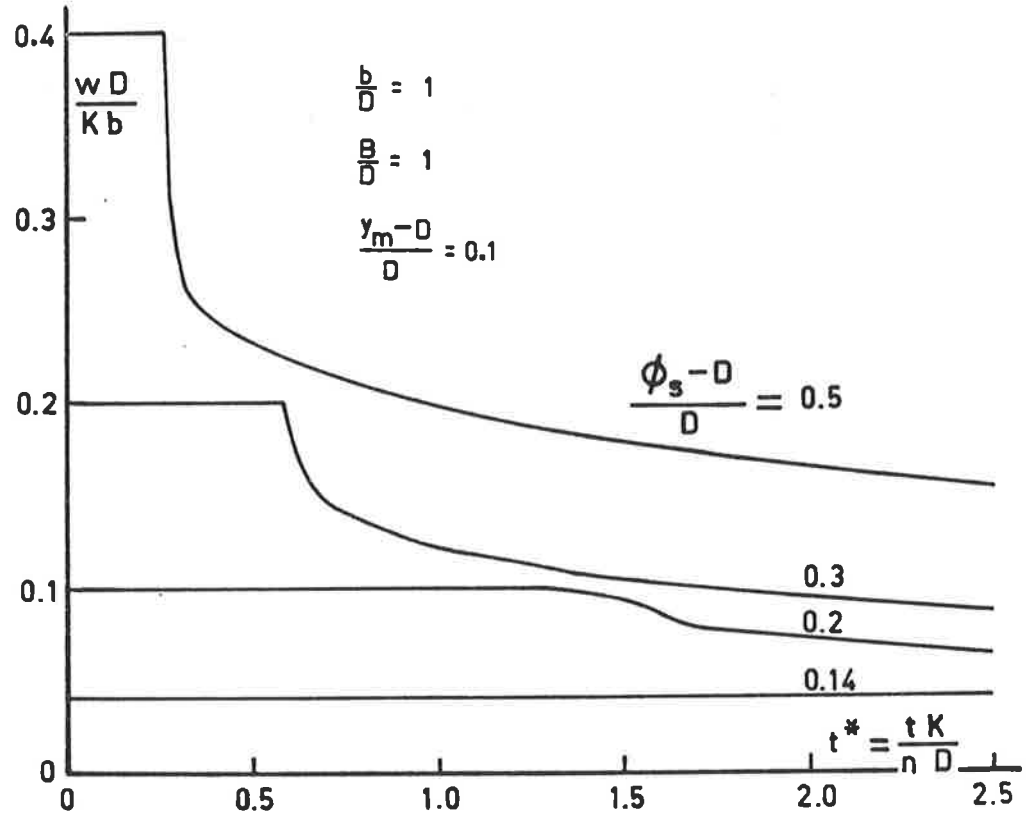

Figure 5.27 (b) Problem RECT : Effect of stream stage, ϕ_s on exchange flow rate, w.

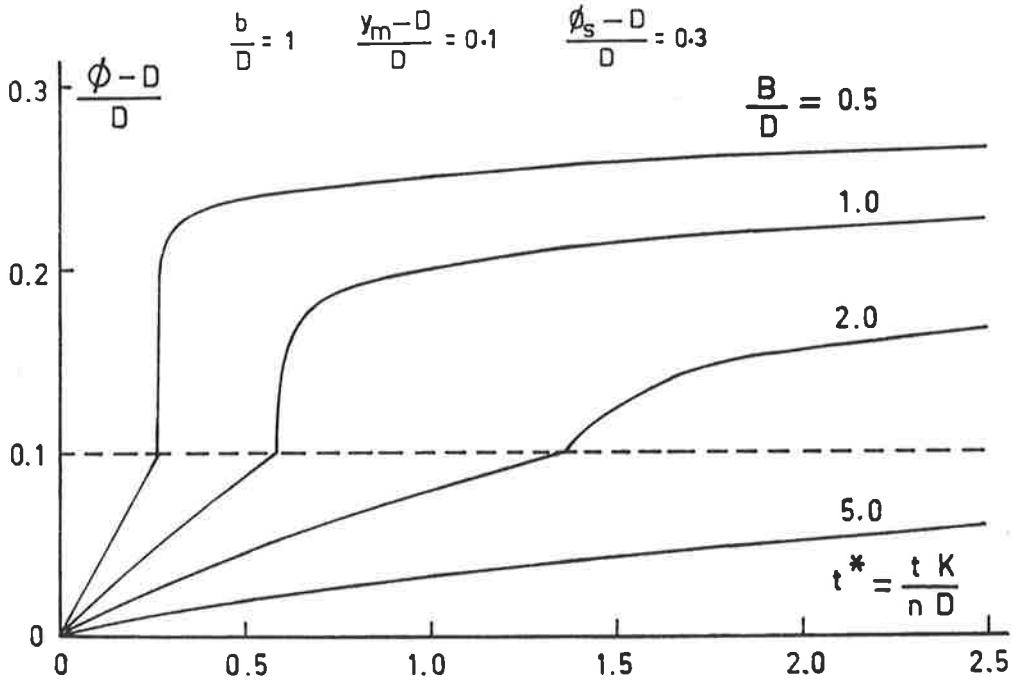

Figure 5.28 (a) Problem RECT : Effect of streambed hydraulic impedance, B on hydraulic head, ϕ at the stream centreline.

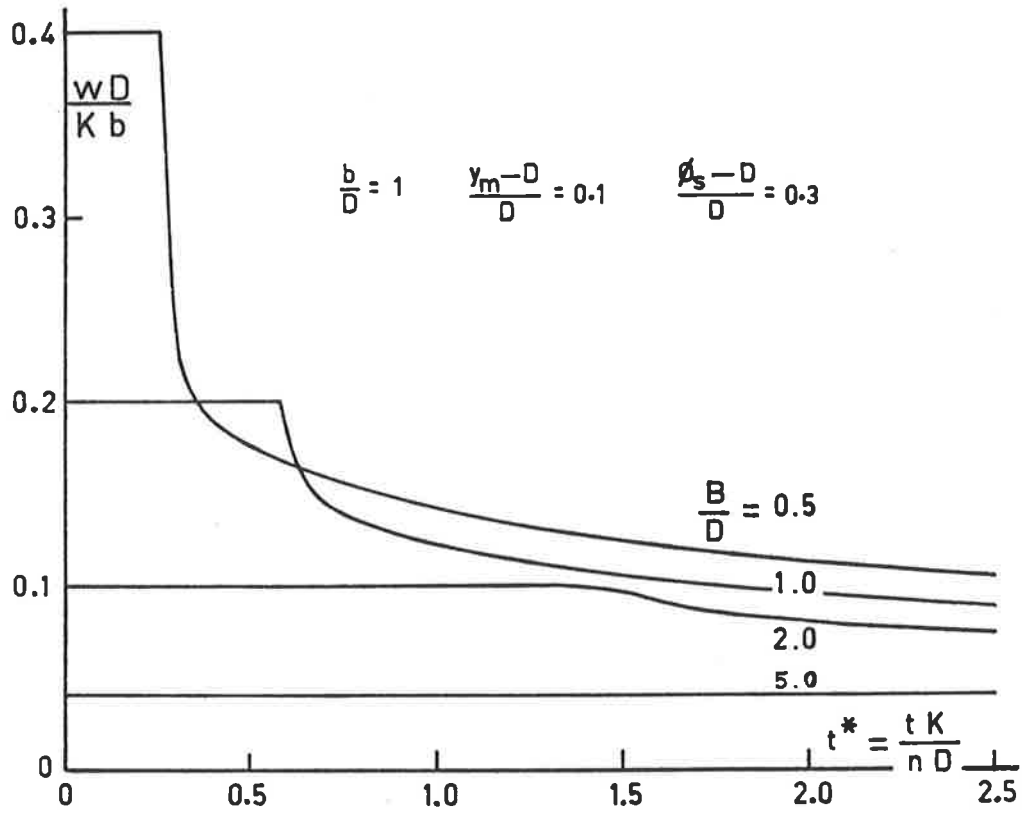

Figure 5.28 (b) Problem RECT : Effect of streambed hydraulic impedance, B on exchange flow rate, w.

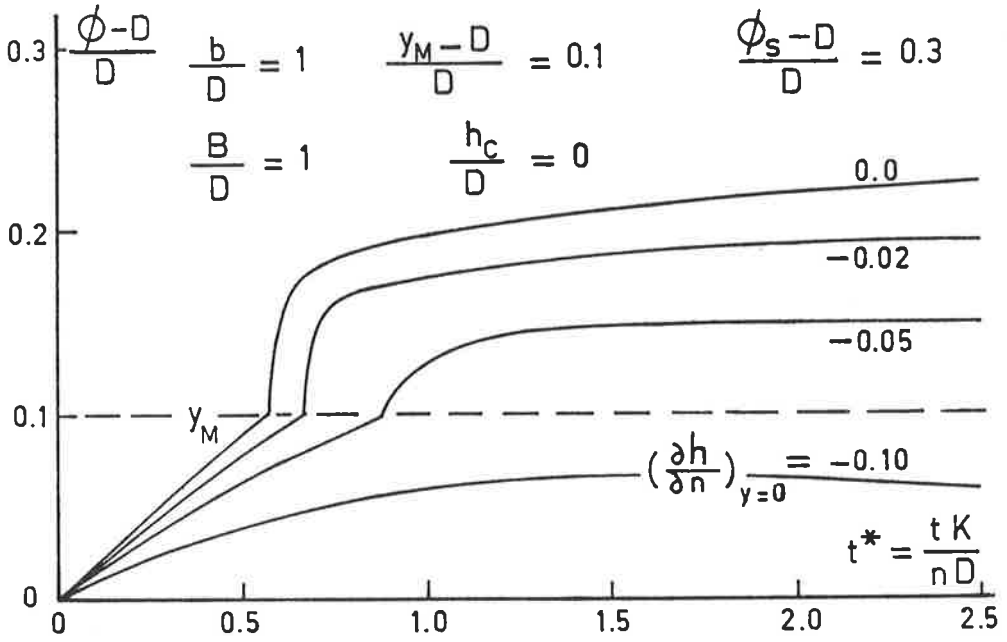

Figure 5.29 (a) Problem RECT : Effect of vertical hydraulic gradient at the base of the aquifer, $(\partial h/\partial n)$ at y=0, on hydraulic head, ϕ at the stream centreline.

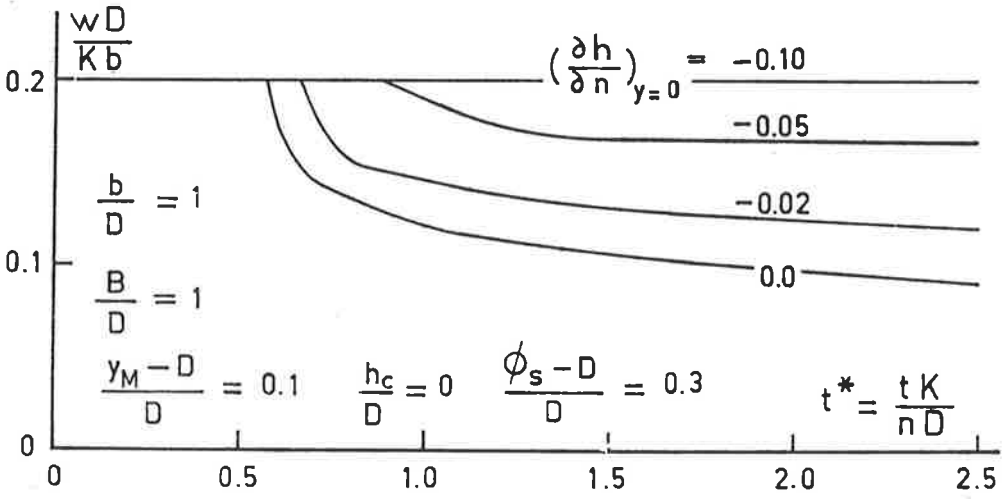

Figure 5.29 (b) Problem RECT : Effect of vertical hydraulic gradient at the base of the aquifer, $(\partial h/\partial n)$ at y=0, on exchange flow rate, w.

The effect of the maximum suction head, h_c below the streambed on the same parameters is shown in figures 5.26a and 5.26b for a single streambed configuration with parameter values as specified in the figure. For higher suction heads the free surface rises more quickly due to higher initial infiltration rates.

An increase in stream stage, ϕ_s results in higher hydraulic heads in the aquifer and higher aquifer intake rates (figures 5.27a and 5.27b). A decrease in the streambed hydraulic impedance, B has a similar effect. (figures 5.28a and 5.28b).

The leakage rate at the base of the aquifer may have a significant effect on the timing of the connection process and may prevent it occurring at all (see figures 5.29a and 5.29b).

These parameter sensitivity tests on a simple rectangular streambed provide a first estimate of their importance in preventing or controlling the timing of hydraulic connection. The BIEM model is subsequently applied to a more realistic streambed geometry.

5.4.2 Reservoir release into a trapezoidal channel (Problem TRAP).

A volume of water is to be released from a reservoir into a trapezoidal ephemeral stream channel for the purpose of recharging the underlying aquifer. The channel surface has a semipervious lining. The question arises as to the effect on aquifer storage of the release rate used to discharge the release volume. This problem is investigated using the BIEM model.

Assuming normal flow in a trapezoidal channel with bottom width, W_b and depth of flow, H_w application of Manning's equation gives

$$Q^* = Qn/W_b^{8/3}S_o^{1/2} = (a+a^2)^{5/3}(1+2.82a)^{-2/3} \qquad 5.29$$

where Q^* = dimensionless discharge rate in open channel.

Q = discharge rate in open channel $[L^3\ T^{-1}]$

n = Manning's n (a surface roughness parameter) $[L^{-1/3}\ T]$

S_o = bed slope of the channel

$a = H_w/W_b$

This equation applies only for bankslopes of 45°.

Dillon (1981b) used this equation to relate steady state seepage rates to streamflow rates for a number of simple hypothetical models of stream-aquifer interaction (Appendix C.2). Setting the release volume in dimensionless form to be

$$Q^*\tau^* = 10$$

where τ^* is the dimensionless form of the release duration τ

$$\tau^* = \tau K/n_e L \qquad 5.30$$

and in this example the characteristic length, L is chosen to be 1 metre. The geometry and boundary conditions of problem TRAP are shown in figure 5.30.

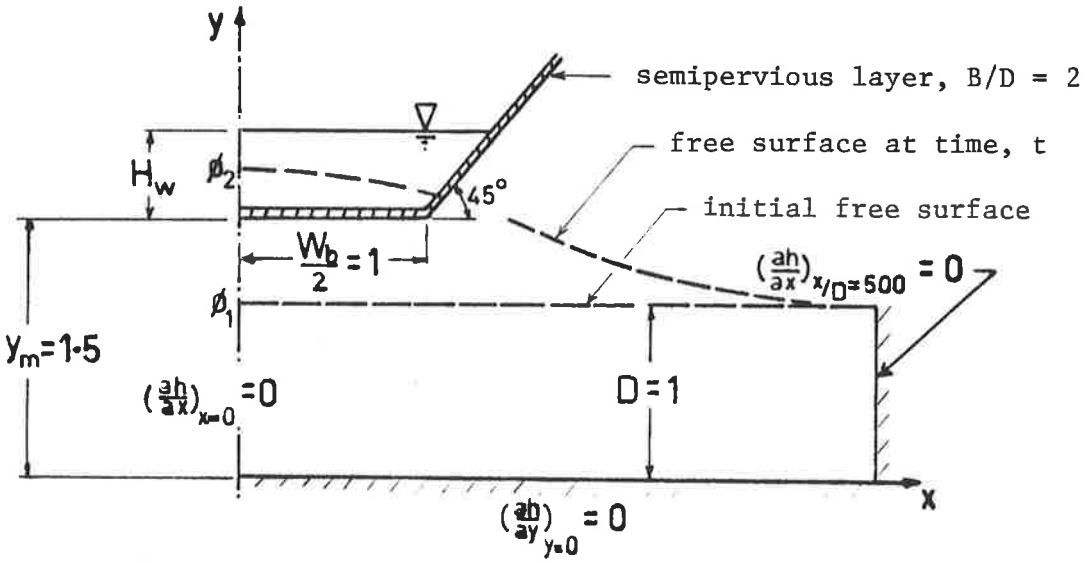

Figure 5.30 Transition from hydraulically disconnected to hydraulically connected stream for a trapezoidal channel : problem TRAP geometry and boundary conditions.

Figure 5.31 shows the variation in exchange flowrate with time for each release pattern. Increasing the streamflow rate increases the aquifer intake rate and the return flow rate during recession. The consequent

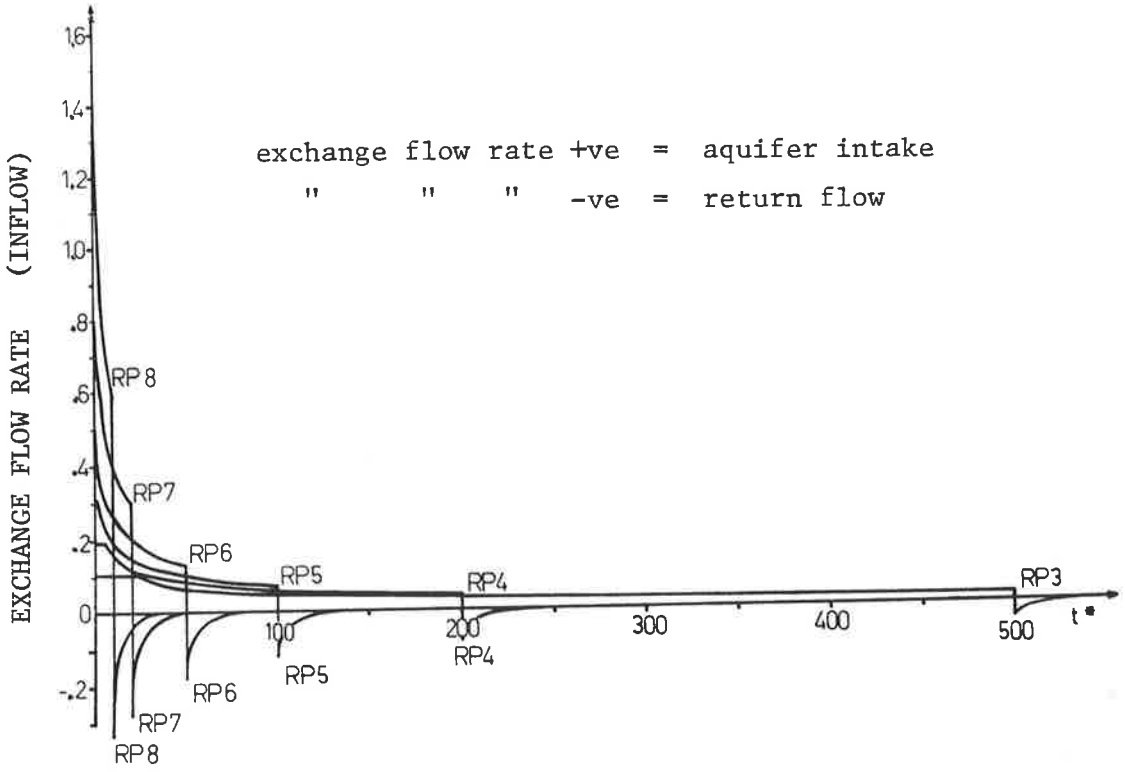

Figure 5.31 Problem TRAP : Effect of release policy on exchange flow rate.

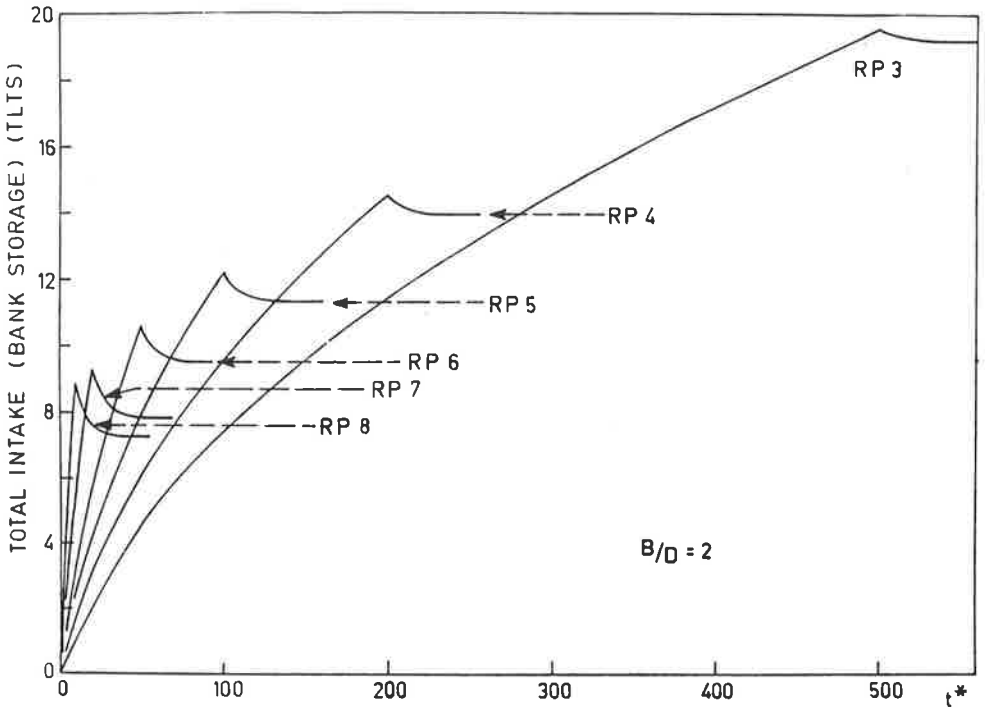

Figure 5.32 Problem TRAP : Effect of release policy on bank storage.

bank storage variations are shown in figure 5.32 and maximum and final bank storages are recorded in Table 5.2.

Table 5.2

Problem TRAP : Release policies and their effect on aquifer storage.

Pattern	Q^*	τ^*	H_w	a	TLTS(max)	TLTS(final)
RP3	0.02	500	.192	.0960	19.52	19.14
RP4	0.05	200	.331	.1657	14.50	13.91
RP5	0.10	100	.498	.2488	12.19	13.35
RP6	0.20	50	.740	.3700	10.59	9.49
RP7	0.50	20	1.223	.6113	9.29	7.85
RP8	1.00	10	1.753	.8767	8.86	7.27

As expected the longer flow durations result in substantially higher peak and final storages. The storage loss due to return flow is larger for the higher flow rates. This is due to the high heads induced adjacent the stream and the narrower spread of the groundwater mound for the shorter duration flows. Figure 5.33 shows the relationship between peak and final bank storage and the duration of the release discharge. Also plotted in this figure is the ratio of peak bank storage to the product of stream depth and the square root of the duration of discharge. Cooper and Rorabaugh showed for their problem of a sinusoidal flood wave in a hydraulically connected stream that this ratio was constant. Although there are a large number of differences between Cooper and Rorabaugh's problem and problem TRAP, it is apparent that where hydraulic connection occurs during a release the efficiency of recharge at lower release rates is higher than that which would be predicted by considering the stream as being hydraulically connected only.

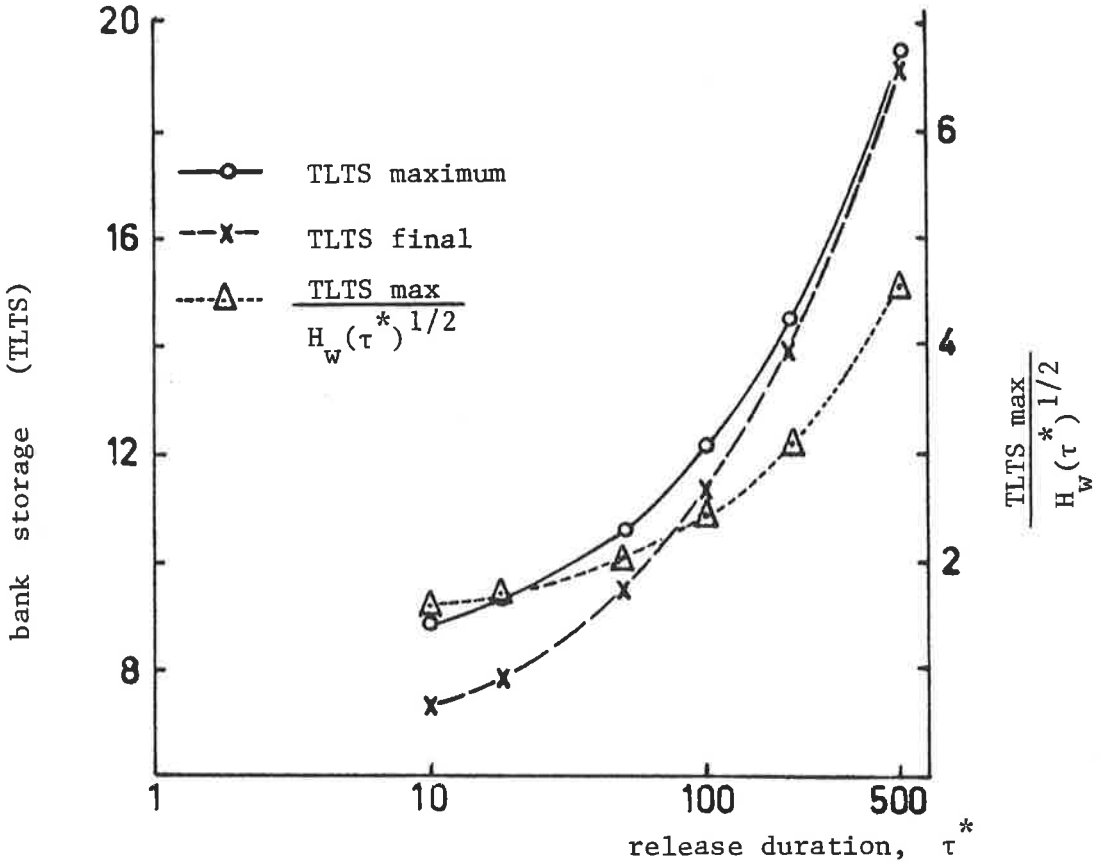

Figure 5.33 Problem TRAP : Effect of duration of release discharge on peak and final bank storage.

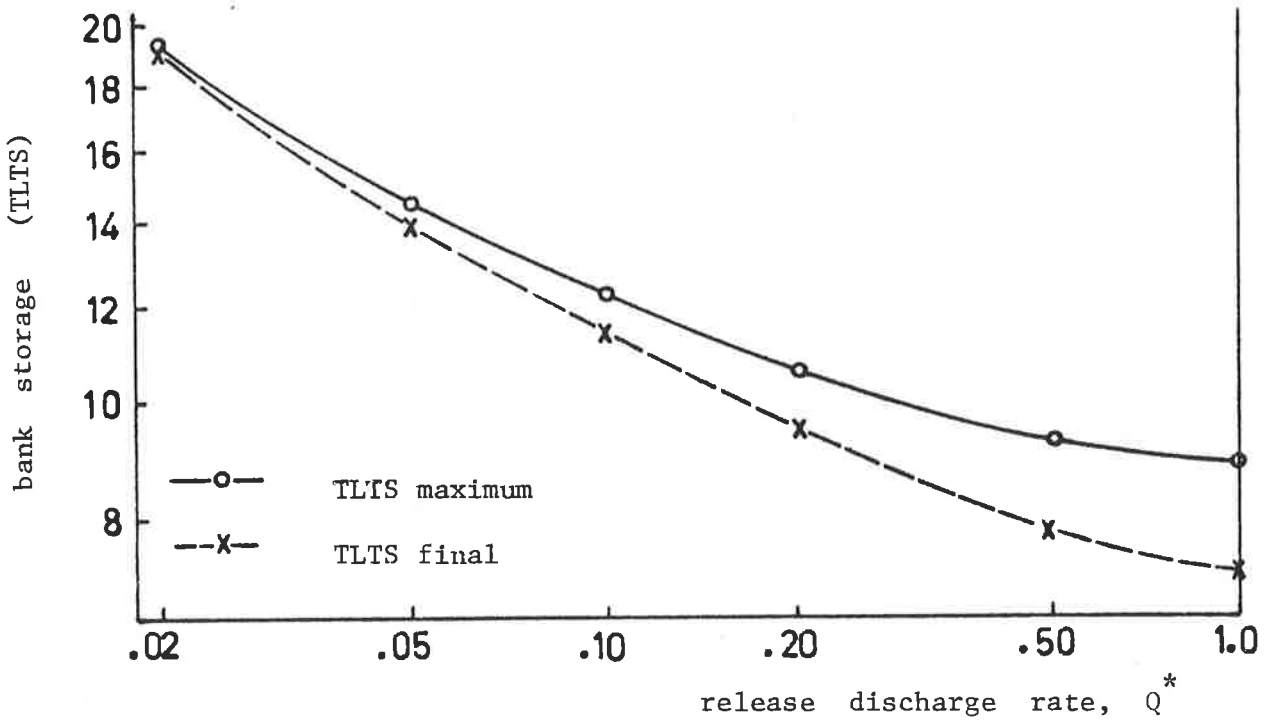

Figure 5.34 Problem TRAP : Effect of release rate on peak and final bank storage (log-log scales).

Peak and final bank storages are also plotted against nondimensional release rate using log-log scales (figure 5.34) and the best fit relationship for peak bank storage, V_{max} found to be

$$V_{max} = 8.2 \ (Q^{*} \ )^{-0.2} \qquad 5.31$$

In order to contain computer execution times, which averaged 90 CP seconds per release pattern (52 time steps), and to maintain solution accuracy, time increment values were changed during execution. Small time steps were required during boundary condition change-over at hydraulic connection and on the formation of the seepage face and disconnection during recession. A pattern of logarithmic and constant time steps were used to produce approximately equal mass balance errors at each time step giving a maximum overall error of 2%.

The hydraulic head variation in the free surface/streambed/seepage face nodes during their boundary condition transitions is represented by some potentiometric surface profiles for release pattern RP8. (See figure 5.35). A rapid rise in hydraulic head occurs once the free surface reaches the semipervious layer. That is the aquifer becomes semi-confined in this vicinity. The model neglects changes in elastic storage, which are neglibible compared with storage changes due to free surface movements. The seepage face condition is approximated crudely as the head profile is expected to be tangent to the stream bank.

Return flow would normally result in an exponential decline in stream stage with time, rather than the step change used in this problem. Hence the boundary condition is more severe than would be encountered in reality. The shape (or time constant) of the recession hydrograph depends on the nature of the stream-aquifer interaction upstream of the section modelled in this problem.

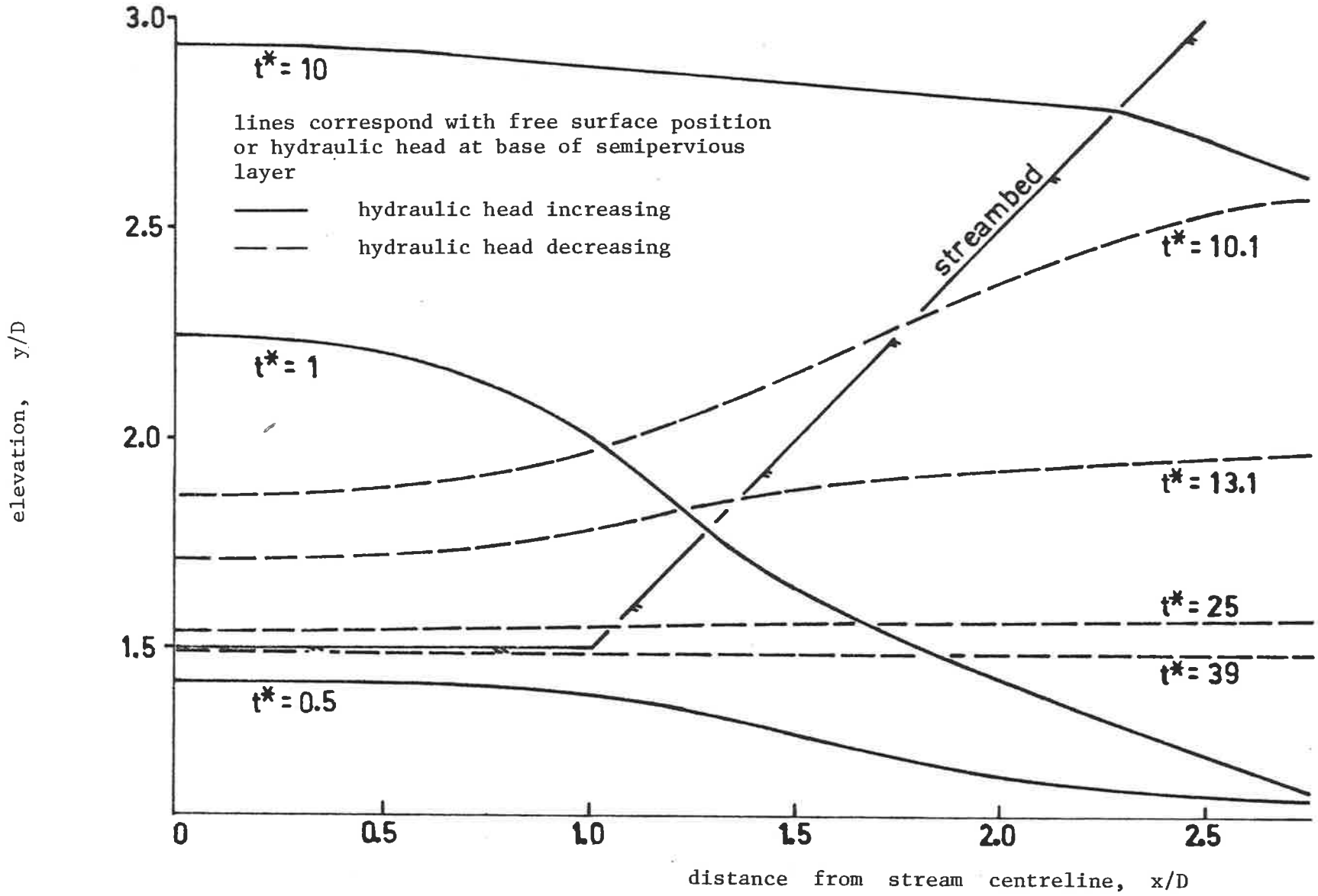

Figure 5.35 Problem TRAP : Hydraulic head profiles near the streambed for release pattern RP8.

5.4.2.1 Effect of streambed hydraulic impedance on bank storage

An indication of the effect of the dimensionless coefficient of streambed hydraulic impedance, B/D (= K 1 / K_B D) on peak bank storage for release pattern RP3 is shown in figure 5.36. If B/D < 0.1 the hydraulic resistance of the semi-pervious layer has negligible effect and aquifer transmissivity limits aquifer intake. For B/D < 10^{-3} very high initial intakes rates occur and very small time steps are required to contain mass balance errors. Figure 5.36 shows a 3% reduction in intake for B/D = 10^{-3} with respect to B/D = 10^{-2}. This reduction is due to these initial errors. The case of no semi-permeable layer (B = 0) would result in theoretically infinite initial infiltration rates (in common with Marino's step change in stream stage, section 5.3.1). Substituting B/D = 10^{-2} for such a case results in negligible error, and avoids the necessity for very small initial time steps.

Hydraulic connection occurred at time $t < \tau$ for cases of B/D < 9. For B/D > 9 no hydraulic connection occurred hence the intake rate $0 < t < \tau$ is inversely proportional to B. For these cases the streambed behaves as a strip recharge source. Figure 5.36 shows the transfer of control of the intake from the aquifer transmissivity to the streambed blanket as the hydraulic resistance of the blanket increases.

5.4.2.2. Linearity

The advantage in approximating aquifer response with linear models is the simplicity of the mathematical solution compared with nonlinear models. The literature contains many examples of impulse response (linear) models relating stream stage to exchange flow. Among them are Venetis (1968 and 1970), Moench and Kisiel (1970), Hall and Moench (1972) and Moench, Sauer and Jennings (1974).

Other modellers relied on linear assumptions for the stream-aquifer interaction process, Morel-Seytoux (1975), Besbes, Delhomme and de Marsily (1978) and Flug, Abi-Ghanem and Duckstein (1980). These models have been

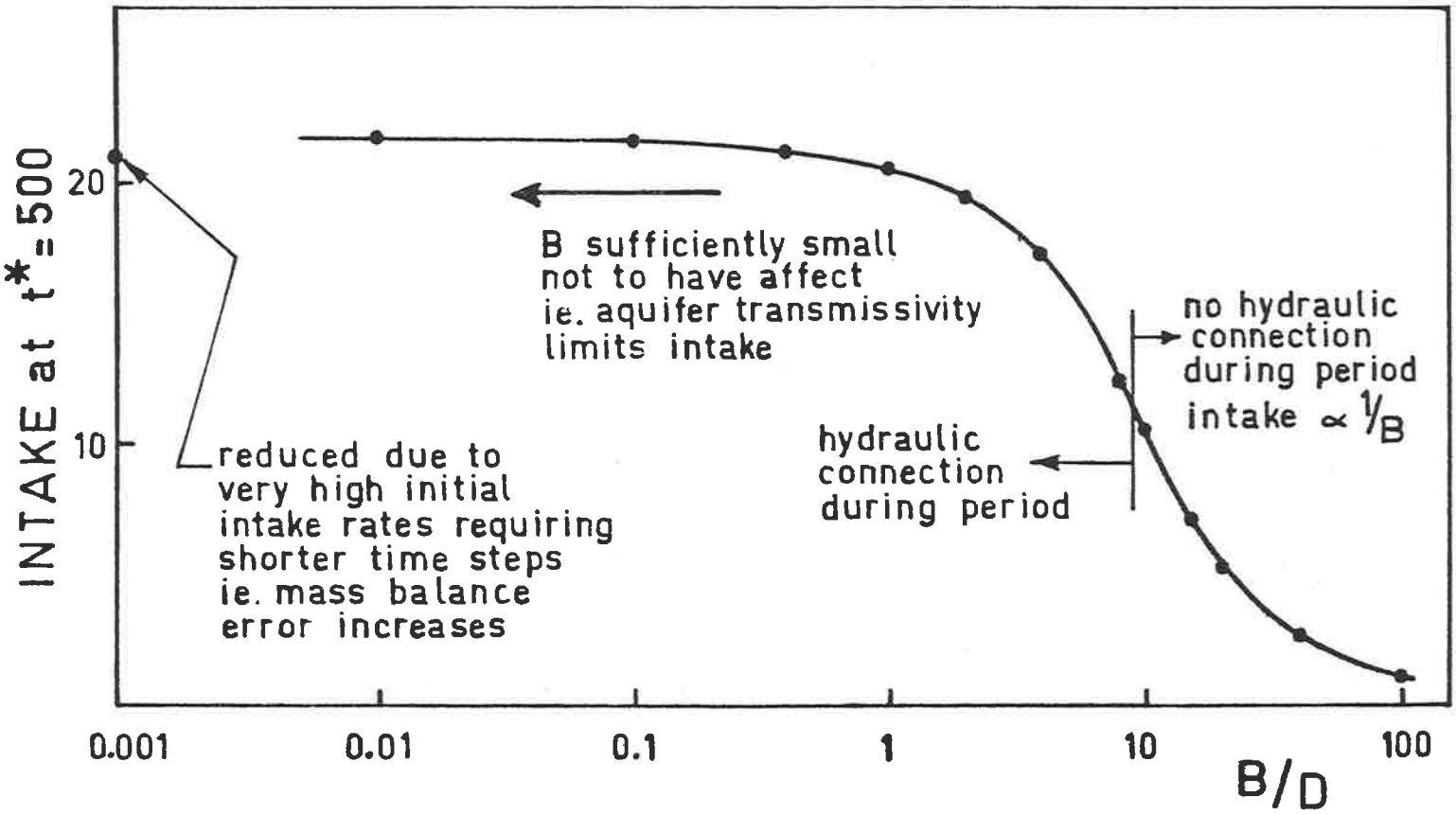

Figure 5.36 Problem TRAP : Effect of hydraulic impedance of the streambed on peak bank storage for release pattern RP3.

used with field data but an examination of linearity of the stream-aquifer interaction process has not been seen by the author. The BIEM model is used again for the problem of reservoir releases into a trapezoidal streambed to determine whether the superposition principle is applicable. The geometry is as shown in figure 5.30. A plot of exchange flow rate with respect to stream depth is shown in figure 5.37.

The initial hydraulically disconnected recharge rate is seen to be nonlinear. An increase in stream depth results in proportionately higher seepage rates through the semipervious layer and also increases the wetted perimeter of this layer. Upon hydraulic connection aquifer intake rates decline and as time progresses intake rates become more linear with respect to stream stage. The timing of hydraulic connection depends on the intake rate history which in turn depends on the stream hydrograph.

As a comparison a similar review of linearity for a rectangular streambed is given in figure 5.38. In this case the effective intake area, being constant, gives a recharge rate to the disconnected aquifer proportional to the depth of flow in the stream. In other respects the graphs take a similar form to those in the previous figure.

Figures 5.37 and 5.38 rely on a uniform semipervious layer over the streambed and on channel geometry and blanket properties being independent of time and discharge rate. Uniform porous media are rarely encountered in field studies and alluvial streams with their braided and lenticular bedding are no exception. Reference has been made to scour due to high discharge by several writers (see assumption 2.1.1.(4)). Hence it is likely that the blanket hydraulic impedance should be reduced at high flows and possibly a change in streambed geometry should also be allowed. The number of permutations of these changes is large for any given channel and only an elementary investigation of these types of effects on model output has been made. Two runs with time-varying streambed hydraulic impedance were performed and these are described in section 5.4.3.2.

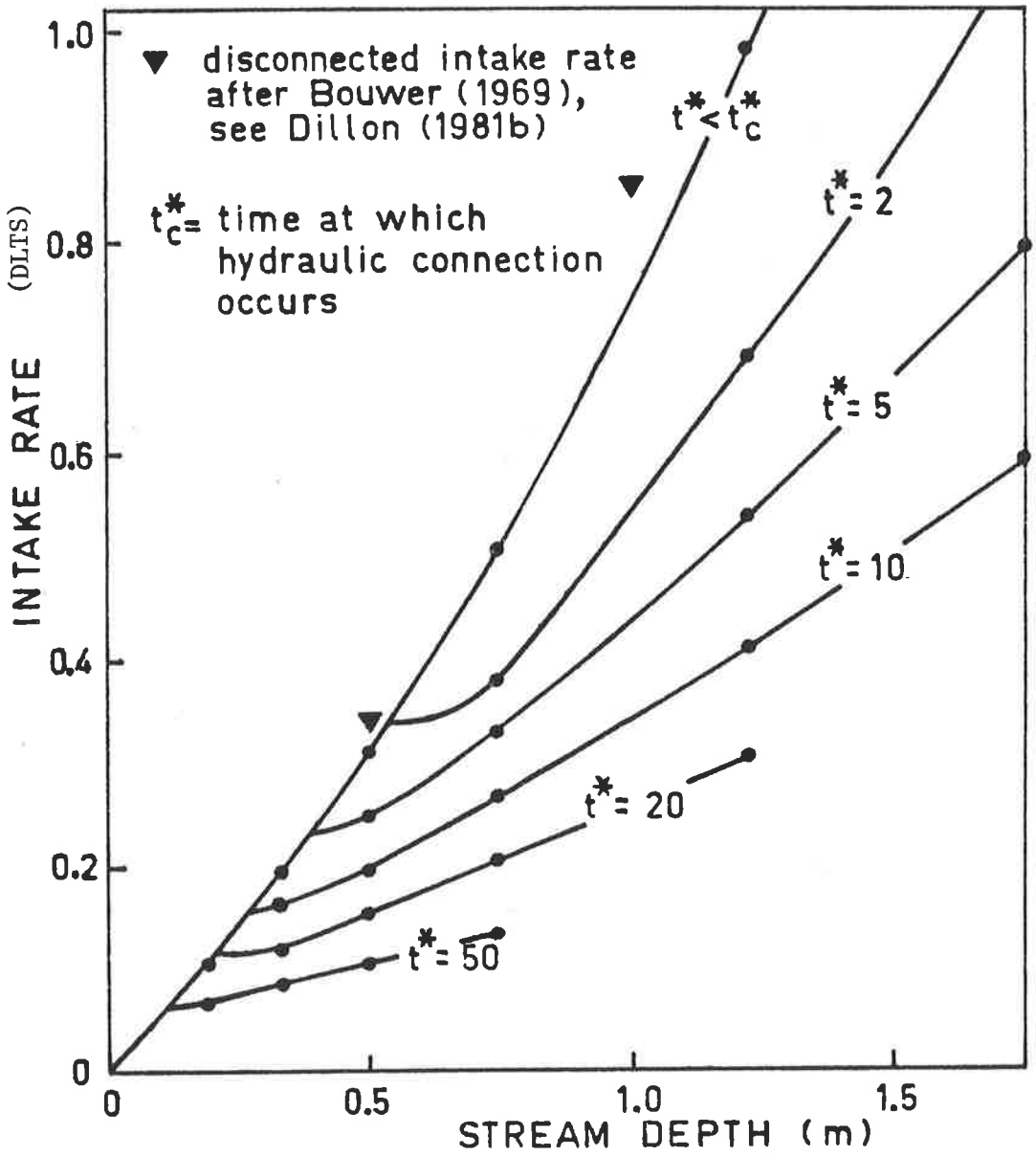

Figure 5.37 Problem TRAP : Exchange flow rate related to stream depth at various times from the commencement of streamflow.

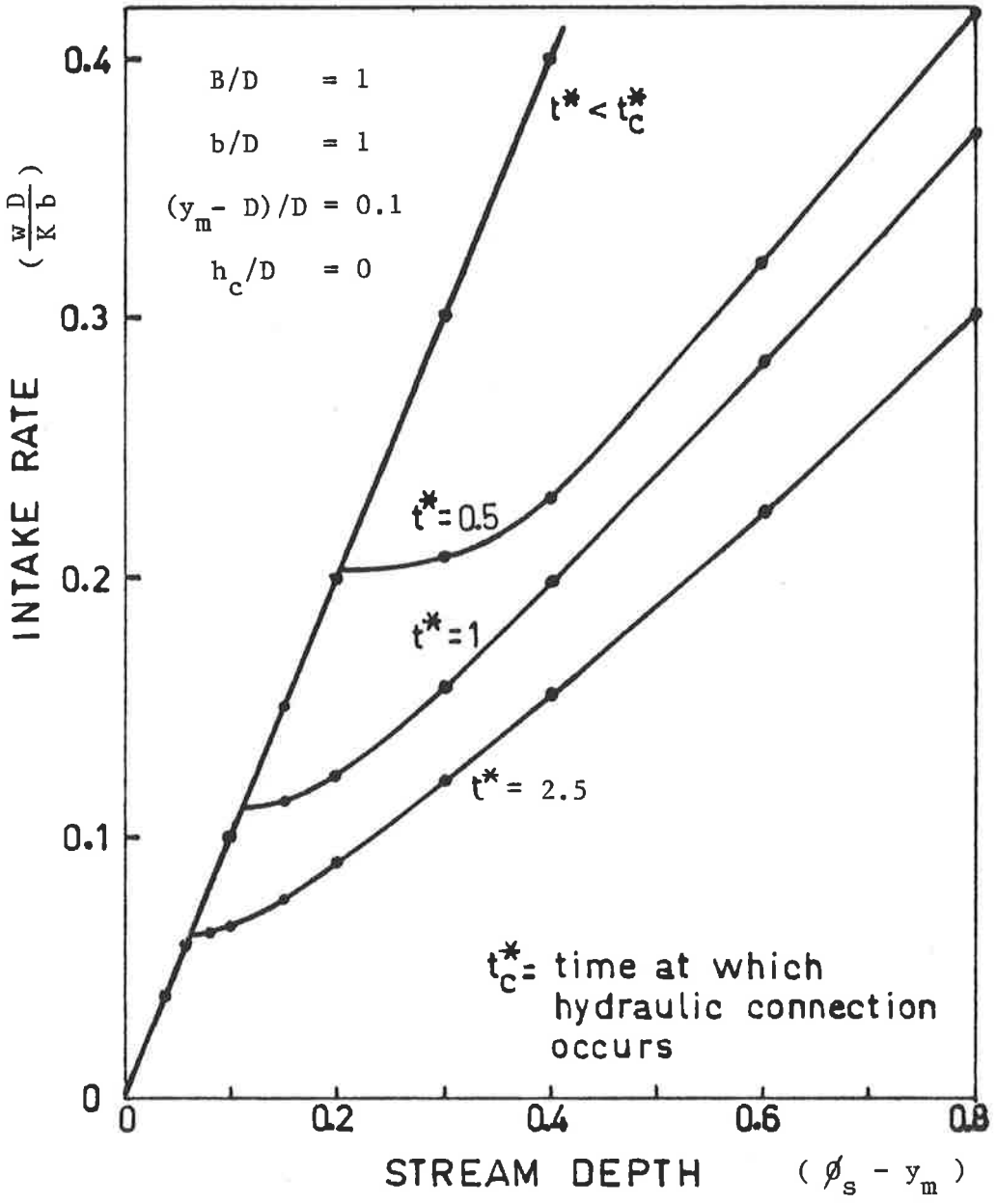

Figure 5.38 Problem RECT : Exchange flow rate related to stream depth at various times from the commencement of streamflow.

The results in figures 5.37 and 5.38 show that the exchange flow rate responds quite differently to a change in stream stage depending on whether or not the stream is hydraulically connected to the underlying aquifer. Secondly as time progresses for constant stream stage, the relationship between stream head and intake rate becomes more linear if the stream and aquifer are hydraulically connected.

5.4.3 Flood wave superimposed on reservoir release.

The effect of a flood wave on exchange flow rate and bank storage during the course of a reservoir release is examined using the BIEM model. It shall be shown later why this particular problem is of interest. Release policy RP3 is chosen and superimposed on asymmetric sinusoidal stream hydrographs having crest heights of 1.0 and 1.5 units and periods of 12 and 24 dimensionless time units. Firstly a brief investigation of the effect of the magnitude and period of the superimposed flood wave on exchange flowrates and bank storage is presented in figures 5.39 and 5.40. In each case the flood wave commenced at $t^* = 50$. Bank storage is shown to be more sensitive to the period of a flood wave than to its peak stage. Figure 5.39 shows that the superimposed wave has a significant effect on exchange flow rates during its passage and for up to two periods afterwards.

5.4.3.1 System Memory.

The problem was extended by considering the effect on bank storage of the arrival time of the flood wave for arrival times $t^* = 50$ and $t^* = 230$. The difference in bank storage at the end of the reservoir release due to the arrival time of the flood wave reflects what Dooge (1973) calls the "memory" of the stream-aquifer system. He defines memory as the length of time of the history of the system and its input which affects the response of the system to an input at any instant. Most literature describing groundwater models avoids consideration of the memory of the system by choosing the initial free surface to be horizontal at the same elevation

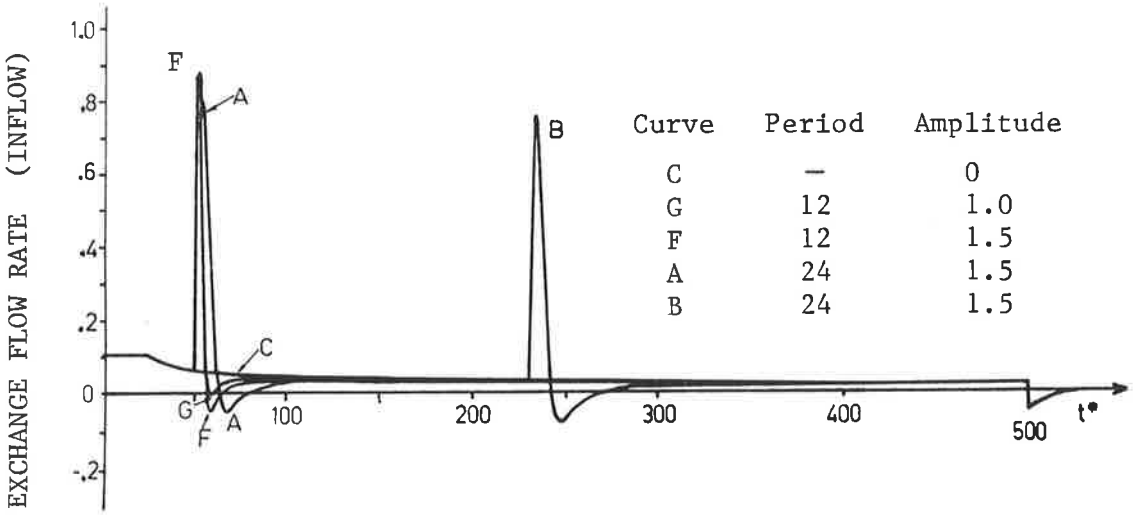

Figure 5.39 Problem TRAP : Exchange flow rate related to asymmetric sinusoidal flood waves of different amplitudes and periods superimposed on release pattern RP3.

as the stream head or at a depth below the streambed such that hydraulic connection need not be considered. However the intial elevation may determine the time at which hydraulic connection occurs. This process is nonlinear as seen in figures 5.37 and 5.38. Hence the exchange flow rate pattern and bank storage pattern are sensitive to the initial free surface elevation.

5.4.3.2 Time-variance

Several model parameters which may change with time are identified in section 5.4.2.2. A token attempt was made to determine the likely effect of varying only the streambed hydraulic impedance. This was varied as a function of stream stage. The value of B was decreased from 2 to 0.1 as the streamstage increased from its initial position to its peak (figure 5.41, curve D). This had the effect of reducing the blanket hydraulic impedance until it was negligible. This corresponded to the stripping of the semipervious blanket without changing streambed geometry during high discharge. The choice of the function relating B to stream

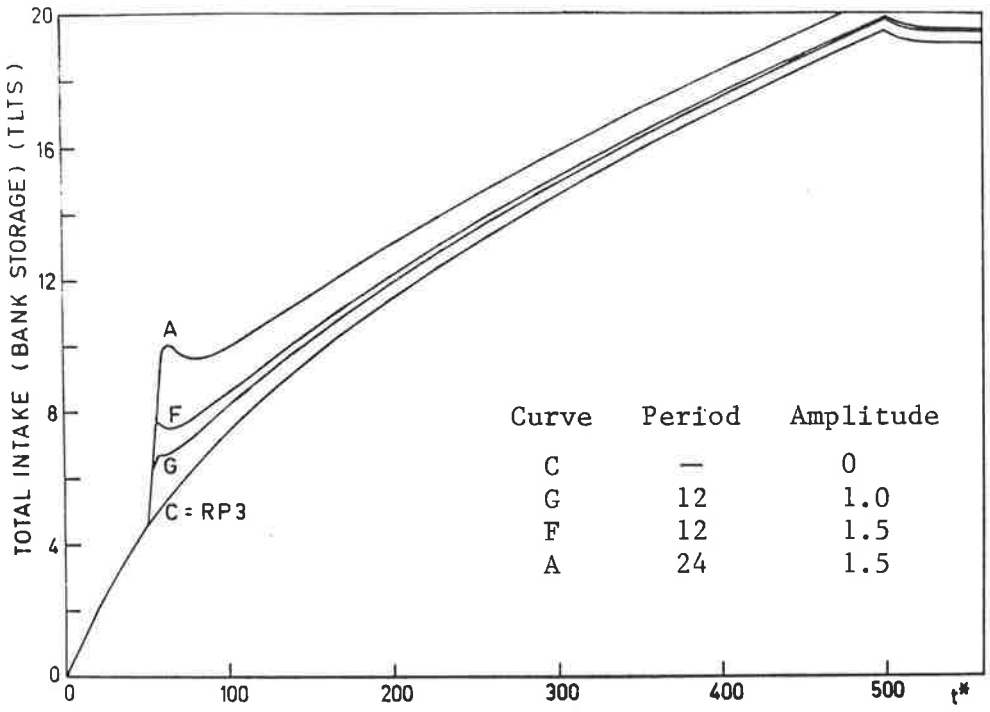

Figure 5.40 Problem TRAP : Bank storage related to asymmetric sinusoidal flood waves of different amplitudes and periods superimposed on release pattern RP3.

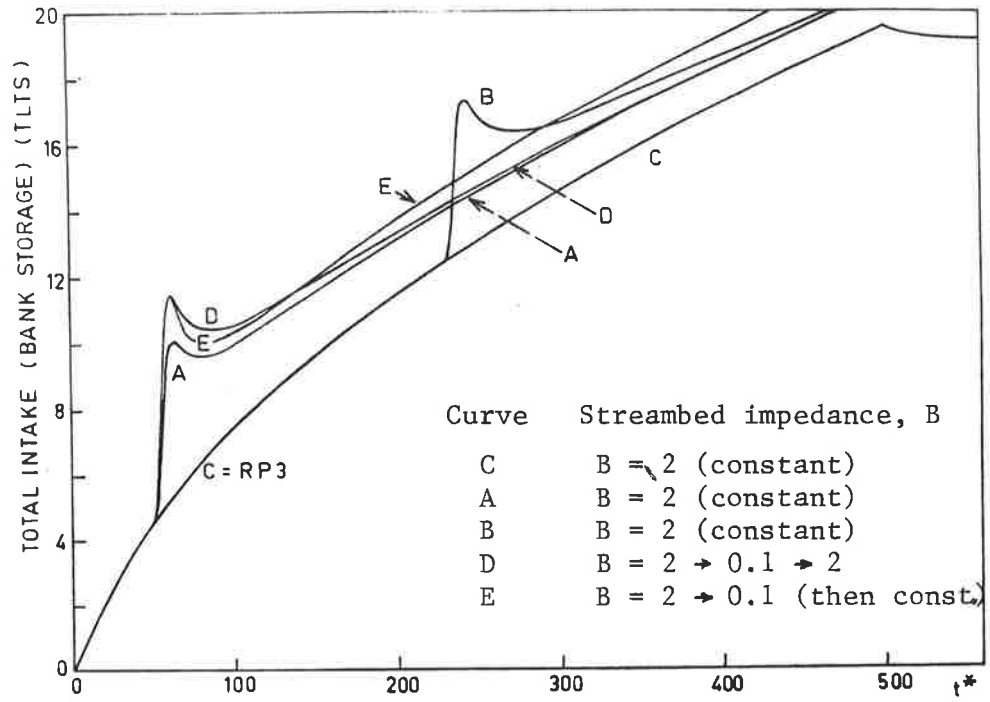

Figure 5.41 Problem TRAP : Bank storage related to a flood wave with amplitude 1.5 and period 24 (dimensionless units) with different arrival times and varying streambed hydraulic impedance.

stage was arbitrary:

$$B = B_o \exp(-2(H_w - H_{wo})) \qquad 5.32$$

where B_o = initial streambed hydraulic impedance = 2L

H_{wo} = stream depth during constant release RP3 = 0.192 L

and L = length scale dimension.

For curve E the streambed hydraulic impedance remains at the lowest value (B = 0.1 L) reached at the peak of the flood. This assumes streambed clogging is a slow process compared with scour.

Bank storage changes for the time-variant and time-invariant cases are shown in figure 5.41. The peak bank storages for these cases are given in table 5.3.

Table 5.3

Problem TRAP : Peak bank storage (at $t^* = 500$) for various cases involving release pattern RP3 and changing streambed hydraulic impedance.

curve	peak bank storage	peak/peak$_{(A)}$	comments
C	19.52	-	RP3 only, B = 2
A	20.56	1	B = 2
B	20.69	1.01	late flood, B = 2
D	20.51	1.00	B = 2 → 0.1 → 2
E	21.50	1.05	B = 2 → 0.1

The temporary change in impedance (curve D) is indistinguishable from the time invariant case (curve A) at $t^* = 500$. However the long term scour case (curve E) results in a 5% increase in peak bank storage, which as expected is smaller than the 11% increase in bank storage due to a reduction in the constant value of B/D from 2 to 0.1 for release pattern RP3 only (from figure 5.36). Figure 5.36 also shows that bank storage is

most sensitive to streambed hydraulic impedance changes when B/D > 2 for problem TRAP with release pattern RP3. Therefore although the effect of varying hydraulic impedance was small in the examples above there may be cases where time varying streambed conditions may not necessarily be adequately modelled using time-invariant parameters.

5.5 Application to a Field Study

The ability of the model to simulate a range of theoretical problems has been conclusively demonstrated. The next step involves testing the model against field data to verify that the governing equation and boundary conditions are applicable to real problems. Chapters 6, 7 and 8 describe a full scale field study of the Little Para River and its interaction with aquifers. Chapter 6 describes the study method and data acquisition and processing. Chapter 7 is an account of a detailed study of seepage from an artificial pond in the streambed. Chapter 8 describes the derivation of a recharge release rule for the Little Para Reservoir using a simple regression model.

In Chapter 9 data acquired in the Little Para study are used to calibrate and validate the BIEM model at several cross-sections on the stream.

CHAPTER 6

LITTLE PARA RECHARGE STUDY

6.1 Purpose

The Little Para River is a small ephemeral stream located 20 kilometres north of Adelaide the capital city of South Australia. (see figure 6.1). The stream rises in a 92 $(km)^2$ catchment in the Mount Lofty Ranges and flows west for 16 km across the Northern Adelaide Plains to the sea. Its annual discharge has a mean of 9.4×10^6 m^3 (9400 ML) and a coefficient of variation (standard deviation divided by the mean) of 0.66. Discharge follows a marked seasonal pattern with on average 85% occuring in the five winter months June to October. On the plains the stream is often dry during summer months.

In 1977 the state government completed construction of the Little Para Dam located on the stream within the Mount Lofty Ranges. The reservoir augmented the metropolitan water supply headworks storage capacity by 18×10^6 m^3 (18000 ML). Its primary function is to store water pumped from the River Murray 80 km away. The dam reduces the effective catchment area to 10$(km)^2$ at the point where the river emerges onto the coastal plain. The river is a known recharge source for aquifers underlying the plain, which provide irrigation water for market gardens. The Parliamentary Standing Committee on Public Works required that the dam should have no adverse affect on aquifer recharge by providing appropriate recharge releases.

The Engineering and Water Supply Department of South Australia, (EWS) and the Civil Engineering Department of the University of Adelaide initiated a joint study in 1978 with the following objectives.

(1) to estimate the recharge due to flow in the Little Para River prior to

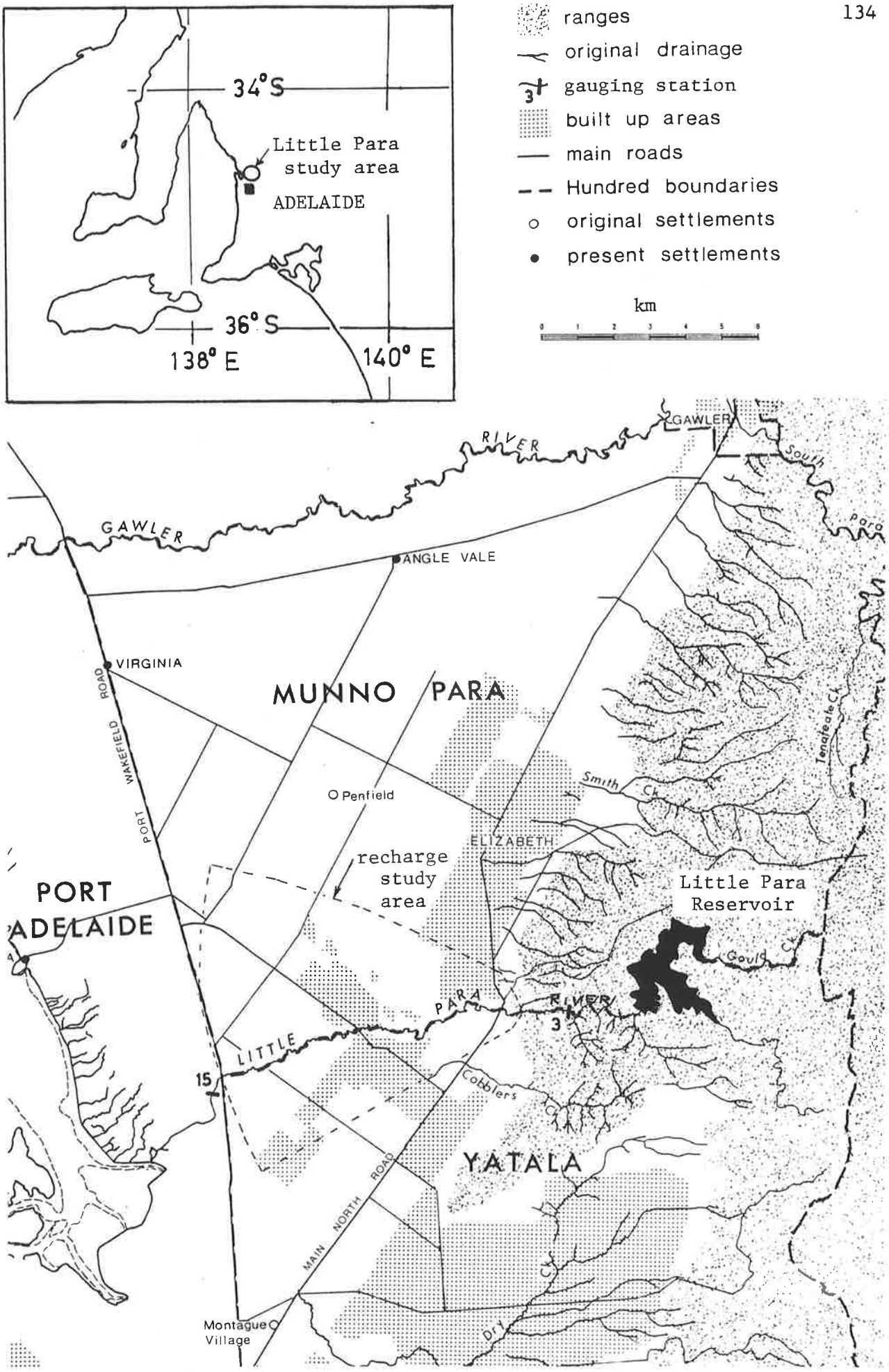

Figure 6.1 Location of Little Para River and recharge study area.

construction of the dam.

(2) to recommend a recharge releases rule for the reservoir to ensure that the dam does not reduce aquifer recharge from the streambed.

(3) to assess the feasibility of conjunctive management of the Little Para Dam and aquifers recharged by the stream.

The author had responsibility for the technical oversight of the study, from planning the field investigation, through three and a half years of day to day activity in data collection and processing, to report writing and submitting detailed recommendations on reservoir operation.

6.2 Study Method

The method used was to release water at various uniform rates from the reservoir and observe the discharge rate at a number of gauging stations and relate discharge losses to water table elevation in piezometers adjacent the stream. A feature of the Little Para River downstream of the dam is the ability to regulate flow and to limit it to the sensitive range of the discharge measurement structures.

The study was conducted in three stages. Firstly discharge and groundwater levels were recorded using existing observation bores and minimal gauging station works. A review of these results led to the construction of a network of observation bores and to the installation of several new gauging stations with continuous water level recorders. A second series of releases was intensively monitored. The third stage using the established installations extended the period of monitoring with a revised and less intense data acquisition programme. The stages of the study occurred as follows.

Stage I February 1979 - May 1979

Stage II February 1980 - April 1981

Stage III July 1981 - June 1982

Almost 6 x $10^6 m^3$ (6000 ML) were released over a period of three and a half years. The reservoir release schedule is given in Table 6.1. The

Table 6.1

RESERVOIR RELEASE SCHEDULE, FEBRUARY 1979 - JUNE 1982

Starting Date	Duration (days)	Nominal Release rate (ℓ/s)	Total Release (ML)	Scour (ML)	Total (ML)	
26.2.79	15.2	140	184			
13.3.79	9.0	220	168			
22.3.79	11.0	140	135			
2.4.79	3.0	300	75			
5.4.79	6.0	140	74			
11.4.79	26.0	70	175			
7.5.79	4.0	140	48			
11.5.79	276.0	0	0		859	Stage I
11.2.80	13.3	140	161			
24.2.80	5.9	0	0			
1.3.80	29.9	140	361			
31.3.80	33.5	220	637			
3.5.80	5.6	0	0			
9.5.80	11.0	140	133			
20.5.80	6.0	220	114			
26.5.80	7.0	300	181			
2.6.80	7.0	220	133			
9.6.80	8.0	140	97			
17.6.80	154.0	0	0		1,817	Stage II(a)
18.11.80	28.0	300	726			
16.12.80	56.0	0	0			
10.2.81	42.0	180	653			
24.3.81	112.0	0	0		1,379	Stage II(b)
14.7.81	10.0	180	156			
24.7.81	20.25	130	227			
13.8.81	0.01	22,000	-	9		Scour
13.8.81	8.0	130	90			
21.8.81	4.13	0	0			
21.8.81						Spill commences
25.8.81	0.25	11,000	-	240		Scour
25.8.81	60.6	130	680			
25.10.81						Spill ceases
26.10.81	2.4	0	0			
28.10.81	19.6	130	220			
17.11.81	21.0	65	118			
8.12.81	7.0	30	18			
15.12.81	126.0	0	0		1,509	Stage III(a)
20.4.82	6.0	140	73			
26.4.82	8.0	0	0			
4.5.82	7.0	140	85			
11.5.82	7.0	0	0			
18.5.82	7.0	140	85			
25.5.82	7.0	0	0			
1.6.82	7.0	140	85			
8.6.82	7.0	0	0			
15.6.82	7.0	140	85			
22.6.82		0	0		413	Stage III(b)
	TOTAL RECHARGE RELEASE				5,977	

RELEASES BY YEAR

9.8.77	reservoir diversion closed
1977/78	0
1978/79	859
1979/80	1,817
1980/81	1,379
1981/82	1,922
Total	5,977
Mean	1,195 ML/year

work was reported in full at the end of each stage by the Civil Engineering Department of the University to the Engineering and Water Supply Department (Dillon 1979, 1981a, 1983a). An outline of field installations, data acquisition and data processing follows but first a brief description of the hydrogeology of the area is provided as this had a major bearing on the number and location of observation bores (collectively the most expensive field installations).

6.3 Hydrogeology of Little Para Region

A number of studies of the hydrogeology of the Northern Adelaide Plains have been reported, Miles (1952), Shepherd (1966 and 1975), Boucaut (1977) and Linke and Eberhard (1981). They reveal that the Little Para River is perched on an alluvial delta varying in thickness between 40 and 60 metres. This formation known as Hindmarsh Clay was deposited from Pleistocene to Recent times. Although consisting mainly of clays it contains beds of sands and gravels some of which provide sufficient water to irrigate market gardens. A geological section of Shepherd (figure 6.2) (located in figure 6.4) displays these Quaternary aquifers, previously described by Miles (1952).

> "River gravels and sands within the flood plains of the principal streams crossing the Adelaide Plains provide numerous aquifers. Individual beds of these gravels are seldom more than 3 or 4 feet thick and are discontinuous and lenticular. They may be separated from each other both laterally and vertically by relatively impermeable clays."

Shepherd (1975) found up to three thin sand layers up to 10 metres thick in the vicinity of the Little Para River less than two kilometres downstream of the Para Fault (the eastern margin of the plains). He summized that "they were deposited during fluviatile stages of the Pleistocene from flood flows in the antecedent river". Sand beds were also found elsewhere. They were poorly developed and contained higher

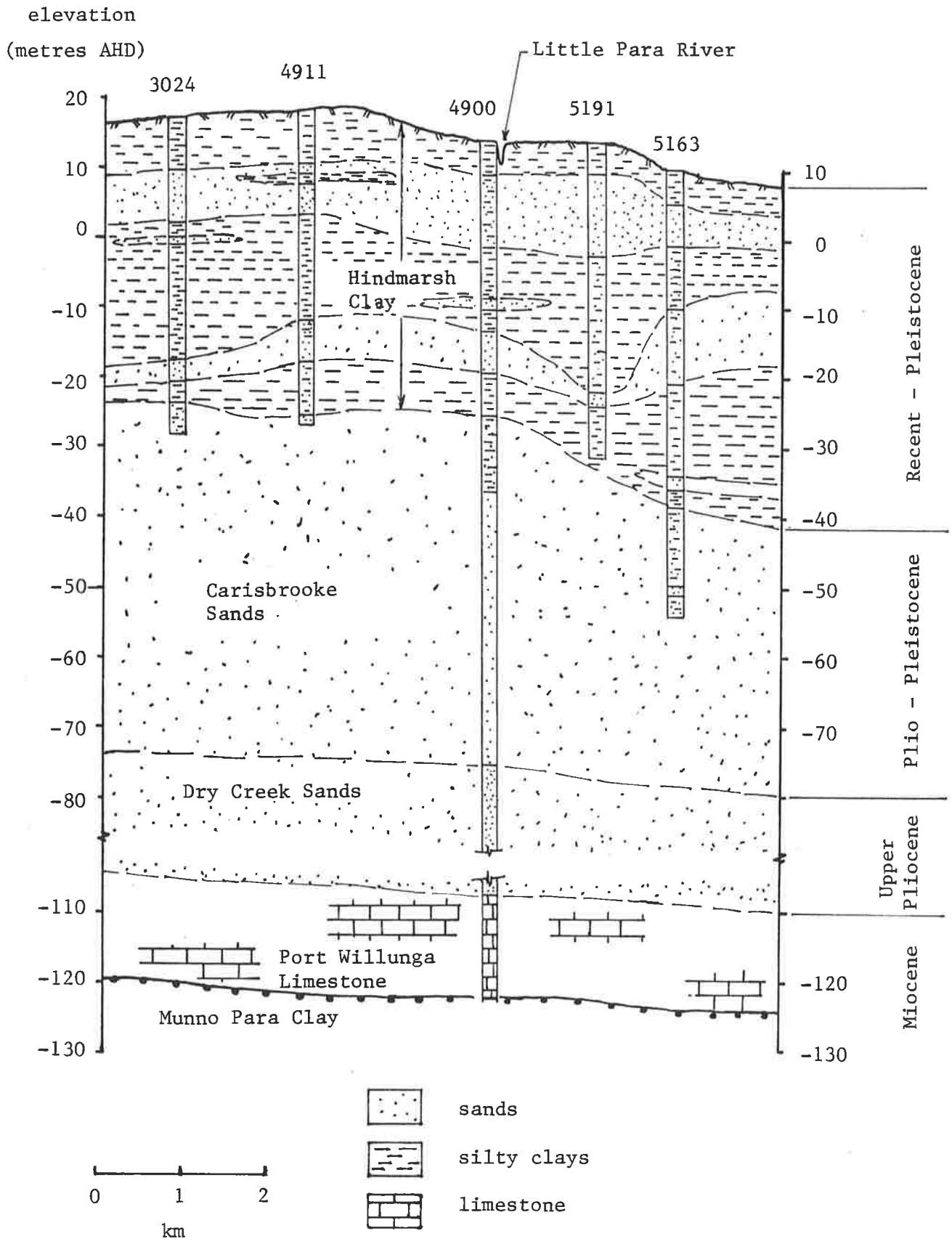

Figure 6.2 Geological section traversing the Little Para River. The Quaternary aquifers are depicted as sandbeds within the Hindmarsh Clay Formation (after Shepherd, 1975).

proportions of clay and silt when more than five kilometres from streams and in the western part of the plain. Miles observed a hydraulic relationship between the rivers and their Quaternary aquifers.

> "Shallow sand beds ..... generally have a direct hydraulic connexion with these streams by both lateral and under-flow and usually yield considerable supplies of goundwater. The yield and water level of these aquifers are however, subject to seasonal variation corresponding to fluctuations in flow of the streams".

Underlying the Hindmarsh Clay are the Carisbrooke Sands - a Plio-Pleistocene transition from the predominantly marine Tertiary to the non-marine Quaternary. These are silty sands reaching a maximum thickness of 50 metres on the eastern side of the plains near the Little Para River. They act as a confined aquifer which appears to be hydraulically connected to the thick underlying marine sand and limestone beds of the Tertiary aquifers. They receive leakage from the Hindmarsh Clay but there is no evidence of any more direct connection with the Little Para River.

A map of the region showing isohalines for total dissolved salts (by electrical conductivity) of water in Quaternary aquifers was drawn by Miles (1952), and revised in a report of the South Aust. Dept. of Mines (1968) and by Linke and Eberhard (1981). See figure 6.3. A plot of Chloride concentrations was compiled from a comprehensive data set also by Linke and Eberhard (not shown). Each map reveals a band of low salinity adjacent the river positively identifying it as a recharge source. The maps indicate the low salinity zone spreads south of the river in the east of the plain and north of the river in the west.

6.4 Field Installations

6.4.1 Gauging stations

A total of fifteen stream gauging stations were used during the study, six of which were equipped with continuous water level recorders for at least part of the study period. The recording stations are situated at

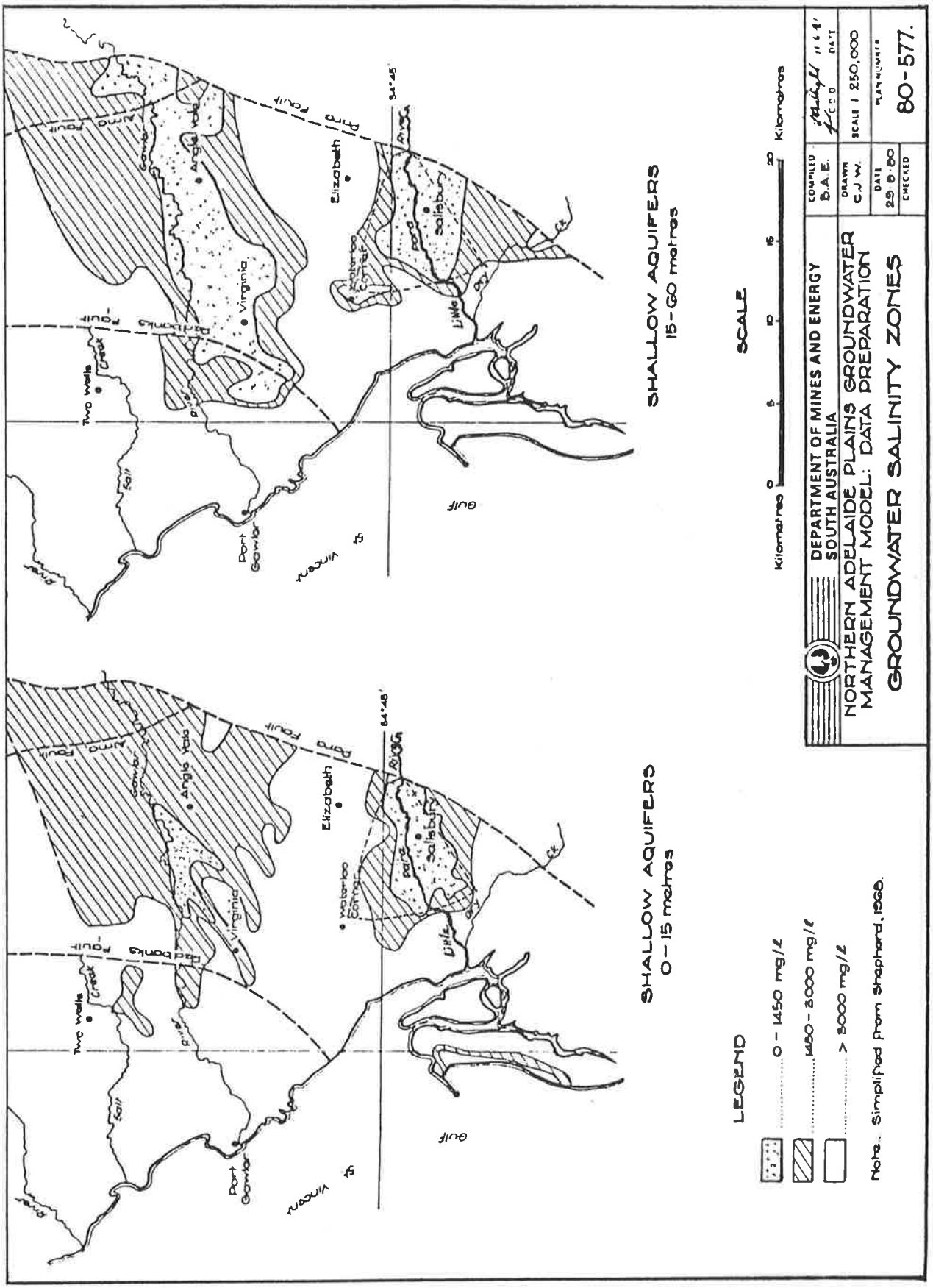

Figure 6.3 Total dissolved salt concentration in Quaternary aquifers in the region surrounding the Little Para River (after Linke and Eberhard, 1981)

sufficiently wide spacings that the difference in discharge rate between station pairs is a significant proportion of the measured discharge rate.

The sites were chosen giving regard to natural controls in the stream, the river channel cross-section and the permeability of streambed materials (to avoid underflow). The control at each recording gauging station took the form of a sharp crested 90^{o} or 120^{o} triangular weir. The steel plate containing the notch was supported by a concrete footing which was keyed into the bed and banks. A two metre wide concrete apron on the downstream side prevented scour from undermining the weir. Stevens F8 (8 day recorders) were replaced by Stevens A71 (3 month recorders) as these became available. A gaugeboard was installed at each station.

A 250mm diameter float inside a stilling well was attached to a punched stainless steel tape. The tape was suspended by a pulley and kept in tension by a counterweight at its other end. Rise or fall of the float was conveyed to the recorder by rotation of the pulley. Sprockets on the pulley engaged punched holes in the tape to prevent slipping.

Gaugings were performed by personnel from the Hydrographic Section of the Engineering and Water Supply Department working under direction of the author. The ratings obtained for each station are shown in Table 6.2. Intermediate gauging stations used either low Crump weirs or natural controls. The natural controls proved to be unstable as can be seen from the square of the correlation coefficient, (r^2) in the table.

Daily discharge was calculated for recording gauging stations. The statistics of these records are displayed in Table 6.3.

6.4.2 Observation bores

During Stage I all available observation bores were monitored. Prior to Stage II a major construction programme was started and 53 observation bores including 14 double piezometers were installed. Ten streambed piezometers were sunk in 1980. A summary of the number of bores is given in Table 6.4.

Table 6.2

LITTLE PARA RIVER GAUGING STATION RATINGS

GS State Number	GS Number LP Study	River km from release valve	Type of Control	EWS Gauging Register Nos	No. of Gaugings	$q = a\ (H-1000)^b$ a	b	r^2	Range of Rating (m)	Highest Gauging m^3/s
504528	-*	-0.30	Notches in crest of reservoir spillway	-	0	-	-	-		
504532	1*	-0.05	Sharp crest 120° triangular weir	1 - 7	7	1.855	2.593	0.970	H<1.16	0.015
504533	2	1.09	Pipe culvert	1 - 6	6	1.738	2.098	0.998	H<1.32	0.16
504503	3**	2.49	Sharp crest 90° triangular weir	33 - 64	31	1.249	2.375	0.998	H≤1.60	
					1	3.040	4.118	-	1.6<H<2.41	12.55
504534	4	3.95	Sharp crest 120° triangular weir	1 - 22	22	2.381	2.493	0.996	H<1.44	0.30
504504	5*	5.04	Short crest 90° triangular weir	78 - 119	40	1.669	2.604	0.995	H≤1.54	
					2	5.501	4.538	-	1.54<H<1.72	1.26
504535	6	6.00	crump V weir	1 - 23	20	14.374	2.824	0.995	H<1.25	0.27
504536	7*	7.98	Sharp crest 120° triangular weir	1 - 30	28	2.054	2.372	0.990	H≤1.40	1.58
					2	8.409	3.909	-	1.40<H<1.65	
504537	8	8.76	Crump V weir	1 - 14	13	39.137	3.278	0.991	H<1.21	0.23
504538	9	9.55	Crump V weir	1 - 15	15	17.513	2.927	0.999	H<1.23	0.23
504539	10	10.26	Natural control	1 - 8	8	2.123	3.440	0.484		
504540	11	11.70	Crump V weir	1 - 12	12	12.936	2.731	0.998	H<1.32	0.58
504451	12**	12.67	Sharp crest 90° triangular weir	1 - 14	12	1.307	2.408	0.996	H≤1.51	1.45
					2	2.767	3.539	-	1.51<H<1.85	
504542	13	14.90	Crump V weir	1 - 12	7	7.981	2.434	0.947	<July 1980) H < 1.22	0.23
					5	9.139	2.456	0.999	>July 1980)	
504543	14	17.22	Natural control	1 - 7	7	0.393	1.289	0.785		
504544	15*	18.95	Sharp crest 90° triangular weir	1 - 12	10	1.297	2.394	0.977	H≤1.51	1.31
					2	2.669	3.464	-	1.51<H<1.81	
				TOTAL	256					

* continuous record available during part of study period.

** base station.

Table 6.3

STATISTICS OF RECORDS FROM RECORDING GAUGING STATIONS

Stn.	Digitized points	Mean no. points / valid day	No. valid days	% valid days from start of record
1	3 676	5.34	688	56.44
3	17 383	13.62	1276	99.92
5	19 031	16.16	1178	96.48
7	6 164	6.85	900	73.71
12	10 615	13.39	793	97.30
15	11 301	14.11	801	92.82

The layout of the fity three observation bores is a compromise between three competing requirements. In the Little Para Recharge Study, it was important to determine the fate of recharged water, requiring estimates of groundwater storage changes and regional groundwater flow directions in the Quaternary aquifers. A grid layout with wide and regular bore spacings is the most cost-effective pattern to meet this information requirement. Secondly, to define the nature of stream-aquifer interaction a concentration of bores in the vicinity of the river is required. For instance Johnston et al (1972) drilled lines of bores perpendicular to a stream to determine the groundwater gradient adjacent to the stream and its affect on exchange flow rates. Thirdly the effect of heterogeneity of the porous medium, which was expected to be most significant on the basis of previous hydrogeological studies, may be determined by clustering together

Table 6.4

TYPES OF FIELD OBSERVATION STATIONS

Stream Discharge Stations

	Stage I	Stage II	Stage III
Recording GS's	3 (1,3,5)	6 (1,3,5,7,12,15)	5 (3,5,7,12,15)
Non rec. GS's	3 (2,4,7)	6 (4,6,8,9,11,13)	5 (4,6,9,11,13)
Natural controls	- -	2 (10,14)	- -

Observation Bores

	Stage I		Stages II and III	
	Shallow	Deep	Shallow	Deep
Existing Mines Dept Obs Bores	12	11	12	11
Private Bores or Wells	1		14	
New Bores 1979 Series	3+3		11+5	
New Bores 1980 Series			*53+14	
River Bed Piezometers Sept 80			**10	
TOTAL	16+3	11	100+19	11

* 3 have been continuously dry
** 4 have been continuously dry
11+5 indicates 5 of the 11 sites have double piezometers
Bores less than 60 metres deep are regarded as shallow.

a number of bores at several locations. Multiple piezometers may be used to determine the vertical hydraulic continuity of the medium.

The approach used in the Little Para Recharge Study is a combination of the above (figure 6.4). Each piezometer was installed with a cable tool rig by Department of Mines and Energy drillers. If more than one distinct water bearing layer in more pervious material was encountered a dual completion in each "aquifer" zone was made using gravel packing around slotted PVC casings and pressure cementing between packings and up to the surface. In the case of single completions the driller used slotted casing at the elevation of the most pervious zone below the water table. Logs of the fifty three holes were recorded by personnel from the Soils and Foundations Section, EWS (South Aust, 1980).

The difference in water elevation between dual piezometers was small in all cases. Vertical hydraulic gradients so obtained were significantly less than horizontal hydraulic gradients. Water quality variations between samples taken from dual piezometers were minor. Where bores were clustered together they gave water elevations which were entirely consistent with the predicted values for those locations based on water elevations in adjacent bores.

The conclusion is drawn that in all observed cases the heterogeneity of the aquifer both horizontally and vertically has an insignificant effect on the representativity of water levels in observation bores. That is the sand beds, although they may be discontinuous and lenticular, are hydraulically connected and the free surface position at any point on a map of the study area may be reliably determined by interpolation from adjacent bores. A contour map of the free surface on 31st March 1980 is shown in figure 6.4 as an example.

Streambed piezometers were hand-augered by Mr. A. Zeluk (laboratory technician) and the author to three metres or to the maximum depth achievable if gravels were encountered below the water table. Each

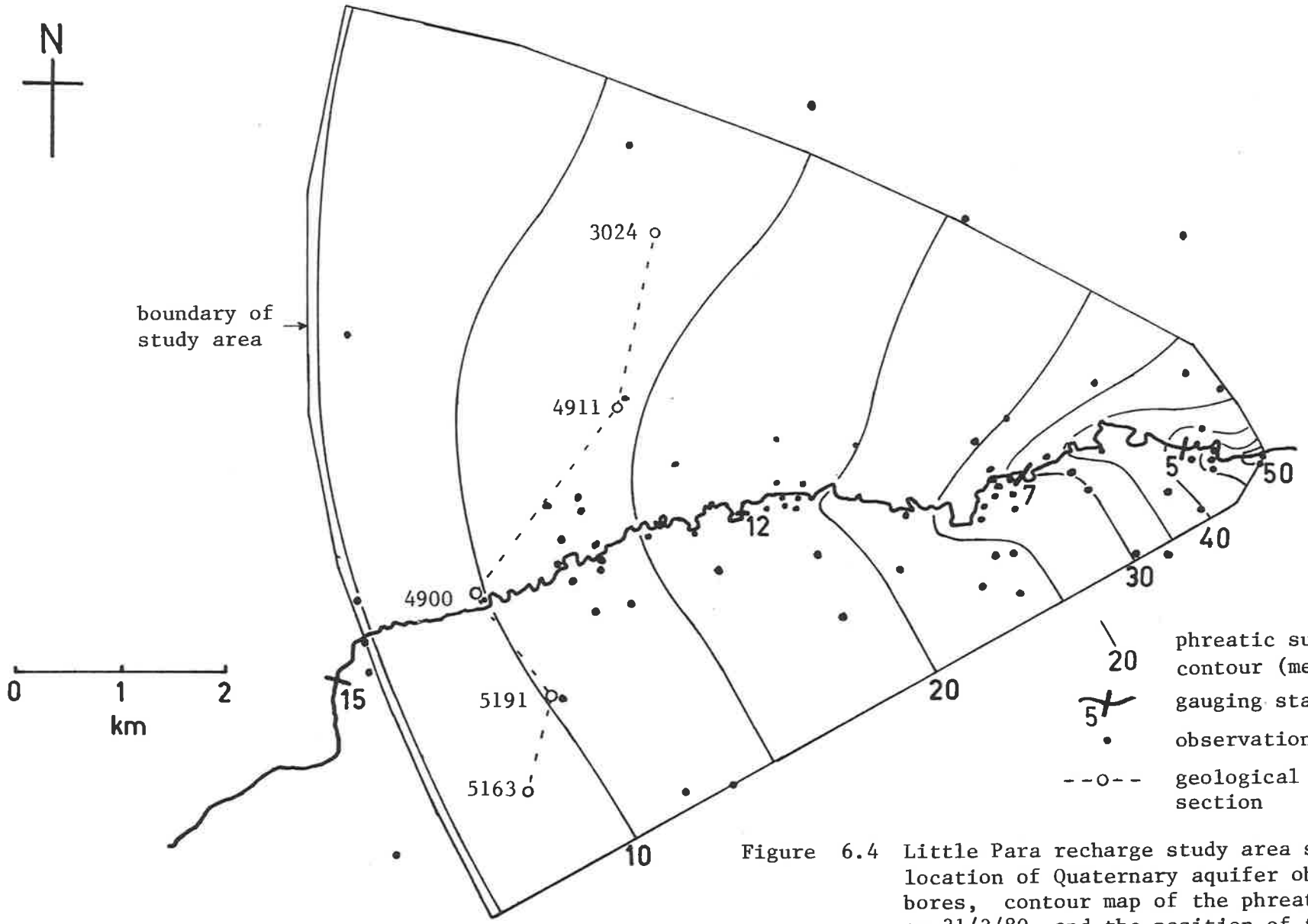

Figure 6.4 Little Para recharge study area showing location of Quaternary aquifer observation bores, contour map of the phreatic surface on 31/3/80 and the position of the geological section (figure 6.2).

consisted of PVC casing, slotted over a 300 mm interval and was completed with gravel packing and cement grouting from the response interval to the surface. These piezometers showed whether hydraulic connection of the stream to the underlying aquifer occurred. The casings extended upwards beyond the expected range of stream stage and were sealed with replaceable PVC caps.

6.4.3 Reservoir release valve

At the start of the joint study the Engineering and Water Supply Department constructed a reservoir release valve chamber and river outlet structure. These were located 200 metres downstream of the dam. The release main is a diversion from the principal reservoir outlet main so water quality was of a high standard, as the elevation range of reservoir water offtake could be selected. The release main bifurcates and passes through two valves before discharging into a vertical concrete outlet pipe near the streambed. The water surges over a small blanket of rip-rap and thereafter follows the natural course of the stream. The use of two valves enables a range of discharge rates to be set up to a maximum of 0.3 m^3s^{-1}. An orifice meter measures discharge rate and this is recorded on a Kent 7 day circular chart recorder and integrated by a clock and cam arrangement to give a digital counter display of accumulated discharge.

6.4.4 Miscellaneous works

Water level recorders were mounted on six bores. For five of these the recorders were contained in a concrete box sunk into the ground at the bore head. The other was located in a frame welded in a 200 litre drum with a steel lid which could be locked down. The drum was secured to the bore casing with a U-bracket and to stakes driven into the ground through eyelets. Although much of the study area is suburban and vandalism was anticipated no equipment in these enclosures was lost or damaged. (Previously the weir at gauging station 5 had been demolished by vandals and had to be reconstructed for this study.)

A concrete well cover was designed by the author and constructed and installed with the help of laboratory staff on a disused well adjacent the river. The land owner permitted the well to be used for groundwater level observations on the condition that the well head was restored to a safe condition. A streambed test pond was constructed in February 1982 and this installation is described in Chapter 7.

6.5 Data Acquisition

A field study of the magnitude and duration of the Little Para Recharge Study demanded considerable human resources. The author's role was to decide on the data collection programme and request personnel or funds from the Engineering and Water Supply Department to enact it. This involved making out a case to support these requests and negotiating with EWS on the priorities for data when considering financial constraints.

Every request for personnel and equipment in the joint study proposal (Dillon, 1978) and the first and second stage progress reports (Dillon, 1979 and 1981a) was granted. However a change of government and policy caused some delay in implementing stage three, which was intended to be continuous with stage two.

An example of the assistance sought for project operation and data acquisition is a list condensed from the first stage progress report: EWS internal supervisor, technical assistant (read gaugeboards, observation bores, groundwater consumption), hydrographers (stream gauging and gauging station maintenance), key- to- disk operator (transfer field data to computer files), programmer (to update and control data files), reservoir keeper (to change valve settings on the release valve), water chemist (to perform chemical analysis on water samples), soils laboratory technicians (to perform streambed infiltrometer tests), drilling crew (observation bore construction and clearing blocked bores), hydrogeologist (for supervision of drilling, bore logging and sampling) and construction personnel (gauging station construction).

Considerable energy was spent in ensuring that each of these people understood their specific task and the value of the information they would provide. The need for accurate observations was stressed. For example the technical assistants were issued with binoculars for taking gaugeboard readings, and the author collected and recalibrated the cables they used for groundwater level observations.

6.5.1 Types of data

Data are classified in two functional groups: those kept on computer files and those not. Models such as the BIEM stream-aquifer interaction model and the regression model (discussed in Chapter 8) are calibrated using data residing on computer files. However the formulation of those models depends largely on information which is unnecessary or inconvenient to store on the computer. This set may be further classified into quantitative data and information (qualitative data).

Maps such as those defining land use or catchment areas and stratigraphic bore logs are examples of the latter. Quantitative data acquired and not saved on computer files consist of chemical analyses of stream and bore water samples, stream gauging data and streambed infiltrometer test results.

Data stored on computer files was derived from a number of sources. The Bureau of Meteorology provided daily A class pan evaporation, rainfall, minimum and maximum temperatures and 9am atmospheric pressure readings. These were hand copied onto standard coding sheets which were treated as described in section 6.5.2. Observations of release rate and integrated discharge were recorded by reservoir keepers. Stream stage readings at nonrecording gauging stations, bore water level observations and water consumption readings at irrigation bores were coded onto standard sheets in the field by technical assistants or the author. Results from surveys of streambed cross-sections and deciles of particle size analyses of streambed soil samples were also hand coded. Data from recording gauging stations

and bores also found their way onto computer files by the process described in sections 6.5.3 or 6.5.4.

6.5.2 Manual data retrieval

A schedule of station observations was drawn up at each stage of the study. Engineering and Water Supply Department personnel carried out these observations under direction of and supplemented by the author during periods of rapid changes in groundwater levels and for occasional check readings. The data was coded in the field onto standard coding sheets designed by the author. EWS personnel collated these and periodically keyed the data into disk storage on the South Australian Public Service Cyber computer and later copied it onto magnetic tape.

After each stage of the study was completed the tape was updated and brought to the University of Adelaide. There it was copied onto disk and backup tape on the University's computer, also a Cyber. This procedure minimized staff time and made best use of existing terminal facilities. The method had the drawback that any systematic data monitoring errors did not become evident to the author until the end of each stage. Instructions were issued to personnel handling data to report to the author any strange observations or difficulties. This circumvented numerous problems but not all of them. The most glaring one was occasional observation bores being overlooked for prolonged periods.

6.5.3 Chart recorder data retrieval

Three types of recorders were used during the course of the study. Initially six surplus Stevens F-type recorders were purchased from EWS for use on key bores and gauging stations. Eventually these were phased out from gauging stations as Stevens A71 recorders became available. The F-type recorders were later replaced at observation bores as the University of Adelaide digital recorders became available.

The F-type charts were hand digitized by part-time assistants and the author at the university and coded onto the field sheets referred to

previously. These were treated in the same way as manually retrieved data except that on installation on the University's computer the data was plotted on a CALCOMP plotter to the scale of the original charts (using Program BPL, see also section 6.6.1 and Appendix D) and the two were overlayed and compared on a light table. Editing corrections were made to the appropriate computer file thereby eliminating errors from the digitizing and the key-to-disk operations.

The A71 charts were digitized by EWS personnel using a digitizing table and pen coupled to a computer. They also plotted the output file and compared it with the original chart to ensure correct digitizing. Normally more digitized points per day were created from A71 charts than from F8 charts and this is reflected in Table 6.3. The digitized A71 data files were added to the tape transferred to the University.

6.5.4 Digital recorder data retrieval

Early in the study the problems associated with the use of Stevens F8 recorders for observation bore monitoring became obvious. Weekly site visits, the length of time spent digitizing and checking bore records, the considerable friction evident in those records and the frequent incidence of recorder failure suggested that an alternative recording method should be found. A survey of commercially available recorders revealed some suitable digital recorders but these were beyond our budget. After consulting Mr. S. Woithe, an instrumentation technician with the Civil Engineering Department, work began on the design of a digital recording system, consisting of a friction-free water level transducer, a solid-state digital recorder and a field reader / computer interface unit. Although taking longer than anticipated the resulting operating system gave most satisfactory performance. At the time of publication it was the subject of an Australian Provisional Patent (No. PF 3149) and under commercial development by Southern Cross Instruments Pty. Ltd., Elwood, Victoria. A brief description of the system developed for this study

appears in Appendix C.5.

Digital recorder data was collected by the author. A digital recorder field data sheet (Appendix C.5, fig. 3) was used to register field data at the times of installing and removing each solid state memory. See Plate 6.1. The memory contents were conveyed through the reader unit into the Civil Engineering Department's PDP computer. A programme was written by Mr. R. Flint (post-graduate student) to allow the real times and data values recorded on the field data sheet to be entered at a terminal and thereby edit the memory contents. Error checks were performed automatically during this process. The resulting files were transmitted to the Cyber for storage and data plotting and processing.

6.5.5 Water quality data collection

Stream water samples were taken at gauging stations and analysed at the State Water Laboratories at Bolivar. A basic analysis of conductivity, total dissolved salts, pH, suspended sediments and turbidity was performed on most samples. On occasions this was extended to include determination of major anions and cations.

Groundwater samples were taken at irrigation bores by market gardeners. The author, accompanied by an Italian interpreter (Mr. P. DeMaria) had previously visited gardeners to inform them of the study and ask permission to monitor bore consumption. In addition the author collected each sample and returned a copy of the results of the chemical analysis to the market gardener.

A double air hose method of collecting piezometer water samples was tested by Mr. D. Clifton (S.A. Dept. Mines and Energy) and the author. Small discharge rates, constrained by small submergence depths, coupled with the undesirable aspect of air mixing with the sampled water ruled out this technique. An unpublished report was provided to the Department of Mines and Energy (Dillon, 1980). Subsequently a small diameter positive displacement pneumatic sampling pump was purchased jointly with the S.A.

Plate 6.3

Fluoroscein dye used as a tracer in the Little Para River downstream of station 7.

Plate 6.2

Trial test of single ring infiltrometer in the Little Para River streambed.

Plate 6.1

Digital recorder replaces a chart recorder (at left) at a piezometer. Mr. S. Woithe inserting the solid state memory.

Dept. of Mines and Energy and the author found it gave a satisfactory discharge rate which succeeded in draining bore casings quickly in a one man operation. It also allowed only minimal mixing of air with the water sample.

At each piezometer the volume of water in the casing was calculated and when twice this volume had been withdrawn a sample was taken. Conductivity measurements were taken during pumping for several bores using a portable meter. In each case the conductivity changed quickly during the first half casing volume and settled to a steady value by one and a half casing volumes. During pumping, water levels were recorded. Water samples were tested for conductivity, pH and major anions and cations at the State Water Laboratories. Results were forwarded on typed sheets via the EWS internal supervisor to the author.

6.5.6 Streambed infiltration tests

Single ring constant head infiltrometers were used to estimate infiltration rates. Initial down hole tests with 90 mm diameter holes gave excessive infiltration rates due to nonuniform flow patterns at the base of holes and disturbance of the soil when hand augering. Thereafter sections of a 200 litre drum, 460 mm diameter were placed on the streambed surface (Plate 6.2) and soil was removed to a depth of 50 mm in a 400 mm wide annulus around each ring. A 5 mm thick layer of bentonite was spread over the cut surface and the topsoil replaced, compacted and dampened. This provided an impermeable skirt to prevent water leaking from the infiltrometer to the surface. In four tests this surface seal failed and results were discarded. Twenty five tests without seal failures were completed at fifteen sites. In all cases the ponded water depth was 300 mm corresponding to the average depth of water in the river during releases.

Infiltration rates varied from 0.05 m/day to 6.5 m/day. Tests at the same site, separated by less than three metres revealed variation of the same order as the mean value of infiltration. No trend in infiltration

rates with river distance from the release valve was observed.

Tests using the rate of decline of water level in natural pools in the stream on the cessation of flow gave infiltration rates which were significantly lower than those from infiltrometer tests. This is due to the reduced proportion of horizontal flow, which is related to the ratio of wetted perimeter to surface area. Secondly pools may be expected to have lower infiltration rates than other parts of the streambed due to deposition of silts and clays during ponding, although this was found to be insignificant for the artificial streambed pond experiment described in Chapter 7.

6.5.7 Cross-sections and particle size analyses

Streambed cross-sections were surveyed at 47 locations, 25 of these under close direction of the author. At the latter sites flow cross-sections were measured and plotted for different reservoir release rates. Stream width, wetted perimeter, wetted cross-section area and elevation of the water surface were derived from the plots by the author and this data was keyed into a disk file on the University's Cyber computer.

Particle size analysis was performed by Mr. A Zeluk and the author on 43 samples of streambed material. Grain sizes at decile intervals for each sample were also keyed into file storage.

6.5.8 Streamflow observations

Manual monitoring of gauging station water levels was performed following some step changes in release rates. Hydrograph data were recorded on field data sheets and subsequently keyed into computer files.

As infiltration is slow with respect to the mean velocity of flow, the residence time of water in a reach has an effect on the proportion of discharge which is infiltrated. Observation of the arrival time of a response to an upstream step discharge change is not a valid indication of residence time (or mean velocity). A mean velocity may be determined by

dividing the discharge rate by the mean wetted cross-section area of a reach, which may be estimated from a series of randomly located cross-sections.

Alternatively a readily detectable tracer such as sodium chloride or a dye may be added to the flow at a known concentration at the upstream end of a reach. A graph of electrical conductivity or fluorescence at a particular frequency, respectively, for the downstream end of the reach provides a measure of the mean velocity of flow. Two undergraduate engineering students, Mr. M. Elford and Mr. T Potter, undertook such a study on a reach of the Little Para River under the direction of the author in 1979. Fluoroscein dye was released into the stream at a constant rate and known concentration at gauging station 7 (Plate 6.3) with the aim of measuring seepage rates in the reach downstream. At various downstream points water samples were taken at regular intervals. These were analysed with a fluorimeter at the State Water Laboratories by Mr. W. Ranford. Fluorescence was calibrated against fluoroscein concentration in solutions of Little Para River water. Hence a mass concentration hydrograph could be developed at a downstream sampling point. The method proved to be unreliable for seepage rate calculations due to absorption losses and insufficient duration of injection compared with the travel time to the first sampling point. However mean travel time could be determined as described in section 6.6.6.

6.6 Data Processing

In this section reference is made to a number of FORTRAN-4 computer programs written by the author. Each program is briefly documented in Appendix D and its listing is given on a microfische in the envelope inside the back cover of this thesis.

6.6.1 Piezometer water elevations

The first operation performed on the University's computer was to screen the data for spurious values. This process has been described for the data retrieved from recorders. Manual bore water level readings were adjusted using a two stage error detection process. (Program BPL). Firstly each reading was compared with the value linearly interpolated from the preceeding and subsequent readings at that bore. If the difference exceeded a specified threshold the estimate for the number of points in error increased by one. This estimate was used as the seed value in the IMSL routine for cubic spline data smoothing by error detection. A list of the points suspected to be in error was produced. These were inspected along with streamflow records, meteorological records and records of adjacent bores for that period and the data was either deleted, corrected or left unchanged.

Data to be corrected were usually obvious due to either a misread measuring tape marker (spaced at 2 metre intervals) or an incorrect bore identification or date. Where a rise in bore water level occurred which could not be attributed to streamflow or rainfall penetration, nor an error in the preceding readings that item of data was deleted from the file. Where a fall occurred it was compared with the historical hydrograph for that bore. Falls too rapid to be attributed to groundwater mound dissipation, and preceded by data in sympathy with recharge, were deleted from the file.

The last operation removed readings affected by short term drawdown from nearby consumption bores. This "valid" data was rejected on the grounds that each bore was to represent regional groundwater conditions not site-specific conditions adjacent to local pumping. If consumption from a bore caused a regional decline in groundwater levels this would be reflected in the readings from the nearby observation bore after the transient drawdown had abated.

Once all groundwater levels had been edited they were corrected to a common datum, Australian Height Datum (AHD), by subtracting observed water depth from the elevation of the top of the bore casing (Program BAHD).

The hydrographs of selected bores were plotted on standard graphs by the CALCOMP plotter using Program BPLOT. An example of the output of this program is shown in figure 6.5. Another program, BSTAT displays the Australian Map Grid coordinates and the mean, standard deviation, minimum, maximum, range and number of readings of groundwater elevation for each bore. An array of interpolated (within time span limits) groundwater elevations on selected dates for all bores is provided by program BORFL. This was used to produce five hand plotted groundwater elevation contour maps at six month intervals during the study period. (Dillon 1983a, chapter 3). After using a planimeter storage changes below the free surface were calculated and knowing recharge and groundwater consumption a shallow aquifer water balance was determined.

6.6.2 Gauging station discharge

The verified stream stage data were combined with the gauging station ratings (Table 6.2) to give a sequence of instantaneous discharge rates. Providing adjacent points were no more than 12 hours apart the discharge rate was assumed to change linearly with time in the intervening period. Hance daily discharges could be calculated. The accounting period started and finished at 9am for consistency with the daily rainfall and evaporation readings which were taken between 8.30am and 9am. The output of program QPL, which performs this task, is in the form of a calendar of daily discharge for each recording gauging station, for example see Table 6.5.

The daily discharges for all recording gauging stations were combined to produce a file, STBMDP which is indexed according to date. In this form the BMDP statistical software could be readily harnessed to give daily discharge correlations between gauging stations. (The BMDP package of programs was produced by the Department of Biomathematics, University of

California, Los Angeles (Dixon et al, 1981) for statistical description and analysis of data.)

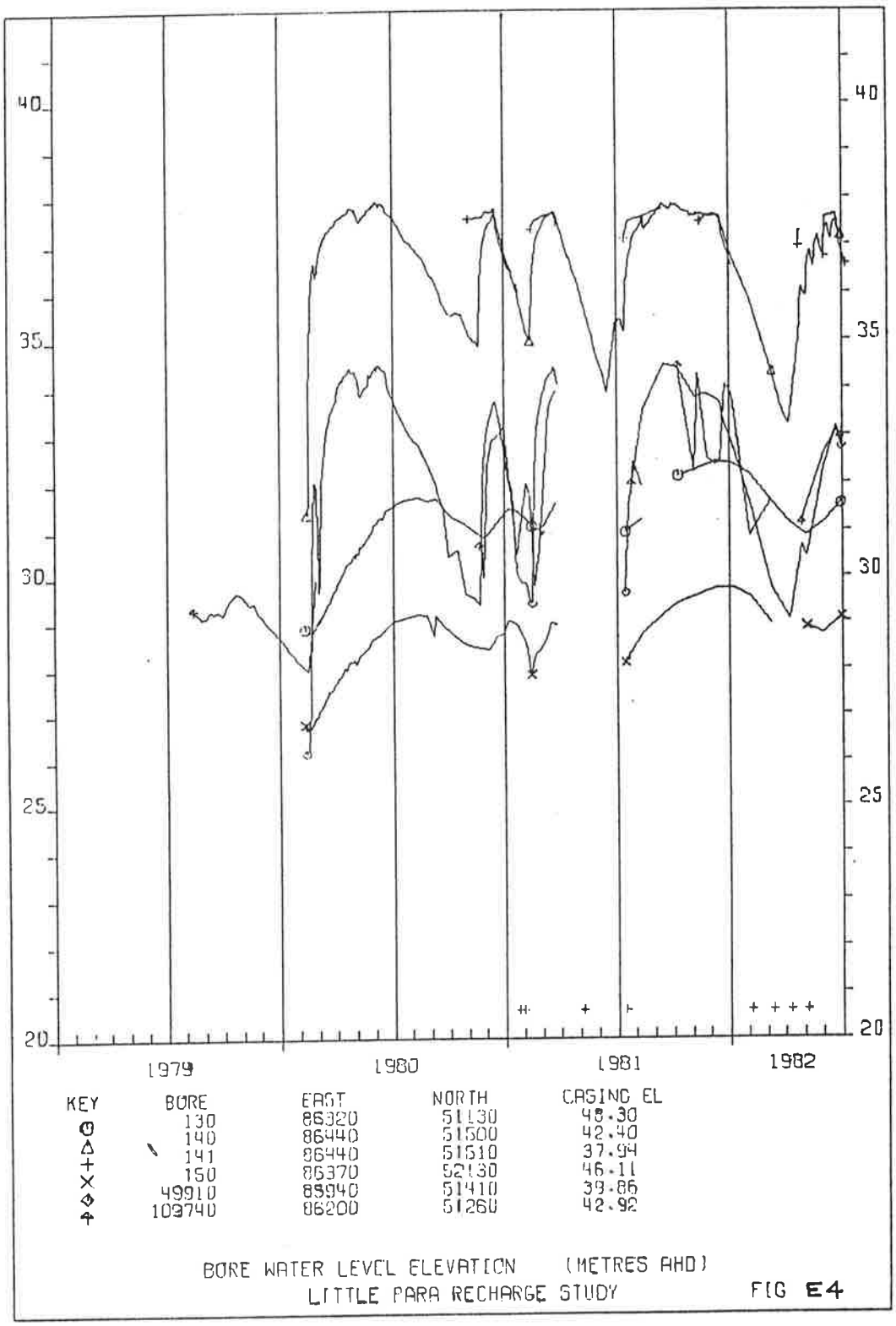

Figure 6.5 Hydrographs of selected observation bores (typical output of program BPLOT).

Table 6.5

Calendar of daily discharge at station 5, 1980 (typical output of Program QPL).

STATION 05 1980
DAILY DISCHARGE (MEGALITRES)

DAY	JAN	FEB	MAR	APR	MAY	JUN	JUL	AUG	SEP	OCT	NOV	DEC
1	.4	.1	.1	15.7	17.9	23.9	1.0	.7	.5	.2	.4	22.5
2	.2	.0	6.1	17.3	17.5	23.9	1.7	.7	.7	.2	.4	23.0
3	.1	.0	10.7	17.5	17.6	19.6	2.2	.8	.5	.1	.3	24.6
4	.0	.1	10.3	17.8	14.3	21.6	2.1	.6	.5	.2	.2	23.5
5	.1	.2	10.7	17.8	.8	18.2	2.0	.6	.4	.1	1.4	23.2
6	.1	.2	10.5	17.7	.5	17.9	1.2	.6	.4	4.6	2.3	23.2
7	.1	.1	10.5	17.6	1.0	17.9	1.1	.6	.4	2.5	1.4	23.1
8	.0	.1	10.5	17.6	.4	17.7	1.1	.6	.4	.6	.6	23.1
9	.0	.1	11.1	17.6	.2	18.2	1.0	.5	.4	.6	.5	22.6
10	.0	.1	10.5	17.6	5.7	14.3	1.0	.5	.8	.4	.4	22.6
11	.0	.0	11.1	17.5	12.0	12.0	1.0	.6	.6	.7	.2	22.6
12	.2	8.3	10.9	17.6	13.1	11.8	.9	.5	.4	2.2	.1	23.1
13	.3	9.2	10.9	17.6	11.7	11.7	.8	.5	.4	2.4	.1	23.2
14	.1	9.6	11.0	17.5	11.6	11.5	.8	.5	.4	.7	.1	24.0
15	.1	9.8	11.1	17.4	11.5	11.5	.7	.7	.5	.5	.1	23.2
16	.0	10.1	11.2	17.4	11.6	12.6	.9	.6	.5	.4	.2	23.5
17	.1	10.2	11.0	17.5	11.8	12.3	.7	.6	.4	.3	.0	10.0
18	.0	10.4	10.8	18.7	11.6	5.4	.9	.6	.5	.4	.1	1.2
19	1.3	10.3	10.6	18.5	11.7	.7	.6	.6	.6	.4	14.0	.7
20	.4	10.3	10.8	17.5	11.9	.5	.6	.6	.6	.5	22.0	.3
21	.1	10.3	10.4	17.8	15.9	.5	.6	1.2	.2	.5	22.3	.1
22	.1	10.7	10.7	18.9	17.7	.5	.6	1.1	.3	.4	22.5	.0
23	.1	10.8	10.8	18.9	17.6	.4	.5	.7	.2	.3	22.8	.1
24	.1	10.8	10.9	18.6	17.6	.4	.5	.6	.2	.4	22.6	.1
25	.0	6.7	10.8	17.8	17.7	.4	.5	.6	.2	.3	22.6	.0
26	.2	.5	10.7	18.2	17.6	.4	.5	.6	.2	.2	22.4	0.0
27	.1	.2	10.7	18.0	22.0	1.1	.5	.6	.2	.1	22.3	0.0
28	.0	.2	10.7	17.8	24.4	4.1	3.9	.5	.2	.7	22.5	0.0
29	.0	.1	10.8	17.7	23.9	2.2	3.3	.5	.2	.4	22.7	0.0
30	.1		11.0	17.7	23.6	1.3	1.2	.5	.1	.3	22.6	0.0
31	.1		10.8		25.5		.8	.5		.3		0.0

MONTHLY DISCHARGE (- = PARTIAL SUM)

4.5	137.5	320.2	532.7	419.3	294.9	35.3	19.4	12.0	21.8	270.2	383.9

MIN AND MAX DISCHARGE RATE (LITRES/SEC)

0.0	0.0	.0	125.3	.9	3.6	4.7	4.4	.4	.2	0.0	0.0
31.6	167.9	131.6	266.0	321.1	286.1	117.5	26.9	36.3	121.0	276.0	374.0

3 MONTHLY DISCHARGE

462.2	1246.8	66.6	675.9

NO OF DAYS DISCHARGE NOT CALCULATED = 0 DISCHARGE FOR YEAR = 2451.5

-1 = ABOVE STN RATING. -2 = MISSING RECORD.

6.6.3 Meteorological data

Meteorological data came directly from EWS observations or was copied from Bureau of Meteorology records which had been checked for obvious errors by Bureau staff. Daily rainfall readings for different stations were compared to ensure that dates of high rainfalls were consistent. Where missing data had been incorrectly set as zero, the subtotal recorded as the first subsequent non-zero reading was partitioned according to daily rainfall or evaporation at adjacent stations, giving an estimate for the missing data. Program EPL was used to print out calendars of daily rainfall and evaporation with or without CALCOMP plots. Program EPLT performed the same function for daily temperature and atmospheric pressure data. The file containing all daily meteorological data was reformatted to give all data indexed with respect to date. The new file named METBMDP was in a form suitable for processing with the BMDP package.

Combining STBMDP and METBMDP provided a file COMBMDP from which correlations of daily discharge and discharge loss for selected meteorological conditions could be readily obtained using BMDP. This information was required to perform the investigation of alternative reservoir release policies, which is reported in chapter 8.

6.6.4 Groundwater consumption

The irrigation bore meter readings were sorted onto a separate file for processing. These data gave considerable trouble due to very frequent meter failures and misreadings. As variations in stream discharge loss rates were not dependent on irrigation pumping on a short term time scale it was more expedient to revert to annual consumption figures held by the Engineering and Water Supply Department. Their readings were taken by meter readers with horticultural experience who could make reasonable estimates of crop water requirements and crop areas. The mean monthly proportions of annual irrigation demands were calculated by Linke and Eberhard (1981) for the Northern Adelaide Plains irrigation area. The

original set of meter readings was regarded as a standby data source if more detailed pumping information was required. Some of these data were used to assist in editing piezometer water elevation records.

Annual irrigation demands for each year of the study were obtained by adding consumptions of each bore within the study area (Table 6.6). Over the study period the mean annual groundwater consumption in the Little Para study area was 700 ML with only 200 ML of this pumped from Quaternary

Table 6.6

GROUNDWATER USED FOR IRRIGATION.
(megalitres)

Year	(a) Northern Adelaide Plains	(b) Little Para study area total	(c) shallow aquifers Little Para study area	(b)/(a) %
1971	17,260			
1972	22,770			
1973	17,820			
1974	14,500			
1975	17,120			
1975/76	17,250			
1976/77	20,330			
1977/78	20,620			
1978/79	19,020	753	197	4.0
1979/80	15,350	675	191	4.4
1980/81	18,990	718	225	3.8
1981/82	17,530	678	220	3.9
Mean	18,210	706	208	3.9

(a) by subtracting ICI quota (1130 ML) from total consumption.

(b) and (c) area defined by figure 6.4.

aquifers. None of this was pumped from near the stream where it was hydraulically connected to the aquifers and the small volumes pumped did not prevent hydraulic connection where the stream was hydraulically disconnected. Hence groundwater consumption induced no additional seepage from the streambed during the study period.

6.6.5 Streambed data

The 10, 50 and 90% passing sizes of streambed materials were plotted with respect to river distance from the release valve (Dillon 1983a, Appendix I) (not shown). No trends were apparent for the 10 and 50% passing sizes but the 90% passing sizes for stream surface material and underlying or bank material both decreased in a downstream direction, as expected. Stream width and cross-section area showed no significant trend with river distance, but both increased with discharge rate, as expected. BMDP scatter plots and regression equations are given in Dillon (1983a, Appendix I) and not shown here.

6.6.6 Fluorometric data

Hand calculations were performed by the author using the data presented by Elford and Potter (1979). A complete dye concentration hydrograph was obtained for only one point 480 metres downstream of station 7 where the dye was injected (figure 6.6). This produced a fluoroscein mass loss of 13% (after compensation for chemical reactions after sampling) comparing favourably with losses of 20% observed by Smart and Laidlaw (1977) in a peaty stream. Losses were mainly due to streambed seepage with some adsorption of dye by streambed materials and photochemical decay. In addition decay with time was observed for samples stored in a dark cupboard at constant temperature. This was possibly due to slow chemical reactions with Chloride ions in Little Para River water. These were also observed and documented by Andre and Molinari (1976). A calibration based on the time lapse between sampling and testing in the fluorimeter was used to correct for this effect.

t_{c7} = time of centre of mass of fluoroscein at station 7.
t_{c480} = " " " " " " " 480 metres downstream of station 7.

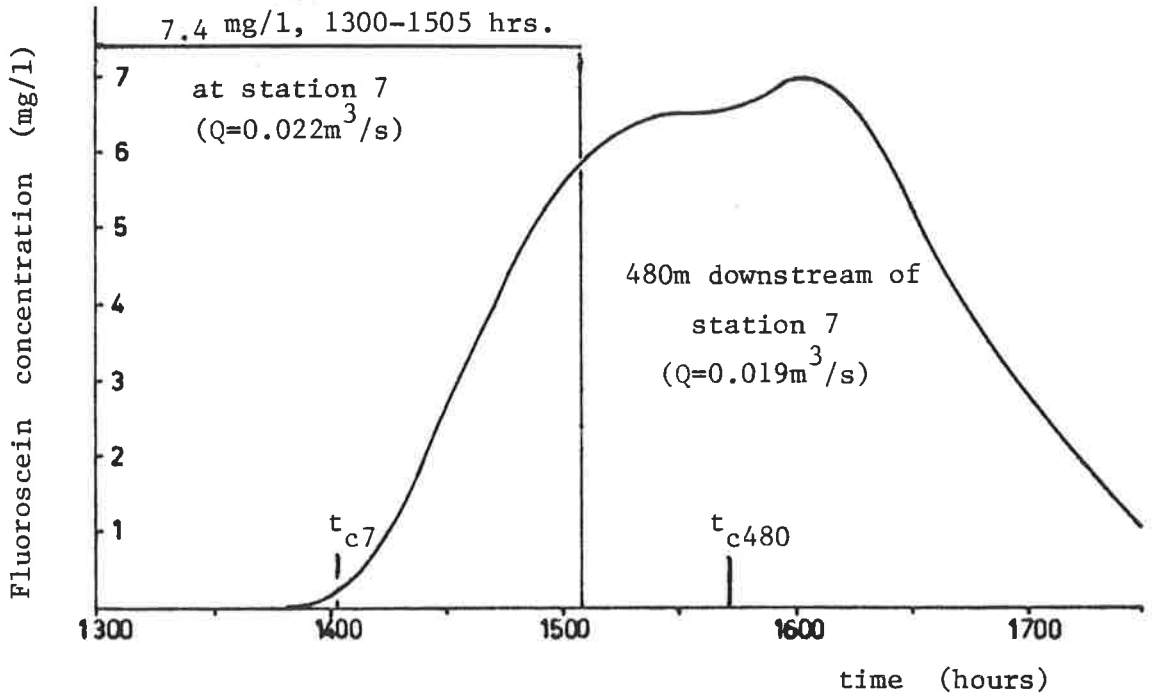

Figure 6.6 Fluoroscein concentration versus time 480 metres downstream of the point of injection, station 7.

The steady discharge rate at station 7 was 0.022 m^3/s and the time lapse between 50% of fluoroscein mass entering the stream and passing the downstream station was 100 minutes. This gave a mean velocity of 0.08 m/s and mean cross-section area of 0.28 m^2. Due to the cost of tracer sampling and analysis this method was not employed for other flow rates or reaches and instead a series of cross-section surveys were used to provide this information.

6.7 Other Sources of Data or Information

Aerial photographs and visual inspection provided information on land use. In particular irrigation areas and residential areas could be defined. Department of Lands 1 in 10,000 scale cadestral maps were used to record this information.

Catchment areas for urban drainage were taken from a flood study

report by consulting engineers B.C. Tonkin and Associates (1981), and the subcatchment areas determined by planimetry.

Geological logs of observation bores were recorded by the Soils and Foundations Section, EWS (South Aust., 1980). This also contained geological sections to a depth of 40 metres. A series of reports of earlier geological or hydrological investigations in the same area, (listed in section 6.3) provided useful background information.

Only data with particular reference to model calibration and validation in Chapters 8 and 9 or small data samples typical of much larger compilations are presented in this thesis. The comprehensive data set is presented in the form of tables and figures in the report and appendices of Dillon (1983a) including ; discharge of recording gauging stations, phreatic surface levels at observation bores, meteorological data, groundwater quality analyses, Little Para River water quality analyses, streambed infiltration test results and river cross-section profiles.

In addition, chapter 5 of the same report identified the data requirements for streambed recharge studies having a range of objectives, with the advantage of hindsight of the Little Para recharge study.

CHAPTER 7

INVESTIGATION OF INFILTRATION FROM A STREAMBED POND

7.1 Introduction

A fourteen metre long test pond was formed in the streambed of the Little Para River by building two embankments across the channel at a selected location and filling the intervening section with water. The inflow of water, storage in the pond and hydraulic gradient and moisture content variation beneath the pond were measured over a six week period.

The aims of the experiment were to reveal the mechanics of water movement below a representative section of the streambed on initial ponding and to show the fate of water in the soil profile when the pond dries. The first could be compared with the Green-Ampt theory used in the BIEM model and the second allowed estimates of evaporation losses from the streambed under various reservoir release patterns.

7.2 Site Selection and Planning

The factors taken into account for site selection were :

- access by vehicle
- risk of vandalism
- proximity to existing piezometers
- narrow channel width at embankment positions.
- stable stream banks
- uniform streambed appearance
- absence of surface gravels (for hand drilling)
- absence of trees (and roots)
- presence of depression and rise in stream invert
- water supply
- equipment storage

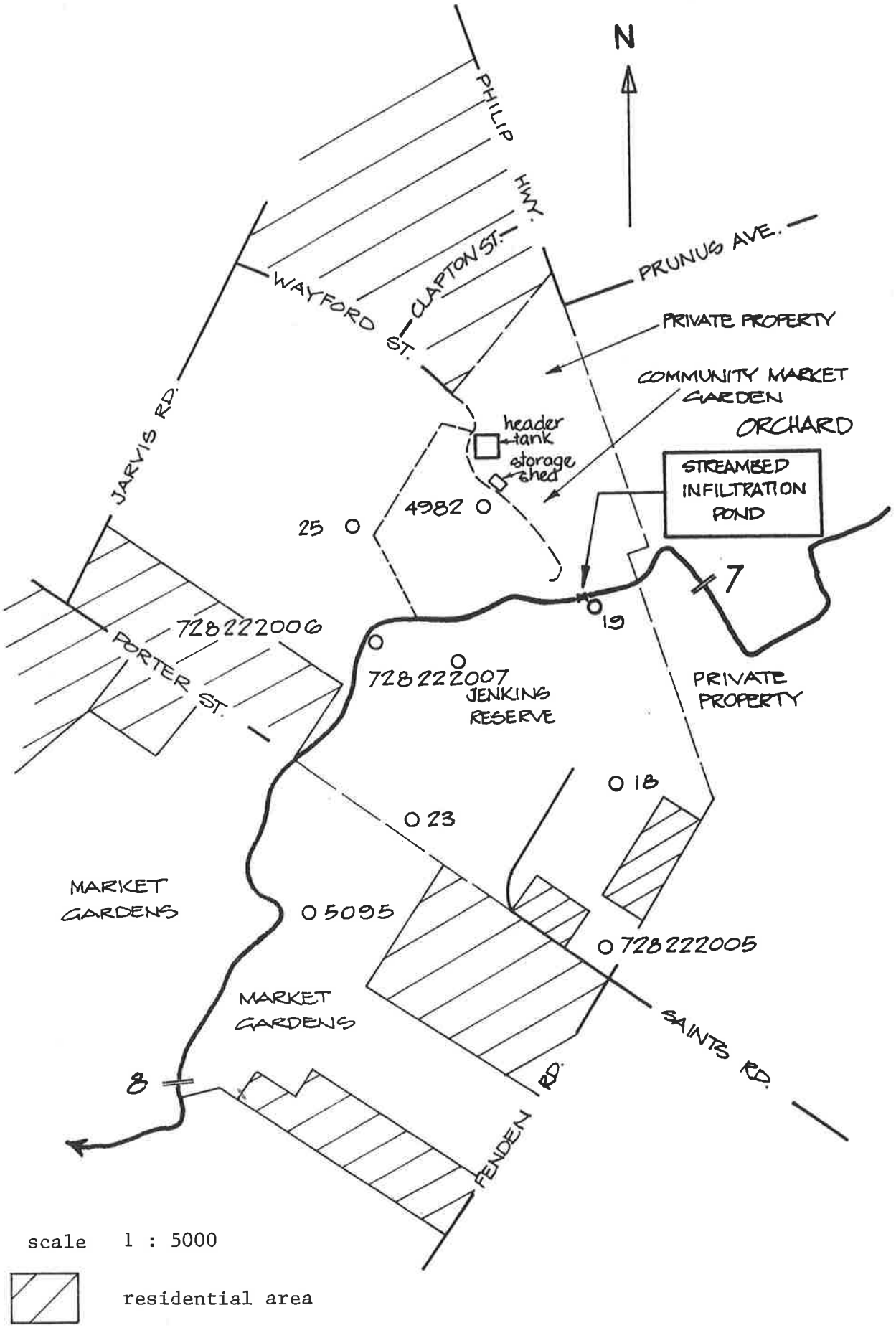

Figure 7.1 Location of streambed infiltration pond.

The selected site (figure 7.1) had the most promising compromise of the above features. Its biggest disadvantages were the relatively wide downstream embankment required and presence of river red gums with their roots invading soil below the pond site.

Vehicular access from the north and south was through Salisbury council property. A community market garden on the northern side provided a water supply from a bore tapping a Quaternary aquifer. As the water was from a shared supply and controlled by the various gardeners the ability to regulate flow was not as simple as expected. When the bore operated water pressure increased considerably. On two occasions gardeners inadvertantly cut off supply to the pond overnight. A site layout diagram appears in figure 7.2.

Hydraulic potential measurements through the soil profile were required to identify the flow mechanism. It was assumed that the heterogeneous mixture of materials would require several flights of tensiometers. Two sets were installed, one on a shoal (elevated streambed invert) and one in a depression. It was suspected that the silts accumulating in the depression would reduce the infiltration rate. With each set of tensiometers neutron moisture meter access tubes were installed. Five tubes reaching a maximum depth of 5.3 metres were positioned adjacent the tensiometers. Temperature measurement probes and meters to record the volume of water entering the pond were installed.

A water balance calculation was performed using the inflow and the volume in storage, to calculate the outflow. The moisture measurements showed changes in water storage in the soil profile above the watertable.

The Little Para River flows through residential areas of Salisbury Park, Elizabeth Vale, Elizabeth South, Salisbury North, Salisbury and Bolivar. The river acts as a recreation focus for residents particularly children. All parts of the river are accessible but some sections are inconvenient to reach. From past experience construction work draws the

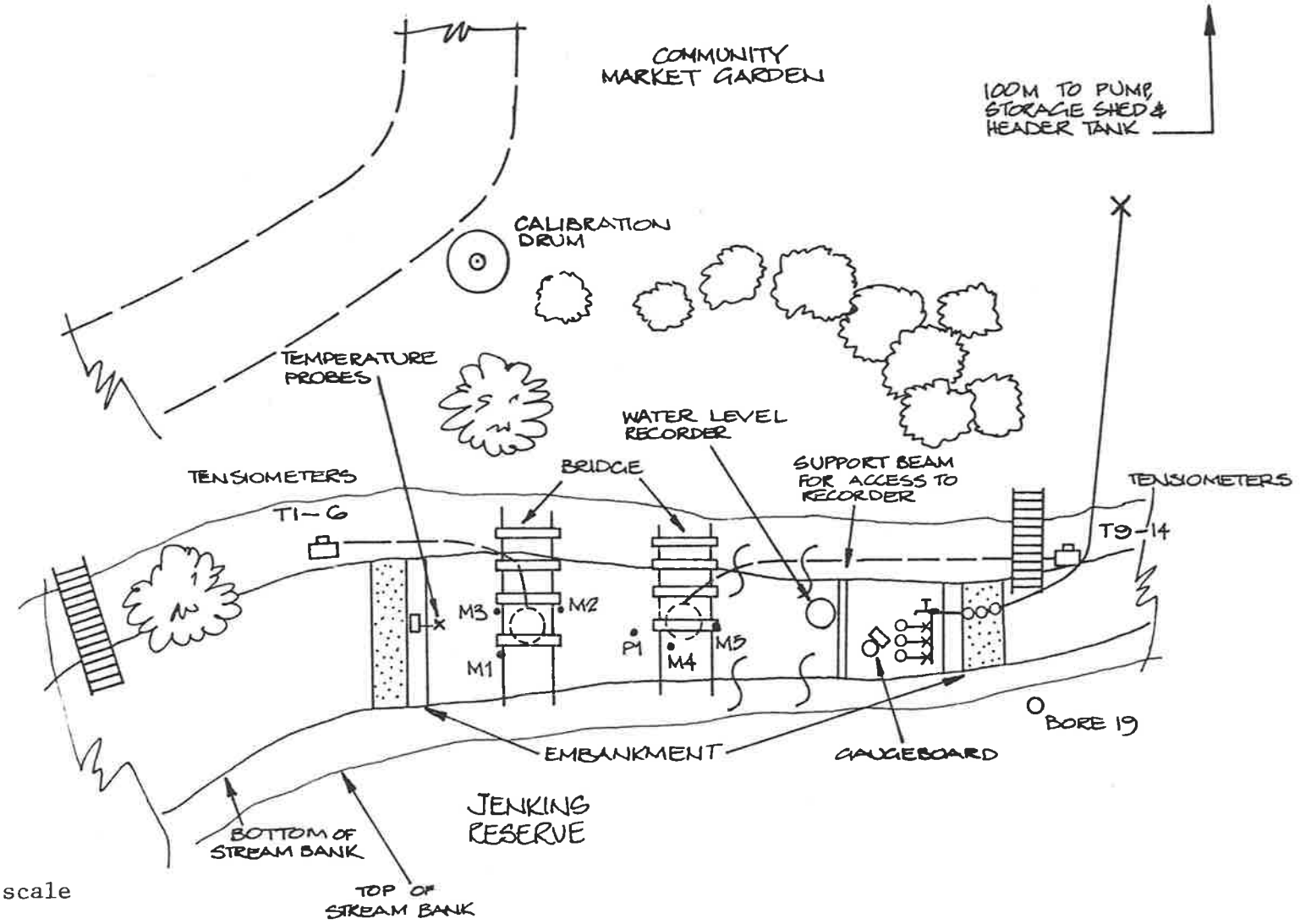

not to scale

Figure 7.2 Infiltration pond site layout diagram.

unwanted attention of children so it was decided to perform no siteworks until the summer school holidays had finished. With the prospect of autumn rains and an academic workload commencing in mid-March it was thought unlikely that the experiment could be extended beyond the first week of April.

7.3 Construction

A tight construction schedule was set to start on the first day of the school year, 8th February 1982 and to be completed two weeks before the commencement of the University academic year 15th March. In order to keep to schedule one of the six proposed neutron moisture meter access holes was not dug, and two others did not reach their intended depth.

7.3.1 Tensiometers

The pattern of the flights of tensiometers is shown in figure 7.3. Separate holes were used to avoid the problem of hydraulic linking of tensiometers through under-compacted backfill. The ceramic cup of each tensiometer was soaked in boiled rainwater for at least 24 hours before installation to saturate the pores. Each cup was 120 mm long and 45 mm in diameter with its centre of response 70 mm from the end to which the tubes were attached. Cups were placed in position at measured depths below the surface datum in 100 mm diameter hand-augred holes. Sifted in-situ material was packed firmly around each cup and the hole was backfilled and compacted in 100 mm layers using soil in the reverse sequence to the stockpiling sequence during excavation. In each case the compacted density approximated the original density as there was only a small handful of soil left over on each occasion.

Each cup was connected to a small bore mercury-water manometer using high pressure nylon brake tubing. Following a procedure outlined by Watson and Ziersch (1977) all air was expelled from the lines by boiled rainwater using a hot water bottle as bellows. After sealing the flushing tube and allowing time for water to flow through the ceramic cup for pressure

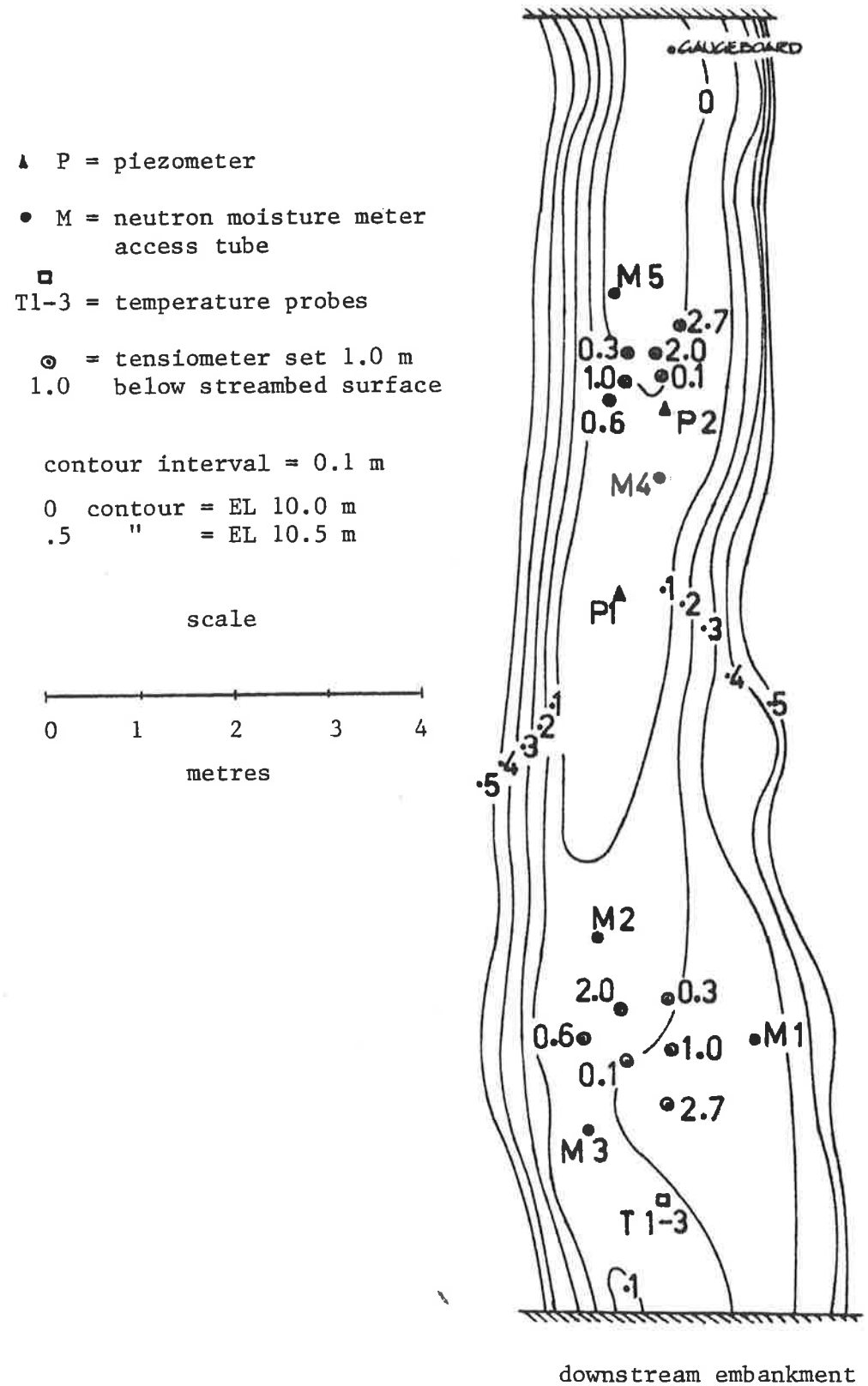

Figure 7.3 Plan of pond showing location of piezometers, access holes, tensiometers and temperature probes.

equilibrium in the cup with the water pressure in the surrounding soil, the tensiometer was ready for use. A level survey related the elevations of the ceramic cups and the datum levels of the manometers to the temporary bench mark. The manometers were held in place in wooden boxes on 50 mm x 50 mm wooden stakes which were concreted into 0.8 m deep holes dug outside the embankments at each end of the pond. Ceramic cups and manometers were loaned by the Soils Division of the S.A. Department of Agriculture.

7.3.2 Neutron moisture meter access holes.

A number of installation techniques are listed in chapter 7 of Greacen (1981). Only one of these was suitable for the test site where drilling rig access was not possible, the soil contained stone layers and the desired depth of the access tubes exceeded 5 metres. It was intended that this method (method 5) be used, by constructing an oversized hole and conveying a measured volume of slurry into its base before pushing in the access tube. A test hole near the site was dug and an attempt made to install an access tube using a slurry mix of 40% kaolinite, 10% Portland cement and 50% water by weight. A major problem arose. The slurry became more viscous when placed in the bottom of the hole due to absorption of water by the soil. This meant that the force required to push the access tube into the slurry was significantly larger and in this case with a 125 mm augred hole and 50 mm diameter PVC tubing, a depth of less than 0.5 m could be reached in a hole more than a metre deep when pushing the tubing by hand.

It may have been possible to persevere with this technique by using more water in the slurry and fixing a tripod with ground anchors to jack the casing into the hole. The risk of an access tube becoming stuck without the slurry reaching the surface and allowing readings over only a fraction of the intended depth appeared to be quite high. An alternative of placing the access tube in position and using a small diameter tube to convey the slurry to the annulus at its base was considered. However this

would have required a larger diameter hole and thicker sheath of slurry than desirable. Also the problem of casing buoyancy in the slurry could not be discounted.

Consequently a new technique was tried. This involved hand-augering a slightly oversized (60 mm diameter) hole and then lowering the aluminium tubing (52 mm diameter) to the full depth. A dry mixture of fine sand and cement were funnelled into the air gap annulus and a small vibrator used on the access tube to encourage the flow of the material to fill the gaps over the length of access tube. The top 150 mm of the annulus was filled with a mixture of bentonite and cement powder and covered with surface soil and moistened.

The objective was to prevent the formation of airgaps even at the expense of partially compacting the soil adjacent to the access tube. Air gaps would be expected to have acted as drains and may have prevented the formation of perched mounds. At the least they would be expected to affect the count rate of the moisture meter. In some access holes gravel up to 40 mm was retrieved, indicating that the hole cross section was enlarged in some parts of the profile. This technique of access tube installation brought some difficulties in neutron moisture meter calibration which are discussed in section 7.5.2.

In order to reach the access tubes during ponding without disturbing the streambed two eight metre span bridges were constructed across the stream. Each consisted of two expanding floor beams spaced at 1.2 metre centres. To these were wired several galvanized iron sleepers, to make access easy from the north bank but to discourage pedestrians from using the bridge as a crossing. Steel pins were driven into the banks at angles under the beam ends to stabilize the bridge supports. PVC casings were placed over the aluminium tubes and tied to the bridges. These were fitted with PVC caps to keep the access tubes dry.

7.3.3 Water supply

A length of 25 mm diameter hose was connected to a tap on an unused gardening plot and three standard water meters were fitted in series at the outlet (Plate 7.1). This branched to give direct discharge from a tap and to feed three ball-cock valves in parallel. Hessian sacks were tied over the direct outlet and placed on the bed where the float actuated discharges occurred. With these measures streambed scour was prevented. The range of water pressures encountered due to the switching of the bore pump was beyond the regulating ability of the ball-cock valves. Hence stable water levels could not be maintained in the pond for periods longer than about 12 hours the usual interval between pumping. The water level rose up to 50 mm due to pumping.

7.3.4 Thermometry

A "Wescor" field psychrometer was used with copper-constantan thermocouples to give temperature readings in the soil near the downstream embankment at depths of 0.1, 0.3 and 1.0 metres below streambed level. A single 100 mm diameter hole was drilled to a depth of one metre, and backfilled with compaction in 100 mm layers with each thermocouple set at the required depth. Water temperature in the pool was measured with a mercury thermometer.

7.3.5 Gaugeboard

A gaugeboard was installed in the streambed adjacent the upstream embankment (Plate 7.1) to allow accurate readings without the use of binoculars. The steel gaugepost was put in a hole one metre deep and set in concrete and the gaugeboard was bolted on later. This provided a reference level for all subsequent elevation measurements. The 1.000 metre mark (near streambed level) was used as a temporary bench mark and assigned a reduced elevation level of 10.000 metres. All elevations given in this chapter are with respect to this benchmark, unless specified otherwise.

Plate 7.1 Upstream embankment at recharge test pond showing tensiometer manometer boxes (left), water meters and outlets, gaugeboard, water level recorder and recorder access beam.

Plate 7.2 Troxler neutron moisture meter taking a count in access hole M1.

Plate 7.3 In-situ calibration sampling around a neutron moisture meter access tube by augering to the selected depth and driving a sampling tube.

Plate 7.6

View of pond from downstream embankment while drying. Note grass is growing in depression. Access hole M3 has been destructively sampled. In foreground is Wescor field psychrometer.

Plate 7.5

Normalizing the neutron moisture meter in an aluminium tube inside a drum of bore water.

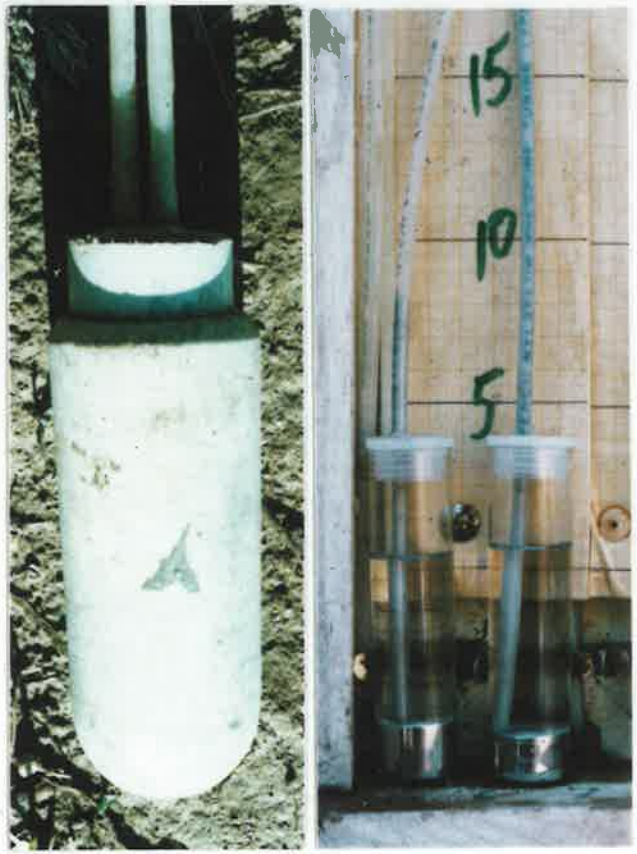

(a) (b)

Plate 7.4

Tensiometer components

(a) ceramic cup (b) mercury-water manometers

7.3.6 Water level recorder

A water level recorder was situated next to the gaugeboard. A Stevens F-Type chart recorder was installed in a frame inside a 200 litre drum (Plate 7.1). This was anchored to the streambed with two droppers driven through cleats on the drum interior walls. The steel lid was hinged to the drum and could be locked down. A 200 mm diameter float was used inside the drum and a punched steel tape ran over the recorder pulley to relate float movements to chart position beneath the ink pen. The pen speed was 30.5 mm/day. A support beam spanning the streambed adjacent the rim of the drum was used to allow easy access to the recorder without applying any load on the drum. In this way the datum of the recorder was not shifted with respect to the benchmark.

7.3.7 Embankments

Upstream and downstream embankments were built by firstly excavating the top 0.25 m material over a width of 0.4 m, including keys inset into the banks to a height of 0.5 m above bed level. Bentonite was liberally sprinked into the base, sides and ends of the cutoff trench. The loose surface material for a width of 0.8 m outside the trench was excavated and bentonite spread on the exposed surface. Heavy duty PVC sheet was spread over the trench and bentonite layer (figure 7.4). Sandbags were filled from streambank material upstream and downstream of the pond. These were packed into the trench. A single width wall of sandbags was constructed up to 0.5 m above streambed level. The area above the plastic was covered with soil sloping up to the top of the sandbags. The contact between the sandbags and the backfill was sprinkled with bentonite during construction. A layer of bentonite extended back from the plastic sheet for a further metre and this was covered with soil.

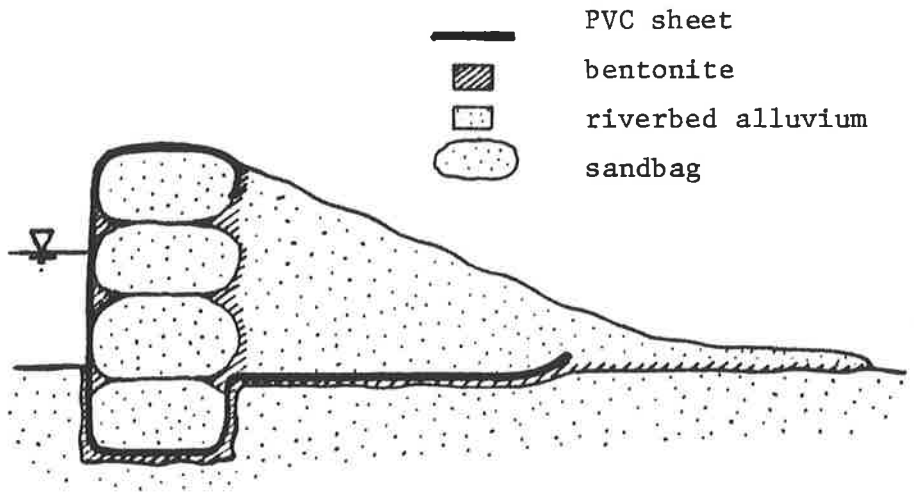

Figure 7.4 Embankment cross-section diagram.

7.4 Experimental Procedures

The water balance was calculated by taking instantaneous readings on the three water meters and the gaugeboard. The three values of discharge registered by the meters had a range of 0.5%. Two of the dials filled with water during the first period of ponding. These gave lower readings than the dry meter which was assumed to give the correct discharge into the pond. On occasions the current gaugeboard reading and time were written on the water level chart record and a mark made. Each week the chart was replaced and the clockwork drive rewound.

Tensiometer readings were taken at intervals on all manometers (Plate 7.4). On three occasions when vandals broke mercury reservoirs (glass vials) or when the mercury column appeared abnormally low the lines were flushed to remove all air. Mercury levels in the reservoirs were measured several times during the experiment to check tensiometer calibration.

Temperature readings were taken with a mercury thermometer at the soil surface and in the water when it was ponded. At the same time the temperature was recorded on the thermocouples set in the streambed. In

this way the temperature profile beneath the streambed could be constructed.

The most time consuming readings were with the neutron moisture meter. A typical reading pattern required the Troxler Portable Scaler Ratemeter to be turned on for 10 minutes to warm up before calibration (normalizing) commenced. The probe was placed in a specified position within a calibration drum (Plate 7.5). The bore water which was used in the pond was also used in calibration. An aluminium tube cut from the same tubing as the access tubes was used in the calibration drum. At least 6 x 1/2 minutes counts consistent to within 0.5% were taken. Usually 10 counts were recorded. Having performed this calibration the first access tube was run, starting from the bottom and working up.

Tape marks on the neutron meter cable at 0.2 metre intervals were used to fix the location of sampling points. The tape marks were calibrated against a steel tape to give an accurate fix on position within the tube. This calibration was repeated at the end of the experiment to determine cable stretch, which was found to be negligible. At each sampling point two half minute counts were recorded (Plate 7.2). If these differed by more than 200 (about 1%) further counts were performed at the same probe position. After logging each bore, a 30 to 40 minute operation, the probe was recalibrated. The mean of the calibrations before and after each hole was used as the reference count. Count rate ratios for the previous hole were calculated during logging of the next hole. Values were rejected if they differed by more than 200 from the mean of the remaining counts at a probe position. The mean of the accepted values was divided by the reference count to give the count rate ratio.

An indicator was required to qualitatively assess whether the moisture meter measurements were increasing during ponding and decreasing during drying. As calibration of count rate ratio with respect to soil moisture content had not yet commenced the indicator used was simply the

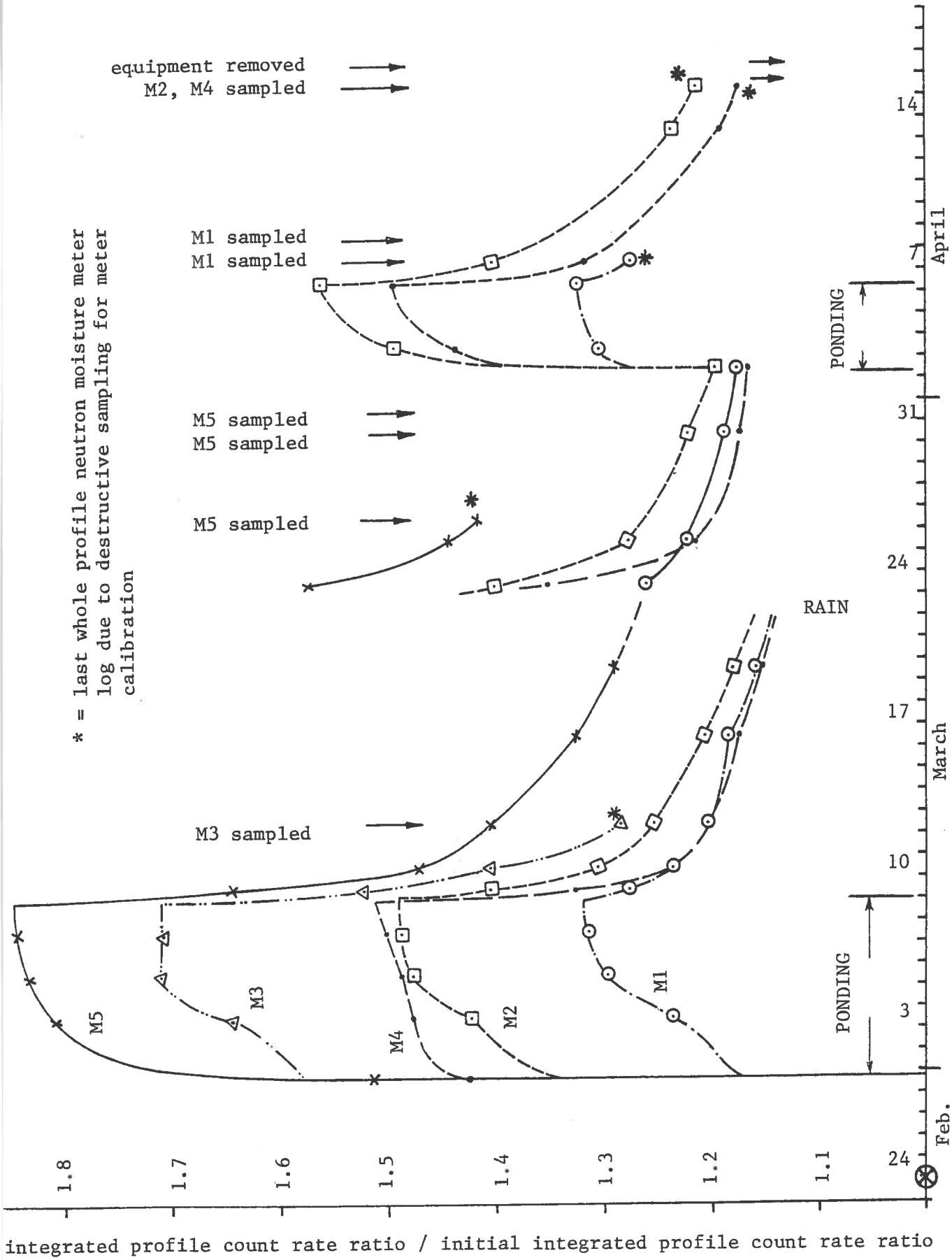

Figure 7.5 Normalized integrated profile count rate ratio variation with time for all access holes.

sum of the count rate ratios for a hole. This was normalized against the sum of the count rate ratios from the first run of logs on 23-24/2/82 for each hole. This value was plotted for each hole (figure 7.5) after each day of neutron moisture meter logging. It was apparent that the meter was responding to moisture changes in the soil profile.

7.5 Neutron Moisture Meter Calibration

The mixture of materials and their irregular distribution below the streambed is a major problem in calibrating the neutron moisture meter. Laboratory calibration, that is packing a drum with representative soil and measuring the count rate at various known moisture contents, was ruled out due to the problem of finding "representative" soil. Field calibration, the selected alternative, suffers from the lack of uniformity of the soil throughout the volume sensed by the meter. This affects the precision of calibration.

7.5.1 Sampling

The procedure adopted was to take core samples at depths where the count rate was uniform over several consecutive probe positions. At each such position the sampling depth was reached by hand augering then the cuttings on the bottom cleared and the sampling tube driven into the bottom of the hole. Five samples were collected at each depth on holes axi-symmetrically arranged at a radius of 0.2 metres from the access tube (Plate 7.3). The sampling tubes were labelled and the ends of the samples coated with wax.

In the laboratory the volumetric water content and bulk density was determined for each sample. The mean of each sample set taken at a depth greater than 0.5 metre was plotted against the corresponding count rate ratio (figure 7.6). Using the estimated equivalent water (Greacen, 1981, p78) calculated from the clay content, the effects of constitutional hydrogen were incorporated with the gravimetric water content to give a total water content. Secondly a square root density correction was

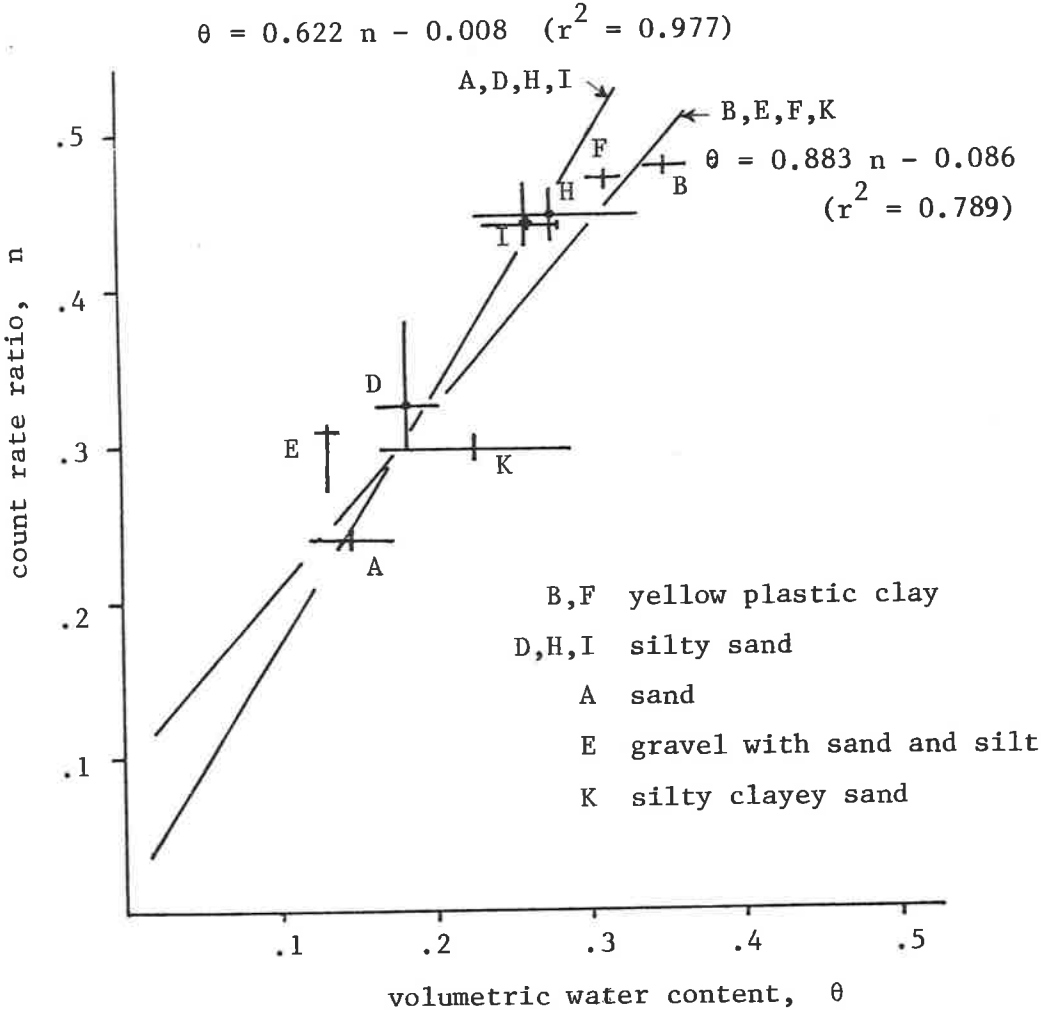

Figure 7.6 Count rate ratio versus volumetric water content.

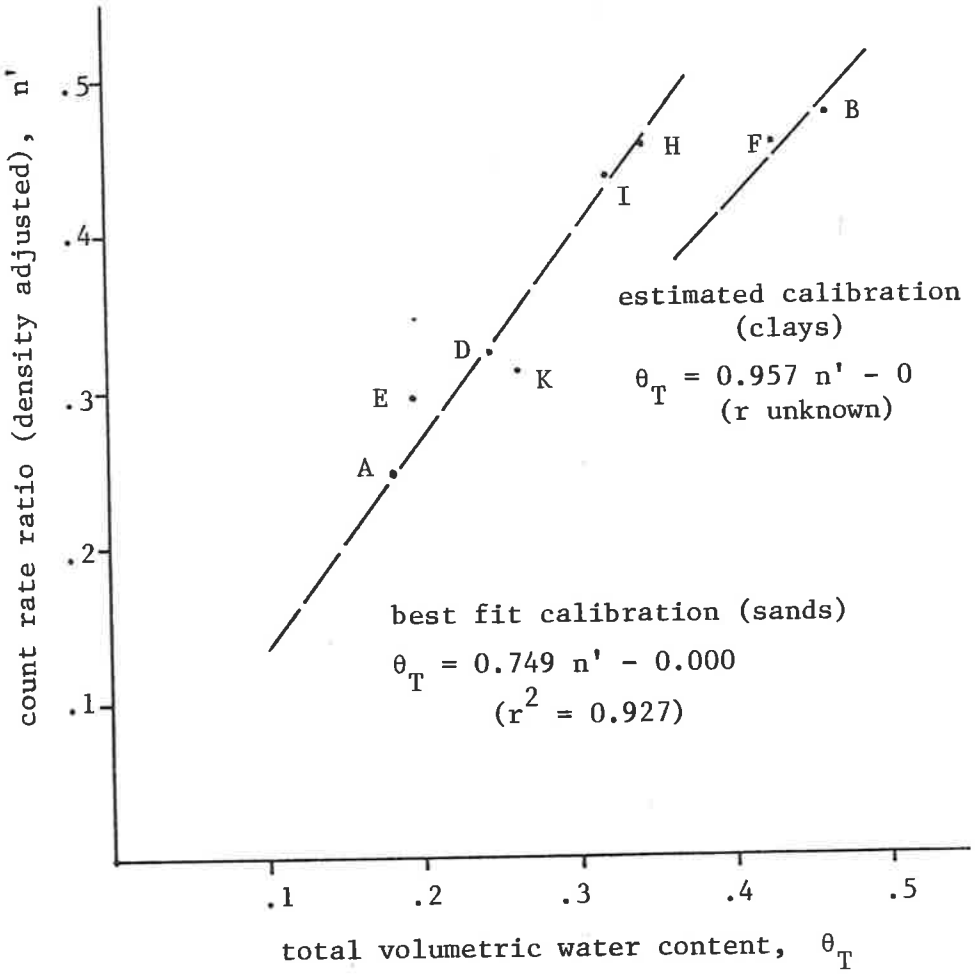

Figure 7.7 Density compensated count rate ratio versus total volumetric water content.

Table 7.1 Neutron moisture meter calibration adjustments

CALIB. NO.	ACCESS TUBE	SAMPLING DATE / /82	MEAN DEPTH (m)	MEAN COUNT RATIO n	MEAN VOL.W.C. θ	MEAN BULK DENS. ρ	CLAY CONTENT C^*	EQUN.VOL. W.C. θ_e	TOTAL W.C. θ_T	DENSITY ADJUSTED COUNT RATIO n'
A	M3	12/3	0.99	.238	.147	1.563	.06	.035	.182	.247
B	M3	13/3	2.70	.478	.352	1.703	.40	.110	.462	.475
C	M5	26/3	0.12	-						
D	M5	26/3	1.47	.327	.184	1.730	.16	.060	.244	.323
E	M5	30/3	2.05	.309	.132	1.848	.16	.064	.196	.295
F	M5	31/3	2.90	.470	.316	1.769	.40	.114	.430	.458
G	M1	7/4	0.16	-						
H	M1	7/4	0.70	.447	.279	1.611	.20	.064	.343	.457
I	M1	8/4	1.80	.440	.262	1.707	.16	.059	.321	.437
J	M2	15/4	0.11	-						
K	M2	15/4	0.51	.297	.228	1.532	.06	.034	.262	.311
L	M4	15/4	0.13	-						

Constitutional hydrogen effects -

Estimation of equivalent water content

$W_e = 0.124\ C^* + 0.015$ (Greacen, 1981, p.78)

C^* = clay content g/g (< 0.002mm)

$\theta_e = W_e \rho$ volumetric equivalent water content

mean bulk density = 1.683 gcm^{-3}

density correction,

$$n' = \left(\frac{1.683}{\rho_i}\right)^{\frac{1}{2}} n$$

performed to standardize the calibration to the mean dry bulk density of all samples 1.683 g cm^{-3} (Table 7.1). This resulted in figure 7.7. Samples B and F were in silty clays which occurred below 2 metres depth in all access hole soil profiles. The samples in shallower more coarse grained materials appeared to conform to a different calibration.

It is likely that if more calibration samples had been taken the number of calibration lines may have increased. With the existing samples two separate neutron responses of materials were evident. Simply based on depth and material gradings two calibration lines were constructed and are assumed to apply to materials within those classifications. Note that no samples were taken of the clays in the dry state. Drainage of these was considerably slower than for the overlying sands, and in the time constraints of the experiment the clays had no opportunity to dry further. An arbitrary (and arguable) choice, to pass this calibration line through the origin was made. Commonly, although not universally, the increase in moisture content is larger for clays than for sands for the same increase in count rate ratio. Hence it may be expected that the slope coefficient for clays 0.957, so obtained, would be greater than that for sands, 0.749. The range in count rate ratios for these silty clays is small so the error in slope of the calibration will result in only small errors in calculated moisture storage changes.

7.5.2 Effect of sand-cement sealant on neutron moisture meter calibration

Greacen (1981,p66) reported that a cement-clay sealant around an access tube increased the value of the calibration slope by 3% compared with adjacent tubes installed by an auger technique without sealant and for which a drum calibration was available. Gravel layers caused variable thicknesses in the cement-sand sealant for the access tubes in the Little Para streambed. The variability in sealant thickness is expected to effect the field calibration. Only one sample set was taken in gravels, set E at a mean elevation of 7.9 m at access tube M5 on 30/3/82. This set deviates

from the best fit calibration for sands by 10% (see figure 7.7) possibly due to moisture retention in the enlarged sealant annulus. The variation of the calibration slope for such layers from the slopes of the two lines given are unknown.

The sement-sand sealant was applied in the dry state. After the first ponding the cement hydrolized. That is water molecules became bound to the cement. This had the effect of increasing the constitutional hydrogen adjacent the access tube. The magnitude of this effect could have been estimated if pond drying had proceeded for a period of 28 days (the duration from the previous discharge in the stream to the running of the initial neutron moisture logs). Projection of the integrated profile count rate ratio in the drying phase suggests that this effect could account for up to 10% of the initial moisture content change. That is the neutron moisture calibration applies only to the hydrolized state of the sealant.

7.5.3 Effect of soil density on moisture meter calibration

Gamma-gamma density logs were run on four access holes and revealed variations in count rate ratio as shown in figure 7.8. These logs show a decrease in count rate ratio at the position of the assumed changeover from the sand to the clay calibration lines (EL 7.3 to 7.8 m). The zone of influence of the soil on the count rate of the back-scattered gamma rays has a radius of less than 0.2 metre. This is small compared with the more penetrating neutron meter emissions having a radius of influence of about 0.5 metre.

An attempt was made to calibrate the density meter count rate ratio against the modified bulk wet density of the soil. The method used followed Schrale (1976) where the modified bulk wet density, ρ'_{wet} is defined by equation 7.1

$$\rho'_{wet} = \rho + 1.11\,\theta \qquad 7.1$$

where ρ is the bulk dry density of the soil and θ is the volumetric moisture content of the soil. The factor 1.11 arises from the ratio of

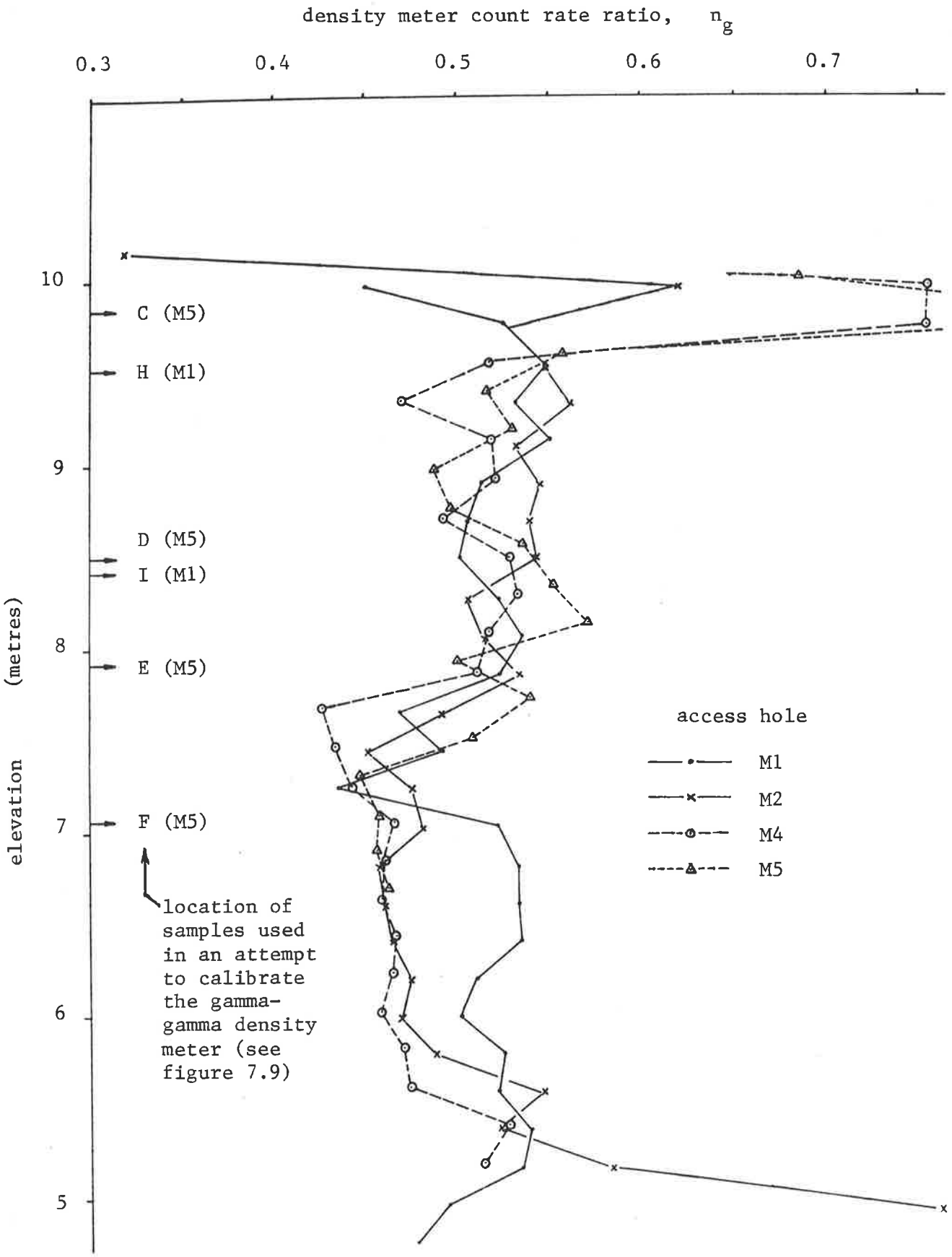

Figure 7.8 Gamma - gamma density meter logs, 6/4/82.

the gamma ray mass attenuation coefficients (at 0.662 Mev) for water with respect to soils.

The following calibration equation was expected.

$$\rho'_{wet} = B - \beta n_g \qquad 7.2$$

where B is a constant, β is a constant (positive) coefficient and n_g is the density meter count rate ratio. The modified bulk wet density on the day of the density log was calculated for the positions from which samples were later taken using equation 7.1. The bulk dry density was determined gravimetrically from the samples and the volumetric moisture content from neutron logs run on the same day and using the neutron meter calibrations of figure 7.7. The resulting graph (figure 7.9) gives only a weak correlation preventing a calibration equation of the form of equation 7.2 from being determined. The exact centre of sensitivity for the probes was not located. This may have reduced the range of count rate ratio, n_g for each sample but would not have diminished the discrepancies enough to give a reliable density calibration.

Without this calibration density correction for the moisture meter logs is not available. As an indication of the variation in moisture content due to an increase in density meter count rate ratio from 0.45 to 0.55, the range of figure 7.8, the change in calculated moisture content for materials in either soil is within the range -0.7% to +4.3%. This results from an arbitrary estimate of β as 1.95 (after Schrale, 1976) and from the square root density effect described in Greacen (1981) as applied to the neutron moisture meter count rate and the linear effect of density on the constitutional hydrogen.

The low sensitivity of moisture content to density over the density range present allows the use of the soil moisture logs in quantifying the change in soil moisture in the profile with time. An estimate of soil moisture changes assuming a uniform profile dry density of 1.683 g cm^{-3}, the mean dry density of all samples, is used as an indicator of water

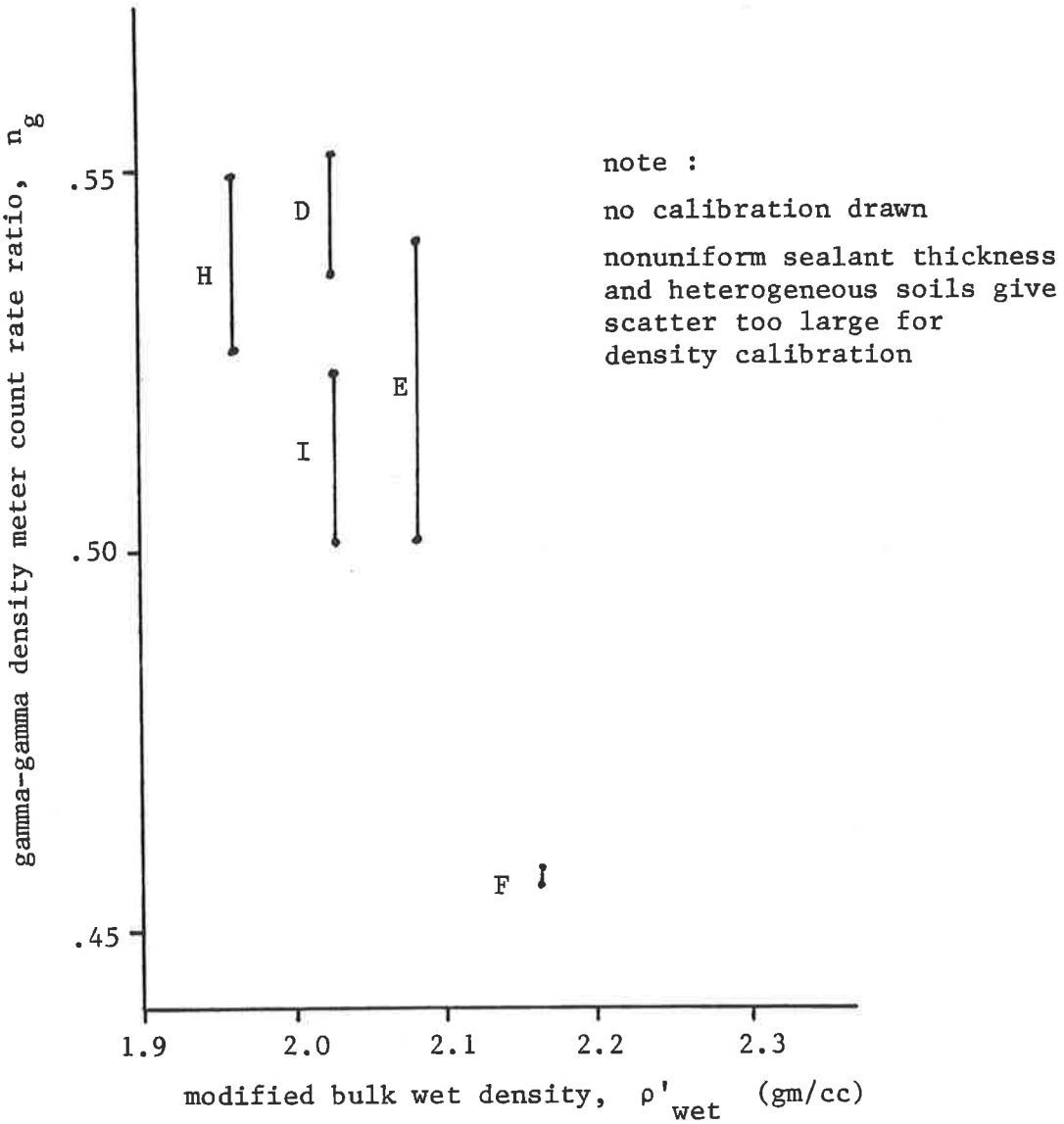

Figure 7.9 Gamma-gamma density meter count rate ratio versus modified bulk wet density.

storage in the soil profile.

7.6 Data Evaluation

Surveyed sections at 1 metre intervals of running distance along the 14 metre length of the pond were used to produce elevation versus volume and elevation versus area curves (figure 7.10).

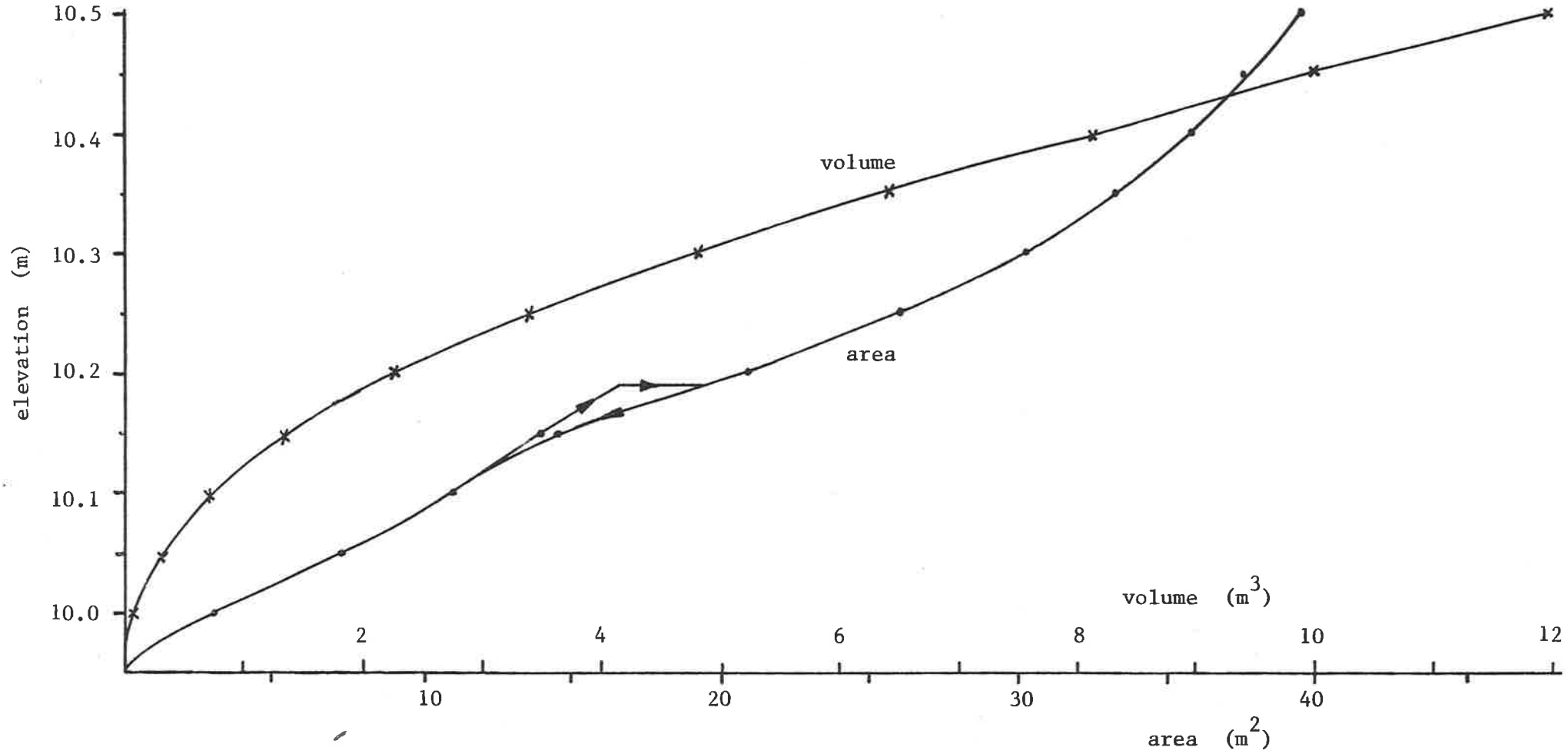

Figure 7.10 Surface area and volume versus elevation curves for streambed infiltration pond.

The hydraulic head at the position of each tensiometer cup was calculated from the tensiometer reading. Solute suction was assumed negligible. The hydraulic head, h, is defined as the sum of the elevation head (with respect to the adopted datum) and the pore water pressure head which may be positive or negative (suction). Plots of the hydraulic head for tensiometers 1 to 6 and 9 to 14 appear in figures 7.11 and 7.12. The hydraulic head profiles through the streambed for selected days are shown in figures 7.13 and 7.14. The elevation of the water table recorded by piezometer 19, slotted over the elevation range -1.55 to -4.55 metres is also shown on figures 7.11, 7.13 and 7.14 using the assumption that the loss in head over approximately 5 metres between the water table and the piezometer response interval is negligible.

Logs of access holes are presented side by side with neutron meter count rate ratio profiles for the driest and wettest conditions (figure 7.15). This figure also shows the position and count rate ratio for each sample set used in calibration. Using the derived calibration equations and assuming uniform dry bulk density the total volumetric water content profiles on the same dates are plotted (figures 7.16 and 7.17). The irregularity in the profiles is attributed to actual variations in moisture content due to the variable nature of the soil and to an error term. The latter comes from applying the calibration derived from a few samples to a range of soil types and densities and variable thickness in the cement-sand sealant. The driest profiles (logged 23-24/2/82) also suffer from a suspected calibration shift of up to 10% as the sealant had not hydrolized until water was first admitted into the pool (28/2/82). In these figures a uniform profile dry bulk density of 1.683 g cm^{-3} is assumed, thereby eliminating density corrections.

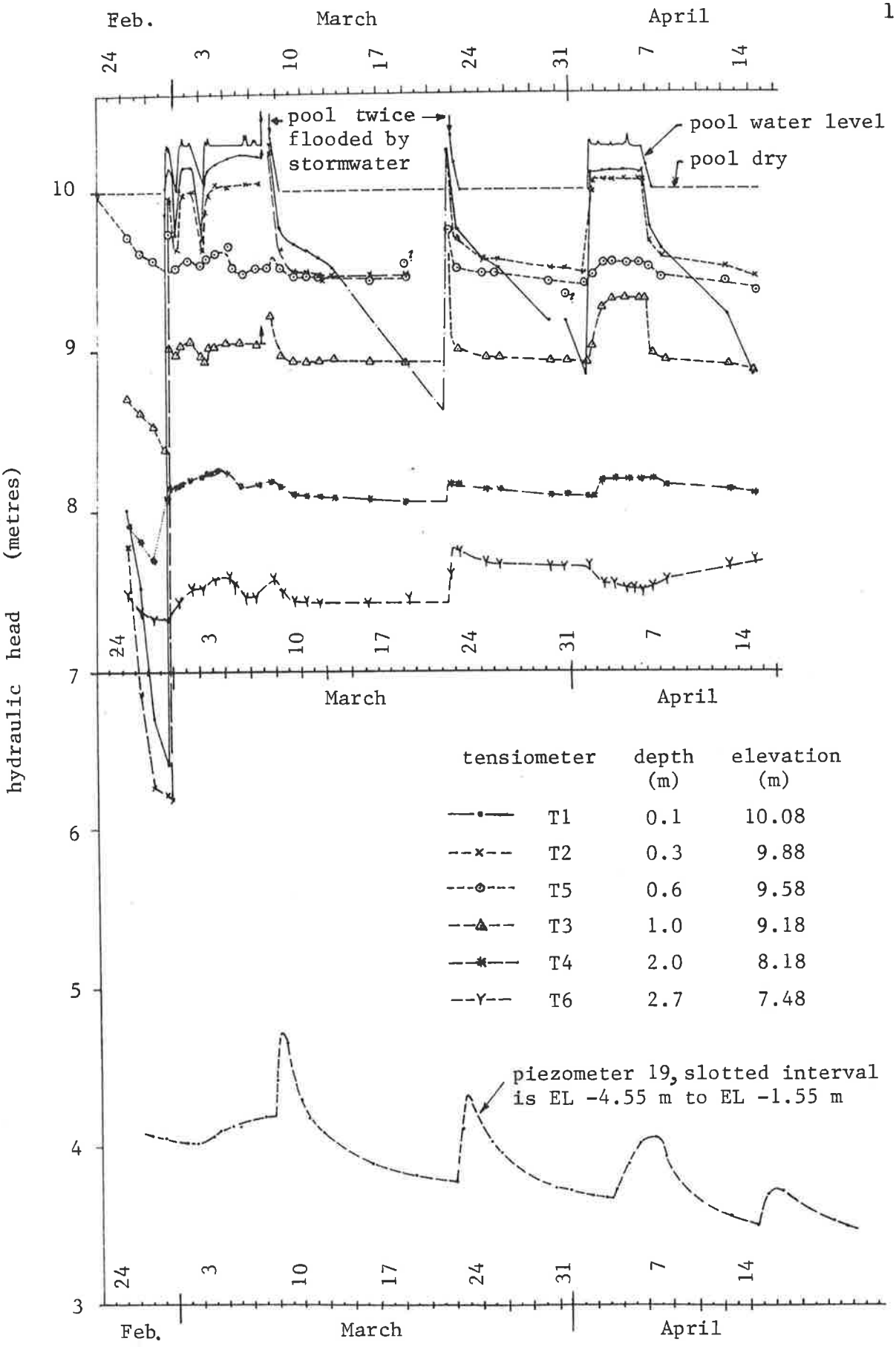

Figure 7.11 Hydraulic head versus time for tensiometers T1 to T6 and piezometer 19.

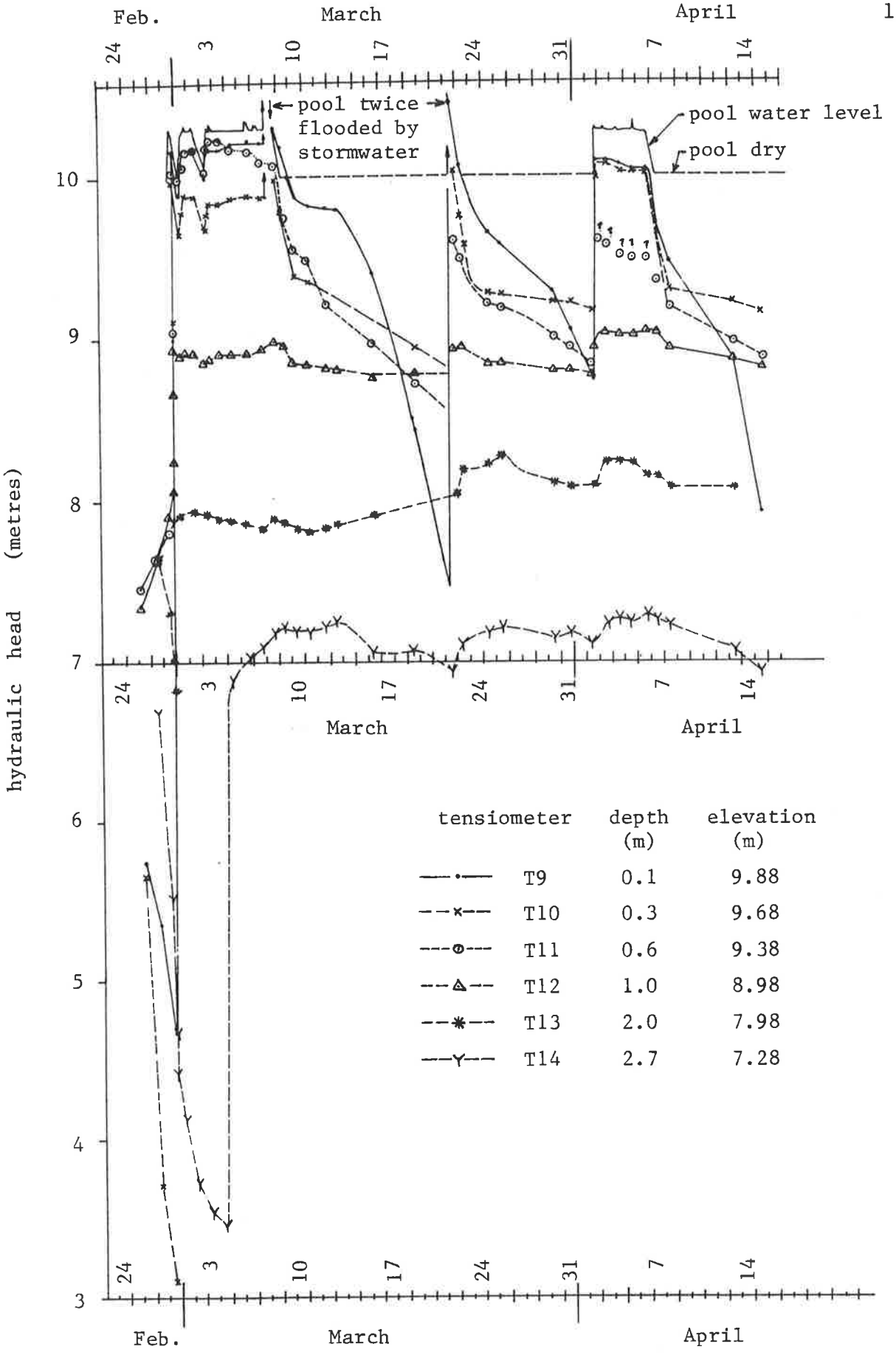

Figure 7.12 Hydraulic head versus time for tensiometers T9 to T14.

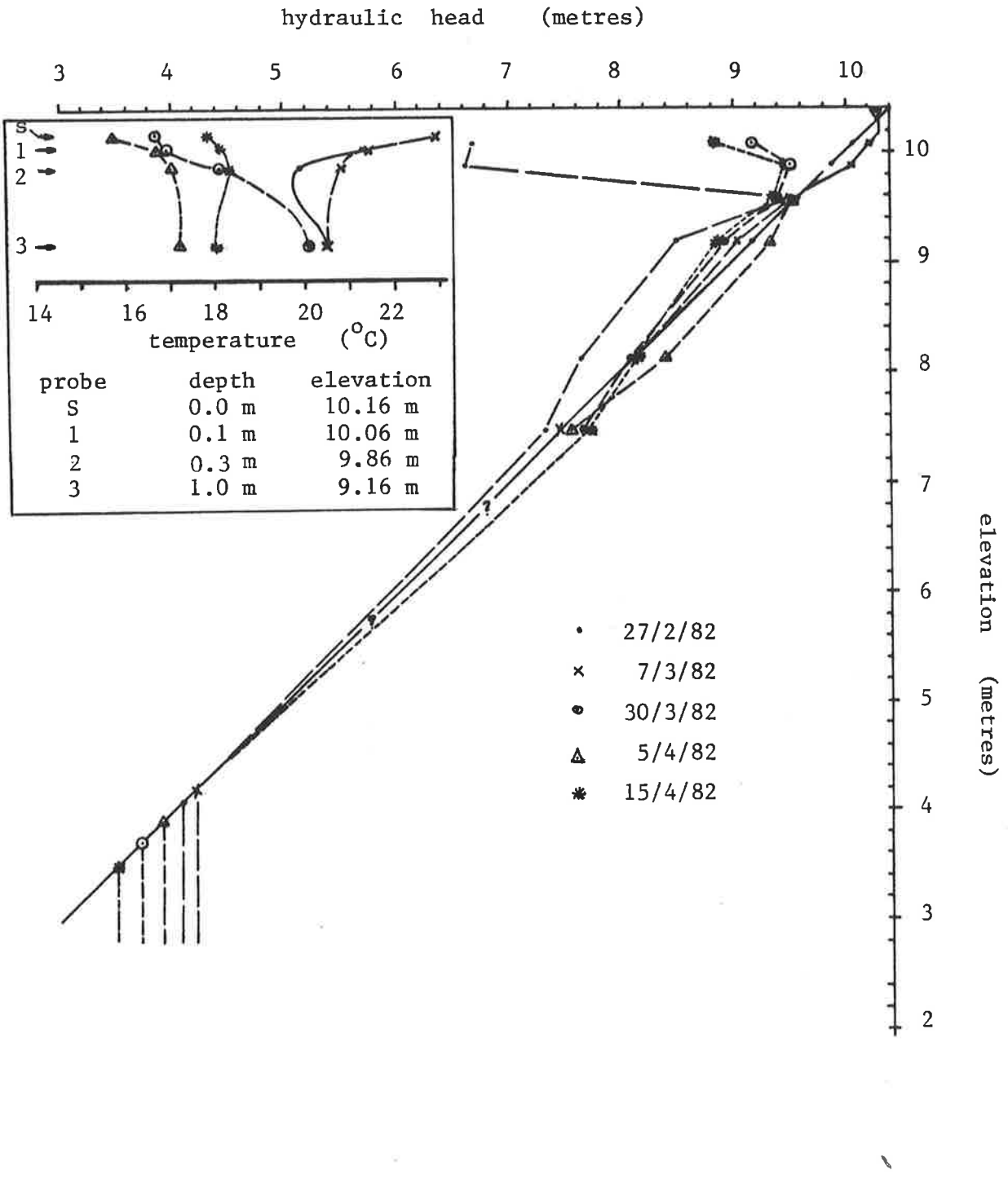

Figure 7.13 Hydraulic head profile for tensiometers T1 to T6 and piezometer 19, and temperature profile near the surface on selected dates.

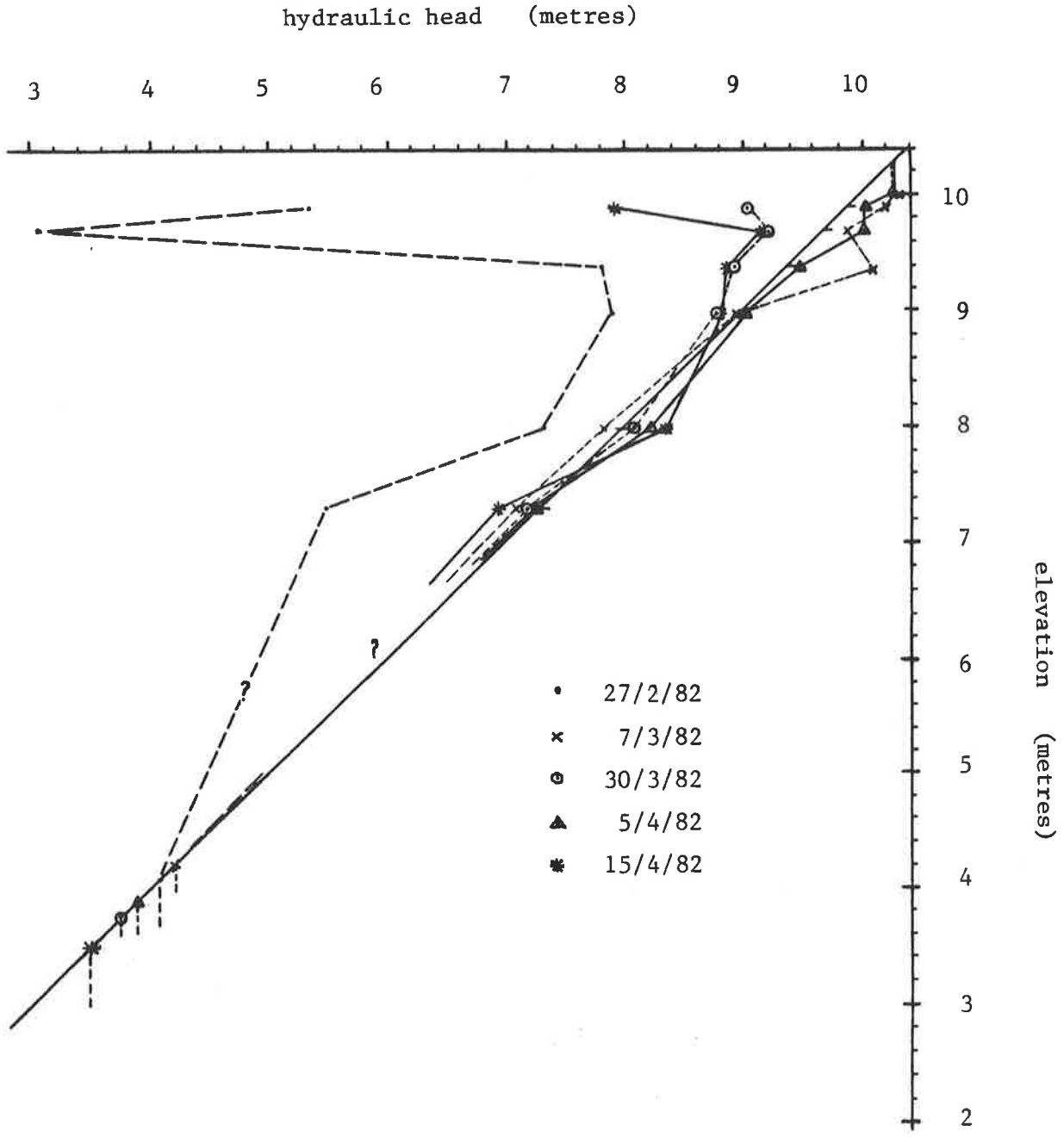

Figure 7.14 Hydraulic head profile for tensiometers T9 to T14 and piezometer 19 on selected dates.

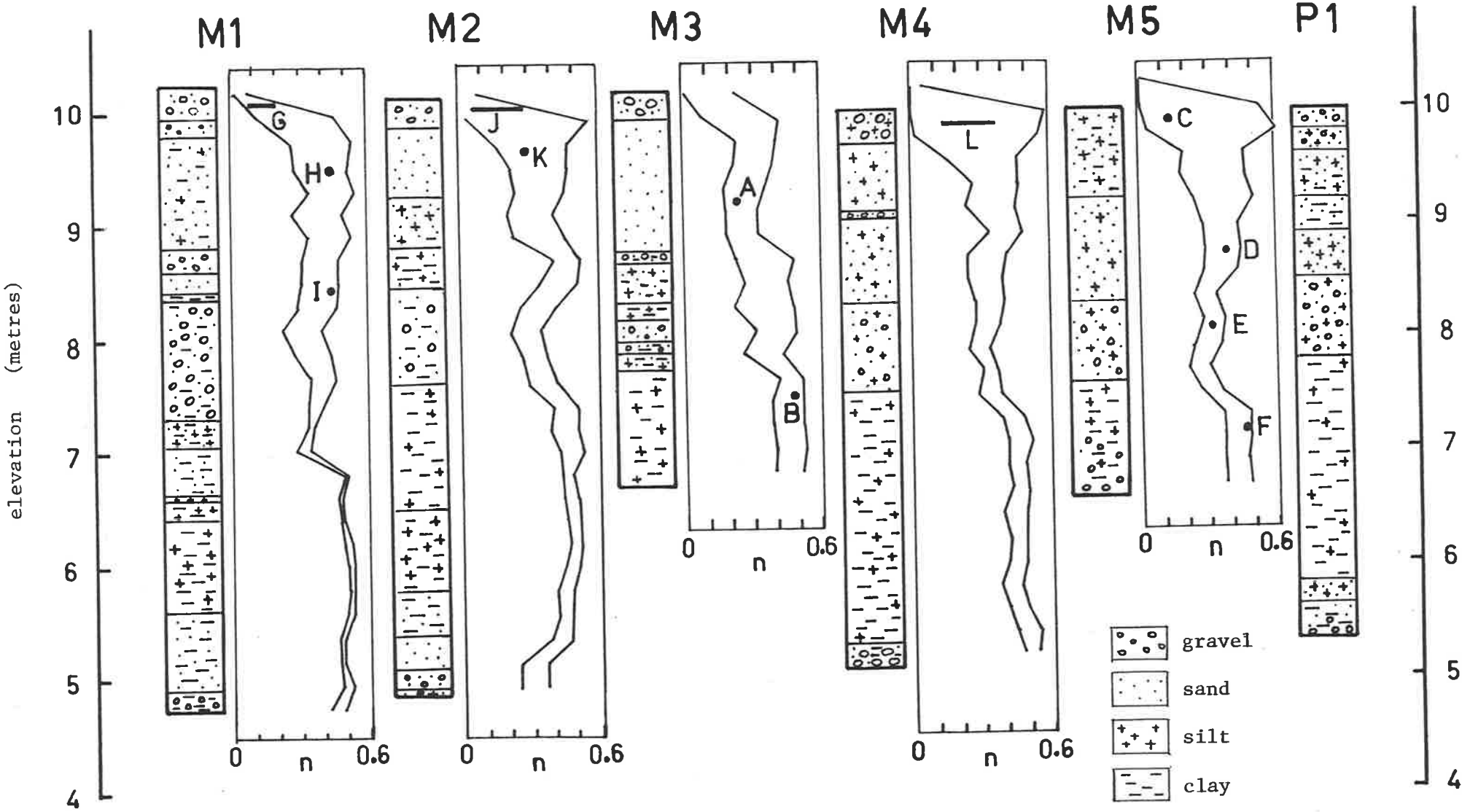

Figure 7.15 Stratigraphic logs of access holes and piezometer P1 and neutron moisture meter count rate ratios for driest (23-24/2/82) and wettest (7/3/82) conditions. Sample positions and count rate ratios are shown.

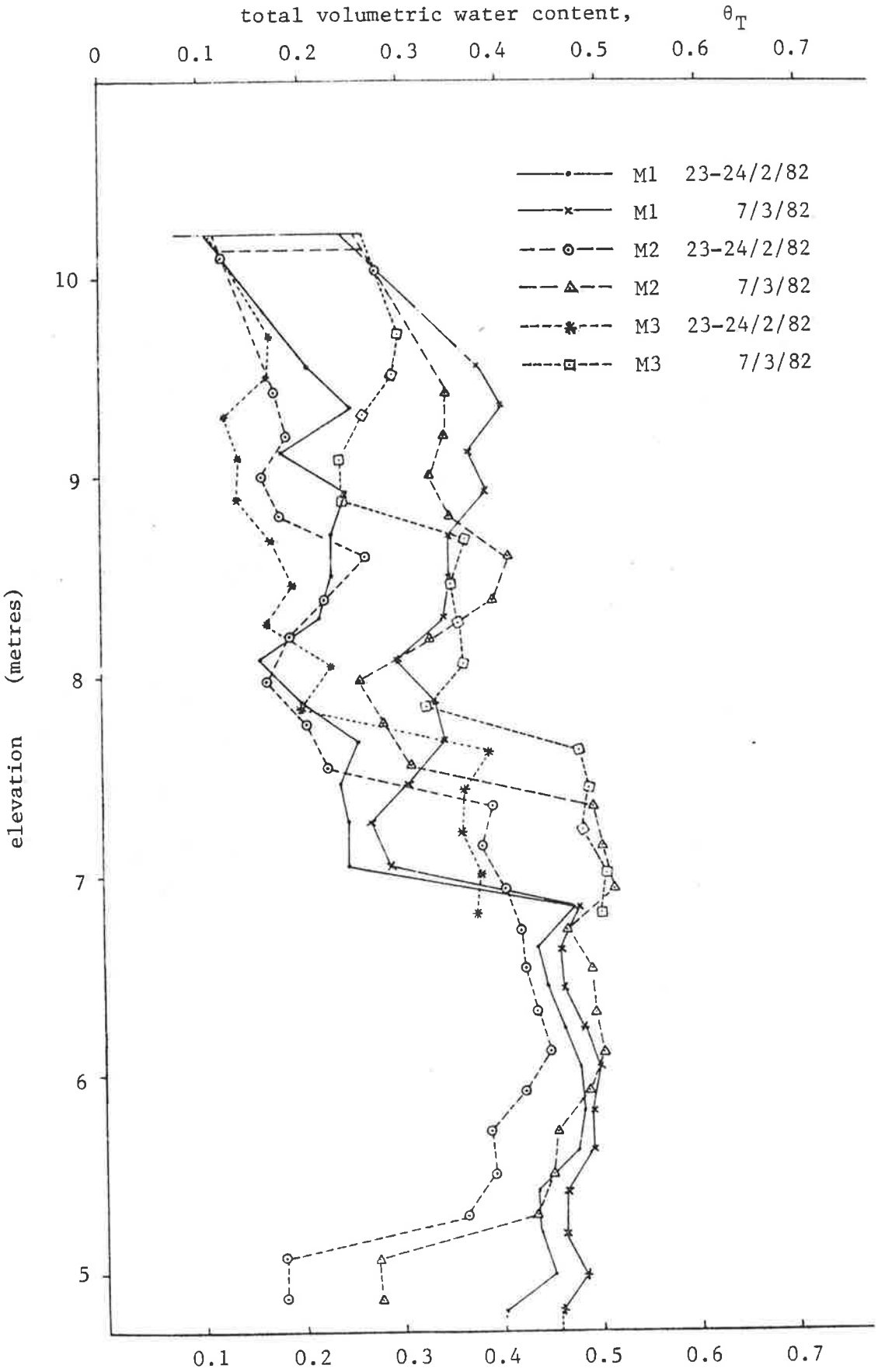

Figure 7.16 Total volumetric water content profiles for access holes M1 to M3 on 23-24/2/82 and 7/3/82.

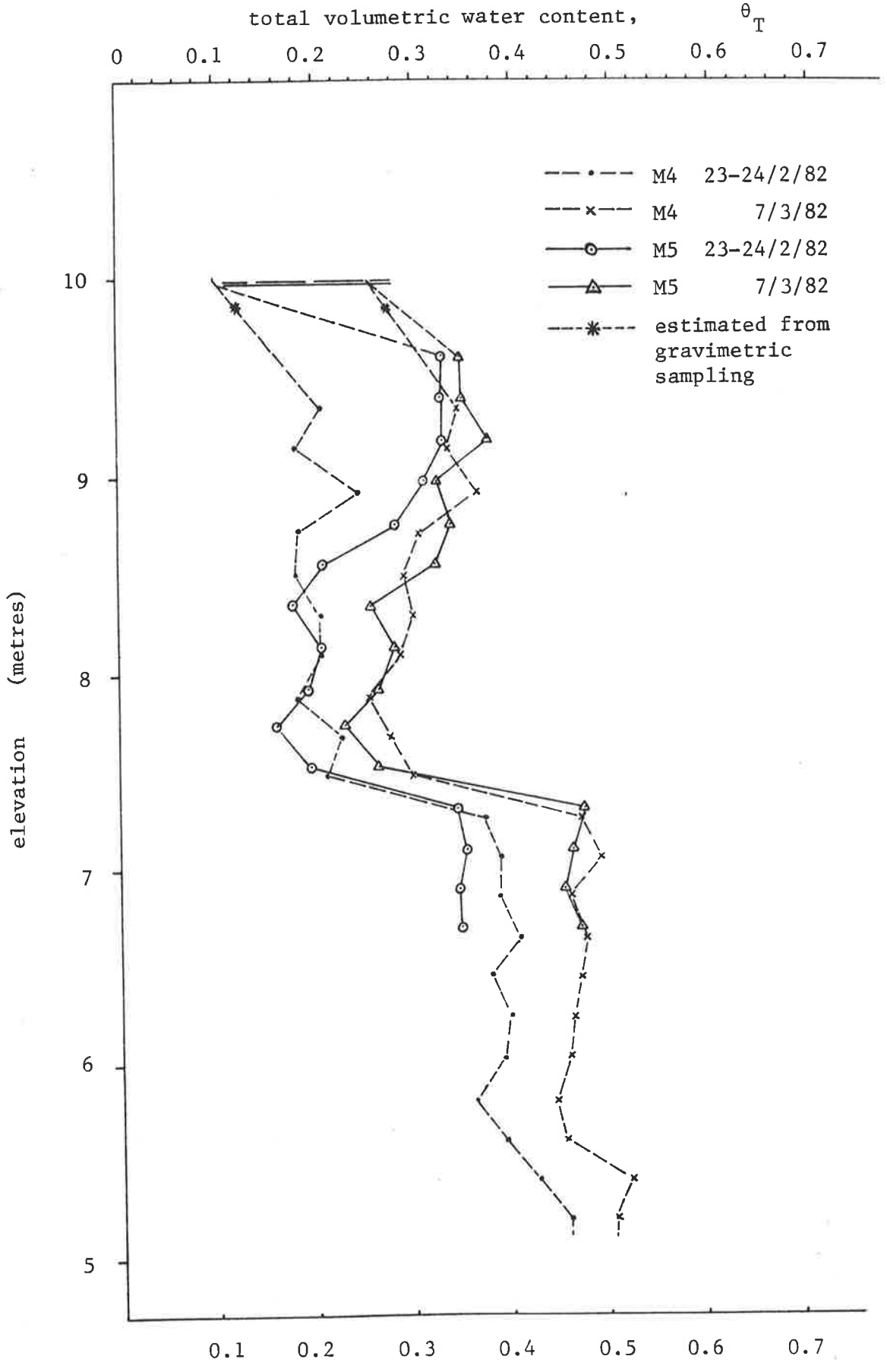

Figure 7.17 Total volumetric water content profiles for access holes M4 and M5 on 23-24/2/82 and 7/3/82.

7.7 Results

7.7.1 Infiltration rate

The infiltration rate was obtained in two ways. Firstly it was calculated from a pool water balance, as the difference between inflow and storage change. Secondly on some occasions inflow was stopped and the rate of decline of the pool water level was observed. The latter method avoids the need to know the volume-elevation relationship, but suffers from seepage from the banks into the pool while the water level declines. It is expected that the consequent infiltration estimates would be marginally smaller than those with steady water level. The fractional difference between the two methods does not exceed 6%. Figure 7.18 shows the variation in infiltration rate with time. Scatter in the infiltration rate calculated by the first method is due to the precision in gaugeboard readings particularly for short period water balance calculations and to water temperature variations. Figure 7.19 shows the infiltration rate as a function of total infiltration.

When the pool water elevation dropped below 10.19 m the downstream end of the pool was no longer in contact with the downstream embankment. This was due to a saddle point in the streambed invert (as detected also in figure 7.10). A steady state infiltration rate of 0.38 m/d, calculated by the falling head method, was observed for pool elevations less than 10.19 m at the end of each period of ponding. Above this level the steady state infiltration rate was 0.48 m/d and 0.76 m/d during the two ponding periods respectively.

On 2nd March a seepage face 1 m wide and 0.5 m long was found on the downstream skirt of the downstream embankment. Its size remained stable until 8th March when stormwater flooded the pond overtopping both embankments. The pond was flooded a second time on 22nd March further weakening the embankments. Repairs using bentonite layers covered with more skirting material were effected on the outer flanks of each

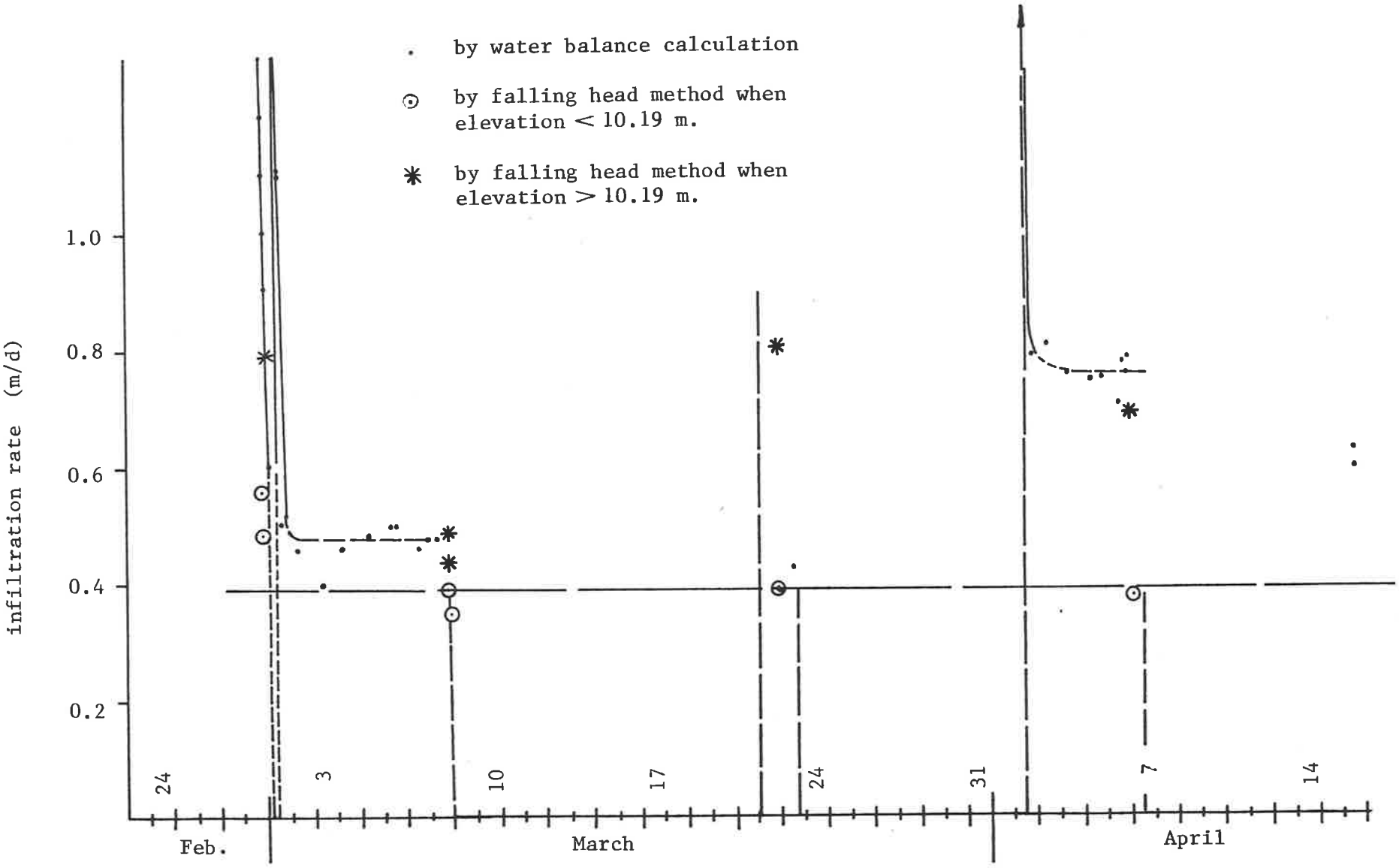

Figure 7.18 Pond infiltration rate versus time.

Figure 7.19 Pond infiltration rate versus total infiltration.

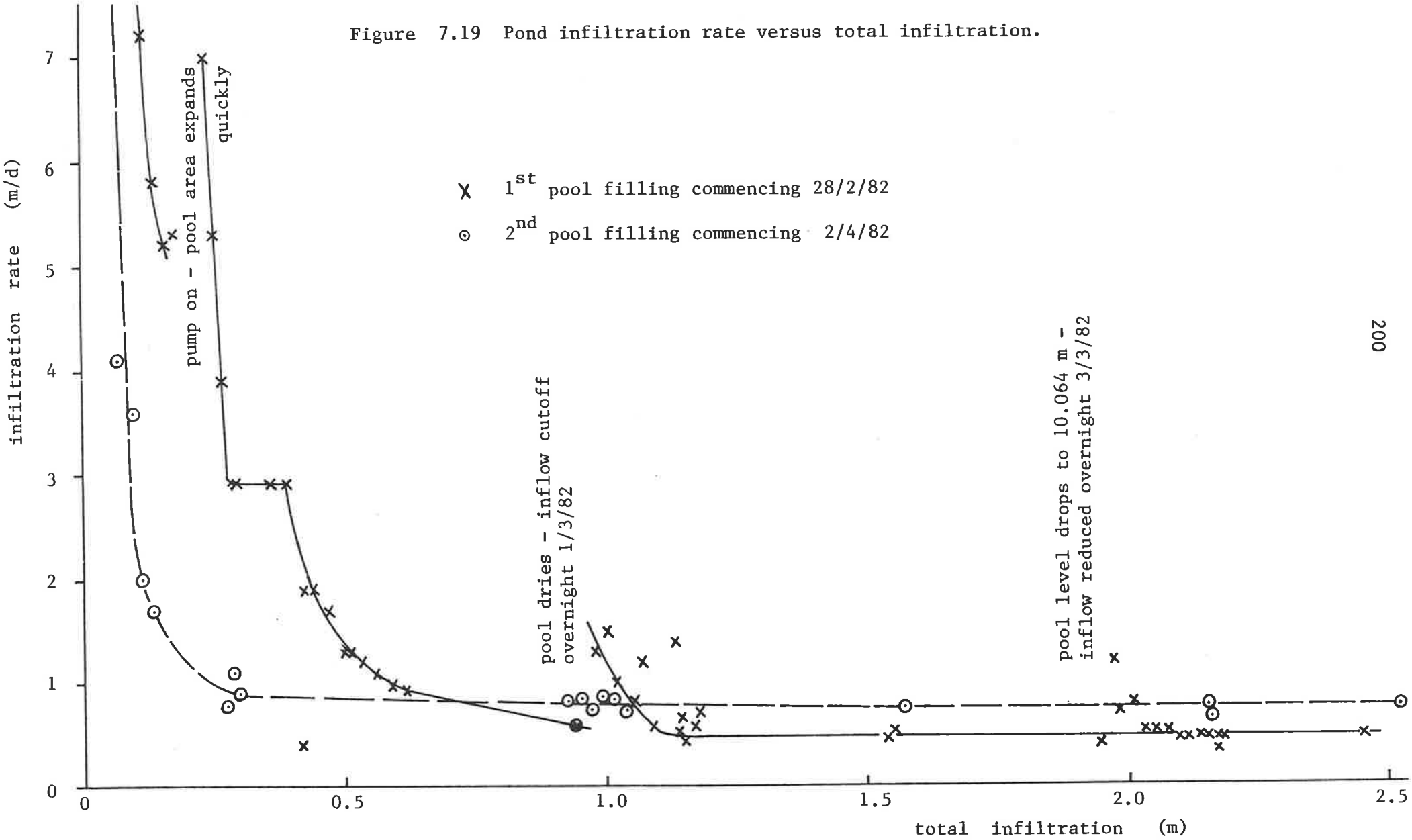

embankment. These were effective for the upstream embankment as the low water level steady state infiltration rate remained unchanged for the second ponding period. However the downstream embankment showed a small seepage face on the downstream flank within 24 hours of the start of the second ponding period. This expanded to an area 1.2 m wide and 1.5 m long on the same day, 3rd April and stabilized.

It had been intended to determine the difference in infiltration rates between the shoal and the depression in the pool. It was expected that during streamflow the suspended sediments would show a preference for settling in the depression rather than on the faster flowing shoal. This was evident by visual inspection of the streambed surface. This may have given rise to lower infiltration rates in the depression due to the formation of a lower permeability surface layer. The hydraulic head at a depth of 0.3 m is marginally lower for tensiometer T10 beneath the depression than for the tensiometer T2 for dates before 8th March, the first flood (from figures 7.13 and 7.14). Otherwise there is no evidence to suggest different surface hydraulic impedance.

Hence it is suggested that the increase of 0.1 m/d and 0.38 m/d in observed infiltration rates for water elevations exceeding 10.19 m for each ponding event respectively is due primarily to seepage through the downstream embankment. The hydraulic gradient for tensiometers T1 to T6 (figure 7.13) is almost identical on 7th March and 5th April when infiltration rates were 0.48 and 0.76 m/d respectively. The ratio of seepage face area for the second ponding to the first (= 3.6) approximates the ratio of infiltration rate increase (= 3.8). This supports the view that most of the increase in infiltration rate is due to leakage through the downstream embankment. Any increase in infiltration rate over the shoaled section of the pool is indetectable.

Piezometers were set in the streambed 2.8 metres and 10 metres downstream of the downstream embankment and slotted just above the first

major clay layer encountered. These piezometers remained dry continuously. In hindsight a flight of tensiometers in the downstream flank of the embankment could have been installed to show the hydraulic gradient. This would have provided a more reliable index of leakage rate but still would not allow it to be quantified.

Temperature of pond water varied through each ponding event (figure 7.20). This had a minor influence on infiltration rates. Comparing figures 7.18 and 7.20, the scatter of the infiltration rate echoes observed temperature variations with infiltration rates increasing as water temperature increases. Note for example the period 1st to 8th March, with minima on the 3rd and maxima on the 6th March.

Biological influences on infiltration rates could not be isolated. On drying the pool after the first ponding event mosquito larvae were abundant on the pool floor. Several days later grass shoots sprang up from the floor of the depression in the pool (Plate 7.6). Some of this grass survived the flood of 22nd March and on 2nd April at the start of the second ponding event grass 50mm high and melon plants were growing in the pool depression. The surface of the shoal was barren, dry and had cracked to a depth of one or two millimetres. This resembled the initial appearance of the whole pool prior to the first ponding.

The bore water used to fill the pond came either directly from the bore or via a header tank in which algal blooms were abundant. There was no doubt that algae entered the pool but no visible evidence for their presence was observed. A pool water sample was taken on 4th March and a basic analysis revealed

Total dissolved salts	743 mg/l
Conductivity @ 25°C	1360 µS/cm
pH	7.2
Suspended solids	5 mg/l

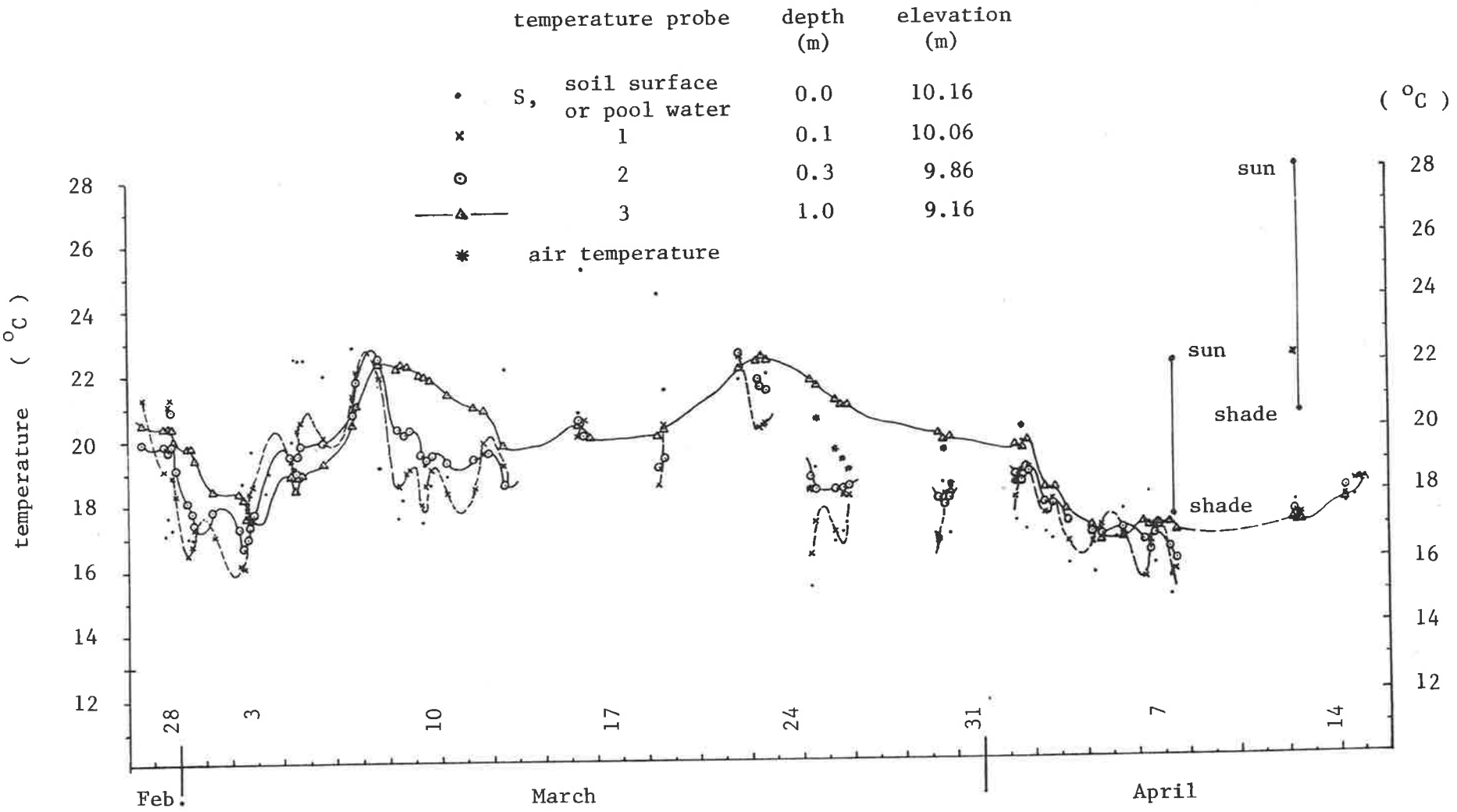

Figure 7.20 Temperature of ponded water and at probe positions versus time.

Neither of these properties suggest that the water quality had any effect on infiltration rates. The following is a quote from an Australian Water Resources Council (1982) report by the working group on aquifer recharge with reclaimed water. "Concentrations of suspended solids in the range 1 - 20 mg/l can reduce infiltration rates in some situations. Generally however, water with suspended solids up to 30 mg/l will be suitable for recharge."

Lastly the bark and grass seeds initially on the streambed surface were allowed to remain. On ponding initially the bulk of the debris floated and this was skimmed from the water surface. Most of the remaining smaller debris became water logged and sank. It is expected that this had no consequential effect on infiltration rates as water could pass freely between the bark and the streambed. Most of this material was flushed out of the pool during the first flooding.

7.7.2 Mechanics of moisture flow

The theoretical models described in section 3.3 assume that a wetting front, either of piston type (Green and Ampt) or diffusion type (Richards), progresses downwards until equilibrium occurs. Above the wetting front the hydraulic head becomes related to the head in the pond by Darcy's law and as the material is saturated the hydraulic head exceeds the elevation head (that is pore pressure is positive). Below the wetting front the hydraulic head is less than the elevation head due to negative pore pressure (capillary head or suction). The wetting front stabilizes at a depth where the hydraulic conductivity equals the infiltration rate.

To apply this theory to the observed hydraulic head profiles gives an understanding of the features controlling infiltration. Figures 7.13 and 7.14 show a change from positive to negative pore pressures at two locations on the last day of each ponding period, 7th March and 5th April. These are the bases of perched groundwater mounds. The uppermost bases occur at a depth of 0.6 m for T1 to T6 and 1.0 m for T9 to T14 (EL 9.6 m

and 9.0 m respectively). For T1 to T6 a second perched mound extends from below 2.7 m to 1.0 m (EL 7.5 to 9.2) on 5th April. T9 to T14 show a second perching layer at a depth of 2.4 m (EL 7.6) on both dates. From the mixed nature of the streambed materials it is not surprising to find that perching occurs at different levels for the two flights of tensiometers.

The mean vertical hydraulic conductivity of the upper perching layer is less than the steady state infiltration rate 0.38 m/d, as the vertical hydraulic gradient through the perching layer exceeds unity and perching produces mound spread beyond the area of the pond. No tensiometers were set into the banks to determine the lateral extent of the mounds. Small mound heights and heterogeneous materials suggest that the spread is unlikely to be significant. That is the predominant direction of flow is vertical.

Tensiometry provides the most reliable guide to soil moisture movement for this field investigation. The finess of a choice between Richards and Green-Ampt models of infiltration is lost in considering the heterogeneity of the porous medium.

Considering figure 7.19 the infiltration rate reached steady state after only 0.3 metres total infiltration on 2nd April. From the discussion of downstream embankment seepage, which accounts for half the infiltration rate, the effective infiltration through the pool base to this time is 0.15m. The average volumetric change in moisture content for the upper ("sand") profile from moisture meter measurements is 0.15. Hence the saturated depth is no greater than 1 m at the time when steady state is reached. This supports the notion that the infiltration rate is controlled by the permeability of the uppermost perching layers located at depths of 0.6 m and 1.0 m at the two tensiometer flights. Significant hydraulic gradients occur up to the streambed above these layers indicating that the hydraulic conductivity does not reduce abruptly at these depths.

In chapter 9 the streambed hydraulic impedance and aquifer hydraulic

conductivity of the calibrated section representing the reach containing the infiltration pond are 4.5 m and 4.0 m/d respectively. In the model it is assumed that the impeding layer occurs at the streambed surface. The hydraulic characteristics of the surface blanket replacing the actual configuration of streambed porous media at the pond are calculated out of interest. Using the model parameters and applying equation 4.32 to the pond steady infiltration rate (0.38 m/day) and the hydraulic gradients across the uppermost perching layers (figures 7.13 and 7.14) gives the equivalent streambed blanket hydraulic conductivity, K_B as 0.12 m/d to 0.25 m/d and corresponding blanket thickness, ℓ as 0.14 m to 0.28 m. Both ranges fall within the realm of physically feasible values.

7.7.3 Fate of infiltrated water

Infiltrated water may recharge the underlying aquifer, evaporate from the ephemeral streambed, become attracted to the roots of vegetation and eventually transpired or remain with the soil profile above the aquifer water table. The proportion of each component may vary depending on the temporal distribution of infiltration, among other factors. Evaporation losses from the streambed alluvium would be expected to depend on reservoir release patterns. It is assumed that the transpiration of phreatophytes is independent of soil moisture in the vadose zone because the roots also extend below the aquifer water table. Hence the transpiration is independent of the streamflow pattern providing the aquifer water table is maintained within the range of plant roots.

During drilling, in preparing the pond, several holes encountered tree roots up to 30 mm in diameter at various depths. The roots belonged to several large river red gums (eucalyptus camaldulensis) which partially shaded the site. A further assumption is made that the effect of roots on the tensiometer readings is non selective or insignificant. That is the measured heads are representative of the body of soil around them and not unduly influenced by the (unknown) presence of isolated nearby roots. (The

effect of the roots on the hydraulic head is uniform throughout the medium.) With these assumptions the effect of transpiration may be neglected when calculating evaporation losses.

It was intended that the method described by Kovacs (1981, p254) be applied. He locates the depth at which a reversal in hydraulic gradient occurs. That is above this depth hydraulic head decreases in an upward direction and below it decreases in a downward direction. Change in soil moisture above this depth is considered to be the evaporative loss while that below is due to downward infiltration beyond the depth of the moisture profile log.

This method could not be used directly to determine evaporation loss for the pond because the changeover depth fell within 0.5 m of the soil surface where the neutron moisture meter is influenced by the surface boundary. Instead surface samples were taken and volumetric soil moisture content determined gravimetrically. The average values at the start and end of the drying period 7th April to 15th April were 0.28 and 0.13 respectively.

At both tensiometer sets the change-over depth was 0.3 m on 15th April. Hence the estimated evaporation loss is 45 mm for this eight day period. The corresponding A-class pan evaporation (mean of Little Para Reservoir and Bolivar stations) is 50 mm for this period. Longer pond drying periods could not be obtained due to streamflow events. However the stream had been dry since 26th January prior to the first filling of the pond on 28th February. This 32 day drying period had an A-class pan evaporation of 296 mm.

Tensiometers T1 to T6 show a hydraulic gradient reversal at a depth of 0.6 m and T9 to T14 show it at 1 m, on 27th February. These depths are identical to those of the uppermost perching layers. It is concluded that these layers limit the depth from which evaporation may occur. Hence after eight days the amount of water remaining in the profile above the mean

evaporation limit 0.8 m is 104 mm. After 28 days most of this, (64 mm) remains here as residual soil moisture storage. (Based on average total moisture content above a depth of 0.8 m from figure 7.16 and 7.17 on 23rd and 24th February minus mean equivalent (constitutional hydrogen) water content, 0.13 - 0.05 = 0.08.) Some proportion of the 40 mm storage reduction drains through the perching layer while the point of hydraulic gradient reversal progresses downwards. Beyond this period hydraulic heads reduce considerably at the soil surface but very little evaporation occurs due to the strong adhesion of the residual moisture to the soil particles. The best estimate for the maximum evaporation loss on pond drying over a sustained period is 85 mm. This is equivalent to less than 6 hrs steady state infiltration.

The change in water content in the profile between logs in the driest conditions 23rd and 24th February and wettest conditions 7th March totals 530 mm over the top 5.3 m in the soil profile. Assuming the mixture of materials between the bottom of the logged profile (EL 4.7) and the mean water table position (EL 4.0) is the same as for the logged profile then the range of soil moisture storage capacity above the water table is 600 mm. Of this capacity approximately 8% is lost to evaporation in the first eight days and up to 14% if dry conditions persist beyond a month. The remainder drains from the soil profile to recharge the aquifer or is transpired by phreatophytes.

CHAPTER 8

DERIVATION OF A RESERVOIR RECHARGE RELEASE RULE

In this chapter a reservoir release rule for the Little Para Reservoir is derived with the use of regression and a simulation model. The BIEM model was not used to determine mean annual natural recharge nor the effect of alternative release policies on recharge from the Little Para River. Daily time steps necessary for investigating streambed hydraulic processes would have been extravagant with computer execution time and impractical for simulating 14 years of historical discharge records. Instead a lumped parameter management model with monthly time steps was used to simulate reservoir operation and the consequences on pumping costs and groundwater recharge from the streambed.

Firstly the principle of enhancing natural recharge by stream discharge regulation is outlined.

8.1 Effect of River Regulation on Aquifer Recharge.

Where a reservoir is located upstream of a reach which recharges an aquifer discharge regulation can be shown to enhance recharge. The relationship between recharge rate, Q_R and discharge rate, Q influences the degree of enhancement of recharge.

The simplest case where the relationship between Q_R and Q is time-invariant is presented for a range of stream-aquifer configurations in Appendix C.2. That analysis assumes stream stage and discharge rate are related by Mannings equation. Figure 2 in Appendix C.2 shows that for all cases Q_R increases with Q but that the proportion Q_R/Q termed "recharge efficiency", decreases as Q increases. In each case, of course, Q_R cannot exceed Q. Streamflow regulation redistributes short duration high discharge rates (low recharge efficiency) into long duration low discharge

rates (high recharge efficiency). Hence a reservoir may be used to enhance groundwater recharge in addition to yielding a surface water supply.

It may also improve the quality of aquifer water. With unregulated flow, infrequent high discharge rates which usually have low salt concentrations contribute most of the total discharge but have only small residence times in the stream in comparison to the longer duration higher salinity baseflow component. Streamflow regulation has the effect of maintaining the water quality in the stream at its volume-averaged concentration thereby improving the quality of recharged water.

Figure 8.1 presents a simple example of the calculation of the reservoir release, D during period, P to provide the target regulated recharge. The reservoir intake during this period is D_u. In this example the target recharge is the recharge, R_u which would have occurred if the stream was unregulated.

Assuming a steady relationship between Q_R and Q (figure 8.1(a)) gives a recharge efficiency shown in figure 8.1 (b). If the discharge rate exceeds Q_c flow extends beyond the recharging reach. A given reservoir inflow discharge record of duration, P may be divided into time increments and the recharge occurring for each of these determined using figure 8.1(a). The sum of these is R_u, the hatched area in figure 8.1(c), which is the total recharge if the flow was unregulated.

If the reservoir release rate is to be uniform figure 8.1(a) may be rescaled by multiplying the vertical and horizontal scales by P to give the relationship between recharge, R during period, P and the reservoir release, D. From figure 8.1 (d) a release D^* provides the target recharge. Higher releases would increase recharge at the cost of reducing reservoir yield. For ephemeral streams it is likely that $R_u < Q_c P$ and recharge enhancement up to $Q_c P$ is most water efficient. Note that reservoir evaporation and phreatophyte transpiration losses are neglected in this simple example.

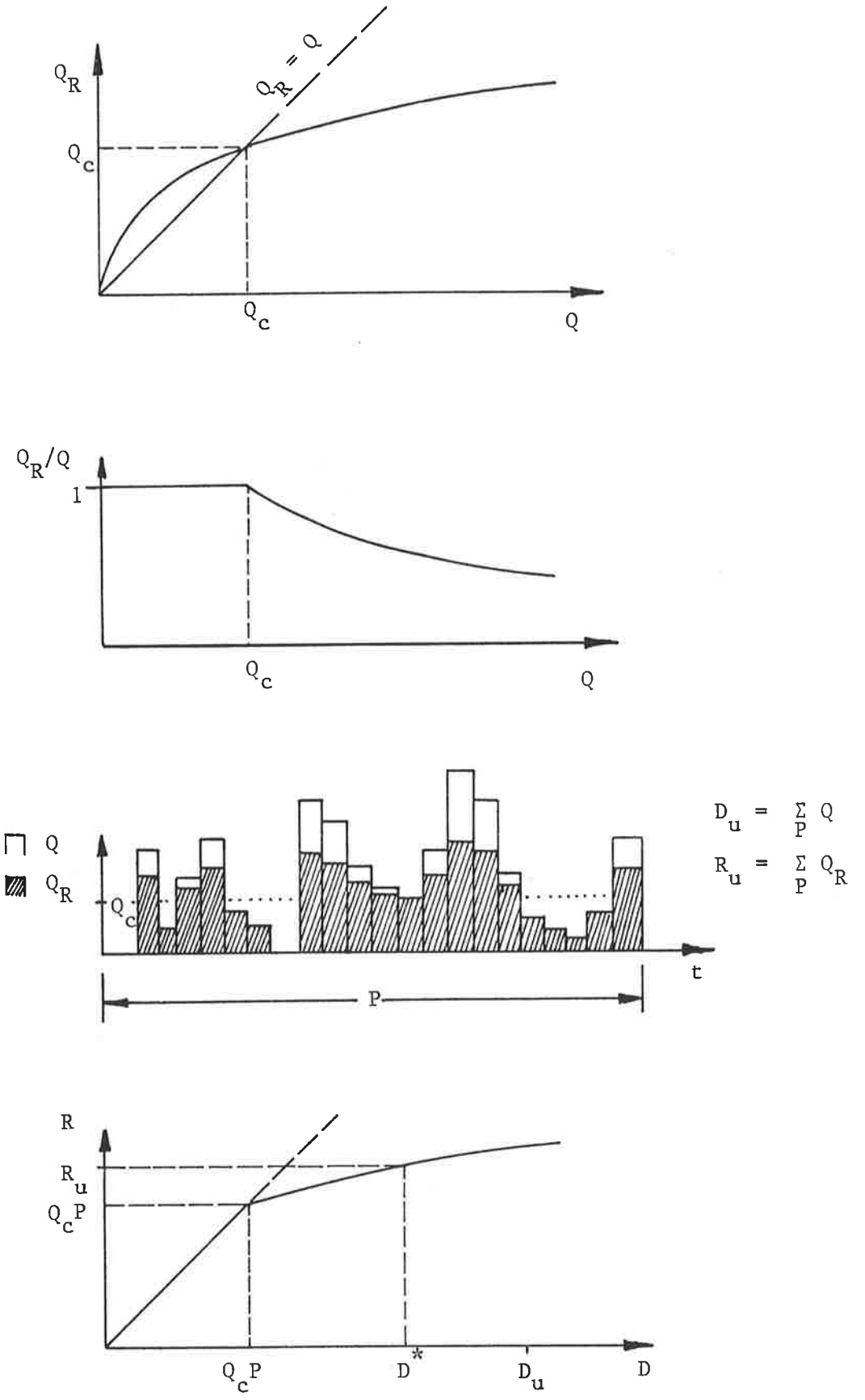

Figure 8.1 Illustration of the principle of discharge regulation for recharge enhancement. (a) recharge as a time-invariant function of discharge (b) recharge efficiency as a function of discharge (c) recharge as a proportion of discharge for unregulated discharge time series (d) recharge due to constant release of water.

This form of recharge calculation was used by Wyatt, Thorn and Mawer (1974). They examined the effect of conjunctive management of an aquifer and a reservoir in order to optimize the size of the surface storage. They defined a maximum recharge rate and all releases at less than this rate were considered recharged. This was applied to the River Stour in Essex, England.

A more sophisticated relationship between discharge rate and recharge rate was chosen by Biere and Lee (1972). They combined two reservoirs and rivers in California's Salinas basin to form a hypothetical ephemeral stream which recharges valley aquifers. They estimated recharge R_t during period, t to be

$$R_t = a_i D_t + b(D_t)^2 \qquad 8.1$$

where i represents the season number (i = 1, 2 or 3)

a_i varies with the season (0.82 to 1.04) to account for recharge from runoff entering the stream downstream of the dam.

b is a negative constant, indicating that percolation efficiency decreases as streamflow increases

and D_t is the reservoir release during period t.

This expression gave recharge efficiencies with respect to releases ranging from 1.02 to 0.57 for the releases used in Biere and Lee's study.

Stewart and Boughton (1983) reviewed a range of empirical relationships between transmission losses and discharge rates in natural hydraulically disconnected streams. However the Little Para River was found to become hydraulically connected in some reaches and the recharge rate depends on groundwater levels adjacent the stream. Thus discharge losses are related to the discharge history of the stream. The total recharge occurring through the streambed depends on the intake capacity of the streambed and the availability of water in the stream. A discussion of these two factors follows.

8.2 Little Para River Streambed Recharge Capacity

Daily discharge linear regressions between adjacent pairs of recording gauging stations were performed using the BMDP computer package (Dixon, 1981). The expressions for the line of best fit to the data for alternative data editing procedures are shown in Table 8.1. The coefficients A and B depend on the editing procedure but the value of Y for any given value of X are similar over the whole flow range. Set iv, the most rigorously edited set is used for subsequent calculations.

A first test (see Table 8.2) for variation in the discharge correlations over the study period year by year revealed no obvious trends. That is the effect of time on the streambed intake capacity was smaller than the effects of antecedent discharge, water temperature, evaporation rate and discharge measurement error.

Hydraulic connection was observed during sustained flow in the reaches between stations 3 and 5, stations 12 and 15 and for the upper part of the reach between stations 5 and 7. The remaining reaches remain hydraulically disconnected. Intake rates for these are more sensitive to discharge rate (see models 2 and 5 in Appendix C.2, table 1 and figure 2) due to the dependence of the wetted area of the semi-pervious layer and the hydraulic gradient across it to stream stage. This is reflected by lower values of the regression coefficient, A between stations embracing the hydraulically disconnected sections of the stream: the downstream part of the reach between stations 5 and 7 and the whole reach between stations 7 and 12.

A plot of the total streamflow loss between stations 3 and 15 for occasions when steady flow was maintained at station 15 in dry weather is shown in figure 8.2. A deduction for evapotranspiration is made and after testing a number of relationships between antecedent flow and recharge capacity the relationship described by figure 8.3 was selected. This provides a simple pattern which is related to the stream-aquifer

Table 8.1

DAILY DISCHARGE CORRELATIONS WITH ALTERNATIVE DATA SETS

Station X	Station Y	Data Set	A	B	R	N
3	5	i	.955	-1.57	0.992	405
		ii	.950	-1.21	0.991	1162
		iii	.957	-1.46	0.996	521
		iv	.927	-1.28	0.995	506
5	7	i	.947	-3.94	0.932	188
		ii	.844	-1.10	0.956	860
		iii	.999	-4.34	0.964	235
		iv	.864	-2.79	0.906	220
7	12	i	.920	-3.81	0.696	75
		ii	.862	+0.10	0.859	753
		iii	.920	-3.37	0.963	144
		iv	.745	-1.65	0.857	130
12	15	i	1.206	-3.12	0.934	63
		ii	0.995	-0.45	0.964	768
		iii	1.050	-2.69	0.994	123
		iv	0.980	-2.22	0.979	111

Y = A * X + B X, Y in ML/day

A = regression coefficient

B = constant of regression

R = correlation coefficient

N = number of days for which correlation could be performed

i = data set used in April 1981 report (Y>0, 26.2.79 - 20.6.80)

ii = complete data set except X, Y > 50 discarded

iii = as for ii except X, Y = 0 discarded and each day that rain was recorded at Little Para Reservoir and the following day were excluded

iv = as for iii except X, Y > 28 discarded

Table 8.2

DAILY DISCHARGE CORRELATIONS BY YEAR

Station X	Station Y	Year	A	B	R	N
3	5	1979	.923	-1.47	.992	112
		1980	.941	-1.25	.997	214
		1981	.896	-1.09	.988	99
		1982	.899	-1.09	.986	81
		All	.927	-1.28	.995	506
5	7	1979	.696	-2.04	.901	41
		1980	.981	-4.92	.937	94
		1981	.799	-1.13	.870	80
		1982	.420	+1.70	.993	5
		All	.864	-2.79	.906	220
7	12	1980	.726	-2.78	.827	56
		1981	.926	-2.23	.939	74
		1982		insufficient	data	
		All	.745	-1.65	.857	130
12	15	1980	.895	-2.23	.963	41
		1981	1.005	-1.97	.988	70
		1982		insufficient	data	
		All	.980	-2.22	.979	111

Y = A * X + B X, Y in ML/day

A = regression coefficient

B = constant of regression

R = correlation coefficient

N = number of days for which correlation could be performed

Set iv data used for all correlations above. MAX = 28.

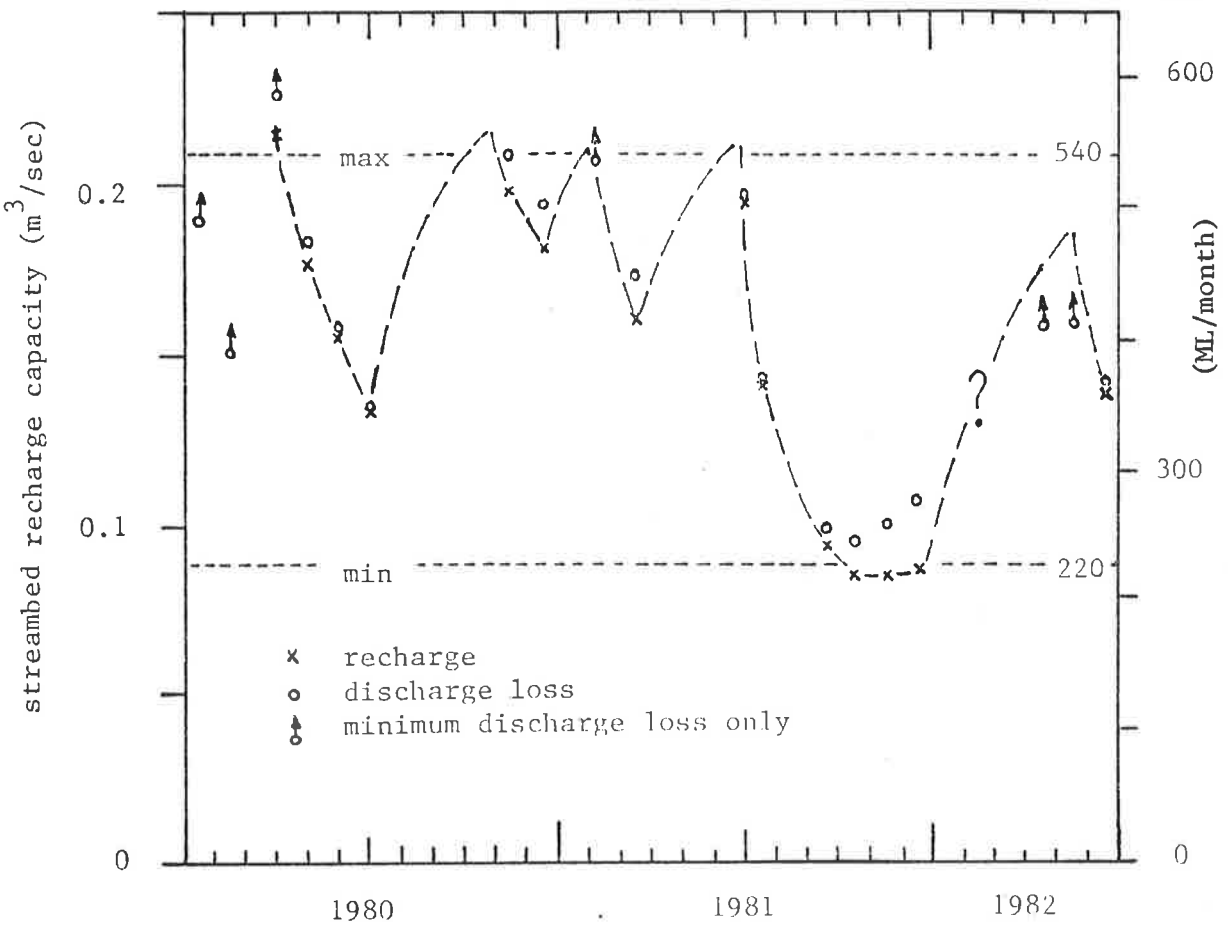

Figure 8.2 Streambed recharge capacity between stations 3 and 15, February 1980 - June 1982.

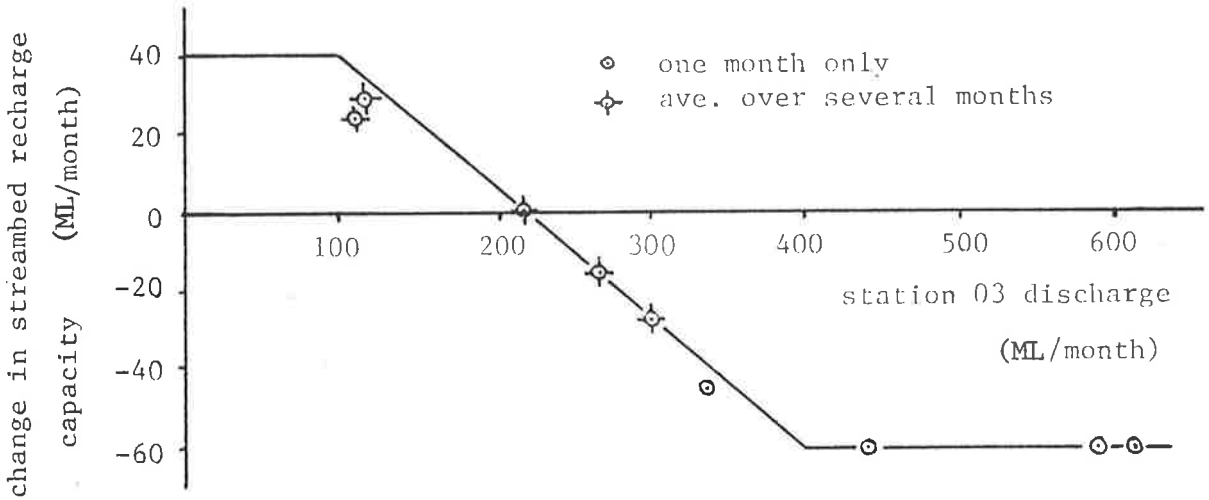

Figure 8.3 Algorithm relating change in streambed recharge capacity to monthly discharge at station 3.

interaction processes. For station 3 discharges in excess of 400 ML/month the loss in streambed recharge capacity is 60 ML/month, due to the reduced hydraulic gradient away from the stream caused by growth of the groundwater mound.

For discharges less than 90 ML/month the groundwater ridge dissipates faster than it is replenished and groundwater slopes increase. In fact some hydraulically connected parts of the stream may become hydraulically disconnected from the aquifer. An increase of 40 ML/month in recharge capacity results. For station 3 discharges between 90 and 400 ML/month the recharge capacity changes by intermediate values. A discharge of 214 ML/month produces no change in streambed capacity.

It is obvious from the above that at the end of a wet winter the recharge which would have occurred without the dam would be restricted by the streambed recharge capacity which would be low due to the high discharges over the previous months. Minimum and maximum streambed recharge capacities of 220 and 540 ML/month have been specified based on figure 8.2 and on calibration runs with monthly discharge and recharge through the study period. A longer study period would be expected to give a better estimate of peak recharge capacity. High flows were well represented in the study so the minimum recharge capacity is a confident estimate.

Having constructed a simple algorithm for changes in streambed recharge capacity based on monthly discharge at gauging station 3 and fitted it to the post dam discharge record the question of the availability of water in the streambed must be addressed.

8.3 Little Para River Temporal Distribution of Discharge

To relate the unmeasured recharge from unregulated (pre-dam) discharge to the measured recharge from regulated discharge the concept of "equivalent uniform flow" is introduced. This is the uniform discharge over a period of one month which would give the same recharge as the

natural flow pattern. Monthly discharge at station 3 was used as the basis because the reservoir release rule was to consist of monthly settings of discharge rate and station 3 had the longest discharge record.

The equivalent uniform flow was calculated as follows. Firstly the daily discharge regression equations for each of the four reaches were combined giving a discharge loss in the vicinity of 12 ML/day when discharge exceeded 12 ML/day at station 3. When the discharge was less than 12 ML/day the entire flow was expected to be lost before station 15. This simple algorithm was applied to the daily discharge record at station 3 from July 1968 to July 1977 in order to find the steady monthly discharge which would give the same monthly recharge (figure 8.4).

A number of assumptions or approximations have been used in finding the equivalent uniform discharge. The effect of antecedent flow on streambed recharge capacity has been neglected. The algorithm gives a recharge capacity of 360 ML/month which lies near the mid-range of the post-dam recharge capacity (figure 8.2). Secondly the regression equations applied to discharges less than 28 ML/day. Refering to Table 8.1 it is observed that the regression coefficient, A is higher for data set iii which includes discharges up to 50 ML/day. Thus it appears that losses become almost constant over the discharge range 28-50 ML/day. Above 50 ML/day discharge losses are unknown. As these high discharges generally occur on isolated rain days and having observed in chapter 5 the importance of the duration of flow on recharge for a hydraulically connected stream, it is thought that the extrapolation was not unreasonable.

Similarly this suggests that only an examination of daily flows is necessary as the distribution of discharge within a 24 hour period could provide only very short duration floodwaves. Therefore, the difference between recharge determined by examination of instantaneous discharge and that determined from daily discharge is expected to be small.

The equivalent uniform flow is equal to monthly discharges up to

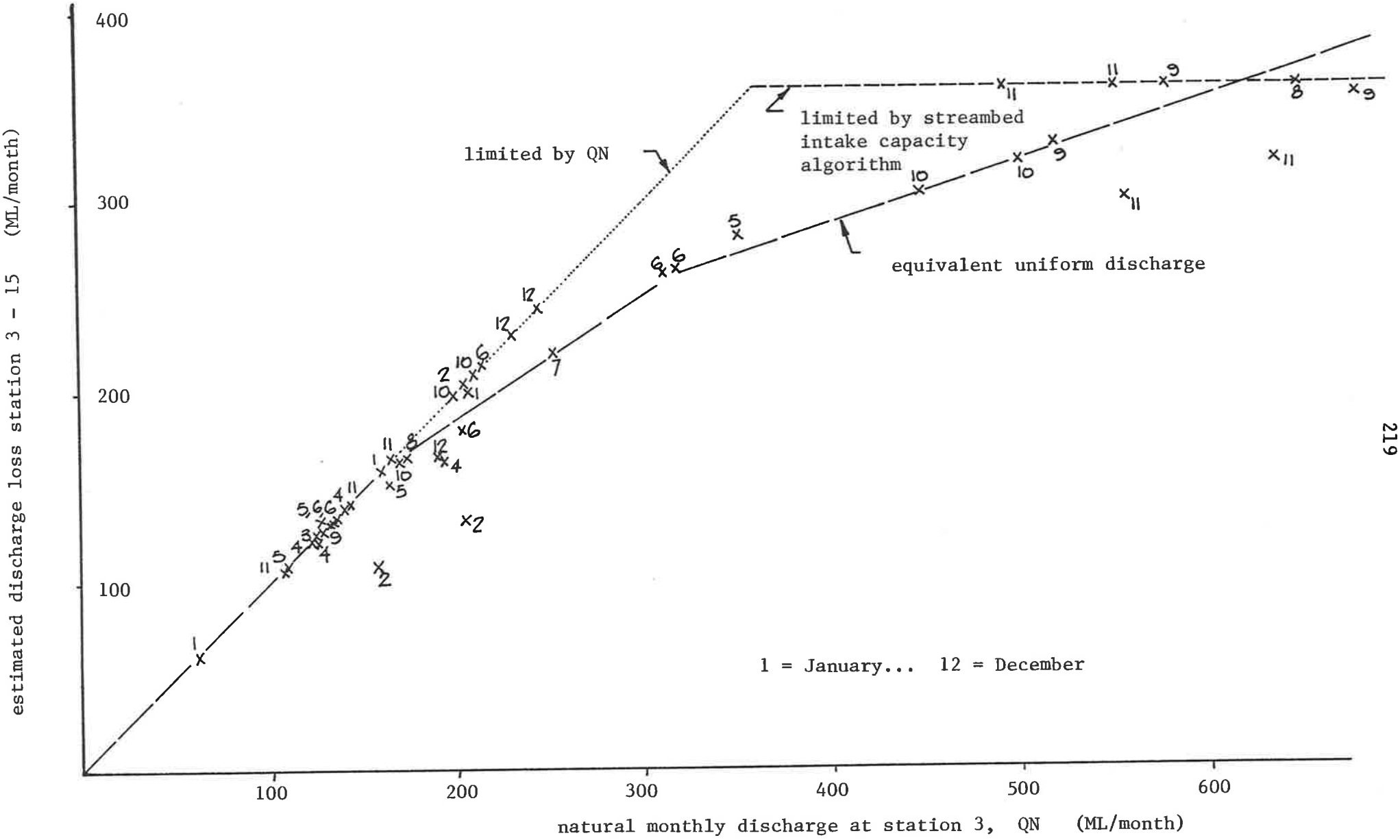

Figure 8.4 Estimated discharge loss between stations 3 and 15 related to monthly discharge at station 3, July 1968 - July 1977.

160 ML/month. Above that discharge some allowance is needed for occasional days when high discharges are conveyed through the channel and out to sea. Beyond 320 ML/month substantially more discharge reaches the sea. No upper bound was placed on the equivalent uniform flow as the channel recharge capacity would limit recharge in most circumstances, and secondly to allow some credit for additional recharge in the hydraulically disconnected reach. This was thought to compensate for the rigid 12 ML/day recharge capacity used in the derivation, and to allow the maximum post-dam recharge capacity to be obtained. The piecewise linear function for equivalent uniform discharge was fitted by eye.

This method could be improved by applying the monthly streambed recharge capacity, as determined from antecedent monthly discharges, to adjust the daily discharge loss algorithm. This was not tried but the effect is expected to be small as only a small number of months had discharges less than the maximum streambed recharge capacity and more than 160 ML/month (the discharge below which the equivalent uniform flow and the actual discharge are the same). That is variations on the function in figure 8.4 while they may be justified would not be expected to cause significant changes to recharge volumes.

8.4 Recharge Due to Runoff From the Catchment Below the Dam

The monthly inflow downstream of station 3 was estimated from each month from the establishment of gauging stations 12 and 15 in February 1980. The daily gain in flow, QID, in each reach was determined from

$$QID = QD - (A * QU + B) \qquad < 0 \qquad 8.2$$

where QU and QD are the daily discharge at the upstream and downstream gauging stations and A and B are the regression coefficients applying to the reach (from Table 8.1). The discharge gain was added for each day and reach to give the monthly discharge gain, QI between stations 3 and 15.

The monthly discharge gain was correlated against the naturally occurring (unregulated) monthly discharge at station 3. The latter was

calculated from

$$QN = NI + Q3 - RL - SC - SP \qquad 8.3$$

where QN represents the monthly discharge which would have been recorded at station 3 if there had been no dam.

NI is the natural catchment intake to the reservoir estimated from the reservoir water balance.

Q3 is the observed discharge at station 3.

RL, SC and SP are the recharge release, scour release and spill from the dam.

While the correlation between runoff downstream of station 3 with that upstream of station 3 was poor (R = 0.53, see figure 8.5) the equation derived

$$QI = 0.18 * QN \qquad 8.4$$

is considered satisfactory given the approximations involved in its derivation. Note that the under-registering of flow gains for summer months having low values of QN reflects the higher streambed intake capacity under dry conditions. The catchment area for QI is 38% of that for QN. Urban development takes up 18% of the downstream catchment compared with none upstream. The downstream catchment however is flat compared with the steep hills of the upstream catchment.

The monthly discharge at station 15, Q15 was correlated with the monthly discharge gain downstream of station 3, QI to determine the discharge loss, RI occurring due to the runoff downstream of station 3 for months with no reservoir release (figure 8.6). The best fit line was used to derive an expression for recharge with respect to flow gain,

$$RI = 0.23 * QI + 12 \quad \not> QI \qquad 8.5$$

Combining equations 8.4 and 8.5 gives an expression for discharge loss arising from runoff downstream of station 3 with respect to the unregulated discharge at station 3

$$RI = 0.041 * QN + 12 \quad \not> 0.18 * QN \qquad 8.6$$

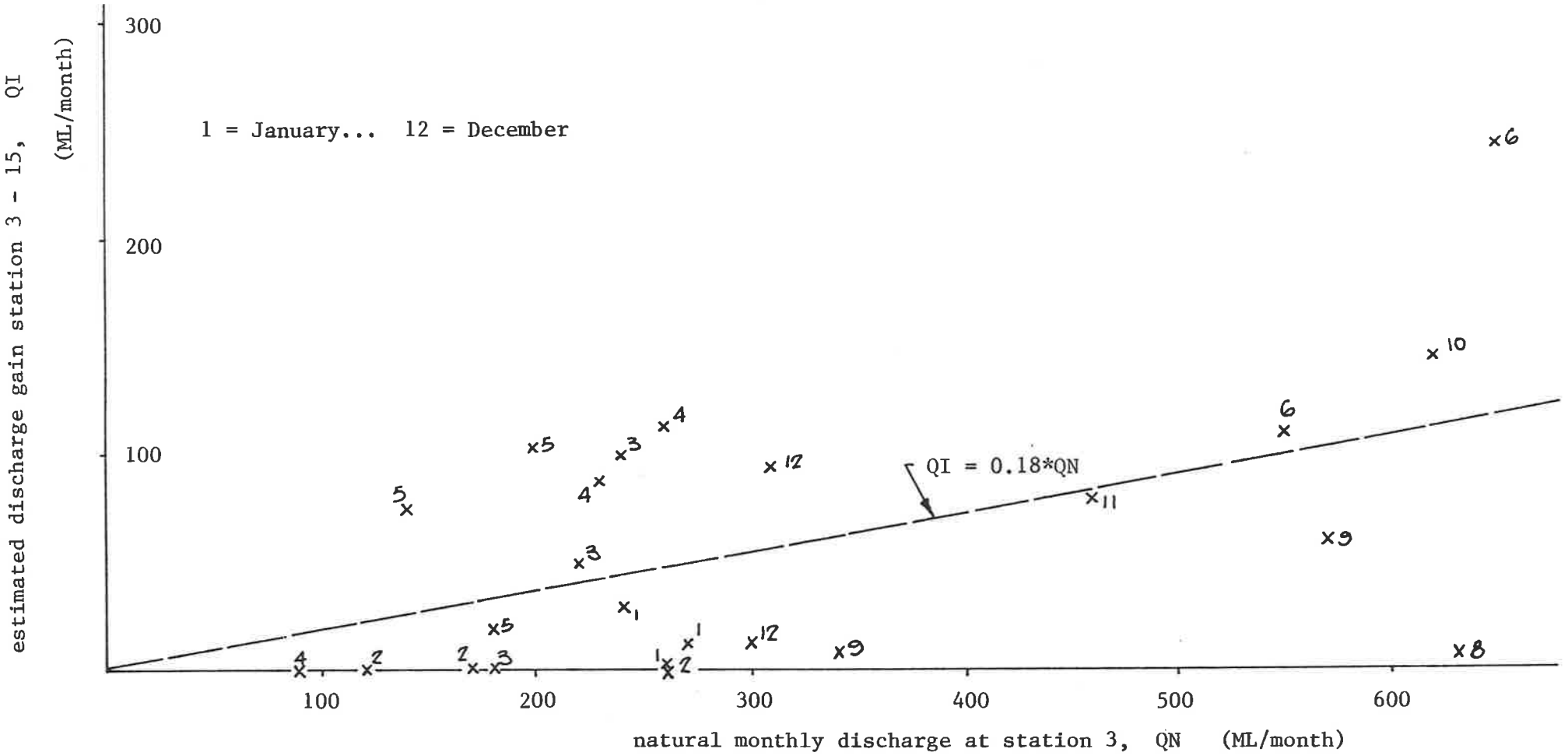

Figure 8.5 Comparing monthly runoff from the catchment between stations 3 and 15 with estimated natural runoff upstream of station 3, February 1980 - June 1982.

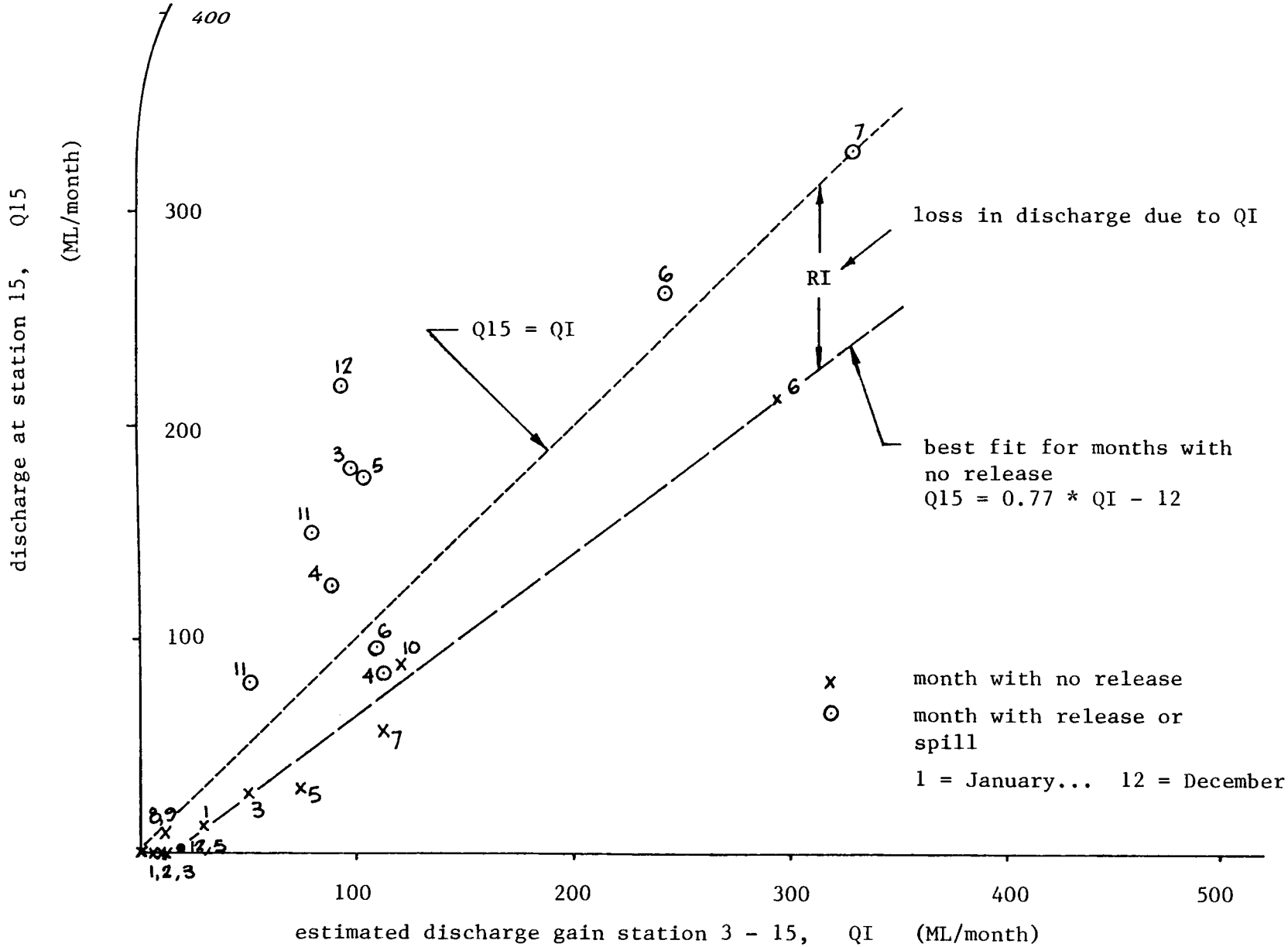

Figure 8.6 Comparing monthly discharge at station 15 with monthly runoff from the catchment between stations 3 and 15 for months with no releases, February 1980 - June 1982.

While the algorithm for discharge loss due to runoff downstream of station 3 is perhaps oversimplified and has wide confidence limits it is thought to be adequate. More sophisticated models relying on more parameters are less capable of calibration with the existing data set. An attempt to correlate QI with monthly rainfall data proved less reliable than the correlation with QN.

Runoff between the dam and station 3 was considered in conjunction with dam leakage.

8.5 Recharge From Dam Seepage

The catchment area between the dam and station 3 is 7.6% of the total catchment upstream of station 3. The gain in flow between the dam and station 3, I3, is correlated against the monthly natural discharge at station 3, QN for the period 1980 to 1982 to determine the dam seepage (figure 8.7).

The equation of the line of best fit is

$$I3 = 0.045 * QN + 31 \qquad 8.7$$

Assuming uniformity of runoff over the station 3 catchment area, the natural runoff I3N, is expected to be

$$I3N = 0.076 * QN \qquad 8.8$$

The resulting difference in flow is attributed to dam seepage, SEEP, where

$$SEEP = I3 - I3N = -0.031 * QN + 31 \not< 0 \qquad 8.9$$

There is no physical significance in the QN coefficient and an inspection of figure 8.7 reveals that the slope of the line of best fit for I3 could be as high as 0.076 without a marked effect on the correlation coefficient. Seepage is expected to be more closely related to reservoir storage level. Due to the very small seepage rates and very small variation of seepage rates predicted by equation 8.9 for the common range of QN no further analysis was performed.

Dam seepage gives a continuous low discharge and never exceeds the streambed intake capacity. However all flow components, dam seepage,

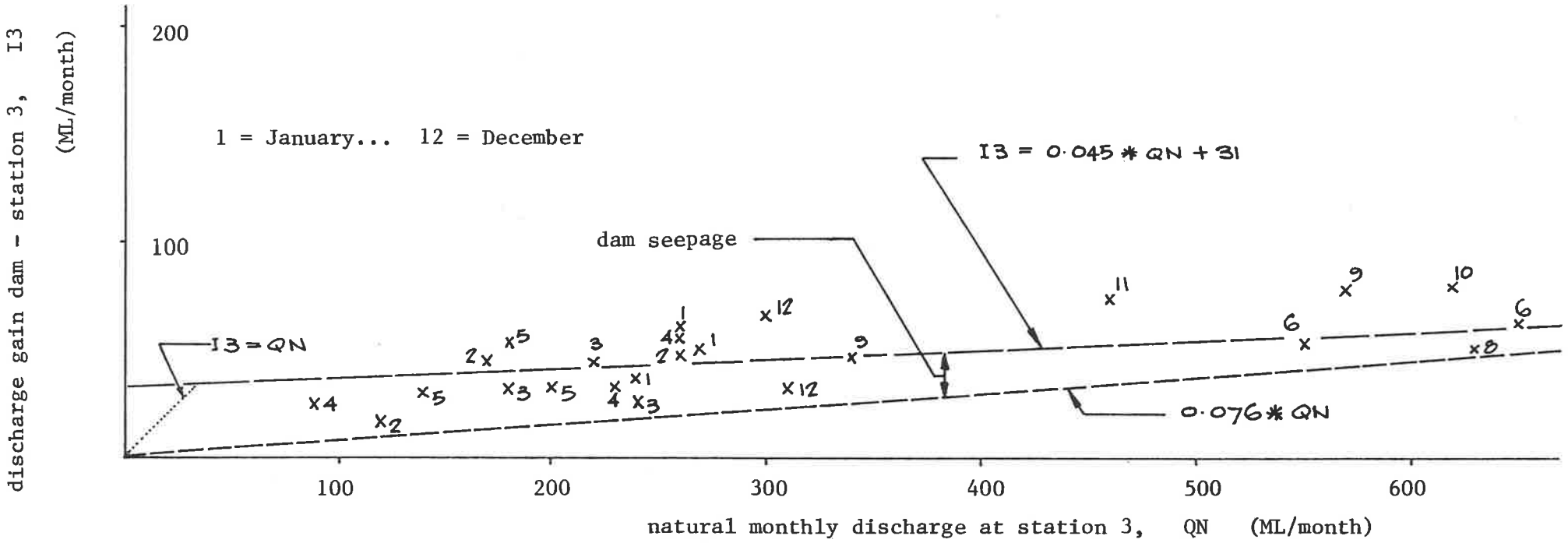

Figure 8.7 Gain in monthly discharge between Little Para Dam and station 3 compared with estimated natural runoff upstream of station 3, February 1979 - June 1982.

runoff below the dam and releases compete for the available recharge capacity. Releases from the reservoir should therefore allow for dam seepage and the expected runoff from the downstream catchment.

8.6 Reservoir Release Simulation

With the relationships between recharge and downstream catchment inflow, dam seepage and stream discharge defined the total recharge associated with alternative reservoir release patterns could be determined. A simulation model DAMSIM was written to calculate total groundwater recharge for alternative reservoir release strategies and the consequent costs of inter-basin pumping to maintain specified target storages in the reservoir. The recharge which would have occurred without the dam was found using the same simulation model.

The model also accounts for streambed evapotranspiration losses and has an option to enable conjunctive management of surface and groundwater storages to be evaluated. Appendix C.5 contains a block diagram (figure 1) of all physical system components considered in DAMSIM. Brief program documentation appears in Appendix D and a listing is given on the microfische.

With only 14 years stream discharge data for station 3 it was decided to test the sensitivity of the simulation results to streamflow record. Two 30 year sets of generated monthly streamflow data were provided by the Engineering and Water Supply Department of South Australia. These were produced by a method described in a report of that Department (South Aust., 1978). The mean annual discharge and coefficient of variation of the annual discharge for the three data sets ranged from 9400 to 10000 ML (1 ML = 10^3 m^3) and 0.49 to 0.67 respectively.

The resulting range in mean annual recharge was 2040 to 2170 ML, that is a spread of 6% of the estimated mean annual recharge from the historical data set.

The historical record gave the highest value due to a lower incidence

of zero flow than the synthetic data. All alternative release policies were simulated for each data set. The variation in recharge from each set was minimal but significant differences in mean annual pumping costs were observed. The ranking of costs of alternative release policies was almost identical for each data set and the same policy was optimal for each set.

8.7 Release Policies and Constraints

More than ten different types of release policies were simulated. These included:

- uniform releases,
- set monthly releases

  and releases dependent on
- the previous month's natural reservoir intake,
- the reservoir storage at the start of the month
- the recharge credit at the start of the month, where credit is defined as the excess of regulated recharge over the natural (no dam) recharge,
- the streambed intake capacity at the start of the month,
- the need for groundwater extraction during the month to replace part of the demand on the reservoir for metropolitan water consumption, and
- various combinations of the above.

The objective of the simulation was to identify the reservoir release rule which would minimize the cost of pumping water from the River Murray to maintain reservoir storages at specified target levels, subject to a number of constraints.

The constraints on release policies include the following considerations.

- Mean annual recharge is to be not less than the mean annual natural (no dam) recharge.
- A minimum annual release of 810 ML is required to secure the irrigation water supply in a shallow leaky aquifer downstream of station 7. This would require at least 3 months a year with release rates of no less

than 270 ML/month.

- Drying periods are required to discourage the growth of algae and to a smaller extent reed beds, both of which may partially clog the streambed and reduce infiltration rates.
- A minimum release of 120 ML/month during December and January is recommended. The stream is the focus of a corridor of parks which attract large crowds in the summer months. The recreational value of water in the stream is considered important by the Salisbury Council, which owns the parks.
- The policy is to consist of monthly changes in release valve settings and release rates should be relatively easily calculated using data readily available to the reservoir keeper.
- The policy should account for the existing recharge deficit, that is the shortfall in recharge due to the effect of the dam, at the date on which the rule is implemented with the view to produce a recharge credit within the planning horizon.

The reservoir target levels embodied a range of constraints such as provision of a level of security for water supply from the reservoir and allowance for the pipeline capacity available for transferring water from the River Murray to the reservoir. This capacity varied monthly according to the demands on other reservoirs fed by the same pipeline.

In addition the unit cost of pumping increases with the pipeline discharge rate (figure 8.8).

The optimal release policy for the specified target storages was tested for an alternative set of target storages (Table 8.3). These allowed a higher risk of the reservoir being incapable of meeting demand.

8.8 Results of Simulation

Table 8.4 gives a comparison of mean annual recharge and mean annual pumping cost for a series of alternative release policies for the three discharge data sets. A plot of pumping cost versus recharge is given

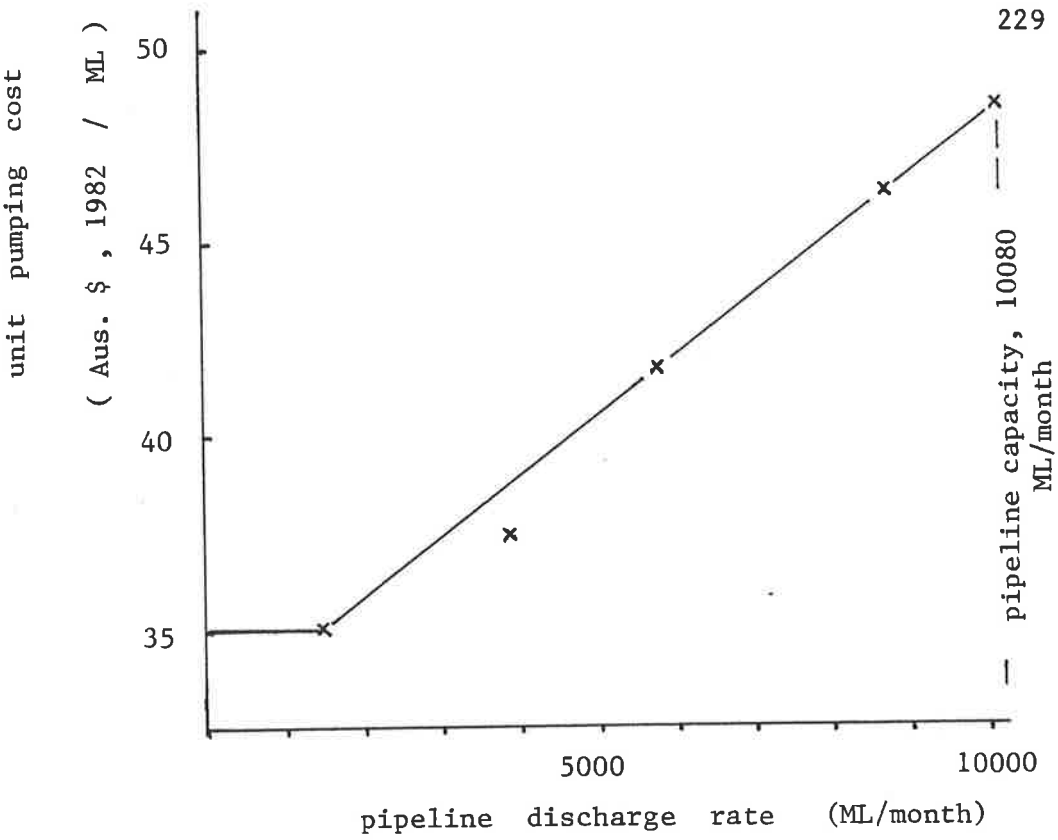

Figure 8.8 Unit cost of pumping water from River Murray to Little Para Reservoir versus pipeline discharge rate.

Table 8.3

Specified and alternative end of month reservoir target volumes and reservoir demand.

Month	Jan	Feb	Mar	Apr	May	Jun	Jul	Aug	Sep	Oct	Nov	Dec
specified	7	5	3	3	5	10	10	10	13	13	11	9
alternative	7	5	3	3	4	5	7	9	11	13	11	9
demand	2	2	2	0	0	0	0	0	0	0	2	2

(thousand megalitres)

Table 8.4

Mean annual recharge and pumping costs associated with a range of release policies for three discharge data sets.

	Annual recharge[b] (ML)			Annual pumping cost $,000		
Data set Policy No.	HIST	11B	11A	HIST	11B	11A
0/0	740	745	744	122	108	96
0/120	2122	2127	2127	165	153	136
0/125	2179	2180	2184	167	155	138
1	2618	2589	2596	189	181	161
2	2335	2318	2312	221	215	191
3	2289	2145	2241	189	173	158
4	2529	2388	2387	229	217	194
5	2137	2175	2186	165	155	140
6	2579	2535	2565	187	178	160[a]
7	2419	2294	2433	175+2[a]	166+2[a]	154+1
8	2256	2234	2337	168	159	147
9	2371	2189	2255	169+3[a]	159+3[a]	144+3[a]
10	2361	2230	2249	243	228	223
10/opt	2344	2260	2291	174	162	145
P5	2201	2195	2204	167	156	139
Natural Recharge:	2173	2037	2066	-	-	-

policy no	description
0/0	no release
0/120	release 120 ML/month
0/125	release 125 ML/month
1	release at streambed capacity minus expected inflow
2	Kingston and Shepherd (1973) - set monthly releases
3	Dillon (1977) rule A - dept. on previous months inflow only
4	Dillon (1977) rule B - dept. on previous months inflow and the season
5	dept. on reservoir volume and streambed capacity
6	dept. on reservoir volume and streambed capacity
7	as for 6 and including groundwater extraction
8	dept. on res. volume, streambed capacity and recharge credit
9	as for 8 and including groundwater extraction
10	simulates natural monthly recharge pattern
10/opt	as for 10 for discharges up to recharge capacity of streambed
P5	set monthly releases pulsed to give recharge in gardening areas.

a. power cost for groundwater extraction

b. includes recharge due to dam seepage and runoff from catchments downstream of the dam.

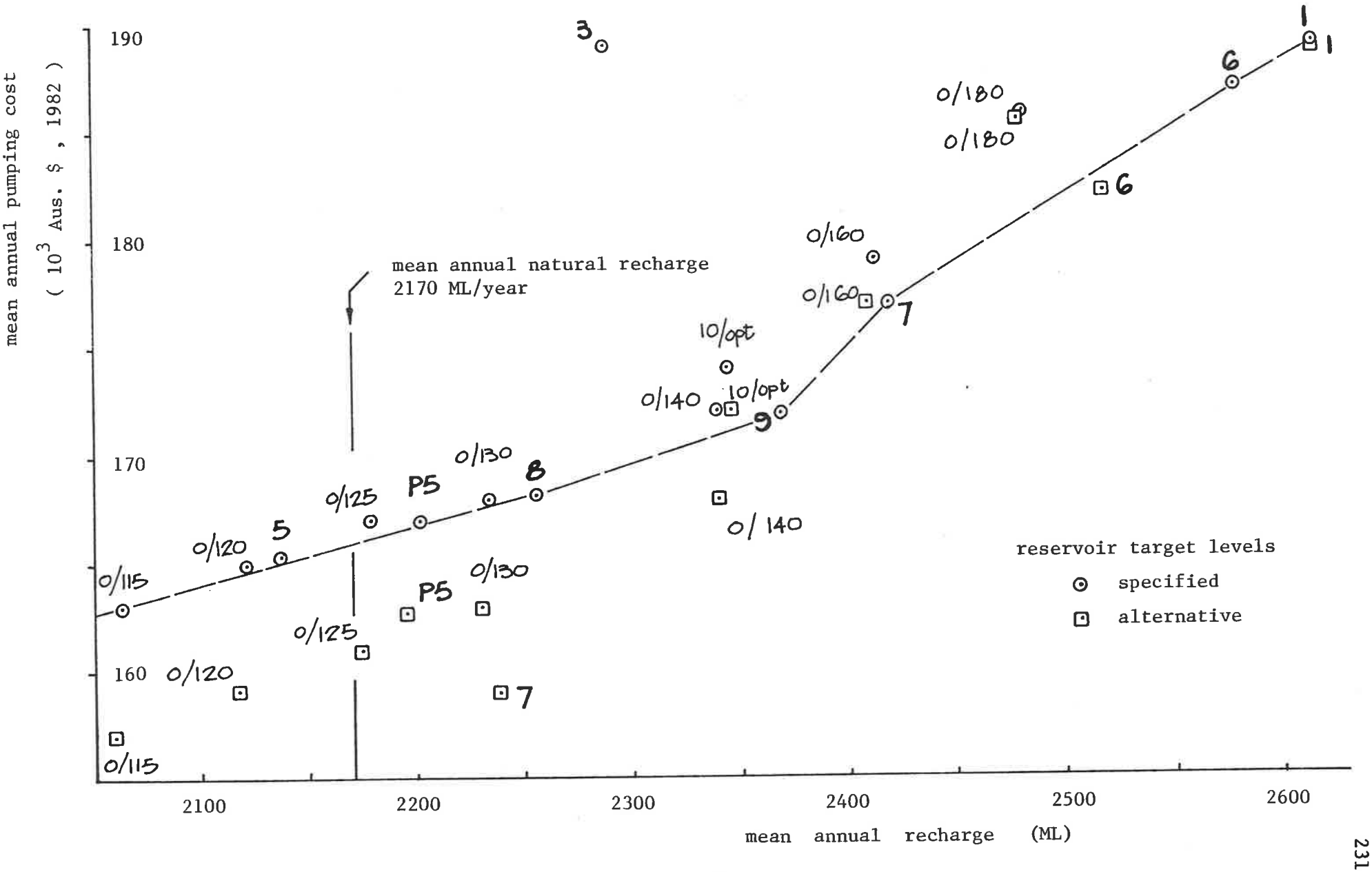

Figure 8.9 Pumping cost versus recharge for several release policies.

in figure 8.9.

It was expected that policies which reduced releases in dry years and increased them in wet years such as policies 5, 6 and 8 would have resulted in lower mean annual pumping costs. However "dry" years, when reservoir natural intake is insufficient to meet reservoir demand (10000 ML), evaporation loss (1070 ML) and mean annual releases (1530 ML) (totalling 12600 ML), occur in almost 80% of all years. This means that in the occasional "wet" year when pumping is not required the recharge must be substantially greater than the mean figure in order to allow any significant reduction in dry year releases. The problem is compounded by the large amount of runoff from the catchment below the dam in wet seasons. Under these conditions releases from the reservoir are in competition with the local runoff for the available streambed intake capacity, which has been reduced by the high discharges. Increasing releases at such times may cause only a marginal increase in recharge and unless spill is imminent pumping would eventually be needed to replace most of the released water.

If reservoir demand had been significantly less it is expected that some form of compensation for low natural intake to the reservoir by reducing releases would result in lower pumping costs. This would be possible because lower target storages could be set and higher carry-over storages would be available leading to a frequent surplus which could be released in summer months when streambed intake capacity had recovered and expected downstream runoff was at a minimum. Hence recharge could be efficiently increased in frequent "wet" years allowing substantial reductions in releases in occasional "dry" years.

The lowest pumping cost is attributed to a uniform annual release. This spreads the pumping volumes more evenly through the years thereby reducing the frequency of pumping large volumes with their attendant higher unit costs. These ranged from \$35/ML for discharges up to 1500 ML/month to a peak of \$48.5/Ml at the pipeline capacity of 10080 ML/month. In the

Table 8.5

Mean annual volumes (megalitres) and statistics using the recommended release rule with specified and alternative end of month reservoir target volumes for three discharge data sets.

Target reservoir volumes	specified			alternative		
Data Set	HIST	11B	11A	HIST	11B	11A
Discharge at GS504503	9353	9954	10048	9353	9954	10,048
(Std. Deviation)	(6169)	(6727)	(4962)	(6169)	(6727)	(4962)
(5) Pumping	4512	4283	3828	4077	3652	3203
(4) Release	1530	1530	1530	1530	1530	1530
Demand	10,000	10,000	10,000	10,000	10,000	10,000
Recharge due to releases	1466	1462	1467	1466	1462	1468
Recharge due to d/s catchment	542	531	549	542	531	549
Recharge due to dam seepage	188	193	183	188	193	183
Recharge due to spill	5	9	5	0	5	0
Total recharge	2201	2195	2204	2196	2192	2200
Natural recharge	2173	2037	2066	2173	2037	2066
Evaporation	1069	1072	1109	788	815	832
Spill	493	879	473	0	505	46
(1) Pumping cost ($)	167,000	156,000	139,000	163,000	147,000	126,000
(2) Pumping Cost No Releases ($)	122,000	108,000	96,000	108,000	93,000	74,000
(3) Cost of Releases = (1) - (2) ($)	45,000	48,000	43,000	55,000	54,000	52,000
(6) $/ML Released = (3) / (4)	29.4	31.4	28.1	35.9	35.3	34.0
(7) $/ML Pumped = (1) / (5)	37.0	36.4	36.3	40.0	40.3	39.3
years of no pumping/yrs record	4/14	5/30	5/30	3/14	8/30	8/30
years of spill / record	3/14	5/30	6/30	0/14	3/30	2/30
Replacement / Release = (6) / (7)	0.79	0.86	0.77	0.90	0.88	0.87
Months of summer pumping/ years	4/2	4/4	1/1	15/7	28/11	26/14
Max month summer pumping (month)	1669 (3)	1985 (3)	128 (3)	2215 (1)	2270 (1)	2091 (3)
Max season summer pumping	1705	1985	128	6387	6674	3863
Final Volume minus Initial Volume	869	0	0	5628	0	2390

management model pumping could occur in May and June to ensure that target volumes were reached. In these months there was no other demand on the pipeline. Pumping in other months would only occur to prevent reservoir storage falling below 500 ML. On these occasions it is assumed that the pipeline is already in use and that to convey water to Little Para Reservoir it must carry its full discharge capacity.

The alternative target volumes increase the incidence of summer pumping from 14% to 50% of years and increase the maximum summer season pumping from 1700 ML to 6400 ML for the historical discharge data set. This also reduces the pumping cost by $4000 pa, which gives the value of allocating additional pipeline capacity to the Little Para Reservoir during summer months. Table 8.5 summarizes the components of the hydrological balance and the costs associated with the recommended release policy for the specified and alternative target reservoir levels.

The recommended release rule P5, shown in table 8.6 provides a constant annual release of 1530 ML which is distributed through the year in accordance with the constraints on release rules previously outlined. The distribution of the annual release between months had only a negligible effect on annual recharge and on pumping costs. Of the total recharge, 2200 ML, the approximate proportions of the components are releases 66%, downstream runoff 25%, dam seepage 8% and spill 1%. The natural recharge, 2170 ML, is exceeded by releasing only 18% of the natural intake to the reservoir.

Table 8.6

Recommended recharge release rule.

Month	Jan	Feb	Mar	Apr	May	Jun	Jul	Aug	Sep	Oct	Nov	Dec	Year
Release (megalitres)	330	30	90	60	270	30	150	60	30	300	60	120	1530

Release rule 1 (in table 8.4) gives 2620 ML recharge, the maximum of the release rules tested. The maximum sustainable mean annual recharge is estimated as 2560 ML based on the discharge at station 3 required to maintain a stable intake capacity (from figure 8.3). This neglects two partially compensating factors, evapotranspiration losses and recharge due to runoff entering the river downstream of station 3. Hence the potential exists for artificial groundwater recharge enhancement by up to 20% through discharge regulation, although at present this is not economically viable.

8.9 Conjunctive Management of Surface and Groundwater Storages

The prospect of drawing metropolitan water supplies from the Little Para Reservoir and Northern Adelaide Plains aquifers was considered in some reservoir release policies listed in Table 8.4. The DAMSIM model allowed for artificial recharge facilities and groundwater extraction for metropolitan water supply. However streambed recharge capacity limits groundwater recharge on average only one year in five. The capital costs of these schemes and their low rate of use rendered them unviable.

The foundation work on conjunctive operation of dams and aquifers was presented by Buras (1963). An example of feasible conjunctive operation of the Burdekin Falls Reservoir and the Budekin Delta aquifer is given by Hadgraft, Volker and Stark (1982).

8.10 Conclusions

A reservoir release rule was found by simulating reservoir operation and the relationship between monthly recharge and discharge in a stream. This relationship was determined empirically based on discharge observations over the period February 1980 - June 1982. In addition to lack of confidence in some of the regression equations used, these relationships may vary with time on a longer time scale.

The geometry, composition and biota of any segment of a stream channel is in dynamic equilibrium with the discharge-frequency function and the sediment and chemical loads of the streamflow. Each of these factors

suddenly changed in August 1977 for the Little Para River when the Little Para Dam was sealed. In addition the artificial expansion of the catchment through urban drainage schemes has already produced obvious changes in the shape and elevation of the streambed. The details of reports of these two effects for other streams and observations on the Little Para River and the implications for streambed recharge capacity are presented in Dillon (1983a, chapter 2). Consequently in the same report a small monitoring programme was recommended to accompany the implementation of the recommended release rule.

Based on this study an annual release of only 18% of mean annual reservoir intake is sufficient to maintain natural streambed recharge. There is potential, though presently it is not economically viable, to enhance groundwater recharge by up to 20% by discharge regulation.

Discharge regulation also has the capacity to improve the quality of recharged water. Baseflow recorded at station 3 prior to dam construction had total dissolved salt (TDS) concentrations between 800 and 1200 mg/l. During high flow TDS fell lower than 100 mg/l, with the volume-averaged TDS of less than 500 mg/l. For unregulated flow the better quality water has a relatively short residence time in the streambed compared with baseflow from the upstream catchment. Discharge regulation has the effect of recharging water at the volume-averaged concentration thereby improving groundwater quality.

CHAPTER 9

CALIBRATION AND VALIDATION OF STREAM-AQUIFER INTERACTION MODEL WITH DATA FROM LITTLE PARA RECHARGE STUDY.

The ability of the BIEM model to simulate theoretical problems has been demonstrated in Chapter 5. Its ability to simulate the interaction between a real stream and aquifer is shown in this chapter. The model is calibrated and validated for five cross-sections of the Little Para River (figure 9.1).

Due to the constraint of computer execution time only daily time steps are considered and runs are limited to no more than fifty days. Node spacings increase logarithmically from the stream to the outer limit of the model, 1200 m. As the duration of flow in the stream increases the groundwater mound curvature distant from the stream also increases. This results in increasing mass balance error due to the approximation of the volume change below the free surface. Additional nodes are needed to overcome this problem, which in turn increases the computer execution time for each time step. Longer runs would provide better estimates of the longer term processes such as percolation through the aquifer base, but these will not be pursued at this stage. The model has already been shown to work for transient problems such as the Cooper and Rorabaugh flood wave independent of the duration of the period providing there are sufficient model time steps to represent the change in stream head.

If say "instantaneous" or hourly discharge periods were used for calibration, a flow routing procedure would be required to obtain the temporal separation of channel storage change and either recharge or baseflow gain. As the objective of the model is to determine recharge for daily periods up to a month, the distribution of recharge during a day is

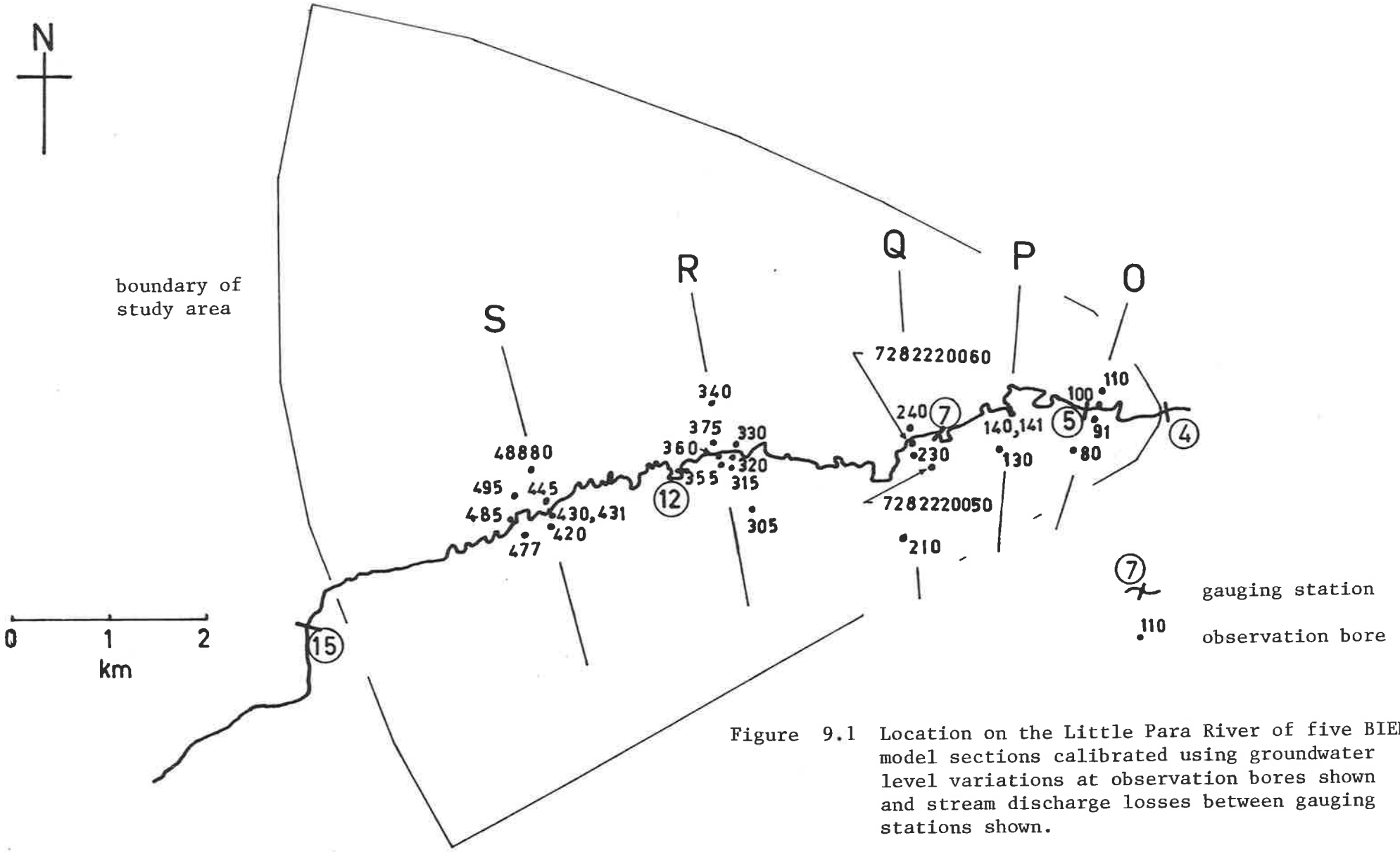

Figure 9.1 Location on the Little Para River of five BIEM model sections calibrated using groundwater level variations at observation bores shown and stream discharge losses between gauging stations shown.

not required. The assumption is made that the net recharge over a day derived from the actual discharge hydrograph is approximated by the recharge due to the mean daily discharge flowing uniformly throughout the day. From the reservoir release pattern study in Chapter 5, it is likely that the model overestimates natural recharge on days when flow rates vary significantly such as on wet days. However no calibration can be obtained for such days due to unaccounted local run off entering the stream between gauging stations. Thus daily time stepping is practical from the perspective of availability of data and for containing computer execution times. The model assumes channel storage changes are negligible compared with daily discharge losses. This assumption is reviewed in section 9.8.8.

At a conference entitled "Verification of Mathematical and Physical Models in Hydraulic Engineering" Wilson and Dettinger (1978) compared the theory of steady state and transient calibration of groundwater models. They concluded that static or slowly responding systems are relatively insensitive to the values of aquifer hydraulic parameters. For rapidly responding or highly stressed systems the parameter sensitivity and information content of measurements is significantly increased. Hence the calibration procedure focused on periods of rapid change in groundwater levels adjacent the Little Para River following periods of no flow. This was expected to give good estimates for the stream-aquifer interaction parameters in the model due to the sensitivity of groundwater elevations adjacent the stream to streamflow.

The FORTRAN-4 computer program BIEMCAL containing the model described in Chapter 4 and all calibration and validation subroutines described in this chapter is documented in Appendix D and its listing given on the microfische.

9.1 Calibration Procedure

A three step calibration procedure was adopted to fit the BIEM model to stream discharge and groundwater elevation data from the Little Para Recharge Study. The unknown parameters to be identified were

(1) streambed cross-section geometry

(2) elevation of aquifer basement, y_b

(3) streambed hydraulic impedance, B

(4) aquifer hydraulic conductivity, K

(5) aquifer effective porosity, n_e

(6) hydraulic gradient through the base of the aquifer, $\left(\frac{\partial h}{\partial n}\right)_b$

and (7) capillary drive in unsaturated flow, h_c

The river was divided into four reaches by five gauging stations equipped with continuous water level recorders. Each reach was modelled by considering a single cross-section of the stream in the vicinity of observation bores (figure 9.1). Two sections were used for the reach between gauging stations 7 and 12, due to quite different groundwater responses upstream and downstream. For each section the parameters above were regarded as constants.

Firstly the streambed geometry was determined from a series of surveyed channel cross-sections. Although stream width varied considerably there was no significant trend with running distance along the stream. The mean water surface width varied between 4 and 4.8 metres for the range of release rates used (70 to 300 l/s). Channel shape varied considerably for the surveyed sections. For convenience, a trapezoidal channel with base width 4 metres and 45° side slopes was selected to represent the "average" streambed geometry for each reach. Calibration was performed regarding this as the fixed streambed geometry. It is subsequently shown in the sensitivity analysis that changes in streambed width or stream bank slope may improve model results.

Secondly a relationship between the stream stage in the "average"

section and discharge rate was required. Flow in the stream was more like rill and pool behaviour than normal flow so in place of Manning's equation a simple exponential relationship was derived using the best fit correlation of wetted cross-section area to discharge. The elevation of the water surface in the "average" cross-section at a given discharge rate was found by equating wetted cross-section area with the mean correlated value. This crude approach assumes equality of average frictional resistance of the wetted perimeter along the reach length with the frictional resistance of the "average" cross-section. While this is not possible for a range of discharge rates this approximation is expected to be insignificant compared with the scatter in the correlations used to derive the "average" section and the stage-discharge relationship:

$$Q = 320. \text{ (depth)}^{2.88} \qquad 9.1$$

where Q is the discharge (ML/day = 10^3 m^3 /day)

and the stream depth is given in metres.

The effect of this equation is examined later in the sensitivity analysis. The remaining unknowns are solved for fixed streambed geometry and using this stage-discharge relationship.

The elevation of the aquifer basement could not be stated simply from examining bore logs, as the aquifers consisted of interbedded and lenticular layers of gravels, sands and silts within the Hindmarsh Clay formation. The thickness of these more permeable layers, known in Eastern Australia as "shoe string sands" varies considerably over short distances.

The calibration procedure increases in complexity with successive stages. In the simplest stage estimates for B and y_b are used to predict K/n_e using a small sample of bore water elevation data. The second stage refines B, y_b, $\left(\frac{\partial h}{\partial n}\right)_b$ and K/n_e using all available bore water elevation data. Stream discharge data is also used in the third stage to finalize B and y_b and to determine K, n_e and h_c. All model parameters have then been defined.

9.2 Stage I Calibration (ICAL=2)

The free surface boundary condition (equation 4.31) involves two of the above unknowns K and n_e. To remove these from the boundary condition a time transformation, equation 4.42 is used. This scales the model time, t^* by a factor of $K/n_e L$ with respect to real time. The characteristic length, L is set to 1 metre for all further reported uses of the model. Hence the time ratio (TR) of model time to real time, t^*/t becomes K/n_e per metre.

Initially the model can be fitted only for time-invariant stream stage as the time ratio is unknown. Hence initial calibration is carried out using data from a period of relatively constant stream discharge and also setting $h_c = 0$. Inspection of discharge records suggested 10/2 - 24/3/81 as the most suitable period.

The time ratio was determined using a set of match points. These are the pairs of time and free surface elevation for observation bores at known distances from the stream. Up to two match points per observation bore were used. The BIEM model was run using first estimates for y_b, B and $\left(\frac{\partial h}{\partial n}\right)_b$. Stream elevation was set at the constant mean value. Logarithmic time stepping was found to be most efficient with computer time while maintaining satisfactory mass balances (within 5%). The free surface elevations corresponding to observation bore locations were computed at each model time step. At the end of each model run these were compared with match point elevations and the model time (if found) at each match point divided by the real time in days since the model start time gave the time ratio for the match point. The mean and standard deviation of the match point time ratios were calculated along with other statistics. The coefficient of variation (standard deviation divided by the mean) was used as a measure of the adequacy of the model.

As a secondary indicator the model times were regressed on the real times for each match point. The slope of the line of best fit, its real

time intercept and correlation coefficient were recorded. Improved model performances were indicated by the slope approaching the mean time ratio, the intercept approaching zero and the correlation coefficient increasing. In general these features were observed for runs producing smaller values of the coefficient of variation, as expected.

A trial and error approach was used to adjust the three parameter estimates to reduce the coefficient of variation. As $\left(\frac{\partial h}{\partial n}\right)_b$ was found to be negligible in all except one case (and confirmed in later calibration stages) it was a relatively simple task to adjust B and y_b. The typical effect of changing these parameters is shown in Table 9.1

Table 9.1

Effect of changing streambed impedance, B, and aquifer basement elevation, y_b on time ratios for observation bores near and far from the stream.

increase	bore adjacent stream	distant bore
B	TR increases	TR increases rapidly
y_b	TR reduces slightly	TR increases

This first phase of calibration provided a screen to reduce the range of B and y_b values for further consideration. It also revealed the range of the time ratio for use in the next stage of calibration.

9.3 Stage II Calibration (ICAL = 3)

The first stage of calibration is particularly sensitive to errors in the small subset of observation bore water level data chosen as match points. The time ratio estimate was refined by extracting from the groundwater elevation file (AHDFILE) the whole data set for each relevant observation bore for the calibration period and recording the root mean sum of squares of the residual (the difference between prototype and model

groundwater elevations), RMSS-B (B refers to bores).

$$RMSS = \sum_{i=1}^{n} \left[\frac{(P_i-M_i)^2}{n}\right]^{\frac{1}{2}} \qquad 9.2$$

where P_i is the i^{th} prototype observation

M_i " " " model prediction, and

and n is the number of observations.

Stream elevations were again set constant and logarithmic time steps employed. This time the best time ratio from stage I was used and in addition ±10%, ±20% and ±40% this value were employed when comparing model results with observation bore water levels. This required only one pass of the BIEM model with multiple arithmetic operations only on the model results.

The values of B and y_b were adjusted in order to minimize RMSS-B. It was found that the mean of residuals also provided a useful guide to parameter adjustments. As further guide the metric, χ_C^2 defined by Cunningham and Sinclair (1979) as

$$\chi_C^2 = \sum_{i=1}^{n} \frac{(P_i-M_i)^2}{M_i} \qquad 9.3$$

was calculated in a modified form

$$\chi_D^2 = \sum_{i=2}^{n} \frac{[(P_i-P_1)-(M_i-M_1)]^2}{M_i-M_1} \qquad 9.4$$

where P_1 and M_1 represent the initial prototype and model groundwater elevations respectively.

In most cases the model parameters producing the minimum RMSS-B also gave the minimum χ_D^2 . The major difference was that χ_D^2 gave a higher weighting to residuals of bores distant from the stream having smaller elevation changes. As the stream-aquifer interaction was of prime concern

the RMSS-B measure of fit was adopted.

Line printer plots of observed and model groundwater elevation changes at observation bores could be performed to allow visual comparison. A second option, the use of a CALCOMP (flat bed) plotter was used only for final results as the line printer plots were faster and satisfactory for calibration purposes. These plots helped in deciding how to adjust parameters when fine tuning the model.

9.4 Stage III Calibration (ICAL = 4)

With the values of y_b, B, $\left(\frac{\partial h}{\partial n}\right)_b$ and TR defined for steady stream stage, time varying boundary conditions were introduced. The file containing daily discharge and meteorological records (COMBMDP) provided the daily discharge at the upstream gauging station. The stream stage was calculated using equation 9.1.

Normally daily time steps were used for the model at this stage, with the stream head adjusted at each step. Six initial logarithmic time steps were used to reach the end of the first day in order to contain the mass balance error. (The initial normal hydraulic gradient, $\frac{\partial h}{\partial n}$ along the free surface must be estimated and for all runs presented this was set to zero. Large successive initial time steps produced large errors in $\frac{\partial h}{\partial n}$ and consequently in free surface position and mass balance error.) Alternative time stepping procedures could also be employed such as solving at preselected times, or using logarithmic time steps, with the model interpolating stream stage linearly with time between pairs of values determined from the discharge record.

Daily discharge losses or gains over the reach between two gauging stations are compared with the instantaneous streambed intake rate at the section multiplied by the reach length. Symmetry of the prototype about the stream centre line and uniform discharge losses or gains along the length of stream are assumed. The latter implies that the time for initial onset of flow to cross the reach is small compared with the time elapsed

since flow commenced for reaches which become hydraulically connected.

In subroutine FLOWFIT, the model and prototype discharge losses or gains each day are compared providing there was no rainfall on the day in question or the preceding day. This screening eliminated spurious correlations involving unaccounted runoff entering the reach between the gauging stations.

The ratio of prototype discharge losses Q_p, to model discharge losses Q_m gives the hydraulic conductivity, K of the aquifer, and K divided by the time ratio gives its effective porosity, n_e.

i.e. $$K = Q_p \; / \; Q_m \qquad 9.5$$

and $$n_e = K \; / \; (t^* \; / \; t).L \qquad 9.6$$

where t^*/t is the time ratio of the model to real time (day^{-1})

and $L = 1$ metre, the adopted characteristic length.

Again the root mean sum of squares of residuals, this time called RMSS-Q, where Q denotes discharge loss residual, is used as a measure of fit of the model to prototype data.

The method adopted for calculating K was to take the mean of Q_p/Q_m ratios for dry weather discharge losses. As a secondary index the slope of the line of best fit of the scatter plot of Q_p versus Q_m was calculated. The latter method proved unreliable as larger scatter for the initial high discharge losses had a significant influence on the slope of the line of best fit.

Days affected by rainfall or with missing discharge data for which the program made an estimate based on a dry weather discharge correlation (subroutine CORRELQ), were not included in calculation of K. However discharge loss for these days was estimated and the total discharge loss during the calibration period calculated. This could be compared with the total discharge loss calculated from the model.

Only minor variations in model parameters were required during stage three to fine tune the model, indicating that the form of the stream-

aquifer interaction process appears acceptable. Line printer and CALCOMP plot options were provided for visual comparison of daily discharge losses.

9.5 Model Validation (ICAL = 5)

The validation period selected was 18th November 1980 to 5th January 1981. It was chosen because of its relative freedom from rainfall interference. Due to its closeness to the calibration period little change in streambed geometry and hydraulic impedance is expected. Statistics on the two periods are presented in Table 9.2.

Both periods start near the beginning of a summer reservoir release after a period of no release. The calibration period contains only the release period whereas the validation period also includes the drying phase at the end of a release. The release rate for validation is the maximum release rate and is 67% higher than the flow rate used in calibration. Day numbers were adopted for convenience in correlating and interpolating data and plotting graphs. Day 1 corresponds to 1st January 1979.

Table 9.2

Comparison of characteristics of calibration and validation periods

	Calibration		Validation	
dates	12/2/81-24/3/81		19/11/80-10/1/81	
day number	774 - 814		689 - 741	
no. of days	41		53	
reservoir release (ML)	726		653	
date/valve setting (l/s)	16/12/80	0	17/ 6/80	0
date/valve setting (l/s)	10/ 2/81	180	18/11/80	300
date/valve setting (l/s)	24/ 3/81	0	16/12/80	0
release duration (days)	42		28	
rain days	11		9	
mean air temp (^{o}C)	20.9		21.8	

The model parameters finalized in the third stage of calibration were employed and RMSS-B and RMSS-Q calculated. Prototype and model bore elevation changes and discharge losses were plotted. While it was not expected that the model would fit as well as for the calibration period, large increases in the measures of fit would indicate that there were faults in the conceptual stream-aquifer interaction model.

9.6 Analysis of Discharge Loss Residuals (ICAL = 6)

To correlate independent variables with the discharge loss residual, a file of these variables was produced by BIEMCAL. This file, together with input text to control the analysis and the BMDP Statistical Software package were used to determine the nature of such correlations. The independent variables included day number, upstream discharge, change in daily discharge, prototype discharge loss, evaporation and mean air temperature, and each or any combination of these parameters may be regressed.

BMDP program P2R was used giving a multiple linear regression in a stepwise manner. At each step the partial correlation coefficient was calculated for all variables not yet in the regression equation. A first order linear regression of the dependent variables on each independent variable was determined and the F statistic appropriate for testing the significance of each regression was calculated. These values are called "F to enter" values, which may not be used with standard F tables to give levels of significance (Draper and Smith, 1981, p311, also Dixon, 1981, p698). For variables already included these are called "F to remove" values.

The variable with the largest "F to enter" value, providing this exceeds a specified threshold is incorporated into the regression equation for the next step. Any variable previously included whose "F to remove" value falls below a specified value is excluded from the regression

equation at the next step. Stepping continues until no excluded variable has an "F to enter" value greater than the permissible threshold and no variable used in the equation has an "F to remove" value less than the specified threshold. The "F to remove" threshold was set marginally lower than the "F to enter" threshold to prevent repeated entry and exit of variables from the regression set.

Analyses were performed using 4 and 3.9 as the "F to enter" and "F to remove" values. A subsequent run with forwards and then backwards stepwise regression was performed with "F to enter" values of 1 and 50 and "F to remove" values of 0 and 49 respectively. The parameters included in the best regression equation in each case were the same except that the best regression equation with the lower F to enter threshold admitted some additional variables which were excluded in the previous runs. The results shown in section 9.8.8 are for the best regression (highest r^2) with "F to enter" = 1.0.

9.7 Temperature-Dependent Streambed Impedance (ICAL = 7)

Prior to a formal analysis of discharge residuals BIEMCAL was modified to allow for variation of streambed impedance, B with stream temperature. An analysis of stream temperature records at station 5 allowed a correlation of mean daily stream temperature with mean air temperature. Hence mean air temperature, recorded on the COMBMDP file, was used to modify the value of B in accordance with the change in hydraulic conductivity due to a change in dynamic viscosity of water. The results of this exercise are given in section 9.8.9.

9.8 Calibration Results

The calibration procedure, resulted in the set of model parameters given in Table 9.3. None of these values trespass outside their expected range. A review of the parameter values in the light of independently determined estimates is given in section 9.8.2. At this stage it is of more interest to examine the fit of the model to the data from the

TABLE 9.3 Calibrated Model Parameters.

Section	REACH (g.s. no's)	LENGTH (metres)	TIME RATIO (day^{-1})	y_b (metres AHD)	B (metres)	K (m/d)	n_e	$(\frac{\partial h}{\partial n})_b$	y_0 (metres AHD)	F.S. CAL. (metres AHD)	F.S. VAL. (metres AHD)	T (m^2/d)	T/n_e (m^2/d)
O	3-5	1090[a]	120	32	2	4.5	.038	-.0002	45.60	43.20→37.01	44.08→37.01	56	1600
P	5-7	2940	100	30	2.25	6.6	.066	0[b]	37.40	34.95→30.20	34.95→30.20	49	700
Q	7-12	4690	140	4-23	4.5	4.0	.029	0[b]	31.90	25.21	25.21	36-112	350-3100
R	7-12		80	0	8.0	7.0	.088	0[b]	23.90	19.58→18.60	20.12→19.00	140	1600
S	12-15	6280	40	-6	10.	4.0	.10	0[b]	14.80	13.58	14.00	80	800

Notes:

a Reach length stn 4-5 only. No aquifer adjacent reach 3-4.

b Approximate only. Smaller than -.00005.

$h_c = 0$, $w_b = 4$ metres, for all sections.

w_b = channel base width

y_b = aquifer base elevation.

$(\frac{\partial h}{\partial n})_b$ = aquifer base normal hydraulic gradient.

B = streambed hydraulic impedance.

K = aquifer hydraulic conductivity.

n_e = aquifer effective porosity.

y_0 = channel base elevation.

T = aquifer transmissivity.

T/n_e = aquifer diffusivity.

F.S. CAL = range of initial free surface elevations for calibration.

F.S. VAL = range of initial free surface elevations for validation.

calibration and validation periods.

9.8.1 Model fit

Table 9.4 summarizes the statistics of fit of the model. Plots of observed data and model results for groundwater elevation changes and daily stream discharge losses are given for the calibration and validation periods for each section in turn in figures 9.2 to 9.11.

In each case the validation results were inferior to the calibration results (columns 4,5,8 and 9). For groundwater levels changes only one section (P) had an increase in RMSS-B of more than 0.04 metres. The discharge loss residual however was not as consistent as all sections had a substantial increase in RMSS-Q. With the exception of section P however the magnitude of the mean discharge loss residual remained less than 300 m^3/d. That is, between 5 and 10% of the mean observed daily discharge loss or about 2% of the reservoir release discharge rate. These results appear satisfactory considering the accuracy of discharge measurements estimated to be ±2 to ±5 1/s (±170 to ±430 m^3/d) from calculations based on Bos (1976) and are sufficiently accurate for reservoir release operation where the tolerance on setting release rates is of the equivalent magnitude. However the large values of RMSS-Q prevent any claim that the nature of stream-aquifer interaction for the Little Para River has been conclusively defined. That is the uniqueness of the model cannot be assured as is discussed in section 9.8.6.

The high values for the RMSS-Q are in part due to unsteady stream discharge. Daily discharge was calculated from 9am to 9am at each station. While it was endeavoured to maintain a constant discharge rate at station 3 this did not always occur due to variations in discharge rate in the Little Para offtake main from which the reservoir release main branched. Hence channel storage changes occurred for which no account was taken in calculating discharge losses.

TABLE 9.4 Statistics of Fit of Calibrated Model for Calibration and Validation Periods.

1	2	3	4	5	6	7	8	9	10	11
SECTION	REACH (g.s. no's)	CAL. OR VAL.	RMSS-B (m)	MEAN-B (m)	χ^2_D	N-B	RMSS-Q (m^3/d)	MEAN-Q (m^3/d)	N-Q	MEAN-Q_p (m^3/d)^p
O	3-5	C	.250	.039	2.44	50	257	-6	30	2954
		V	.287	-.217	9.62	66	425	-36	28	2673
P	5-7	C	.171	.036	0.99	40	372	8	27	6161
		V	.327	.184	5.18	60	1119	-868	21	6672
Q	7-12	C	.263	.200	6.45	65	1104	35	23	5424
		V	.296	-.210	174.4	78	1527	-288	21	6238
R	7-12	C	.139	-.053	17.1	83	1107	119	23	5424
		V	.138	-.061	6.7	97	1507	-186	21	6238
S	12-15	C	.130	.042	53.8	50	378	-29	15	2776
		V	.142	-.065	16.9	67	922	19	18	3443

Notes: $B \equiv P_i - M_i$ (prototype minus corresponding model groundwater elevation)

$Q \equiv Q_p - Q_m$ (prototype minus corresponding model daily discharge loss)

N - B = number of groundwater elevation observations

N - Q = number of daily discharge loss comparisons.

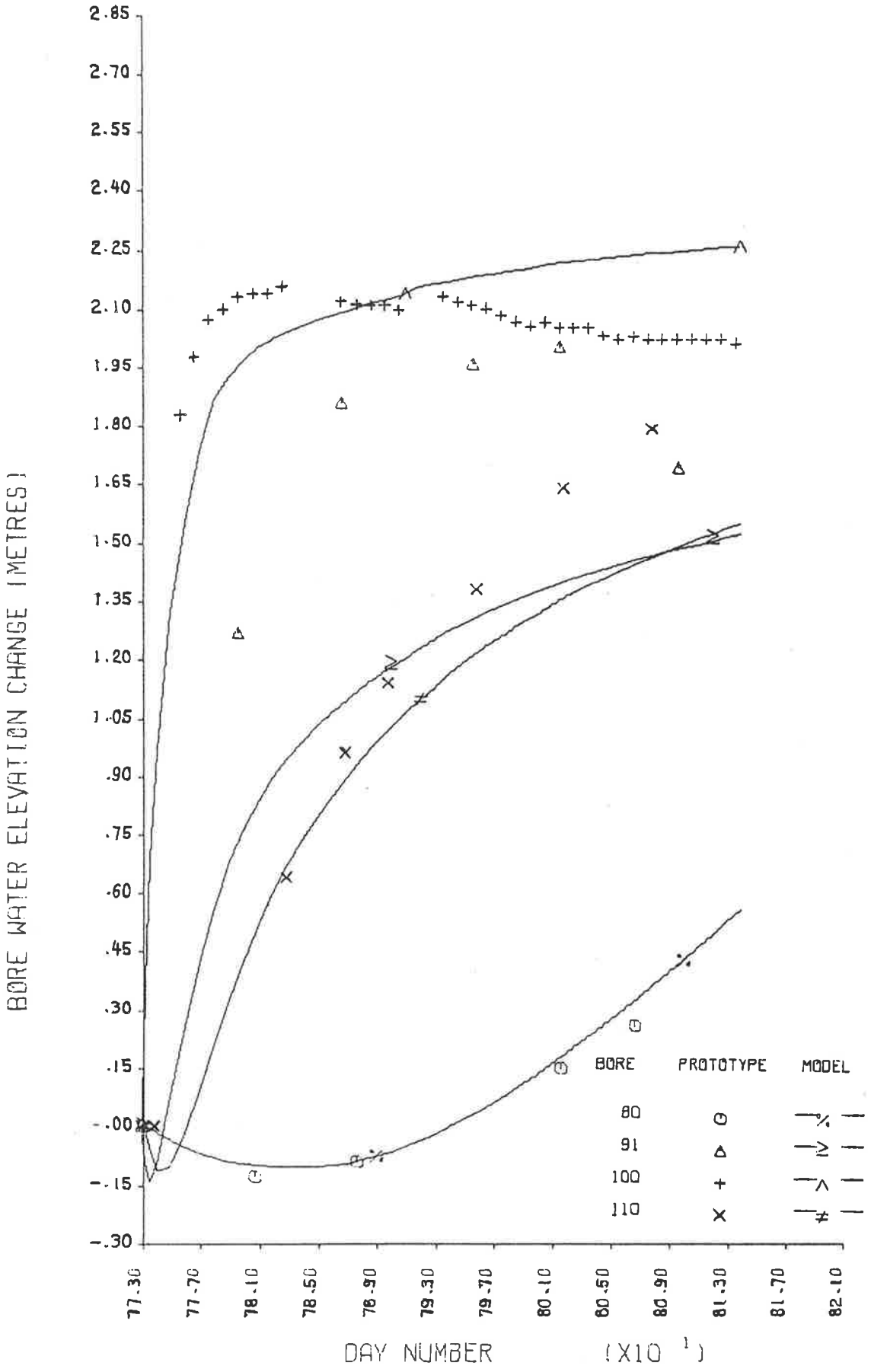

Figure 9.2 (a) Section 0 - calibration period - groundwater levels.

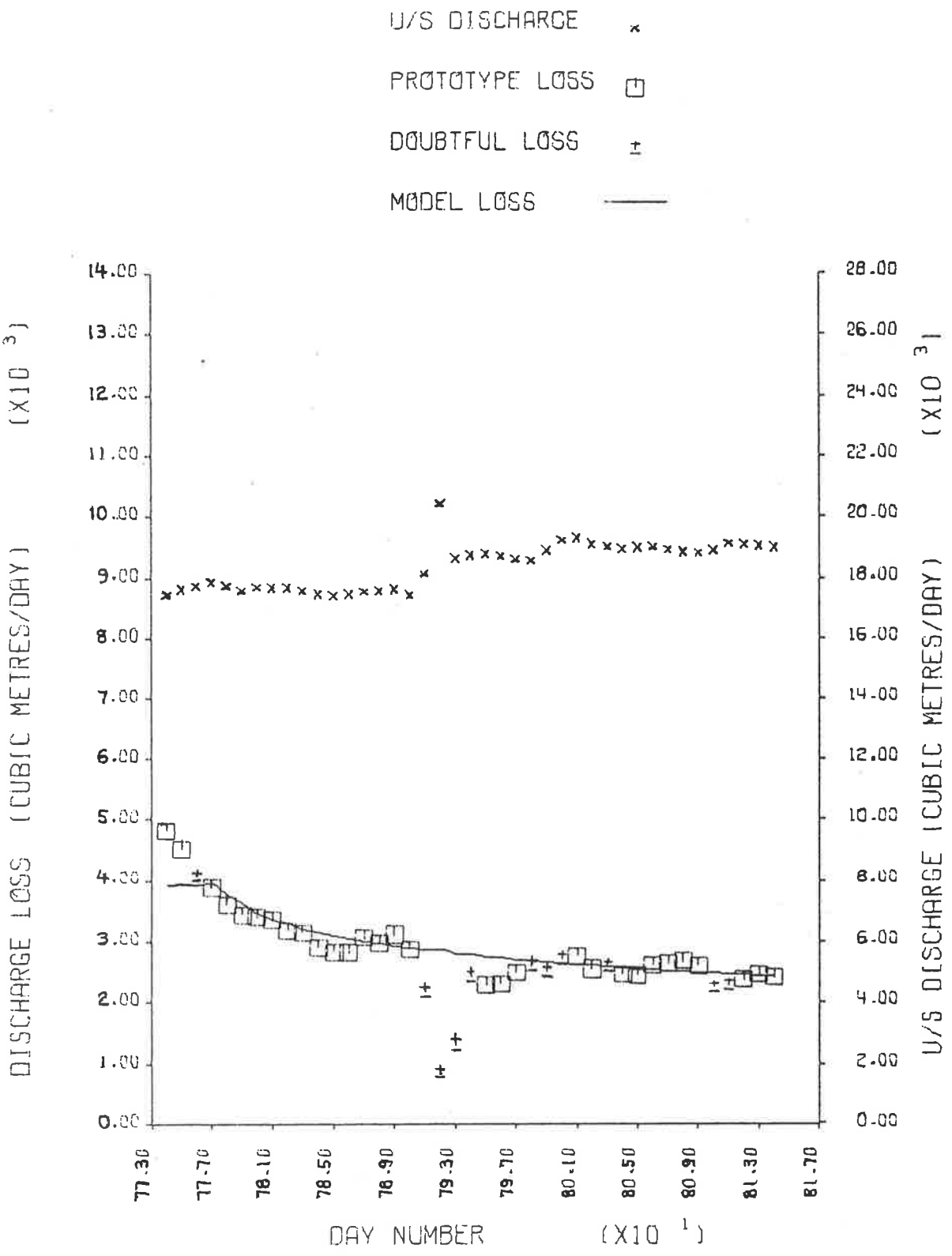

Figure 9.2 (b) Section 0 - calibration period - discharge losses.

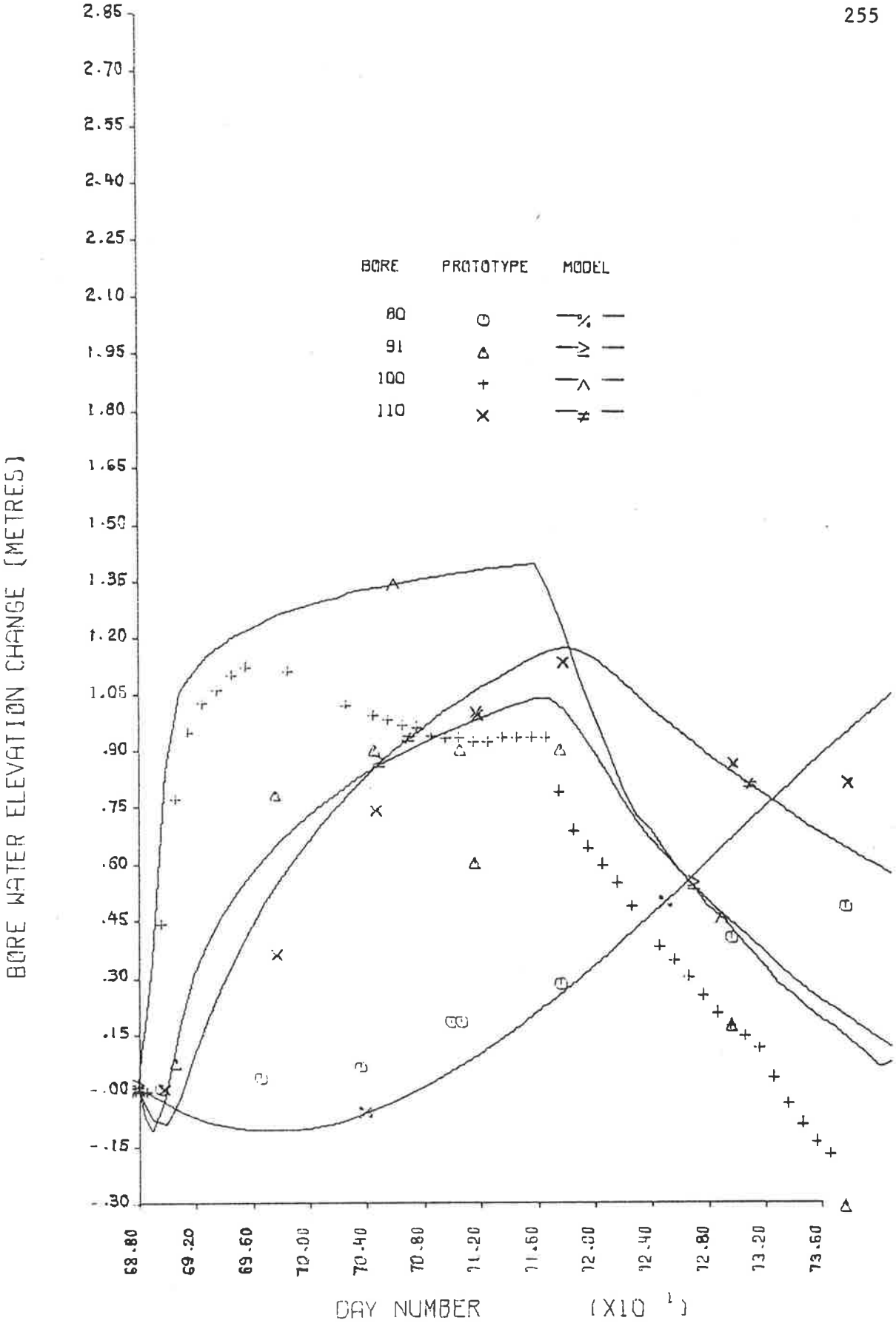

Figure 9.3 (a) Section 0 - validation period - groundwater levels.

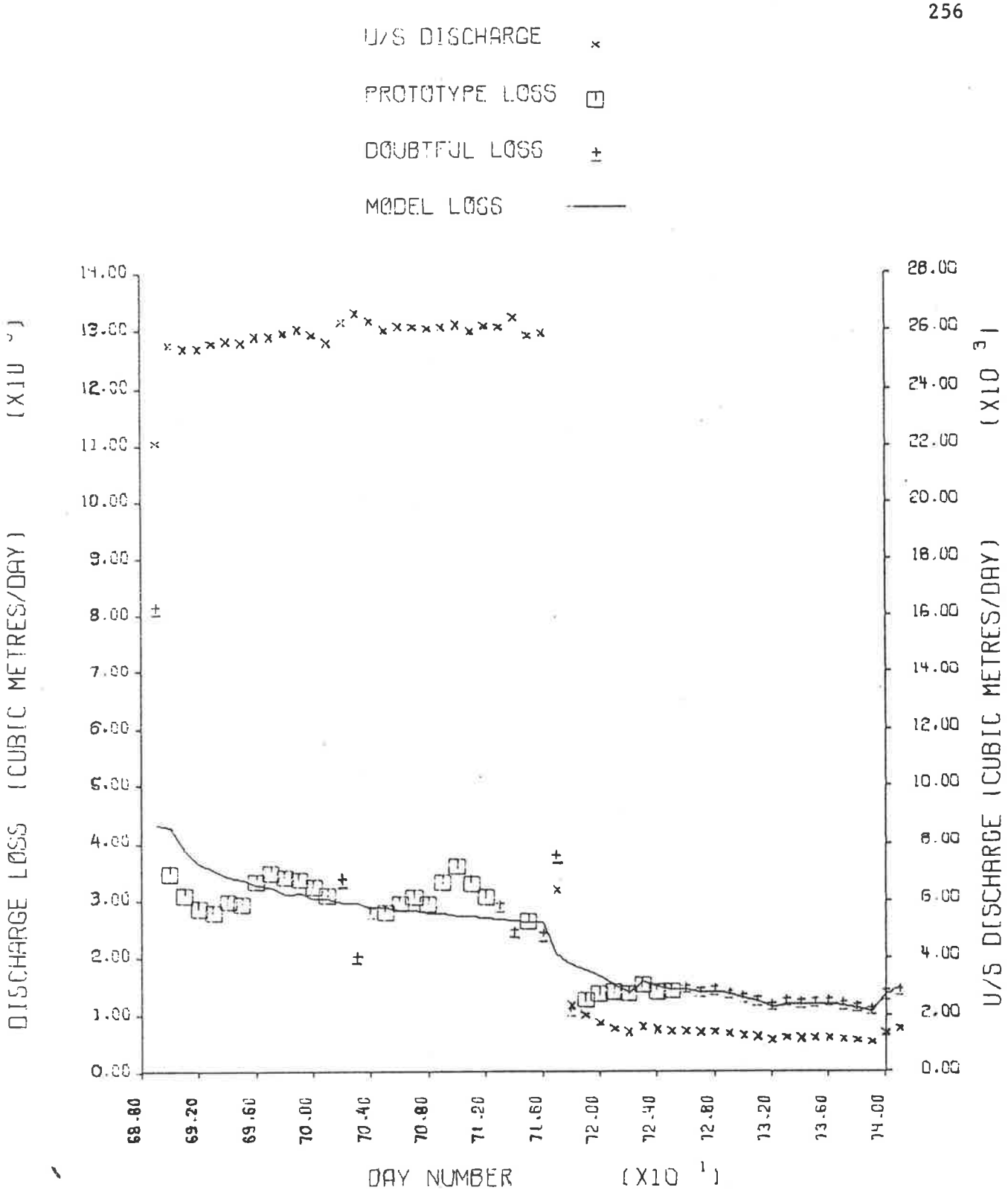

Figure 9.3 (b) Section 0 - validation period - discharge losses.

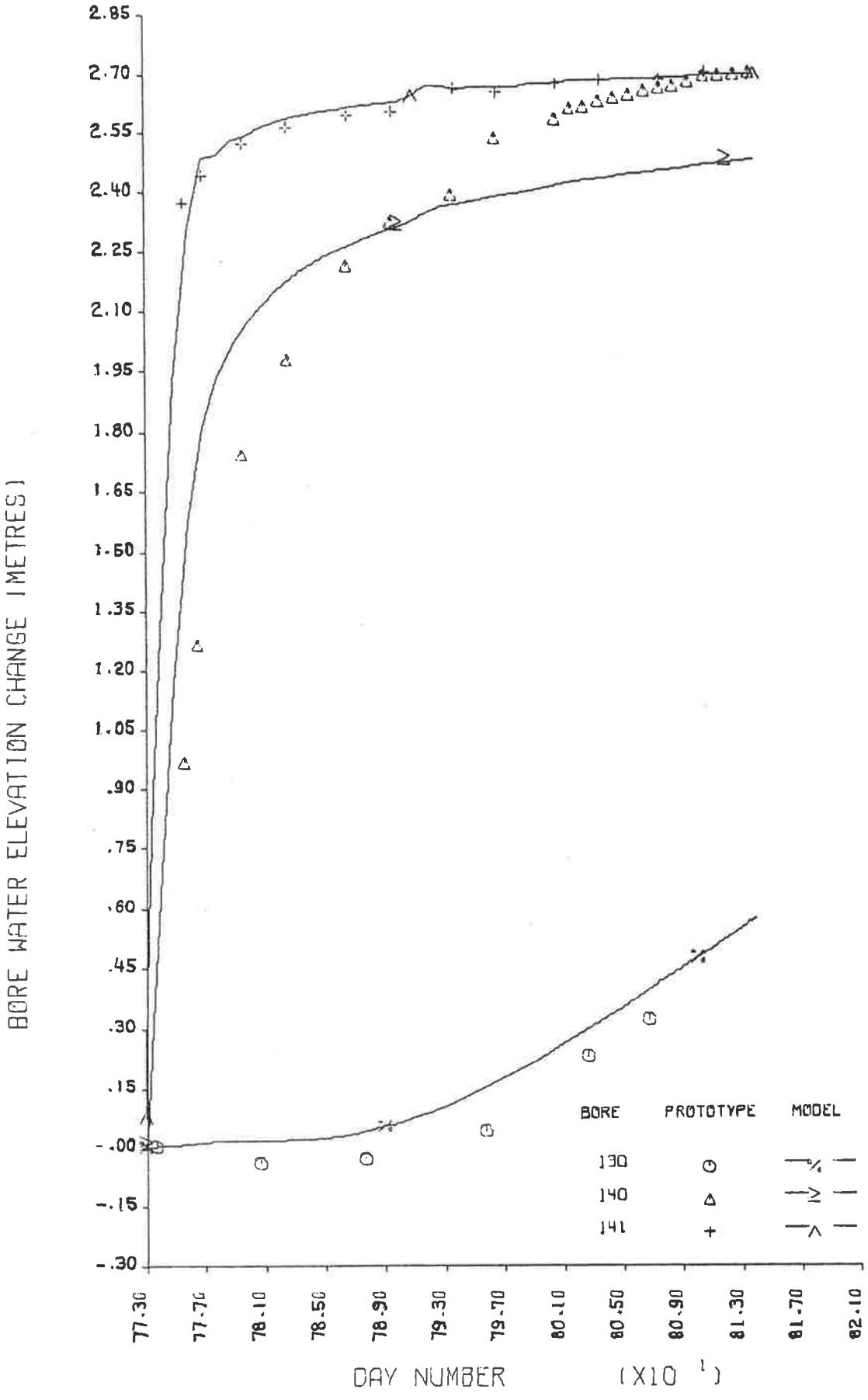

Figure 9.4 (a) Section P - calibration period - groundwater levels.

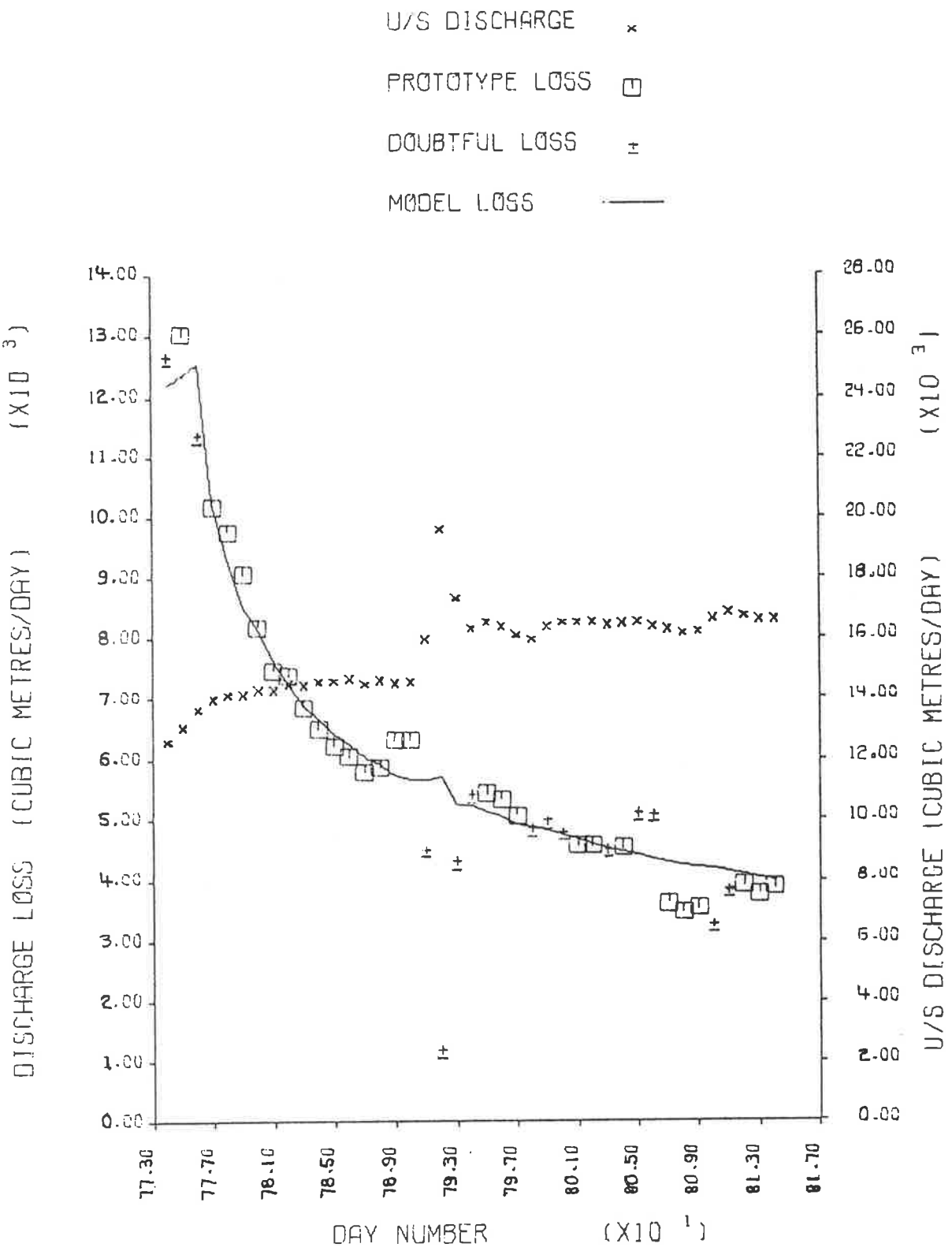

Figure 9.4 (b) Section P - calibration period - discharge losses.

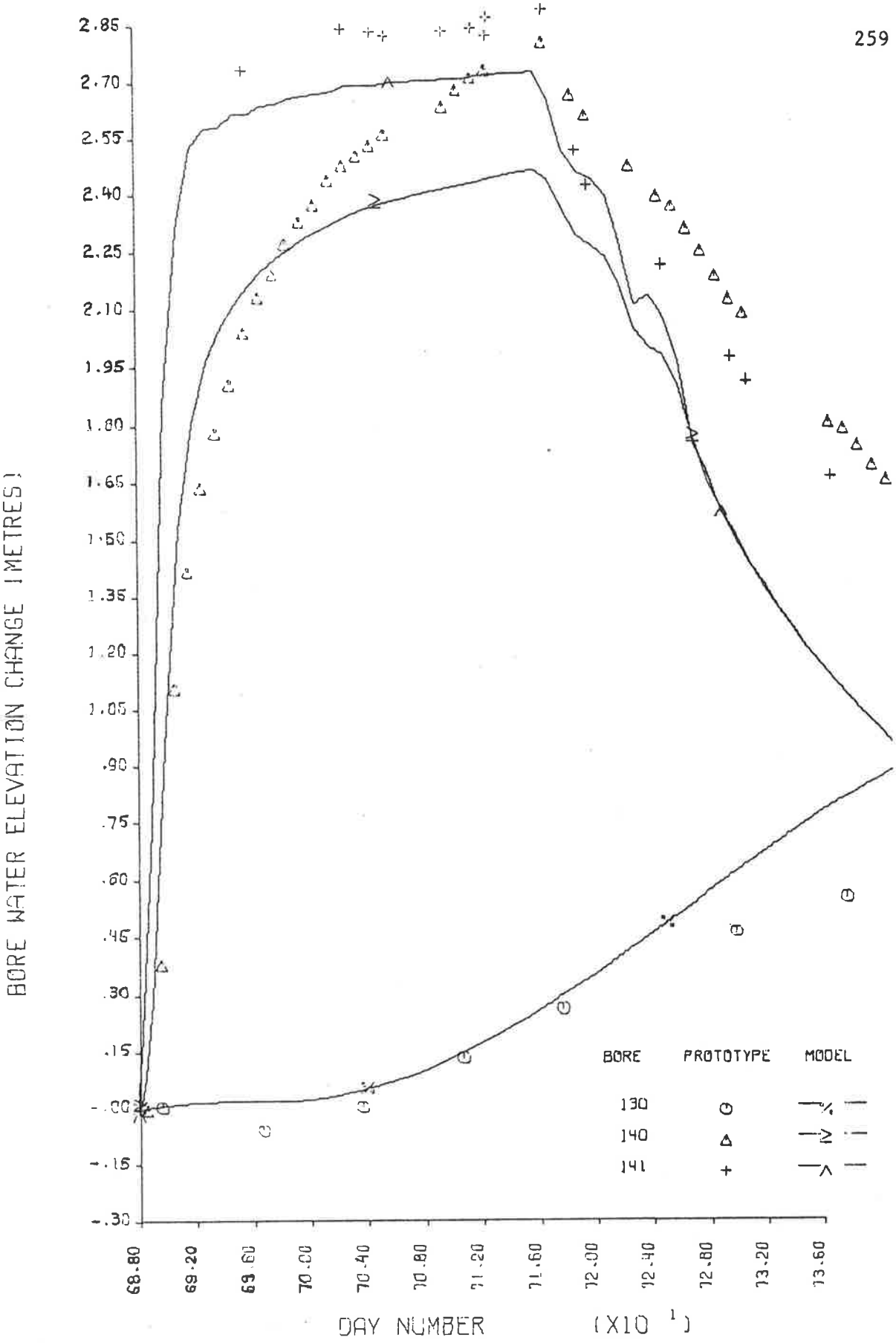

Figure 9.5 (a) Section P - validation period - groundwater levels.

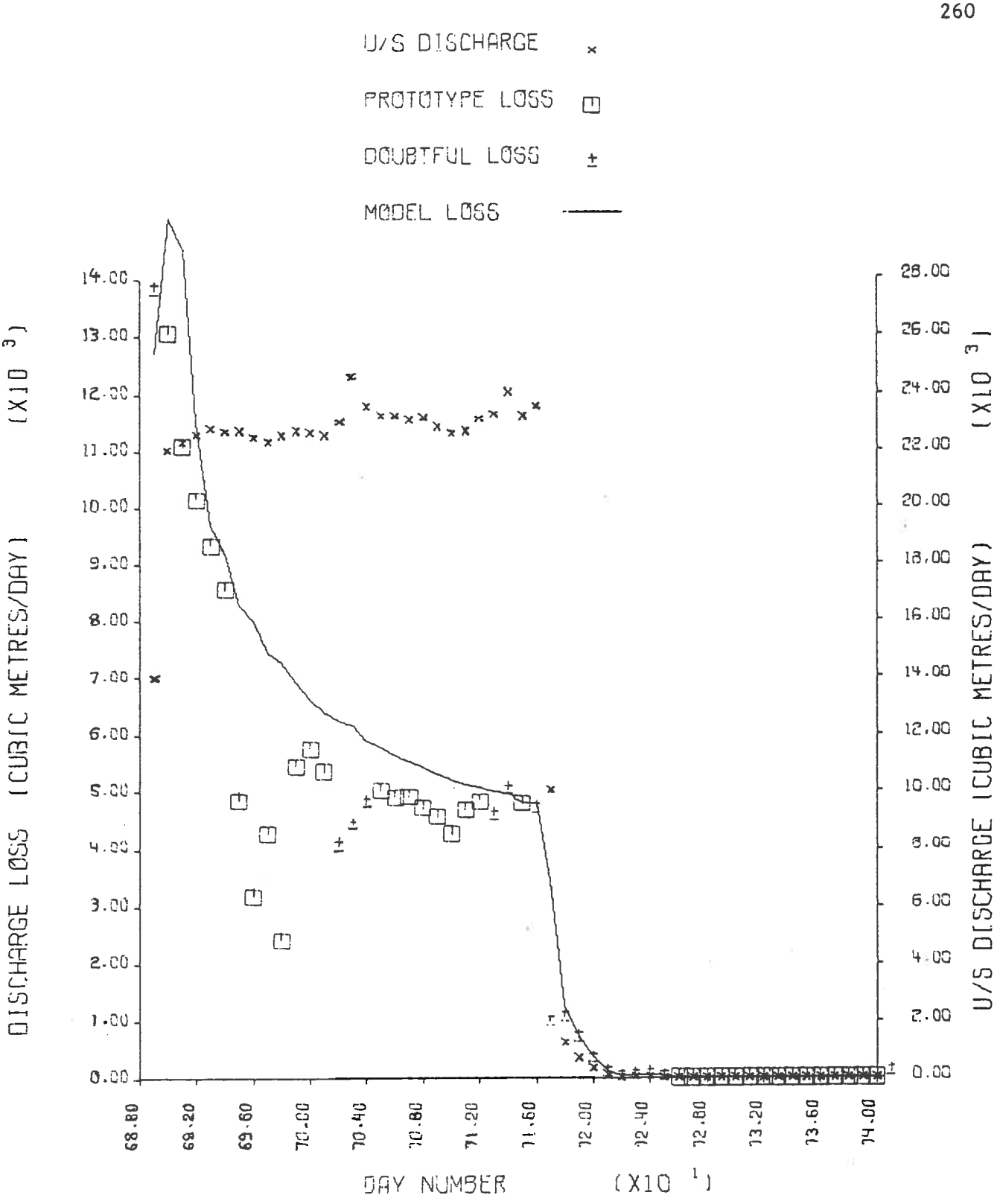

Figure 9.5 (b) Section P - validation period - discharge losses.

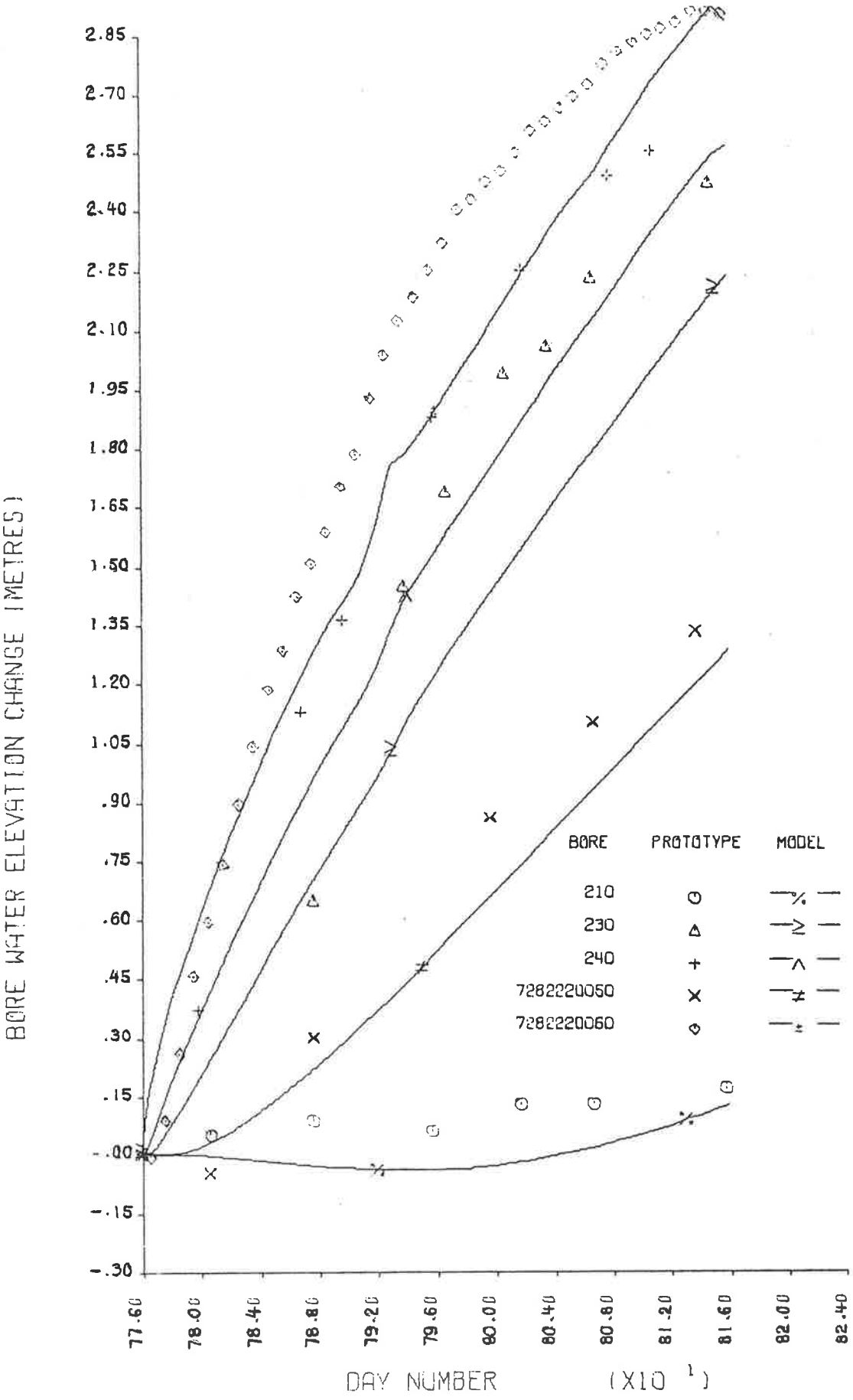

Figure 9.6 (a) Section Q - calibration period - groundwater levels.

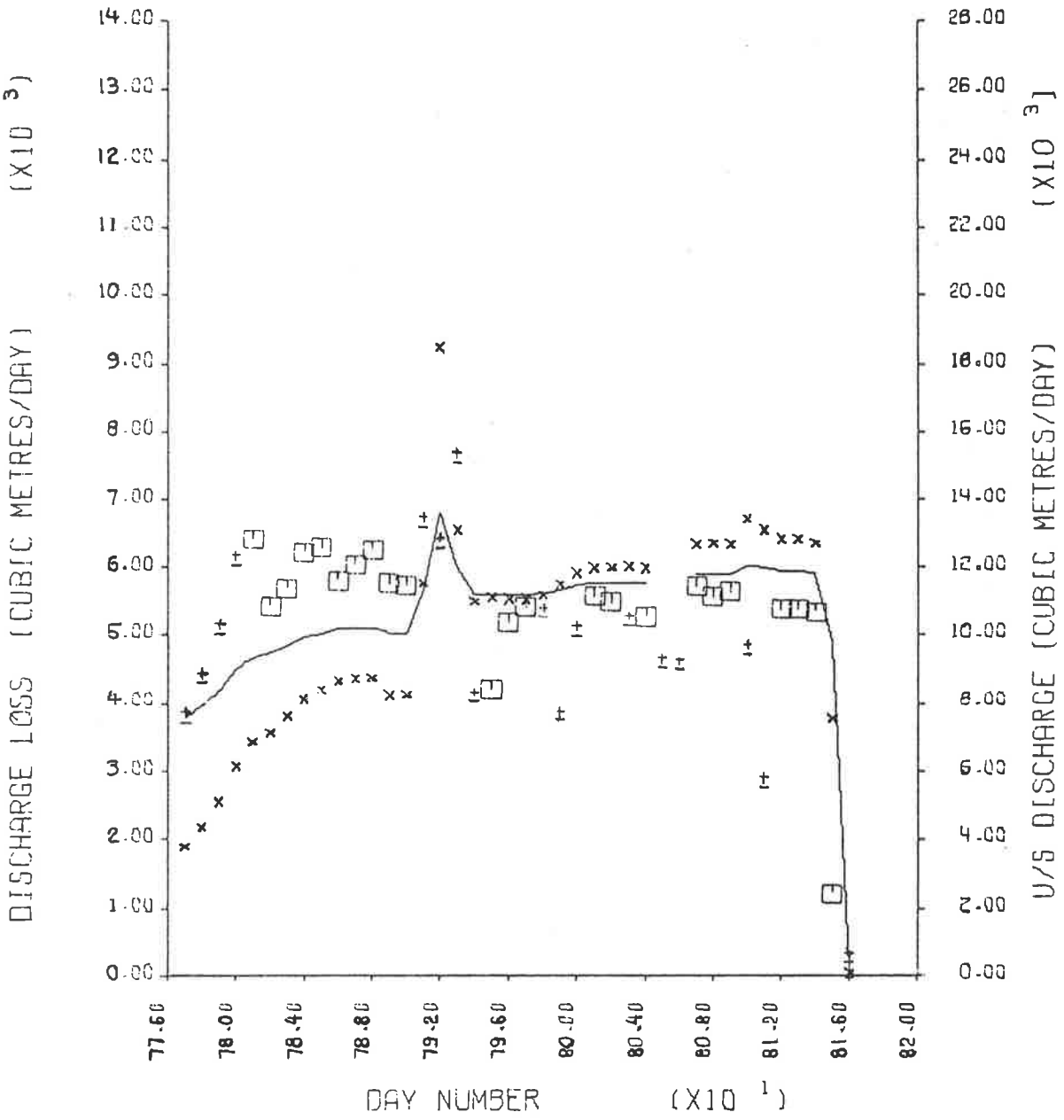

Figure 9.6 (b) Section Q - calibration period - discharge losses.

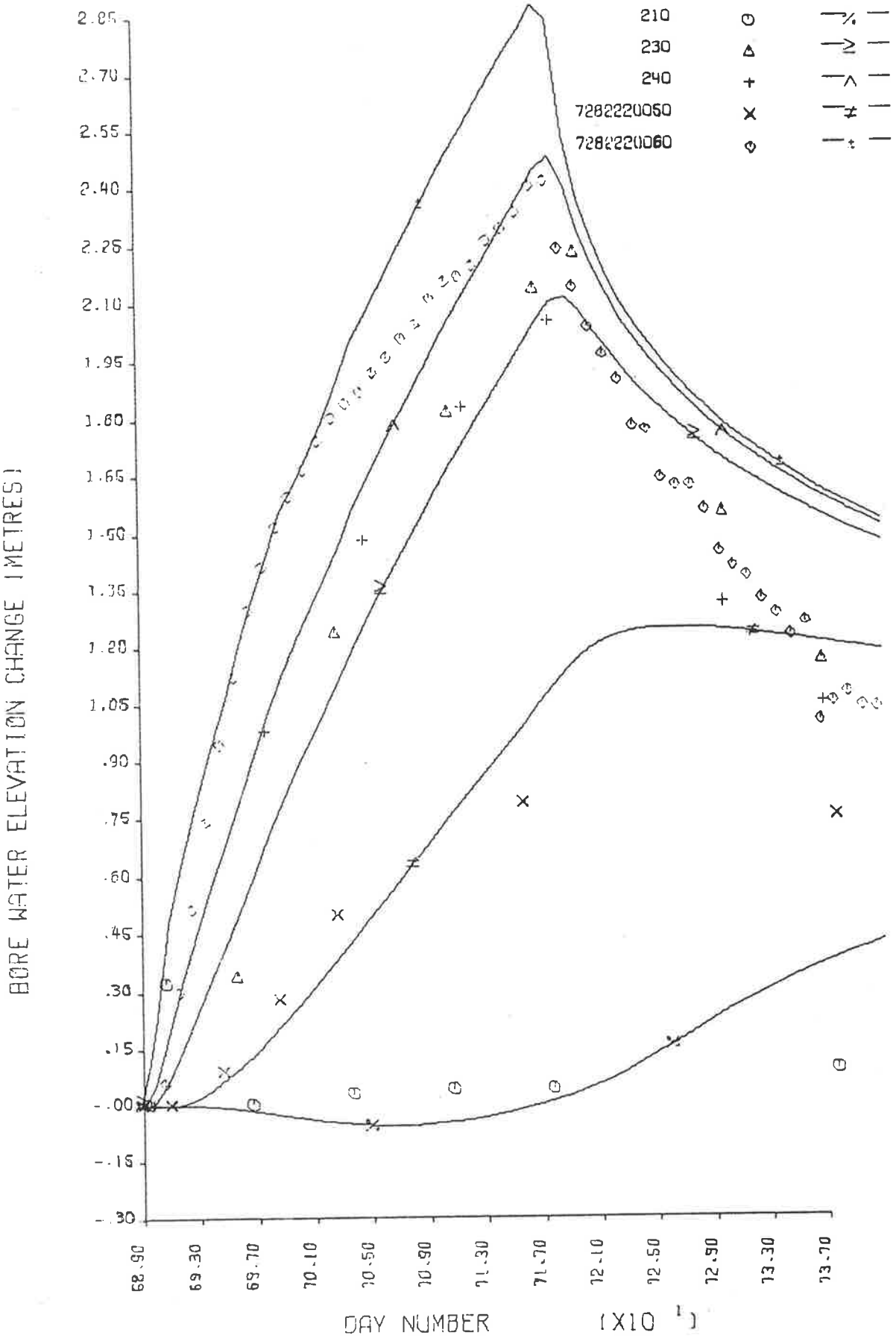

Figure 9.7 (a) Section Q - validation period - groundwater levels.

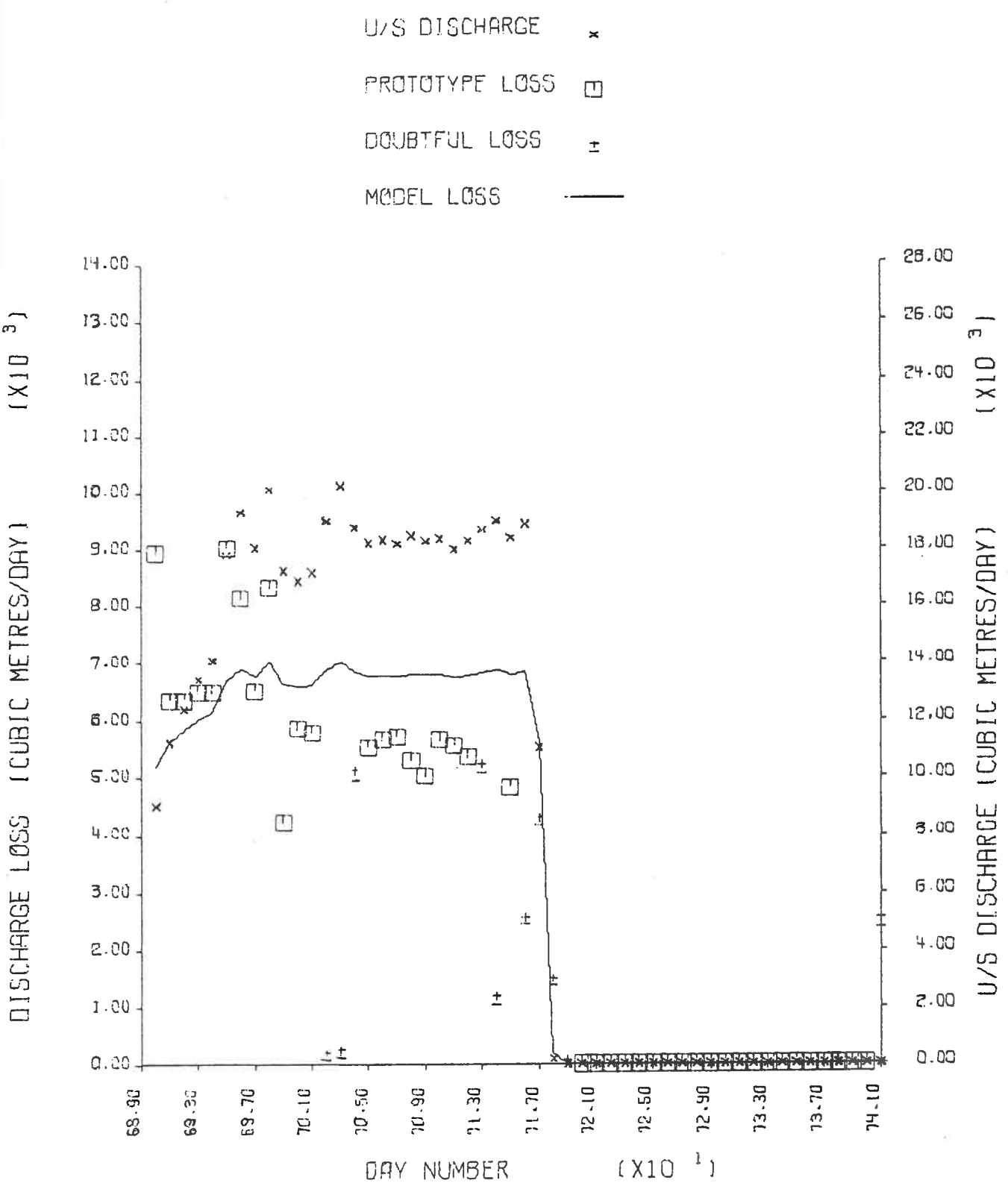

Figure 9.7 (b) Section Q - validation period - discharge losses.

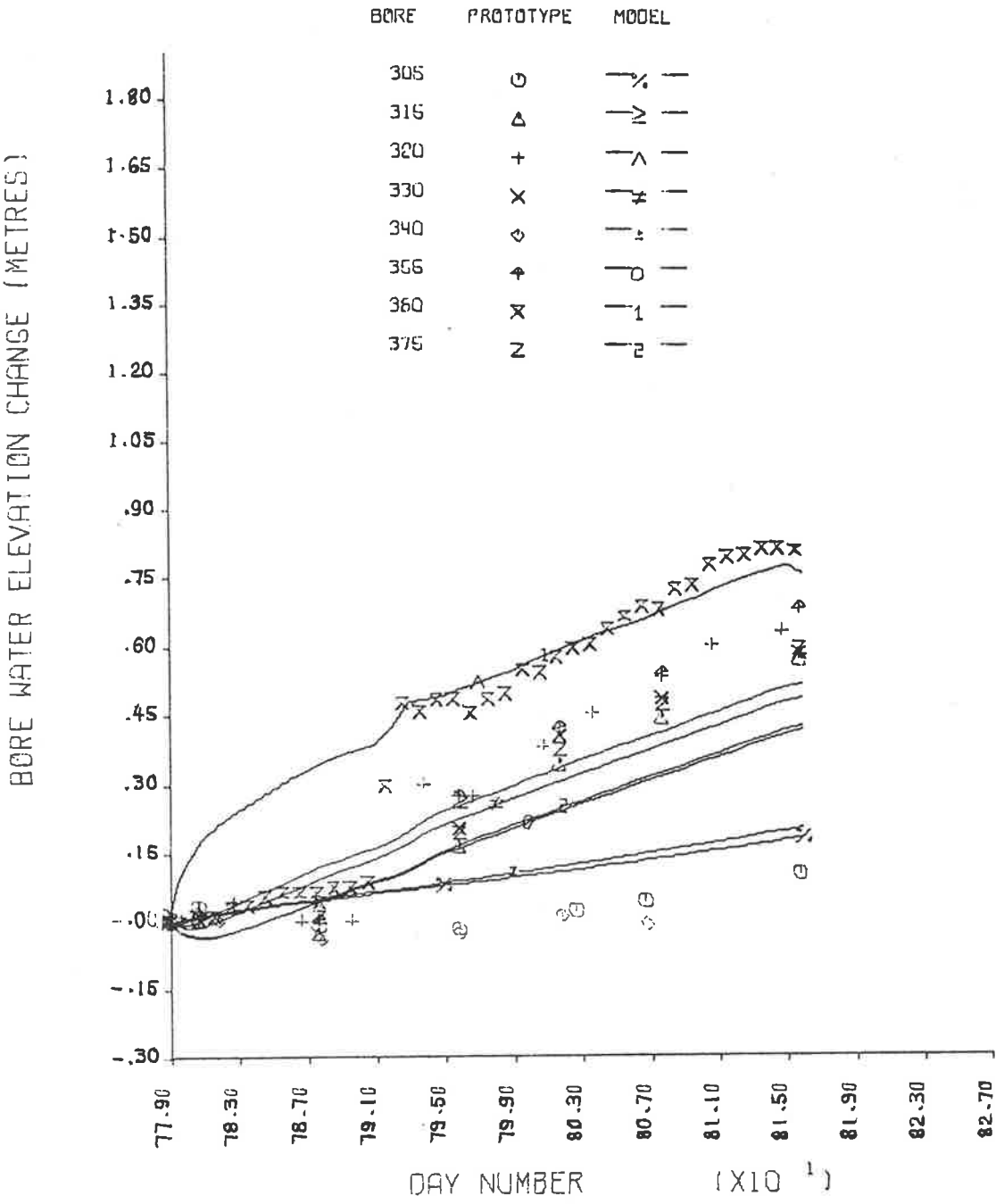

Figure 9.8 (a) Section R - calibration period - groundwater levels.

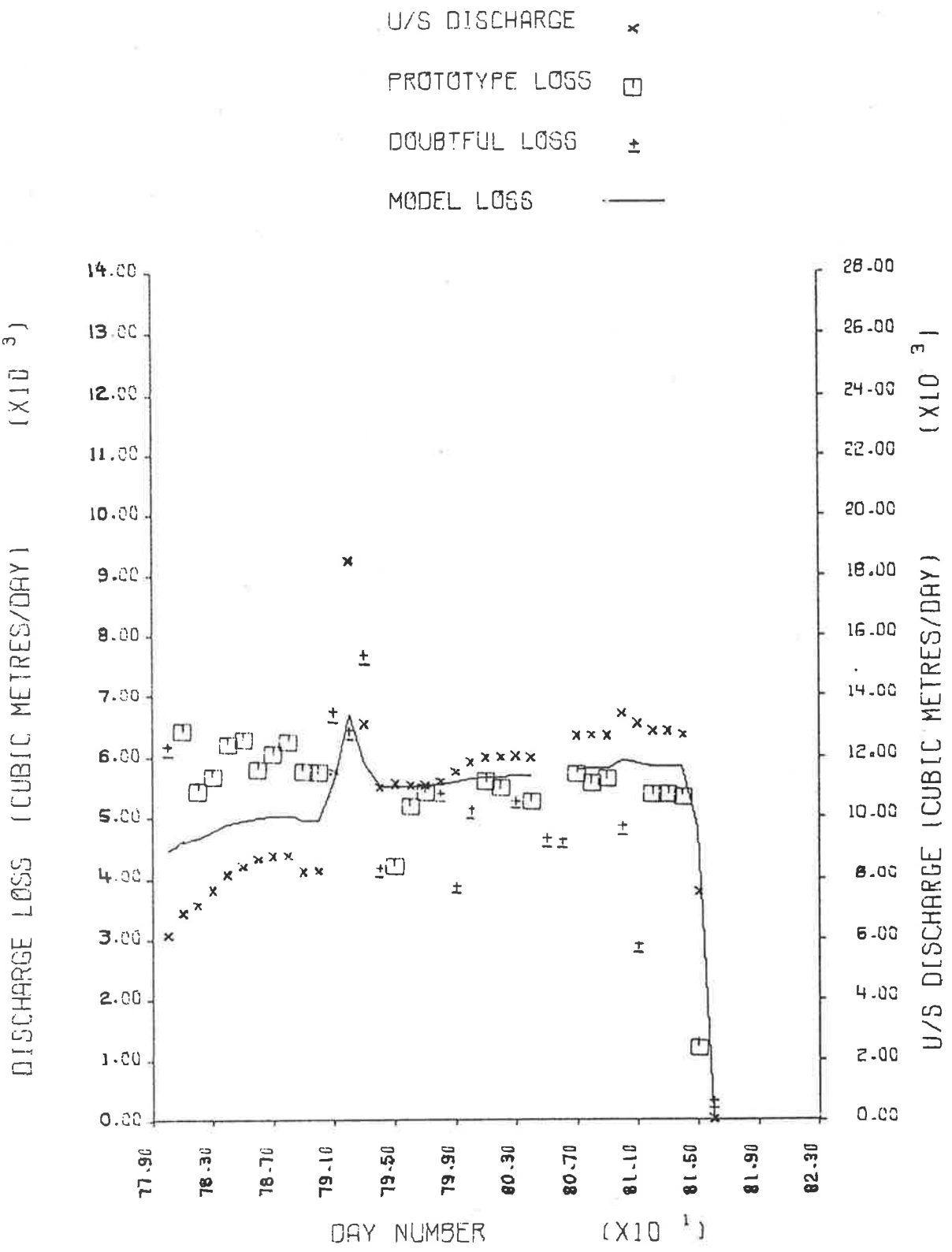

Figure 9.8 (b) Section R - calibration period - discharge losses.

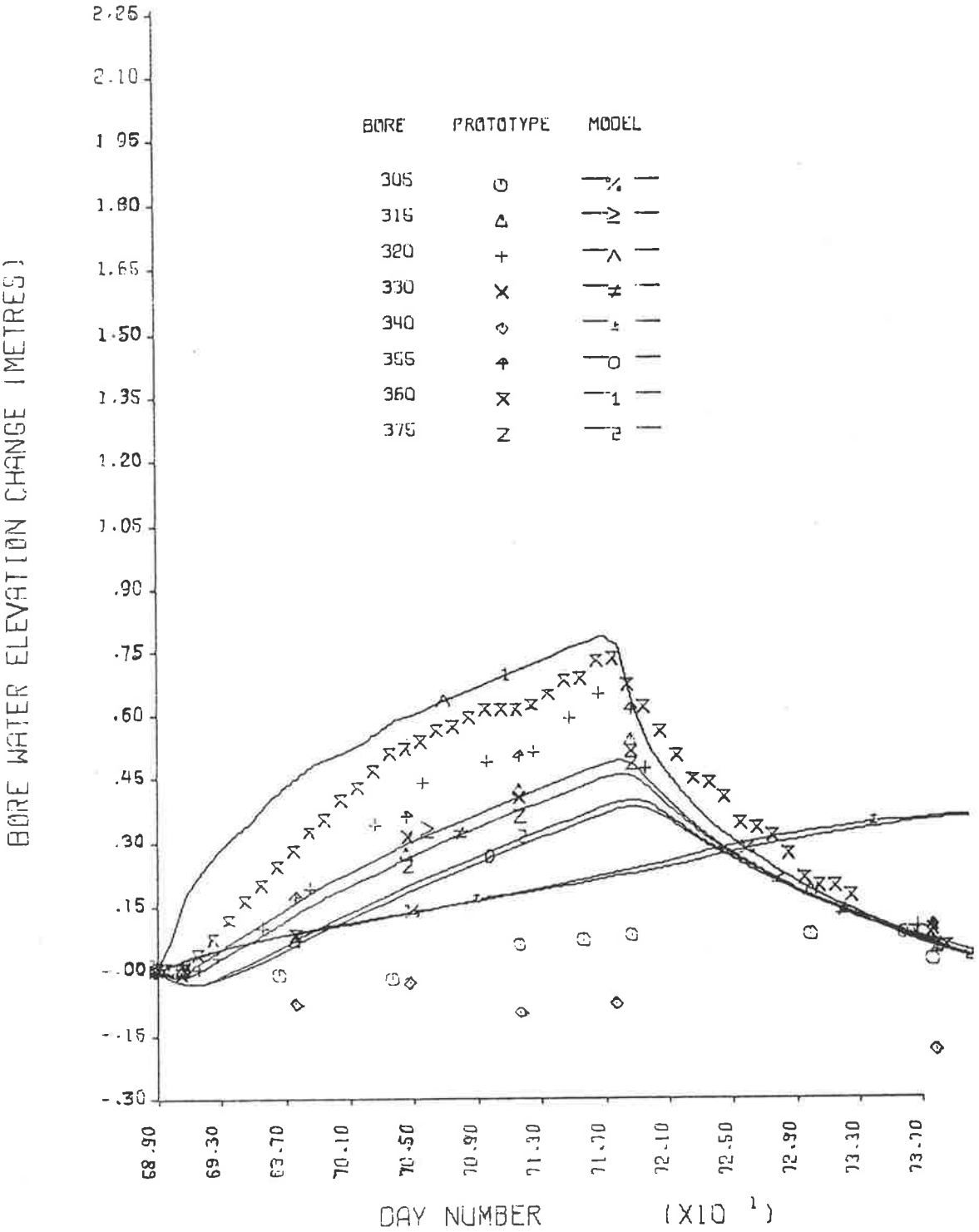

Figure 9.9 (a) Section R - validation period - groundwater levels.

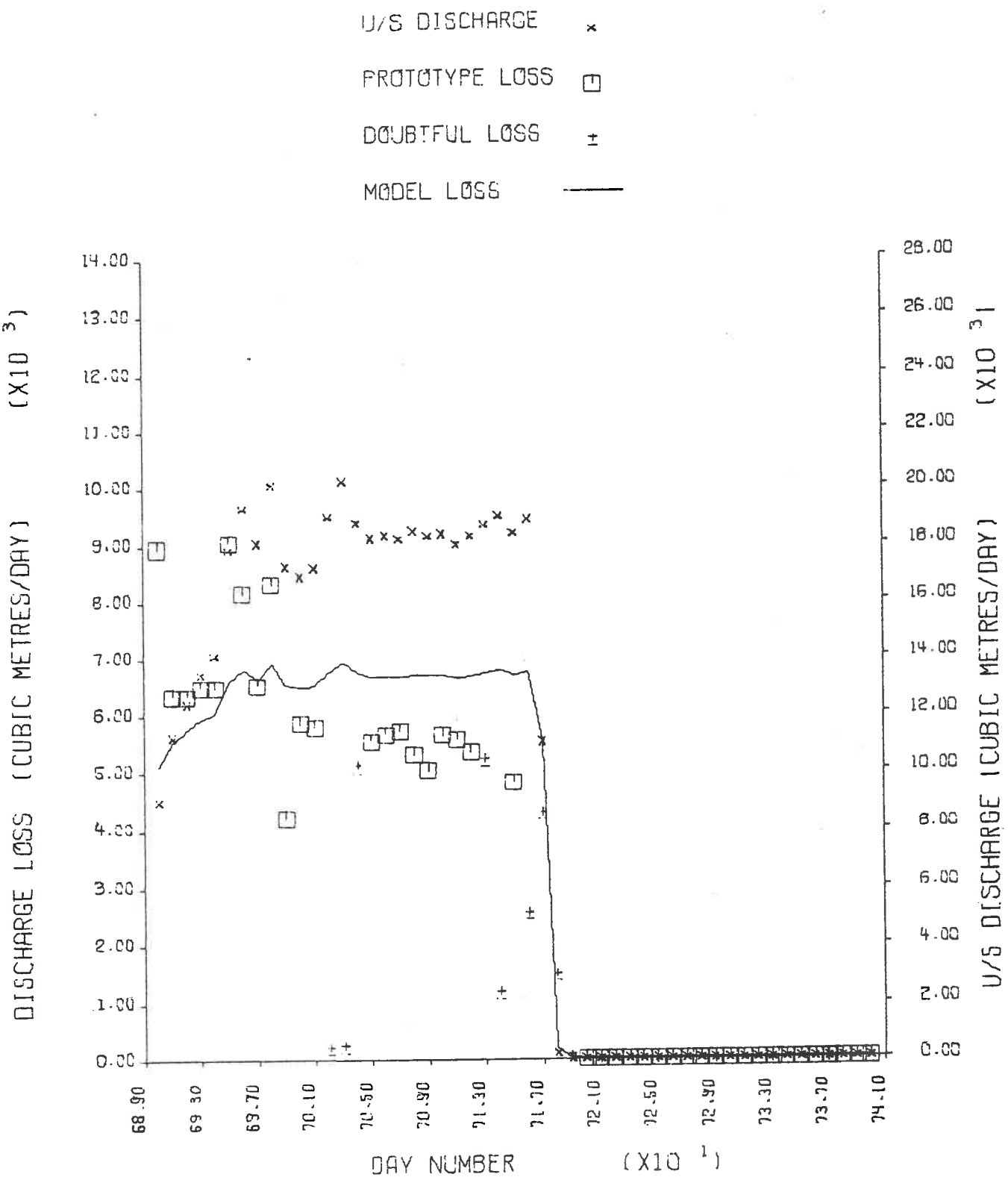

Figure 9.9 (b) Section R - validation period - discharge losses.

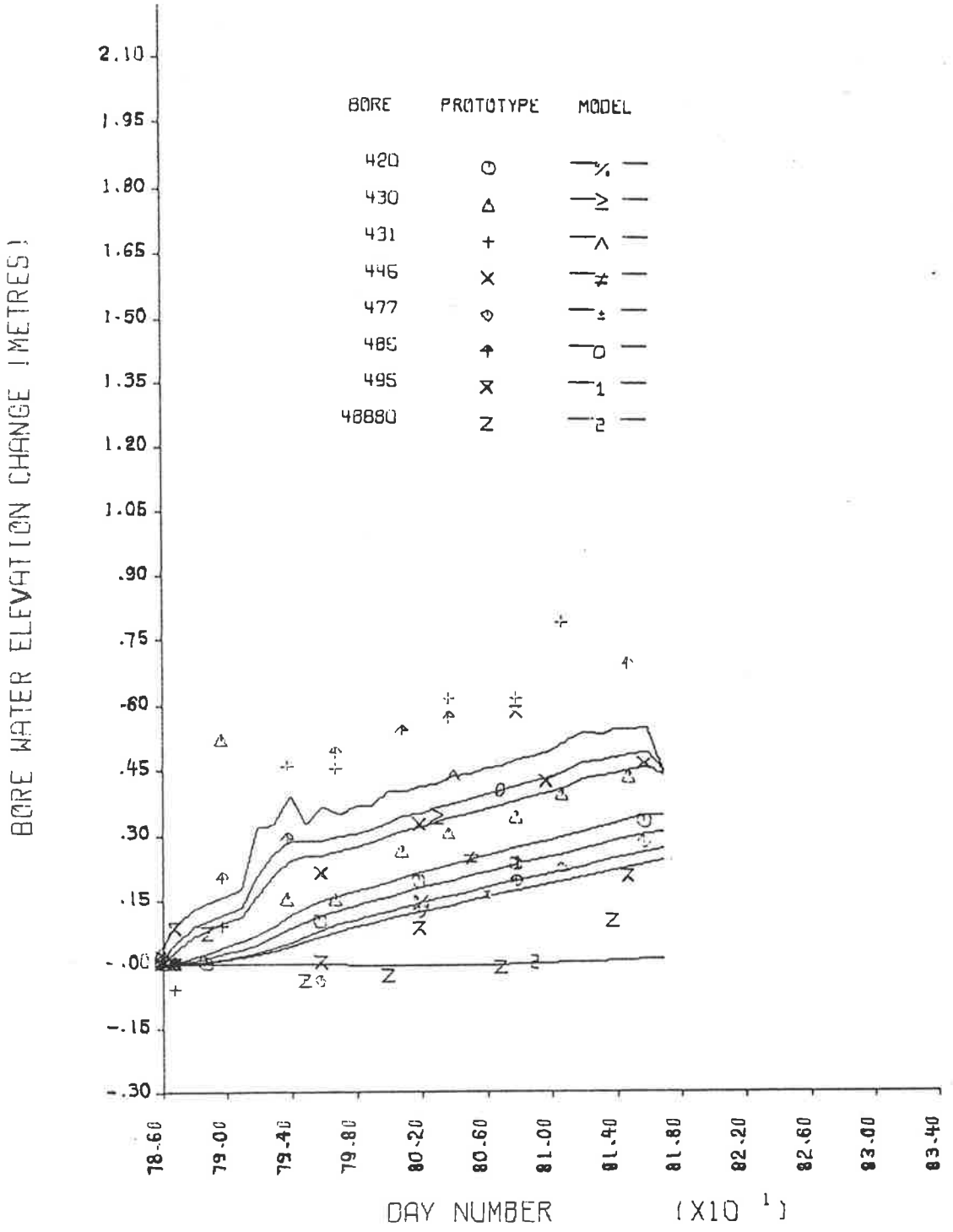

Figure 9.10 (a) Section S - calibration period - groundwater levels.

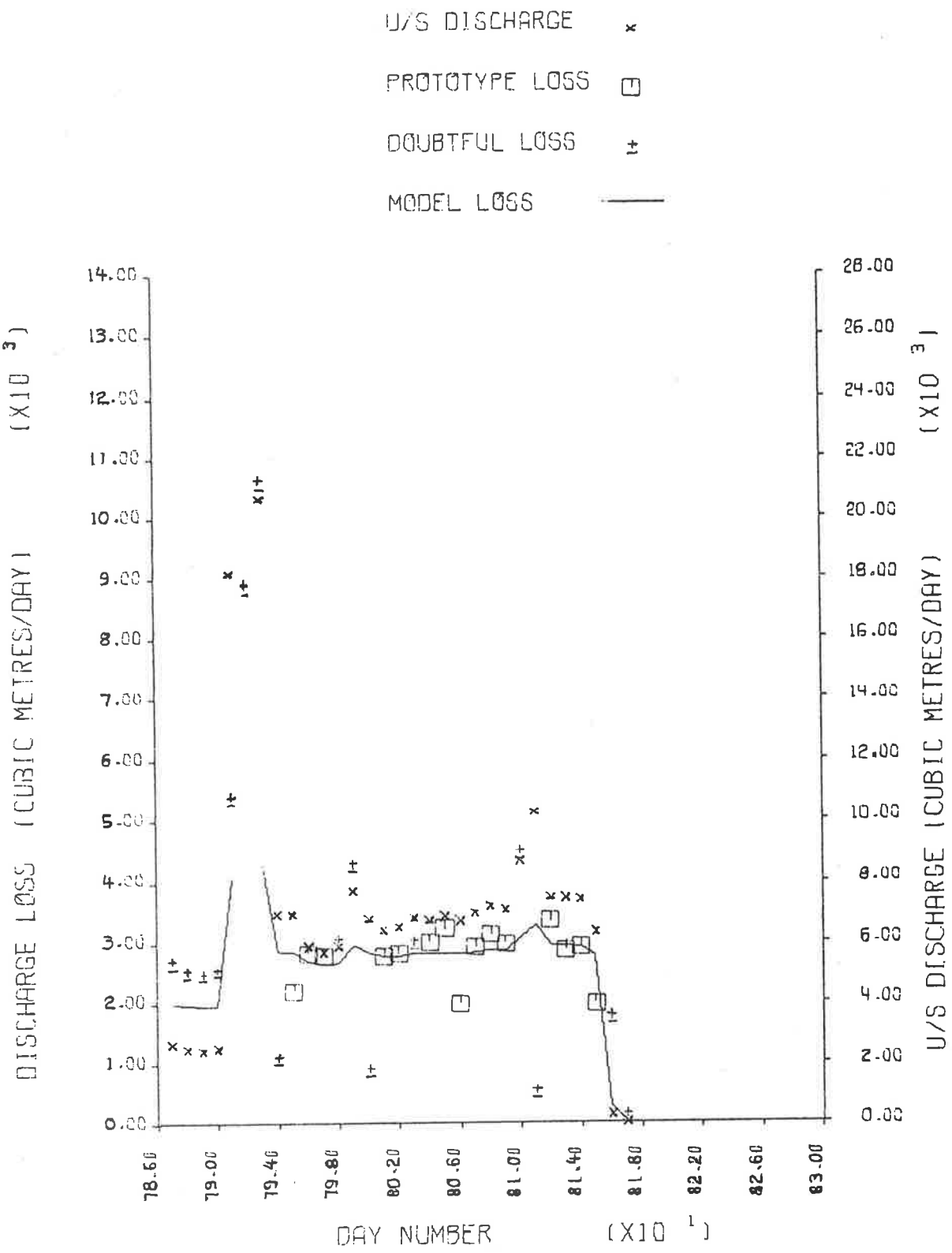

Figure 9.10 (b) Section S - calibration period - discharge losses.

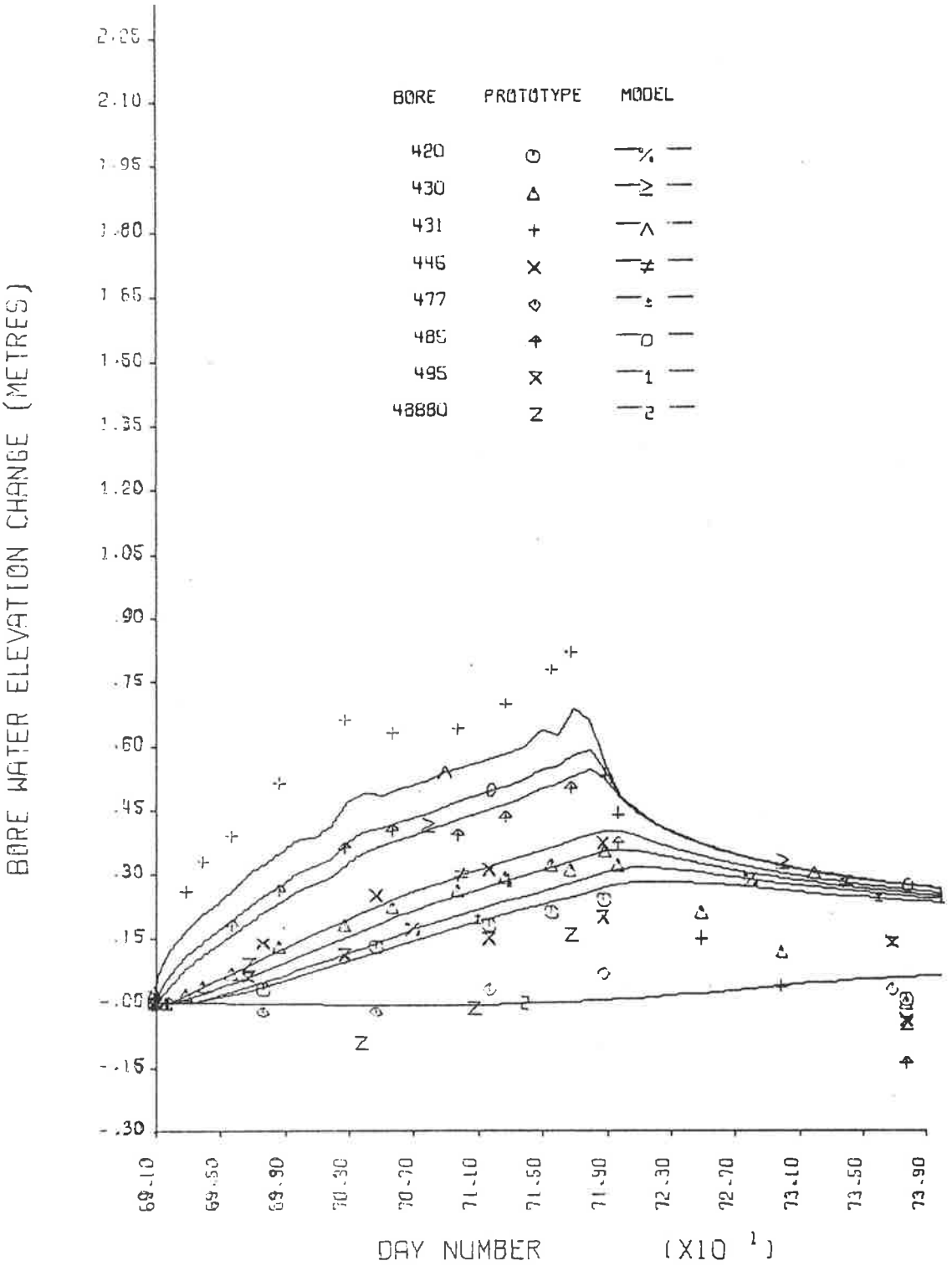

Figure 9.11 (a) Section S - validation period - groundwater levels.

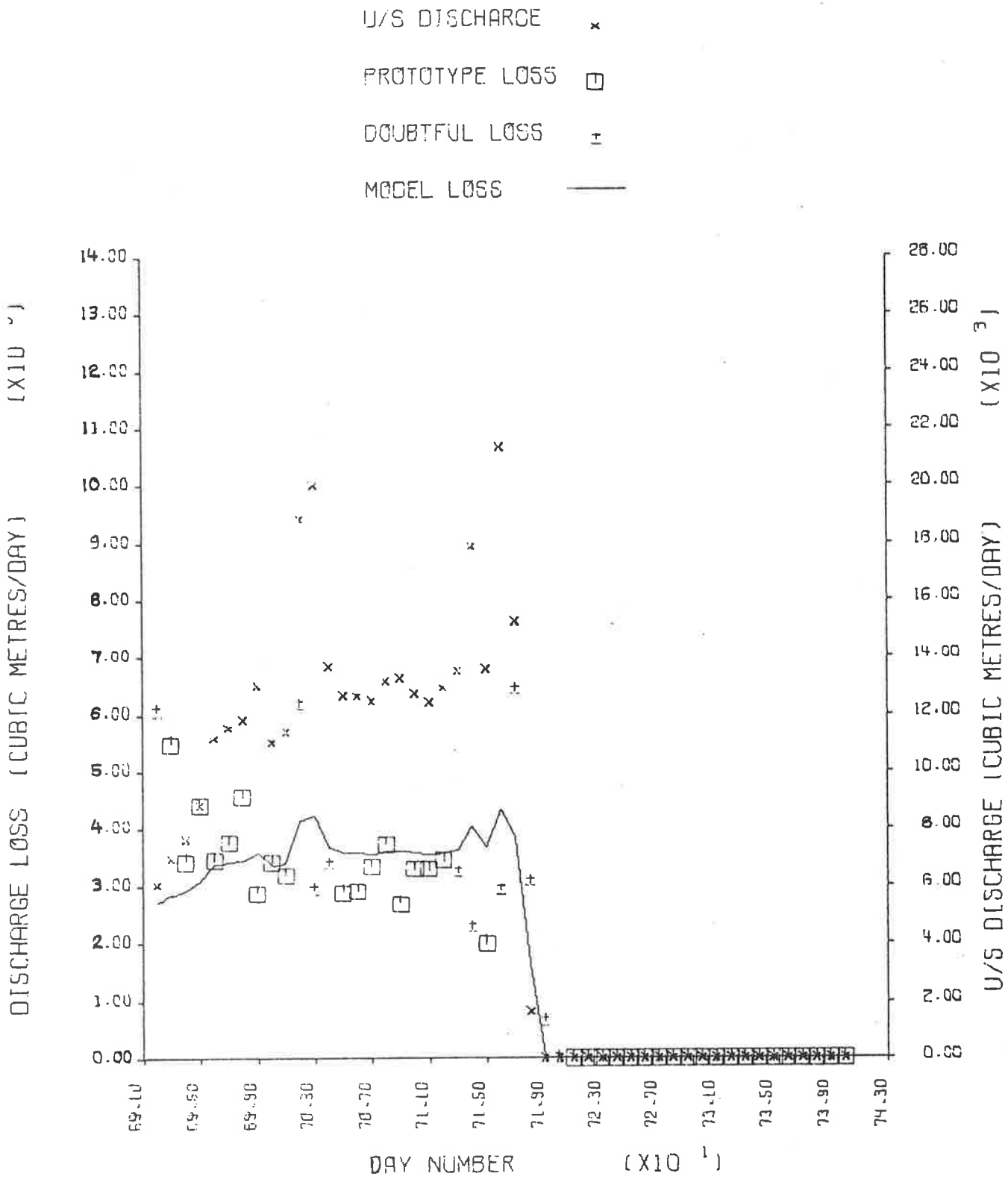

Figure 9.11 (b) Section S - validation period - discharge losses.

Due to the rill and pool nature of the stream the data requirements for validating a routing model were considered excessive and no attempt was made to account for channel storage changes even though these could be of some significance. In section 9.8.8 the discharge loss residual is regressed on the change in daily discharge at the upstream gauging station, which is an index of channel storage change. The validation period also covers the closure of the reservoir release valve from 25900 m^3/d (300 l/s) which produced channel storage changes contributing to the RMSS-Q value.

From figures 9.2 to 9.11, discharge loss rates declined significantly on days following rain induced high stream discharges. This indicates return flow to the stream from bank storage occurs even where the aquifer is not hydraulically connected (as in sections Q and R, figures 9.6 to 9.9). The discrepancy between prototype and model discharge losses for the hydraulically disconnected reach is at least partially due to channel storage changes (from section 9.8.8). However this does not discount the possibility of unsaturated return flow through the stream banks. Alternatively the semipermeable layer may be located beneath the streambank surface in places giving saturated return flow from perched bank storage.

Table 9.5 presents details of the bores used in model calibration and validation including statistics of fit for each bore and the aggregated bore data. This table amplifies the calibration problem of section P. With only one bore further than 15 metres from the river available for calibration the information on the transmissivity of the aquifer is not as good as for other sections. Secondly with the very rapid hydraulic connection of the aquifer after streamflow commences, the precision of the time ratio estimates from the bores adjacent the stream is low and the weighting of time ratio estimates from the only distant bore is enhanced, resulting in an "unbalanced" calibration.

Table 9.5 also shows the distribution of the groundwater elevation residual root mean sum of squares (RMSS-B) and mean (MEAN-B) between bores

TABLE 9.5 Bores Used in Model Calibration and Validation - with Statistics of Fit.

1 SECTION	2 REACH	3 NO OF BORES	4 BORE ID	5 DISTANCE FROM C/L RIVER (metres)*	6 CALIBRATION NO OF DATA	7 CALIBRATION RMSS-B (m)	8 CALIBRATION MEAN-B (m)	9 CALIBRATION OBS. BORE MEAN CHANGE (m)	10 VALIDATION NO OF DATA	11 VALIDATION RMSS-B (m)	12 VALIDATION MEAN-B (m)	13 VALIDATION OBS.BORE MEAN CHANGE (m)
O	3-5	4	80	500	4	.037	-.030	.047	8	.208	-.018	.201
			91	60	5	.558	.557	1.756	8	.253	-.146	.501
			100	-7	34	.183	-.052	2.064	42	.327	-.306	.621
			110	-110	7	.187	.149	1.079	8	.108	-.021	.736
			ALL		50	.250	.039	1.734	66	.287	-.217	.570
P	5-7	3	130	380	6	.070	-.062	.087	7	.121	-.086	.191
			140	15	22	.222	.076	2.388	38	.378	.232	2.097
			141	2.1	12	.068	.010	2.593	15	.242	.188	2.543
			ALL		40	.171	.036	2.104	60	.327	.184	1.986
Q	7-12	5	210	600	6	.104	.098	.105	6	.184	.042	.087
			230	120	7	.388	.347	1.791	7	.195	-.016	1.497
			240	-60	7	.283	.261	1.719	7	.332	-.266	1.243
			7282220050	300	5	.144	.103	.708	6	.209	-.068	.402
			7282220060	8	40	.260	.191	1.969	52	.320	-.274	1.566
			ALL		65	.263	.200	1.654	78	.296	-.210	1.328
R	7-12	8	305	550	6	.078	-.066	.027	8	.175	-.153	.035
			315	70	6	.075	-.020	.250	6	.048	.003	.233
			320	7	11	.213	-.198	.291	12	.196	-.178	.326
			330	-80	6	.074	.039	.283	6	.041	.023	.232
			340	-500	5	.108	-.098	-.014	6	.296	-.246	-.080
			355	110	6	.169	.130	.318	6	.155	.133	.290
			360	7	37	.138	-.073	.429	47	.095	-.048	.385
			375	-100	6	.108	.079	.272	6	.047	.037	.202
			ALL		83	.139	-.053	.312	97	.138	-.061	.284
S	12-15	8	420	100	5	.044	.035	.170	6	.104	-.071	.133
			430	15	9	.152	.007	.282	16	.158	-.146	.178
			431	2	7	.159	.084	.421	15	.152	.046	.459
			445	-60	5	.099	.085	.282	5	.137	-.056	.206
			477	120	6	.049	-.001	.128	5	.163	-.154	.018
			485	-7	8	.166	.080	.371	10	.144	-.086	.275
			495	-80	5	.178	.026	.188	5	.103	-.087	.132
			48880	-410	5	.056	.019	.018	5	.102	.008	.020
			ALL		50	.130	.042	.250	67	.142	-.065	.226

* + = south of river, - ve = north of river.

for each section (columns 7,8 11 and 12). These are compared with the mean observed groundwater elevation changes for each bore. (columns 9 and 13). The ratio of RMSS-B with mean observed changes (columns 7/9 and 11/13) is commonly between 20% and 50% for all bores. Bores with small elevation changes give higher ratios. Hence the two sections furthest downstream, (R and S) run into the problem of being insufficiently stressed. That is, after Wilson and Dettinger (1978), the information content of measurements is low and corresponding parameter sensitivity may be low. An example of this effect is given later (in section 9.8.6).

In summary the fit of the BIEM model to the observed data is clearly satisfactory for most engineering purposes but does not fully account for all the fine scale hydraulic processes occurring at the streambed nor in the aquifer.

9.8.2 Model parameter estimates

The values of the calibrated model parameters are given in Table 9.3. Independent estimates for some of these parameters may be used for comparison.

Hydraulic conductivity, K

Geological logging of bores on the Northern Adelaide Plains reveals increases in the fines content of the Quaternary aquifers in the downstream (westerly) direction. This is consistent with the formation of a fluviatile delta where river slope and water velocity decrease in a downstream direction giving a size-graded deposition of sediment. A similar variation in particle size accurs across the delta perpendicular to its principal direction with the proportion of silts and clays increasing with distance from the principal axis. Hydraulic conductivity was expected to follow the pattern of particle sizes.

A regional multiple-aquifer finite element (FEM) model calibrated by Close and Linke (1981) did not give a distribution of hydraulic conductivity conforming to the above pattern. Results from pump tests on

seven bores in the Quaternary aquifers revealed a large variation in hydraulic conductivity. (Linke and Eberhard, 1981). The range of results for these independent tests are compared with the hydraulic conductivity for the calibrated BIEM sections in Table 9.6.

TABLE 9.6: Aquifer properties obtained by independent methods.

Aquifer property	Method		
	7 pump tests	FEM model	BIEM sections
(1) Hydraulic conductivity (m/d)	5-99	0.3-5	4-7
(2) Thickness (m)	5-17	50-65	7-23
(3) Transmissivity (m^2/d)	46-800	20-300	50-140
(4) Effective porosity	-	0.1	0.029-0.10
(5) Diffusivity (m^2/d)	-	200-3000	700-3100

The pump tests reflect the transmissivity of sand beds within the Hindmarsh Clay formation, whereas the FEM model considers the whole thickness of the formation. The BIEM model treats the aquifer as a uniform medium thicker than a sand bed but much thinner than the full depth of the Hindmarsh Clays. (It attempts to represent the thickness of the medium contributing significantly to groundwater flow.) The calibration procedure in effect determines the diffusivity from observation bore responses and transmissivity from stream discharge losses, such that the depth chosen minimizes the RMSS-B. The interaction of aquifer basement elevation y_b with hydraulic conductivity on RMSS-B is illustrated later (section 9.8.6).

Table 9.6 reflects the different methods in rows 1 and 2 but shows

satisfactory agreement in the range of transmissivity and diffusivity. The natural heterogeneity of porous media is reflected by each method. While the BIEM sections gave the smallest range of transmissivity, the range is not so small as to suggest that the calibration procedure artificially constrains these parameter values.

Effective porosity, n_e

Typical effective porosity for sands is in the range 0.1 to 0.3. Silty or clayey sands have lower values, typically up to 0.1. The specific yield of clays is similar but the time for equilibrium drainage of pore spaces may be many days or months. Row 4 of Table 9.6 reveals a satisfactory range of values by the BIEM method for effective porosity. The aquifer diffusivity which is inversely related to the effective porosity is seen to be comparable with results of Close and Linke.

Aquifer basement hydraulic gradient, $\left(\frac{\partial h}{\partial n}\right)_b$

During periods of no flow at section 0, the groundwater levels were observed to decline at a rate which indicated outflow from the model. This could have been caused by percolation through the base of the aquifer to underlying aquifers or by an increase in groundwater flow in the downstream direction (perpendicular to the model cross-section) over the length of this reach, or both. A negative hydraulic gradient was assigned to the aquifer base to account for this outflow. The value of the hydraulic gradient was assigned by matching prototype and model rates of decline at bores distant from the river prior to the arrival of the recharge mound. As the initial free surface for the model replicated the prototype free surface, dissipation of the initial groundwater mound is taken into account by the model.

For all other sections RMSS-B was higher when the aquifer basement hydraulic gradient was changed from zero to -0.00005, the smallest outflow gradient tested. The calibration period was not long enough to determine leakage rates smaller than this hence impermeable aquifer bases were

assumed. Numerical dispersion for the model gave rise to small declines in free surface elevations at observation bores distant from the river prior to the arrival of the recharge mound. These declines while insignifant for model fitting could be expected to complicate determination of hydraulic gradients smaller than .00005 even if longer calibration periods were used.

Close and Linke's regional finite element model contained a separating layer between the Quaternary and Tertiary aquifers. The calibrated value of the vertical permeability of the separating layer is shown in row 1 of Table 9.7 for positions corresponding to the locations of the BIEM sections.

TABLE 9.7: Aquifer basement hydraulic gradient from Finite Element Model of Close and Linke.

	Section O	Section P	Sections Q,R,S
(1) Vertical permeability (m/d)	.0005	.0005	.0002
(2) Mean vertical hydraulic gradient through aquifer base	0.7	0.25	0.25
(3)=(1)×(2) vertical leakage rate (m/d)	.00035	.00013	.00005
(4) Hydraulic conductivity from BIEM section (m/d)	4.5	6.6	4.0-7.0
(5)=(3)/(4) Equivalent vertical hyd. gradient through base of aquifer for BIEM ($\times 10^6$)	78	19	7-13
(6) BIEM section hyd. gradient ($\times 10^6$)	200	0	0
(7) BIEM minimum significant gradient ($\times 10^6$)	50	50	50

From known vertical hydraulic gradients, (row 2), the vertical leakage rate corresponding to the FEM model were found (row 3). Using the BIEM isotropic hydraulic conductivities the corresponding vertical hydraulic gradients were calculated (row 5) and compared with the calibrated BIEM model values (row 6). At section 0, this is significantly higher than the corresponding FEM value. The BIEM model does not account for net groundwater outflow in the downstream direction, hence it may compensate by over estimating vertical leakage. For other sections the FEM derived value of vertical hydraulic gradient at the aquifer base is less than the minimum significant gradient detectable by the BIEM model over the calibration period.

Streambed hydraulic impedance, B

It can be seen from Table 9.3 that the calibrated streambed hydraulic impedance increased with distance downstream. This is consistent with the expected pattern of hydraulic conductivity due to streambed morphology as previously described. It may also correspond with an increasing concentration of organic matter in the streambed arising from a series of stormwater outfalls draining residential and industral areas of the cities of Salisbury and Elizabeth.

Suction head, h_c

The effect of suction head was investigated only for the sections which became hydraulically connected. For disconnected sections, changing the streambed hydraulic impedance could account for the effect of changing the suction head (for suction heads of smaller magnitude than the minimum vertical distance separating the streambed and the groundwater mound). Hence for these cases h_c was arbitrarily set to zero, and the case of h_c exceeding the difference in elevation of the streambed and the maximum free surface elevation below it was neglected. For hydraulically connected sections, h_c had a negligible effect on model groundwater elevations, except those immediately adjacent the stream prior to hydraulic connection

which rose more rapidly as h_c became more negative. Non-zero values of h_c were found to produce no improvement (with one exception, discussed below) in the fit of discharge losses, so h_c was set to zero.

It was observed for the calibration period of section 0 that a finite suction head (h_c = 1.0 m) reduced the RMSS-Q (see sensitivity analysis, Table 9.8). This occurred due to an increase in model discharge losses at the start of flow corresponding more closely with observed losses. Channel storage increases were considerable during this period hence overestimating observed discharge losses. Also h_c was found to have a most significant adverse effect on the validation fit. It was also observed that minor damped oscillation of discharge loss rates on alternate days occurred. These oscillations increased in amplitude from 2.4% to 3.1% maximum discharge loss as h_c was increased from 0.5 to 2.0 metres. This is caused by the strong dependence of exchange flowrate on groundwater elevation while this is rising rapidly. Smaller time steps would reduce the magnitude of this minor temporary instability.

9.8.3 Sensitivity of model output to parameter values.

Sensitivity analyses were performed for two sections 0 and S which are hydraulically connected and disconnected respectively. Parameter values were changed by 10%, except for y_b which was reduced to increase the aquifer thickness by 10% and h_c and $\left(\frac{\partial h}{\partial n}\right)_b$ which were originally zero for at least one of the sections. The calibration period was used for all runs.

Cunningham and Sinclair described sensitivity in terms of an index,

$$S_C = \frac{100}{n} \sum_{i=1}^{n} \left| \frac{P_i - M_i}{P_i} \right| \qquad 9.7$$

where all symbols are as defined at equation 9.3. They defined sensitivity as the change in S_C (percentage change in model output with respect to prototype response) for a given change in the value of a model parameter.

This means that sensitivity depends on the initial set of model parameters. A similar index, S_D was chosen to define the change in bore water levels with respect to initial bore water levels.

$$S_D = \frac{100}{n-1} \sum_{i=2}^{n} \left| \frac{(P_i - P_1) - (M_i - M_1)}{P_i - P_1} \right| \qquad 9.8$$

Tables 9.8 and 9.9 contain two rows for each observation bore and the aggregate of observation bore data : the model mean change in groundwater level, $\bar{M}$ (metres) and the change in sensitivity index, ΔS_D due to the change in parameter value. The value of S_D for the calibrated model is shown in brackets. Also shown are RMSS-B and RMSS-Q and the change in each due to the change in parameter value. Finally the sum of discharge losses during the calibration period on days with no rainfall interference, MEAS-Q is presented along with its fractional change due to the change in parameter value.

The ranking of sensitivity of parameters is seen to depend on the nature of the connection between the stream and aquifer. For the hydraulically connected section, O, y_b hence aquifer thickness is shown to have a significant effect on model output, particularly MEAS-Q, as aquifer transmissivity controls the exchange flow. For the hydraulically disconnected section, S, MEAS-Q is independent of aquifer thickness and K/n_e but is most sensitive to the stream stage - discharge relationship, streambed width and hydraulic impedance.

The sensitivity of output to section head for section S which remains hydraulically disconnected is high as expected. Changing the suction head by 0.1 m increases the hydraulic head loss through the semipermeable blanket by 0.1 m causing hydraulic gradients to increase by 33% on the flat streambed with larger percentage increases on the sloping banks. Hence the 40% increase in discharge loss causing a large increase in RMSS-Q.

The change in sensitivity index, ΔS_D did not yield a convincing

TABLE 9.8 Sensitivity analysis - section O.

PARAMETER			Streambed width (m)	Streambank slope (tan)	y_b (m.AHD)	K/n_e (m/d)	K (m/d)	$(\frac{\partial h}{\partial n})_b$	B (m)	h_c (m)	Stream depth $[h_{s_0}=]$	No. of nodes streambed/ total
Calibrated model value			4	1	32	120	4.5	-.0002	2	0	$(\frac{Q}{320})^{1/2.88}$	8/43
Sensitivity test value (only one changed)		None changed	4.4	0.9	30.6	108	4.95	-.00022	2.2	1.0	$1.1 * h_{s_0}$	18/65
bore 80	$\bar{M}$(m)	0.077	0.082	0.078	0.257	0.033		0.022	0.073	0.084	0.081	0.070
SL=500m	ΔS_D	(16.6)	2.2	0.3	113.	3.0		5.8	1.2	2.9	1.3	0.7
bore 91	$\bar{M}$(m)	1.199	1.247	1.205	1.140	1.154		1.180	1.139	1.237	1.253	1.221
SL=60m	ΔS_D	(32.0)	3.0	0.4	3.7	2.7		1.1	4.0	2.6	3.3	1.3
bore 100	$\bar{M}$(m)	2.116	2.169	2.122	2.045	2.095		2.108	2.053	2.149	2.178	2.127
SL=-7m	ΔS_D	(7.8)	0.1	0.0	0.4	0.1		0.2	1.0	1.4	0.4	0.1
bore 110	$\bar{M}$(m)	0.929	0.966	0.934	0.906	0.874		0.906	0.886	0.963	0.970	0.951
SL=-110m	ΔS_D	(9.9)	1.1	0.2	1.6	4.4		1.2	3.7	0.0	1.2	0.7
all bores	$\bar{M}$(m)	1.695	1.742	1.701	1.652	1.665		1.680	1.640	1.727	1.748	1.707
	ΔS_D	(11.2)	0.2	0.0	9.9	1.2		0.6	1.5	1.0	0.1	0.1
RMSS-B		.250	.234	.247	.289	.269		.255	.292	.225	.237	.244
(m)	Δ	-	-.016	-.003	.039	.019		.005	.042	-.025	-.013	-.006
RMSS-Q		250	187	243	368	276	368	257	334	209	179	244
(m^3/d)	Δ	-	-63	-7	118	26	118	7	84	-41	-71	-6
MEAS-Q		88800	89600	89000	95300	90700	97700	89600	88200	87400	89800	87400
(m^3)	Δ%	-	0.8	0.2	7.3	2.1	10.0	0.9	-0.7	-1.6	1.2	-1.6

$\bar{M}$(m) = mean model groundwater level change, in metres.

ΔS_D = change in sensitivity index, S_D, from its calibrated model value, shown in brackets.

TABLE 9.9 Sensitivity analysis - section S.

PARAMETER		Streambed width (m)	Streambank slope (tan)	y_b (m.AHD)	K/n_e (m/d)	K (m/d)	$(\frac{\partial h}{\partial n})_b$	B (m)	h_c (m)	Stream depth $[h_{s_0} =]$	No. of nodes streambed/ total
Calibrated model value		4	1	-6	40	4.0	0	10	0	$(\frac{Q}{320})^{1/2.88}$	8/43
Sensitivity test value (only one changed)	None changed	4.4	0.9	-8	36	4.4	-.0001	11	0.1	$1.1 * h_{s_0}$	18/65
bore 420	$\bar{M}$(m)	.135	.147	.136	.134	.121	.071	.123	.190	.149	.137
SL=100m	ΔS_D	(17.4)	5.8	0.4	0.1	6.7	29.2	5.7	9.2	6.7	0.9
bore 430	$\bar{M}$(m)	.275	.300	.276	.265	.259	.217	.250	.385	.304	.279
SL=15m	ΔS_D	(28.5)	8.7	0.6	3.3	4.7	1.9	6.2	37.0	10.1	1.3
bore 431	$\bar{M}$(m)	.337	.368	.339	.328	.323	.288	.307	.474	.373	.342
SL=2m	ΔS_D	(62.9)	0.6	0.2	0.9	0.5	4.8	0.8	11.0	1.0	0.7
bore 48880	$\bar{M}$(m)	-.001	-.001	.001	.000	-.002	-.060	-.001	-.001	-.001	.002
SL=-410m	ΔS_D	(89.6)	0.8	0.1	3.7	2.0	146.5	1.0	3.7	1.1	10.8
all bores	$\bar{M}$(m)	.208	.227	.209	.203	.195	.149	.189	.292	.230	.211
	ΔS_D	(45.7)	0.7	0.0	0.2	0.0	19.9	0.3	9.6	0.8	1.0
RMSS-B		.130	.123	.130	.134	.137	.168	.142	.129	.122	.129
(m)	Δ	-	-.007	.000	.004	.007	.038	.012	-.001	-.008	-.001
RMSS-Q		170	240	172	170	170	247	170	185	645	253	170
(m^3/d)	Δ	-	70	2	0	0	77	0	15	475	83	0
MEAS-Q		42100	46000	42300	42100	42100	46300	42100	38300	59000	46500	42000
(m^3)	Δ%	-	9.4	0.5	0.0	0.0	10.0	0.0	-9.1	40.3	10.5	-0.2

$\bar{M}$(m) = mean model groundwater level change, in metres.

ΔS_D = change in sensitivity index, S_D, from its calibrated model value, shown in brackets.

estimate of sensitivity as bores with smaller mean model groundwater level changes in general gave higher values of ΔS_D. For example see Table 9.8, bore 80 for y_b and Table 9.9, bore 48880 for $\left(\frac{\partial h}{\partial n}\right)_b$. For each section in general water levels in bores close to the stream were sensitive to the same parameters as exchange flow. Groundwater levels in bores distant from the stream were sensitive to $\left(\frac{\partial h}{\partial n}\right)_b$ but relatively insensitive to the streambed parameters. As expected MEAS-Q is directly proportional to K when K/n_e is constant.

During calibration the streambed geometry was fixed. The sensitivity analysis reveals RMSS-B and/or RMSS-Q could be reduced by adjusting the streambed geometry. No doubt subsequent iterative changes of other parameters could further improve the calibration fit. Such an exercise was not attempted. The analysis of discharge loss residuals (section 9.8.8) and reflections on the uniqueness of model parameters (section 9.8.6) indicate that further parameter refinement to improve calibration fit may not necessarily improve model predictive performance.

The effect of the choice of the number of nodes (43) is shown in Tables 9.8 and 9.9 to be satisfactory for both cases of stream aquifer interaction. The effect of node numbers on execution time and mass balance error at the end of each run are shown in Table 9.10. All runs were on the University of Adelaide CDC Cyber 73 computer. Execution time is approximately proportional to the square of the number of nodes.

9.8.4 Comparisons between two sections in one reach

The reach between gauging stations 7 and 12 was modelled using two independent sections, Q and R. They produce the same discharge loss time series due to the discharge loss calibration procedure and because the stream remains hydraulically disconnected. As could be expected due to the differences in groundwater responses the parameters of the models are quite different (Table 9.3). This implies that model parameters including streambed hydraulic impedance are sensitive to the groundwater records

TABLE 9.10: Effect of number of nodes on computer execution times and field length.

	SECTION O		SECTION S	
1. Number of nodes	43	65	43	65
2. Number of potential streambed nodes	8	18	8	18
3. Max field length (octal)	104000	105200	104000	105200
4. Execution time (CP sec)	84	225	68	152
5. Final mass balance error (%)	-4.5	-2.5	-0.7	-0.1
6. Number of time steps	47	47	37	37
7. Exec. time/timestep (sec)	1.8	4.8	1.8	4.1

used for calibration. Thus if other sets of bores had been chosen for any section different values for model parameters would have resulted.

9.8.5 Observations on stage I calibration (ICAL=2)

Stage I calibration aims at estimating the time ratio for use in the second stage. The time ratio matching operation was very efficient with computer time (due to logarithmic time stepping) and assisted in reducing the ranges of parameter values to consider in subsequent stages. The values of time ratio for the calibrated sections were in all cases within 50% of the best time ratios derived from stage I (Table 9.11) even though runs in the second stage used a wide span of time ratios. The problems associated with noisy data are not as severe in subsequent calibration stages where data sets are larger.

The first stage of calibration was rerun substituting the final calibrated parameter values for B, y_b and $\left(\frac{\partial h}{\partial n}\right)_b$ to predict time ratio.

TABLE 9.11 Comparison of best parameter values for first and second stages of calibration with stage III calibrated values.

SECTION	TRIAL	STAGE I (ICAL = 2)										STAGE II (ICAL = 3)						STAGE III (ICAL = 4)	
		TR		Best fit t^* V_s t															
		Mean (d^{-1})	s.d./mean	Slope (d^{-1})	t at t^*=0 (days)	r	no. match pts./max.	B (m)	y_b (m.AHD)	$(\frac{\partial h}{\partial n})_b$	TR (d^{-1})	RMSS-B (m)	MEAN-B (m)	B (m)	y_b (m.AHD)	$(\frac{\partial h}{\partial n})_b$	RMSS-B (m)	MEAN-B (m)
O	B.A.S.	119	.19	145	1.9	.98	6/8	2	32	0	120	.235	-.074	3	32	-.00012	-	-
	C	337	.66	39	-64	.21	6/8	2	32	-.0002	120	.393	.205	2	32	-.0002	.250	.039
P	B.A.S.	62	.34	117	1.3	.55	4/6	1	25	0	100	.194	.092	2.25	30	0	-	-
	C	122	.44	136	1.4	.74	6/6	2.25	30	0	100	.194	.092	2.25	30	0	.171	.036
Q	B.A.S.	98	.43	107	-1.4	.62	8/10	2.5	12	0	100	.222	-.061	3	4-23	0	-	-
	C	226	1.16	145	-4.7	.70	8/10	4.5	4-23	0	140	.240	.133	4.5	4-23	0	.263	.200
R	B.A.S.	109	.73	132	1.1	.33	9/14	16	12	0	80	.156	-.051	8	0	0	-	-
	C	73	.64	80	0.5	.27	9/14	8	0	0	80	.156	-.051	8	0	0	.139	-.053
S	B.A.S.	70	.50	85	2.9	.45	8/15	16	4	0	40	.134	-.008	10	-6	0	-	-
	C	45	.46	55	2.9	.50	8/15	10	-6	0	40	.134	-.008	10	-6	0	.130	.042

B.A.S. = best parameter estimates at that stage.

C = parameters of stage III calibrated sections.

If the first stage is a reliable indicator of the final parameter values, the mean time ratio so obtained should approach its (stage III) calibrated value and have a lower coefficient of variation than the previous best run for stage I. In fact this occurred for sections R and S but not the other three. One may argue that guesses of time ratio values could be an equally satisfactory way to commence calibration at the second stage.

9.8.6 Observations on stage II calibration (ICAL=3)

Due to the ability to regulate dry weather discharge in the Little Para River at the reservoir release valve, relatively steady discharge rates could be maintained for quite long periods. Consequently the assumption of constant stream stage at a section was tolerable. In practice beside occasional rainfall induced runoff from the catchment downstream of the dam, there was a trend towards increased discharge rates with time for downstream reaches, due to the decline in discharge loss rates in hydraulically connected upstream reaches.

Using a constant stream head allowed the results of a single model run to be compared with sets of observed groundwater elevations for a range of time ratios. During stage II model parameters changed significantly from their stage I value and for three of the five sections (P, R and S) the parameter estimates could not be improved in the third stage of calibration.

It was discovered at stage II that model uniqueness could not be assured, due to the interaction between parameters B and y_b on RMSS-B. Figures 9.12 and 9.13 illustrate this interaction clearly. An increase in streambed impedance B reduces the aquifer recharge rate thus reducing the rate of rise of the free surface. An equivalent effect is observed at bores distant from the stream if y_b is increased, causing a reduction in transmissivity of the aquifer. In these two cases two sets of model parameters were selected for testing at the third stage of calibration, (B,y_b) = (10,6) and (8,0) for section R and (12,0) and (10,-6) for

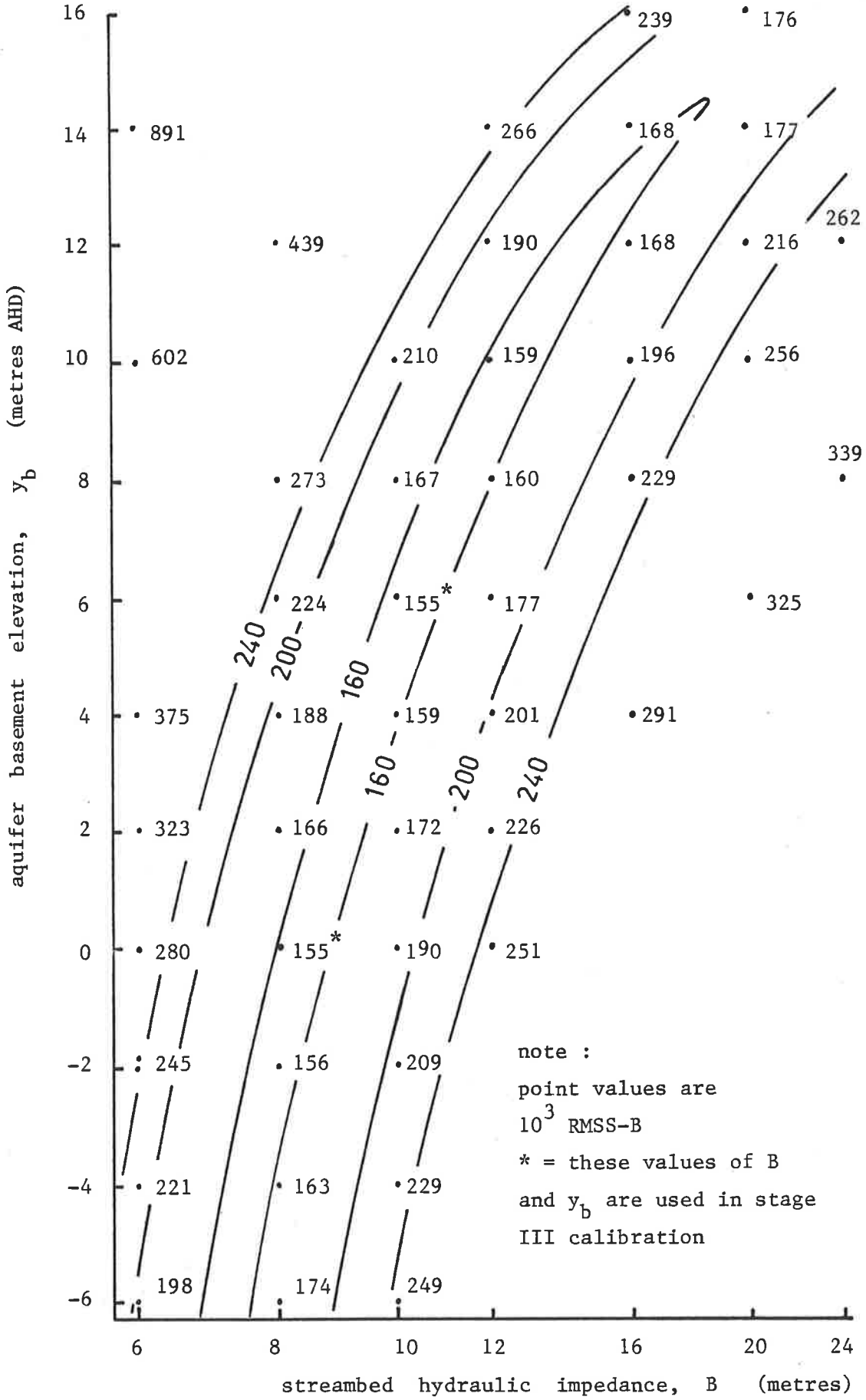

Figure 9.12 Effect of B and y_b on RMSS-B in stage II calibration of section R for time ratio = 80.

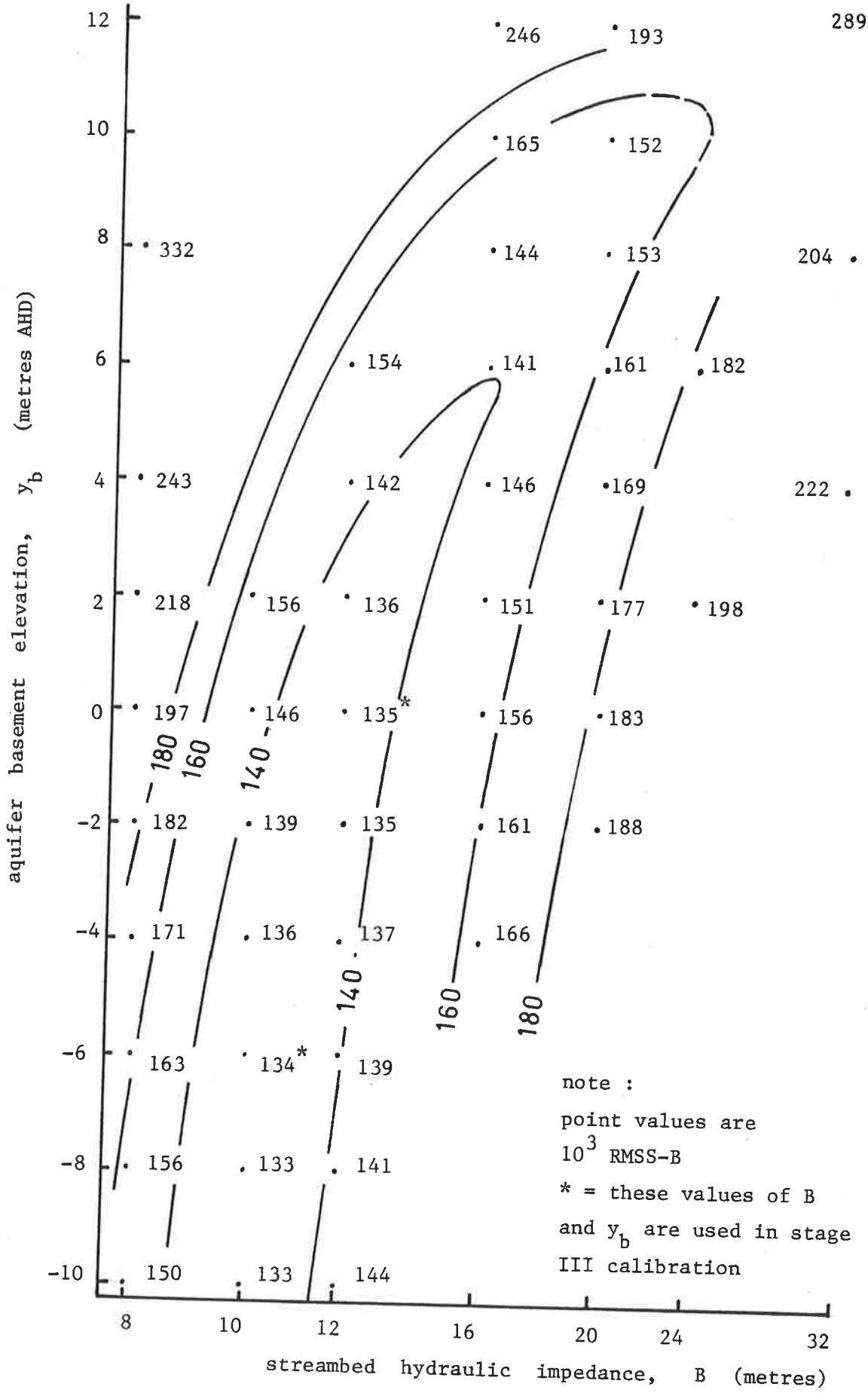

Figure 9.13 Effect of B and y_b on RMSS-B in stage II calibration of section S for time ratio = 40.

section S.

The dependence of RMSS-B on the time ratio is illustrated in Table 9.12 for each of these (B,y_b) pairs. RMSS-B is a parabolic function of time ratio and for each section the range in RMSS-B is approximately equal for the two (B,y_b) pairs. That is RMSS-B appears to exhibit the same sensitivity to time ratio for each pair of B and y_b values for each section.

TABLE 9.12: Effect of time ratio on RMSS-B for sections R and S in second stage calibration.

Section	B (m)	y_b (m)	TR=	48	64	72	80	88	96	112
R	10	6		.180	.161	.157	.156	.158	.162	.177
	8	0		.178	.160	.156	.156	.159	.165	.183
			TR=	24	32	36	40	44	48	56
S	12	0		.160	.142	.137	.135	.135	.137	.147
	10	-6		.150	.136	.133	.134	.137	.142	.157

For sections of the stream exhibiting a change from hydraulic disconnection to hydraulic connection, the time ratio for the time at which the free surface intersects the streambed is used as a constraint and limits the range of B and y_b combinations. If B is too large or y_b too low the model does not allow hydraulic connection.

For section Q, the rise in groundwater levels within 200 metres of the river were significantly higher than would be expected in proportion to

rises in groundwater levels further from the stream. This could be due to a number of factors such as a reduction in aquifer transmissivity with distance from the stream or a reduction in net groundwater outflow in the downstream direction (perpendicular to the model cross-section) in the vicinity of the stream. The first of these was simplest to model and the aquifer basement adjacent the stream was lowered to provide the transmissivity range required to reproduce the observed groundwater level changes.

9.8.7 Observations on stage III calibration

The effect on model parameters of the variation in model stream stage due to variation in actual discharge rate was found to be insignificant. Model parameters varied only marginally if at all during this third stage. This was in part attributed to the choice of a calibration period with minimal discharge variation. The question as to whether the model could be adequately calibrated without sustained periods of constant discharge remains open to further investigation. Computer runs for stage three calibration having daily time steps required more execution time (typically 80 sec) than second stage runs, (typically 60 sec) having logarithmic time steps.

The choice of fitting bore water elevations before rather than after stream discharge losses is parametrically efficient and consequently reduces the aggregate computer execution time for calibration.

9.8.8 Results of analysis of discharge loss residuals

Larger discharge losses were expected to occur on days of higher stream temperature, due to reduced water viscosity in the semipermeable layer and on days of higher evaporation. Along with a number of other factors these were investigated for their impact on the difference between dry weather prototype and model discharge losses. The BMDP program P2R for stepwise regression was used as described in 9.6.

Table 9.13 summarizes the best regression equations and "F to remove"

TABLE 9.13 Regression of discharge loss residual on selected independent variables.

Section	Calib. or valid	No. of days	Standard error of estimate initial/ best regression (m^3/d)	Multiple r-square best regression	Regression coefficient (2 dec. places), above *F to remove value (1 dec. place)* DAY NO	STN U/S (m^3/d)	LPEVAP (mm)	MEANTMPX (^oC)	DELU (m^3/d)	Regression constant
O	C	24	198/176	.31	6.39 *2.7*			12.11 *1.7*	1.17 *8.3*	-5307
	V	24	425/217	.77	43.11 *26.4*	.046 *31.2*		26.29 *6.8*		-31970
P	C	21	395/314	.43	-7.64 *1.03*		53.28 *4.55*			5520
	V	18	702/604	.39	-55.72 *1.2*	2.37 *5.0*		82.51 *3.0*		-17453
Q	C	18	1204/288	.95		-.23 *46.*		41.59 *3.4*	0.85 *234.1*	1740
	V	18	1259/289	.96	-126.12 *72.9*	.12 *10.4*		39.14 *6.3*	0.56 *106.8*	84810
R	C	18	1202/288	.95		-.23 *44.7*		41.60 *3.4*	0.85 *234.0*	1791
	V	18	1257/289	.96	-126.12 *72.9*	.12 *10.8*		39.11 *6.3*	0.56 *106.8*	84870
S	C	11	390/303	.58	-58.24 *6.1*	.64 *6.3*	41.21 *1.5*			42395
	V	16	883/539	.65		-.36 *26.3*				4308

values for each variable admitted. The independent variables were day number (DAY NO), daily discharge at the upstream gauging station (STN U/S), Little Para Reservoir A class pan daily evaporation (LPEVAP), Adelaide mean daily air temperature (MEANTMPX) and the incremental change in daily discharge at the upstream gauging station (DELU).

Each data set consisted of between eleven and twenty four dry days for which all data were available. The standard error of the initial estimate corresponds to the case of setting the predictor to the mean of the discharge loss residual. The standard error of the best regression is reduced significantly for sections Q and R and to a smaller extent for the other sections. This is also represented in the square of the multiple regression correlation coefficient. In no case does the standard error of the best fit regression fall below 175 m^3/d (2.0 l/s) which corresponds with the accuracy of the discharge measurements (quantified in section 9.8.1). The validation runs for sections P and S result in best regression standard errors of 500-600 m^3/d (6 to 7 l/s) which exceed the tolerance on discharge measurements. There is therefore a moderate uncorrelated component of discharge losses for these sections, indicating minor deficiencies in the model structure.

Apart from section 0, the regression coefficient for day number is negative revealing that discharge losses decline with time more rapidly than the model predicted. For the hydraulically disconnected sections day number was significant for the calibration run or the validation run but not both. It had been suggested that for some parts of the stream either permeability may reduce with time, due to saturation of cracking/swelling clays and organic components of the substrate or that hydraulic gradient may be reduced due to formation of local perched water tables which may intersect the streambed. The lack of consistent significance of the day number suggests that the effect of these features on discharge losses during the calibration and validation periods is unimportant.

The upstream station discharge was included to determine whether the discharge-stage relationship introduced systematic discrepancies. For each section the calibration and validation regression coefficients for upstream discharge were of opposite sign or one was insignificant. One is led to conclude that the stage-discharge relationship is suitable for the given streambed geometry as no consistent trend was observed.

Evaporation was highly correlated with mean temperature having a correlation coefficient of 0.87 and 0.70 for the calibration and validation periods respectively. Hence it is not surprising that only one of evaporation or temperature find their way into the equation. In most cases temperature had a more significant correlation with discharge loss residuals. The regression coefficient usually varied between 12 and 42 $m^3/d/^oC$ with the shorter reach, containing section O having the lower coefficient. For section S evaporation was more significant for the calibration period and the regression coefficient 41 $m^3/d/mm$ corresponds to a pan coefficient of 1.4 which exceeds the maximum likely pan coefficient 0.8. Due to the small number of degrees of freedom for this equation, stream discharge measurement error could influence the regression coefficient and no further explanations are attempted.

It was expected that changes in channel storage due to flow variations would have featured more strongly in the discharge loss residual regression equation. Sections Q and R and section O for calibration only found the discharge change significant. While the regression coefficient is strictly limited in the range 0 to 1 it is observed that more than 50% of the discharge change on average contributed to a channel storage change for these sections.

The regression constant is given in Table 9.13 in order to complete the regression equation. As this corresponds to the mean of the residual between the dependent variable and the sum of the product of independent variables and their regression coefficients it has no F to remove value.

In conclusion no uniform trend was observed to link the independent variables to discharge loss residuals, although some variables were found to be significantly correlated for some sections during one or both periods of interest. Regressions including these parameters significantly reduced the standard error of estimate for the reach between stations 7 and 12, and also between station 3 and 5 for the validation period. However for the remaining sections, P and S the uncorrelated component of error remains high indicating that improvements could be made to the model. For example lowering the elevation of the semipermeable blanket to some finite depth below streambed level would provide a small drainable bank storage for hydraulically disconnected streams and alter the temporal pattern of exchange flow rates following stage changes in hydraulically connected streams. Such changes fall beyond the scope of this thesis.

In general the standard error of estimate for the best regression was consistent with the expected error in discharge measurement with the exception of sections P and S.

9.8.9 Effect of temperature compensation on discharge loss residuals

For ICAL=7, the streambed hydraulic impedance was adjusted daily in accordance with stream temperature. This was found to have negligible impact on the fit of groundwater levels, but a significant effect on discharge losses. Table 9.14 summarizes the multiple regression of the discharge loss residual on selected independent variables.

One would expect that the regression coefficient for temperature would be zero or that it would not be significant if the temperature compensation algorithm was correct. On the contrary it is observed that the regression coefficient for temperature has increased from values in Table 9.13 for most cases. The F to remove value has declined in some instances. However in all except two cases, the calibration periods for sections P and S, the strong correlation between temperature and evaporation causes the regression coefficient for evaporation to be forced

TABLE 9.14 Regression of discharge loss residual on selected independent variables for temperature compensated steambed hydraulic impedence model.

Regression coefficient (2 dec. places), above
F to remove value (1 dec. place)

Section	Calib. or valid	No. of days	Standard error of estimate initial/best regression (m^3/d)	Multiple r-square best regression	DAY NO	STN U/S (m^3/d)	LPEVAP (mm)	MEANTMPX (^oC)	DELU (m^3/d)	Regression constant
O	C	24	186/168	.33	16.29 *5.4*	-.23 *3.3*	-29.52 *2.2*	28.42 *4.2*		-9218
	V	24	435/332	.47			-32.19 *2.7*	72.89 *15.8*		-1322
P	C	21	415/319	.50	-33.45 *4.2*	.30 *2.4*		41.48 *5.8*		21053
	V	18	573/513	.34		.82 *3.1*	-49.59 *1.7*	60.72 *3.6*		-20292
Q	C	18	1127/296	.95	35.91 *1.7*	-.45 *12.5*	-132.90 *8.7*	61.29 *2.3*	1.09 *45.8*	-23885
	V	18	1691/650	.89	-156.69 *26.5*		-144.42 *8.9*	64.74 *1.8*	.41 *10.9*	109073
R	C	18	1124/294	.95	35.08 *1.6*	-.45 *12.2*	-131.31 *8.6*	61.32 *2.4*	1.09 *45.8*	-23230
	V	18	1679/643	.89	-155.57 *26.7*		-143.01 *8.9*	65.41 *1.9*	.41 *11.2*	108366
S	C	11	338/302	.28					.39 *3.5*	115
	V	16	1118/652	.71		-.41 *22.6*	-73.43 *5.0*			5462

negative, implying that prototype discharge losses are reduced, with respect to model values, as evaporation increases. Clearly the effect of temperature is over-compensated in this model and based on the physical incongruity of the regression coefficients, and the generally poorer performance of the best regression equation as evidenced in the standard error of estimate and the square of the multiple regression coefficient, one is led to reject this model in favour of the uncompensated model.

The physical significance of this is illustrated in chapter 7 where an impeding layer for the infiltration pond is located 0.8 metres below the streambed and temperature variations at that depth have lower amplitude than surface temperature variations and reflect only longer term variations in water temperature. Temperature compensation using say mean monthly streambed temperatures may possibly be justified after further investigation.

9.9 Summary

Firstly the BIEM model is shown to be capable of calibration for a field problem involving interaction of an ephemeral stream and an aquifer. The three stage calibration procedure used is computationally efficient and is capable of further refinement as outlined in the next chapter (section 10.2).

Secondly the fit of model predictions to prototype observations of stream discharge losses and groundwater elevation changes is satisfactory for reservoir release operation purposes. However an analysis of discharge loss residuals reveals that for some sections moderate uncorrelated discrepancies may exceed the bounds of discharge measurement errors. While the form of the model appears to represent the major features of stream-aquifer interaction improvements which may account for these discrepancies are possible and some suggestions for model alterations arising from calibration observations are presented in chapter 10.

CHAPTER 10

CONCLUSIONS

10.1 Summary and Conclusions

This study was aimed at exploring the nature of the interaction between a 16 km length of the Little Para River and the underlying Quaternary aquifer, through monitoring and numerical modelling. After a review of the literature revealed no investigation of the process of hydraulic connection of ephemeral streams and aquifers, a numerical model was constructed to satisfy this need. The model was successfully applied to a range of conceptual stream-aquifer interaction problems for which solutions were available. It was then used to explore the process of hydraulic connection.

A field study was undertaken over a period of three and a half years, involving controlled releases from Little Para Reservoir, to monitor discharge losses in the Little Para River and groundwater elevation changes on a regional scale. In addition a streambed test pond experiment was conducted to observe hydraulically disconnected streambed infiltration on a smaller scale. Data from this overall study was used to derive a reservoir recharge release rule for the new reservoir upstream of the study zone. Field data was also used to calibrate and validate the numerical model at five cross-sections on the stream. An analysis of stream discharge loss residuals was performed.

The study met its original objectives of exploring the fundamentals of streambed hydraulics which govern the exchange of water between ephemeral streams and aquifers, and of solving an operation problem for the Little Para Reservoir.

The boundary integral equation model gave excellent agreement with

solutions to a range of theoretical problems. It provided answers to new problems accounting for the process of hydraulic connection. An example reservoir release problem demonstrated the usefulness of the model, as configured, for short term simulations. When applied to the Little Para River it gave reasonable fit to the observed data in validation, but indicated that in its present form it did not account for all processes occurring at the streambed. Execution times on the available computers at the time were too long to apply the model to determine mean annual recharge or to compare recharge from various release policies.

The field study provided a valuable data set from which algorithms could be derived and used to determine mean annual recharge due to unregulated discharge. Similarly recharge due to different release strategies could be estimated. In this way the policy producing the lowest pumping costs and satisfying all recharge and in-stream requirements could be isolated. It was found to be a constant annual release volume, rather than any policy which attempted to conjunctively operate the surface storage and aquifers.

10.2 Suggestions for Additional Research

With the use of a faster computer the BIEM model could be calibrated and validated using all of the available period, February 1980 to June 1982, rather than month long extracts. The calibrated model could then be used with the historical discharge record to estimate the recharge history. It would be interesting to compare that figure with the recharge estimate derived in chapter 8.

Incorporation of an open channel flow routing equation in the BIEM model may appeal to surface water hydrologists wishing to distinguish between channel storage changes and bank storage changes during the passage of a floodwave. A series of sections could be linked and stream discharge at downstream stations determined by routing the upstream discharge and adding or subtracting the exchange flow for the intervening reach.

An ability to vary the depth of the semipervious layer below the streambed may have advantages if it is known that the stream becomes hydraulically connected with a perched watertable overlying the regional water table. This would involve treating the aquifer as two zones separated by the semipervious layer. The same streambed boundary conditions would apply and the hydraulic impedance, B of the streambed reduced to eliminate its effect if necessary.

An extension to a three dimensional model would enable an appropriate treatment of regional groundwater flow, but computation time is likely to be excessive even on a very fast computer. A model similar to that of Henry (1979) where the stream is represented by a single line of nodes is more likely to be of value for regional flow problems. The model reported in this thesis could be used to examine stream cross-sections where difficulties occur in fitting a horizontal plane model.

The calibration phase could be semi-automated by the use of successive approximations. That is each parameter estimate is improved by comparing paired values of previous estimates and the corresponding values of the objective function (eg. RMSS). The relationship between the parameter estimate and the objective function may be used to forecast the parameter estimate which would minimize the objective function. This could be repeated parameter by parameter and step by step until no further improvement in the objective function was obtained. A series of initial, parameter values and orders of stepping through parameters should be used to check that the global value of the objective function within the range of feasible parameter values is obtained. This approach is expected to considerably reduce the man hours required for calibration at the expense of additional computer execution time.

The physical dependencies occurring at the streambed on a micro-scale are diverse and include the following examples:

. Erosion and sediment deposition rates change with water velocity.

- Growth and transpiration rates of algae vary with light, temperature, water velocity, suspended sediments, nutrients, and water chemistry.
- Growth and decay of streambed vegetation and biota occur with time.
- Burrowing of organisms, crustacea and animals in the streambed causes local perturbations.
- Evaporation from a drying streambed depends on moisture content.
- Cracking and swelling of soil depends on moisture content.
- Hydraulic conductivity varies with moisture content.
- Moisture content varies with suction head, usually with hysteresis.

Due to the large variations in soil types over small areas of streambed and the combined effects of the factors listed above which vary in space and time it is unlikely that a comprehensive model of streambed processes will ever be useful at a field scale. However studies of the effects of these processes may be valuable in accounting for macroscopic (average) changes in streambed geometry and hydraulic impedance due to changes in catchment land use or streamflow regime.

10.3 Implications of Results

The release rule recommended in chapter 8 has been adopted by the Engineering and Water Supply Department for the operation of the Little Para Reservoir to ensure the replenishment of Northern Adelaide Plains aquifers.

The potential for groundwater recharge enhancement by discharge regulation in ephemeral streams is demonstrated. This is an important principle to consider in constructing a dam on an ephemeral stream upstream of a recharge zone. In the case of the Little Para River only 18% of natural reservoir intake was required to be released in order to maintain the natural recharge. Additional releases could efficiently enhance natural recharge by up to 20%. In arid and semi-arid areas where fresh

groundwater is a valuable resource streamflow regulation to enhance recharge and improve groundwater quality may be a valuable means of water conservation.

APPENDIX A

DERIVATION OF THE UNSTEADY FREE SURFACE BOUNDARY CONDITION

1. Method 1

For steady flow the free surface is a streamline, hence the derivative of hydraulic head normal to the free surface is zero, and the free surface boundary conditions are

$$\frac{\partial h}{\partial n} = 0 \qquad \text{A.1}$$

and $h = \eta$ where $y = \eta(x)$ A.2

where η is the elevation of the free surface.

The unsteady free surface is not a streamline and without accretion is always composed of the same fluid particles (De Wiest, 1961). Writing the equation of the free surface as

$$y(t) = \eta(x(t),t) \qquad \text{A.3}$$

, an identity in t, and differentiating with respect to time gives

$$\frac{\partial y}{\partial t} = \frac{\partial \eta}{\partial x}\frac{\partial x}{\partial t} + \frac{\partial \eta}{\partial t} \qquad \text{A.4}$$

This is equivalent to taking the "substantial derivative" as described by Bear (1972). That is partial differentiation of a fluid property following a particular particle where that property of the fluid is conserved. In this case, following a fluid particle on the surface, the pressure, p, is always zero.

$\frac{\partial x}{\partial t}$ and $\frac{\partial y}{\partial t}$ are the fluid particle velocity components in the x and y directions.

Applying Darcy's law gives

$$\frac{\partial x}{\partial t} = \frac{-K}{n_e}\frac{\partial h}{\partial x}, \text{ and } \frac{\partial y}{\partial t} = \frac{-K}{n_e}\frac{\partial h}{\partial y} \qquad \text{A.5}$$

where K is the saturated hydraulic conductivity of the medium and

n_e is the effective porosity of the medium.

Substituting into equation A.4 and rearranging gives

$$\frac{n_e}{K}\frac{\partial \eta}{\partial t} = \frac{\partial h}{\partial x}\frac{\partial \eta}{\partial x} - \frac{\partial h}{\partial y} \qquad \text{A.6}$$

Using the same transformation as used in chapter 4 to make each variable and coefficient dimensionless

$$\left.\begin{aligned} \phi &= h/L \qquad \tau = tK/n_e L \\ X &= x/L \qquad w = W/K \\ Y &= y/L \qquad \bar{\eta} = \eta/L \end{aligned}\right\} \text{A.7}$$

where L is a characteristic length.

Equation A.6 becomes

$$\frac{\partial \bar{\eta}}{\partial \tau} = \frac{\partial \phi}{\partial X}\frac{\partial \bar{\eta}}{\partial X} - \frac{\partial \phi}{\partial Y} \qquad \text{A.8}$$

On the free surface

$$\phi(X,Y,\tau) = \bar{\eta}(X,\tau) \qquad \text{A.9}$$

Differentiating with respect to X at constant time τ gives

$$\frac{\partial \phi}{\partial X} + \frac{\partial \phi}{\partial Y}\frac{\partial Y}{\partial X} = \frac{\partial \bar{\eta}}{\partial X} \qquad \text{A.10}$$

and using equation A.3 gives

$$\frac{\partial \phi}{\partial X} = \frac{\partial \bar{\eta}}{\partial X}\left(1 - \frac{\partial \phi}{\partial Y}\right) \qquad \text{A.11}$$

Similarly differentiating A.9 with respect to time at constant X gives

$$\frac{\partial \phi}{\partial Y}\frac{\partial Y}{\partial \tau} + \frac{\partial \phi}{\partial \tau} = \frac{\partial \bar{\eta}}{\partial \tau} \qquad \text{A.12}$$

again using equation A.3 gives

$$\frac{\partial \phi}{\partial \tau} = \frac{\partial \bar{\eta}}{\partial \tau}\left(1 - \frac{\partial \phi}{\partial Y}\right) \qquad \text{A.13}$$

Substituting for $\frac{\partial \bar{\eta}}{\partial \tau}$ and $\frac{\partial \bar{\eta}}{\partial X}$ in equation A.8 using A.11 and A.13 gives

$$\frac{\partial \phi}{\partial \tau} = \left(\frac{\partial \phi}{\partial X}\right)^2 + \left(\frac{\partial \phi}{\partial Y}\right)^2 - \frac{\partial \phi}{\partial Y} \qquad \text{A.14}$$

Using the inverse of transform A.7 yields the equation given by Bear (1972)

$$\frac{n_e}{K}\frac{\partial h}{\partial t} = \left(\frac{\partial h}{\partial x}\right)^2 + \left(\frac{\partial h}{\partial y}\right)^2 - \frac{\partial h}{\partial y} \qquad \text{A.15}$$

for the rate of change of hydraulic head of a point on the free surface.

To obtain a boundary condition in terms of h and $\frac{\partial h}{\partial n}$ as required for the BIEM this equation is not useful in this form. Instead, equation A.8 is transformed by rotating the co-ordinate axes to make them parallel and normal to the slope of the free surface at a point on the surface (fig. A.1).

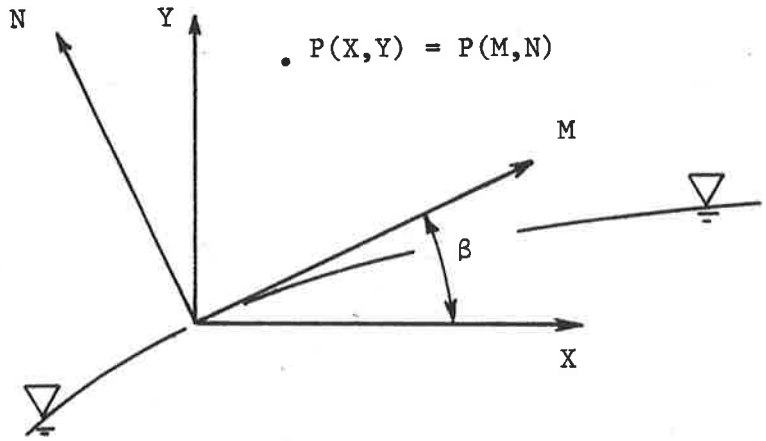

Figure A.1 Axis rotation.

Any point may now be defined

as $P(X,Y) = P(M,N)$

where

$$M = X \cos \beta + Y \sin \beta$$
$$N = -X \sin \beta + Y \cos \beta \qquad \text{A.16}$$

using the chain rule

$$\frac{\partial \phi}{\partial X} = \frac{\partial \phi}{\partial M}\frac{\partial M}{\partial X} + \frac{\partial \phi}{\partial N}\frac{\partial N}{\partial X} \quad \text{and} \quad \frac{\partial \phi}{\partial Y} = \frac{\partial \phi}{\partial M}\frac{\partial M}{\partial Y} + \frac{\partial \phi}{\partial N}\frac{\partial N}{\partial Y} \qquad \text{A.17}$$

$$\frac{\partial \phi}{\partial X} = \frac{\partial \phi}{\partial M}\cos\beta - \frac{\partial \phi}{\partial N}\sin\beta \qquad \frac{\partial \phi}{\partial Y} = \frac{\partial \phi}{\partial M}\sin\beta + \frac{\partial \phi}{\partial N}\cos\beta \qquad \text{A.18}$$

Substituting A.18 into A.8, noting that

$$\frac{\partial \bar{\eta}}{\partial X} = \tan\beta \quad , \quad \text{gives}$$

$$\frac{\partial \bar{\eta}}{\partial \tau} = \left(\frac{\partial \phi}{\partial M}\cos\beta - \frac{\partial \phi}{\partial N}\sin\beta\right)\tan\beta - \frac{\partial \phi}{\partial M}\sin\beta - \frac{\partial \phi}{\partial N}\cos\beta \qquad \text{A.19}$$

$$= \frac{-\partial \phi}{\partial N}\left(\frac{\sin^2\beta + \cos^2\beta}{\cos\beta}\right) + \frac{\partial \phi}{\partial M}(\sin\beta - \sin\beta)$$

$$= -\frac{1}{\cos\beta}\frac{\partial \phi}{\partial N} \qquad \text{A.20}$$

Using the universe of transform A.7 gives

$$\frac{n_e}{K}\frac{\partial \eta}{\partial t} = \frac{-1}{\cos \beta}\frac{\partial h}{\partial n} \qquad A.21$$

This is the equation used in the BIEM model described in chapter 3 for the free surface without accretion.

The free surface with accretion, having recharge rate $W\,[LT^{-1}]$ follows the same equations up to A.4. However, the free surface is not composed of the same fluid particles throughout time. Again following the path of zero pressure, $\frac{\partial y}{\partial t}$ is the rate of vertical movement of the point of zero pressure and not of a fluid particle instantaneously coincident with the free surface.

Equation A.5 changes to

$$\frac{\partial y}{\partial t} = \frac{-K}{n_e}\frac{\partial h}{\partial y} + \frac{W}{n_e} \qquad A.22$$

$\frac{\partial x}{\partial t}$ is unchanged. Substituting A.22 into A.4 gives

$$\frac{n_e}{K}\frac{\partial \eta}{\partial t} = \frac{\partial h}{\partial x}\frac{\partial \eta}{\partial x} - \frac{\partial h}{\partial y} + \frac{W}{K} \qquad A.23$$

Using the substitution $w = W/K$ equation A.23 under the non-dimensional transform becomes

$$\frac{\partial \bar{\eta}}{\partial \tau} = \frac{\partial \phi}{\partial X}\frac{\partial \bar{\eta}}{\partial X} - \frac{\partial \phi}{\partial Y} + w \qquad A.24$$

Note that this differs from equation A.8 only by the inclusion of the last term. Following the same development, equations A.14, A.15, A.20 and A.21 can be shown to become respectively:

$$\frac{\partial \phi}{\partial \tau} = \left(\frac{\partial \phi}{\partial X}\right)^2 + \left(\frac{\partial \phi}{\partial Y}\right)^2 - (1 + w)\frac{\partial \phi}{\partial Y} + w \qquad A.25$$

$$\frac{n_e}{K}\frac{\partial h}{\partial t} = \left(\frac{\partial h}{\partial x}\right)^2 + \left(\frac{\partial h}{\partial y}\right)^2 - (1 + w)\frac{\partial \phi}{\partial y} + w \qquad A.26$$

$$\frac{\partial \bar{\eta}}{\partial \tau} = -\frac{1}{\cos \beta}\frac{\partial \phi}{\partial N} + w \qquad A.27$$

and

$$\frac{n_e}{K}\frac{\partial \eta}{\partial t} = -\frac{1}{\cos \beta}\frac{\partial h}{\partial n} + w \qquad A.28$$

Note that the above derivations assume the effective porosity, n_e, is filled or drained instantaneously as the free surface rises or falls. This assumption is discussed in chapter 2 and is referred to again in chapter 4.

An alternative derivation of equation A.21 which the author has not seen elsewhere follows. A third alternative is given in Liggett and Liu (1983).

2. Method 2

A simpler derivation follows from observation that the free surface always consists of the same fluid particles when there is no recharge (or evaporation). Figure A.2 shows the change in free surface position during a time interval Δt. The slope of the initial free surface at P is tan β.

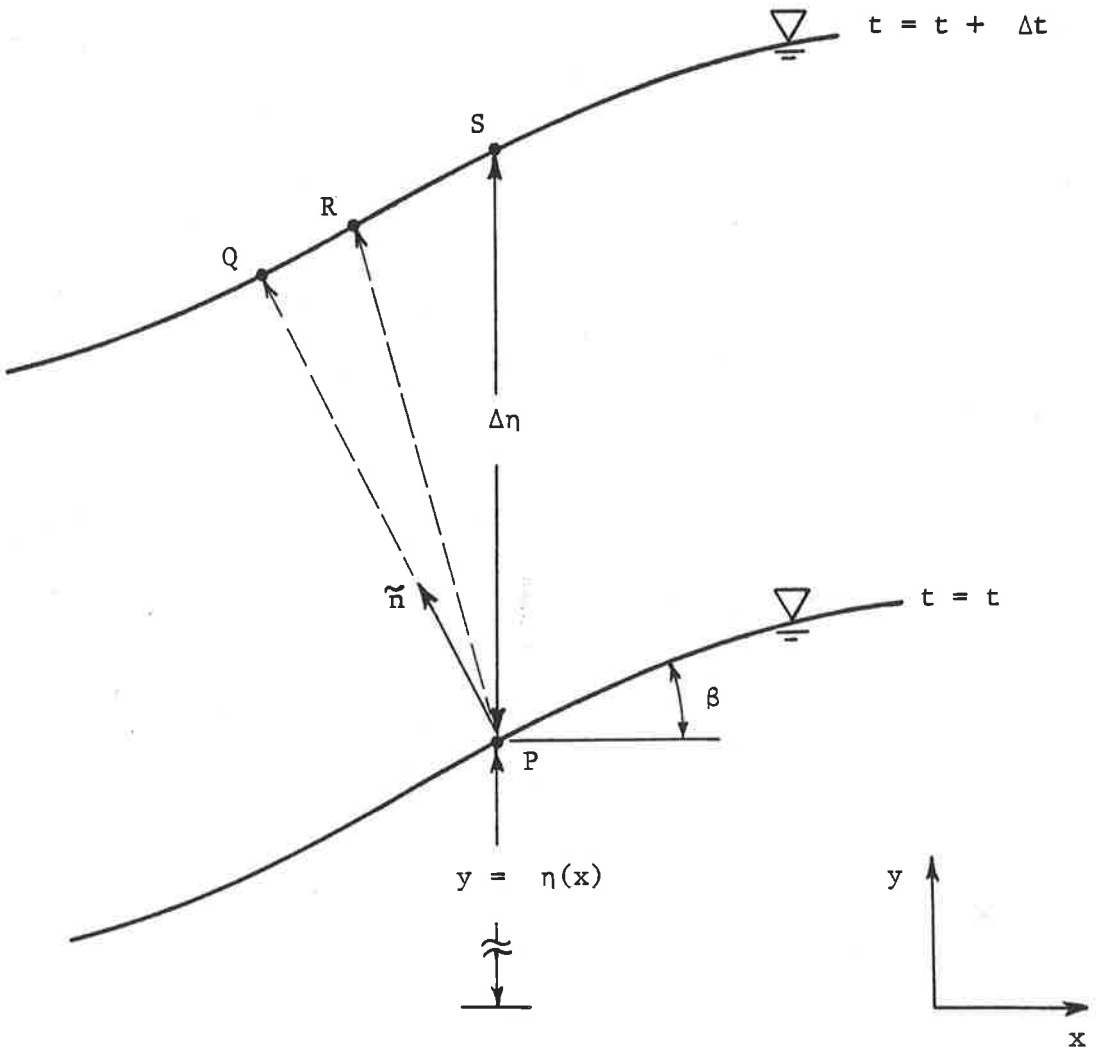

Figure A.2 The unsteady free surface boundary condition.

Applying Darcy's law to the velocity of fluid particles at P in the direction of the outward normal $\tilde{n}$ to the free surface, gives

$$v_n = \frac{-K}{n_e} \frac{\partial h}{\partial n} \qquad \text{A.29}$$

Over a time period Δt the particle on the free surface at P is displaced to R due to the seepage velocity caused by the hydraulic gradient field at P. In most problems it is desirable to keep the x co-ordinate constant for each free surface node. Therefore it is the y co-ordinate of S which requires description. From figure A.2

$$PQ = v_n \Delta t \qquad \text{A.30}$$

and

$$PS = \Delta\eta = \frac{v_n \Delta t}{\cos \beta} \qquad \text{A.31}$$

where β is the angle the free surface makes with the horizontal. Taking the limit as $\Delta t \to o$ and substituting equation A.29 into A.31 gives

$$\frac{\partial \eta}{\partial t} = \frac{-K}{n_e} \frac{1}{\cos \beta} \frac{\partial h}{\partial n} \qquad \text{A.32}$$

which is identical to equation A.21.

In the case when there is vertical recharge to the free surface this is superimposed on the rate of vertical movement of the free surface

$$\frac{\partial \eta}{\partial t} = \frac{-K}{n_e} \frac{1}{\cos \beta} \frac{\partial h}{\partial n} + \frac{W}{n_e} \qquad \text{A.33}$$

where W is the recharge rate $\left[LT^{-1}\right]$ or the evaporation rate if W is negative. This equation agrees with equation A.28.

APPENDIX B

CONFIRMATION OF EQUATIONS FOR OBSERVING THE STABILITY OF IMPLICIT INTEGRATION OF THE FREE SURFACE BOUNDARY CONDITION

1. Proof that equation 5.2 is a solution to problem SINE

It is shown that equation 5.2 satisfies all boundary and initial conditions of problem SINE, described in figure 5.1. Equation 5.2 is repeated here for convenience.

$$h(x,y,t) = a \sin mx \frac{\cosh (my + mH)}{\cosh (mH)} \exp (- \sigma t) \qquad B.1$$

where $\sigma = m \tanh (mH)$ and $m = \frac{\pi}{L}$ B.2

(a) side boundary conditions, at $x = \pm L/2$, $\frac{\partial h}{\partial x} = 0$

differentiating equation B.1 with respect to x gives

$$\frac{\partial h}{\partial x} = ma \cos mx \frac{\cosh (my + mH)}{\cosh (mH)} \exp (- \sigma t) \qquad B.3$$

$= 0$ at $x = \pm L/2$ q.e.d.

(b) base and linearized free surface boundary conditions,

at $y = -H$, $\frac{\partial h}{\partial y} = 0$

at $y = 0$, $\frac{\partial h}{\partial y} = \frac{-\partial h}{\partial t}$

differentiating equation B.1 with respect to y gives

$$\frac{\partial h}{\partial y} = a \sin mx \frac{m \sinh (my + mH)}{\cosh (mH)} \exp (- \sigma t) \qquad B.4$$

hence at $y = -H$, $\frac{\partial h}{\partial y} = 0$ q.e.d.

at $y = 0$, $\frac{\partial h}{\partial y} = ma \sin mx \tanh (mH) \exp (- \sigma t)$ B.5

differentiating equation B.1 with respect to t and substituting equation B.2 gives

$$\frac{\partial h}{\partial t} = a \sin mx \frac{\cosh (my + mH)}{\cosh (mH)} (-m) \tanh (mH) \exp (- \sigma t) \qquad B.6$$

at $y = 0$, $\frac{\partial h}{\partial t} = - ma \sin mx \tanh (mH) \exp (- \sigma t)$ B.7

$= - \frac{\partial h}{\partial y}$ at $y = 0$, q.e.d.

(c) initial conditions, at $y = 0$, $h = a \sin mx$

final condition, as $t \to \infty$, $h(x,y) \to 0$

these conditions are satisfied for $m > 0$ by inspection of equation B.1.

2. Derivation of equation 5.4

Substituting equation 5.2 (= B.1) into equation 5.1 (repeated here as B.8) at $y = 0$

$$h^{k+1} = h^k - \Delta t \left[\varepsilon \left(\frac{\partial h}{\partial y}\right)^{k+1} + (1 - \varepsilon) \left(\frac{\partial h}{\partial y}\right)^{k} \right] \qquad \text{B.8}$$

and making use of equation B.5 and B.2 gives

$$a \sin mx \exp(-\sigma(k+1)\Delta t) = a \sin mx \exp(-\sigma k \Delta t) - \Delta t\, \sigma\, a \sin mx \left[\varepsilon \exp(-\sigma(k+1)\Delta t) + (1 - \varepsilon) \exp(-\sigma k \Delta t) \right] \qquad \text{B.9}$$

dividing by $a \sin mx$ and renaming the damping coefficient for the numerical approximation to the free surface, as σ_N gives

$$\exp(-\sigma_N(k+1)\Delta t) = \exp(-\sigma_N k \Delta t) - \sigma \Delta t \left[\varepsilon \exp(-\sigma_N(k+1)\Delta t) + (1 - \varepsilon) \exp(-\sigma_N k \Delta t) \right]$$

dividing by $\exp(-\sigma_N k \Delta t)$ gives

$$\exp(-\sigma_N \Delta t) = 1 - \sigma \Delta t \left[\varepsilon \exp(-\sigma_N \Delta t) + (1 - \varepsilon) \right] \qquad \text{B.10}$$

which is the same as equation 5.4.

APPENDIX C.1

Stream-Aquifer Interaction Models: A Review

P.J. DILLON, Grad. I.E. Aust.

SUMMARY The assumptions upon which models of stream-aquifer interaction are based are examined. This provides a starting point to compare model performance for the large variety of existing models including integrated stream-aquifer models.

1 INTRODUCTION

Stream-aquifer interaction models are classified in this paper according to the hierarchy shown in Figure 1. Integrated models solve two systems of equations - one for open channel flow and the other for porous media flow. Freeze (1972) describes the union of the two parts of the model as external coupling when the output of one part becomes the input to the other without satisfying any condition on the internal boundary connecting the two parts. Internal coupling is said to occur when an internal boundary condition is satisfied at each time step.

Definition sketches for hydraulic connection and disconnection between streams and aquifers are given in Figure 2. Sheshtakov and Kravchenko (1967) and Ward (1974) describe a hydraulically connected stream as one where the streambed below the water level in the stream is completely saturated. Bear (1979) and Rushton and Tomlinson (1979) also considered cases where different parts of the same streambed exhibited each type of behaviour. Transition from one type of connection to the other may occur and has been described by Walton et al (1967) and observed by Burkham (1970).

2 SURFACE WATER MODELS

Surface water models (see Table I) consist firstly of observation based models of gain or loss of open channel flow along a reach. These are only useful for hydraulically disconnected streams as seepage rates are assumed to be independent of phreatic surface position. Besbes et al (1978) and Flug et al (1980) used historical data to produce an impulse response function for recharge from ephemeral streams, to predict recharge from subsequent streamflow records. Analytical response functions for seepage between streams and hydraulically connected aquifers were developed by Cooper and Rorabaugh (1963).

These have found frequent reuse in linear models. They have also been applied by deconvolution in determining aguifer diffusivity for aquifers hydraulically connected to rivers. Success in this application is restricted by the extreme sensitivity of diffusivity to head measurements in observation bores (Pinder et al (1969), Singh and Sagar (1977). Smith (1972) modelled ephemeral flood wave advance by considering time dependent infiltration rates. This method appears successful for hydraulically disconnected streams. The abundant literature on seepage losses from canals is not included in this review. Models of baseflow are described in a review paper by Hall (1968).

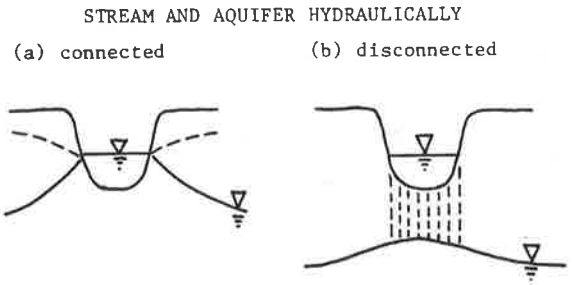

Figure 2

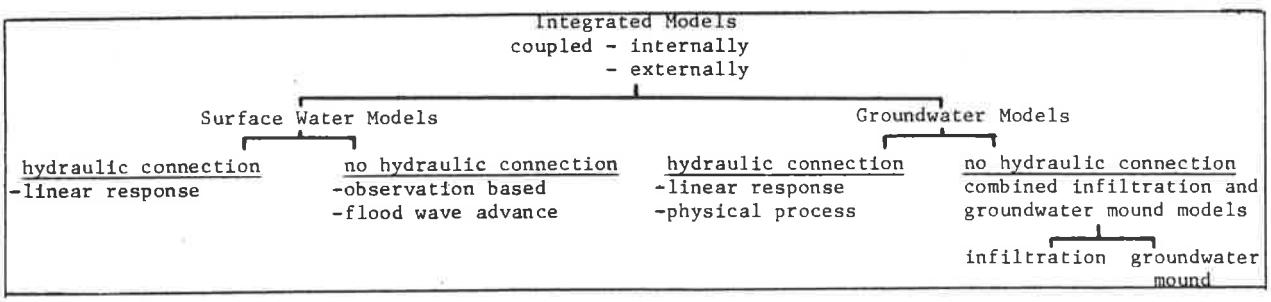

Figure 1 Hierarchy of Stream-Aquifer Models

(Paper C1408 submitted to The Institution of Engineers, Australia on 19 May 1982).

TABLE I

SURFACE WATER MODELS

No hydraulic connection
observation based models - Todd (1955)
Burkham (1970)
Dillon (1981)
linear response -Besbes et al (1978)
Flug et al (1980)
flood wave advance - Smith (1972)
Hydraulic connection
analytical model review-Walton(1979,Table II)
linear response - Cooper and Rorabaugh (1963)
Venetis (1968) and (1970)
Moench and Kisiel (1970)
Hall and Moench (1972)
Moench et al (1974)
identification-using linear theory-Ferris (1959)
Rowe (1960)
Pinder et al (1969)
Yeh (1975)
Singh and Sagar(1977)
Sagar and Singh (1979)

3 GROUNDWATER MODELS

Groundwater models are reviewed within this paper according to the assumptions which they do not make. This provides a ready reference to the effect of these assumptions. Table II lists each assumption together with an index code to cross reference with Table IV. The notation C and D refers to hydraulically connected and hydraulically disconnected streams respectively, where these are itemised separately in Table IV. Asterisks indicate the assumptions which are generally poor and for which compensation would significantly improve a model.

The items in Table IV under the headings "effect on output" and "limitations" contain quantitative and qualitative information from the references on the right. The columns "reality" and "mathematical advantage" represent the author's opinions only. "Reality" indicates the likelihood of encountering field study conditions falling within the limits of validity of an assumption. "Mathematical advantage" expresses the reduction in data requirements and saving in computer time and memory upon using an assumption.

There is no single model which is best, however the literature describes models which are suitable for various applications. This table may be useful in determining the relative merits and deficiences of existing models for particular applications. An excellent review of infiltration models is given by Freeze (1969). Hunt (1972) and Reddy and Basu (1976) using analytical steady state models concluded that infiltration rates are insensitive to channel shape and soil anisotropy respectively.

Combined models of infiltration and groundwater mound are referenced in Table III . The few common assumptions of the saturated - unsaturated flow models are attributed to experimental convenience for model verification rather than on limitations of the applicability of the theory or numerical procedure. Computer time and storage is a problem for each of these models. The paper by Vauclin et al (1979) in particular provides insight into the physical process of infiltration from a hydraulically disconnected stream.

4 INTEGRATED STREAM AQUIFER MODELS

Harrold (1934) was the first to use groundwater levels in wells to predict future baseflow in a stream. However, it was not until the 1970s that

TABLE II

ASSUMPTIONS USED FOR GROUNDWATER MODELS

1	C&D	The alluvial aquifer has a horizontal impermeable base
2	C	All porous media flow is saturated
2	D	see four infiltration model assumptions below
3		Water is discharged instantaneously upon reduction in head
*4	C&D	The alluvial aquifer is homogeneous, isotropic and infinite in extent
5	C&D	The Dupuit-Forchheimer conditions are valid
*6	C	The stream penetrates the full thickness of the aquifer (or alternatively the head throughout the aquifer below the streambed is always equal to the river stage).
*6	D	The groundwater accretion rate is constant once the wetting front reaches the water table
7		The aquifer is solely confined or unconfined. If it is unconfined the fluctuations of the watertable are a small fraction of aquifer thickness so the transmissivity remains constant.
*8		The system is isothermal
9		The quality of water in the stream has no cumulative effect on the stream-aquifer interaction process
10		Groundwater flow in a direction parallel to the stream does not affect the stream-aquifer interaction
		Infiltration models
I1		Flow is one dimensional (vertical)
I2		The porous medium is unsaturated below a wetting front
*I3		The soil is initially dry
*I4		Resistance to flow of air displaced by water is negligible

* significant assumptions
C = hydraulically connected
D = hydraulically disconnected

modellers incorporated streamflow and groundwater flow within a single model. These models, listed in Table V, include linear models and models based on physical processes. The tradeoff between computer execution time and storage and model complexity differs for each model. External coupling requires significantly less computer time but should only be used when the mathematical description of the stream-aquifer interaction is sufficiently representative of the physical process occurring at the internal boundary. For the internally coupled models the convergence criterion is the change in either stream stage or seepage rate between successive iterations. Stream stage is derived directly from solving the streamflow routing equations and is less sensitive than seepage rate to changes in groundwater levels.

A sensitivity analysis by Cunningham and Sinclair (1979) indicates that river discharge, water table elevation and seepage rate are most sensitive to Manning's roughness coefficient n, river channel slope and only moderately sensitive to the hydraulic conductivity of the streambed. These results are encouraging as the order of decreasing importance of parameters is also the order of increasing difficulty in measurement.

It should be noted that Cunningham and Sinclair defined sensitivity as the fractional change in model output when parameters are changed by stated frac-

TABLE IV

CONSEQUENCES OF ASSUMPTIONS USED FOR GROUNDWATER MODELS

ASSUMP-TION	EFFECT ON OUTPUT	LIMITATIONS	REALITY	MATH ADVANTAGE	REFERENCES
1C	over est. gw levels/under est.recharge	K base < K aq/10 base slope small	good	small	leaky base: McWhorter-(1972),Singh(1968), De Wiest(1967),Bouwer(1975),Bouwer(1969,p 148)
1D	under est. recharge	K base very low base slope small	poor to good	small	observ. perched mounds: Wilson-(1968), Mousavi-(1978). perched mound models: Brock (1976),Khan-(1976).inclined base: Baumann(1965)
2C	under est. seepage	capillary fringe << aq. thickness	good	small	Bouwer(1964),Skaggs-(1976),Luthin-(1975) Marino(1981)
3	over est. seepage	n.a. in bank very close to stream	moderate	large: θ = const repl-aces θ = f(dh/dt,t)	Vachaud(1967),Narasimhan-(1980)
4C	may be sig.	medium uniform to depth of 5xstream width/bed scour negligible	poor	large (usually insufficient data)	K variation: Sharp(1977),Bianchi-(1968),Bouwer (1969,p 147). bed scour: Jordan(1977),Lang-(1962),Norris(1970),Randall(1978). finite aq: Marino(1973), Cooper-(1963),Sharma-(1979)
4D	sig. for mound shape	clay layers absent	poor	"	drains at finite distance: Amar(1975),Baumann (1965),Maasland(1959),Marino(1974a),(1974b)
5C	small except below stream	phreatic surface slope is small	poor to moderate	large -1D	Sharp(1977),Lin(1972),Bear(1972),Gelhar(1974)
5D	under est. mound height	mound height < ½ init.sat.thickness	moderate to good	large -1D	Brock(1976),Khan-(1976),Marino(1967),Singh (1976),Smiles-(1979)
6C	over est. seepage	½ aq. thickness penetrated by stream	poor	large allows assumption 5C	observations:Grannemann-(1979),Lang-(1962), Pluhowski-(1962),Walton-(1967). partial penetration: Ferris-(1962,p 129),Hall-(1972),Marino (1973). analogue: Bouwer(1978,p 288),Herbert (1970). analytical:Ernst(1979),Streltsova(1974) FEM: Narasimhan-(1978). non-Darcy:Rushton(1979)
6D	sig.for intermittent infiltration	sustained period of infiltration	poor to good	small	Glass-(1977),Youngs(1977),Smiles-(1979), Marino(1974a)
7	increases with proximity to stream	transition is distant from stream	moderate to good	allows simpler mesh for num.mod	regional scale: Rushton-(1975) local scale: Sharp(1977)
8	sig.inc.in recharge rate for temp rise	small temp. range or hyd. connection	poor to good	small	observations: Norris(1970),Walton-(1966) gas pressure changes: Worstell(1976)
9	may be sig. in long term	low concs. of SS. and reactive chemicals	poor to good	moderate	siltation: James-(1977),Webb-(1977). algae: Jackes(1981).chem reactions: Warner-(1967),Nightingale(1977). density diff: Grodzensky(1967)
10	may be sig.	no change in type of connection d/s.	poor to good	large -1D	
I1	under est. recharge	stream width >> depth	good	sig. unsat. zone -1D	gravity: Bouwer(1969). adsorption: Talsma(1969),Bruch-(1978),Bruch et al (1978)
I2	v.sensitive to h_e value	steady infiltrn. K inc. with depth	poor to good	sig.saves defining unsaturated K(h)& θ(h)	Freyberg-(1980),Reeder-(1980) Whisler-(1970),Bouwer(1969,p 158) & (1976)
I3	under est. recharge	long drying period prior to infiltrn.	poor	sig.saves computing θ profile	Freeze (1969), Wallace-(1977),Philip(1969, p 282), Bouwer(1969,p 157)
I4	over est. recharge	narrow stream-easy air escape	poor	sig.saves 2 phase flow computation	De Backer(1975),Curtis-(1980)

TABLE V

INTEGRATED STREAM - AQUIFER MODELS - STRUCTURE AND APPLICATIONS

Reference	Stream Model	Aquifer model, main assumptions	Coulping	Applications	Interaction Process	Limitations, comments
Taylor and Luckey (1972)	not stated	linear response for stream depletion due to pumping 4, 6, 8	ext-ernal	est.recharge Arkansas River, Colorado 200km reach	Stream is line source, indept. of gw levels -from Jenkins (1968)	time invariant response assumed
Kokinow and Bredehoeft (1974)	not stated	2D lin. Boussinesq eqn. FD soln with IADI. Solute trans port with MAC 4, 5, 6C	ext-ernal	interaction & water quality Arkansas River Colorado 16km reach, 1mth time steps	hydraulic con-nection only	gw levels & stream & gw salinities agree w/-obs stream discharge poorly modelled
Moench, Sauer and Jennings (1974)	step res-ponse after Sauer(1973)	1D step response semi-infinite aq. semi pervious banks 4, 5, 6C	ext-ernal	flow routing Nth Canadian River, Oklahoma 100km, 12 days	stream penetr-ates aquifer completely. af-ter Hall-(1972)	simple linear model no attempt to represent physical processes
Knapp et al (1975)	Muskingum eqn.	2D lin. Boussinesq eqn. FD soln with ADI. 3 soil water stores 5, 6C	ext-ernal	Little Arkansas River Basin, Kansas. 25 year water managemt.	Hydraulic con-nection only	sensitive to soil moist ure parameters too many params(40) for satisfactory calibratn.
Rovey (1975)	Mannings eqn	2D and 3D Richards eqn. for sat-unsat. flow. FD implicit solution 8 (D only)	ext-ernal	Arkansas Valley Colorado, 40km reach	hyd. connected & disconnected streams	gw levels agree w/- obs stream discharge poorly modelled sensitive to unsat. flow parameters
Morel-Seytoux (1975)	Muskingum eqn. in response fn. form explicit FD soln	2D lin. Boussinesq eqn. in response fn. form Soln. by convolution using FD with ADI 4, 6C	ext-ernal	management of pumped stream-connected aq. case study?	hydraulic con-nection only	v. large computer time & storage required crude description of stream-aq interaction
Fraser and Jones(1979)	Mannings eqn with variable flow width	1D lin. Boussinesq FD central diff. soln. 5, 6C	ext-ernal	Callide-Don River Basin Queensland, 100km, 35 days	hydraulic con-nection only	dendritic stream with phreatophyte evapotrans sensitive to streambed K & specific yield
Pinder and Sauer(1971)	1D dynamic eqn. FD explicit soln.	2D Boussinesq eqn FD, IADI solution 5, 6C	int-ernal (seepage rate)	bank storage model for flood routing theoretical example only	hydraulic con-nection only	does not account for gw flow parallel to stream
Freeze (1972)	1D dynamic eqn FD explicit soln.	2D & 3D Richards eqn (unsat-sat. flow) with hysteresis FD implicit LSOR	int-ernal (stream head)	baseflow pre-diction for broad shallow streams 2D theoretical examples only	sat. flow bet-ween stream & aq. seepage from seepage face on stream bank	most general of all models reviewed excessive data require-ments and computer time & storage
Henry (1979)	Muskingum eqn. FD	2D Lin. Boussinesq eqn. FD solved simult-aneously 5, 6, 8 (D only)	int-ernal (stream head)	Callide-Don River Basin Queensland 20km, 50 days Henry & Palmer (1981), Proser-pine River Pearce(1981)	hydraulically connected and disconnected streams	solves prediction, detec tion or inverse problem solves for stream and aq. heads concurrently iterates until converg-ence achieved includes irrecoverable stream storage term
Cunningham and Sinclair (1979)	1D Dynamic eqn. space-FEM time-FD, ex plicit soln.	2D lin. Boussinesq eqn. space-FEM time- FD, IADI solution 5, 6C	int-ernal (seepage rate)	Truckee River, Nevada 6km reach	hydraulic con nection only	sensitive to Mannings n channel slope assessment of predict-ive uncertainty and uniqueness of model

TABLE III

COMBINED MODELS OF INFILTRATION AND GROUNDWATER MOUND

Green-Ampt infiltration	Glass et al (1977)
Richards eqn models	Freeze (1971)
	Taylor and Luthin (1969)
	Luthin et al (1975)
" with sand tank	Vauclin et al (1979)

tions from their assumed values. If other assumed values had been used the ranking of the sensitivities of parameters would be different. It is not surprising to find that output was only moderately sensitive to streambed hydraulic conductivity as its assumed value was more than four times the hydraulic conductivity of the aquifer.

5 CONCLUSIONS

The assumptions which poorly represent actual physical conditions and processes and which have been shown in the literature to have a significant effect on model output are:

a) 4C,4D The alluvial aquifer is homogeneous, isotropic and infinite in extent.
b) 5C The Dupuit-Forchheimer conditions are valid (for hydraulic connection).
c) 6C The stream penetrates the full thickness of the aquifer.
d) 6D The groundwater accretion rate is constant.
e) 8 The system is isothermal (hyd. disconnection only).
f) I3 The soil is initially dry (infiltration models).
g) I4 Resistance to flow of air displaced by water is negligible.

Simple methods have been used to compensate for some of these assumptions. However, assumptions 4C and 4D can only be overcome by further data collection. The cost of acquiring these data may not be justified by the advantages in reducing uncertainty in model output. This leads to the concept of terminal model accuracy for a given budget.

A balance between the amount of data acquisition and model complexity should be sought. Reduction in the number of model parameters to be identified will greatly reduce calibration effort. Table IV indicates those assumptions which are satisfactory and may be used to simplify models without impairing their performance.

6 NOTATION

Abbreviations used in tables:

aq	- aquifer
gw	- groundwater
h_e	- effective suction head
infiltrn	- infiltration
θ	- moisture content
n	- Mannings roughness coefficient
sig	- significant
ADI	- alternating direction implicit solution
FD	- finite difference
FEM	- finite element method
IADI	- iterative alternating direction implicit solution
K	- hydraulic conductivity
LSOR	- line successive over-relaxation
MAC	- marker and cell method
-ID	- reduces problem by one dimension
n.a.	- not applicable
d/s	- downstream

7 REFERENCES

AMAR, A.C. (1975). Groundwater recharge simulation, ASCE J. Hydraul. 101 (HY9) pp 1235-1247.

BAUMANN, P. (1965). Technical development in groundwater recharge, Advances in Hydroscience, Vol. 2, pp 209-279.

BEAR, J. (1972). Dynamics of Fluids in Porous Media, American Elsevier.

BEAR, J. (1979). Hydraulics of Groundwater, McGraw Hill, New York.

BESBES, M., DELHOMME, J.P. and de MARSILY, G.(1978). Estimating recharge from ephemeral streams in arid regions, Water Resour.Res. 14(2) pp 281-290.

BIANCHI, W.C. and HASKELL, E.E.(1968). Field observations compared with Dupuit-Forchheimer Theory for mound heights under a recharge basin, Water Resour. Res. 4(5) pp 1049-1057.

BOUWER, H. (1964). Unsaturated flow in groundwater hydraulics, ASCE J. Hydraul. 90(HY5) pp 121-144.

BOUWER, H. (1969). Theory of seepage from open channels, Advances in Hydroscience, Vol. 5,pp 121-172.

BOUWER, H. (1975). Predicting reduction in water losses from open channels by phreatophyte control, Water Resour.Res. 11(1) pp 96-101.

BOUWER, H. (1976). Infiltration into increasingly permeable soils, ASCE J. Irrig and Drain, 102(IR2) pp 127-136.

BOUWER, H. (1978). Groundwater Hydrology, McGraw Hill, New York.

BROCK, R.R. (1976). Dupuit-Forchheimer and potential theories for recharge from basins, Water Resour.Res. 12(5) pp 909-911.

BRUCH, J.C. and SLOSS, J.M. (1978). A variational inequality method applied to free surface seepage from a triangular ditch. Water Resour Res. 14(1) pp 119-124.

BRUCH, J.C., SAYLE, F.C. and SLOSS J.M. (1978). Seepage from a trapezoidal and a rectangular channel using variational inequalities, J. Hydrol, 36 pp 247-260.

BURKHAM, D.E. (1970). A method for relating infiltration rates to streamflow rates in perched streams, USGS Prof.Paper 700-D, pp 266-271.

COOPER, H.H. and RORABAUGH, M.I. (1963). Groundwater movements and bank storage due to flood stages in surface streams, USGS Water Supply Paper 1536-J pp 343-366.

CUNNINGHAM, A.B. and SINCLAIR, P.J. (1979). Application and analysis of a coupled surface and groundwater model, J. Hydrol, 43, pp 129-148.

CURTIS, A.A. and WATSON, K.K. (1980) Numerical analysis of infiltration into a sand profile bounded by a capillary fringe, Water Resour. Res, 16(2), pp 365-371.

De BACKER, L. (1975). Experimental artificial recharge, Proc. Work. Conf. on Computer Simulation of Water Resour. Systems, Ghent, Belgium, Jul 1974, pp 279-289.

De WIEST, R.J.M. (1967). Artificial recharge through augmented bank storage, Int. Assoc. Sci. Hydrol, pub. no 72, pp 53-68.

DILLON, P.J. (1981). Simple models of groundwater recharge for ephemeral streams, Proc. Aust. Water Resour. Council Groundwater Recharge Conf., Townsville, July 1980 pp. 60-71.

ERNST, L.F. (1979). Groundwater flow to a deep well near a rectilinear channel, J. Hydrol, 42 pp 129-146.

FERRIS, J.G., KNOWLES, D.B., BROWN, R.H. and STALLMON, R.W. (1962). Theory of aquifer tests, USGS Water Supply Paper 1536-E. (particularly p 122)

FERRIS, J.G. (1959). Groundwater, ch 7 in Whisler C.O. and Brater, E.F. (eds) Hydrogeology, Wiley, New York.

FLUG, M., ABI-GHANEM, G.V. and DUCKSTEIN, L.(1980) An event-based model of recharge from an ephemeral stream, Water Resour. Res. 16(4) pp 685-690.

FRASER, C.J. and JONES, N.O. (1977). A model of water flows in the quaternary alluvium of the Callide-Don river basin, Queensland. Aust. Water Resour. Council Groundwater Modelling Seminar, Sydney, July 1977.
FREEZE, R.A. (1969). The mechanism of natural groundwater recharge and discharge (1), Water Resour. Res. 5(1) pp 153-171.
FREEZE, R.A. (1971). Three dimensional transient saturated-unsaturated flow in a groundwater basin, Water Resour. Res. 7(2) pp 347-366.
FREEZE, R.A. (1972). Role of subsurface flow in generating surface runoff. (1) Baseflow contributions to channel flow, Water Resour. Res 8(3) pp 609-623.
FREYBERG, D.L, REEDER, J.W., FRANZINI, J.B. and REMSON , I. (1980). Application of the Green-Ampt model to infiltration under time dependent surface water depths, Water Resour. Res. 16(3) p 517-528.
GELHAR, L.W. (1974). Stochastic analysis of phreatic aquifers, Water Resour. Res. 10(3), pp 539-545.
GLASS, J.P., CHRISTENSEN, B.A. and RUBIN, H. (1977). Analysis of transient groundwater flow from seepage ponds, Proc. 3rd Intl. Hydrol Symp. Fort Collins, Colorado pp 246-256.
GRANNEMAN, N.G. and SHARP, J.M. (1979). Alluvial Hydrogeology of the lower Missouri River, J. Hydrol 40, pp 85-99.
GRODZENSKY, V.D. (1967). Formation of fresh ground water lenses as a result of percolation from canals and pits, Int. Assoc. Sci. Hydrol. pub. no 72 pp 360-364.
HALL, F.R. (1968). Base-flow recessions - a review, Water Resour. Res, 4, pp 973-983.
HALL, F.R. and MOENCH, A.F. (1972). Application of the convolution equation to stream-aquifer relationships, Water Resour. Res., 8(2) pp 487-493.
HARROLD, L.L. (1934). Relation of streamflow to groundwater levels,Trans. Am. Geophys. Union, pt 2, pp 414-416.
HENRY, J.L. (1979). Integrated Finite Difference Modelling of Groundwater Flow, Queensland Water Resources Commission Report, Volumes I and II.
HENRY, J.L. and PALMER, J.R. (1981). Natural and artificial recharge of groundwater in the Callide Valley, Proc. Aust. Water Resour. Council Groundwater Recharge Conference, Townsville, July 1980 pp 72-87.
HERBERT, R. (1970). Modelling partially penetrating rivers on aquifer models, Groundwater, 8 pp 29-36.
HUNT, B.W. (1972). Seepage from shallow open channel, ASCE J. Hydraul. 98 (HY5) p 779-785.
JACKES (1981). Burdekin artificial groundwater recharge study: biological problems, Proc.Aust.Water Resour. Council, Groundwater Recharge Conference Townsville, July 1980 pp 119-130.
JAMES, S.E. and HENRY, J.J. (1977). Effects of siltation on rates of recharge, Aust. Water Resour. Council Tech. Paper No. 23.
JENKINS, C.T. (1968). Techniques for computing rate and volume of stream depletion by wells, Ground Water 6, (2), pp 37-46.
JORDAN, R.R. (1977). Streamflow transmission losses in Western Kansas,ASCE J. Hydraul. 103(8) pp 905-919.
KHAN, M.Y., KIRKHAM, D. and HANDY, R.L. (1976). Shapes of steady state perched groundwater mounds, Water Resour. Res. 12(3) pp 429-436.
KNAPP, R.M., GREEN, D.W., POGGE, E.C. and STANFORD, C. (1975). Development and field testing of a basin hydrology simulator, Water Resour. Res. 11(6) pp 879-888.
KOKINOW, L.F., BREDEHOEFT, J.D. (1974). Modelling flow and chemical quality changes in an irrigated stream-aquifer system. Water Resour. Res., 10(3) pp 546-562.
LANG, S.M. and RHODEHAMEL, E.C. (1962). Movement of groundwater beneath the bed of the Mullica River in the Wharton Tract, New Jersey, USGS Prof. Paper 450-B pp 90-92.
LIN, C.L. (1972). Digital simulation of the Boussinesq equation for a water table aquifer, Water Resour. Res, 8(3), pp 691-698.
LUTHIN, J.N., ORHUN, A., TAYLOR, G.S. (1975) Coupled saturated-unsaturated transient flow in porous media: experimental and numerical model, Water Resour. Res., 11(6) pp 973-978.
MAASLAND, M. (1959). Water table fluctuations induced by intermittent recharge, J. Geophys, Research, 64 pp 549-559.
McWHORTER, D.B. and BROOKMAN, J.A. (1972). Pit recharge influenced by subsurface spreading, Ground Water 10(5) pp 6-11.
MARINO, M.A. (1967) Hele-Shaw model study of the growth and decay of groundwater ridges, J. Geophys. Research 72(4) pp 1195-1205.
MARINO, M.A. (1973). Water table fluctuation in semi-pervious stream-aquifer systems, J. Hydrol 19, pp 43-52.
MARINO, M.A. (1974a) Rise and decline of the water table induced by vertical recharge, J. Hydrol 23, pp 289-298.
MARINO, M.A. (1974b) Water table fluctuation in response to recharge,ASCE J. Irrig. and Drain, 100 (IR2) pp 117-125.
MARINO, M.A. (1981). Analysis of transient movement of water and solutes in stream-aquifer systems, J. Hydrol. 49, pp 1-17.
MOENCH, A.F. and KISIEL, C.C. (1970). Application of the convolution relation to estimating recharge from an ephemeral stream, Water Resour. Res. 6(4) pp 1087-1094.
MOENCH, A.F. SAUER, V.B. and JENNINGS, M.E. (1974) Modification of routed streamflow by channel loss and baseflow, Water Resour. Res. 10(5) pp 963-968.
MOREL-SEYTOUX, H.J. (1975). A combined model of water table and river stage evolution, Water Resour. Res. 11(6) pp 968-972.
MOUSAVI, S.F. and KIRKHAM, D. (1978). Porous media tests of groundwater mounds, Soil Sci. 125 (3) pp 160-164.
NARASIMHAN, T.M., NEUMAN, S.P. and WITHERSPOON, P.A. (1978). Finite element method for subsurface hydrology using a mixed explicit-implicit scheme, Water Resour. Res. 15(5), pp 863-877.
NARASIMHAN, T.N. and YANEHIRO, B.Y. (1980). A note on the meaning of storage coefficient, Water Resour. Res. 16(2) pp 423-429.
NIGHTINGALE, H.I., BIANCHI, W.C. (1977). Groundwater turbidity resulting from artificial recharge, Ground Water, 15(2), pp 146-152.
NORRIS, S.E. (1970). The effect of stream discharge on streambed leakage to a glacial outwash aquifer, USGS Prof Paper 700-D, pp D262-D265.
PEARCE, B.R. (1981). The use of temporary sand dam storages in determining the river recharge in the Proserpine area, Proc. Aust. Water Resour. Council Groundwater Recharge Conf., Townsville, July 1980 pp 88-97.
PHILIP, J.R. (1969). Theory of infiltration, Advances in Hydroscience, Vol. 5 pp 215-305.
PINDER, G.F., BREDEHOEFT, J.D. and COOPER, H.H. (1969). Determination of aquifer diffusivity from aquifer response to fluctuations in river stage, Water Resour. Res. 5(4) pp 850-855.
PINDER, G.F. and SAUER, S.R. (1971). Numerical simulation of floodwave modification due to bank storage effects, Water Resour. Res. 7(1) pp 63-70.
PLUHOWSKI, E.J. and KANTROWITZ, I.H. (1962). Source of groundwater runoff at Champlin Creek, Long Island New York, USGS Prof. Paper 450-B pp B95-B97.
RANDALL, A.D. (1978). Infiltration from tributary streams in Susquehanna river basin, J. Research USGS, 6(3) pp 285-297.
REDDY, A.S. and BASU, U. (1976). Seepage from trapezoidal canal in anisotropic soil, ASCE J. Irrig and Dr, 102 (IR3) pp 349-361.

REEDER, J.W., FREYGERG, D.L., FRANZINI, J.B. and REMSON , I. (1980). Infiltration under rapidly varying surface water depths , Water Resour. Res., 16(1) pp 97-104.
ROVEY, C.E.K. (1975). Numerical model of flow in a stream-aquifer system, Colorado State Uni, Fort Collins, Hydrology Papers no 74.
ROWE, P.P. (1960) An equation for estimating transmissibility and coefficient of storage from river level fluctuations, J. Geophys. Research. 65(10) pp 3419-3424.
RUSHTON, K.R. and TOMLINSON, L.M. (1975). Numerical analysis of confined-unconfined aquifers, J. Hydrol 25 pp 259-274.
RUSHTON, K.R. and TOMLINSON, L.M. (1979). Possible mechanisms for leakage between aquifers and rivers. J. Hydrol. 40 pp 49-65.
SAGAR, B. and SINGH, S.R. (1979). Aquifer diffusivity from noisy boundary data, ASCE J. Hydraul. 105 (HY8) pp 943-954.
SAUER, V.B. (1973). Unit response method of open channel flow routing, ASCE J. Hydraul. 99 (HY1) pp 179-193.
SHARMA, H.D. and CHAWLA, A.S. (1979). Canal seepage with boundary at finite depth, ASCE J. Hydraul, 105 (HY7) pp 877-897.
SHARP, J.M. (1977). Limitations of bank storage model assumptions. J. Hydrol. 35, pp 31-47.
SHESHTAKOV, V.M. and KRAVCHENKO, I.P. (1967). A contribution to the technique for the evaluation of natural and workable resources of near-canal fresh water lenses, Intl. Assoc. Sci. Hydrol, Pub.no. 72, pp 83-90.
SINGH, K.P.(1968). Some factors affecting baseflow, Water Resour Res, 4(5) pp 985-999.
SINGH, R. (1976). Prediction of mound geometry under recharge basins Water Resour Res, 12(4) pp 775-780.
SINGH, S.R. and SAGAR, B.(1977). Estimation of aquifer diffusivity in stream-aquifer systems, ASCE J Hydraul. 103(HY11) pp 1293-1302.
SKAGGS, R.W. and TANG, Y.K.(1976). Saturated and unsaturated flow to parallel drains, ASCE J Irrig and Dr, 102(IR2) pp 221-238.
SMILES, D.E. and KNIGHT, J.H.(1979). The transient water table beneath a leaking canal, J Hydrol 44, pp 149-162.
SMITH, R.E. (1972). Border irrigation advance and ephemeral flood waves, ASCE J. Irrig and Dr, 98 pp 289-307.
STRELTSOVA, T.D. (1974). Method of additional seepage resistances-theory and application, ASCE J Hydraul, 100 (HY8) pp 1119-1131.
TALSMA, T. (1969). Infiltration from semi-circular furrows in the field. Aust. J. Soil Res., 7, pp 277-284.
TAYLOR, G.S. and LUTHIN, J.N.(1969). Computer method for transient analysis of water table aquifers, Water Resour. Res. 5 (1) pp 144-152.
TAYLOR, O.J. and LUCKEY, R.R. (1972). New technique for estimating recharge using a digital model, Ground Water, 10(6) pp 22-26.
TODD, D.K. (1955). Ground-water flow in relation to a flooding stream. Proc. ASCE Vol 81, separate no 628, pp 1-20.
TODD, D.K. (1959). Annotated bibliography on artificial recharge of groundwater through 1954, USGS Water Supply Paper 1477.
VACHAUD, G.(1967). On the storage coefficient of free surface aquifers considering the flow in the unsaturated zone, Int.Assoc.of Sci. Hydrol.pub no 72, pp 69-82.
VAUCLIN, M.,KHANJI, D. and VACHAUD, G.(1979). Experimental and numerical study of a transient two dimensional unsaturated-saturated water table recharge problem, Water Resour.Res. 15(5) pp 1089-1101.
VENETIS, C. (1968). On the impulse response of an aquifer, Int. Assoc. Sci. Hydrol, Bull no 13(3) pp 136-139.
VERETIS, C. (1970). Finite aquifers: characteristic responses and applications, J.Hydrol. 12,pp 53-62.
WALLACE, K., HINES, N. and GOLDING, W.(1977).A laboratory study of the infiltration characteristics of coarse grained soils, James Cook Univ, Interim Road Rept. no 14.
WALTON, W.C. and ACKROYD, E.A.(1966). Effects of induced streambed infiltration on water levels in wells during aquifer tests, Minnesota Univ. Water Resour Res Centre Bulletin no 2.
WALTON, W.C., HILLS, D.L. and GRUNDEEN, G.M.(1967). Recharge from induced streambed infiltration under varying groundwater level and stream stage conditions, Minnesota Univ., Water Resour Res Centre Bulletin no 6.
WALTON, W.C. (1979). Progress in analytical groundwater modelling, J Hydrol. 43, pp 149-159.
WARD, R.C. (1974). Principles of Hydrology, 2nd edition, McGraw Hill.
WARNER, D.L. and DOTY, L.F. (1967). Chemical reaction between recharge water and aquifer water, Int. Assoc. Sci. Hydrol.pub no 72, pp 278-288.
WEBB and WATSON K.K. (1977). Analysis of the movement of water from recharge channels and pits, Aust. Water Resour Council Tech Paper no 24.
WHISLER, F.D. and BOUWER, H. (1970). Comparison of methods for calculating vertical drainage and infiltration for soils, J Hydrol. 10 pp 1-19.
WILSON, L.G. and de COOK, K.J. (1968). Field observations on changes in the subsurface water regime during influent seepage in the Santa Cruz River, Water Resour Res., 4(6) pp 1219-1234.
WORSTELL, R.V. (1976). Estimating seepage losses from canal systems, ASCE J. Irrig and Dr., 102 (IR1) pp 137-147.
YEH, W.W.G. (1975). Aquifer parameter identification, ASCE J. Hydraul, 101(9) pp 1197 - 1209.
YOUNGS, E.G. (1977). The unsteady groundwater mound below an irrigation ditch or leaky canal, J Hydrol, 34, pp 307 - 314.

P.J. DILLON

Peter Dillon worked in the Water Resources Branch of the Engineering and Water Supply Department of South Australia between graduating from, (1975) and returning to tutor, (1977) in the Department of Civil Engineering at the University of Adelaide. He is studying groundwater recharge from the Little Para River for his former employer and is a PhD candidate.

CORRESPONDENCE ON THIS PAPER WILL BE ACCEPTED FOR PUBLICATION UNTIL 30 SEPTEMBER 1983

Dillon, P. (1980, July). Simple models of groundwater recharge for ephemeral streams In *Proceedings of the Groundwater Recharge Conference*. (p. 60-71). James Cook University, Townsville, Queensland.

APPENDIX C.3

WATER RESOURCES RESEARCH, VOL. 19, NO. 3, PAGES 621–626, JUNE 1983

An Ephemeral Stream-Aquifer Interaction Model

P. J. DILLON

Department of Civil Engineering, University of Adelaide, Adelaide, South Australia

J. A. LIGGETT

School of Civil and Environmental Engineering, Cornell University, Ithaca, New York 14853

The boundary integral equation method is applied to the interaction between an ephemeral stream and an unconfined aquifer through a semipervious streambed. The resulting two-dimensional vertical slice model describes groundwater flow when the stream and aquifer are hydraulically disconnected or connected as well as the transition between these two states. It incorporates the Green-Ampt equation with the hydraulically disconnected boundary conditions. The model was successfully calibrated using stream discharge and bore hydrograph data from the Little Para River recharge study, South Australia. It predicts with sufficient accuracy the inflow and outflow from the stream to the aquifer during fluctuating water levels in the stream.

INTRODUCTION

Since early 1979 the Department of Civil Engineering, University of Adelaide, in cooperation with the Engineering and Water Supply Department of South Australia, has been conducting experiments and gathering data on the North Adelaide Plains aquifer. The aquifer is heavily pumped for agricultural purposes and is recharged largely by ephemeral streams, including the Little Para River. A primary objective of the study is to develop an operating rule for a storage reservoir on this river so as to maintain the natural recharge with the minimum reservoir release volume. Thus the interaction between the stream and the aquifer is an important aspect.

This stream-aquifer system is typical of ephemeral streams traversing alluvial plains. The streambed is usually covered by silts that are less pervious than the sands of the aquifer, and thus the efficiency of streambed recharge is reduced. The stream is subject to rapid changes in flow, either by rainfall runoff or by releases from the Little Para Dam. The water table fluctuates with the seasons and depends on the relative levels of pumping and recharge. At various times and places the water table is below the streambed (hydraulically disconnected), and accretion must pass through an unsaturated zone. At other times and/or places the water table is above the streambed (hydraulically connected).

These two situations and the transition between them are studied by a two-dimensional (horizontal normal to the stream and vertical) numerical model based on the boundary integral equation method (BIEM). Traditionally, the stream boundary conditions in groundwater models have been specified heads or specified exchange flow rate for hydraulically connected and disconnected streams, respectively. *Henry* [1979], in his integrated stream-aquifer model, accounted for hydraulic transition by specifying a 'changeover head' below which the recharge rate was dependent only on the stream head and above which it depended only on the head difference between the stream and the aquifer. Henry's stream aquifer interaction process has been extended in the current model by (1) introducing a suction head, (2) applying the Green-Ampt equation to approximate unsaturated flow, and (3) using the boundary conditions that result naturally as the groundwater mound intersects various parts of the streambed. No attempt has been made to solve Richard's equation for unsaturated flow, as was done by *Freeze* [1972] and *Rovey* [1975]. The simpler model requires less computer time and storage and is more suited to the availability of field data.

Paper number 3W0147.
0043-1397/83/003W-0147$05.00

THE MATHEMATICAL MODEL

The physical situation is indicated in Figure 1. The region is divided vertically by a line of symmetry, across which there is no flow. The water table may be either (1) disconnected or (2) connected, as shown in the figure. The aquifer basement ($y = 0$) may be either impermeable or leaky.

The solution in the saturated zone is governed by Laplace's equation:

$$\frac{\partial^2 \phi}{\partial x^2} + \frac{\partial^2 \phi}{\partial y^2} = 0 \tag{1}$$

in which ϕ is the hydraulic or piezometric head, defined as

$$\phi(x, y) = \frac{p(x, y)}{\gamma} + y$$

where $p(x, y)$ is the water pressure at (x, y) $(M L^{-1} T^{-2})$, γ is the weight density of water $(M L^{-2} T^{-2})$, and y is the height above an arbitrary datum chosen as the elevation of the aquifer basement (L). The boundary conditions are

$$\frac{\partial \phi}{\partial n} = q_b / K \qquad y = 0 \tag{2a}$$

$$\frac{\partial \phi}{\partial n} = 0 \qquad x = 0 \tag{2b}$$

$$\phi = y$$

$$\frac{\partial \phi}{\partial t} = \frac{K}{n_e}\left[-\frac{1}{\cos \beta}\frac{\partial \phi}{\partial n} + \frac{w(t)}{K}\right] \quad \text{free surface} \tag{2c}$$

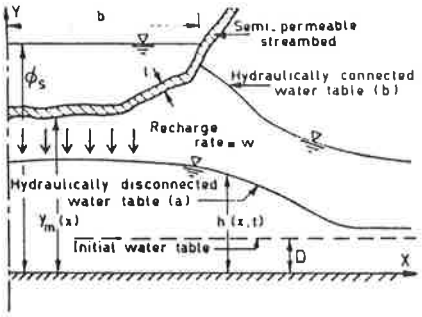

Fig. 1. The stream-aquifer system. The water table may be either (*a*) hydraulically disconnected or (*b*) hydraulically connected.

$$\phi = \phi_s - B\frac{\partial\phi}{\partial n} \qquad \text{on bed when } \phi \geq y_m \qquad (2d)$$

in which

$$\frac{\partial\phi}{\partial n} = \nabla\phi \cdot \mathbf{n}$$

where **n** is the outward unit normal to the boundary, q_b is the leakage through the aquifer basement (usually taken to be zero), t is time (T), K is the aquifer hydraulic conductivity (LT^{-1}), n_e is effective porosity, β is the angle the free surface makes with horizontal, w is recharge rate (LT^{-1}), ϕ_s is the head in the stream (L), and $B = Kl/K_B$ (L) where l is the thickness of the semipermeable blanket and K_B is its hydraulic conductivity.

The nondimensional recharge is given by

$$w/K = (\phi_s - y_m - h_c)/B \qquad \phi < y_m + h_c \qquad (3a)$$

$$w/K = (\phi_s - \phi)/B \qquad y_m + h_c \leq \phi \leq y_m \qquad (3b)$$

in which y_m is the elevation of the semipermeable blanket and h_c is the capillary potential or suction head at the base of the blanket. This relationship between exchange flow rate w and aquifer head ϕ is different from that proposed by *Rushton and Tomlinson* [1979]. The streambed and aquifer heads appears here as two independent parameters instead of being combined into a single head difference term, thus providing the flexibility to account for arbitrary streambed cross sections.

A time delay t_d for recharge to reach the water table after the onset of streamflow is obtained by integrating the Green-Ampt equation [*Green and Ampt*, 1911; *Bouwer*, 1969] to give

$$t_d = \frac{n_e}{K}\left[y_m - D - (\phi_s - h_c)\ln\left(\frac{\phi_s - h_c + y_m - D}{\phi_s - h_c}\right)\right] \qquad (4)$$

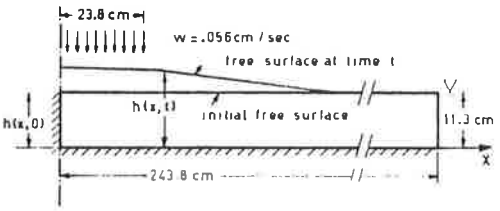

Fig. 2. Diagram of the Hele-Shaw model of strip recharge used by *Marino* [1967].

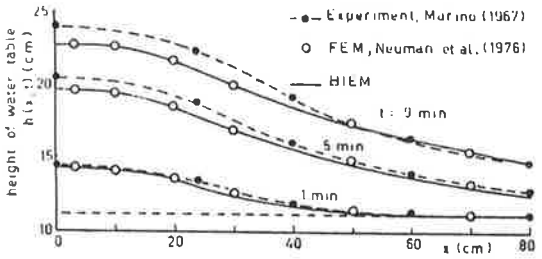

Fig. 3. Results of experiment and numerical calculations.

in which D is the initial saturated aquifer thickness (Figure 1). *Freyberg et al.* [1980] have indicated the suitability of the Green-Ampt equation for modelling infiltration under time-dependent surface water depths. Equation (4) and the inclusion of a suction head in (3*a*) represent the only recognition of the unsaturated zone. Both data requirements and computing time would be high for a complete calculation of unsaturated flow. The limits on accuracy of this model are considered to be in the determination of the streambed leakage factor ($K/B = K_B/l$), hydraulic conductivity of the aquifer (K), and the fact that these quantities are taken as constant.

NUMERICAL CALCULATIONS

The solution of (1) with boundary conditions (2) is accomplished by the boundary integral equation method (BIEM). The BIEM reduces this two-dimensinal problem to one computational dimension, it computes with relative ease the unsteady, nonlinear free surface, it requires minimal data to specify the spacial domain of the model, and it is efficient compared to finite element and finite difference methods. The BIEM is based on the integral equation [*Liggett and Liu*, 1983]

$$\alpha\phi(P) - \int_\Gamma \left[\phi(Q)\frac{\partial}{\partial n}(\ln r) - \ln r\frac{\partial}{\partial n}\phi(Q)\right] ds \qquad (5)$$

in which Γ is the boundary of the solution domain, P is any point on Γ or in the domain, Q is the succession of points on Γ over which the integration is performed, $\alpha = 2\pi$ if P is inside the domain, $\alpha = \pi$ if P is on a smooth part of Γ, and α is the interior angle of the boundary if P is located at a kink on Γ. The $\ln r$ is the two-dimensional, free space Green's function for Laplace's equation where r represents the distance between point P and point Q. If ϕ and $\partial\phi/\partial n$ are known on Γ, (5) yields ϕ anywhere in the solution domain by a simple boundary integration. In a well-posed problem, either ϕ or $\partial\phi/\partial n$ but not both are given at each boundary point, and (5) is used to find the missing condition by choosing P at a succession of boundary points. The boundary integration is carried out by choosing a succession of node points and assuming the behavior of ϕ and $\partial\phi/\partial n$ between nodes. In this paper that behavior (the interpolation

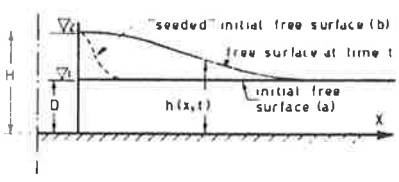

Fig. 4. Diagram of a hydraulically connected aquifer with a sudden rise in stream level.

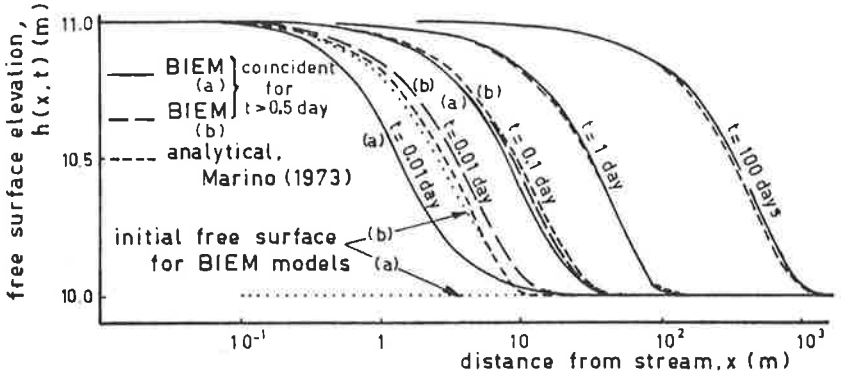

Fig. 5. Free surface profiles for a hydraulically connected aquifer with a sudden rise in stream level.

functions) is assumed linear. The resulting integration can be carried out explicitly, leaving simultaneous equations in the boundary unknowns. *Liggett and Liu* [1983] provide a comprehensive description of the method as applied to flow in porous media. Verification of the mathematical and numerical models is presented subsequently.

Hydraulically Disconnected Stream

When the horizontal outflow from the aquifer is sufficiently high, when the groundwater leaks vertically through the aquifer base, and/or when recharge is low, the groundwater mound does not intersect the streambed. The stream then provides strip recharge. Comparisons of the current calculations with the results of *Marino* [1967] for a Hele-Shaw model study (Figure 2) of the growth of groundwater mounds beneath a strip recharge source are given in Figure 3. The results of *Neuman et al.* [1976], who used a finite element model, are shown in the same figure and give excellent agreement. The BIEM results satisfy conservation of mass to 0.3%, whereas the experimental results at 5 and 9 minutes show a net mass gain (mass balance error) of about 9%. Mass balance error is defined as the change in storage below the free surface since the start minus the net accumulated inflow across the model boundaries all divided by the change in storage below the free surface. See also the work of *Liggett and Liu* [1983] for applications of BIEM to recharge problems.

Hydraulically Connected Stream

For a hydraulically connected stream the rate of flow between stream and aquifer is dependent on the head in the aquifer beneath the streambed. In general, the river bed is assumed to be lined by a semipermeable blanket of fine material which significantly reduces the exchange of water between the stream and aquifer. Analytical models based on impermeable bed and semipervious banks have been described by *Marino* [1973] and by *Hall and Moench* [1972]. However, *Sharp* [1977] found that the major alluvial aquifers of central United States were only partially penetrated by their streams and that most of the interchange of water takes place through the river bed.

To test the BIEM model for a hydraulically connected stream for which an analytical solution is available, the configuration in Figure 4 was chosen, noting that this does not represent a good model for real stream-aquifer interaction. The lateral progression of a rise in the phreatic surface over time following a step change in stream head is given by *Marino* [1973] as

$$h^2(x, t) = D^2 + (H^2 - D^2)\,\mathrm{erfc}\,[x/(4\alpha t)^{1/2}] \qquad (6)$$

where $\alpha = KD/n_e$, the aquifer diffusivity. His analytical solution is based on the Dupuit-Forchheimer (D-F) assumptions. In the example $(H\text{-}D)/D = 0.1$ was chosen to give shallow free surface slopes. *Marino* [1967] found that the D-F results agreed within 5% of Hele-Shaw analog results for mounds having $(H\text{-}D)/D$ up to 0.5.

The exchange flow q between stream and aquifer is obtained by differentiating (6) with respect to x at $x = 0$:

$$q(0, t) = KH \frac{\partial}{\partial t} h(0, t) = K(H^2 - D^2)/(4\pi\alpha t)^{1/2} \qquad (7)$$

which, when integrated with respect to time, gives the bank storage. Equation (7) gives initially an infinite exchange flow

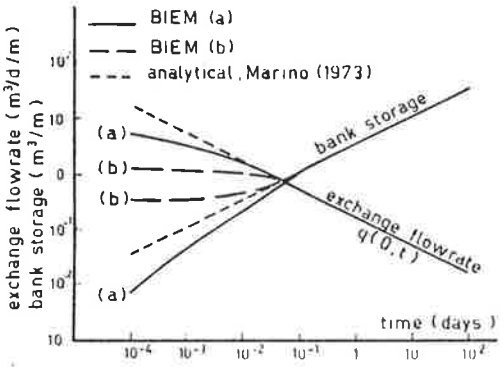

Fig. 6. Exchange flow rate and bank storage for a hydraulically connected aquifer.

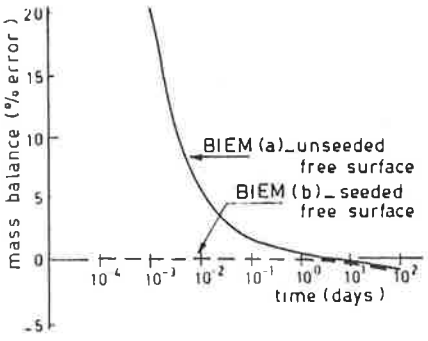

Fig. 7. The numerical mass balance error.

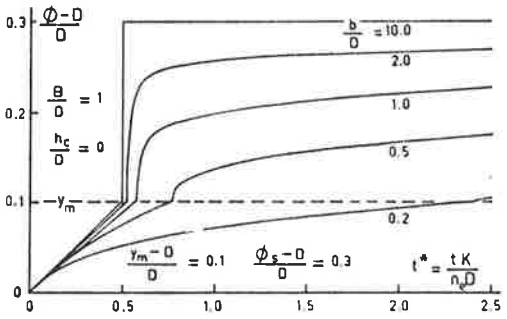

Fig. 8*a*. Centerline potential during the process of hydraulic connection for various stream widths.

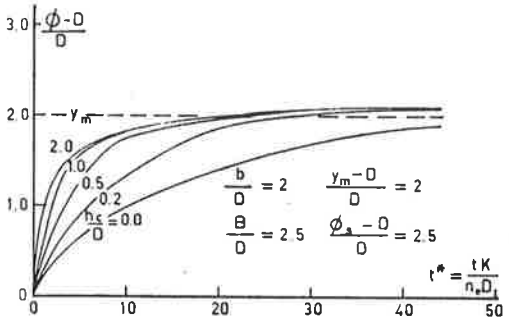

Fig. 9*a*. Centerline potential during hydraulic connection for various suction heads.

rate corresponding to an infinite free surface slope at the stream bank. Errors in a discrete numerical model are to be expected when faced with such discontinuities.

In the example problem the parameters took the following values: H = 11 m, D = 10 m, K = 10 m/d, n_v = 0.1, and $\alpha = KD/n_v = 10^3$ m^2/d. The BIEM model gives consistent results for the shape of the free surface and the exchange of flow between stream and aquifer except, as anticipated, during the short period immediately following the step change in stream head (see Figures 5 and 6). The effect of artificially 'seeding' the initial free surface (see Figure 4) in the immediate vicinity of the stream was investigated as a means of reducing the initial errors. These tests showed that the initial free surface shape had no significant effect (less than 0.5%) on the free surface profile, exchange flow, and bank storage after 0.5 day, and the effect continued to diminish with time. Secondly, seeding the free surface could significantly reduce the mass balance error, automatically calculated in the program at each time step, for the time period up to 0.5 day (see Figure 7). The initial mass balance error for the unseeded surface is largely due to the extremely steep initial free surface adjacent to the stream boundary. The mass balance error of almost −1% at 100 days is due to curvature of the free surface over a zone where node spacings are large. The errors are the result of approximating the curved free surface by a series of straight line segments. Such errors can be reduced by using more nodes or higher order elements. These tests indicate that in the extreme case of infinite rate of change in stream head the BIEM gives satisfactory results for the free surface, exchange flow rate and bank storage after a dimensionless time of $t^* = Kt/n_vD = 5$.

Transition from Hydraulically Disconnected to Hydraulically Connected Streambed

During sustained flow in an ephemeral stream the induced groundwater ridge may rise until it intersects the streambed. As this occurs, the rate of groundwater accretion diminishes due to the reduction in potential gradient across the semipervious streambed material. This boundary condition is given as equation (2*d*).

The potential at the stream centerline and the groundwater accretion rate are plotted with respect to time on nondimensional graphs for a number of cases (see Figures 8 and 9). The effects of streambed width on the transition are illustrated by the potential at the streambed centerline (Figure 8*a*) and the exchange flow rate divided by streambed width (Figure 8*b*). As streambed width increases with respect to aquifer thickness, the duration of the transition process is reduced.

An examination of the effect of the suction head h_c on the same parameters is given for a single streambed configuration with a dimensionless streambed leakage factor, B/D = 2.5 (See Figures 9*a* and 9*b*). For higher suction heads the free surface rises more quickly due to higher initial infiltration rates. If the leakage rate through the base of a perched groundwater mound is sufficiently high or if the ratio between streambed leakage and aquifer permeability is sufficiently low, hydraulic connection will not occur. These principles may be applied in field studies of ephemeral stream-aquifer interaction to provide some constraints on the values of model parameters during the model calibration phase. An example of such an application follows.

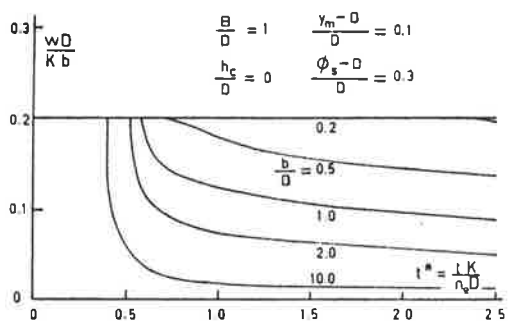

Fig. 8*b*. Recharge rates during the process of hydraulic connection for various stream widths.

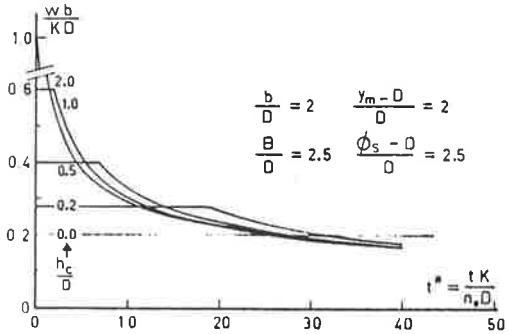

Fig. 9*b*. Recharge rates during hydraulic connection for various suction heads.

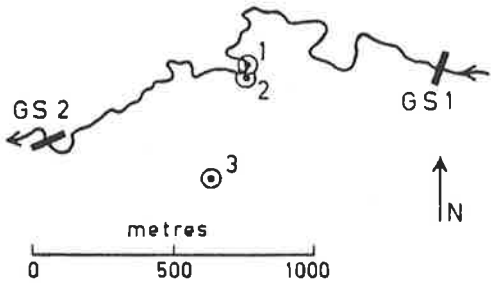

Fig. 10. Test reach of the Little Para River.

BIEM APPLIED TO THE LITTLE PARA RECHARGE STUDY

Two reaches of the Little Para River undergo a transition from hydraulic disconnection to connection with an underlying aquifer during sustained streamflow. Figure 10 shows the location of two gauging stations and several piezometers encompassing one of these reaches. During a reservoir release into the river in late summer 1981, discharge rates were recorded at the two gauging stations (Figure 11). Groundwater levels, as observed in piezometers 1, 2, and 3, were adjusted to account for the regional groundwater slope, which is in southwesterly direction. The BIEM was applied and model results for groundwater elevations at the three piezometer are compared with the corrected observations in Figure 12. Fitting model output to the groundwater data provided estimates for the nondimensional recharge w/K and the aquifer diffusivity α. It was hoped that the value of leakage through the base of the aquifer could be quantified in the same way. However, only an upper bound on the leakage rate could be determined ($|\partial\phi/\partial n|$ at base $< 10^{-4}$) because in this example the leakage rate proved to be so small that its effect on groundwater levels was insignificant during the modeling period compared with the dominant process of streambed recharge.

Drilling has revealed that the unconfined aquifer consists of a series of interconnected lenticular beds of silty sands to gravels within clays which in the model is approximated by a homogeneous medium. The model does not account for the meandering nature of the stream nor the variation in exchange flow rates along the 3-km length of reach. With these practicalities in mind and although model uniqueness has not been determined, the model calibration is considered satisfactory for its proposed use. Next the BIEM output was fitted against the observed stream discharge loss rate (Figure 13), which allowed the value of K, the representative hydraulic conductivity of the aquifer, to be calculated. Consequently, the effective porosity could be obtained. The values found (K = 11 m/d, n_e = 0.09) lie comfortably within independently determined ranges for these parameters. (A calibrated regional groundwater model gives K = 0.3 m/d, n_e = 0.1. A pump test on a sand bed in this vicinity gave K = 17.6 m/d. Regional water balance calculations give n_e = 0.085. As the piezometers tapped the more pervious strata, one would expect that the value of K necessary to model their response would be higher than the regional average.) Note that the BIEM gives an instantaneous recharge rate at the section. The field data give an average recharge rate for the reach, which is not spacially constant due to stream lag time and is always limited by the available streamflow.

The calibrated model is to be used to predict stream losses and aquifer recharge for various reservoir operations, thus providing information which is used in determining release rules so as to give the desired recharge rates with minimal wastage. Also, the recharge rates are to be used in a regional groundwater model which will predict the behavior of the overall system.

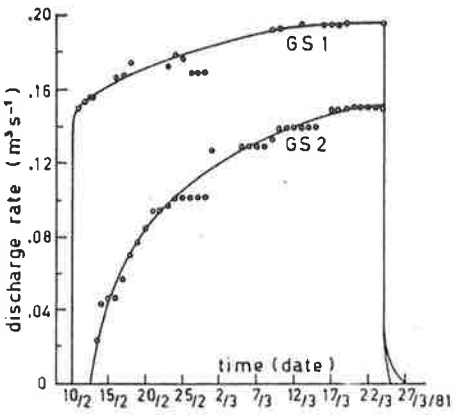

Fig. 11. Discharge rate at gauging stations GS1 and GS2 due to reservoir release into the Little Para River.

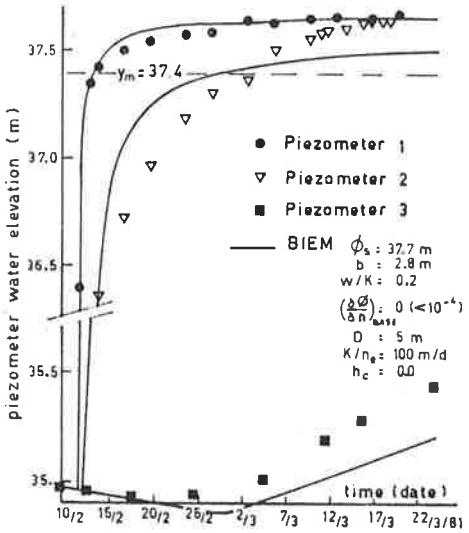

Fig. 12. Groundwater elevations at the piezometer sites.

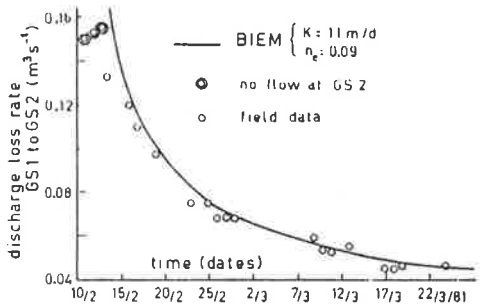

Fig. 13. Recharge rate over the reach.

CONCLUSION

This paper was focused on the transition between hydraulic disconnection and connection of ephemeral streams with aquifers. The results contained in this paper indicate that the simple specified head/specified exchange flow rate models are acceptable for broad streambeds ($b/D > 10$) when the streambed and the head in the stream are close to the initial water table, i.e., when

$$\frac{y_m - D}{D} < 0.1 \qquad \frac{\phi_s - D}{D} < 0.3$$

For narrower streams the semipermeable bed conditions are necessary to describe the transition process. The model has been applied to a field study with satisfactory results.

Acknowledgments. The writers would like to thank the Director General–Engineer-in-Chief of the Engineering and Water Supply Department of South Australia for financial assistance and cooperation on the field studies. Also we acknowledge partial support from the National Science Foundation, grant CEE-7902803. The second author is grateful to the University of Adelaide for a Distinguished Scholar grant and for providing facilities during the course of this and other research.

REFERENCES

Bouwer, H., Theory of seepage from open channels, *Advan. Hydrosci.*, *5*, 121–172, 1969.

Freeze, R. A., Role of subsurface flow in generating surface runoff, 1, Baseflow contributions to channel flow, *Water Resour. Res.*, *8*(3), 609–623, 1972.

Freyberg, D. L., J. W. Reeder, J. B. Franzini, and I. Remson, Application of the Green-Ampt model to infiltration under time-dependent surface water depths, *Water Resour. Res.*, *16*(3), 517–528, 1980.

Green, W. H., and G. A. Ampt, Studies on soil physics, 1, The flow of air and water through soils, *J. Agric. Sci.*, *4*, 1–24, 1911.

Hall, F. R., and A. F. Moench, Application of the convolution equation to stream-aquifer relationships, *Water Resour. Res.*, *8*(2), 487–493, 1972.

Henry, J. L., Integrated finite difference modelling of groundwater flow, Queensland Water Resources Commission Report, *Vol. I, II*, Brisbane, Australia, 1979.

Liggett, J. A., and P. L-F. Liu, *Boundary Integral Equation Method for Porous Media Flow*, Allen and Unwin, London, 1983.

Marino, M. A., Hele-Shaw model study of the growth and decay of groundwater ridges, *J. Geophys. Res.*, *72*(4), 1195–1205, 1967.

Marino, M. A., Water table fluctuation in semipervious stream-unconfined aquifer systems, *J. Hydrol.*, *19*, 43–52, 1973.

Neuman, S. P., T. N. Narasimhan, and P. A. Witherspoon, Application of mixed explicit-implicit finite element method to nonlinear diffusion-type problems, in *Finite Elements in Water Resources*, Pentech, Plymouth, Massachusetts, 1976.

Rovey, C. E. K., Numerical model of flow in a stream-aquifer system, *Hydrol. Pap. 74*, Colo. State Univ., Fort Collins, 1975.

Rushton, K. R. and L. M. Tomlinson, Possible mechanisms for leakage between aquifers and rivers, *J. Hydrol.*, *40*, 49–65, 1979.

Sharp, J. M., Limitations of bank-storage model assumptions, *J. Hydrol.*, *35*, 31–47, 1977.

(Received September 3, 1982;
revised January 10, 1983;
accepted January 21, 1983.)

Dillon, P. J. (1983, November). Boundary Integral Model of Stream-aquifer Interaction. In *preprints of papers / organised by the National Committee on Hydrology and Water Resources of the Institution of Engineers, Australia.* (pp. 195-199). Hobart, Tasmania.

APPENDIX C.5

DIGITAL HYDROLOGIC DATA
ACQUISITION SYSTEM

P.J. Dillon
Department of Civil Engineering
University of Adelaide, Australia

Abstract

A data aquisition system which monitors groundwater or surface water levels and loads the recorded data into a computer is described. It features a novel bore water level transducer and a portable multi-purpose data reader. The equipment is relatively inexpensive, adaptable to other applications and has proved to be reliable and accurate in a field study. The system requires minimal operator time to load and verify the data.

Résumé

Une description d'un système d'acquisition des données qui contrôle les niveaux d'eaux souterraines et d'eaux de surface, et qui alimente un ordinateur en données enregistrées. Il y a un nouveau transducteur de niveaux d'eau souterraine et une mémoire portative et multi-usages pour fournir des données. L'équipement est relativement bon marché, adaptable à d'autres applications, et s'est révélé fidèle et précis au cours des essais sur le terrain. L'alimentation et la vérification des données demandent peu de temps dans ce système.

1 Introduction

A study of groundwater recharge from a regulated stream overlying a heavily exploited aquifer has been undertaken jointly by the Engineering and Water Supply Department of South Australia and the University of Adelaide. Flow exchange between the stream and the groundwater was found to depend on the position of the phreatic surface adjacent the stream. This was monitored at selected observation bores. Initially a chart recorder with a pulley and float arrangement for detecting water level changes was installed at each site. However this produced staircased records due to pulley stiction and the small water plane cross-section of the float, whose size was restricted by the casing dimensions. Charts had to be replaced weekly and the recorders were unreliable in the humid environment in which they were placed. There remained the onerous task of manually digitizing the charts and entering the data into computer files for subsequent analysis. Alternative commercially available recording equipment was beyond the study's budget. To resolve these problems a digital recording system was designed, developed and constructed chiefly by Mr. S. Woithe an instrumentation technician at the University of Adelaide. This system has been in routine operation for nine months, recording groundwater levels at six observation bores and stream stage and water temperature at several river gauging stations. The recorded data is fed into computer files.

2 System Operation

The data aquisition system is composed of five pieces of equipment in addition to a computer. See figure 1. The transducer and recorder are located at the observation bore or gauging station. At regular intervals the battery and solid state memory of the recorder are replaced and date, time and an independent measurement of water level are recorded on a field data sheet. Warning lights on the recorder indicate whether the recorder is operating correctly. The portable reader is plugged into the recorder at site visits to give a direct reading of momory contents as an additional check.

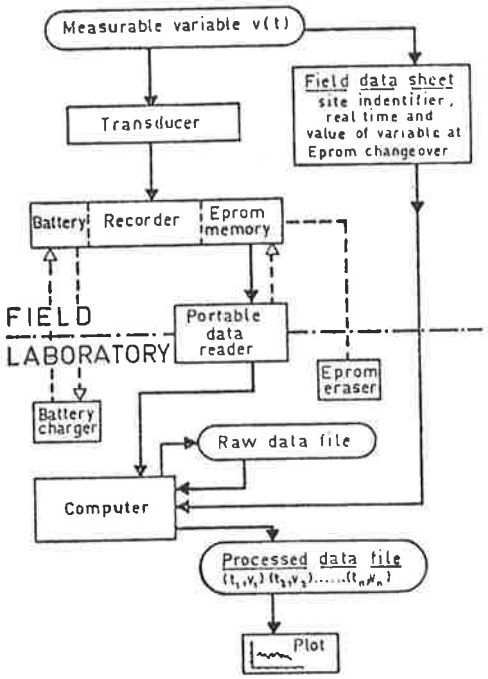

Figure 1 Data aquisition system block diagram

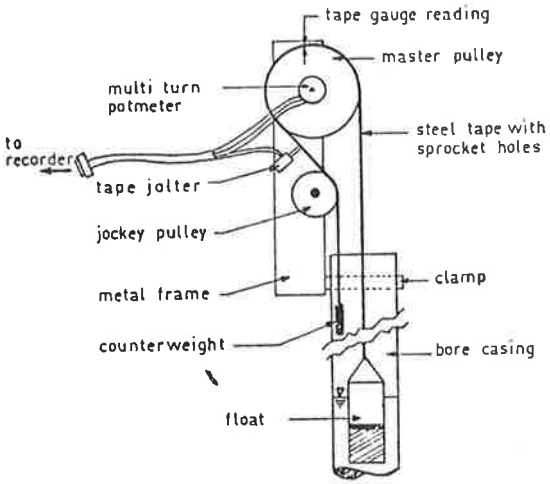

Figure 2 Groundwater level transducer

Later back in the laboratory the memory is plugged into the reader and this is coupled to a port on a PDP11 computer. The data is fed down the line and stored on a floppy disk. An interactive editing program is engaged on a computer terminal and the contents of the field data sheet are keyed in. The raw data file is automatically edited, scaled, reformatted and saved as a processed data file. The program also performs basic checks on data quality. A calcomp (automated) graphical plot is obtained as an additional check. Such checks are a vital component of any recording system (Brown, 1980). The verified data is then merged into the data bank. The solid state memory is erased using ultraviolet light and the battery is recharged ready for the next change over.

3 System components

3.1 Transducer

A rise in groundwater level lifts the float (figure 2) attached to a punched stainless steel tape which is wrapped around a sprocketted master pulley. As the pulley turns, the shaft of a multi-turn potentiometer rotates causing a variation in electrical resistance. The voltage across the potentiometer terminals is the transducer output. A jockey pulley directs the counterweight down inside the bore casing. A tape jolter is activated prior to the recorder taking a reading and the impact is sufficient to overcome pulley stiction and friction between float and casing. The jolter and potentiometer circuits are only powered for a short time before and during readings. Where water levels are monitored in bore casings greater than 250 mm diameter the jolter and jockey pulley are not required. The transducer has a range of 3750 mm with a resolution of 1 mm and is linear to ±2 mm over the full range. Transducer output is insensitive to temperature from 0° to 50°C. In straight casing the jolter allows floats as small as 50 mm diameter to give water levels within ±2 mm of their true value for static and dynamic tests. For water temperature recording a thermocouple is used as the transducer.

3.2 Recorder

The recorder is of modular design and consists of four standard size printed circuit boards. These provide regulated power supplies, microprocessor control, a transducer interface and solid state memory.

3.2.1 Power supply

The power supply board produces a number of independent regulated supplies for operating the recorder and transducer.

3.2.2 Microprocessor control

A reprogrammable chip on the microprocessor board controls the operation of the recorder and gives it remarkable versatility. The recorder takes readings at time intervals of either 10 seconds, 1 minute, 10 minutes or 1 hour, selected by setting a switch on the recorder. Each reading is started by activating the jolter, and pausing. The voltage reading across the potentiometer is then converted to a digital value.

If the reading is different to the last reading stored in the solid state memory by more than a specified threshold value, then this reading and the time increment number are stored in the next memory location. If more than a specified period of time has passed since the last value was stored then the new reading and time increment number are stored regardless. If neither of these conditions apply no new values are stored and the recorder 'rests' until the next time interval has elapsed. At the time of removing the solid state memory, a manual over-ride ensures that the current data are stored.

This data compression procedure reduces the number of data stored without loss of information, giving more efficient use of memory storage in the recorder and later also in the computer. If spectral analysis is required the threshold values are set to zero to comply with Fast Fourier Transform routines.

After 65000 time increments (45 days at one minute time increments) the time value is reset to zero and continues counting. Therefore only data storage and power supply capacity limit the length of unattended field operation. In the event of a power failure the memory is not erased.

3.2.3 *Transducer interface*

One board is used to interface the water level transducer with the recorder. This contains scaling potentiometers which enable very fast calibration of the transducer. The analogue voltage from the transducer is converted to a digital signal on this board. When monitoring temperatures only this board need be replaced.

3.2.4 *Solid state memory*

The fourth board contains a bank of eight semi conductor chips (eproms) each of which store 500 pairs of time and data value readings. Thus one board can record a total of 4000 reading pairs. The time reading is stored as a four digit hexidecimal number (resolution 1:65000) and the data value is stored as a four digit decimal number (resolution 1:10000). The eproms are erasible using ultra-violet light. Two boards are required for each recorder so that one can be brought in for reading while the other has its turn in the recorder.

3.3 Reader

A microprocessor unit mounted in a briefcase serves as a recorder checking tool and as a computer interface for the eprom boards. When plugged into a recorder it displays the last time and value stored in the memory and the current time and value. Back in the laboratory the contents of an eprom board are fed into the computer by plugging the board into a socket on the reader which is connected to a computer terminal line. No additional hardware is required. One reader can service a data network of many recorders.

3.4 Memory Eraser

A pair of ultraviolet light tubes are used to erase up to four eprom boards simultaneously. Erasure takes approximately 30 minutes. The reader is used to check that each board is completely erased and ready for re-use.

3.5 Battery charger

A safe unit to fast charge sealed rechargeable batteries has been developed. A fully drained 8 Amp-hour 12 Volt battery can be fully recharged in 6 hours. The buildup of gas within the battery is minimized with a consequent reduction in the likelihood of explosion. Lead-acid batteries are used as they are relatively cheap and do not have the "memory" problems of Nickel-cadmium batteries. Each gives about 8 weeks power supply for a transducer and recorder at one minute resolution.

4 Example of data aquisition

The Little Para River recharge study is located in a metropolitan area so the likelihood of undesirable interference with equipment was averted by concealing it underground. Concrete boxes 400 mm deep were constructed and covered by steel-rimmed fitted concrete lids 600 mm x 450 mm set at ground level. The top of the observation bore casing penetrated the bottom of the box. Temperatures ranging from 3° to 44°C were observed and humidity frequently reached dew point. This harsh environment did not impede recorder performance.

Thresholds of 50 mm and 4 hours were programmed in the recorder microprocessor as the maximum change in groundwater level and maximum time lapse between successive data entries in memory. A time increment of 1 minute was set. Eproms and batteries were exchanged at intervals of about 6 weeks. These values of the thresholds were chosen to allow detection of diurnal fluctuations in groundwater levels due to evaporation and transpiration of phreatophytes flanking the stream. The data

value threshold was only triggered when streamflow commenced after the bed had been dry or when nearby irrigation bores were in use.

Examples of the field data sheet, raw data file, processed data file and calcomp plot for a short period of record from an observation bore adjacent the river are given in Figures 3, 4, 5 and 6 respectively.

5 Costs

This system was designed to keep the capital outlay below Aus$600 per field installation and to minimize operator intervention at all stages of system operation. The materials costs and the labour involved in producing the equipment is outlined below:

	AUS$	Manhours
Transducer - bore	50	10
- temperature*	20	2
Recorder**	420	18
Reader + battery charger + eprom erasor	560	40
Batteries (2)	80	-

*includes temp transducer interface board

** includes bore water level interface board and 2 eprom boards.

Prices are in 1981 Australian dollars and labour times cover fabrication and an electronics technician's time in assembling and testing the equipment.

AUS $1 = 2.6 Dutch Guilders; 6.6 Fr Francs; 2.4 Deutsche Marks; 0.56 Pounds; US$0.98 (August 1982).

Operation costs depend principally on travel time to reach the recording equipment. Changeover of memory and battery and equipment checks at a field station take only ten minutes. Reading the data and producing a processed data file requires about twenty minutes per station. Perusing the calcomp plot and sorting the processed file into the data bank requires a further ten minutes. Memory erasure and battery recharging require minimal operator time.

Little Para recharge study field data sheet.

Bore No. 36 Eprom No: 12 Battery No: 8

	ON	OFF	Δ=CHANGE(MM / Mins)	ERRORS
Date / Time } T	18/9/81 1805	9/10/81 1524	30079	δ_T = ΔT - ΔET δ_V = ΔTG+(ΔEV)
GL (m)	4.928	4.840	−88 ±14	D=mean(TG-GL)
TG (m)	8.535	8.442	−93 ±2	= 3.602 m. (15 readings)
ET (min)$_{16}$	0001	7592	30097 (dec)	δ_T = −18 min
EV (mm)	1865	1961	96	δ_V = 3 mm
checks	✓	✓		
initials	PJD	PJD		$GL_1 = TG_1 - D$ = 4.933 m

GL = sounding gauge reading (st error = ±7 mm/reading)

TG = tape gauge reading (st error = ±1 mm/reading)

ET = eprom recorded time

EV = eprom recorded data value

File Names: Raw data file: R361081 Processed data file: P361081

Figure 3 Example field data sheet

time	value	time	value	time	value	time	value
0001	1865	00F1	1863	01E1	1869	02D1	1868
03C1	1869	04B1	1869				
				7261	1978	7351	1970
7441	1964	7531	1961	7592	1961	FFFF	FFFF

Figure 4 Example raw data file

```
                M.T. LAGGED R.T. BY     -18 MINS
                 TIME SCALE FACTOR =  0.999
                 TIME CORRECTION APPLIED
                ERROR IN LEVEL CHANGE =    3 MM
                % ERROR IN LEVEL CHNG =  -3.2 %
                 LEVEL CORRECTION APPLIED

 36   180981 1805        GL      4.933
 36   180981 2204        GL      4.935
 36   190981 0204        GL      4.929
 36   190981 0604        GL      4.930
 36   190981 1004        GL      4.937
 36   091081 1347        GL      4.840
 36   091081 1524        GL      4.840
```

Figure 5 Example processed data file

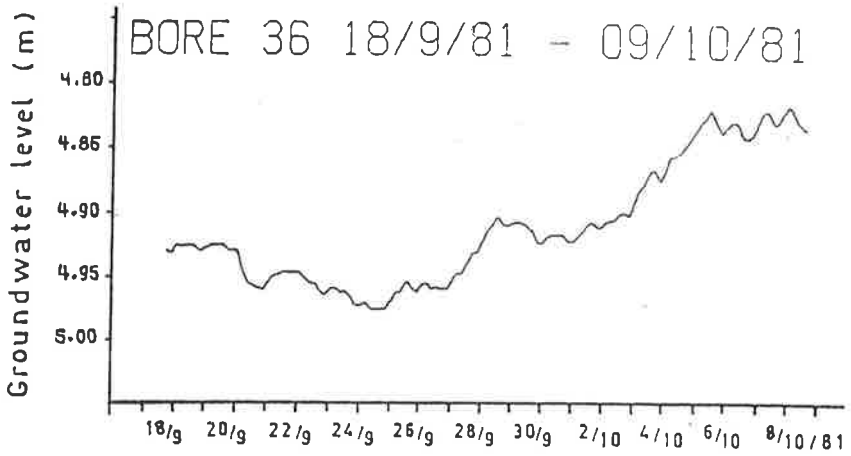

Figure 6 Example calcomp plot

6 Summary

The system described in this paper has proven reliable and accurate and was economically viable for a field study of groundwater recharge. Interested instrument manufacturers and users of hydrologic data aquisition systems are invited to correspond with the author.

Acknowledgements

The author expresses his appreciation to Mr. S. Woithe who undertook most of the design, development, construction and testing of the recording system. The support of the Director-General and Engineer-in-Chief of the Engineering and Water Supply Department of South Australia which funded the field study is gratefully acknowledged.

Reference

Brown, J.A.H. 1980. A review of the design of water resources data networks. Australian Water Resources Council Technical Paper No. 52, 372 pp.

APPENDIX C.6

INTERNATIONAL CONFERENCE ON GROUNDWATER AND MAN
SYDNEY, 1983

MANAGEMENT OF A PUMPED SURFACE STORAGE AND AN AQUIFER

P. J. Dillon

Civil Engineering Department, University of Adelaide,
Box 498 GPO, Adelaide 5000
AUSTRALIA

ABSTRACT

A regression model is used to relate groundwater recharge to releases from a pumped surface storage into an ephemeral stream. This enables the operation of the reservoir to be simulated to identify the release policy which meets a given recharge requirement at the least pumping cost. The method has been applied to the Little Para Reservoir and in so doing the possibility of its conjunctive operation with the Northern Adelaide Plains aquifers was investigated.

INTRODUCTION

When a reservoir is constructed there is often a requirement for releases to be made for in-stream uses, environmental reasons or to supply those with a prior-right to the water. When it is constructed upstream of a reach recharging an aquifer by streambed seepage provision should be made for recharge releases from the reservoir. It is shown later that releasing even a small proportion of the natural reservoir intake may yield the natural recharge. Larger releases would artificially enhance recharge.

In the case where the reservoir requires inter-basin transfer of water to meet demands, the volume of water pumped is related in some way to the volume of water released for recharge, figure 1. The pumping cost associated with any release policy may be determined by simulation. If the relationship between releases and recharge is time-dependent the release rule which minimises pumping costs while meeting the recharge requirement may not be immediately obvious.

STREAMFLOW-RECHARGE RELATIONSHIP

The stream and aquifer may be either *hydraulically connected* or *hydraulically disconnected,* figure 2, where the hydraulic head in the aquifer below the streambed has an influence or no effect, respectively, on the exchange flow (recharge) rate. In cases where hydraulic connection occurs during streamflow, the shape of the stream hydrograph has a significant effect on exchange flow and bank storage.

A simple example of releasing a constant volume of water using alternative uniform release rates is considered. The channel is assumed to have a constant trapezpodal cross-section, uniform slope and lined with a thin semi-permeable blanket as shown in figure 3. A boundary integral equation model, described by Dillon and Liggett (1983) was used to simulate groundwater flow on a stream cross-section assuming a homogeneous isotropic aquifer on an impermeable horizontal base. These last assumptions are reviewed in Dillon, 1983a. The peak and final bank

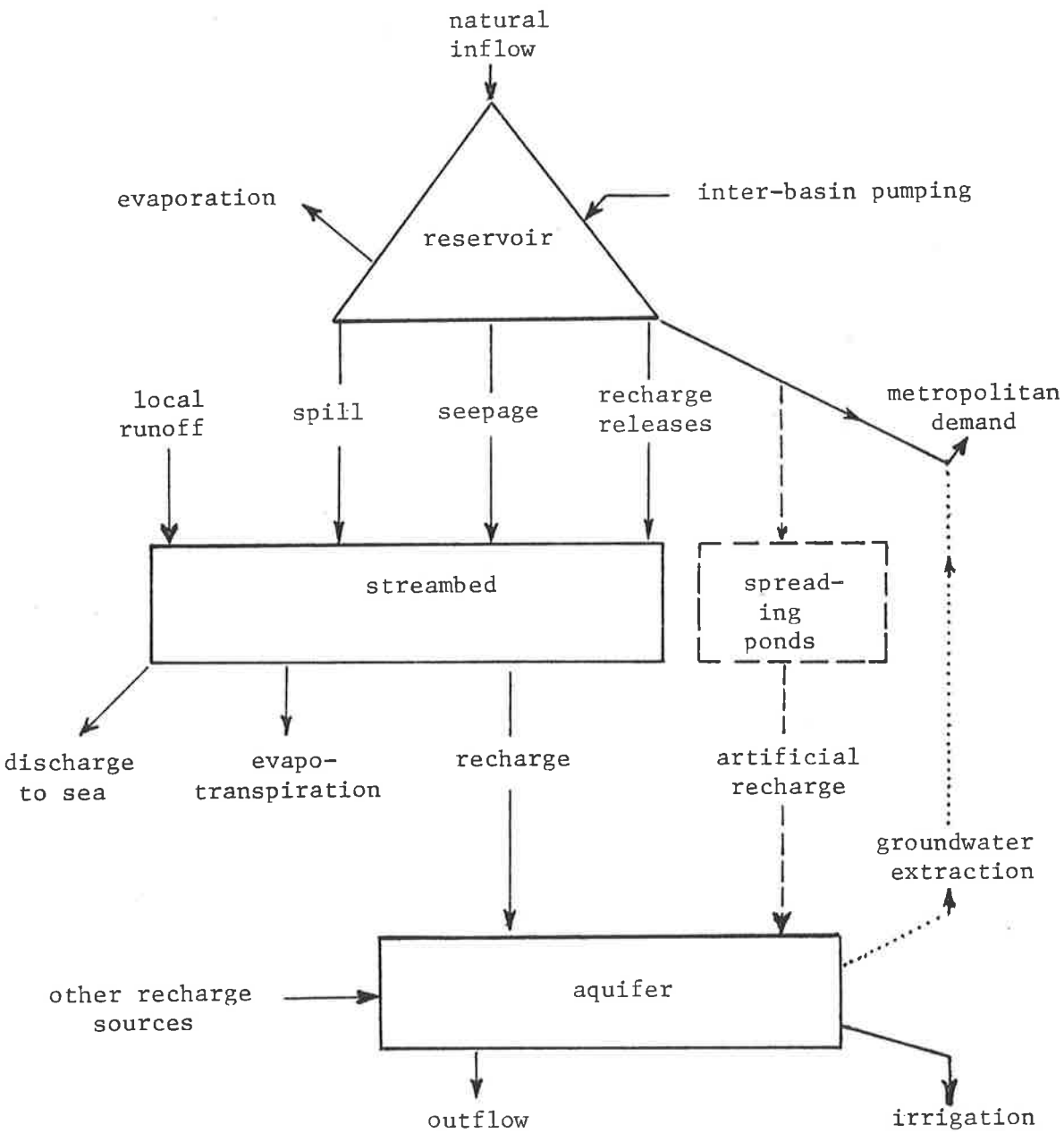

System block diagram
FIGURE 1

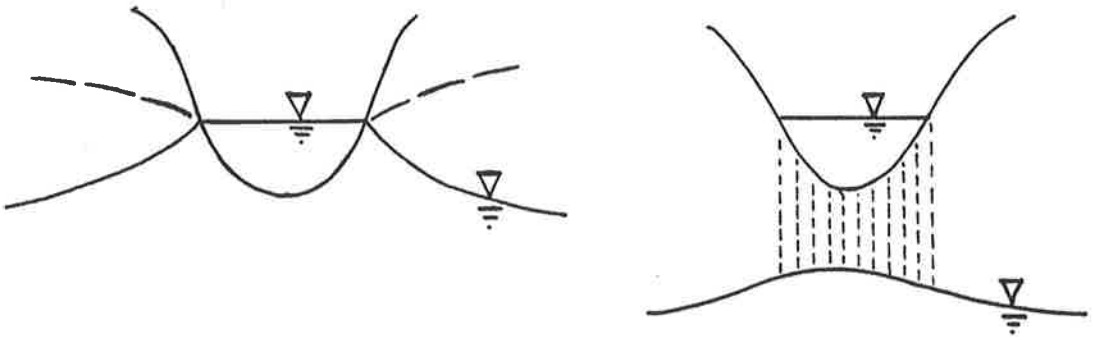

Stream and aquifer
hydraulically connected (a) and hydraulically disconnected (b)

FIGURE 2

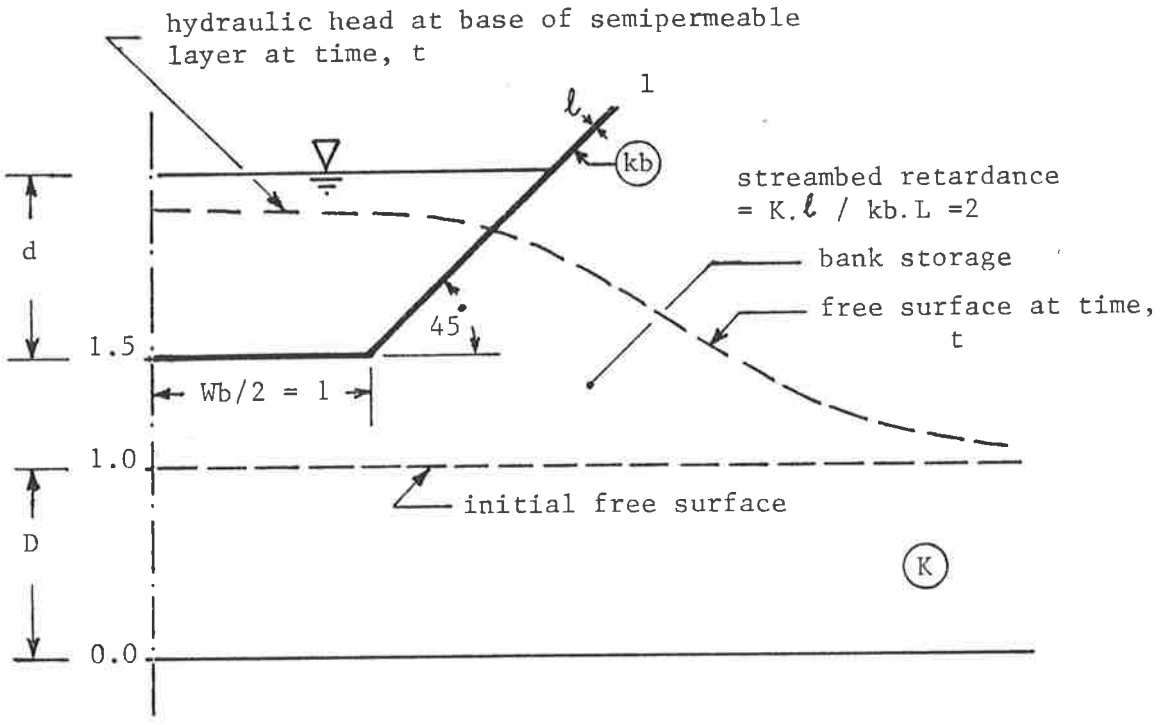

Stream and aquifer cross-section for BIEM reservoir release - recharge problem

FIGURE 3

storage induced in the aquifer as a result of each release pattern appear in Table 1. Extending the duration of flow significantly improves recharge.

This, together with other model runs, not shown, indicate that reservoirs or flow control structures may be used to enhance the natural groundwater recharge by streamflow regulation. The percolation tanks of the Baramati district, Maharashtra, India, are an established example of this principle (Dillon, 1983b). These impound monsoon runoff and allow time for the water to percolate through the streambed enhancing the yield of wells in the valley alluvium.

TABLE 1

Effect of release pattern on recharge.

Release Rate Q*	Duration T*	Depth d	Bank Storage, V* peak	final
0.02	500	0.096	19.52	19.14
0.05	200	0.166	14.50	13.91
0.10	100	0.249	12.19	11.35
0.20	50	0.370	10.59	9.49
0.50	20	0.611	9.29	7.85
1.00	10	0.877	8.86	7.27

$Q^* = Q\ n\ Wb^{-8/3}\ So^{-1/2} = (a + a)^{5/3}\ (1 + 2.82a)^{-2/3}$

$T^* = T\ K\ Ne^{-1}\ L^{-1}$

$V^* = V\ Ne^{-1}\ L^{-2}$

where Q = discharge rate in open channel $[L^3\ T^{-1}]$
n = Manning's roughness coefficient $[L^{-1/3}\ T]$
So = channel bed slope
Wb = bottom width of channel [L]
a = depth/Wb = d/Wb
T = release duration [T]
K = aquifer hydraulic conductivity $[LT^{-1}]$
Ne = effective porosity
L = characteristic length, chosen here to be 1 metre [L]
V = bank storage/unit length of stream $[L^2]$

LITTLE PARA RIVER, SOUTH AUSTRALIA

In 1977 a dam was built on the Little Para River to supplement the Adelaide metropolitan water supply by 10 x $10^6 m^3$/year. The reservoir stores water pumped from the River Murray and harvests a mean annual 9.4 x $10^6 m^3$ runoff from its own catchment. Downstream the Little Para River crosses the Northern Adelaide Plains and recharges 2.2 x $10^6 m^3$/year to the underlying aquifers. These are also recharged from other sources and supply 18 x $10^6 m^3$/year for irrigation of market gardens. Two thirds of the length of the stream becomes hydraulically connected to the aquifers during sustained streamflow. Hence the recharge rate declines during a release as the hydraulic gradient across the streambed diminishes.

An undertaking was made prior to dam construction that releases would be provided to ensure that not less than the natural recharge occurred. However there was insufficient data with which to quantify natural recharge. In response to this need the Little Para Recharge Study commenced in 1979

with the dual aims of:

1. identifying the natural recharge, and
2. recommending a release policy, giving consideration to the possibility of conjunctive operation of the Little Para Reservoir and the Northern Adelaide Plains aquifers.

ESTIMATION OF NATURAL RECHARGE

Prior to the study there were insufficient data to reliably determine the mean annual recharge. So, over a period of 3½ years releases from the reservoir, discharge at downstream gauging stations and water table elevations near the streambed were monitored. From this comprehensive data set a regression model was developed to relate streambed intake rates to the post-dam stream discharge record. (Dillon, 1983c.)

Firstly dry weather daily discharge correlations between adjacent pairs of gauging stations were found. A test for variation in these correlations over the study period revealed no obvious trends. The sum of discharge losses over the four reaches in the recharge zone was not constant. After allowing for phreatophyte evapotranspiration the aquifer recharge rate was found to range between 0.085 and 0.210 m^3/sec. depending on antecedent streamflow and watertable elevation. The intake rate declines during periods of high discharge due to the reducing hydraulic gradient in the connected sections of the aquifer as the groundwater ridge rises and spreads. A simple formula for the change in streambed recharge capacity as a function of monthly discharge at the gauging station (station 03) upstream of the recharge zone was found by a data best-fit procedure, figure 4.

With this simple model the recharge capacity of the streambed at each month of post-dam discharges could be determined. To project this relationship to pre-dam conditions, the term *equivalent uniform discharge* is introduced. This is the uniform discharge over a month which would give the same discharge loss over the recharge zone as the natural flow pattern. It is estimated by applying the regression equation for daily discharge loss with respect to daily discharge at station 03 irrespective of the flow history. This algorithm was applied to the 10 year pre-dam daily discharge record at station 03. Daily discharge loss is limited by the available discharge or the streambed intake capacity. The daily losses in each month are added to produce the equivalent uniform discharge, figure 5.

Using the dry weather inter-station discharge loss correlations the discharge gain over the recharge zone due to local runoff could be estimated. More significantly the recharge resulting from this runoff could be calculated for the post-dam period. Hence a relationship between recharge from local runoff and the natural (pre-dam) discharge at station 03 was found. Similarly recharge from dam seepage was determined. With these relationships defined, the total recharge associated with alternative reservoir release patterns could be calculated. The recharge which would have occurred without the dam was found using the same simulation model.

RESERVOIR RELEASE SIMULATION

With only 14 years stream discharge data for station 03, it was decided to test the sensitivity of the simulation results to streamflow record. Two 30 year sets of generated streamflow data were provided by the Engineering and Water Supply Department of S.A. These were produced by a method described in a report of that Department (1978). The mean annual discharge and coefficient of variation of the annual discharge for the three

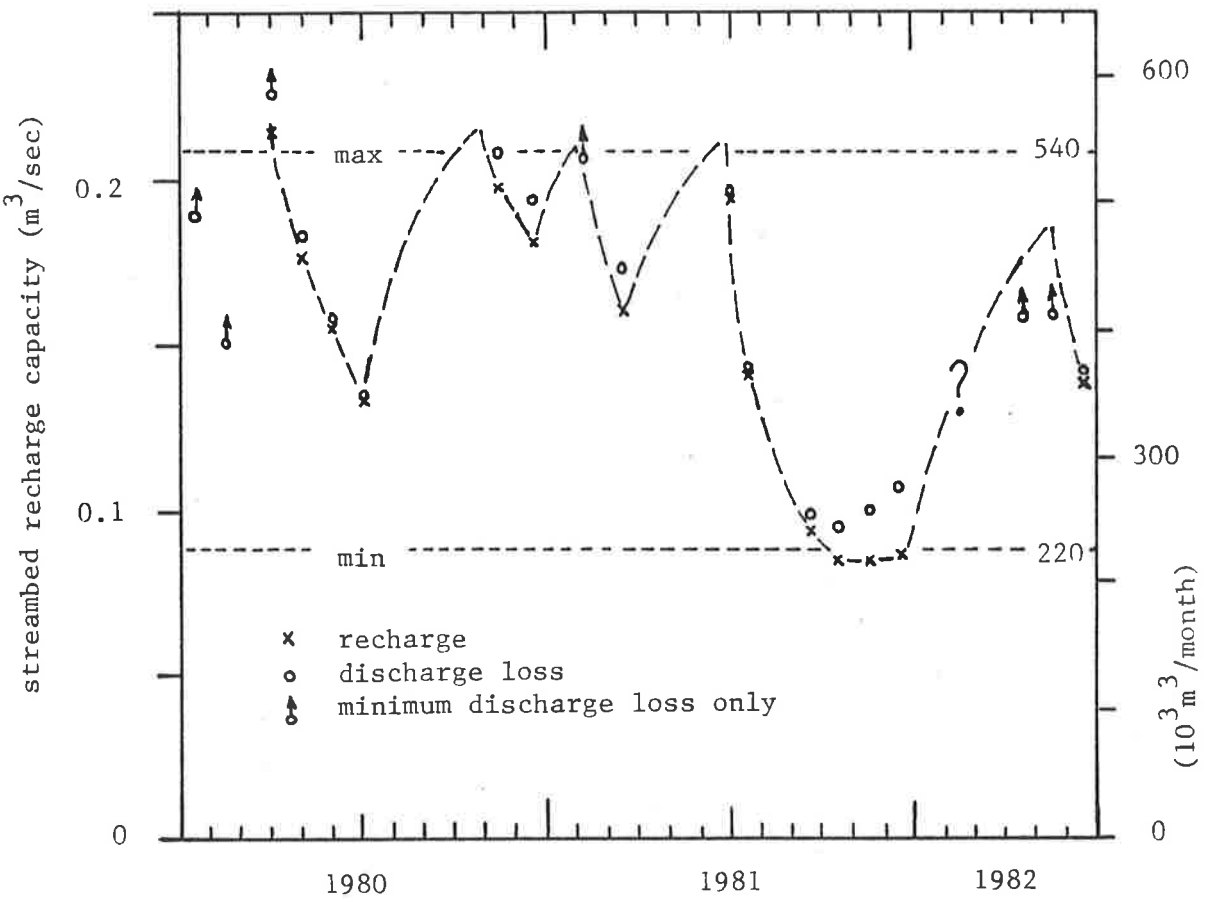

(a) Streambed recharge capacity during study period

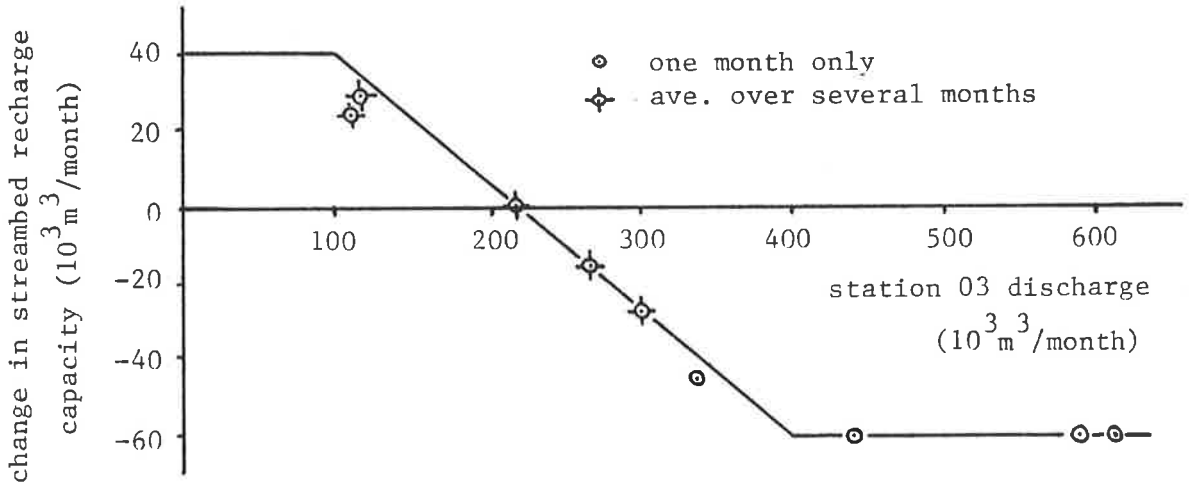

(b) Change in streambed recharge capacity related to discharge

Streambed Recharge Capacity

FIGURE 4

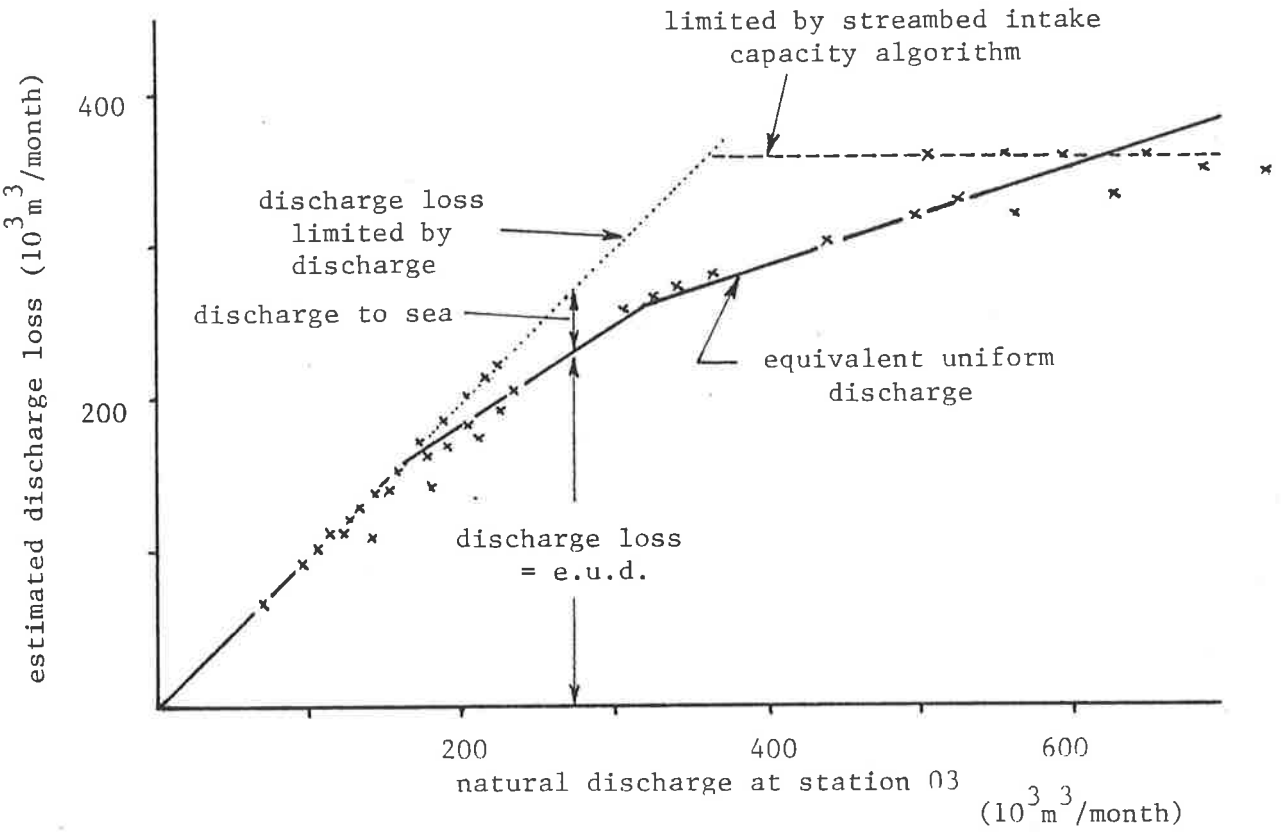

Equivalent Uniform Discharge

FIGURE 5

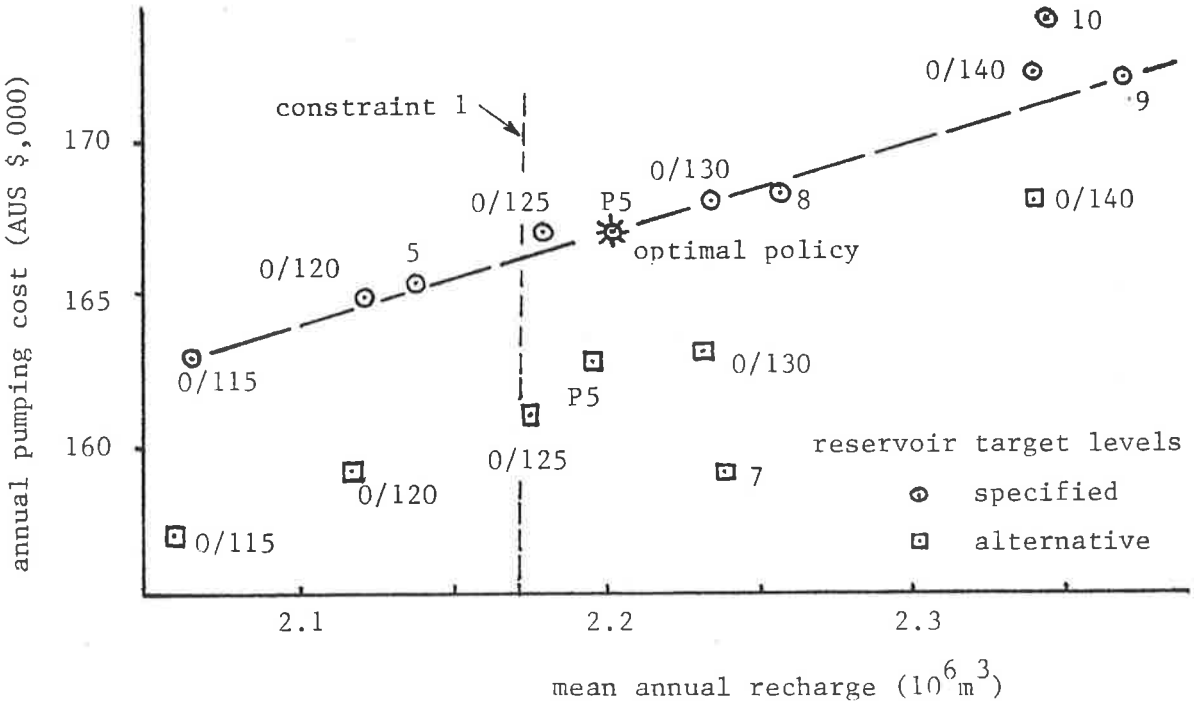

Pumping cost and recharge for several release policies

FIGURE 6

data sets ranged from 9.4×10^6 to $10.0 \times 10^6 m^3$ and 0.49 to 0.67 respectively. The resulting range in mean annual natural recharge was 6% with the historical record giving the highest value due to a lower incidence of zero flow than the synthetic data. All alternative release policies were monitored for each data set. The variation in recharge from each set was minimal but significant differences in mean annual inter-basin pumping costs were observed. The ranking of these costs was almost identical for each data set and the same policy was optimal in each case.

A range of alternative release policies were simulated. These included uniform or set monthly releases and releases dependent on

- the previous month's natural reservoir intake,
- the reservoir volume at the start of the month,
- the recharge credit at the start of the month, where credit is defined as the excess of actual recharge over the natural (without dam) recharge,
- the streambed intake capacity at the start of the month,
- the need for groundwater extraction to provide part of the metropolitan water consumption during the month

or various combinations of these factors.

The constraints on release policies include the following considerations:

1. Mean annual recharge is not to be less than the mean annual natural recharge.
2. To secure the irrigation water supply in a shallow leaky aquifer adjacent the stream in the upstream part of the recharge zone a minimum annual release $0.8 \times 10^6 m^3$ is required.
3. To discourage growth of algae and to a smaller extent reed beds, both of which may partially clog the streambed and reduce infiltration rates, drying periods are required.
4. The stream is the focus of a corridor of parks through residential areas. The parks attract large crowds in the summer months and the recreational value of releases at these times was considered.
5. The policy is to consist of monthly changes in release valve settings and release rates should be relatively easily calculated using data readily available to the reservoir keeper.
6. The policy should account for the existing recharge deficit at the date on which the rule is implemented with the view to produce a recharge credit over a finite number of years.

Computing CP time for a simulation run of eleven alternative policies for 360 months of stream discharges was 19 seconds for a FORTRAN IV program run on a CYBER 173 computer.

RESULTS

The policy resulting in the least pumping cost has a constant annual release, figure 6. It was expected that policies which reduced releases in dry years and increased them in wet years would have given lower pumping costs. Two factors militated against this. Firstly, the high demand on the reservoir requires between 77% and 86% of releases to be replaced by pumping. In the occasional wet year, when pumping is not required recharge must be substantially greater than the mean value in order to allow any significant reduction in dry year releases. This is compounded by the large amount of runoff from the catchment downstream of the dam in wet seasons. Hence reservoir releases compete with local runoff for the streambed intake capacity which has been reduced by the high discharges. Only a marginal increase in recharge results and unless spill occurs pumping would eventually be required to replace most of the released water.

Conjunctive operation of the aquifer and reservoir was also found to be economically less attractive than constant annual releases with no groundwater extraction for mains supplies. The potential reduction in spill and evaporation losses from the reservoir by artificial recharge enhancement in wet years using out-of-stream recharge facilities could not cover the cost of groundwater extraction. The viability of conjunctive operation is limited by the high commitment of the natural inflow of the dam to meeting the metropolitan water consumption, and the relative costs of inter-basin pumping and artificial recharge and extraction.

OPTIMAL RELEASE POLICY

The optimal release policy has a constant annual release of $1.5 \times 10^6 m^3$. The monthly release rates were assigned by satisfying constraints 2 to 4. This procedure implicitly satisfied constraint 5 and a simple arithmetic check showed that constraint 6 was observed. The distribution of the annual release between months had only a minor effect on recharge and a negligible effect on pumping costs. The mean annual recharge from dam seepage and downstream runoff is $0.2 \times 10^6 m^3$ and $0.5 \times 10^6 m^3$ respectively. The total mean annual recharge using the optimal release policy marginally exceeds the mean annual natural recharge of $2.2 \times 10^6 m^3$.

A test of the effect of monthly reservoir target levels on pumping and recharge for the optimal release policy revealed a negligible effect on recharge and significant changes in pumping costs. Lowering target levels increased the proportion of releases to be replaced by pumping, but decreased evaporation and spill resulting in reduced inter-basin pumping. This required larger pumping rates and increased the incidence of pumping in the dry season when pipeline capacity is at a premium.

CONCLUSIONS

Reservoirs on ephemeral streams allow recharge to be regulated and enhanced. In streams where hydraulic connection with underlying aquifers occurs the effect of regulation is more pronounced. A method of evaluating natural recharge and predicting recharge due to reservoir releases has enabled alternative release policies to be compared. This has been applied to the Little Para Reservoir in South Australia to find the most economical release policy. Conjunctive operation of the reservoir with aquifers was examined and found economically infeasible. The methods used could also be applied to reservoirs which do not receive water from other river basins, by making reliability of supply the objective function.

ACKNOWLEDGEMENTS

The Little Para Recharge Study was a joint study by the Engineering and Water Supply Department of South Australia and the Civil Engineering Department of the University of Adelaide. The author wishes to thank the Director-General, Engineer-in-Chief of the Engineering and Water Supply Department for permission to present this paper. Insofar as this report carries recommendations on proposals for action it must not be assumed from this paper that they form part of any approved policy.

REFERENCES

Dillon, P.J. (1983a). "Stream-aquifer interaction models: a review", Civ. Engg. Trans., I.E. Aust., Vol CE25, No 2, pp 107-113.

Dillon, P.J. (1983b). "Artificial groundwater recharge: a case study in Maharashtra India", University of Adelaide, Civil

Engg. Dept., Report G15.

Dillon, P.J. (1983c). "Little Para Recharge Study final report", University of Adelaide, Civil Engg. Dept, Report to Engineering and Water Supply Department of South Australia.

Dillon, P.J. and Liggett, J.A. (1983?). "An ephemeral stream-aquifer interaction model", Water Resources Research, paper submitted August 1982.

South Australia. Engineering and Water Supply Department, "Metropolitan Adelaide Water Resources Study", Volume 1, EWS 77/42, 1978, Chapter 5.

APPENDIX D.1

PROGRAM BIEMCAL DOCUMENTATION

Description

Program BIEMCAL uses the boundary integral equation method to solve potential flow problems in a 2-D vertical plane. It is particularly suited to porous media flow and can solve problems involving confined steady state flow or free surface transient flow in homogeneous isotropic porous media. It can account for recharge at the free surface and time-varying boundary conditions.

It gives comprehensive treatment of stream-aquifer interaction and allows for transition between hydraulic disconnection and hydraulic connection of an ephemeral stream with a semipermeable streambed. A mass balance check is performed at each time step and provision is made for shifting nodes on shifting boundaries.

Calibration and validation subroutines provide measures of model performance in simulating groundwater elevation changes at observation bores and stream discharge losses between gauging stations. Line printer or CALCOMP plots of groundwater elevation changes and stream discharge losses are available options.

Input

TAPE 5 - Control parameters, coordinates of boundary nodes and boundary element types.

TAPE 7 - Daily stream discharge and meteorological data (COMBMDP) (section 6.6.3).

TAPE 8 - Bore water elevation data (AHDFILE) (section 6.6.1).

Output

TAPE 6 - Line printer output of head and normal hydraulic gradient at each node, stream head, infiltration rates, number of connected nodes

components of mass balance and mass balance error at each time step. Optional summary table of selected parameters for all time steps. Optional line printer plot of prototype and model groundwater elevation changes and daily discharge losses.

TAPE 9 - Optional file of prototype and model discharge losses and selected independent variables. (Used for regression analysis of discharge loss residuals with BMDP Package. eg section 9.6)

PLOT - Optional CALCOMP (in-house flat bed plotter at Univ. of Adelaide) plot of prototype and model groundwater elevation changes at piezometers and discharge losses.

Note : For a description of control parameters and the format of input and output refer to the comments on the listing of BIEMCAL on the microfische. The listing distinguishes between code from the original seed program of Prof. J. Liggett, code written by the author and code (also by the author) which is used only in calibrating and validating the model.

Summary of Subroutine Functions

BIEMCAL (main program)

Reads conrol parameters, node coordinates and boundary element types and determines node types. Initializes all parameters and matrices. Contains time stepping loop (which solves for h and $\frac{\partial h}{\partial n}$ on the boundary) and checks at each time step whether a second iteration is required and if so initiates it. Supervises termination of time stepping and depending on control parameters calls subroutines for calibration or validation of the model with field data.

CNRANG - calculates corner angles for boundary nodes

ASSMBL - assembles matrix [E] and vector {c} of equation 4.27

SORT - sorts out each unknown as either h, $(\frac{\partial h}{\partial n})_1$ or $(\frac{\partial h}{\partial n})_2$

INTG - performs boundary integration to produce matrices [R] and [L] and vector {FCORN } of equation 4.56.

FDCOMP - rearranges matrix [E] of equation 4.27 for solving.

FSOLVE - rearranges vector {c} of equation 4.27, which now also includes {FCORN} of equation 4.57, and solves for the vector of unknowns

BETA - calculates the angle of slope of the free surface

CHECK - calculates components of mass balance for the time step and since the start (t=0) and finds the mass balance error (see section 4.6)

SHIFT - provides optional shifting of mid-side nodes on boundaries with moving end nodes (see section 4.7)

QUAD - gives quadratic interpolation for h and $\frac{\partial h}{\partial n}$ when shifting nodes (called only from SHIFT)

INTERP - interpolates head between nodes to correspond to bore positions (required only for calibration or validation runs, ICAL > 1)

MATCH - scans bore hydrographs produced by model to find model times at which elevation changes are equal to prototype elevation changes of the specified match points (only for stage I calibration, ICAL = 2, see section 9.2)

COMPARE - compares prototype and model match times to give estimate for time ratio hence K/n_e (only for stage I calibration, ICAL = 2, see section 9.2)

BOREFIT - reads observation bore water levels (from TAPE 8) and compares with model output and calculates statistics of fit, calls optional line printer or CALCOMP plots of bore prototype and model groundwater elevation changes (only for ICAL > 2, see section 9.3)

STREAM - reads daily stream discharge and meteorological data file, TAPE 7, and calculates prototype daily discharge loss and stream head for the model at the current time step (only for ICAL > 3, see section 9.4)

CORRELQ - estimates daily discharge at a gauging station using discharge from an upstream gauging station and mean dry weather discharge correlations (Table 8.1) when record is missing (called only from STREAM)

FLOWFIT - compares prototype and model daily discharge loss giving statistics of fit and optional line printer or CALCOMP plot (only for ICAL > 3). Determines best estimate for K (for stage III calibration, ICAL = 4, see section 9.4). Validates model when ICAL = 5, see section 9.5. Produces file (TAPE 9) for discharge loss residual regression analysis (see sections 9.6 and 9.8.8) when ICAL > 5.

LPLOT - performs line printer plot of superimposed prototype and model groundwater elevation changes or discharge losses (called from BOREFIT and STREAMFIT)

TCOMP - a function which adjusts streambed hydraulic impedance according to water temperature (see sections 9.7 and 9.8.9) when ICAL = 7.

PROGRAM BIEMCAL FLOWCHART

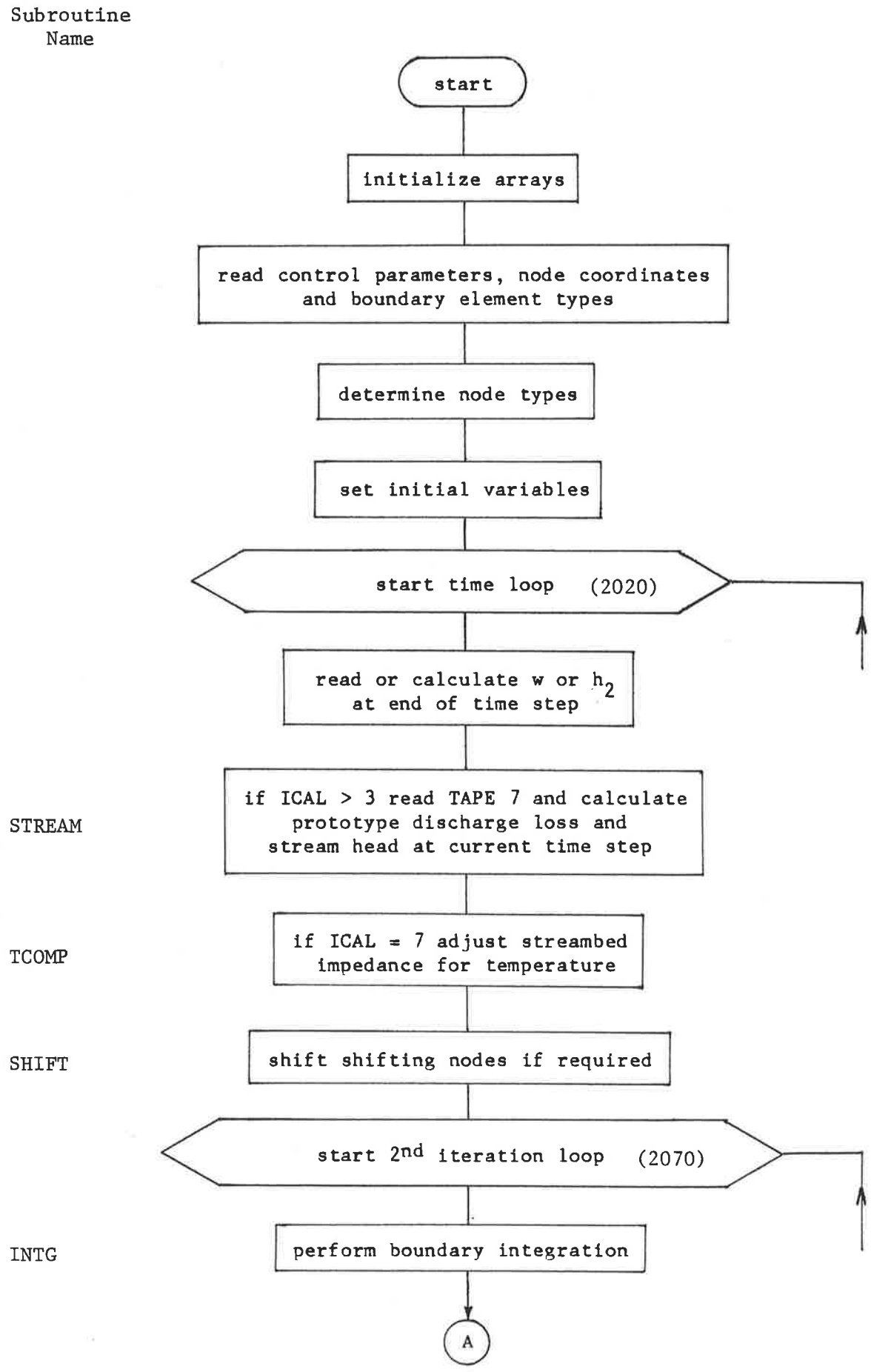

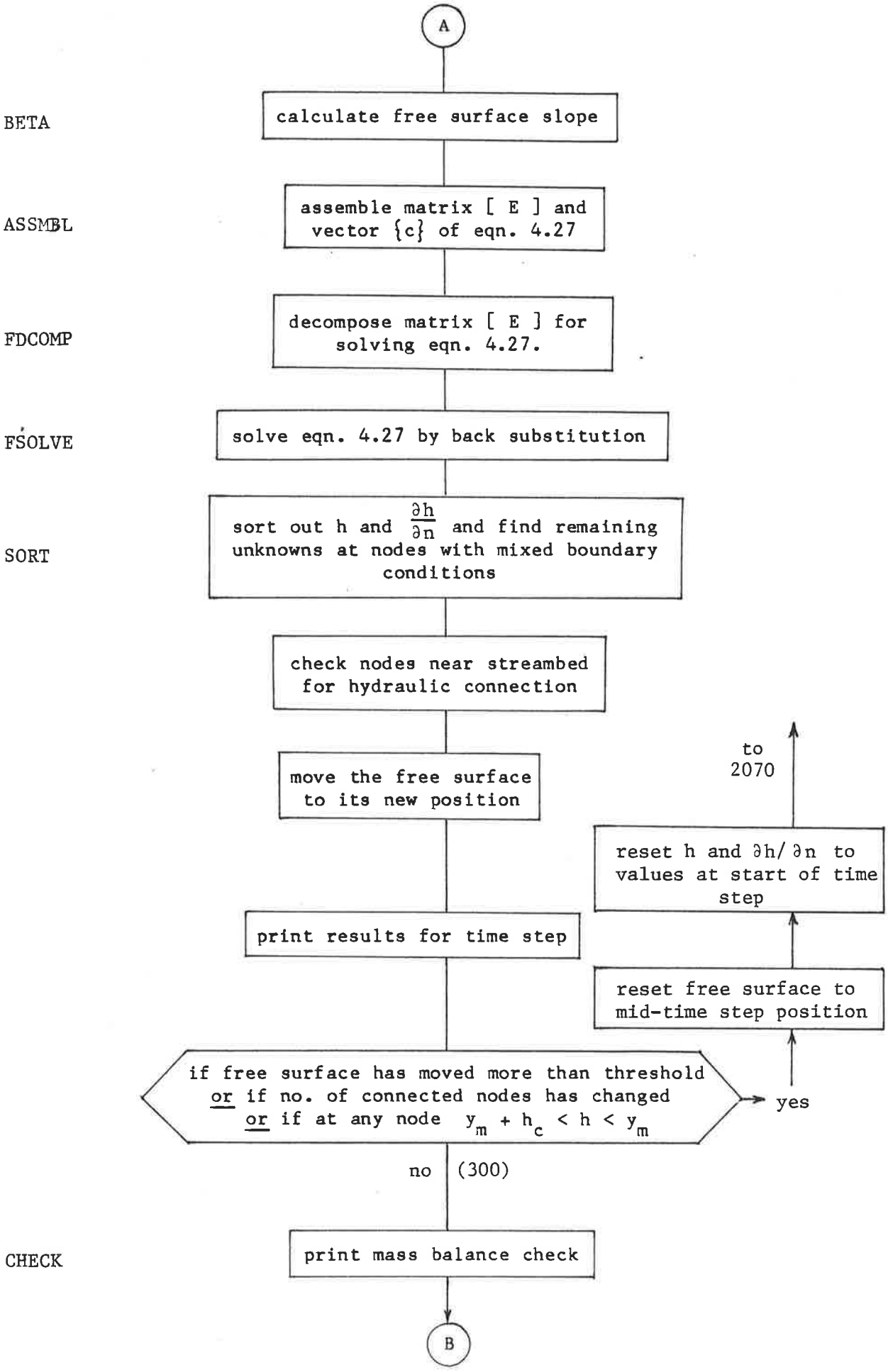
A
BETA
calculate free surface slope
ASSMBL
assemble matrix [E] and vector {c} of eqn. 4.27
FDCOMP
decompose matrix [E] for solving eqn. 4.27.
FSOLVE
solve eqn. 4.27 by back substitution
SORT
sort out h and ∂h/∂n and find remaining unknowns at nodes with mixed boundary conditions
check nodes near streambed for hydraulic connection
move the free surface to its new position
print results for time step
if free surface has moved more than threshold or if no. of connected nodes has changed or if at any node $y_m + h_c < h < y_m$
yes
to 2070
reset h and ∂h/∂n to values at start of time step
reset free surface to mid-time step position
no
(300)
CHECK
print mass balance check
B

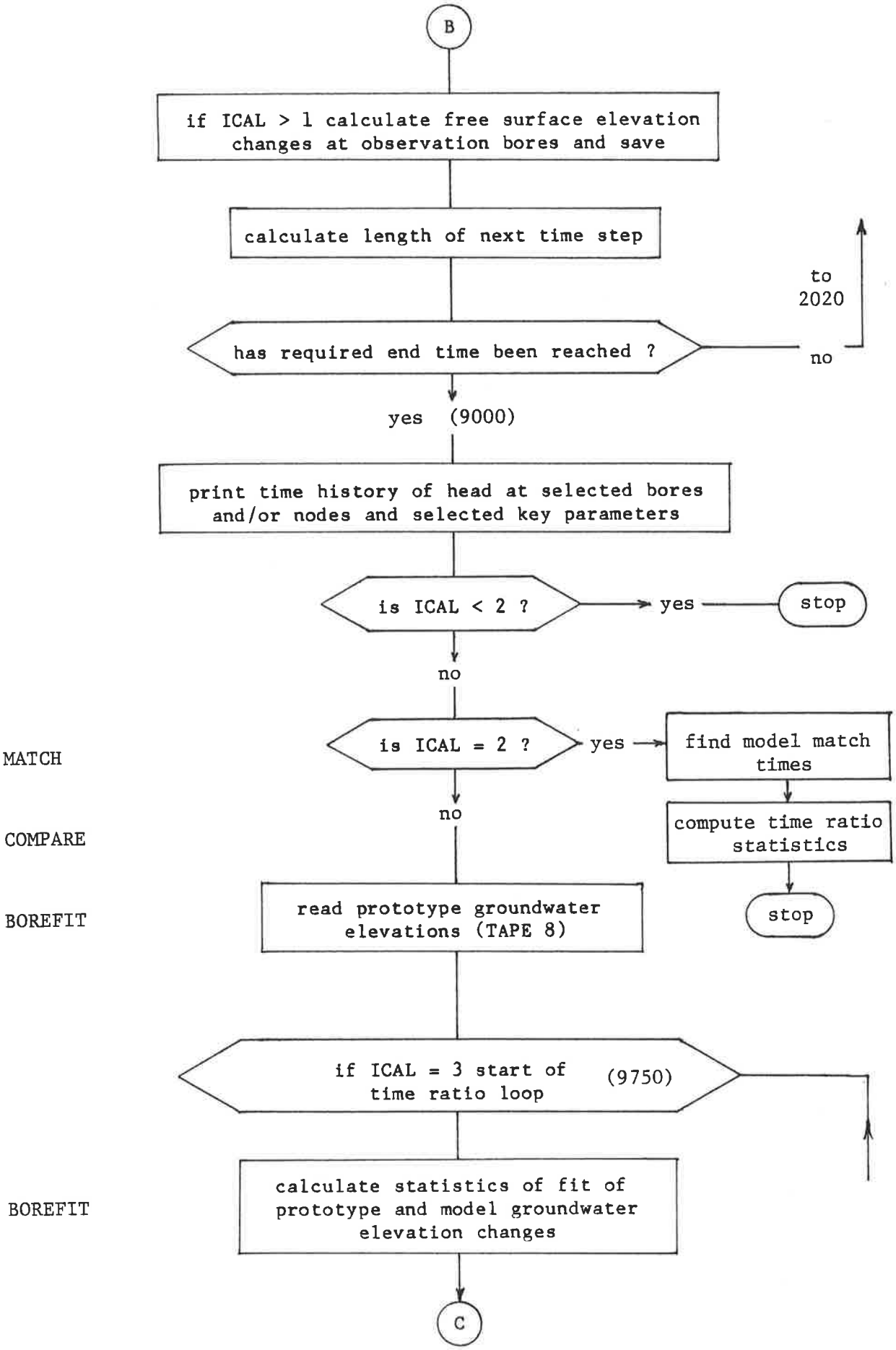
B
if ICAL > 1 calculate free surface elevation changes at observation bores and save
calculate length of next time step
to 2020
has required end time been reached ?
no
yes (9000)
print time history of head at selected bores and/or nodes and selected key parameters
is ICAL < 2 ?
yes
stop
no
MATCH
is ICAL = 2 ?
yes
find model match times
no
COMPARE
compute time ratio statistics
stop
BOREFIT
read prototype groundwater elevations (TAPE 8)
if ICAL = 3 start of time ratio loop (9750)
BOREFIT
calculate statistics of fit of prototype and model groundwater elevation changes
C

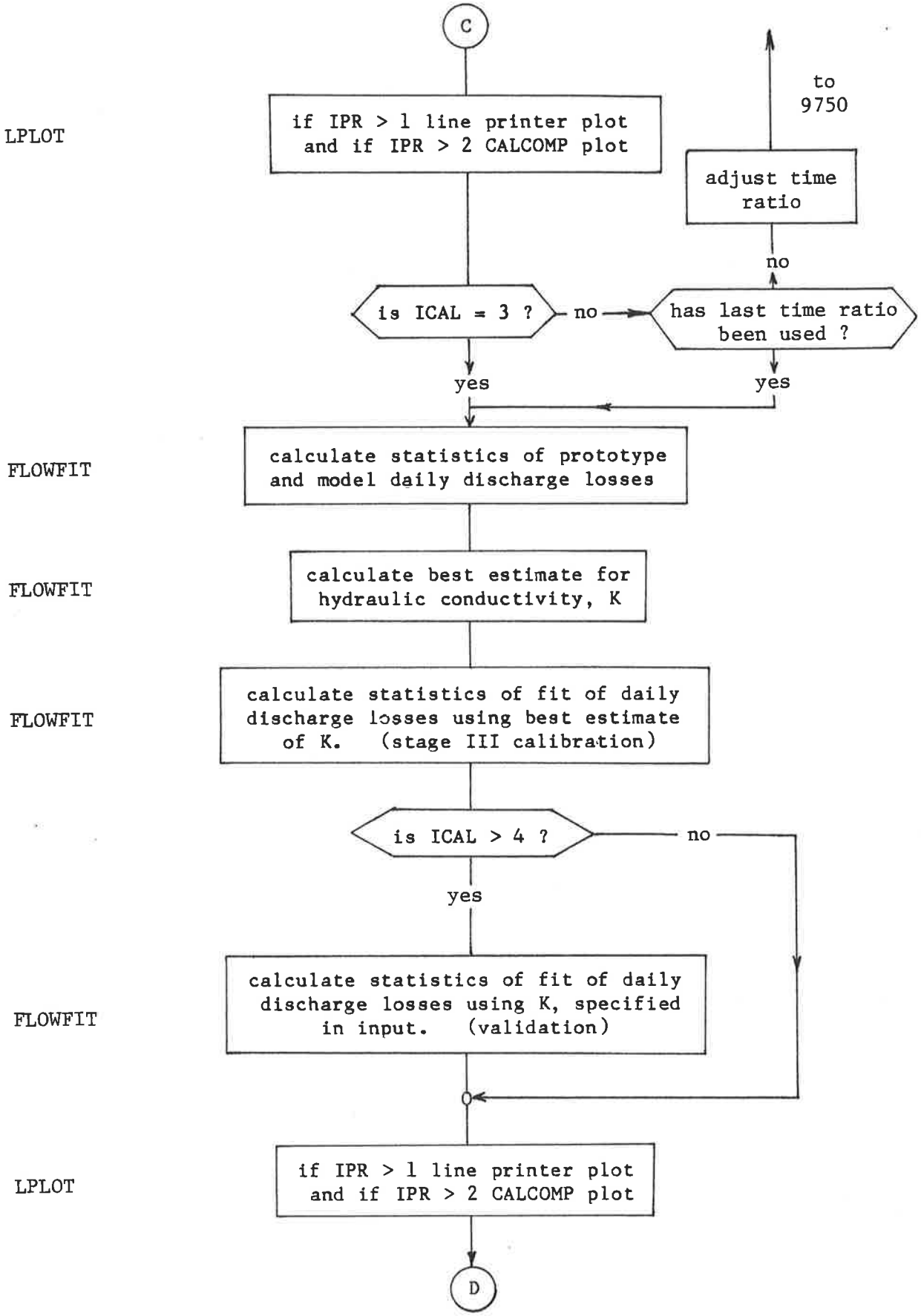
C
LPLOT
if IPR > 1 line printer plot
and if IPR > 2 CALCOMP plot
is ICAL = 3 ?
no
has last time ratio
been used ?
yes
yes
no
adjust time
ratio
to
9750
FLOWFIT
calculate statistics of prototype
and model daily discharge losses
FLOWFIT
calculate best estimate for
hydraulic conductivity, K
FLOWFIT
calculate statistics of fit of daily
discharge losses using best estimate
of K. (stage III calibration)
is ICAL > 4 ?
no
yes
FLOWFIT
calculate statistics of fit of daily
discharge losses using K, specified
in input. (validation)
LPLOT
if IPR > 1 line printer plot
and if IPR > 2 CALCOMP plot
D

FLOWFIT

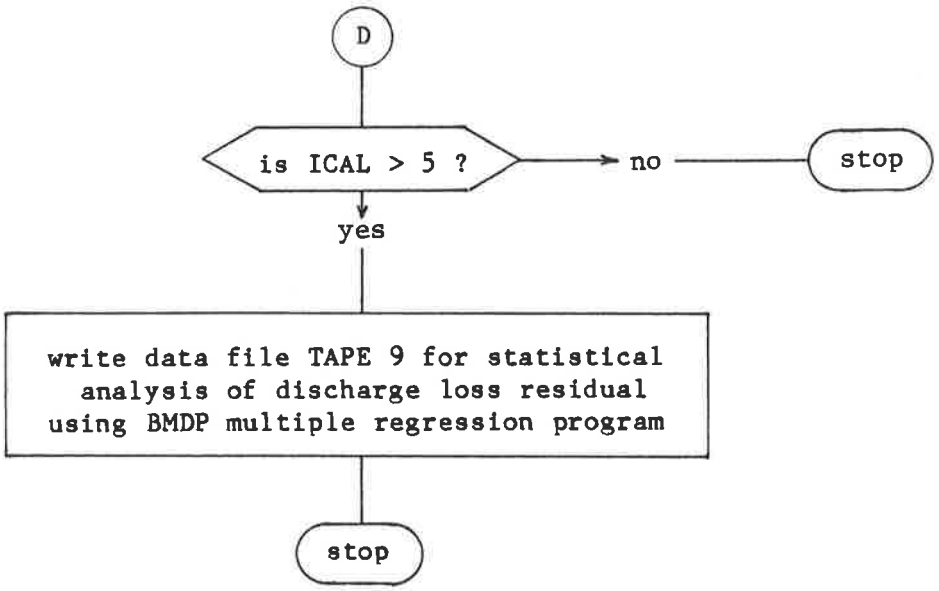
D
is ICAL > 5 ?
no
stop
yes
write data file TAPE 9 for statistical analysis of discharge loss residual using BMDP multiple regression program
stop

APPENDIX D.2

DOCUMENTATION OF MAIN DATA PROCESSING PROGRAMS

Description

A suite of programs was written to perform data checking, editing, tabulating, plotting, interpolation, statistical description and various transformations. These functions are described in section 6.6 and a brief resume is given in Table D2.1.

These programs originated from a multipurpose program which evolved as data processing needs were defined and successively refined. Eventually the program grew cumbersome to modify and its efficiency in accomplishing any one function was impeded by its size. Hence the base program was subdivided into a number of separate entities each having a limited number of functions. This improved the efficiency of computer execution times considerably. A legacy of the common origin of the programs is that substantial amounts of code, whole subroutines in particular, are identical in some programs.

A listing of each program is given on the microfische. To avoid repetition in listing subroutines these are given only once (in alphabetical order) at the end of the eight program listings. Slight variations in code to satisfy particular requirements of the calling programs occur in subroutines named GRF and SETUP. Where this occurs both versions are listed and the program to which each belongs is indicated. The set of subroutines called by each program is shown in its listing. This information also appears in Table D2.2.

TABLE D2.1

Summary of input, output and functions of data processing programs.

Program	Input	Output	Function
BPL	GLFILE	list of suspect data and predicted values	manual bore water depth readings checked using a 2-stage error detection algorithm
BAHD	GLFILE	AHDFILE	subtract depth to water from AHD elevation of top of bore casing
BPLOT	AHDFILE	CALCOMP plot of bore hydrographs	plot selected bore hydrographs on A4 graphs (eg. figure 6.5)
BSTAT	AHDFILE	table of statistics of bore water levels	tabulates Aust. map grid coords. no. of obs., range, mean, etc. for all observation bores
BORFL	AHDFILE	table of groundwater elevations at all obs bores on selected dates	interpolates all obs bore water levels at regular intervals and prints table (assists plotting of contour maps)
QPL	STNREC	STBMDP, calendars of daily discharge, plots of discharge	from stream stage file calculate daily discharge at all recording gauging stations, tabulates and plots daily discharge for study period
EPL	METALL	METBMDP, calendars and plots of daily rainfall and evaporation	tabulates and plots meteorological data which is integrated over time periods
EPLT	METALL	METBMDP, calendars and plots of daily temperature and air pressure	tabulates and plots meteorological data which is averaged over time periods

TABLE D2.2

Subroutines used by data processing programs.

Program	Subroutines
BPL	AHD DATE DECDAY GRF ICSMOU MINMAX SFOWN SMOOTH.
BAHD	DATE DECDAY GRF IREF READREF SETUP.
BPLOT	DATE DECDAY GRF IREF READREF SETUP.
BSTAT	DATE DECDAY GRF IREF MINMAX READREF SETUP.
BORFL	CONST DATE IREF READREF.
QPL	DATE DECDAY FLORATE GRAPH MINMAXL RATING SETUP.
EPL	DATE DECDAY GRAPH MINMAXL NDAYF SETUP.
EPLT	DATE DECDAY GRAPH MINMAXL NDAYF SETUP.

Summary of Subroutine Functions

AHD - function assigning bore casing elevation to bore number

CONST - interpolates between observations to find groundwater elevations on specified days, tests time span between readings to check validity of interpolated values

DATE - given day number calculate the date

DECDAY - given date and time calculate day number with decimal fraction

FLORATE - given station rating and stream stage calculate discharge rate

GRAPH - plots graphs on one pair of axes to common scales

GRF - prints headings on bore water elevation plots

ICSMOU - (IMSL LIBRARY SUBROUTINE) data smoothing by error detection with cubic spline

IREF - finds an index no. for a bore to determine its map coordinates and datum elevation from table set up in READREF

MINMAX - finds minimum and maximum elements in an array

MINMAXL - as for MINMAX when maximum may be undefined or data is missing

NDAYF - given a date calculate the day number (integer)

RATING - given a gauging station select constants for discharge rating - up to 3 indept. sub-range ratings allowed

READREF - read all bore coordinates and datum elevations from file TAPE 9

SETUP - (from BPLOT) plot standard sheet for bore hydrographs

- (from QPL) plot standard sheet for gauging station hydrographs or meteorological records

SFOWN - calculates origin and scale factors for plots based on range of data and specified maximum axis lengths

SMOOTH - performs linear interpolation test to give first estimate of the number of gw level observations in error then calls IMSL subroutine ICSMOU which uses this estimate in cubic spline data smoothing

In addition to these subroutines calls are made to some in-house CALCOMP plotter subroutines. (Some of these are also used in program BIEMCAL.) These include:

AXIS - draws axis in specified position with specified scale

LINE - draws line connecting specified coordinate pairs

NUMBER - allows numbers to be drawn on plot

PAUPLOT - gives instructions to plotter operator

PLOT - moves pen to specified coordinates

PLOT25 - initiates all calls to the 25cm wide CALCOMP plotter

SYMBOL - allows words and symbols to be drawn on plot

PROGRAM BPL FLOWCHART

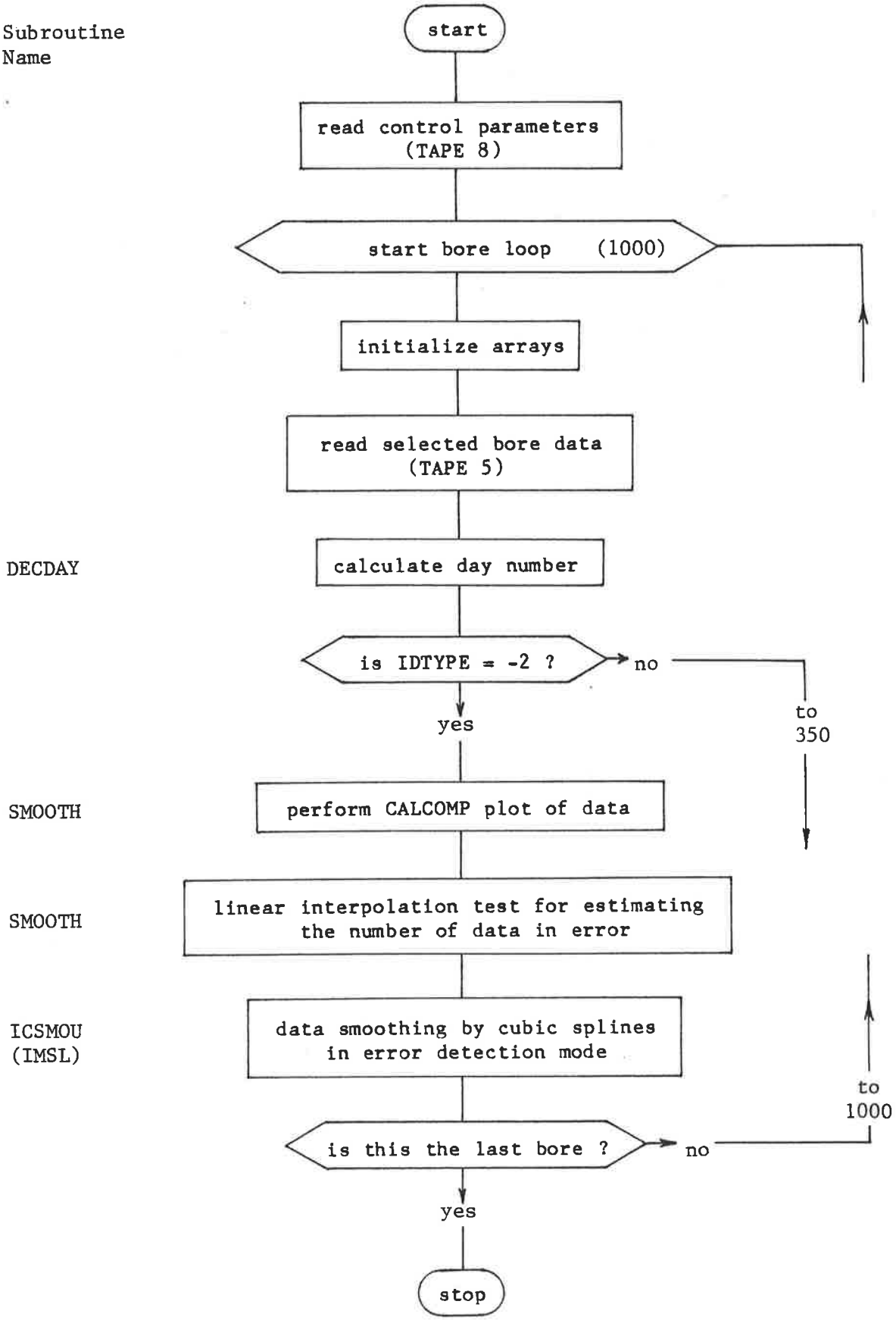

GRF

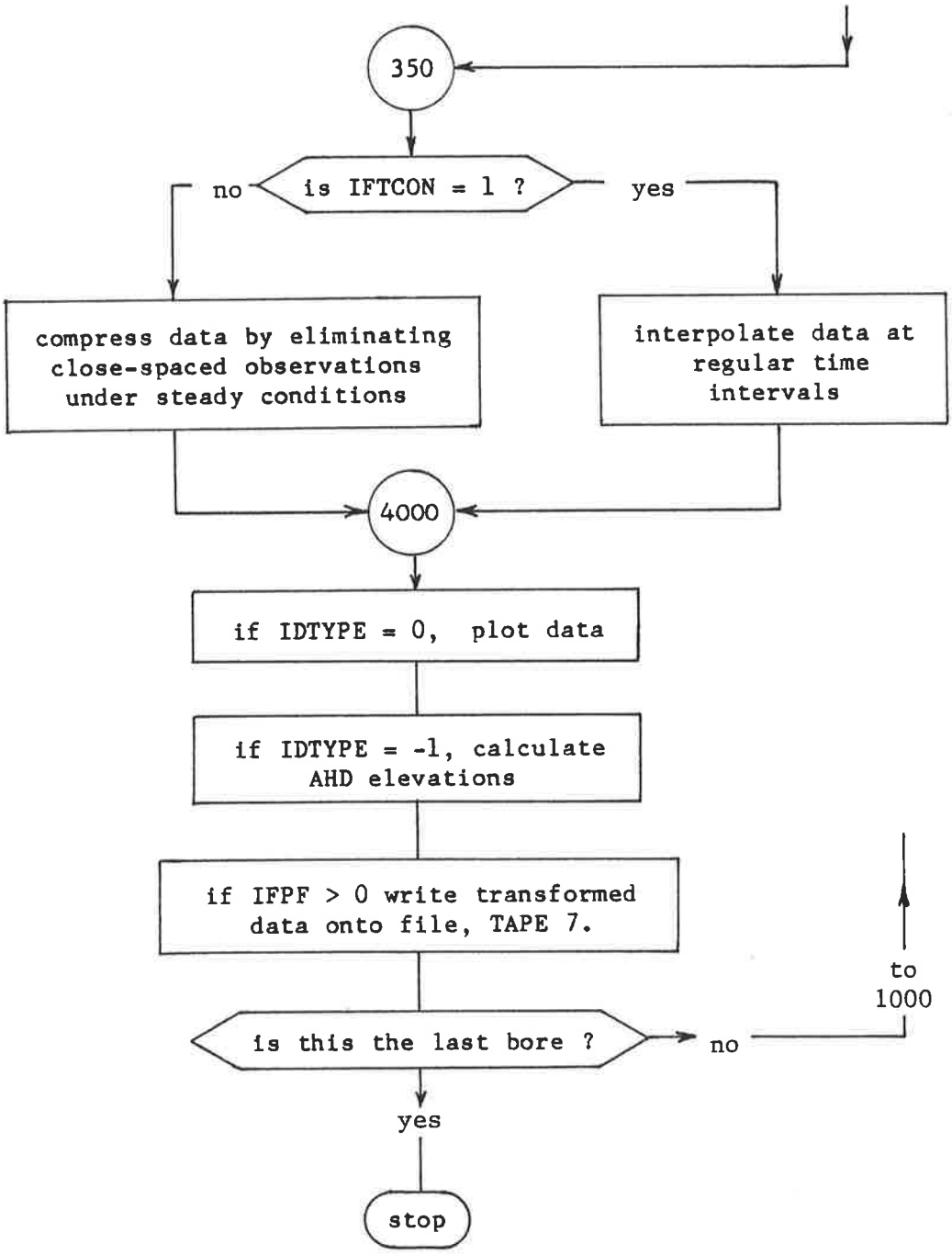
350
is IFTCON = 1 ?
no
yes
compress data by eliminating close-spaced observations under steady conditions
interpolate data at regular time intervals
4000
if IDTYPE = 0, plot data
if IDTYPE = -1, calculate AHD elevations
if IFPF > 0 write transformed data onto file, TAPE 7.
is this the last bore ?
no
to 1000
yes
stop

PROGRAMS BAHD and BPLOT FLOWCHART

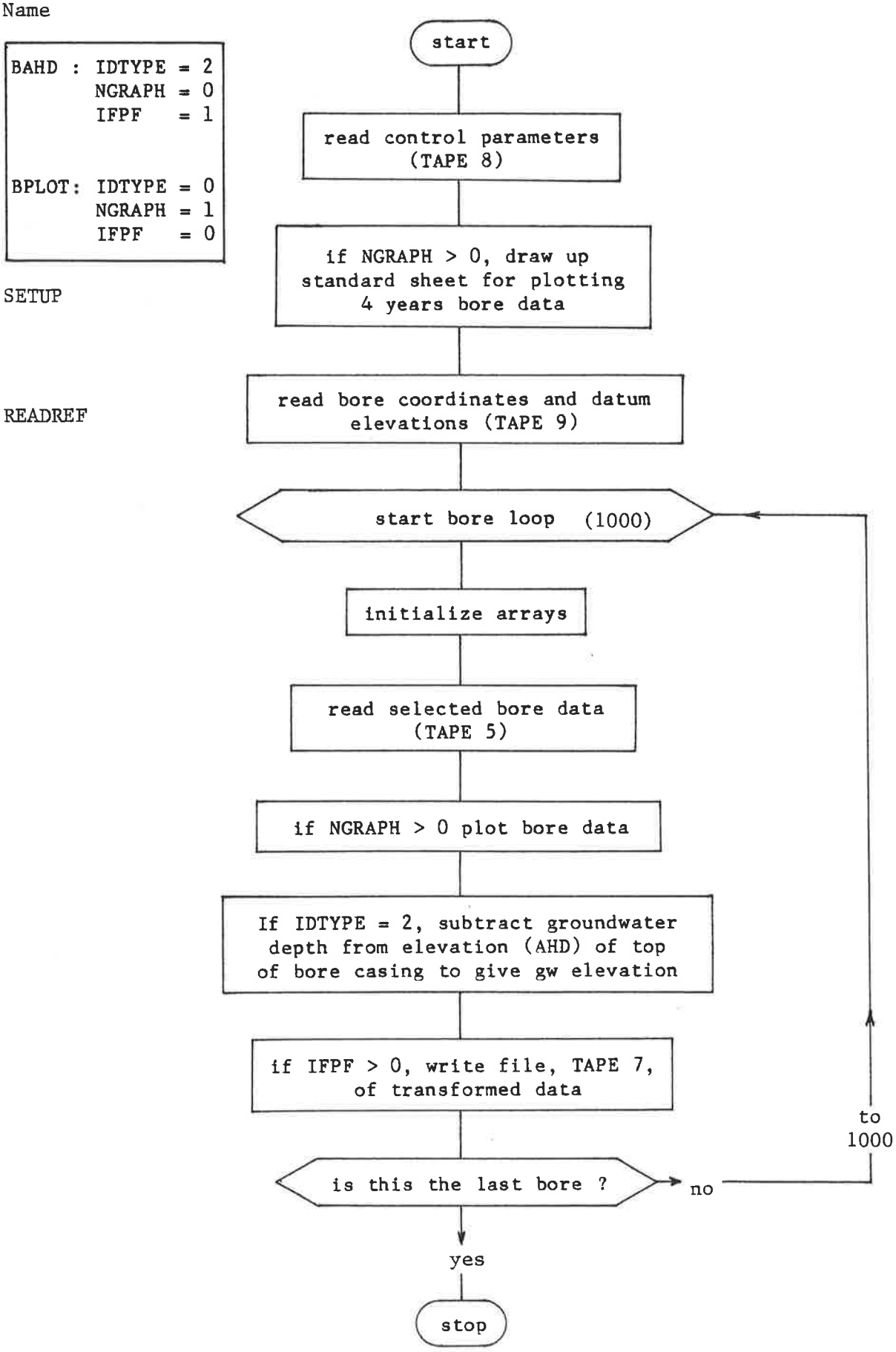

PROGRAM BSTAT FLOWCHART

Subroutine Name

READREF

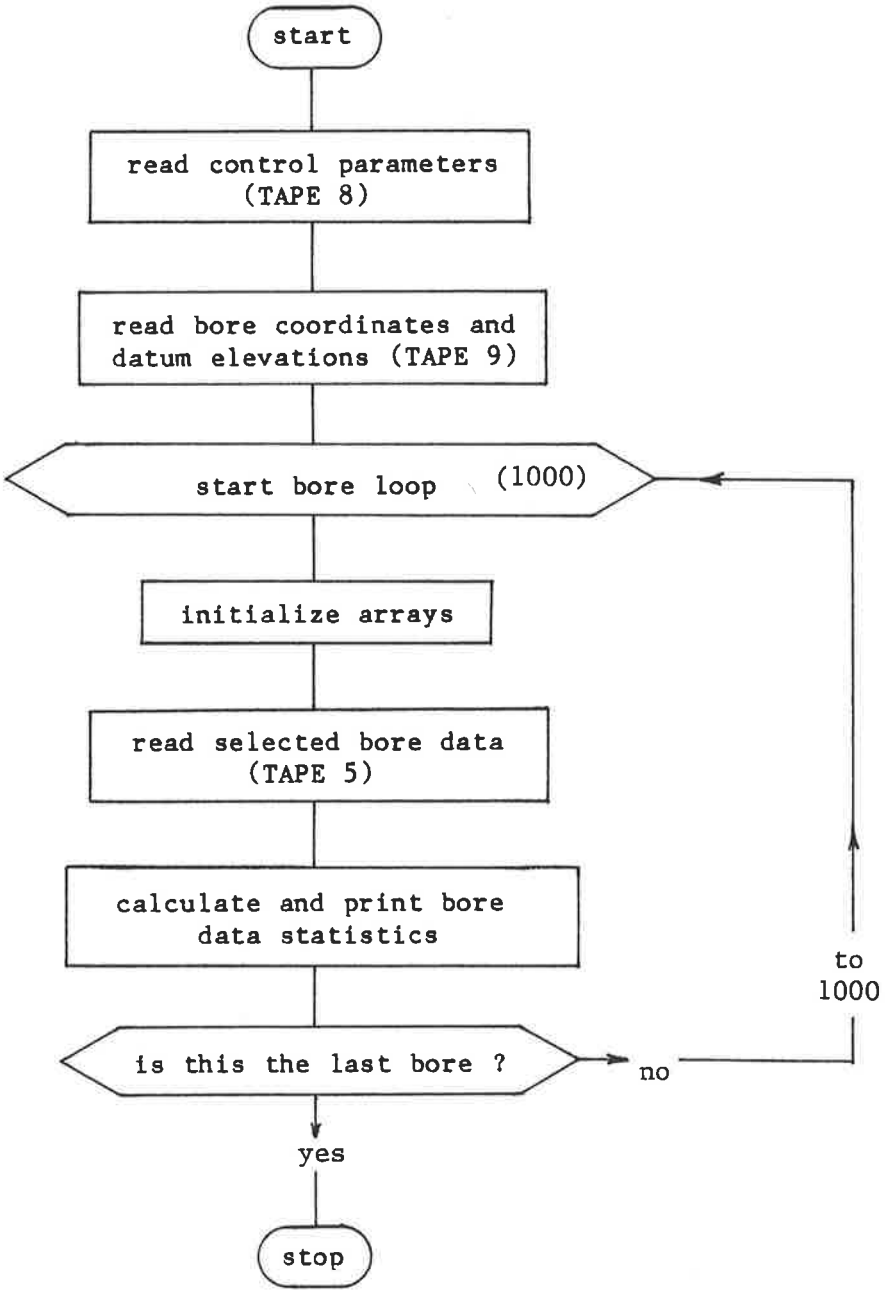

PROGRAM BORFL FLOWCHART

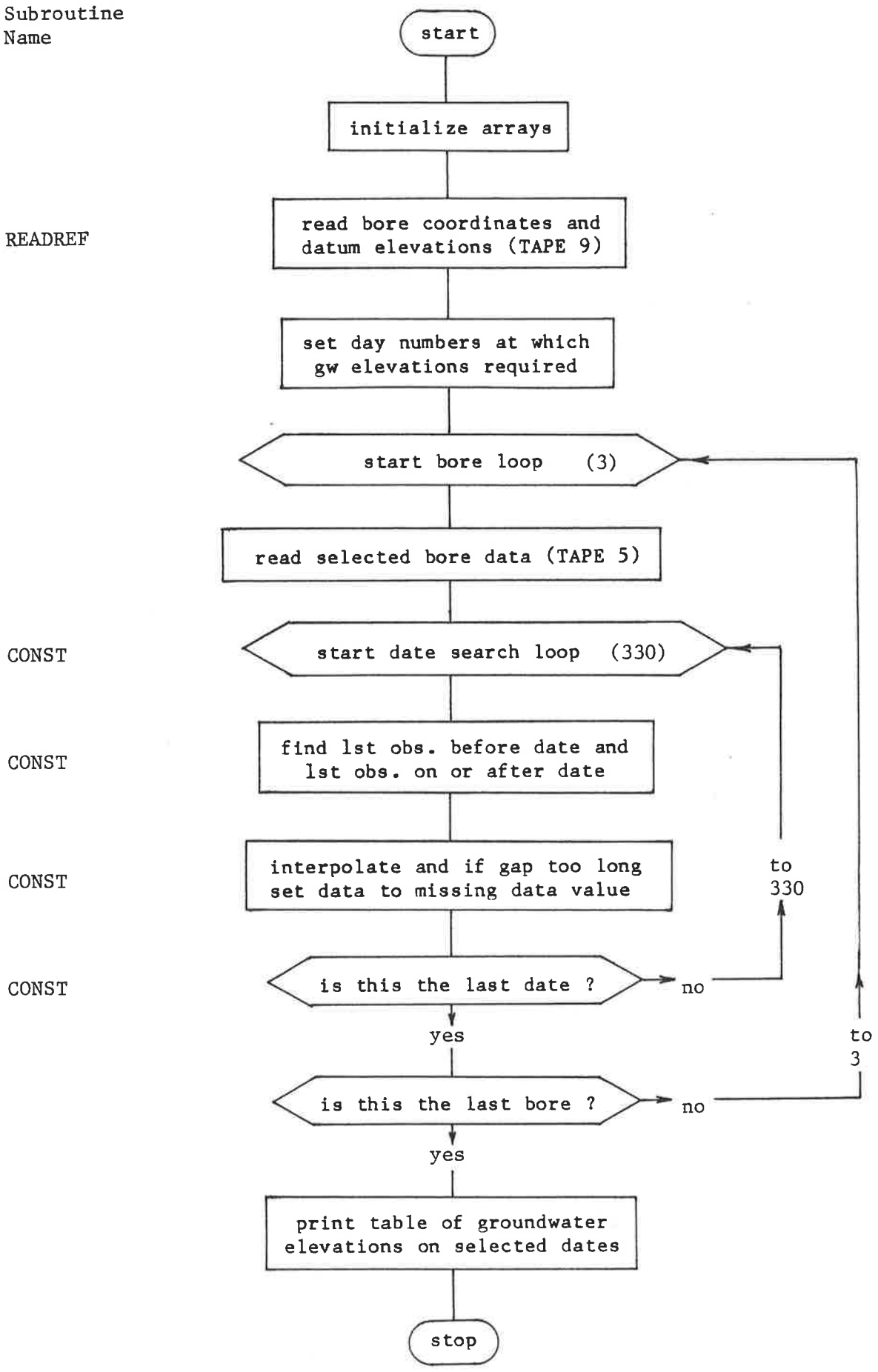

PROGRAM QPL FLOWCHART

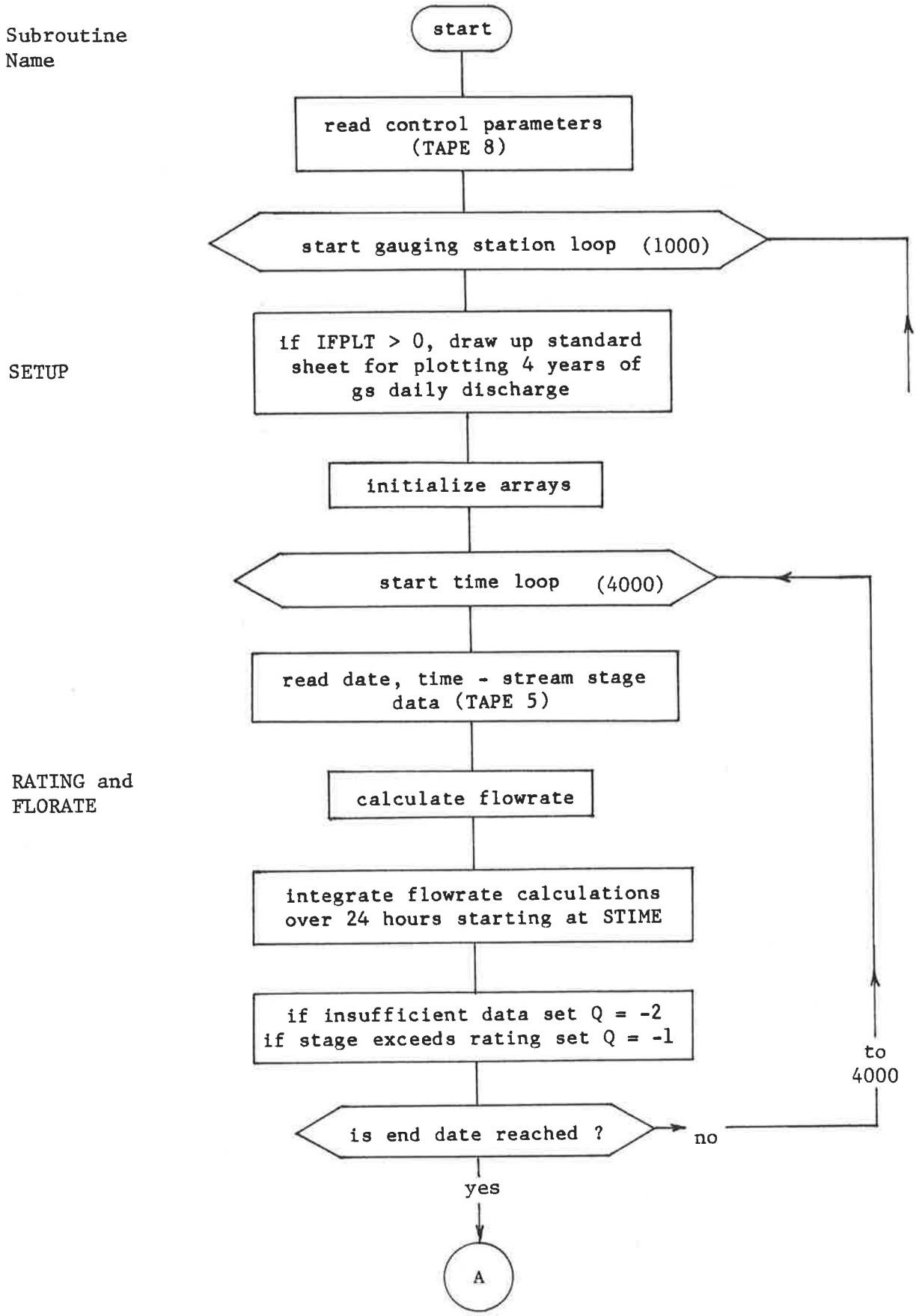

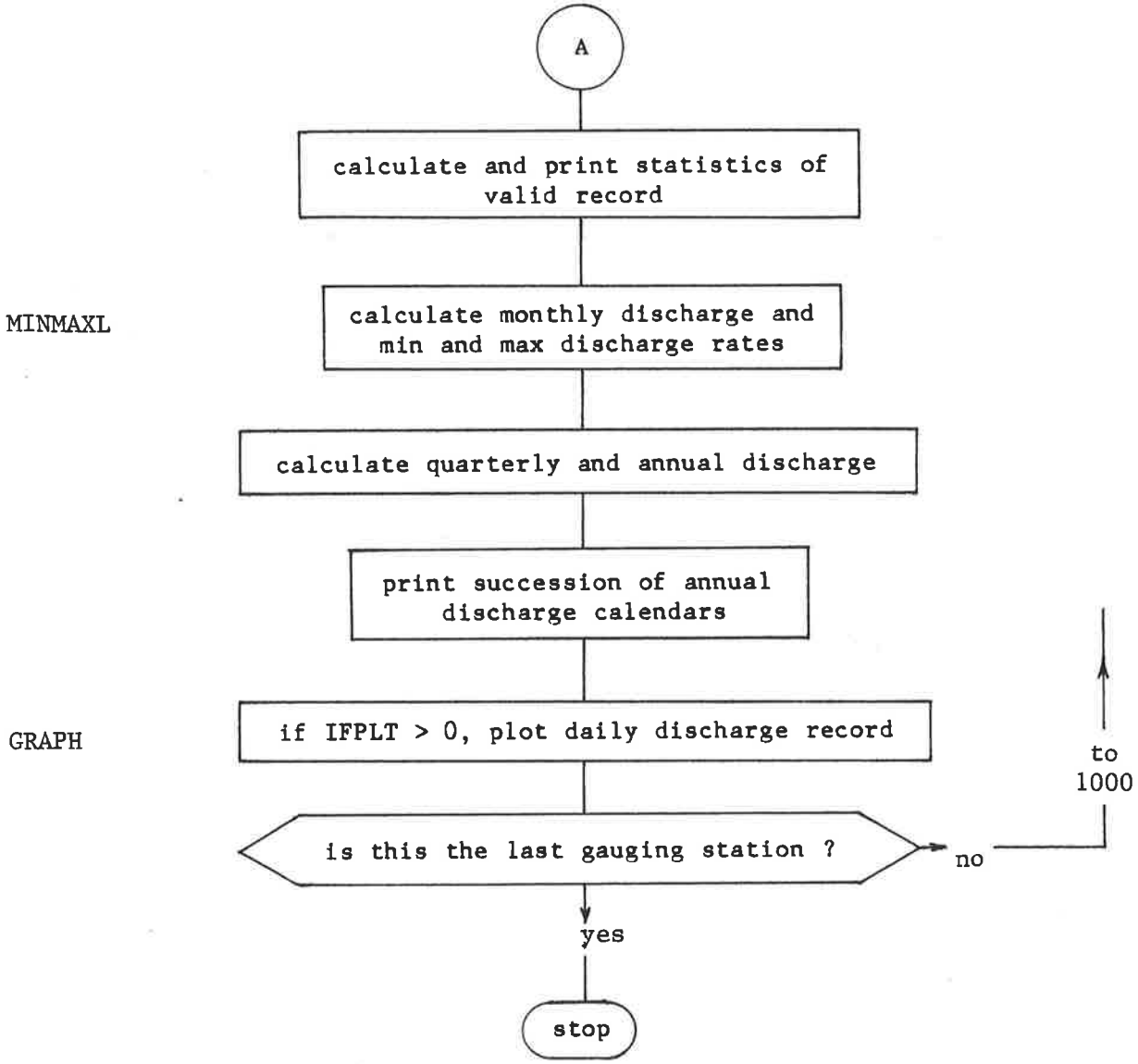
A
calculate and print statistics of valid record
MINMAXL
calculate monthly discharge and min and max discharge rates
calculate quarterly and annual discharge
print succession of annual discharge calendars
GRAPH
if IFPLT > 0, plot daily discharge record
is this the last gauging station ?
no
to 1000
yes
stop

PROGRAMS EPL and EPLT FLOWCHART

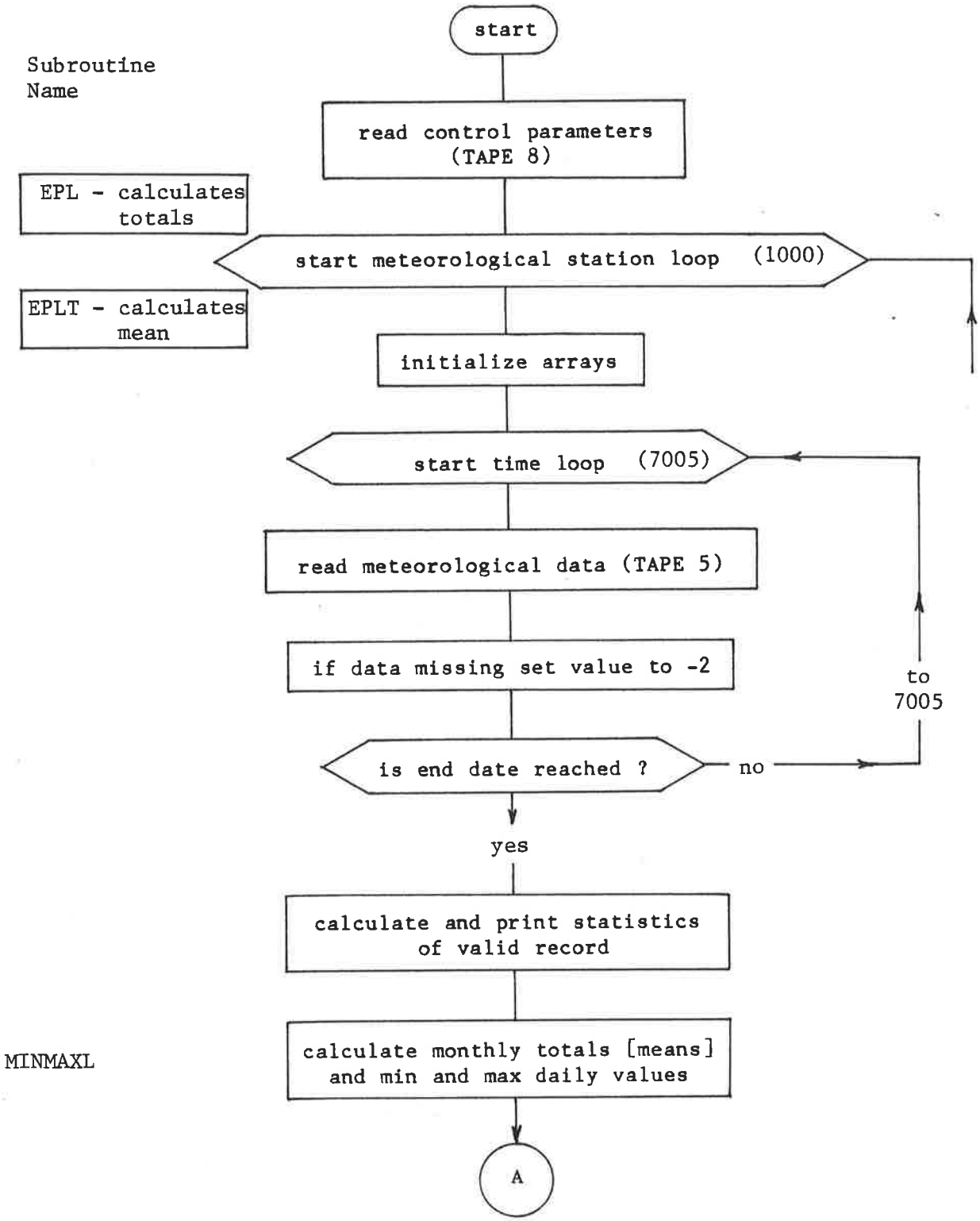

SETUP and GRAPH

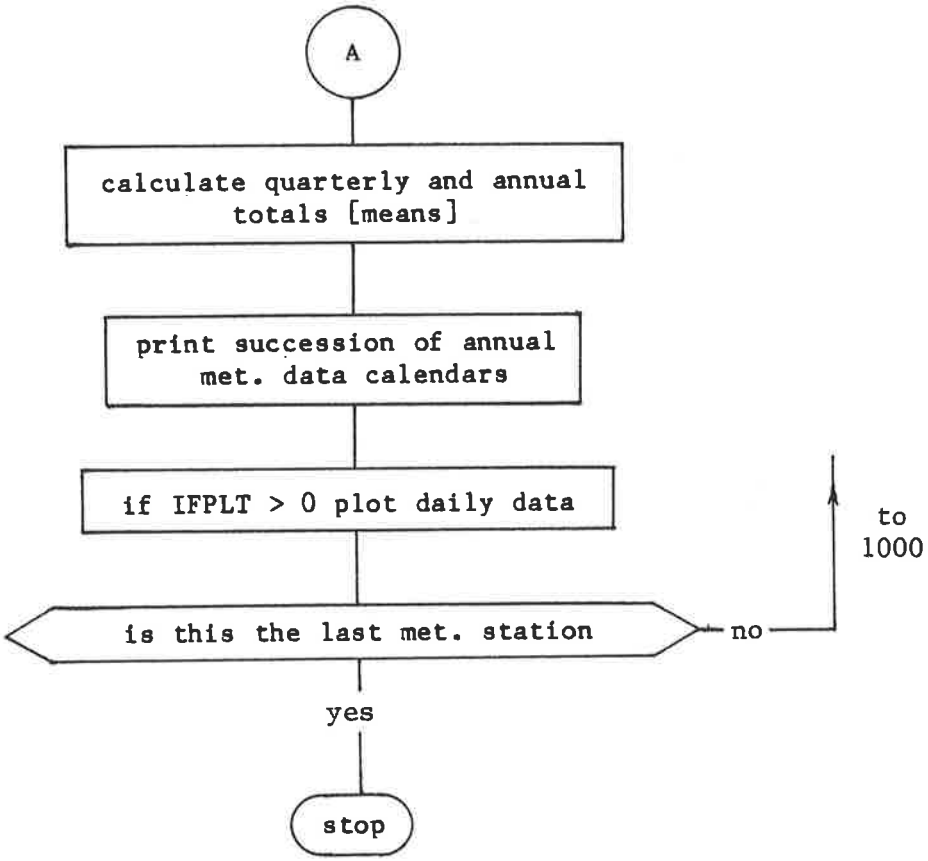

APPENDIX D.3

PROGRAM DAMSIM DOCUMENTATION

Description

Program DAMSIM simulates the operation of a water supply reservoir which acts as a pumped storage and also receives catchment inflow. The reservoir is required to release water to recharge aquifers associated with the river on which it lies. Alternative reservoir release policies are similated to determine their effect on groundwater recharge and pumping cost.

The model can account for artificial recharge facilities to augment the streambed and can allow for groundwater extraction to supply some of the reservoir water demand. It considers recharge attributed to releases, dam leakage and runoff from the downstream catchment. Allowance is made for reservoir evaporation and evapotranspiration from the streambed. Using the concept of equivalent uniform flow (figure 8.4) the recharge which would have occured without the dam can be estimated.

The model was applied, using monthly time steps, to the Little Para Reservoir and the Northern Adelaide Plains aquifers enabling a release rule satisfying all recharge constraints and minimizing pumping costs to be identified. This operating policy has subsequently been adopted by the Engineering and Water Supply Department of South Australia.

Input

TAPE 5 - Control parameters, constants and specified variables. Monthly demand on reservoir and aquifer, target end of month reservoir volumes, monthly evaporation and mean temperature, monthly pipeline capacity availability, expected (median) monthly discharge at gauging station 3 and historical or synthetic monthly discharge record at gauging station 3 (see figure 6.1).

Output

TAPE 6 - Mean annual flow components, frequency of spill and failure of reservoir to meet demand, mean annual pumping costs for each release policy. Summary table of these principal statistics for all release policies.

Summary of Subroutine Functions

DAMSIM (main program)

Reads control parameters, constants and data; initializes parameters and matrices; contains release policy loop (to iterate through a range of policy types); runs through monthly discharge record simulating reservoir operation in monthly time steps; prints table of flow components and costs for each release policy and one summary table for all release policies.

RECH - calculates recharge capacity of streambed based on antecedent discharge and using figure 8.3.

- ENTRY QlREL - calculates recharge due to reservoir release
- ENTRY ERN - calculates natural recharge which reservoir inflow would have given if there was no dam
- ENTRY CRN - calculates recharge occurring due to dam seepage and runoff from the catchment downstream of the dam
- ENTRY ECN - calculates the recharge due to expected (median monthly) discharge from the catchment downstream of the dam

RELPOL - selects the release rate and the groundwater extraction rate according to the assigned release policy number (IREL) descriptions of release policies appear later

EVAP - a function to calculate evaporation loss from the reservoir

EQVQN - a function to calculate the equivalent uniform flow which produces the same stream discharge loss as the natural reservoir inflow (or the expected inflow, as required) using figure 8.4.

Release Policies

The monthly reservoir release, Q1, is determined according to a release policy number, IREL. Each policy has one or more constants which are defined in the program input file, TAPE 5. A full sensitivity analysis of all constants and model parameters was not performed, however the values assigned to constants were varied to improve the ratio of mean annual recharge to pumping cost. The range of possible policy types is large and those listed here and contained in program DAMSIM are intended to be a representative sample.

IREL=0 constant release rate (=C4)

IREL=1 release discharge loss capacity of streambed and artificial recharge ponds, QCAP, minus the expected recharge from downstream runoff, CEN (which approximates expected equivalent uniform monthly downstream discharge). ie. mimimize water wastage while maximizing groundwater recharge.

IREL=2 fixed monthly releases with an annual pattern based on estimated mean monthly flow losses from a report by Kingston and Shepherd (1973).

IREL=3 set the release as a function of reservoir natural intake in the preceding month, see figure D3.1, after release rule A of Dillon (1977).

IREL=4 as for IREL=3 for summer months but for winter months (April to September) the range of release rates is restricted, see figure D3.1, after release rule B of Dillon (1977).

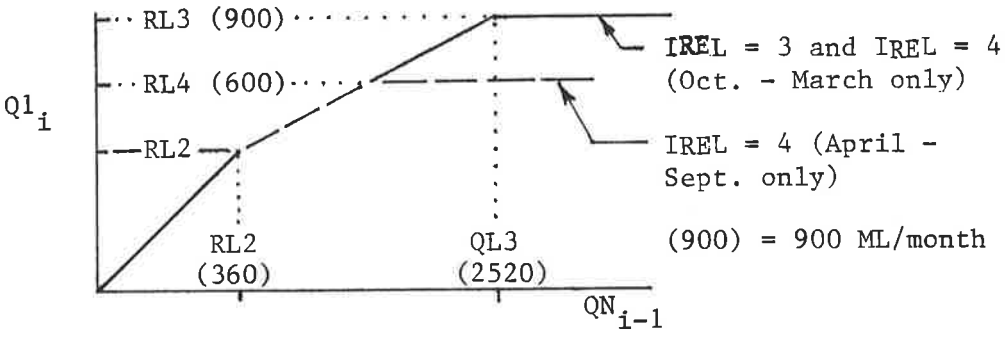

Figure D3.1 Release related to natural reservoir intake in the preceding month for policies IREL = 3 and 4.

IREL=5 if reservoir storage is lower than target at end of previous month, no release (unless there have been 4 consecutive months without releases in which case release nominal discharge, RL11). If reservoir has potential to spill, release (QCAP-CEN), if reservoir storage is in intermediate range, release a fraction, RL12 of (QCAP-CEN) unless releases have been continuous over 4 months (then no release).

IREL=6 adjust release rate (QCAP-CEN) if pumping rate into reservoir exceeds PCRIT (the rate above which the unit cost of pumping increases). Release rate reduces from (QCAP-CEN) to zero as pumping rate increases from PCRIT to PMAX, the pipeline capacity.

IREL=7 as for IREL=6 and in addition groundwater extraction is allowed to supply up to half the reservoir demand (constrained also by groundwater extraction capacity for mains supply and an arbitrary deficit limit on the difference between actual recharge minus groundwater extraction and recharge which would have occurred without the dam).

IREL=8 as for IREL=5 but in the intermediate range of reservoir storage no limit is imposed on continuous releases and if a recharge deficit (as defined above) exists the release rate is (QCAP-CEN).

IREL=9 if reservoir storage exceeds the target at the end of the previous month release (QCAP-CEN). Otherwise no release (unless there have been 4 consecutive months without releases in which case release RL11) and groundwater extraction may supply up to half the reservoir demand subject to the same constraints as in IREL=7.

IREL=10 release the equivalent uniform monthly flow of the reservoir natural intake in the current month. This simulates the natural recharge which would have occurred without the dam.

IREL=11 as for IREL=10 using the historical discharge record until the reservoir began impounding water in July 1977. Thereafter release according to the historical release record, contained in vector, RREAL.

variations on above:

0/125 as for IREL=0 with C4=125 ML/month.

10/opt as for IREL=10 except that releases do not exceed the discharge loss capacity, QCAP.

P5 fixed monthly releases pulsed to give recharge adjacent market gardening areas. Obtained by substituting values of Table 8.6 for vector, SHEP in IREL=2.

Table 8.4 contains mean annual recharge and pumping costs for each of the above policies where each constant is assigned a specific value defined in Dillon (1983a). Figure 8.9 shows a graph of pumping cost versus recharge for the subset of these policies which give the most cost efficient recharge. The recommended policy (Table 8.6) gives the most cost efficient recharge of all policies tested which satisfied all constraints. It is not claimed that this is a globally optimum policy, but it is simple and has been adopted by the Engineering and Water Supply Dept. of South Aust. for operating releases from the Little Para Reservoir.

PROGRAM DAMSIM FLOWCHART

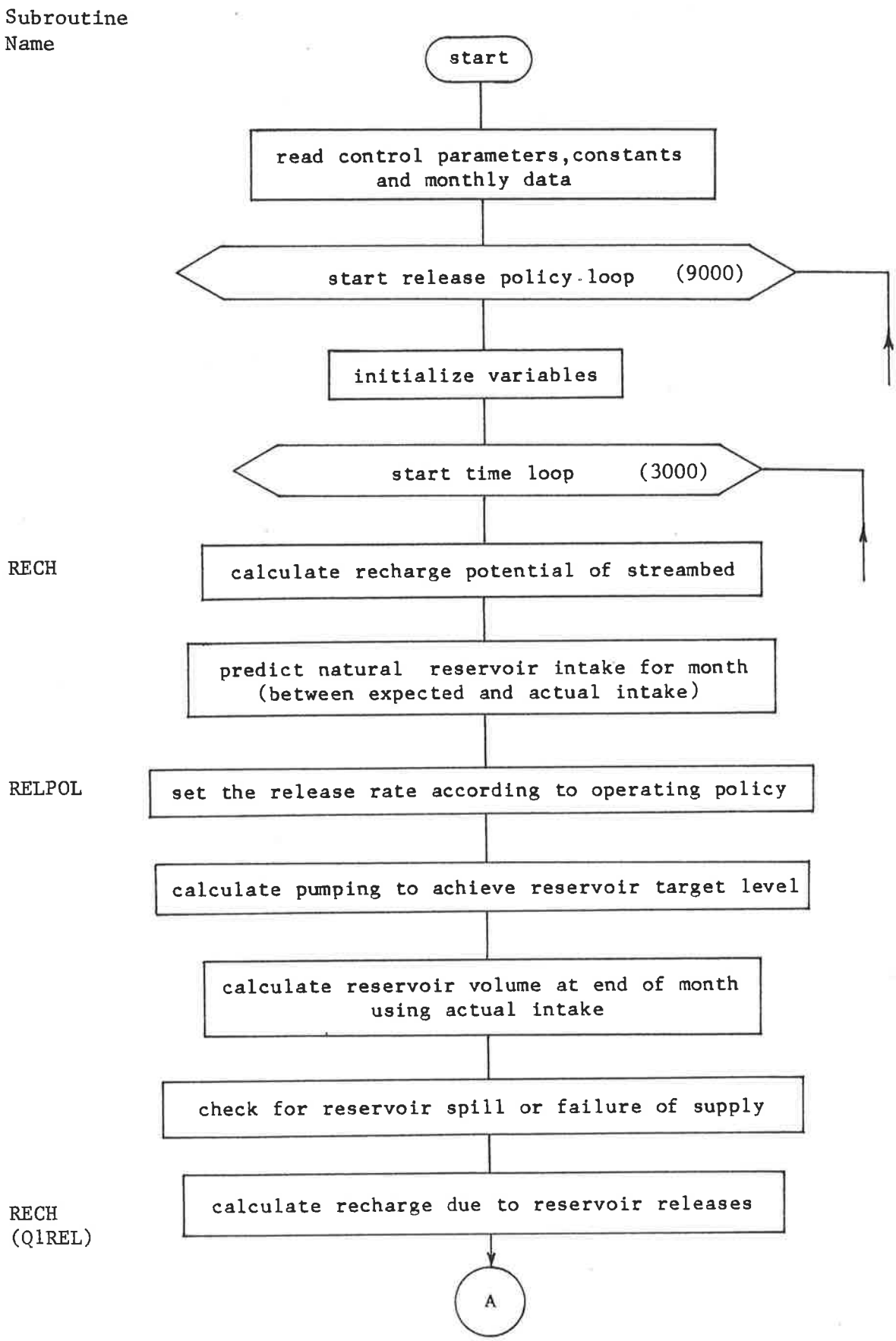

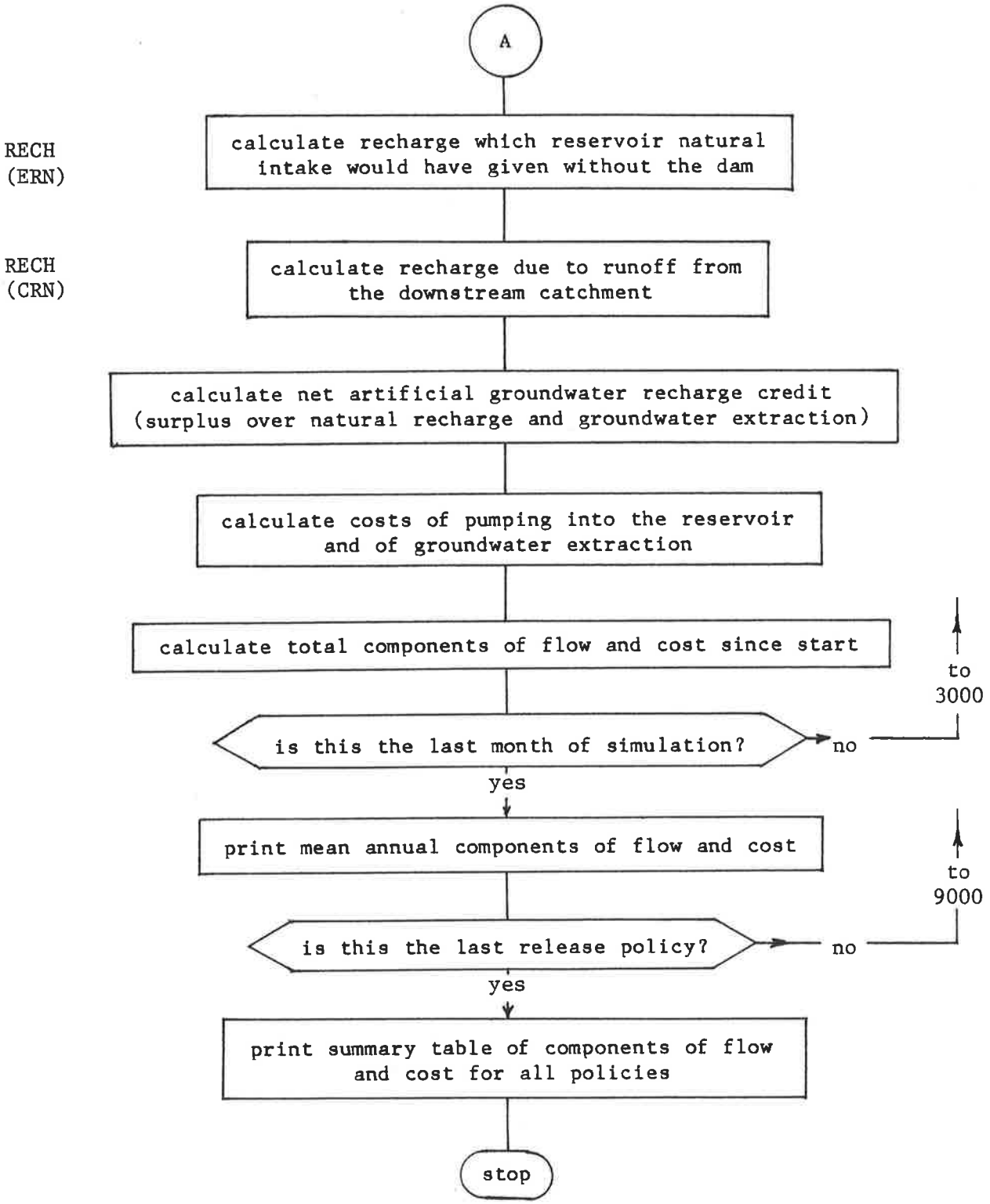
A
RECH (ERN)
calculate recharge which reservoir natural intake would have given without the dam
RECH (CRN)
calculate recharge due to runoff from the downstream catchment
calculate net artificial groundwater recharge credit (surplus over natural recharge and groundwater extraction)
calculate costs of pumping into the reservoir and of groundwater extraction
calculate total components of flow and cost since start
to 3000
is this the last month of simulation?
no
yes
print mean annual components of flow and cost
to 9000
is this the last release policy?
no
yes
print summary table of components of flow and cost for all policies
stop

BIBLIOGRAPHY

AMAR, A.C. (1975). Groundwater recharge simulation, ASCE J. Hydraul. 101 (HY9) pp 1235-1247.

ANDRE, J.C. and MOLINARI, J. (1976). Mises au point sur les differents facteurs physico- chemiques influant sur la mesure de concentration de traceurs fluorescents et leurs consequences practiques en hydrologie, J. Hydrol. 30 pp 257-285.

AUSTRALIAN WATER RESOURCES COUNCIL (1982). Guidelines for the use of reclaimed water for aquifer recharge, AWRC Water Management Series No 2, Aust. Govt. Publishing Service, Canberra.

BACHMAT, Y., BREDEHOEFT, J., ANDREWS, B., HOLTZ, D. and SEBASTIAN, S. (1980). Groundwater Management : the use of numerical models, Am. Geophys. Union Water Resources Monograph 5, Washington D.C..

BAUMANN, P. (1965). Technical development in ground-water recharge, Advances in Hydroscience, Vol. 2, pp 209-279.

BEAR, J. (1972). Dynamics of Fluids in Porous Media, American Elsevier.

BEAR, J. (1979). Hydraulics of Groundwater, McGraw Hill, New York.

BESBES, M., DELHOMME, J.P. and De MARSILY, G. (1978). Estimating recharge from ephemeral streams in arid regions, Water Resour. Res. 14(2) pp 281-190.

BIANCHI, W.C. and HASKELL, E.E. (1968). Field observations compared with Dupuit-Forchheimer theory for mound heights under a recharge basin, Water Resour. Res. 4(5) pp 1049-1057.

BIERE, A.W. and LEE, I.M. (1972). A model for managing reservoir water releases,Amer. J. Agr. Econ. 54(3) pp 411-421.

BOS, M.G. (ed.) (1976) Discharge measurement structures, Publication No. 161, Delft Hydraulics Laboratory, Delft, The Netherlands.

BOUCAUT, W.R.P. (1977) Northern Adelaide Plains - Groundwater Hydrological Summary, South Aust. Dept. of Mines, unpublished report.

BOUWER, H (1964). Unsaturated flow in groundwater hydraulics, ASCE J. Hydraul. 90(HY5) pp 121-144.

BOUWER, H. (1969). Theory of seepage from open channels, Advances in Hydroscience, Vol. 5, pp 121-172.

BOUWER, H. (1975). Predicting reduction in water losses from open channels by phreatophyte control, Water Resour. Res. 11(1) pp 96-101.

BOUWER, H. (1976). Infiltration into increasingly permeable soils, ASCE J. Irrig. and Drain. 102(IR2) pp 127-136.

BOUWER, H. (1978). Groundwater Hydrology, McGraw Hill, New York.

BROCK, R.R. (1976a). Hydrodynamics of perched mounds, ASCE J. Hydraul. 102(HY8) pp 1083-1100.

BROCK, R.R. (1976b). Dupuit-Forchheimer and potential theories for recharge from basins, Water Resour. Res. 12(5) pp 909-911.

BRUCH, J.C. and SLOSS, J.M. (1978). A variational inequality method applied to free surface seepage from a triangular ditch. Water Resour. Res. 14(1) pp 119-124.

BRUCH, J.C., SAYLE, F.C. and SLOSS J.M. (1978). Seepage from a trapezoidal and a rectangular channel using variational inequalities, J. Hydrol. 36 pp 247-260.

BURAS, N. (1963). Conjunctive operation of dams and aquifers, ASCE J. Hydraul. 89(HY6) pp 111-131.

BURKHAM, D.E. (1970). A method of relating infiltration rates to streamflow rates in perched streams, USGS Prof. Paper 700-D, pp 266-271.

CLOSE, A.F. and LINKE, G.K. (1981). Northern Adelaide Plains Groundwater Management Model: Calibration Report, Engg. and Water Supply Dept. of South Aust. Report No. EWS 81/39.

COOPER, H.H. AND RORABAUGH, M.I. (1963) Groundwater movements and bank storage due to flood stages in surface streams, USGS Water Supply Paper 1536-J, pp 343-366.

CORDERY, I. (1976). Some effects of urbanization on streams, Inst. of Engineers Aust. Civil Engg. Trans. CE18(1) pp 7-11.

CUNNINGHAM, A.B. and SINCLAIR, P.J. (1979). Application and analysis of a coupled surface and groundwater model, J Hydrol. 43 pp 129-148.

CURTIS, A.A. and WATSON, K.K. (1980). Numerical analysis of infiltration into a sand profile bounded by a capillary fringe, Water Resour. Res, 16(2) pp 365-371.

DAKSHANAMURTHY, V. and FREDLUND, D.G. (1981). A mathematical model for predicting moisture flow in an unsaturated soil under hydraulic and temperature gradients, Water Resour. Res. 17(3) pp 714-722.

De BACKER, L. (1975). Experimental artificial recharge, Proc. Work. Conf. on Computer Simulation of Water Resour. Systems, Ghent, Belgium, Jul 1974, pp 279-289.

De WEIST, R.J.M. (1967). Artificial recharge through augmented bank storage, Int. Assoc. Sci. Hydrol., pub. no 72, pp 53-68.

DILLON, P.J. (1977). Recharge releases from Little Para Reservoir, Engg. and Water Supply Dept. of South Aust. Report No. EWS 77/15.

DILLON, P.J. (1978). Unsteady Groundwater Recharge - proposal for a joint study by Engg. and Water Supply Dept. of South Aust. and the Dept. of Civil Engg. Univ. of Adelaide, EWS File No 6207/78 (unpublished).

DILLON, P.J. (1979). Little Para Recharge Study Stage I Progress Report, Univ. of Adelaide Civil Engg. Dept. Report to Engg. and Water Supply Dept. of South Aust. (unpublished).

DILLON, P.J. (1980). Air lift water sampling test 27/6/80, Univ. of Adelaide Civil Engg. Dept. report to South Aust. Dept. of Mines and Energy (unpublished).

DILLON, P.J. (1981a). Little Para Recharge Study Stage II Progress Report, Univ. of Adelaide Civil Engg. Dept. report to Engg. and Water Supply Dept. of South Aust. (unpublished).

DILLON, P.J. (1981b). Simple models of groundwater recharge for ephemeral streams, Proc. Aust. Water Resour. Council Groundwater Recharge Conf., Townsville, July 1980, pp 60-71. (see Appendix C.2)

DILLON, P.J. (1983a). Little Para Recharge Study Final Report and Appendices, Univ. of Adelaide Civil Engg. Dept. report to Engg. and Water Supply Dept. of South Aust. (2 volumes, unpublished).

DILLON, P.J. (1983b). Boundary integral model of stream-aquifer interaction, Preprints Inst. of Engineers Aust. Hydrol. and Water Resour. Symp., Hobart, Nov. 1983, pp 195-199. (see Appendix C.4)

DILLON, P.J. (1983c). Management of a pumped surface storage and an aquifer, Proc. Intl. Conf. on Groundwater and Man, Sydney, Dec. 1983, Aust. Water Resour. Council Conf. Series No. 8, Vol 1, pp 69-78. (see Appendix C.6)

DILLON, P.J. (1983d). Stream-aquifer interaction models : a review, Inst. of Engineers Aust. Civil Engg. Trans. CE25(2) pp 107-113. (see Appendix C.1)

DILLON, P.J. (1983e). Artificial groundwater recharge : a case study in Maharashtra, India, Univ. of Adelaide, Dept. of Civil Engg. Report No. G15.

DILLON, P.J. (1983f). Digital hydrologic data acquisition system, Proc. UNESCO Symp. on Methods and Instrumentation for the Investigation of Groundwater Systems, Noordwijkerhout, The Netherlands, May 1983, pp 528-537. (see Appendix C.5)

DILLON, P.J. and LIGGETT, J.A. (1983). An ephemeral stream-aquifer interaction model, Water Resour. Res. 19(3) pp 621-626. (see Appendix C.3)

DIXON, W.J. ed. (1981). BMDP Statistical Software 1981, Dept. of Biomathematics Univ. of California, Los Angeles, Univ. of California Press.

DOOGE, J.C.I. (1973). Linear Theory of Hydrologic Systems, U.S. Dept. Agric. Tech. Bull. Vol. 1468.

DRAPER, N.R. and SMITH, H. (1981). Applied Regression Analysis, (2nd edition), John Wiley and Sons, New York.

ELFORD, M.T. and POTTER, T.J. (1979). Numerical modelling of open channel transient flow, Univ. of Adelaide Civil Engg. Dept. student project report.

ERNST, L.F. (1979). Groundwater flow to a deep well near a rectilinear channel, J. Hydrol. 42 pp 129-146.

FERRIS, J.G., KNOWLES, D.B., BROWN, R.H. and STALLMON, R.W. (1962). Theory of aquifer tests, USGS Water Supply Paper 1536-E. (particularly p 122).

FERRIS, J.G. (1959). Groundwater, ch 7 in Whisler C.O. and Brater, E.F. (eds) Hydrogeology, Wiley, New York.

FLUG, M., ABI-GHANEM, G.V. and DUCKSTEIN, L (1980). An event-based model of recharge from an ephemeral stream, Water Resour. Res. 16(4) pp 685-690).

FRASER, C.J. and JONES, N.O. (1977). A model of water flows in the quaternary alluvium of the Callide-Don river basin, Queensland, Aust. Water Resour. Council Groundwater Modelling Seminar, Sydney, July 1977.

FREEZE, R.A. (1969). The mechanism of natural groundwater recharge and discharge (1), Water Resour. Res. 5(1) pp 153-171.

FREEZE, R.A. (1971). Three dimensional transient saturated-unsaturated flow in a groundwater basin, Water Resour. Res. 7(2) pp 347-366.

FREEZE, R.A. (1972). Role of subsurface flow in generating surface runoff (1) Baseflow contributions to channel flow, Water Resour. Res. 8(3) pp 609-623.

FREYBERG, D.L., REEDER, J.W., FRANZINI, J.B. and REMSON, I. (1980). Application of the Green-Ampt model to infiltration under time dependent surface water depths, Water Resour. Res. 16(3) p 517-528.

GELHAR, L.W. (1974). Stochastic analysis of phreatic aquifers, Water Resour. Res. 10(3), pp 539-545.

GLASS, J.P., CHRISTENSEN, B.A. and RUBIN, H. (1977). Analysis of transient groundwater flow from seepage ponds, Proc. 3rd Intl. Hydrol. Symp., Fort Collins, Colorado, pp 246-256.

GRANNEMAN, N.G. and SHARP, J.M. (1979). Alluvial hydrogeology of the lower Missouri River, J. Hydrol. 40 pp 85-99.

GREACEN, E.L. ed. (1981). Soil water assessment by the neutron method, CSIRO Aust. publication, Melbourne.

GREEN, W.G. and AMPT, G.A. (1911). Studies on soil physics, 1, The flow of air and water through soils, J. Agric. Sci. 4 pp 1-24.

GRODZENSKY, V.D. (1967). Formation of fresh ground water lenses as a result of percolation from canals and pits, Int. Assoc. Sci. Hydrol. pub. no 72, pp 360-364.

HADGRAFT, R.G. and VOLKER, R.E. (1981). A model for predicting aquifer recharge from rainfall and river flow, Proc. Aust. Water Resour. Council Groundwater Recharge Conf., Townsville, July 1980, pp 108-118.

HADGRAFT, R.G., VOLKER, R.E. and STARK, K.P. (1982). Investigation of reservoir release rules using dynamic programming and simulation, Preprints Inst. of Engineers Aust. Hydrol. and Water Resour. Symp., Melbourne, May 1982, pp 64-68.

HALL, F.R. (1968). Base flow recessions - a review, Water Resour. Res. 4 pp 973-983.

HALL, F.R. and MOENCH, A.F. (1972). Application of the convoluation equation to stream-aquifer relationships, Water Resour. Res. 8(2) pp 487-493.

HANTUSH, M.S. (1967). Growth and decay of groundwater mounds in response to uniform percolation, Water Resour. Res. 3(1) pp 227-234.

HARROLD, L.L. (1934). Relation of streamflow to groundwater levels, Trans. Am. Geophys. Union, pt 2, pp 414-416.

HENRY, J.L. (1979). Intergrated Finite Difference Modelling of Groundwater Flow, Queensland Water Resources Commission Report, Volumes 1 and II.

HENRY, J.L. and PALMER, J.R. (1981). Natural and artificial rechage of groundwater in the Callide Valley, Proc. Aust. Water Resour. Council Groundwater Recharge Conference, Townsville, July 1980, pp 72-87.

HERBERT, R. (1970). Modelling partially penetrating rivers on aquifer models, Groundwater, 8 pp 29-36.

HUNT, B.W. (1972). Seepage from shallow open channel, ASCE J. Hydraul. 98 (HY5) p 779-785.

JACKES (1981). Burdekin artificial groundwater recharge study: biological problems, Proc. Aust. Water Resour. Council, Groundwater Recharge Conference Townsville, July 1980, pp 119-130.

JACOB, C.E. (1950). Flow of Groundwater, chapter V in, Engineering Hydraulics, edited by ROUSE, H., Wiley, New York.

JAMES, S.E. and HENRY, J.L. (1977). Effects of siltation on rates of recharge, Aust. Water Resour. Council Tech. Paper No. 23.

JENKINS, C.T. (1968). Techniques for computing rate and volume of stream depletion by wells, Groundwater 6(2), pp 37-46.

JOHNSTON, P.R., LAURENSON, E.M. and HOWELL, D.T. (1972). Procedure for the conjunctive use of surface and groundwater storages, Aust. Water Resour. Council Tech. Paper No. 3, Aust Govt. Publishing Service, Canberra.

JORDAN, R.R. (1977). Streamflow transmission losses in Western Kansas, ASCE J. Hydraul. 103(HY8) pp 905-919.

KHAN, M.Y., KIRKHAM, D. and HANDY, R.L. (1976). Shapes of steady state perched groundwater mounds, Water Resour. Res. 12(3) pp 429-436.

KINGSTON, D and SHEPHERD, R.G. (1973). Proposed Little Para Dam - effect on intake to aquifers of Northern Adelaide Plains, South Aust. Dept. of Mines Report Book No. 73/246.

KNAPP, R.M., GREEN, D.W., POGGE, E.C. and STANFORD, C. (1975). Development and field testing of a basin hydrology simulator, Water Resour. Res. 11(6) pp 879-888.

KOKINOW, L.F. and BREDEHOEFT, J.D. (1974). Modelling flow and chemical quality changes in an irrigated stream-aquifer system, Water Resour. Res. 10(3) pp 546-562.

KOVACS, G. and associates (1981). Subterranean Hydrology, Water Resources Publications, Littleton, Colorado.

LANG, S.M. and RHODEHAMEL, E.C. (1962). Movement of groundwater beneath the bed of the Mullica River in the Wharton Tract, New Jersey, USGS Prof. Paper 450-B, pp 90-92.

LIGGETT, J.A. and LIU, P.L. (1983). Boundary Integral Equation Method for Porous Media Flow, Allen and Unwin, London.

LIN, C.L. (1972). Digital simulation of the Boussinesq equation for a water table aquifer, Water Resour. Res. 8(3) pp 691-698.

LINKE, G.K. and EBERHARD, B. (1981). Northern Adelaide Plains Groundwater Management Model : Data Preparation, Engg. and Water Supply Dept. of South Aust. Report No. EWS 81/38.

LIU, P.L. and LIGGETT, J.A. (1980). Numerical stability and accuracy of implicit integration of free surface groundwater equations, Water Resour. Res. 16(5) pp 897-900.

LUTHIN, J.N., ORHUN, A. and TAYLOR, G.S. (1975). Coupled saturated-unsaturated transient flow in porous media: experimental and numerical model, Water Resour. Res. 11(6) pp 973-978.

MAASLAND, M. (1959). Water table fluctuations induced by intermittent recharge, J. Geophys. Research 64 pp 549-559.

McCUEN, R.H., RAWLS, W.J. and BRAKENSIEK, D.L. (1981). Statistical analysis of the Brooks- Corey and the Green- Ampt parameters across soil textures, Water Resour. Res. 17(4) pp 1005-1013.

McWHORTER, D.B. and BROOKMAN, J.A. (1972). Pit recharge influenced by subsurface spreading, Ground Water 10(5) pp 6-11.

MARINO, M.A. (1967). Hele-Shaw model study of the growth and decay of groundwater ridges, J. Geophys. Research 72(4) pp 1195-1205.

MARINO, M.A. (1973). Water table fluctuation in semi-pervious stream-aquifer system, J. Hydrol. 19 pp 43-52.

MARINO, M.A. (1974a). Rise and decline of the water table induced by vertical recharge, J. Hydrol. 23 pp 289-298.

MARINO, M.A. (1974b). Water table fluctuation in response to recharge, ASCE J. Irrig. and Drain. 100 (IR2) pp 117-125.

MARINO, M.A. (1981). Analysis of transient movement of water and solutes in stream-aquifer systems, J. Hydrol. 49 pp 1-17.

MARMION, K.R. (1962). Hydraulics of artificial recharge in non- homogeneous formations, Univ. of California, Berkeley, Water Resour. Centre Contribution No. 48.

MILES, K.R. (1952). Geology and underground water of the Adelaide Plains area, Geol. Survey of South Aust. Bulletin No. 27.

MOENCH, A.F. and KISIEL, C.C. (1970). Application of the convolution relation to estimating recharge from an ephemeral stream, Water Resour. Res. 6(4) pp 1087-1094.

MOENCH, A.F. SAUER, V.B. and JENNINGS, M.E. (1974). Modification of routed streamflow by channel loss and baseflow, Water Resour. Res. 10(5) pp 963-968.

MOREL-SEYTOUX, H.J. and KHANJI, J. (1974). Derivation of an equation of infiltration, Water Resour. Res. 10(4) pp 795-800.

MOREL-SEYTOUX, H.J. (1975). A combined model of water table and river stage evolution, Water Resour. Res. 11(6) pp 968-972.

MOUSAVI, S.F. and KIRKHAM, D. (1978). Porous media tests of groundwater mounds, Soil Sci. 125 (3) pp 160-164.

NAKANO, Y. (1981). A travelling wave solution to the problem of simultaneous flow of water and air through homogeneous porous media, Water Resour. Res. 17(1) pp 57-64.

NARASIMHAN, T.N., NEUMAN, S.P. and WITHERSPOON, P.A. (1978). Finite element method for subsurface hydrology using a mixed explicit-implicit scheme, Water Resour. Res. 15(5) pp 863-867.

NARASIMHAN, T.N. and YANEHIRO, B.Y. (1980). A note on the meaning of storage coefficient, Water Resour. Res. 16(2) pp 423-429.

NEUMAN, S.P., NARASIMHAN, T.N. and WITHERSPOON, P.A. (1976). Application of mixed ewplicit- implicit finite element method to nonlinear diffusion- type problems, in, Finite Elements in Water Resources, GRAY, W.G. et al (ed), Pentech Press, London, pp 1.153-1.186.

NIGHTINGALE, H.I. and BIANCHI, W.C. (1977). Groundwater turbidity resulting from artificial recharge, Ground Water 15(2) pp 146-152.

NORRIS, S.E. (1970). The effect of stream discharge on streambed leakage to a glacial outwash aquifer, USGS Prof. Paper 700-D, pp D262-D265.

PEARCE, B.R. (1981). The use of temporary sand dam storages in determining the river recharge in the Proserpine area, Proc. Aust. Water Resour. Council Groundwater Recharge Conf., Townsville, July 1980, pp 88-97.

PHILIP, J.R. (1969). Theory of infiltration, Advances in Hydroscience, Vol. 5 pp 215-305.

PINDER, G.F., BREDEHOEFT, J.D. and COOPER, H.H. (1969). Determination of aquifer diffusivity from aquifer response to fluctuations in river stage, Water Resour. Res. 5(4) pp 850-855.

PINDER, G.F. and SAUER, S.R. (1971). Numerical simulation of floodwave modification due to bank storage effects, Water Resour. Res. 7(1) pp 63-70.

PLUHOWSKI, E.J. and KANTROWITZ, I.H. (1962). Source of groundwater runoff at Champlin Creek, Long Island, New York, USGS Prof. Paper 450-B, pp B95-B97.

RANDALL, A.D. (1978). Infiltration from tributary streams in Susquehanna river basin, J. Research USGS, 6(3) pp 285-297.

RAUDKIVI, A.J. (1979). Hydrology, Pergamon Press, Oxford.

REDDY, A.S. and BASU, U. (1976). Seepage from trapezoidal canal in anisotropic soil, ASCE J. Irrig. and Drain. 102 (IR3) pp 349-361.

REEDER, J.W., FREYBERG, D.L., FRANZINI, J.B. and REMSON, I. (1980). Infiltration under rapidly varying surface water depths, Water Resour. Res. 16(1) pp 97-104.

RICHARDS, L.A. (1931). Capillary conduction of liquids through porous mediums, Physics, Vol. 1, pp 318-333.

ROVEY, C.E.K. (1975). Numeridal model of flow in a stream-aquifer system, Colorado State Uni, Fort Collins, Hydrology Papers No. 74.

ROWE, P.P. (1960). An equation for estimating transmissibility and coefficient of storage from river level fluctuations, J. Geophys. Research 65(10) pp 3419-3424.

RUSHTON, K.R. and TOMLINSON, L.M. (1975). Numerical analysis of confined-unconfined aquifers, J. Hydrol. 25 pp 259-274.

RUSHTON, K.R. and TOMLINSON, L.M. (1979). Possible mechanisms for leakage between aquifers and rivers, J. Hydrol. 40 pp 49-65.

SAGAR, B. and SINGH, S.R. (1979). Aquifer diffusivity from noisy boundary data, ASCE J. Hydraul. 105 (HY8) pp 943-954.

SAUER, V.B. (1973). Unit response method of open channel flow routing, ASCE J. Hydraul. 99 (HYl) pp 179-193.

SCHRALE, G. (1976). Studies of underground water storage and recharge by means of nuclear well logging techniques, PhD. Thesis, School of Earth Sciences, Flinders Univ. of South Aust.

SHARMA, H.D. and CHAWLA, A.S. (1979). Canal seepage with boundary at finite depth, ASCE J. Hydraul, 105 (HY7) pp 877-897.

SHARP, J.M. (1977). Limitations of bank storage model assumptions, J. Hydrol. 35 pp 31-47.

SHEPHERD, R.G. (1966). The hydrogeology of the Northern Adelaide Plains basin, Mining Review Vol. 125 pp 8-20.

SHEPHERD, R.G. (1975). Northern Adelaide Plains Groundwater Study Stage II 1968- 1974, South Aust. Dept. of Mines Report Book No. 75/38.

SHESHTAKOV, V.M. and KRAVCHENKO, I.P. (1967). A contribution to the technique for the evaluation of natural and workable resources of near-canal fresh water lenses, Intl. Assoc. Sci. Hydrol. Pub. No. 72, pp 83-90.

SINGH, K.P. (1968). Some factors affecting baseflow, Water Resour. Res. 4(5) pp 985-999.

SINGH, R. (1976). Prediction of mound geometry under recharge basins, Water Resour. Res. 12(4) pp 775-780.

SINGH, S.R. and SAGAR, B. (1977). Estimation of aquifer diffusivity in stream-aquifer systems, ASCE J. Hydraul. 103(HY11) pp 1293-1302.

SKAGGS, R.W. and TANG, Y.K. (1976). Saturated and unsaturated flow to parallel drains, ASCE J. Irrig. and Drain. 102(IR2) pp 221-238.

SMART, P.L. and LAIDLAW, I.M.S. (1977). An evaluation of some fluorescent dyes for water tracing, Water Resour. Res. 13(1) pp 15-33.

SMILES, D.E. and KNIGHT, J.H. (1979). The transient water table beneath a leaking canal, J. Hydrol. 44 pp 149-162.

SMITH, R.E. (1972). Border irrigation advance and ephemeral flood waves, ASCE J. Irrig. and Drain. 98 pp 289-307.

SOUTH AUSTRALIA, Dept. of Mines. (1968). Northern Adelaide Plains Groundwater Study to May 1968, Report No. DM 1974/67, Volumes I and II.

SOUTH AUSTRALIA, Engg. and Water Supply Dept. (1978). Metropolitan Adelaide Water Resources Study, Report No. EWS 77/42.

SOUTH AUSTRALIA, Engg. and Water Supply Dept. (1980). Little Para Recharge Study Site Investigation Report, Soils and Foundations Section, Design Services Branch (unpublished).

STEWART, B.J. and BOUGHTON, W.C. (1983). Transmission losses in natural streambeds- A review, Preprints Inst. of Engineers Aust. Hydrol. and Water Resour. Symp., Hobart, Nov. 1983, pp 226-230.

STRELTSOVA, T.D. (1974). Method of additional seepage resistances-theory and applicaiton, ASCE J. Hydraul. 100 (HY8) pp 1119-1131.

TALSMA, T. (1969). Infiltration from semi-circular furrows in the field, Aust. J. Soil Res. 7 pp 277-284.

TAYLOR, G.S. and LUTHIN, J.N. (1969). Computer method for transient analysis of water table aquifers, Water Resour. Res. 5(1) pp 144-152.

TAYLOR, O.J. and LUCKEY, R.R. (1972). New technique for estimating recharge using a digital model, Ground Water 10(6) pp 22-26.

TIXERONT, J. and DANIEL, J.M. (1967). Alimentation et suralimentation des nappes souterraines, Int. Assoc. Sci. Hydrol. Pub. No. 72, pp 173-181.

TODD, D.K. (1955). Ground-water flow in relation to a flooding stream, Proc. ASCE Vol 81, Separate No. 628, pp 1-20.

TODD, D.K. (1959). Annotated bibliography on artificial recharge of groundwater through 1954, USGS Water Supply Paper 1477.

TONKIN, B.C. and ASSOCIATES (1981). Little Para River Drainage Basin Hydrology, consulting engineers report to local government authorities, B.C. Tonkin and Assocs., Adelaide.

VACHAUD, G. (1967). On the storage coefficient of free surface aquifers considering the flow in the unsaturated zone, Int. Assoc. Sci. Hydrol. Pub. No. 72, pp 69-82.

VAUCLIN, M., KHANJI, D. and VACHAUD, G. (1979). Experimental and numerical study of a transient two dimensional unsaturated-saturated water table recharge problem, Water Resour. Res. 15(5) pp 1089-1101.

VENETIS, C. (1968). On the impulse response of an aquifer, Int. Assoc. Sci. Hydrol. Bull. No. 13(3) pp 136-139.

VENETIS, C. (1970). Finite aquifers: characteristic responses and applications, J. Hydrol. 12 pp 53-62.

WALLACE, K., HINES, N. and GOLDING, W. (1977). A laboratory study of the infiltration characterisitcs of coarse grained soils, James Cook Univ. Interim Road Rept. No. 14.

WALTON, W.C. and ACKROYD, E.A. (1966). Effects of induced streambed infiltration on water levels in wells during aquifer tests, Minnesota Univ. Water Resour. Res. Centre Bulletin No. 2.

WALTON, W.C., HILLS, D.L. and GRUNDEEN, G.M. (1967). Recharge from induced streambed infiltration under varying groundwater level and stream stage conditions, Minnesota Univ. Water Resour. Res. Centre Bulletin No. 6.

WALTON, W.C. (1979). Progress in analytical groundwater modelling, J. Hyrol. 43 pp 149-159.

WARD, R.C. (1974). Principles of Hydrology, 2nd edition, McGraw Hill.

WARNER, D.L. and DOTY, L.F. (1967). Chemical reaction between recharge water and aquifer water, Int. Assoc. Sci. Hydrol. Pub. No. 72, pp 278-288

WATSON, K.A. and ZIERSCH, R.L. (1977). Tensiometers: installation, servicing and usage, South Aust. Dept. Agric. and Fisheries, Horticulure Branch Handbook.

WATSON, K.K. and WHISLER, F.D. (1977). Profile desaturation during sediment deposition in a groundwater recharge trench, J. Hydrol. 33 pp 397-401.

WATSON, K.K. (1981). Numerical analysis of natural groundwater recharge under intermittent surface inputs, Proc. Aust. Water Resour. Council Groundwater Recharge Conf., Townsville, July 1980, pp 98-107.

WEBB, S.N. and WATSON, K.K. (1977). Analysis of the movement of water from recharge channels and pits, Aust. Water Resour. Council Tech. Paper No. 24.

WHISLER, F.D. and BOUWER, H. (1970). Comparison of methods for calculating vertical drainage and infiltration for soils, J. Hydrol. 10 pp 1-19.

WILSON, J.L. and DETTINGER, M. (1978). Steady state versus transient parameter estimation in groundwater systems, Proc. ASCE Hydraul. Div. Conf. on Verification of Mathematical and Physical Models in Hydraulic Engineering, Univ. of Maryland, Aug. 1978, pp 112-119.

WILSON, L.G. and De COOK, K.J. (1968). Field observations on changes in the subsurface water regime during influent seepage in the Santa Cruz River, Water Resour. Res. 4(6) pp 1219-1234.

WORSTELL, R.V. (1976). Estimating seepage losses from canal systems, ASCE J. Irrig. and Drain. 102(IRl) pp 137-147.

WYATT, T., THORN, D.G. and MAWER, P.A. (1974). Streamflow regulation by artificial recharge fed from upstream surface storage- derivation of control rules, Int. Assoc. Hydrol. Sci., Studies and Reports in Hydrology, Vol 15(2) pp 989-1000.

YEH, W.W.G. (1975). Aquifer parameter identification, ASCE J. Hydraul. 101(HY9) pp 1197-1209.

YOUNGS, E.G. (1977). The unsteady groundwater mound below an irrigation ditch or leaky canal, J. Hydrol. 34 pp 307-314.